Atmospheric processing and relevance of biomass burning aerosols over the Amazon and the Atlantic

Dissertation

zur Erlangung des Grades
"Doktor rerum naturalium (Dr. rer. nat.)" der Fachbereiche:
08 - Physik, Mathematik und Informatik,
09 - Chemie, Pharmazie und Geowissenschaften,
10 - Biologie und Universitätsmedizin

verfasst und vorgelegt von
Bruna Amorim Holanda
geb. in São Paulo

Max Planck Graduate Center
mit der Johannes Gutenberg-Universität Mainz

angefertigt am Max-Planck-Institut für Chemie

Mainz, 2021

MAX-PLANCK-GESELLSCHAFT
Max Planck Graduate Center
mit der Johannes Gutenberg-Universität Mainz
JOHANNES GUTENBERG UNIVERSITÄT MAINZ

Tag der mündlichen Prüfung: 08. Dezember 2021

I hereby declare that I wrote the dissertation submitted without any unauthorized external assistance and used only sources acknowledged in the work. All textual passages which are appropriated verbatim or paraphrased from published and unpublished texts as well as all information obtained from oral sources are duly indicated and listed in accordance with bibliographical rules. In carrying out this research, I complied with the rules of standard scientific practice as formulated in the statutes of Johannes-Gutenberg-Universität Mainz to ensure standard scientific practice.

Mainz, 07.09.2021, Bruna Amorim Holanda

Abstract

Biomass burning aerosols from vegetation fires affect the Earth's radiation balance and hydrological cycle and, thus, have profound influences on atmospheric circulation and the climate system. This is particularly true for the atmosphere over the Amazon rain forest, which oscillates between pristine aerosol conditions in the wet season and the heavily polluted dry season with the widespread use of fire in deforestation, agricultural expansion, and infrastructure projects. Accordingly, the role of fires as a destructive and transformative force in the Amazon ecosystem has been a focal point of research for decades. Especially, the atmospheric effects of the large amounts of emitted smoke, comprising black carbon (BC) along with organic and inorganic aerosols, have been investigated intensely. Yet, significant uncertainties remain on the smoke's spatial and temporal variability as well as its optical and microphysical properties.

This dissertation characterizes the sources, abundance, properties, and atmospheric significance of biomass burning aerosols over the Amazon and the tropical Atlantic region. Black carbon has been characterized systematically, along with a broad spectrum of complementary aerosol and trace gas parameters. This work is based on large-scale field campaigns, including multi-year measurements at the Amazon Tall Tower Observatory (ATTO) as well as five missions with the High Altitude and LOng Range research aircraft (HALO). The analysis yielded a comprehensive and fundamental aerosol characterization with a particular focus on biomass burning smoke and its microphysical and optical properties. The ATTO data emphasize the aerosol's pronounced seasonality and diurnal cycles as well as the response to climate extremes such as El Niño periods. It is shown that the Amazonian pollution burden is not solely defined by local and regional fires but also receives large amounts of African smoke via long-range transport. This African contribution cannot be neglected in the analysis and modelling of the life cycle of Amazonian aerosols.

The ATTO results are complemented by the HALO aircraft observations, resolving the transatlantic transport of BC-rich African smoke in defined layers in the free troposphere, followed by its entrainment into of the Amazonian boundary layer. Even after mixing, the Amazonian and African smoke can efficiently be distinguished through characteristic microphysical signatures. This approach has been used systematically to analyze the physical and chemical properties of both smoke fractions. Finally, a comparison of all HALO missions links the detailed characterization of the Amazonian and African smoke to further combustion aerosols worldwide suggesting distinct differences in the relationship between BC and cloud condensation nuclei concentration.

Zusammenfassung

Aerosole aus der Biomasseverbrennung wirken sich auf die Strahlungsbilanz und den Wasserkreislauf der Erde aus und haben somit tiefgreifenden Einfluss auf die atmosphärische Zirkulation und das Klimasystem. Dies gilt besonders für die Atmosphäre des Amazonas-Regenwalds, die zwischen weitgehend unberührten Aerosol-Bedingungen in der Regenzeit und einer stark verschmutzten Trockenzeit mit weit verbreitetem Einsatze von Feuer im Zuge von landwirtschaftlicher Expansion, Bergbau und Infrastrukturprojekten oszilliert. Dementsprechend ist die Rolle von Bränden als zerstörerische und transformative Kraft im Amazonas-Ökosystem seit Jahrzehnten ein wesentliches Forschungsthema. Insbesondere die atmosphärischen Auswirkungen der großen Mengen an emittiertem Rauch, der neben organischen und anorganischen Aerosolen auch schwarzen Kohlenstoff enthält, wurden intensiv untersucht. Dennoch bestehen nach wie vor erhebliche Unsicherheiten hinsichtlich der räumlichen und zeitlichen Variabilität des Rauches sowie seiner optischen und mikrophysikalischen Eigenschaften.

In dieser Dissertation werden die Quellen, die Häufigkeit, die Eigenschaften und die atmosphärische Bedeutung von Aerosolen aus der Biomasseverbrennung über dem Amazonas und den tropischen Atlantik charakterisiert. Schwarzer Kohlenstoff wurde zusammen mit einem weiten Spektrum anderer Aerosol- und Spurengasparameter charakterisiert. Diese Arbeit basiert auf groß angelegten Feldkampagnen, einschließlich mehrjähriger Messungen am Amazon Tall Tower Observatory (ATTO) sowie fünf Missionen mit dem Forschungsflugzeug HALO. Basierend auf den Messdaten wird eine umfassende Analyse grundlegender Aerosolparameter mit besonderem Schwerpunkt auf Rauch aus Biomasseverbrennung und dessen mikrophysikalischen und optischen Eigenschaften präsentiert. Die ATTO-Beobachtungen heben dabei die ausgeprägte Saisonalität und die täglichen Aerosol-Zyklen, sowie die Auswirkungen von Klimaextremen wie El-Niño-Perioden hervor. Die Ergebnisse verdeutlichen, dass die Schadstoffbelastung im Amazonas nicht nur durch lokale und regionale Brände bestimmt wird, sondern auch durch große Mengen afrikanischen Rauchs über den Atlantik nach Südamerika transportiert werden. Dieser afrikanische Beitrag sollte bei künftigen Analysen und Modellierungen des Lebenszyklus von Aerosolen im Amazonas Berücksichtigung finden.

Die ATTO-Beobachtungen werden durch die HALO-Missionen ergänzt, die den Transport des afrikanischen Rauchs in definierten Schichten in der freien Troposphäre, gefolgt von seinem Eintrag in die Amazonas-Grenzschicht, darlegen. Aufgrund der beachtlich unterschiedlichen mikrophysikalischen Signaturen können der südamerikanische und afrikanische Rauch auch nach ihrer Durchmischung klar voneinander abgegrenzt werden. Dieser Ansatz wurde systematisch genutzt, um die physikalischen und chemischen Eigenschaften der Rauchfraktionen im Amazonasgebiet zu

analysieren. Schließlich verknüpft ein Vergleich aller HALO-Missionen die detaillierte Charakterisierung des amazonischen und afrikanischen Rauchs mit weiteren Aerosolen aus Verbrennungsprozessen und legt nahe, dass auch die Beziehungen zwischen schwarzen Kohlenstoff und der Anzahl an Wolkenkondensationskeimen deutlich variiert, abhängig von der Emissionsquelle.

Contents

CHAPTER 1

Introduction

1.1 Atmospheric aerosols in the Anthropocene

Human activities have exerted profound and manifold influences on Earth's climate and environment over the last two centuries. The rapid population and economic growth as well as the associated increase in the demand for food, energy, and goods have made humankind a major geological force on Earth (Monastersky, 2015). We are witnessing fundamental and fast transformations in essentially all parts of the Earth system, such as the atmosphere, land cover, the oceans, and biodiversity. As these changes are mostly driven by human activities, the current epoch has been termed the *Anthropocene* (Steffen et al., 2011). The changes in the atmospheric composition along with the associated adjustments in the climate system have been particularly fast. Both, the atmospheric trace gas and aerosol compositions have changed profoundly. While the atmosphere in the pre-industrial era mostly comprised natural aerosols, such as sea spray, mineral dust, biological particles and sulfates e.g. from the oxidation of oceanic dimethyl sulfide or volcanic sulfur dioxide (Andreae, 2007; Després et al., 2012; Fröhlich-Nowoisky et al., 2016), the industrialization greatly enhanced the number and strength of aerosol sources worldwide (Andreae, 2009; Carslaw et al., 2017; Crutzen, 2006). Combustion of biomass and fossil fuels has become an aerosol source of particular importance as it is the basis for modern agriculture, land clearing and management, energy production, and mobility (Bond et al., 2013; Ramanathan and Carmichael, 2008). The large-scale atmospheric circulations distribute anthropogenic aerosols over thousands of kilometers and, thus, the number of places on Earth free of human aerosols have become rare (Andreae, 2007).

Aerosols are solid or liquid particles suspended in the atmosphere, which play important role in atmospheric chemistry, climate, and public health (Andreae and Rosenfeld, 2008; Lelieveld et al., 2019; Shiraiwa et al., 2017). Figure 1.1 illustrates the dynamic life cycle of ambient aerosols in the atmosphere. They comprise a complex mixture of different species, including sulfate, nitrate, ammonium, mineral dust, sea spray, as well as carbonaceous materials, such as black carbon (BC) and organic aerosols. Their sizes span from a few nanometers to hundreds of micrometers (Boucher et al., 2013; Seinfeld and Pandis, 2006). They can be emitted directly from their sources into the atmosphere or be formed secondarily in the atmosphere through the oxidation and subsequent nucleation of precursor gases, such as volatile organic compounds (Hallquist et al., 2009; Kulmala, 2003). During atmospheric transport, airborne particles undergo complex physical (e.g., coagulation and condensation) and chemical (e.g., oxidation) transformations through interactions with solar radiation and reactive atmospheric constituents. These aging processes can alter the particles' initial size, shape, and composition substantially and, therefore, their atmospheric influence and relevance (Pöschl, 2005; Zhang et al., 2008). After typical atmospheric residence times of up to days or even weeks, aerosol particles are removed from the atmosphere by wet deposition, in which aerosols are nucleated as cloud droplets with subsequent precipitation (rain-out) or mechanically incorporated into falling raindrops (wash-out). Particles can also be removed by dry deposition in the course of diffusion or sedimentation.

Atmospheric aerosols play fundamental roles in the climate system (Andreae and Crutzen, 1997). They alter Earth's energy balance directly, by scattering and absorbing solar and terrestrial radiation, known as aerosol-radiation interactions (ARI)

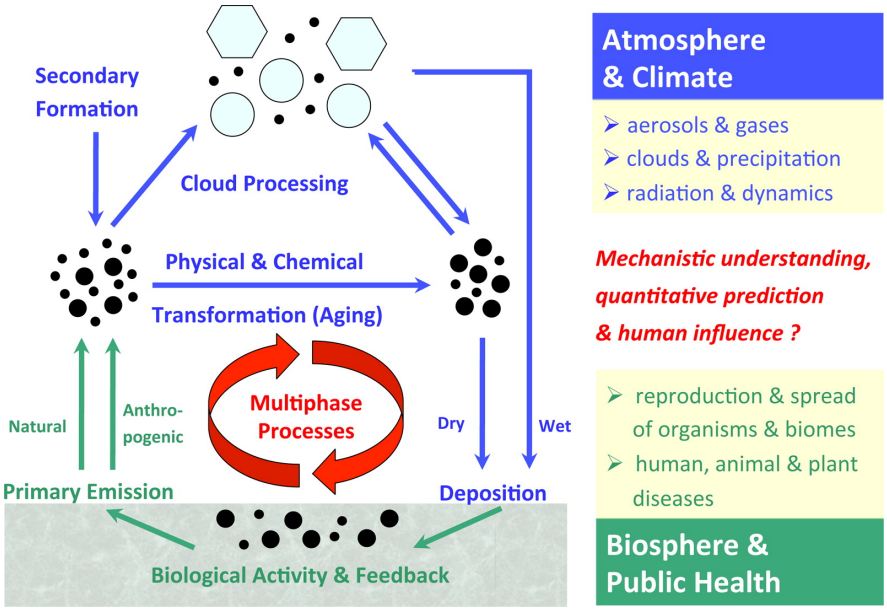

Figure 1.1: Life cycle and atmospheric processing of aerosol particles and gases. Adopted from Pöschl and Shiraiwa (2015)

.

(Boucher et al., 2013). As a result of ARI, aerosols induce rapid adjustments in the distribution of atmospheric radiative fluxes and heating rates, which then modify temperature and water vapor profiles, atmospheric stability, and the conditions for cloud formation (Stjern et al., 2017). The efficiency at which particles absorb or scatter light depends on the wavelength of the radiation, the particle size distributions, shape, and refractive index, which is determined by their chemical composition and mixing state (Bohren and Huffman, 1998; Hansen and Travis, 1974). Both, aerosol scattering and absorption contribute to the extinction of radiation. In atmospheric sciences, the wavelength dependence of scattering and absorption within an aerosol population is expressed by the Ångström exponent (AE), and the contribution of scattering to total extinction is termed the single-scattering albedo (SSA). Aerosols can also affect the climate system indirectly through aerosol-cloud interactions (ACI) (Boucher et al., 2013; Mülmenstädt and Feingold, 2018). Here fractions of the aerosol population can act as cloud condensation nuclei (CCN) or ice nuclei (IN) and, thus, influence the processes involved in cloud and precipitation formation on microphysical (i.e., cloud droplet number concentration and size distribution) and macrophysical scales (i.e., cloud reflectivity and lifetime) (Ackerman et al., 2000; Andreae and Rosenfeld, 2008; Rosenfeld et al., 2014; Rosenfeld et al., 2008; Twomey, 1974; Twomey, 1977).

1.2 Black Carbon: the climate's dark forcing

Black carbon is a primary pollutant emitted directly into the atmosphere in processes of incomplete combustion and most of it originates from anthropogenic sources(Bond et al., 2013). Black carbon consists of aggregates of small carbon spherules, which are insoluble in water and have very low chemical reactivity in the atmosphere (Bond

et al., 2013). Because of its ability to absorb solar radiation throughout all visible wavelengths, BC is "the climate's dark forcing" and of major significance for the Earth energy balance (Andreae and Ramanathan, 2013; Ramanathan and Carmichael, 2008). In fact, BC exerts a positive forcing on climate, contributing to global warming (Bond et al., 2013). According to the most recent assessment report of the Intergovernmental Panel on Climate Change (IPCC), the best estimate of industrial-era climate forcing of BC is $+0.063\,W\,m^{-2}$, with an uncertainty spanning from -0.28 to $+0.42\,W\,m^{-2}$ (Naik et al., 2021. In Press; Thornhill et al., 2021).

As a result of the highly heterogeneous distribution of atmospheric BC in space and time, large uncertainties persist in assessing its influence on the climate system (Laj et al., 2020). Moreover, the climate effects of BC and its atmospheric residence time depend on the physicochemical properties of the particles. Generally, freshly emitted BC particles are too small and too hydrophobic to activate as cloud nuclei (Fierce et al., 2015; Weingartner et al., 1997). Shortly after emission, however, condensation of semivolatile gases and coagulation with co-emitted or preexisting particles alter BC morphology and mixing state. The addition of external coatings onto BC cores can enhance their absorption of solar radiation – through the so-called lensing effect (Cappa et al., 2012; Fuller et al., 1999; Yuan et al., 2021) – as well as increase their ability to activate as CCN (Liu et al., 2013; Zuberi et al., 2005). Wet scavenging is the main removal mechanisms of BC particles from the atmosphere, however, clouds can also re-evaporate releasing modified BC particles back to the atmosphere. Therefore, there is a clear need to measure BC and its mixing state in order to better understand its atmospheric life cycle and to model its climate impacts.

Biomass burning is a major source of BC particles in the atmosphere, contributing about 60 % of the global BC emissions (Andreae, 2019; Bond et al., 2013). In biomass burning plumes, BC particles are co-emitted with organic and inorganic particulate matter as well as numerous gases of different volatility (Andreae, 2019; Lobert and Wamatz, 1993). The emitted smoke can be transported over long distances, getting diluted into the background remote troposphere and lower stratosphere where they can persist for long time periods with strong radiative impacts (Ditas et al., 2018; Ohneiser et al., 2020; Samset et al., 2013; Schill et al., 2020). While BC strongly absorbs solar radiation, the organic and inorganic species generally scatter light. Moreover, there is a fraction of the organics that can absorb light called brown carbon (BrC) (Andreae and Gelencsér, 2006). The climate impact of biomass burning smoke is thus determined by the complex mixture of BC with non-absorbing species with proportions and properties that depends on the type of fuel or vegetation burnt and combustion conditions (flaming vs smoldering).

Different methods have been used to measure BC based on its light absorption, such as photoacoustic spectrometers, aethalometers, multi angle absorption photometers and particulate soot absorption photometers (Patrick Arnott et al., 1999; Pileci et al., 2021; Slowik et al., 2007). Retrieving BC mass from absorption measurements, however, requires assumptions about the mass absorption coefficient (MAC), which can be biased by the presence of internally mixed BC or other chemical components, such as brown carbon. Therefore, an alternative method based on laser-induced incandescence (LII) has been introduced for measuring refractory BC (rBC) mass in single particles and implemented in the single particle soot photometer (SP2) (Gao et al., 2007; Schwarz et al., 2008; Stephens et al., 2003). The instrument quantifies the mass of rBC by measuring the intensity of the incandescent signal emitted by

single rBC particles upon vaporization while crossing an intense laser beam. The retrieved rBC mass using the LII method is independent of the particles' mixing state and morphology (Moteki and Kondo, 2007; Slowik et al., 2007).

1.3 The Amazon rain forest

The Amazon is the largest rain forest in the world and of high global relevance for its key roles in carbon and water cycling and climate change (Andreae et al., 2015; Lenton et al., 2008). In parts of the wet season (February to May), the atmospheric conditions can approach those of a pre-industrial era, with regional climate being regulated by the trace gas and aerosol emissions from the regional biosphere (e.g., Pöhlker et al., 2012; Pöschl et al., 2010). In contrast, the dry season (August to November) is characterized by intense and widespread biomass burning emissions, changing substantially the atmospheric composition and cycling (e.g., Artaxo et al., 2013; Rizzo et al., 2013). In the last decades, biomass burning became very frequent and ubiquitous across the basin, since fire is the tool of choice for land clearing and management in the course of agricultural expansion, infrastructure development, and mining (e.g., Davidson et al., 2012). The disturbance of forests is most severe along the 'arc of deforestation' in the southeast basin and along the major roads that lead into previously inaccessible regions (e.g., Laurance et al., 2009; Pöhlker et al., 2019a). In 2019 and onward, the number of detected fires in the Amazon region sharply increased in comparison to previous years, raising public concerns worldwide (Artaxo, 2019; Escobar, 2020). During the strongest 'days of fires', thick smoke layers covered a large extent of the Amazon basin, as shown by satellite images in Fig. 1.2.

In addition to the regional pollution, the Amazonian atmosphere is strongly influenced by the transport of biomass burning smoke from Africa across the Atlantic Ocean throughout the year (Moran-Zuloaga et al., 2018a; Saturno et al., 2018a). The effective transatlantic transport is favored by the large-scale trade wind circulation, in which the Amazon is located directly 'downwind' of the African continent, which is one of the strongest aerosol sources worldwide (e.g., Baars et al., 2011; Baars et al., 2012; Barkley et al., 2019; Pöhlker et al., 2019a; Saturno et al., 2018c; Wang et al., 2016). In the wet season, northeasterly air masses episodically transport Saharan dust and smoke from African fires north of the equator (i.e., in the Sahel region and West Africa) towards the Amazon (Moran-Zuloaga et al., 2018a; Wang et al., 2016). In the dry season, southeasterly winds transport large amounts of smoke from southern Africa towards the Amazon (Adebiyi and Zuidema, 2016; Saturno et al., 2018c). The interplay of the different aerosol populations throughout the year is mainly driven by the north–south oscillation of the Intertropical Convergence Zone (ITCZ) (Andreae et al., 2015; Andreae et al., 2012; Martin et al., 2010), which places the Amazon under the dominant influence of the northern hemisphere in the wet season and the southern hemisphere in the dry season, as shown in Fig. 1.3 (Pöhlker et al., 2019a). This makes the Amazon Basin a suitable environment to study atmospheric and biogeochemical processes under strong biomass burning influence as a function of aging time and source regions, in stark contrast to the pristine atmospheric conditions.

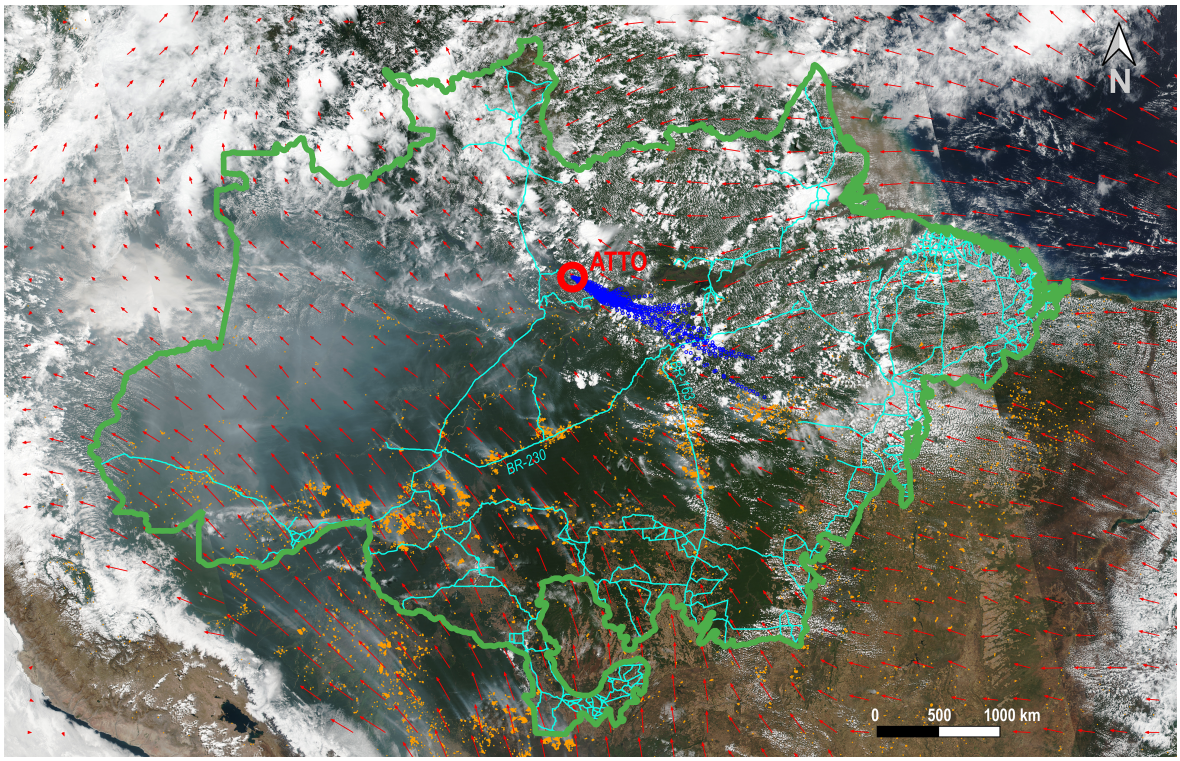

Figure 1.2: Composite map of the Amazon Basin on 14 August 2019, showing dense smoke from regional fires covering an extensive area of basin. The figure shows (i) corrected reflectance satellite images showing cloud cover and smoke plumes, (ii) individual detected fires shown as yellow points, (iii) wind vectors (red) at 950 hPa showing overall wind fields in agreement with HYSPLIT 1 d backward trajectory (BT) ensembles (blue), started at the ATTO site. Green boundary shows legal Amazon region. Blue lines show major highways in the Amazon basin. Adapted from Holanda et al. (2021).

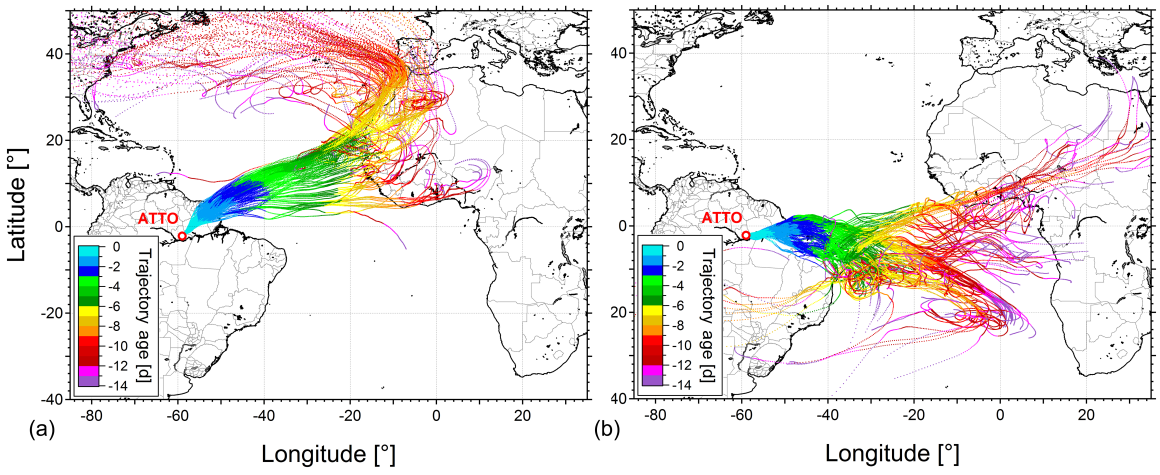

Figure 1.3: HYSPLIT backward trajectory (BT) ensembles contrasting the atmospheric conditions during the wet and dry seasons at ATTO: (a) northeast tracks of BTs from 1 to 31 March 2014, representing the wet season and (b) southeast tracks of BTs from 1 to 30 September 2014, representing the dry season. Starting height of BTs was 1000 m a.g.l. Color coding represents BT transport times. Adopted from Pöhlker et al. (2019a).

1.4 Research objectives and thesis outline

Anthropogenic aerosol emissions are known to have a strong – though yet highly uncertain – influence on atmospheric circulation and the climate system. This is particularly true for the role of biomass burning smoke in the Amazon basin. Therefore, in this doctoral project I analyzed and interpreted comprehensive aerosol data from the Amazon Basin and the tropical Atlantic region, as well as other relevant locations worldwide to extend our knowledge on the emissions, transport, and atmospheric relevance of biomass burning aerosols. This project used sophisticated research platforms, including the Amazon Tall Tower Observatory (ATTO) in central Amazonia as well as the High Altitude LOng-range (HALO) research aircraft in five missions. While the atmospheric observations at ATTO provided unique multiyear time series with high temporal resolution from the Amazon ecosystem, the HALO missions are an ideal complement providing high spatial resolution over extended geographic regions for the Amazon and beyond.

The **ATTO** site has been operated since 2012 as a research facility for long-term and in-depth investigations of meteorology, trace gases, atmospheric aerosols, and rain forest ecology (e.g., Andreae et al., 2015; Botía et al., 2020; Löbs et al., 2020; Saturno et al., 2018c; Yáñez-Serrano et al., 2018). In the context of this dissertation, the characterization of aerosol chemical composition as well as the physical (concentration, size distribution, mixing state) and optical properties (spectral light absorption and scattering) has been carried out. The two focal points have been to understand aerosol-radiation and aerosol-cloud interactions in a highly polluted biomass burning atmosphere in contrast to near-pristine conditions, and the impact of the aged African smoke in contrast to the local biomass burning emissions over the Amazon.

In addition to the ground-based ATTO measurements, this dissertation includes airborne observations with the HALO aircraft, which performed highly resolved atmospheric profiling flights up to 15 km altitude over different target environments. In this PhD project, the same set of instruments to measure black carbon and cloud condensation nuclei was successfully operated during five large field experiments as outlined below. The flight tracks and target regions of the HALO missions as well as the ATTO location are shown in Figure 1.4.

ACRIDICON-CHUVA: Aerosol, Cloud, Precipitation, and Radiation Interactions and Dynamics of Convective Cloud Systems–Cloud Processes of the Main Precipitation Systems in Brazil: A Contribution to Cloud Resolving Modeling and to the Global Precipitation Measurement. The campaign was based at the international airport in Manaus and comprised 14 scientific flights covering the large geographical extent of the Amazonian Basin in September and October 2014, during the dry season (Andreae et al., 2018a; Machado et al., 2017; Wendisch et al., 2016). The sampled regions relevant for this study include the northern part of Amazonia under comparatively clean conditions, the Atlantic Ocean off the Brazilian coast, where a layer of aged African aerosol was probed in the free troposphere, and the so called 'arc of deforestation' in southern Amazon, which is subject of intense deforestation.

CAFE-Africa: Chemistry of the Atmosphere: Field Experiment in Africa. The campaign took place in August-September 2018 in the course of 14 scientific flights over Western Africa and the Atlantic Ocean, with base at Sal international airport, Cape Verde. During the flights conducted over the Southern Atlantic Ocean, several smoke

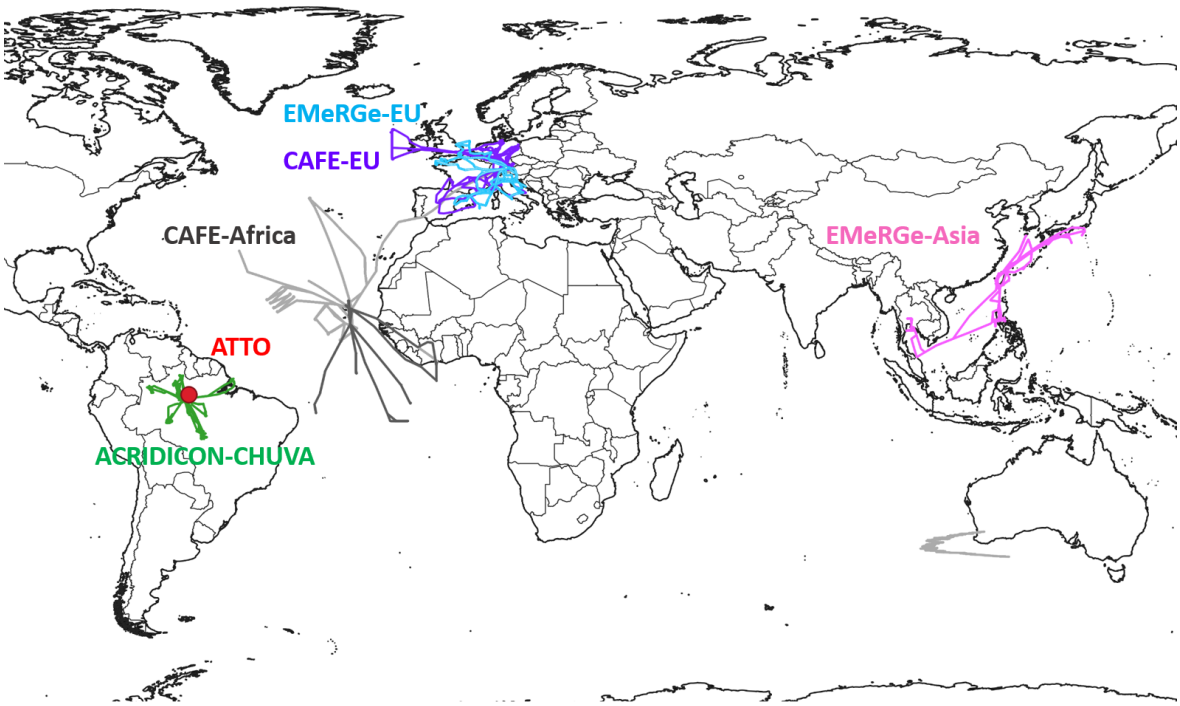

Figure 1.4: Geographic locations of the field experiments relevant for this dissertation, including the ATTO site as well as the flight tracks of the five HALO aircraft missions. This PhD project entailed a participation in all campaigns shown here, except ACRIDICON-CHUVA.

layers containing African biomass burning being transported in the free troposphere were probed. The plumes were intercepted at different locations over the Atlantic Ocean and at different distances from the African continent, therefore with different aging times.

EMeRge-EU & EMeRge-Asia: Effect of Megacities on the Transport and Transformation of Pollutants on the Regional to Global Scales in Europe and Asia. Both campaigns aimed to investigate the emissions and transformation of major megapopulated centers in Europe and Asia. The first part of the campaign was based in Oberpfaffenhofen, Germany, and took place in July 2017 probing the outflow of large cities in Germany, Italy, Spain, and England (Andrés Hernández et al., 2021a). The second part was based in Tainan, Taiwan, and took place in March–April 2018 probing the outflow of major cities in Taiwan, China, Korea, Japan, and Thailand.

CAFE-EU/BLUESKY: Chemistry of the Atmosphere: Field Experiment in Europe. The campaign took place in May–June 2020 during the rigorous restrictions for societal activities in many countries worldwide because of the COVID-19 pandemic (Voigt et al., 2021a). The significant reduction of industrial production and mobility in 2020 created an unprecedented atmospheric state of high relevance for atmospheric research. Therefore, the European airspace with reduced air pollution conditions was intensively probed during the 8 scientific flights of the CAFE-Europe campaign.

Based on this wide spectrum of measurements, this dissertation addresses the following specific research objectives:

1. *Characterization of the aerosol optical properties in the central Amazon under pristine and highly polluted atmospheric conditions*. Nowadays, the Amazon Basin represents one of the few continental places worldwide where atmospheric conditions approach a pre-industrial state. Thus, an assessment of the effects of anthropogenic emissions on atmospheric processes and climate requires a detailed understanding of the underlying natural processes. Chapter 2.1 presents multi-year measurements (2012-2017) of aerosol optical properties at the ATTO site, underlining its seasonality, diurnal cycles as well as its response to climate extremes such as El Niño periods. It is shown that the Amazonian aerosol population is not only influenced by regional fires but also by the long-rang-transport from Africa smoke, which significantly affects the optical aerosol properties in the Amazon.
2. *Characterization of aerosols in freshly emitted and long-range transported biomass burning plumes*. Extended smoke layers containing aged African biomass burning aerosols were observed both in and off the Brazilian coast during flight AC19 of the ACRIDICON-CHUVA campaign. The smoke originated from vegetation fires in Southern Africa and carried over the Atlantic Ocean for at least 10 days before reaching South America. In addition to the highly aged smoke, a visible forest fire plume in the Northern Amazon was probed during the same scientific flight, allowing a direct comparison between the two distinct smoke plumes. In chapter 2.2, consistent differences in the physico-chemical properties of biomass burning aerosols from deforestation fires over the Amazon on one hand, and from fires in African savannas after transatlantic transport, on the other, are discussed. Moreover, dynamics and seasonality of the transatlantic transport of African smoke are investigated by combining long-term measurements at ATTO, remote sensing and modelling data.
3. *Quantification of the African aerosol burden over the central Amazon Basin*. In order to assess climate effects of widespread biomass burning aerosols over the Amazon, the influence of African aerosols cannot be neglected. Based on the distinct differences in BC microphysical properties within South American and African smoke plumes, a classification scheme to quantify both smoke influences at ATTO is presented in chapter 2.3. This approach is systematically employed over two years of BC measurements (2019-2020) at the ATTO site, providing a time-resolved assessment of the African contribution to the BC burden. This study comprises the longest time series of BC microphysical properties derived from SP2 measurements ever reported in literature. This approach further allowed the analysis of the aerosol physical and chemical properties of both smoke types at ATTO.
4. *Investigation of the spatial distribution of biomass burning aerosols over the Tropical Atlantic and Amazon Basin*. To date, the long-range transport of African smoke over the Atlantic Ocean and its influx into the Amazon Basin remains underestimated in global models (Carter et al., 2021; Lund et al., 2018; Shinozuka et al., 2020). Thus, further aerosol measurements near sources as well as in remote regions are required. In chapter 2.4, systematic vertical profiles of BC mass concentration, size distribution and mixing state over the Amazon Basin and the Tropical Atlantic are presented. The results combine aircraft data from two large scale field experiments that took place during the Amazonian dry season: the ACRIDICON-CHUVA in September-October 2014 and CAFE-

AFRICA in August-September 2018. Together, the aircraft campaigns provide new insights about the atmospheric aging of African biomass burning aerosols over the Atlantic as well as its vertical and geographical distribution over the Amazon Basin.

5. *Investigation of the number of CCN particles produced per BC mass in different combustion processes*. In the Anthropocene, essentially all human-driven emissions include the burning of biomass or fossil fuel. The ratio of BC to non-BC particles depends on the emissions source, combustion conditions and atmospheric aging. In chapter 2.5 the number of cloud condensation nuclei at a supersaturation of $0.38\,\%$ produced per BC mass in different combustion sources is investigated. This study combines data from five HALO field campaigns in order to obtain characteristic ratios between BC and CCN in environments dominated by urban and/or biomass burning emissions. New insights on the significance of anthropogenic emissions to the climate system are expected from the relationship between highly absorbing BC with the typically scattering CCN particles.

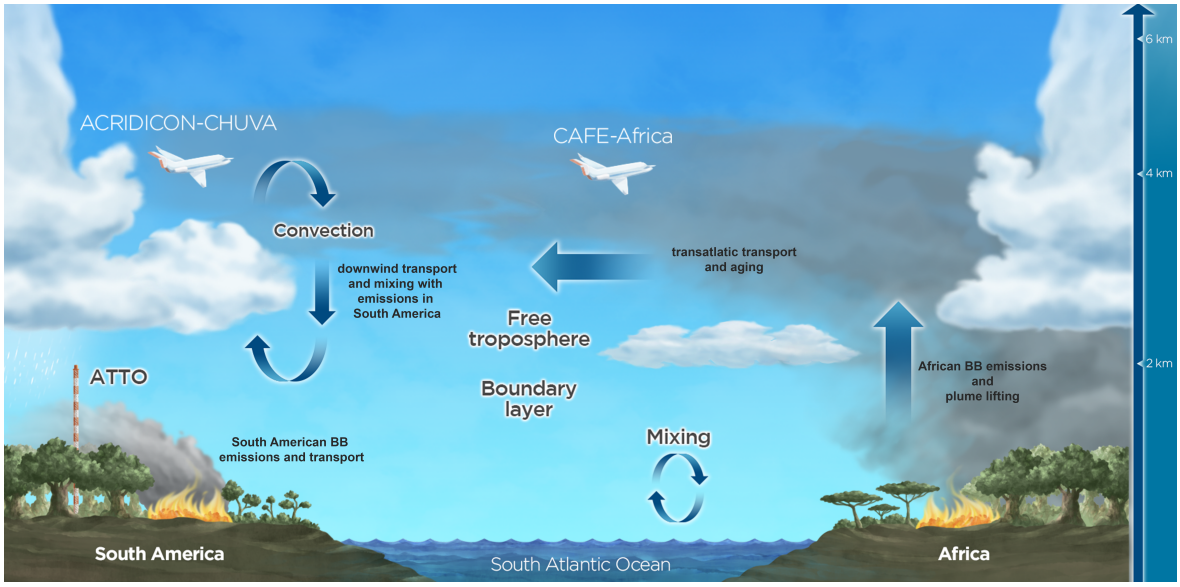

Figure 1.5: Schematic of the main processes investigated within this PhD project. After being lifted at high altitudes over western or southern Africa, biomass burning aerosols are horizontally transported westwards over the South Atlantic Ocean in stable atmospheric layers. The transport and transformation of the aged African smoke during transatlantic transport was investigated during the CAFE-Africa campaign. After reaching South America and during transport inland, the African smoke is mixed into the convective Amazonian boundary layer. The aerosols are added to the South American natural or anthropogenic emissions. The influx of African smoke layers into the Amazonian atmosphere was investigated during the ACRIDICON-CHUVA campaign, and their seasonality and effects on optical properties were investigated at the ATTO site.

The scheme in Figure 1.5 illustrates and summarizes the main aerosol processes over the Amazon and Atlantic Ocean investigated in this dissertation. The investigation of aerosol properties in this focal region has been based on the measurements at ATTO, as well as in the context of ACRIDICON-CHUVA and CAFE-Africa. The results can be found in the following chapters 2.1 to 2.4, corresponding to one published second-author paper, one published first-author paper, one first-author paper as final draft

before submission, and one first-author papers as draft in early state. Further, a comparative study of all five HALO missions yielded another first-author paper as draft in early state, which is presented in chapter 2.5. In addition, the research performed in the course of this dissertation contributed so far to 17 additional articles which are published, in preparation or currently undergoing peer-review in international scientific journals (for details, see Personal List of Publications).

CHAPTER 2

Results

2.1 Black and brown carbon over central Amazonia: long-term aerosol measurements at the ATTO site

This chapter has been published as:

Saturno, J.; Holanda, B. A.; Pöhlker, C.; Ditas, F.; Wang, Q.; Moran-Zuloaga, D.; Brito, J.; Carbone, S.; Cheng, Y.; Chi, X.; Ditas, J.; Hoffmann, T.; Angelis, I. Hrabe de; Könemann, T.; Lavrič, J. V.; Ma, N.; Ming, J.; Paulsen, H.; Pöhlker, M. L.; Rizzo, L. V.; Schlag, P.; Su, H.; Walter, D.; Wolff, S.; Zhang, Y.; Artaxo, P.; Pöschl, U., and Andreae, M. O.: "Black and brown carbon over central amazonia: long-term aerosol measurements at the atto site". *Atmos. Chem. Phys.*, 18, 17. (2018), pp. 12817–12843. DOI: 10.5194/acp-18-12817-2018. URL: https://www.atmos-chem-phys.net/18/12817/2018/

Supplementary Material: The Supplementary Material for this article can be found online at: https://doi.org/10.5194/acp-18-12817-2018-supplement

This manuscript includes data sets from the following field experiment:
ATTO

Contribution to this publication by Bruna A. Holanda: Together with Jorge Saturno, I conducted the measurements of aerosol optical properties at ATTO, which are the core piece of the paper. I broadly supported the data acquisition and data quality assurance as well as maintenance and calibrations of the five relevant aerosol instruments at ATTO. Further, I contributed to the data processing and analysis as well as the writing of this paper.

Atmos. Chem. Phys., 18, 12817–12843, 2018
https://doi.org/10.5194/acp-18-12817-2018

Atmospheric Chemistry and Physics
Open Access
EGU

Black and brown carbon over central Amazonia: long-term aerosol measurements at the ATTO site

Jorge Saturno[1,a], Bruna A. Holanda[1], Christopher Pöhlker[1], Florian Ditas[1], Qiaoqiao Wang[1,2], Daniel Moran-Zuloaga[1], Joel Brito[3,4], Samara Carbone[3,5], Yafang Cheng[1], Xuguang Chi[6], Jeannine Ditas[1,2], Thorsten Hoffmann[7], Isabella Hrabe de Angelis[1], Tobias Könemann[1], Jošt V. Lavrič[8], Nan Ma[1,2], Jing Ming[1], Hauke Paulsen[9], Mira L. Pöhlker[1], Luciana V. Rizzo[10], Patrick Schlag[3], Hang Su[1], David Walter[1], Stefan Wolff[1], Yuxuan Zhang[1], Paulo Artaxo[3], Ulrich Pöschl[1], and Meinrat O. Andreae[1,11]

[1]Multiphase Chemistry & Biogeochemistry Departments, Max Planck Institute for Chemistry, 55128 Mainz, Germany
[2]Jinan University Institute for Environmental and Climate Research, Guangzhou, 510630, China
[3]Institute of Physics, University of São Paulo, São Paulo, 05508-900, Brazil
[4]Laboratory for Meteorological Physics, Université Clermont Auvergne, 63000 Clermont-Ferrand, France
[5]Institute of Agrarian Sciences, Federal University of Uberlândia, Uberlândia, Minas Gerais, 38408-100, Brazil
[6]Institute for Climate and Global Change Research & School of Atmospheric Sciences, Nanjing University, Nanjing, 210093, China
[7]Department of Chemistry, Johannes Gutenberg University, 55128 Mainz, Germany
[8]Biogeochemical Systems & Biogeochemical Processes Departments, Max Planck Institute for Biogeochemistry, 07701 Jena, Germany
[9]Institute of General Botany, Johannes Gutenberg University, 55128 Mainz, Germany
[10]Departamento de Ciencias Ambientais, Universidade Federal de Sao Paulo, Diadema, SP, Brazil
[11]Scripps Institution of Oceanography, University of California San Diego, La Jolla, CA 92098, USA
[a]now at: Physikalisch-Technische Bundesanstalt, Bundesallee 100, 38116 Braunschweig, Germany

Correspondence: Jorge Saturno (j.saturno@mpic.de) and Christopher Pöhlker (c.pohlker@mpic.de)

Received: 24 November 2017 – Discussion started: 12 December 2017
Revised: 2 June 2018 – Accepted: 10 August 2018 – Published: 6 September 2018

Abstract. The Amazon rainforest is a sensitive ecosystem experiencing the combined pressures of progressing deforestation and climate change. Its atmospheric conditions oscillate between biogenic and biomass burning (BB) dominated states. The Amazon further represents one of the few remaining continental places where the atmosphere approaches pristine conditions during occasional wet season episodes. The Amazon Tall Tower Observatory (ATTO) has been established in central Amazonia to investigate the complex interactions between the rainforest ecosystem and the atmosphere. Physical and chemical aerosol properties have been analyzed continuously since 2012. This paper provides an in-depth analysis of the aerosol's optical properties at ATTO based on data from 2012 to 2017. The following key results have been obtained.

– The aerosol scattering and absorption coefficients at 637 nm, $\sigma_{sp,637}$ and $\sigma_{ap,637}$, show a pronounced seasonality with lowest values in the clean wet season (mean ± SD: $\sigma_{sp,637} = 7.5 \pm 9.3\,M\,m^{-1}$; $\sigma_{ap,637} = 0.68 \pm 0.91\,M\,m^{-1}$) and highest values in the BB-polluted dry season ($\sigma_{sp,637} = 33 \pm 25\,M\,m^{-1}$; $\sigma_{ap,637} = 4.0 \pm 2.2\,M\,m^{-1}$). The single scattering albedo at 637 nm, ω_0, is lowest during the dry season ($\omega_0 = 0.87 \pm 0.03$) and highest during the wet season ($\omega_0 = 0.93 \pm 0.04$).

– The retrieved BC mass absorption cross sections, α_{abs}, are substantially higher than values widely used in the literature (i.e., $6.6\,m^2\,g^{-1}$ at 637 nm wavelength), likely related to thick organic or inorganic coatings on the BC cores. Wet season values of $\alpha_{abs} = 11.4 \pm$

$1.2\,m^2\,g^{-1}$ (637 nm) and dry season values of $\alpha_{abs} = 12.3 \pm 1.3\,m^2\,g^{-1}$ (637 nm) were obtained.

- The BB aerosol during the dry season is a mixture of rather fresh smoke from local fires, somewhat aged smoke from regional fires, and strongly aged smoke from African fires. The African influence appears to be substantial, with its maximum from August to October. The interplay of African vs. South American BB emissions determines the aerosol optical properties (e.g., the fractions of black vs. brown carbon, BC vs. BrC).
- By analyzing the diel cycles, it was found that particles from elevated aerosol-rich layers are mixed down to the canopy level in the early morning and particle number concentrations decrease towards the end of the day. Brown carbon absorption at 370 nm, $\sigma_{ap,BrC,370}$, was found to decrease earlier in the day, likely due to photo-oxidative processes.
- BC-to-CO enhancement ratios, ER_{BC}, reflect the variability of burnt fuels, combustion phases, and atmospheric removal processes. A wide range of ER_{BC} between 4 and 15 $ng\,m^{-3}\,ppb^{-1}$ was observed with higher values during the dry season, corresponding to the lowest ω_0 levels (0.86–0.93).
- The influence of the 2009/2010 and 2015/2016 El Niño periods and the associated increased fire activity on aerosol optical properties was analyzed by means of 9-year σ_{sp} and σ_{ap} time series (combination of ATTO and ZF2 data). Significant El Niño-related enhancements were observed: in the dry season, $\sigma_{sp,637}$ increased from 24 ± 18 to $48 \pm 33\,M\,m^{-1}$ and $\sigma_{ap,\,637}$ from 3.8 ± 2.8 to $5.3 \pm 2.5\,M\,m^{-1}$.
- The absorption Ångström exponent, $å_{abs}$, representing the aerosol absorption wavelength dependence, was mostly <1.0 with episodic increases upon smoke advection. A parameterization of $å_{abs}$ as a function of the BC-to-OA mass ratio for Amazonian aerosol ambient measurements is presented. The brown carbon (BrC) contribution to σ_{ap} at 370 nm was obtained by calculating the theoretical BC $å_{abs}$, resulting in BrC contributions of 17 %–29 % (25th and 75th percentiles) to $\sigma_{ap\,370}$ for the entire measurement period. The BrC contribution increased to 27 %–47 % during fire events under El Niño-related drought conditions from September to November 2015.

The results presented here may serve as a basis to understand Amazonian atmospheric aerosols in terms of their interactions with solar radiation and the physical and chemical-aging processes that they undergo during transport. Additionally, the analyzed aerosol properties during the last two El Niño periods in 2009/2010 and 2015/2016 offer insights that could help to assess the climate change-related potential for forest-dieback feedbacks under warmer and drier conditions.

1 Introduction

Atmospheric aerosol particles affect the Earth's climate through different mechanisms. Direct mechanisms include the aerosol particle interactions with radiation by scattering and absorption. The balance between scattering and absorption can lead to warming or cooling of the atmosphere (IPCC, 2013). Moreover, indirect mechanisms, like aerosol–cloud interactions during cloud formation and cloud microphysical modifications, are accompanied by high uncertainties, especially due to the lack of knowledge on pre-industrial levels of cloud condensation nuclei (CCN) (Carslaw et al., 2013) and aerosol spatial distribution in the atmosphere (Andreae, 2007).

Continuous aerosol measurements at remote continental locations are crucial to understand atmospheric conditions prior to industrialization and reduce the uncertainties in climate models (Seinfeld et al., 2016). The Amazon Basin is one of the few continental areas in the world where the atmosphere approximates pristine conditions during some periods of the year (Andreae et al., 2015; M. L. Pöhlker et al., 2018). However, anthropogenic pollution is rather persistent and, thus, reaches almost every place on the planet (Andreae, 2007; Chi et al., 2013; Hamilton et al., 2014). The Amazon rainforest has been impacted substantially by intensified agriculture and the associated deforestation and infrastructural development in the last 50 years (Artaxo et al., 2013; Davidson et al., 2012). Given these circumstances, only when air masses travel over clean marine areas and rain-related scavenging is significant do the observations approach near-pristine to pristine levels (Andreae et al., 2012, 2015; M. L. Pöhlker et al., 2018).

Biogenic primary and secondary organic aerosol particles over the Amazon rainforest are ubiquitous throughout the year (Martin et al., 2010b). During the dry season (August–November), when fires are frequent in the forest and its peripheries, the background biogenic aerosol is overwhelmed by BB smoke (Andreae et al., 1988; Artaxo et al., 2002; Fuzzi et al., 2007; Guyon et al., 2003a; Roberts et al., 2003). Despite the rare occurrence of natural tropical forest fires (Cochrane, 2003; Nepstad et al., 2008), most of the fire episodes in the Amazon rainforest peripheries occur due to human activity, including land use change, brush clearing for agricultural activities, burning of agricultural waste (Andreae, 1991; Crutzen and Andreae, 1990), and cooperative burning of savannas by indigenous communities, which is done to prevent larger wildfires (Bilbao et al., 2010). Starting in August, the dry season is characterized by aerosol number concentrations of 1000–3000 cm^{-3} (Andreae et al., 2015). Another characteristic of the dry season is the occurrence of abundant black carbon (BC) in the atmosphere. This type of aerosol particles is primarily emitted by flaming and smoldering fires together with large amounts of organic aerosols (OA) (Andreae and Merlet, 2001) and is considered an important short-lived climate forcing agent (Andreae, 2001;

Bond et al., 2004, 2013). The light absorbing fraction of OA, which is co-emitted with BC, is called *brown carbon* (BrC) (Andreae and Gelencsér, 2006). The BC + BrC aerosol fraction is commonly defined as *light-absorbing carbonaceous* (LAC) matter (Petzold et al., 2013). A list of frequently used acronyms and symbols can be found in Table A1.

During combustion, aerosol particles are co-emitted with carbon monoxide (CO). The ratio between aerosol mass or number concentrations and CO has been used to trace the origin and age of air masses (Guyon et al., 2005; Janhäll et al., 2010). Enhancement ratios (ER_{BC}) for open biomass burning measured for boreal forest smoldering fires have an average ER_{BC} of 1.7 ng m^{-3} ppb^{-1} (Kondo et al., 2011). In contrast, agricultural fires exhibit higher ER_{BC} compared to forest fires, with reported values varying between 2.2 and 30 ng m^{-3} ppb^{-1} (Mikhailov et al., 2017, and references therein).

Biomass burning plumes are usually dominated by accumulation mode aerosol particles, which are efficient to scatter radiation in the UV-visible range and are also rich in BC. In the absence of BB aerosol particles, the biological coarse mode particles become dominant in terms of mass and the aerosol optical properties are affected (Moran-Zuloaga et al., 2018). Therefore, clear seasonal trends in scattering and absorption have been observed by long-term measurements in the Amazon region (Rizzo et al., 2013).

The light absorption of BC has a wavelength dependence that depends on the BC mixing state, its size distribution, and the composition of co-emitted particles (Andreae and Gelencsér, 2006; Kirchstetter et al., 2004; Lack et al., 2013; Schuster et al., 2016). The wavelength dependence is described by the absorption Ångström exponent ($å_{abs}$) (Ångström, 1929). It varies from low values ($å_{abs} = 1.0 \pm 0.1$, weak spectral dependence), usually associated with fossil fuel emitted BC (Bond and Bergstrom, 2006), up to high values ($å_{abs} = 6$–7, strong spectral dependence) for organic-rich aerosol, e.g., humic-like substances (Hoffer et al., 2006). Measurements at an Amazonian forest site during the dry season resulted in $å_{abs}$ average values below 1.0 for absorption coefficients lower than 15 M m^{-1} at 450 nm (Rizzo et al., 2011). For BB aerosol particles, the $å_{abs}$ is usually higher than 1.0. However, it depends on the burning conditions, the BC-to-OA ratio (Saleh et al., 2014), and the BC–BrC size distributions and morphologies (Kirchstetter et al., 2004; Womack et al., 2017). Several studies have used the absorption spectral dependence to apportion the fossil fuel and BB contributions to total absorption (Favez et al., 2010; Massabò et al., 2015; Sandradewi et al., 2008). However, the $å_{abs}$ values do not always reflect the combustion type, and using it as a source apportionment parameter can lead to erroneous results (Garg et al., 2016; Lack and Langridge, 2013; Lewis et al., 2008; Wang et al., 2016b). Several studies assume a BC $å_{abs}$ of 1.0, but models show that pure BC could exhibit a broader range of $å_{abs}$ values (Moosmüller et al., 2011). In order to retrieve the ambient BC wavelength dependence, Wang et al. (2016b) proposed the use of the wavelength dependence of $å_{abs}$ instead of $å_{abs}$ itself. The so-called *wavelength dependence of* $å_{abs}$ (WDA) is calculated as the difference of two wavelength pairs: one for short to long wavelengths (e.g., 440–870 nm) and another for medium to long wavelengths (e.g., 675–880 nm).

Precise BC mass measurements are required to retrieve the correct relationship between absorptivity and BC mass, defined as the mass absorption cross section (MAC or α_{abs}). The BC mass concentration has traditionally been measured by using thermal or thermal–optical techniques (Cachier et al., 1989; Chow et al., 2007). However, these methods suffer from several biases, like organic carbon charring that increases the apparent BC concentration, especially when high organic fractions are present (Andreae and Gelencsér, 2006). More recently, laser-induced incandescence (LII) techniques have been introduced (Snelling et al., 2005). These techniques measure the volume-equivalent mass of refractory black carbon (rBC) that vaporizes at temperatures of 2800–4000 K. The MAC is used by atmospheric radiative transfer models to obtain absorption coefficients from mass concentration data. The MAC of BC varies between 4 and 11 m^2 g^{-1} at 550 nm, with an average of 6.5 m^2 g^{-1} at 637 nm for fresh soot (Bond and Bergstrom, 2006). In case of condensation of non-BC material on the BC particles, the MAC can be enhanced due to the well-known "lensing effect" (Fuller et al., 1999). This commonly happens when BC is emitted by BB, since it is co-emitted with large amounts of organic vapors that can condense on BC particles (Saleh et al., 2014). In the central Amazon, black carbon particles have been shown to be coated by organic and inorganic matter (Pöhlker et al., 2014; Pöschl et al., 2010). It has been found that the coating mass significantly affects the absorption enhancement of BC particles, but no significant changes are caused by variations in the coating's oxygen-to-carbon ratio (Tasoglou et al., 2017). A wide range of MAC values can be found in the literature for different fire conditions (smoldering and flaming).

Commonly, the absorption properties of an aerosol population are reported as the single scattering albedo (SSA, ω_0), which is defined as total scattering divided by total extinction (absorption + scattering). Therefore, a lower ω_0 is associated with a stronger absorption. Tropical Amazonian forest fires have moderately high ω_0 values (0.93 ± 0.02 at 670 nm), given the high amount of scattering aerosols which are co-emitted with LAC, compared to African savanna fires that have lower ω_0 values (0.84 ± 0.015 at 670 nm) (Reid et al., 2005). In the Amazon rainforest, long-term measurements by Rizzo et al. (2013) have found similar values for ω_0 during the dry and wet seasons, 0.87 ± 0.06 and 0.86 ± 0.09, respectively. The low ω_0 in the wet season is attributed to long-range transported aerosols that include mineral dust and aged BB aerosol particles. Aged BB aerosol is proven to have increased MAC, and therefore lower ω_0 (Reid et al., 2005). Moreover, the biogenic part of the aerosol can contribute up to 35 % of total light absorption (Guyon et al., 2004).

When present in large amounts in the atmosphere, mineral dust can significantly absorb light, with a MAC of 0.02–0.1 $m^2\,g^{-1}$ at 550 nm (Clarke and Charlson, 1985). It is mobilized from soils and suspended in the atmosphere by windstorms in areas like the Saharan desert in Africa. Dust aerosol particles in the atmosphere efficiently scatter visible radiation and are able to absorb infrared radiation (Andreae, 1996), having a $\mathring{a}_{abs} \gg 1.0$ (Caponi et al., 2017; Denjean et al., 2016). Mineral dust plumes travel over the Atlantic Ocean and are able to reach the American continent. Depending on the circulation patterns over the tropical Atlantic, the African dust plumes will be transported to South America or to the Caribbean Sea and central America (Prospero et al., 1981). The average transport time from emission to deposition in the Amazon Basin during winter is $\sim$ 10 days (Gläser et al., 2015). Ground measurements of aerosol physical and chemical properties have confirmed that between January and April mineral dust plumes from Africa episodically dominate the aerosol load over large parts of the Amazon rainforest (Formenti et al., 2001; Guyon et al., 2004; Moran-Zuloaga et al., 2018; Talbot et al., 1990; Wang et al., 2016a). Moreover, the dust-enriched aerosol usually arrives together with BB aerosol emitted by fires in sub-Sahelian western Africa and also aerosol particles emitted by industrial activities in Morocco and the western Saharan coast (Moran-Zuloaga et al., 2018; Salvador et al., 2016). In spite of anthropogenic disturbance of soils in Africa that could enhance the flux of mineral dust to the atmosphere (Andreae, 1991), a decreasing trend in mineral dust emissions since the 1980s has been observed and is mainly caused by a reduction of surface winds in the Sahel region (Ridley et al., 2014).

This study provides a comprehensive and in-depth analysis of the aerosol optical properties in the Amazonian atmosphere. A continuous long-term data set (2012–2017) of different optical properties is provided. We particularly focus on the impact of BB emissions from long-range transport and from regional/local open fires during the dry season. By using data from another central Amazonian remote sampling site, we extend our time series back to 2008 and provide the longest data set on optical properties measured in the Amazon rainforest so far. By these means, we are able to study the perturbations caused by the El Niño–Southern Oscillation (ENSO), which has been reported to cause droughts in the Amazon Basin (see Fig. S1 in the Supplement), with increasing fire activity and forest degradation (Aragão et al., 2007; Cochrane, 2003; Davidson et al., 2012; Lewis et al., 2011).

2 Materials and methods

2.1 Sampling site and measurement period

Aerosol particles and trace gases have been measured at the Amazon Tall Tower Observatory (ATTO) site, located in the Uatumã Sustainable Development Reserve, Amazonas State, Brazil, in central Amazonia since 2011 (Andreae et al., 2015). The large-scale meteorological conditions of the site are determined by the seasonal migration of the intertropical convergence zone (ITCZ) (C. Pöhlker et al., 2018). From August to November, during the *dry season*, the ITCZ is located in the north of South America, and mostly Southern Hemisphere air masses reach the ATTO site, bringing BB emissions from deforestation hotspots in southeastern Brazil (i.e., the so-called arc of deforestation) as well as transcontinental emissions from southern Africa. During the *wet season*, from February to May, when the ITCZ shifts to southern latitudes, the air masses generally come from the Northern Hemisphere, following a path over the Atlantic Ocean from the African continent and then over mostly untouched forest areas upwind of the ATTO site. The transition seasons, *dry to wet* and *wet to dry*, occur in December–January and June–July, respectively.

At the ATTO site, systematic aerosol measurements were started in March 2012, being continuously extended and intensified since then. In the course of this process, the aerosol inlet system was modified and upgraded step-wise. A detailed list of the different inlet configurations and characteristics can be found in Table S1. On 4 May 2014, a PM_1 cyclone was installed in the common inlet line for the aerosol optical measurements. The rest of the instrumentation kept sampling total suspended particles (TSP). The sample air was dried by diffusion driers filled with silica gel to guarantee a relative humidity around 40 % or below. An automatic regenerating adsorption aerosol dryer (Tuch et al., 2009) was installed in January 2015.

Another sampling site, the ZF2/TT34 tower, located $\sim$ 60 km NNW of Manaus and $\sim$ 140 km WSW of ATTO (Fig. S2), has been the location of long-term aerosol observations and intensive measurement campaigns (Martin et al., 2010a; Rizzo et al., 2013). Given that most of the air masses that reach the ZF2 site are similar to those transported over the ATTO site (C. Pöhlker et al., 2018), the ZF2 data are usually comparable to the ATTO data and the time series presented in this study can complement previous ZF2 time series already reported for the period 2008–2011 (Rizzo et al., 2013). Additionally, two intensive observation periods (IOP) and long-term measurements of the GoAmazon2014/5 experiment took place at several measurement sites in the Amazon Basin, including the ATTO site. More details can be found in Martin et al. (2016, 2017).

2.2 Instrumentation

2.2.1 Aerosol light scattering measurements

Scattering coefficients at ATTO were measured using different nephelometers. Figure S3 shows the measurement periods of the different instruments. The first one was a three-wavelength integrating nephelometer (model 3563, TSI, St.

Paul, USA) (14 August 2012 to 24 November 2013). The instrument measures aerosol scattering (σ_{sp}) and backscattering (σ_{bsp}) at 450, 550, and 700 nm (Anderson et al., 1996). Calibrations were periodically done by using CO_2 as a span gas. Given the optical configuration of the instrument, the truncation of forward scattered radiation constitutes the largest source of error and was corrected by following the procedure described by Anderson et al. (1996). The estimated error of the nephelometer measurements is 8 % for scattering coefficients on the order of $10\,M\,m^{-1}$ (Rizzo et al., 2013). Using an averaging time of 30 min, the detection limit at 550 nm was $0.14\,M\,m^{-1}$ (Rizzo et al., 2013).

Later, in February 2014, the TSI nephelometer was replaced by an Aurora 3000 (Ecotech Pty Ltd., Knoxfield, Australia), which measures at 450, 525, and 635 nm wavelength. Over the measurement period studied in this work, we used two different Aurora instruments, with and without backscattering measurement. The Aurora nephelometer was set up to work with an integration time of 1 min. Similar to the TSI nephelometer, CO_2 calibrations were periodically performed. The data were corrected for truncation according to Müller et al. (2011b). Uncertainty in scattering measurements by the Aurora nephelometers was estimated to be 5 % (Müller et al., 2011b).

2.2.2 Aerosol light attenuation and absorption measurements

Light absorption coefficients at 637 nm wavelength, $\sigma_{ap,637}$, were measured by a multi-angle absorption photometer, (MAAP, model 5012, Thermo Electron Group, Waltham, USA). This instrument measures the transmission of light through a glass-fiber filter on which aerosol particles are collected. Additionally to the forward hemisphere transmission measurement, the MAAP measures the light back scattering at 130 and 165°. By using a radiative transfer model (Petzold and Schönlinner, 2004), the instrument is able to provide absorption coefficients. The instrument was set up to provide data at 1 min resolution. By averaging the data at 30 min intervals, the MAAP detection limit is $0.13\,M\,m^{-1}$, which corresponds to a BC_e mass concentration of $20\,ng\,m^{-3}$ (calculated with a MAC of $6.6\,m^2\,g^{-1}$). The MAAP was generally operated at a flow rate of $10\,L\,min^{-1}$, but for some periods the flow rate was reduced to $8.3\,L\,min^{-1}$. According to Müller et al. (2011a), the MAAP measures at a wavelength of 637 ± 1 nm, instead of the 670 nm reported in the instrument's manual. In our calculations, we use 637 nm as the default MAAP wavelength and do not apply any interpolation factor to scale up the data from 670 to 637 nm since it would be within the instrument's ~ 5 % uncertainty range. The total uncertainty of the MAAP absorption measurements is of the order of 10 % for 30 min average times (Rizzo et al., 2013).

An aethalometer was used to measure attenuation of light by aerosol particles at different wavelengths. This instrument uses an LED light source to irradiate an aerosol-laden quartz-fiber filter and a detector, located in the forward hemisphere, to measure the light transmission (Hansen et al., 1984). The measured transmission is compared to a blank measurement in order to obtain a change in light transmission (i.e., attenuation). This attenuation is then converted to BC mass concentration by using a mass attenuation cross section that depends on the instrument model (14 625 and $6837.6\,m^2\,g^{-1}\,\lambda^{-1}$ for the AE31 and AE33 aethalometer models, respectively).

Aethalometer measurements started at the ATTO site in April 2012 using model AE31 (Magee Scientific, Berkeley, USA). The instrument was operated at different flow rates during the measurement period (varying from 2.0 to $3.7\,L\,min^{-1}$) and measured attenuation every 15 min. In January 2015, a new aethalometer, model AE33 (Aerosol d.o.o., Ljubljana, Slovenia), was installed. The overlapping measurement time of the AE31 and AE33 models (27 November to 15 December 2014) enabled the comparison of both data sets. We found good agreement between both models (difference < 10 %) for measurements at 470, 520, 590, and 660 nm. However, the wavelength dependence did not fit very well during this intercomparison period. Similar deviations in the wavelength dependence of AE31 and AE33 have been reported previously (ACTRIS, 2014). Nevertheless, it is still not clear whether the higher wavelength dependence of the AE33 compared to the AE31 is the result of an artifact of the instrument. An independent multi-wavelength absorption measurement can help to clarify the aforementioned AE31–AE33 deviation in $\mathring{a}_{abs}$ (Saturno et al., 2017). The comparison between compensated AE31 and AE33 data was used to correct the AE33 wavelength dependence deviation by applying intercomparison factors to AE33 data. The obtained AE31–AE33 intercomparison fits are shown in Fig. S4.

Aethalometer data require several corrections to account for different artifacts related to multiple scattering by the filter fibers, scattering by embedded aerosol particles, and filter-loading effects. The correction applied in this study has been described in a previous article (Saturno et al., 2017). The compensation algorithm is based on the correction scheme proposed by Collaud Coen et al. (2010). It uses MAAP data as a reference absorption measurement, which could introduce uncertainties related to the modification that aerosol particles can suffer by being deposited on a filter matrix. We retrieved the $\mathring{a}_{abs}$ from applying a log–log fit to aethalometer data corrected for filter-loading and multiple scattering effects. In the case of aethalometer AE33, the measurements do not require a filter-loading correction because this model uses the dual-spot technology which accounts for this artifact (Drinovec et al., 2015). The AE33 internal algorithm applies a multiple scattering correction using the correction factor reported by Weingartner et al. (2003). In this study, this compensation was reverted and the multiple scattering correction was calculated according to a comparison with MAAP measurements, in a similar fashion to the one applied to AE31 data mentioned above.

2.2.3 rBC mass measurements and MAC calculations

Refractory black carbon (rBC) was measured using a single particle soot photometer (SP2) revision C (Droplet Measurement Technologies, Longmont, USA). Initially, the measurements were done with a four-channel SP2 and the instrument was upgraded on 19 January 2015 to the eight-channel configuration. Figure S3 shows the different measurement periods of this instrument. The SP2 uses a high-intensity Nd:YAG laser beam (1 MW cm^{-2}, $\lambda = 1064$ nm) to irradiate aerosol particles that are provided by an air jet at 90°, with a flow rate of 0.12 L min^{-1}. All particles scatter the light from the laser beam and some of them, which are able to absorb radiation at the given wavelength (e.g., rBC), will incandesce and vaporize at high temperatures (Moteki and Kondo, 2008; Stephens et al., 2003). Four avalanche photo-diode (APD) detectors are installed in the instrument to measure (a) scattering, (b) broadband incandescence (350–800 nm), (c) narrowband incandescence (630–880 nm), and (d) scattering with a split detector. Time-dependent data are recorded from each particle as it passes through the laser beam. The ratio between broadband and narrowband signals can provide information on the particle's composition since it is related to the boiling point temperature of the sampled particles (Schwarz et al., 2006). The instrument was periodically calibrated using fullerene soot (Alfa Aesar Inc.) as the rBC reference material. A quadratic fit was applied to the recorded incandescence peak heights vs. the mass of mobility size-selected fullerene particles. The fullerene effective densities were taken from Gysel et al. (2011). The scattering detector was calibrated using polystyrene latex (PSL) spheres by relating the scattering signal to the PSL scattering cross section. The SP2 rBC dynamic ranges were 80–280 and 80–450 nm for the four-channel and eight-channel configurations, respectively.

The narrow dynamic range of the four-channel SP2 was preventing us from measuring rBC mass concentration values comparable to MAAP measurements. In a comparison with another eight-channel instrument during the GoAmazon2014/5 experiment we found that the four-channel instrument was underestimating the rBC mass concentration by a factor of 40 %. This factor was stable during the wet season 2014, but we could not measure its stability during the following dry season. Due to instability of this factor over the sampling period, a proper data correction was not possible. Therefore, in this paper we use only the eight-channel instrument's data, which were available from 9 February 2015 until 31 July 2016 with some interruptions due to hardware failures. The eight-channel SP2 rBC size-dependent counting efficiency was obtained by comparing the counts of fullerene particles measured by the SP2 and a condensation particle counter (CPC). This way, an underestimation factor of 5 % was found to affect SP2 rBC mass measurements and a scaling factor of 1.05 was applied to the data to account for this systematic error. Similar underestimation factors have been previously reported (Liu et al., 2017; Wang et al., 2014). The cumulative uncertainty of the SP2 measurements associated with the counting efficiency and mass calibration of the instrument has been estimated to be around 25 % (Wang et al., 2014).

The BC mass absorption cross section, α_{abs}, was calculated by running daily fits of 30 min averaged MAAP $\sigma_{ap,637}$ vs. SP2 rBC mass concentration data, using a standardized major-axis estimation (as explained in Sect. 2.6). Fits with $R^2 < 0.9$ were filtered out, resulting in a total of 106 out of 220 days included in the final result. Given the mentioned SP2 and MAAP uncertainties, the α_{abs} values presented here have uncertainties around ±40 %. The obtained α_{abs} values (shown in Sect. 3.1) were used to convert MAAP absorption measurements into BC_e mass concentrations.

2.2.4 Complementary measurements

Online chemical composition of aerosol particles has been measured since August 2014 using an aerosol chemical speciation monitor (ACSM) (Aerodyne Research Inc., Billerica, USA). Initial results on non-refractory aerosol chemical composition at the ATTO site have already been reported by Andreae et al. (2015) and a detailed paper on the long-term ACSM observations is being prepared by Carbone et al. (2018). This online mass spectrometry technique detects organics, nitrate, sulfate, ammonium, and chloride in the submicron (< 1 µm) aerosol size range (Ng et al., 2011).

A Picarro cavity ring-down spectrometer G1302 analyzer (Picarro Inc., Santa Clara, USA) measured CO_2 and CO at the ATTO site. Three calibration tanks were used to calibrate the instrument every 100 h. A Nafion™ dryer was installed in front of the instrument in order to reduce the noise in the CO measurements, which are affected by the high relative humidity of the tropical forest air. Calibration and performance checks will be reported in an upcoming paper. The instrument samples at five different heights, but we restrict our analysis to the data measured at 79 m. All CO measurements have been conducted on the walk-up tower. The measurement setup is largely inspired by a setup operational at another location since 2009 (see Winderlich et al., 2010). In order to calculate the BC enhancement ratios with respect to CO (ER_{BC}), we used a major-axis estimation fit that was applied to the bivariate data (Falster et al., 2006) where the slope represents the enhancement ratio. The 5th percentiles were used as background values.

Condensation nuclei (CN) number concentrations, N_{CN}, and size distributions from 10 nm to 10 µm, were continuously measured using several instruments including mobility and optical particle sizers (more details can be found in Andreae et al., 2015). In this study, we used coarse mode (> 1 µm) number and mass concentrations obtained by means of an optical particle sizer (OPS), model 3330 (TSI Inc., Shoreview, USA), to identify mineral dust transport events. A detailed analysis of the Saharan dust plume

arrivals at the ATTO site can be found in Moran-Zuloaga et al. (2018). Aerosol particle size distributions (10–430 nm diameter) were measured with scanning mobility particle sizer (SMPS) models 3080 and 3081 (TSI Inc., Shoreview, USA) using a CPC, model 3772 (TSI Inc., Shoreview, USA).

2.3 Wavelength dependence and BrC contribution calculations

Light scattering and absorption wavelength dependence are represented by the Ångström exponents, $\mathring{a}_{\mathrm{sca}}$ and $\mathring{a}_{\mathrm{abs}}$, respectively. The Ångström exponent can be retrieved when measurements at two or more different wavelengths are available; for example, the $\mathring{a}_{\mathrm{abs}}$ can be calculated as

$$\mathring{a}_{\mathrm{abs}} = -\frac{\ln\left(\frac{\sigma_{\mathrm{ap}}(\lambda_1)}{\sigma_{\mathrm{ap}}(\lambda_2)}\right)}{\ln\left(\frac{\lambda_1}{\lambda_2}\right)}, \quad (1)$$

where σ_{ap} is the absorption coefficient at two different wavelengths, λ_1 and λ_2.

When measurements at more than two wavelengths are available, a linear fit can be used to retrieve the Ångström exponent from the logarithm of the absorption (or scattering) coefficients vs. the logarithm of the wavelength, as follows:

$$\ln\sigma_{\mathrm{ap}} = -\mathring{a}_{\mathrm{abs}}\ln(\lambda) + \ln(\mathrm{constant}). \quad (2)$$

Black carbon is commonly taken to be wavelength-independent with $\mathring{a}_{\mathrm{abs}} = 1$. However, this assumption is theoretically wrong and the BC-related $\mathring{a}_{\mathrm{abs}}$ is very sensitive to the size of the particles (Moosmüller et al., 2011). Wang et al. (2016b) proposed a method to calculate the *wavelength dependence of the Ångström exponent* (WDA) in order to estimate the BrC contribution to total light absorption by aerosol particles. They use the difference between two $\mathring{a}_{\mathrm{abs}}$ calculated for two different wavelength pairs (440–870 and 675–880 nm) using aerosol robotic network (AERONET) and aethalometer data. We use a similar approach to retrieve WDA using aethalometer data from the ATTO site. In this study the WDA is calculated as follows:

$$\mathrm{WDA} = \mathring{a}_{\mathrm{abs},370-950} - \mathring{a}_{\mathrm{abs},660-950}, \quad (3)$$

where $\mathring{a}_{abs,370-950}$ and $\mathring{a}_{\mathrm{abs},660-950}$ correspond to the absorption Ångström exponents calculated for the 370–950 and 660–950 nm wavelength pairs, respectively. This way, a theoretical BC WDA was calculated from the modeled $\mathring{a}_{\mathrm{abs}}$ for BC (BC WDA $= \mathring{a}^{\mathrm{BC}}_{\mathrm{abs},370-950} - \mathring{a}^{\mathrm{BC}}_{\mathrm{abs},660-950}$).

Theoretical WDA values were calculated following conceptual Mie theory models for (i) polydisperse BC particles (Mishchenko et al., 1999), and (ii) core-shell internally mixed monodisperse BC (Bohren and Huffman, 1983). Characteristic BC core size distributions measured by the SP2 during the wet and dry seasons were used in the polydisperse BC-only model to retrieve extinction efficiency and single scattering albedo. The refractive indices used were 1.95–0.79i for BC (Bond and Bergstrom, 2006) and 1.55–0.001i for the coating material (Liu et al., 2015). The latter value was only used for the internally mixed BC case. The BC core diameters used in the internally mixed case were 100, 125, 150, 175, 200, 225, and 250 nm, with a coating thickness to core size ratio from 0.1 to 1. These values are in accordance with rBC mass size distributions observed at the ATTO site; see Fig. S5. Black carbon density was set to 1.8 g cm^{-3} (Schkolnik et al., 2007). Calculated BC WDA thresholds (25th and 75th percentiles), shown in Fig. S6, were compared to the ambient data in order to identify BrC influenced periods. For a general analysis, data with WDA lower than the 75th percentile were considered to be in the *BC-only* regime. The presence of BrC, in addition to BC, occurred when the modeled BC absorption at 370 nm was exceeded. A sensitivity study of this model was done by changing the refractive indices and the core size of the model input. These results are presented in Table S2 as relative overestimation of the BrC contribution to $\sigma_{\mathrm{ap},370}$. The calculated BC absorption Ångström exponents $\left(\mathring{a}^{\mathrm{BC}}_{\mathrm{abs}}\right)$ for the two wavelength pairs mentioned in Eq. (3) were used to calculate BrC absorption at 370 nm, as follows:

$$\sigma^{\mathrm{BC}}_{\mathrm{ap},370} = \sigma_{\mathrm{ap},950} \times \left(\frac{370}{950}\right)^{-\mathring{a}^{\mathrm{BC}}_{\mathrm{abs},370-950}}, \quad (4)$$

$$\sigma^{\mathrm{BrC}}_{\mathrm{ap},370} = \sigma_{\mathrm{ap},370} - \sigma^{\mathrm{BC}}_{\mathrm{ap},370}, \quad (5)$$

where $\mathring{a}^{\mathrm{BC}}_{\mathrm{abs},370-950}$ is obtained from the Mie model calculations. The uncertainties of the BrC contribution to total absorption at 370 nm were calculated using the theoretical minimum and maximum BC WDA values. They were below 37 % overall, and decreased to below 19 % when the BrC contribution was higher than 30 % at 370 nm. The relative overestimation of the BrC contribution obtained by using different BC core sizes and different refractive indices in the Mie model calculations can be found in Table S2.

2.4 HYSPLIT backward trajectories and clustering

The systematic backward trajectory (BT) analysis used here is described in C. Pöhlker et al. (2018). Briefly summarized: three-day backward trajectories were calculated by running the NOAA hybrid single-particle Lagrangian integrated trajectory (HYSPLIT) model (Draxler and Hess, 1998) using 1° resolution meteorological data from the global data assimilation system (GDAS1). The trajectories were calculated for 1000 m above ground level at 1 h intervals for the period January 2008 to June 2016. The entire trajectory ensemble was classified into 15 BT clusters using a *k*-means cluster analysis. The clusters represent different air mass transport tracks and velocities. The different cluster average trajectories and their frequency of occurrence are

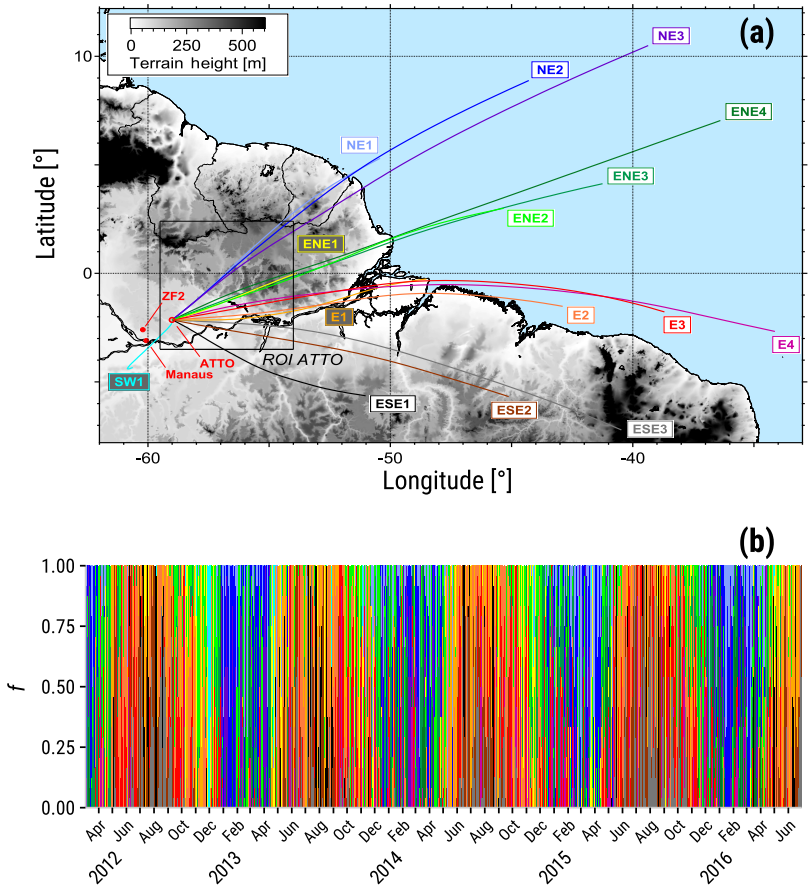

Figure 1. (a) Map of the northeastern Amazon Basin including averaged backward trajectory clusters and the region of interest (ROI) (59–54° W; 3.5° S–2.4° N), as a black rectangle, used to retrieve precipitation in the ATTO area. **(b)** Time series of the frequency of occurrence of each BT cluster during the sampling period. Adapted from C. Pöhlker et al. (2018).

shown in Fig. 1a and b, respectively. The clusters are classified as northeasterly ("NE1", "NE2", and "NE3"), east-northeasterly ("ENE1", "ENE2", "ENE3", and "ENE4"), easterly ("E1", "E2", "E3", and "E4), southeasterly ("ESE1", "ESE2", and "ESE3"), and southwesterly ("SW1") trajectory clusters. In some parts of the analysis presented here the trajectory clusters are grouped by main directions (NE, ENE, E, and ESE).

South American fire count data were retrieved from the satellite observations database available online by the Instituto Nacional de Pesquisas Espaciais (INPE), Brazil, at https://prodwww-queimadas.dgi.inpe.br/bdqueimadas/, last access: 4 April 2017. The fire data covered the same period as the HYSPLIT clustering analysis period, January 2008 to June 2016. Fire counts were classified at hourly resolution according to the corresponding BT cluster where they occurred. The fire counts reported in this study were weighted according to the trajectory density as (trajectory counts) / 100 km^2. Since the fire count number depends on the amount of satellite data available, we use these data with caution and only as a qualitative reference. For an extended discussion on fire geographical locations and land cover types, see C. Pöhlker et al. (2018).

2.5 Satellite data

The aerosol optical depth (AOD) at 550 nm, measured by the moderate resolution imaging spectroradiometer (MODIS) onboard the satellites Terra and Aqua, was retrieved for two domains of interest (see Fig. 2a).

– DOI1: over the Atlantic Ocean. Used to monitor the westward transport of BB aerosol particles from southern Africa, which are mostly emitted during the Amazon dry season, especially between August and September (Das et al., 2017). There is no guarantee that the observed aerosol over this area will necessarily reach the

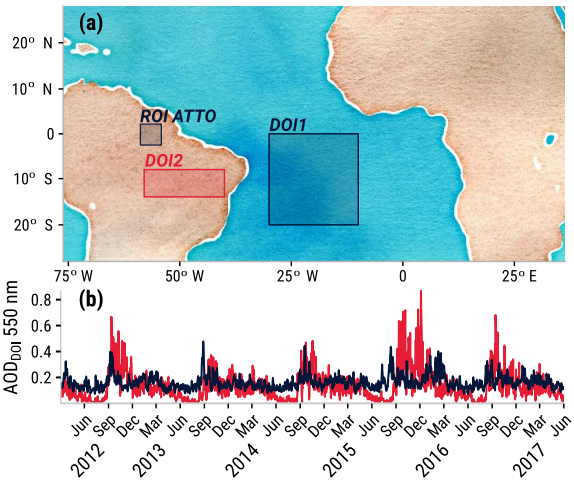

Figure 2. Aerosol optical depth (550 nm) observations in two different domains of interest shown in **(a)** DOI1 (boundaries: 30° W; 20° S; 10° W; 0° S) and DOI2 (boundaries: 58° W; 14° S; 40° W; 8° S). Time series of area-averaged AOD are shown in **(b)** for DOI1 (dark blue) and DOI2 (red). As a reference, the ATTO region of interest (ROI ATTO) is shown as a black rectangle in **(a)**.

ATTO site, but it is used as an indication of LRT events from southern Africa that will likely reach the Amazon Basin.
Boundaries: 30° W; 20° S; 10° W; 0° S.

– DOI2: over the southern Amazon. Used to monitor BB in this region where fire activity is related to deforestation and agriculture-related activities.
Boundaries: 58° W; 14° S; 40° W; 8° S.

The MODIS products can be found online at the Goddard Earth Science Data and Information Services Center at https://giovanni.gsfc.nasa.gov/giovanni/, last access: 17 July 2017, (GES-DISC, 2017).

Terra and Aqua data were averaged over the two different domains. The averaged AOD at 550 nm time series corresponding to DOI1 and DOI2 can be found in Fig. 2b. The seasonality observed for both data sets is similar, but the AOD for DOI1 (Atlantic Ocean) generally increased in August and decreased after the end of September, with some peaks in January–February, especially in 2016. On the other hand, high AOD values in DOI2 (southern Amazon) increased sharply in the beginning of September and decreased continuously until the middle of December, with the exception of the dry season 2015, when high AOD was observed until February 2016.

2.6 Data treatment

The analyzed data were averaged to 30 min intervals and corrected to standard temperature and pressure (STP, 273.15 K and 1013.25 hPa). Furthermore, the scattering data were interpolated to 637 nm to compare directly to the absorption data obtained by the MAAP, in order to avoid the uncertainty associated with the absorption spectral dependence calculation. The time periods of major and medium dust influence were taken from a study by Moran-Zuloaga et al. (2018). During the dry season, BB pulses were segregated by using the 75th percentile of $\sigma_{ap\,637}$ as a threshold. When examining correlations between independent measurements, we applied standardized major-axis estimations (SMA) by using the SMATR package (Falster et al., 2006) in the R statistical software environment (R Development Core Team, 2009). This method minimizes the error on the x and y axes, and not only at the y axis, like a linear regression does. Therefore, it provides unbiased estimates of the slope (Warton et al., 2006).

3 Results and discussion

3.1 Overview of aerosol optical properties (2012–2017)

This section summarizes the aerosol optical properties from 5 years of continuous measurements at the ATTO site. The corresponding time series are shown in Fig. 3 and descriptive statistics can be found in Table 1. The wet and dry season statistics were calculated excluding the transition periods.

The scattering coefficients, σ_{sp}, are shown in Fig. 3a, averaging 7.5 ± 9.3 and $33 \pm 25\,M\,m^{-1}$ at 550 nm during the wet and dry seasons, respectively (see Table 1). These values agree well with previously reported results at ZF2 of 8.1 ± 7.2 and $36 \pm 48\,M\,m^{-1}$ at 550 nm during the wet and dry seasons, respectively (Rizzo et al., 2013). Good agreement was also found for our results at 450 and 700 nm and the corresponding data from Rizzo et al. (2003). The proximity of both sites, ATTO and ZF2, frequently allows probing of comparable air masses of similar origin and atmospheric history. The long-term measurements also show a pronounced year-to-year variability in σ_{sp} (compare, e.g., 2014 and 2015 in Fig. 3a). The largest observed deviations from the dry-season average were found during the dry season 2015, with an average increase of 38 % in σ_{sp} at 550 nm. Similar increases were observed in σ_{sp} at 450 and 637 nm. These increases can be directly related to the higher occurrence of fire episodes during the strong ENSO period 2015/2016 with its negative precipitation anomaly, as discussed in more detail in Sects. 3.5 and 3.6.

The absorption coefficients, σ_{ap}, at 637 nm (MAAP) are shown in Fig. 3b, and averaged 0.68 ± 0.91 and $4.0 \pm 2.2\,M\,m^{-1}$ during the wet and dry seasons, respectively. Also for this parameter, comparable values were measured at the ZF2 site, with averages of 1.0 ± 1.4 and $3.9 \pm 3.6\,M\,m^{-1}$ at 637 nm during the wet and dry seasons, respectively (Rizzo et al., 2013). The higher increase in the absorption coefficient (factor of 5.9) from wet to dry season compared to

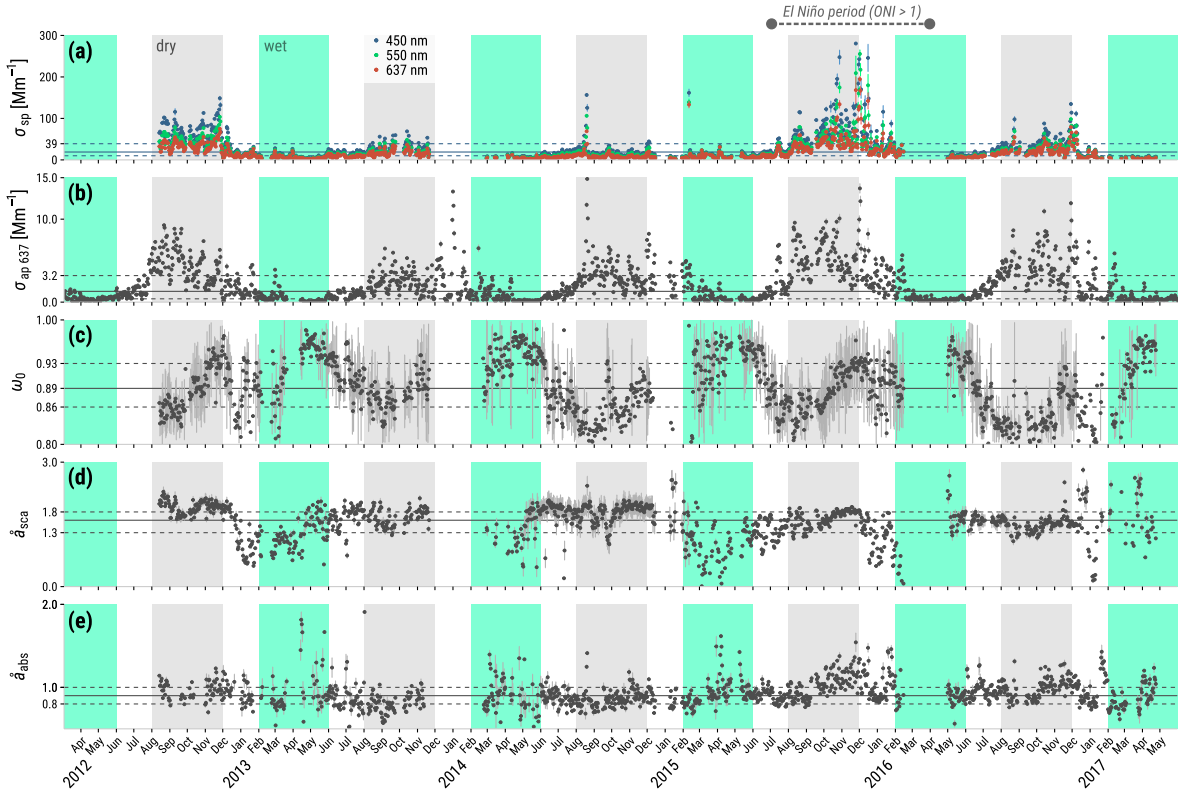

Figure 3. Overview of aerosol optical properties during the measurement period. **(a)** Scattering coefficient, **(b)** absorption coefficient at 637 nm, **(c)** single scattering albedo at 637 nm, **(d)** scattering Ångström exponent, and **(e)** absorption Ångström exponent. All data were averaged on 24 h intervals and standard errors are presented as vertical gray bars. Green and gray shaded areas correspond to the wet and dry seasons, respectively. First and third quartiles are represented as horizontal dashed lines, and medians as horizontal solid lines.

the increase in scattering (factor of 4.4) affected the ω_0 (see Fig. 3c). Lower values were observed during the dry season (0.87 ± 0.03 at 637 nm, 0.81 ± 0.08 at 550 nm) compared to the averages observed in the wet season (0.93 ± 0.04 at 637 nm, 0.88 ± 0.08 at 550 nm). At the ZF2 site, Rizzo et al. (2013) have found small differences between ω_0 values during the dry and wet seasons (0.87 ± 0.06 and 0.86 ± 0.09 at 637 nm, respectively) for over 2 years (2008–2011) of measurements. However, measurements during the wet season in 1998 at a sampling site closer to ATTO (Balbina, 60 km NW of ATTO and 140 km NE of Manaus) showed higher ω_0 values: 0.92–0.95 at 550 nm (Formenti et al., 2001). These values are within our measurement range for the same season (0.88 ± 0.08 at 550 nm). Single scattering albedo retrieved from multi-year ground-based radiometer measurements in the Amazonian forest had an average of 0.93 ± 0.02 (Dubovik et al., 2002). Given that we sampled dried aerosol particles, our average ω_0 are expected to be lower than these ambient-humidity values during the entire measurement period and the dry season. Measurements close to BB sources in Brazil have shown a wide range of ω_0; e.g., Chand et al. (2006) found an ω_0 of 0.92 ± 0.02 (550 nm) for dried aerosol over Rondônia, whereas Guyon et al. (2003a) calculated lower ω_0 values during BB events at the end of the LBA-EUSTACH 1 campaign in Rondônia, reaching 0.85 ± 0.02 at 550 nm. Freshly emitted smoke has an even lower ω_0, of 0.79 ± 0.05 at 550 nm (Reid et al., 1998).

The scattering Ångström exponent, $å_{sca}$, is a function of the aerosol particle size distribution. However, some studies have found that this relationship is only evident for surface and volume mean diameters and was not clearly valid between $å_{sca}$ and count mean diameters (Rizzo et al., 2013; Virkkula et al., 2011). We obtained higher $å_{sca}$ values during the dry season (1.71 ± 0.24) compared to the wet season (1.29 ± 0.50) as shown in Fig. 3d. This is an indication of the dominance of fine mode aerosol (mostly BB-related) during the dry season over the coarse mode aerosols that become more important in the wet season (i.e., PBAP, Saharan dust and sea salt), as previously observed at the ATTO site (Andreae et al., 2015; Moran-Zuloaga et al., 2018). A simi-

Table 1. Descriptive statistics (mean ± standard deviation and interquartile range, IQR) of daily averaged aerosol optical properties over the Amazon rainforest during the different seasons and the entire measurement period.

		Wet season (Feb–May)		Dry season (Aug–Nov)		Entire period (2012–2017)	
	Wavelength	Mean ± SD	IQR	Mean ± SD	IQR	Mean ± SD	IQR
Scattering coefficient σ_{sp} ($M\,m^{-1}$)	450 nm	9 ± 11	(5.1–11)	47 ± 35	(24–64)	31 ± 35	(10–39)
	550 nm	7.5 ± 9.3	(3.8–8.7)	33 ± 25	(17–46)	22 ± 25	(7–28)
	637 nm	6.4 ± 8.9	(3.0–7.4)	26 ± 19	(13–35)	17 ± 19	(6–23)
Absorption coefficient σ_{ap} ($M\,m^{-1}$)	637 nm	0.68 ± 0.91	(0.17–0.72)	4.0 ± 2.2	(2.4–5.1)	2.1 ± 2.2	(0.43–3.2)
Single scattering albedo ω_0	637 nm	0.93 ± 0.04	(0.91–0.96)	0.87 ± 0.03	(0.84–0.89)	0.89 ± 0.04	(0.86–0.93)
Scattering Ångström exp.[1] $\mathring{a}_{sca}$		1.29 ± 0.50	(0.98–1.65)	1.71 ± 0.24	(1.53–1.89)	1.54 ± 0.42	(1.32–1.84)
Absorption Ångström exp.[1] $\mathring{a}_{abs}$		0.91 ± 0.19	(0.80–0.98)	0.94 ± 0.16	(0.84–1.03)	0.93 ± 0.16	(0.83–1.01)
Mass absorption cross section α_{abs} ($m^2\,g^{-1}$)[2]	637 nm	11.4 ± 1.2	(10.8–12.0)	12.3 ± 1.3 [3]	(11.4–13.3)[3]	11.9 ± 1.4	(11.0–13.0)

[1] Calculated by applying a log–log linear fit to measurements at all available wavelengths. [2] Calculated by fitting eight-channel SP2 and MAAP data. [3] Including data from July 2015/16 (wet-to-dry transition season).

lar seasonal trend has been observed at the ZF2 site, where $\mathring{a}_{sca}$ was 1.70 ± 1.41 and 1.48 ± 1.12 (30 min averages) for the dry and wet seasons, respectively (Rizzo et al., 2013). A detailed analysis of the coarse mode aerosol abundance and properties measured at the ATTO site is presented elsewhere (Moran-Zuloaga et al., 2018).

Regarding the absorption Ångström exponent, $\mathring{a}_{abs}$, the overall average during the whole sampling period was 0.93 ± 0.16 (see Fig. 3e). Although no significant difference was found between dry and wet season averaged values, the averaged $\mathring{a}_{abs}$ was slightly higher during the dry season, reaching 0.94 ± 0.16 compared to 0.91 ± 0.19 during the wet season. It was found that the $\mathring{a}_{abs}$ only increased significantly during hours or days-long episodes, typically caused by nearby burning during the dry season. Details on the absorption wavelength dependence are discussed in Sect. 3.7. The aethalometer compensation calculation could potentially affect the retrieved $\mathring{a}_{abs}$ values. It has been shown that the raw attenuation Ångström exponent can represent a good approximation to the real $\mathring{a}_{abs}$ (Saturno et al., 2017). High absorption and scattering coefficients coincide with ESE and E trajectories, which are mostly dominant, but not exclusively, during the dry season; see Fig. 1. On the other hand, during the "cleanest" periods in the wet season, when light absorption reaches its minimum and ω_0 its maximum, the dominant trajectories are ENE and NE.

3.2 Black carbon mass absorption cross section

Accurate MAC values are required to retrieve BC mass concentrations from absorption measurements. During the entire measurement period, the calculated MAC was $11.9 \pm 1.4\,m^2\,g^{-1}$ (mean ± standard deviation) at $\lambda = 637$ nm. Daily calculated MAC values in the wet season were slightly lower on average compared to the dry season values (11.4 ± 1.2 and $12.3 \pm 1.3\,m^2\,g^{-1}$, respectively; see Table 1). As an illustration of the different MAC values obtained in the wet and dry seasons, $\sigma_{ap,637}$ vs. M_{rBC} scatter plots are presented in the Supplement as Fig. S7. Lower MAC values measured in the wet season 2016 could be associated with less coated BC compared to more aged particles in the dry season, which could have thicker coatings. Nevertheless, both values are much higher than the $6.6\,m^2\,g^{-1}$ suggested by Bond and Bergstrom (2006), especially considering that mineral dust and BrC do not strongly absorb at this wavelength and would therefore have little influence on the apparent MAC. However, they are in agreement with a modeled absorption enhancement of 1.6 calculated for open biomass burning in Brazil (Liu et al., 2017). In any case, there are large discrepancies that make it difficult to compare different MAC values obtained from ambient measurements due to systematic analytical uncertainties that dominate over the natural variability (Zanatta et al., 2016). These uncertainties are introduced by filter-based absorption measurement biases and BC mass overestimation or underestimation when

thermal–optical methods are used. In the case of the SP2, the rBC mass measurements are free of the different biases that affect thermal–optical techniques and are a wavelength-independent measurement. In the case of absorption measurements, a positive bias is introduced when organic aerosol deposits on the filter, enhancing the scattering by the filter fibers and the absorption by previously deposited BC particles when coating them. This artifact can be between 12 % and 70 % for particle soot absorption photometer (PSAP) measurements and will depend on the OA-to-BC ratio and the aging state of the organic aerosol particles (Lack et al., 2008). We expect a lower artifact for the MAAP since the scattering by filter fibers is accounted for by the reflectance measurements, but using our instrumentation we are not able to estimate the artifact coming from embedded BC absorption being modified by organic aerosol deposition. There are only a few field studies that present comparisons of rBC measurements and light absorption measurements, like MAAP, photoacoustic spectrometry (PAS), or aethalometer, and especially long-term measurements are scarce. Raatikainen et al. (2015) reported SP2 (eight-channel) and MAAP measurements in the Finnish Arctic and found that SP2 rBC mass concentrations were 5 times lower than MAAP BC_e mass concentration measurements, which is equivalent to MAC values of $\sim 30\,m^2\,g^{-1}$ at 637 nm. Some other studies have found values in closer agreement with our ATTO MAC results. For example, Laborde et al. (2013) found that air masses over Paris had an average MAC of 11.9 and $10.8\,m^2\,g^{-1}$ (interpolated to 637 nm), for aged and fresh BB aerosol, respectively. Additionally, Liu et al. (2010) calculated a median MAC of $10.2 \pm 3.2\,m^2\,g^{-1}$ during a measurement campaign at the Jungfraujoch research station in Switzerland. Another study in Mexico City, using PSAP for absorption measurements at $\lambda = 660$ nm, found a MAC of $11.2\,m^2\,g^{-1}$ (interpolated to 637 nm) (Subramanian et al., 2010).

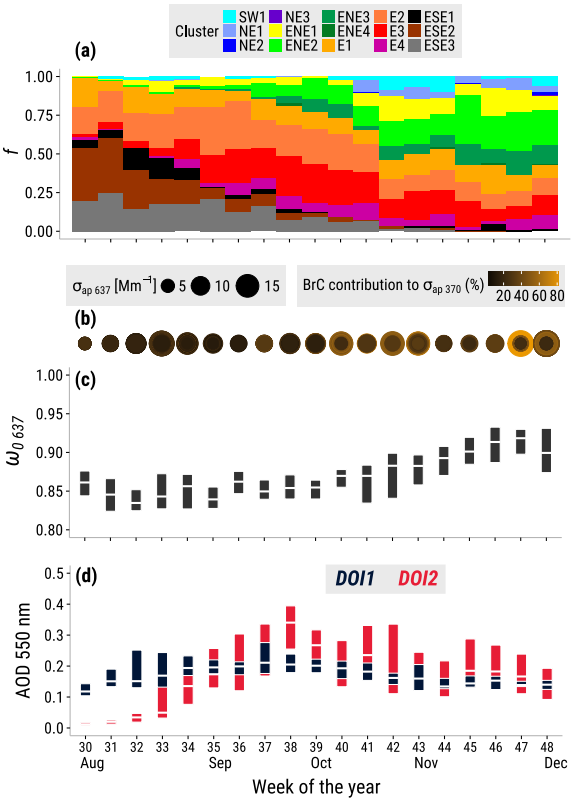

Figure 4. Multi-year (2012–2017) dry season weekly averages of **(a)** frequency of occurrence of BT clusters, f, **(b)** absorption coefficients at 637 nm, $\sigma_{ap,637}$, shown as circles with increasing diameters, the color scale corresponding to the relative BrC contribution to $\sigma_{ap,370}$, **(c)** single scattering albedo at 637 nm, $\omega_{0\,637}$, and **(d)** aerosol optical depth at 550 nm (AOD) for the different domains of interest, DOI1 and DOI2, which cover regions of the South Atlantic Ocean and the southern Amazon, respectively. Boxplots in **(c)** and **(d)** represent the median (white segment) and the 25th and 75th percentiles (lower and upper box edges, respectively).

3.3 Variability of optical properties during the dry season

The Amazonian dry season is generally impacted by BB aerosol particles that cause an increase in scattering and absorption coefficients (see Fig. 3a–b). However, the aerosol optical properties vary with the burning material (and region), as well as the aging process prior to reaching the ATTO site. In order to study the dry season variability of BB aerosol particles, multi-year (2012–2017) weekly averages were analyzed. The air mass trajectories, presented as BT clusters in Fig. 4a, show a decreasing dominance of ESE winds from August to November, whereas from October to November there is an increasing influence of ENE winds, indicating the south-to-north air mass trajectory shift that occurs during the transition from the dry to wet seasons. It is important to note that southerly and easterly winds are most likely to bring BB aerosol to the ATTO site during the dry season, given that very active open fire areas during this period are located in the southern Amazon and the Cerrado region (Andreae et al., 2012; Guyon et al., 2005) and, more remotely, in southern Africa (Andreae et al., 1994; Barbosa et al., 1999; Das et al., 2017). Aerosol optical depth at 550 nm is used in this study as a parameter to study the seasonal pattern of BB emission transport from both areas. In Sect. 2.5, we defined two domains of interest to study the aerosol seasonal patterns in these two areas: DOI1 for the LRT of South African smoke over the Atlantic Ocean, and DOI2 for the fires occurring in the southern Amazon. For the southern African fires (DOI1), the seasonal pattern shows an important influence during August–October, slightly decreasing towards the end of the Amazonian dry season (see Fig. 4d). For the southern Amazon region (DOI2), the typi-

cal fire seasonality during the dry season is observed in the AOD over this area (Fig. 4d), with the highest values observed in September and October. It is important to note that August seems to be the period when African LRT is a more important source than regional emissions and could be considered the main contributor of BB aerosol to the ATTO site during this time. For the rest of the dry season, it is likely that the aerosol properties are defined by South American BB emissions. In fact, the shift in air mass trajectories and variation of BB sources drive the BrC contribution to $\sigma_{ap,370}$, as shown in Fig. 4b. The BrC contribution (associated with high $\mathring{a}_{abs}$) is more important at the end of the dry season and is lower during August, when the aerosol particles likely arrive from Zambian woodland savanna fires (Barbosa et al., 1999), which burn more efficiently and emit aerosol particles with lower ω_0, 0.84 ± 0.015 at 670 nm on average (Dubovik et al., 2002). Additionally, on average, high $\sigma_{ap,637}$ events (see the increasing circle size in Fig. 4b) are more likely to bring high BrC containing aerosol, which is another indication that closer fires have a higher probability of providing BrC-rich aerosol particles to the ATTO site. The absorption wavelength dependence and BrC contribution are discussed in detail in Sect. 3.6. The differences between both identified BB sources in terms of BrC can be explained by two reasons: (i) the BrC photochemical oxidation and destruction of chromophores during transport (Sumlin et al., 2017) that would strongly affect LRT aerosol, and (ii) a lower rain scavenging rate for BC during transport, which would lead to an increased BC fraction in the aerosol population. The increase in the single scattering albedo (ω_0, Fig. 4c) towards the end of the dry season confirms that the aerosol particles during this time are scattering more radiation, not only due to higher BrC presence, but also due to other light-scattering aerosol particles.

3.4 Diel cycles

Figure 5 presents the diel cycles observed during the dry and the wet seasons for the following selected aerosol properties and meteorological parameters: Accumulation mode particle number concentration (N_{acc}), absorption coefficient at 637 nm ($\sigma_{ap,637}$), BrC absorption coefficient at 370 nm ($\sigma_{ap,BrC,370}$), precipitation rate (P_{ATTO}), and equivalent potential temperature (θ_e). In order to study the typical diel cycles in each season, extreme events like mineral dust transport in the wet season and nearby BB during El Niño in 2015–2016 have been excluded by using data within the 90 % confidence interval. The diel cycle of the equivalent potential temperature (Fig. 5i–j), calculated according to Stull (1988), reflects the evolution of the planetary boundary layer (PBL). Shortly before sunrise ($\sim$ 10:00 UTC), θ_e exhibits its minimum and increases afterwards reaching its maximum values in the early afternoon hours. The pronounced increase in θ_e in the early morning hours reflects the onset of solar warming and the initiation of vertical mixing, leading to the evolution of the convective boundary layer. After sunset, a stable nocturnal boundary layer is formed close to the forest canopy. A detailed analysis of the planetary boundary layer of the Amazon can be found in Fisch et al. (2004). Figures 5a–b show diel cycles of accumulation mode (100–430 nm) particle number concentration, N_{acc}. The diel patterns are similar during both seasons, with a minimum at sunrise, and an increase that starts in the morning at 12:00 UTC (08:00 LT) and maximum concentrations between 17:00 and 18:00 UTC (13:00–14:00 LT). This diel pattern observed in N_{acc} is driven by the diurnal evolution of the planetary boundary layer. On the one hand, the stable nocturnal layer leads to a concentration of particles and gases close to the canopy. On the other hand, the canopy acts as an effective particle sink, resulting in a concentration decrease towards the early morning (Ahlm et al., 2009). After sunrise, vertical mixing breaks up the stable nocturnal boundary layer. While the subsequent increase in N_{acc} is likely due to entrainment of particles from the elevated aerosol-rich layers, the decrease in the afternoon hours can be attributed to effective deposition in the forest canopy, as also discussed in Ahlm et al. (2009). The absorption coefficient at 637 nm, $\sigma_{ap,637}$, which is mostly related to BC, follows a diel pattern (Fig. 5c–d) similar to the N_{acc} trend for both seasons. Since BC is usually not emitted by nearby sources and it is generally transported in the accumulation mode, the similarities with N_{acc} diel patterns were expected. However, the wet season diel cycle of $\sigma_{ap,637}$ exhibits a decreasing tendency that starts two hours earlier than the decrease in N_{acc}. This difference can be explained by the fact that $\sigma_{ap,637}$ and N_{acc} are mass and number-related measurements, respectively. Therefore, a size-dependent deposition would affect mass and number-related aerosol properties differently. This difference was more evident in the wet season when BC concentrations were not as dominant as in the dry season. The diel pattern of BrC contribution during the dry season is significantly different from the $\sigma_{ap,637}$ (BC) pattern. Brown carbon absorption at 370 nm, $\sigma_{ap,BrC,370}$, shows its highest values between 12:00 and 14:00 UTC (08:00–10:00 LT) in the dry season and starts decreasing at 14:00 UTC (10:00 LT), earlier than $\sigma_{ap,637}$ and N_{acc} (Fig. 5e). This observation implies that the BrC aerosol particles measured at the ATTO site are mixed down into the boundary layer in the early morning and are then quickly photo-degraded during the day (Forrister et al., 2015; Laskin et al., 2015; Rincón et al., 2010; Wang et al., 2016b; Wong et al., 2017). This pattern is not observed during the wet season, when $\sigma_{ap,BrC,370}$ exhibits no significant diel variability.

Other remote site observations have found no significant diel variation of the absorption coefficient, due to efficient mixing of the PBL and low anthropogenic emissions (Chi et al., 2013). At ATTO, the high convectivity and related entrainment of high-altitude air masses, containing regional and/or LRT aerosols, result in a pronounced diel cycle in σ_{ap}.

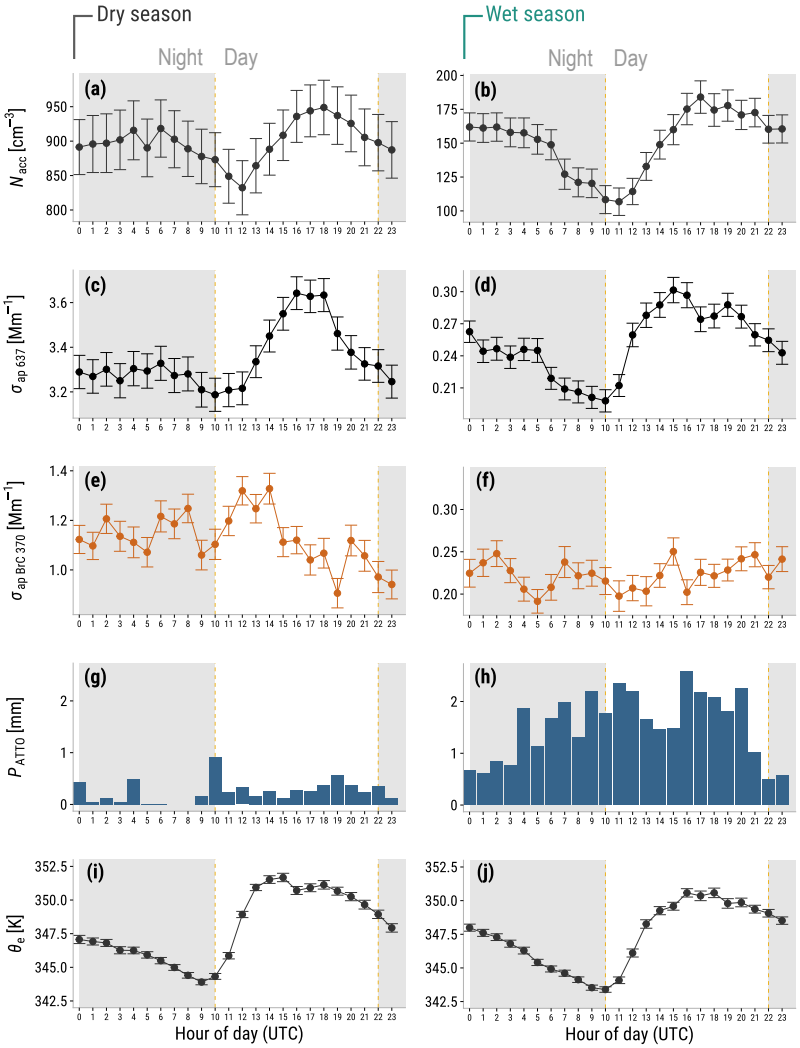

Figure 5. Diel variation of **(a, b)** median of the accumulation mode particle number concentration, N_{acc}, **(c, d)** median of the absorption coefficient at 637 nm, **(e, f)** median of the BrC absorption coefficient at 370 nm, **(g, h)** precipitation rate, and **(i, j)** median of the equivalent potential temperature. Gray and white backgrounds correspond to the night and day times, respectively. Error bars correspond to the standard error. Please note the different y axis scales.

This is in good agreement with previous dry season results from another Amazonian site (Brito et al., 2014).

3.5 BC-to-CO enhancement ratio

Agricultural clearing fires, like savanna fires, are dominated by the flaming combustion phase, in contrast to deforestation fires, where less than 50 % of the biomass is burned in the flaming phase (Dubovik et al., 2002). An important part of forest fires occurs in the form of smoldering combustion due to higher fuel moisture and larger fuel diameters (Guyon et al., 2005). Under smoldering fire conditions, when the combustion is less efficient and, thus, tends to emit more CO, observations tend to show lower ER_{BC} and higher single scattering albedo, ω_0, as well as a higher organic carbon (OC) enhancement ratio, ER_{OC}. On the other hand, flaming fires, which produce abundant BC aerosol particles, tend to exhibit lower ω_0 and higher ER_{BC} (Akagi et al., 2011). The smoke that arrives at the ATTO site during the dry season is a mixture of smoldering and flaming emissions with varying relative fractions. The air mass origin (i.e., the backward trajectories) largely defines whether emissions are advected

from regions with predominantly smoldering or flaming fires (C. Pöhlker et al., 2018).

The ER_{BC} and ω_0 values allow us to distinguish between flaming and smoldering-derived smoke and help locate the different sources. Figure 6 shows the ER_{BC} and ω_0 values at ATTO, being classified by grouped BT clusters. Mainly, the ESE and E trajectory clusters have ER_{BC} higher than 8 ng m^{-3} ppb^{-1}. From the two predominant BT cluster groups in the dry season (ESE and E), the ESE trajectories seem to be more influenced by flaming fires since the measurements are more shifted to high ER_{BC} and lower ω_0. In fact, the ESE clusters are dominated by the 0.80–0.90 ω_0 range, which means they are highly loaded with light-absorbing aerosol. This is consistent with the land cover information, which indicates that agricultural lands account for 6 %–20 % of the ESE clusters' total land cover, 3 %–5 % of the E clusters, and < 1 % of the ENE and NE clusters (C. Pöhlker et al., 2018). The eastern clusters (E) are more equally distributed in the ω_0 range and tend to be lower in terms of ER_{BC} compared to the ESE clusters. Therefore, we expect E trajectories to be more influenced by smoldering fires during the dry season compared to the ESE trajectories, even though, as already mentioned, the arrival of African savanna fire smoke from easterly trajectories in August–September provides BB aerosol particles that have lower ω_0 and higher ER_{BC}.

During the wet season, when ENE and NE BT clusters are dominant, we observed a trend towards lower ER_{BC} and higher ω_0, since the frequency of regional fires is much lower than in the dry season. Actually, when including data from the beginning of 2016, under the influence of ENSO, we observed a shift towards higher ER_{BC} in the NE directions due to the occurrence of fires in the Guyanas area. These atypical data were excluded from Fig. 6 to improve the contrast between the different air mass trajectory clusters. The NE and ENE trajectories were very similar in terms of ω_0 and ER_{BC}. Occasional dust transport events from the Sahara, mixed with BB aerosol from the Sahel region, brought aerosol particles with lower ω_0 compared to the wet season average.

The lower ER_{BC} observed in the wet season was likely due to aerosol scavenging during the transatlantic advection (Moran-Zuloaga et al., 2018), while CO is not affected by wet deposition (Liu et al., 2010). Note that ER_{BC} decreased more steeply with increasing ω_0, and their correlation was closer during the dry season (E and ESE BT clusters) in comparison to the wet season. This feature might be related to the age of the aerosol particles, because aging would make the BC become less hydrophobic (M. L. Pöhlker et al., 2018), so that it can be more efficiently removed by wet scavenging.

3.6 El Niño impact on aerosol optical properties

The aerosol optical properties measured at ATTO changed during the El Niño period at the end of 2015 and the beginning of 2016 (Fig. 3). To have a broader view of the relationships between El Niño-related drought conditions, increased fire abundance, and the Amazonian aerosol properties, we added scattering and absorption data from the ZF2 site published in Rizzo et al. (2013) and extended with recent data to the current ATTO time series in Fig. 7a–b. Overlapping data in 2013 (Fig. 7a and b) are statistically equivalent, with only a few days affected by probable near-site sources. Positive Oceanic Niño Index (ONI) values (Fig. 7c) were found to be related to higher scattering and absorption coefficients in the dry season. However, the ENSO is not the only cause of precipitation anomalies in the Amazon Basin. The Atlantic Multi-Decadal Oscillation (AMO) has also been found to be causing droughts (Aragão et al., 2008). The non-ENSO daily mean average (ZF2 and ATTO) scattering coefficient at 637 nm during the dry seasons was 24 ± 18 M m^{-1}. This average increased up to 48 ± 33 M m^{-1} during the ENSO periods (2009 and 2015 dry seasons). The wet season scattering coefficient average was also affected during El Niño, increasing from a non-ENSO average of 7 ± 7 to 10 ± 11 M m^{-1} during the wet season 2016. A similar pattern was observed for $\sigma_{ap,637}$, which increased from a non-ENSO average in the dry seasons of 3.8 ± 2.8 M m^{-1} to an ENSO average of 5.3 ± 2.5 M m^{-1} (2009 and 2015 dry seasons' average). It is remarkable that high absorption coefficients were also measured during the dry season 2010 (5.6 ± 4.7 M m^{-1}), a year with a mostly negative ONI. However, it has been shown that an increased sea surface temperature in the Atlantic Ocean

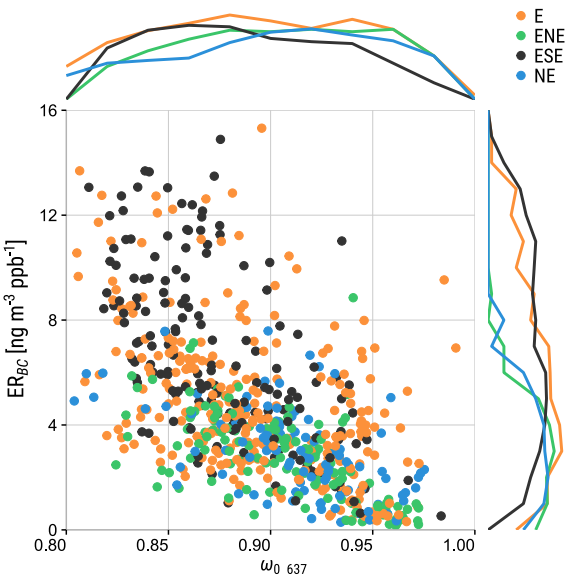

Figure 6. Scatter plot of 2012–2017 daily average of the BC-to-CO enhancement ratio, ER_{BC} vs. single scattering albedo at 637 nm, $\omega_{0\ 637}$, with marginal probability density plots (normalized counts in log scale) for data corresponding to grouped BT clusters.

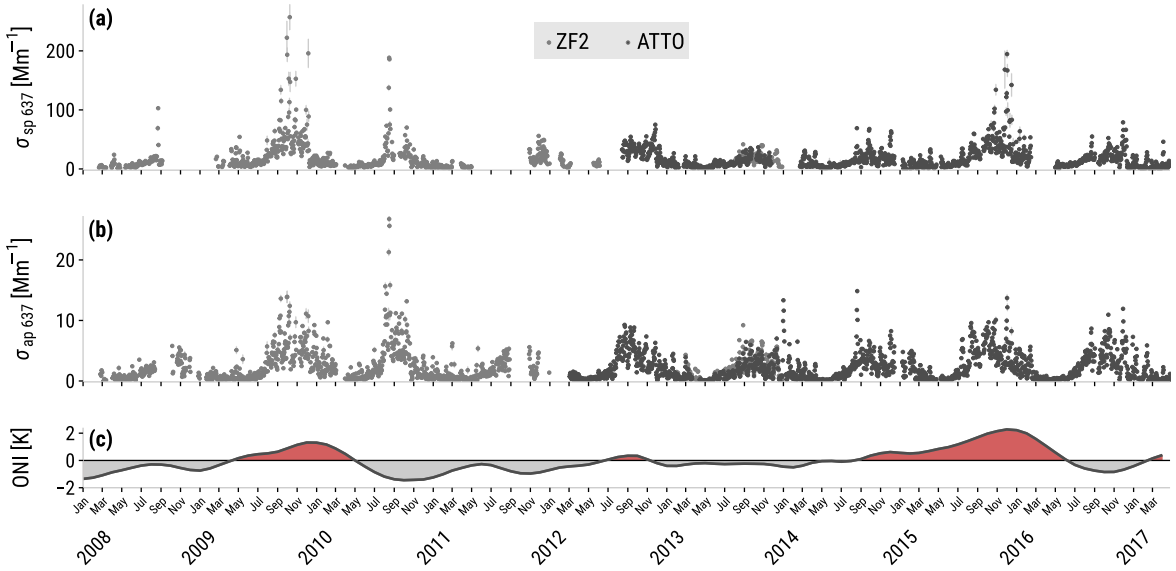

Figure 7. Scattering **(a)** and absorption **(b)** coefficient (637 nm) time series measured at the ZF2 and the ATTO sites from 2008 to 2016 (24 h averaged data). Increased scattering and absorption coefficients were observed under the influence of El Niño. **(c)** High ONI indicates active ENSO periods, shown as red shaded areas.

(not ENSO-related) in 2010 caused a special drought period in the Amazon rainforest (Lewis et al., 2011).

3.7 Absorption wavelength dependence and BrC contribution

Open biomass burning emits a mixture of BC and OA with high absorption wavelength dependence (Andreae and Gelencsér, 2006; Hoffer et al., 2006; Kirchstetter et al., 2004). However, our observations show that sometimes LAC measured at the ATTO site can fall in the BC-only regime, with $\mathring{a}_{abs} \approx 1$. To understand this pattern, we have analyzed the relationship between the WDA and other parameters, like the OA-to-sulfate ratio and ω_0. In Fig. 8a, WDA is presented as a function of the OA-to-sulfate mass ratio. According to the result of an orthogonal fit (not shown), there is a significant correlation between these variables ($R^2 = 0.61$), and the aerosol light absorption is in the BC-only regime (shaded area in Fig. 8a) when the OA-to-sulfate ratio is lower than ~ 6.5, which occurred 15 % of the time in the high-absorption periods ($\sigma_{ap,637}$ higher than the 75th percentile). On the other hand, higher OA-to-sulfate ratios correspond to likely BrC-rich aerosol masses, which were the majority of the cases. The ω_0 at 637 nm of the BC-only regime (interquartile range, IQR: 0.82–0.86) was clearly lower than the one corresponding to the BrC-rich regime (IQR: 0.85–0.90).

In Fig. 8b, the BC-only regime data have been segregated by BT clusters. The air masses that are more likely to bring wavelength-independent LAC to the site are those with the faster wind speed: E3, E4, and ESE3. These emissions could be related to ship traffic in the Atlantic Ocean, BB in southern Africa, or power plant emissions from the western African coast. Low OA-to-sulfate ratios with high ω_0 occurred a few times and could be explained by high sulfate input from volcanic emissions in the Congo (Fioletov et al., 2016; Saturno et al., 2018a), rather than fossil fuel emissions, which are typically rich in BC.

In an effort to identify the BrC-rich trajectories, the WDA was studied for the different BT clusters that are mostly active during the dry season. Box plots corresponding to each trajectory cluster, together with the average fire counts in the geographical cluster area, are presented in Fig. 9. From the group of ESE trajectory clusters (ESE1, ESE2, and ESE3), the ESE1 trajectories exhibit the highest WDA values, with a decreasing tendency towards faster trajectories, ESE3 being the one with the lowest WDA values. Even though ESE3 is the trajectory cluster with more fire counts, the fact that those fires occur farther from the ATTO site compared to the ones in the slowest trajectory, ESE1, could be related to a decrease in absorption wavelength dependence during transport. A similar pattern is observed for the easterly trajectory clusters (E1, E2, E3, and E4), where the slowest air mass trajectories comprised of the E1 cluster exhibit the highest WDA median compared to the rest of the E clusters. In the case of E4, the WDA 25th percentile is lower than the rest of the E trajectories, but it shows an increased median that can not be explained by the occurrence of fire events, which is

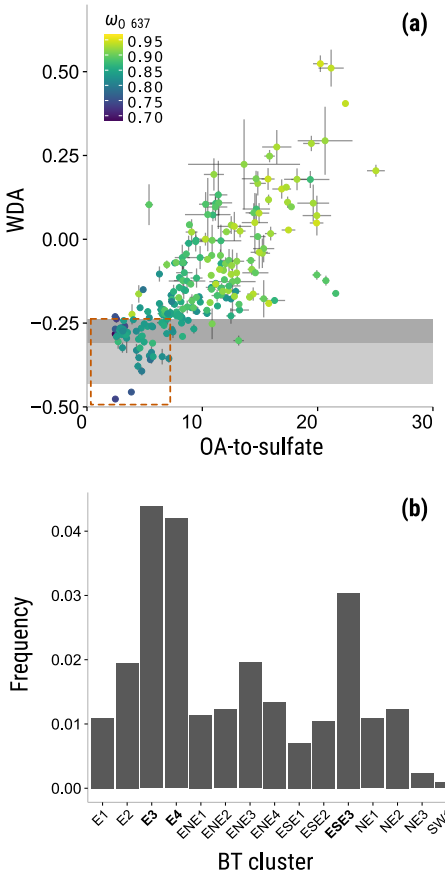

Figure 8. (a) Absorption wavelength dependence (WDA) as a function of the OA-to-sulfate mass ratio during high-absorption periods in the dry season. The color scale indicates the ω_0 at 637 nm. Gray shaded areas correspond to theoretical WDA for internally mixed BC (light gray) and externally mixed BC (dark gray). The data inside the dashed rectangle in **(a)** are used in **(b)** to identify the BT clusters that are more likely to bring wavelength-independent LAC to the ATTO site.

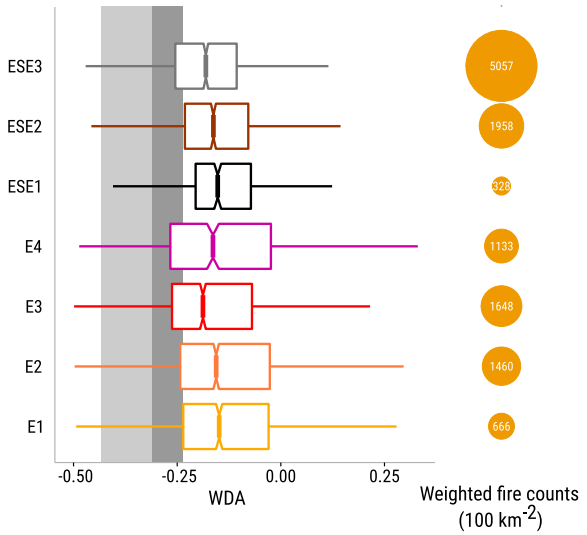

Figure 9. Wavelength dependence of $\mathring{a}_{abs}$ (WDA) for different trajectories in the dry season presented as box and whisker plots (left). The light and dark gray shaded areas correspond to the pure BC and internally mixed BC regimes, respectively. Notches correspond to 1.58 IQR $n^{-1/2}$. If notch ranges do not overlap, the medians are statistically different (95 % confidence). The trajectory weighted fire counts for each BT cluster are shown as circles on the right side. The data presented here correspond to 1 h averages.

lower than the observations for the other clusters (E2, E3, and E4). The E4-weighted fire counts are anyhow on the same order of magnitude as E2 and E3 and the wavelength dependence differences could be related to different fuel types or combustion phases. Actually, the long E clusters (E3 and E4) cover more southern areas than the shorter ones (E1 and E2) and have some overlap with ESE3. By comparing grouped E and ESE clusters, it can be observed that WDA in the E clusters has higher variability compared to the ESE ones. This pattern could be associated with a wider range of sources in the E trajectories compared to ESE. The E trajectories travel over the Amazon River, where ship traffic is quite significant. In fact, as can be observed in Fig. 9, for the E3 and E4 trajectories, there is a significant number (> 25th percentile) of measurements that fall in the BC-only regime. Something similar is only observed for the ESE3 trajectories among the ESE group. Most of the agricultural land is located along the southern margins of the Amazon rainforest (C. Pöhlker et al., 2018). This area is within the ESE clusters footprint. The narrower range of WDA values measured for the ESE trajectories compared to the E ones indicates that sources in the ESE footprint are more homogeneous compared to the sources located in the E footprint. These WDA tendencies could be useful for understanding the BrC emissions and atmospheric transformations in the context of the Amazon rainforest and its surroundings.

Using the calculated BC-only WDA thresholds, we were able to estimate the BrC contribution to total absorption during the measurement period (2012–2017) (Fig. 10). We found that BrC contributes 24 % (IQR: 17 %–29 %) of total light absorption at 370 nm wavelength. A slight seasonal variability was observed for the BrC relative contribution, with the medians and IQR during the wet and dry season being 27 % (19–34) and 22 % (16–27), respectively. However, most of the wet season data had to be excluded, because they were from air masses rich in mineral dust, which introduces large uncertainties into the WDA method. During El Niño, at the end of 2015, open fire events were more frequent (with weighted fire counts of 1756 km^{-2} compared to the 2008–2016 average of 1076 km^{-2}), and the CO 95th percentile was

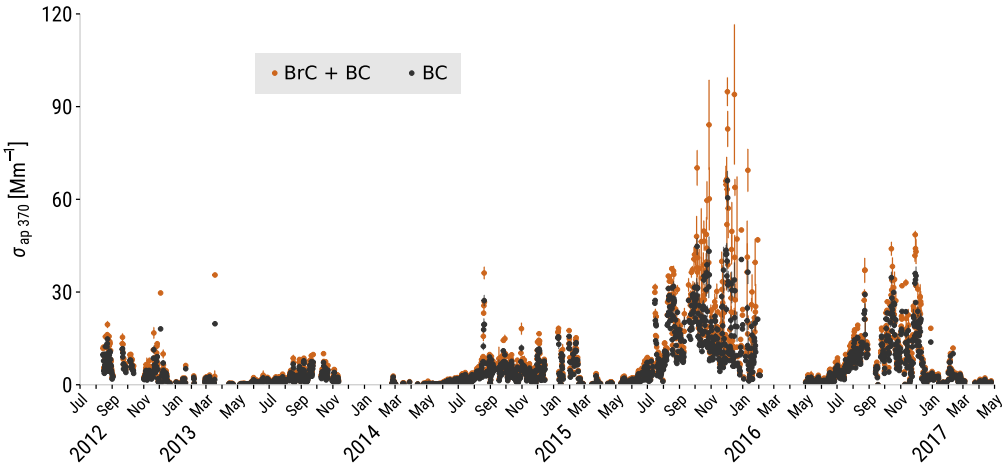

Figure 10. Total absorption at 370 nm (12 h average data) segregated by BC only (gray points) and BrC + BC (brown points). Error bars are equivalent to ±1 standard error. Long-range transport dust events have been excluded from the analysis.

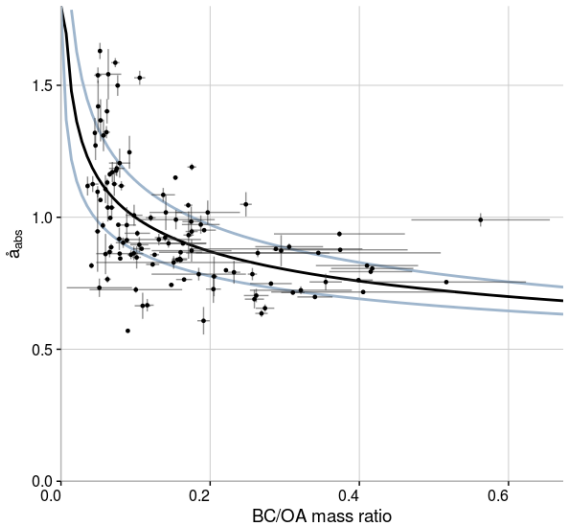

Figure 11. Absorption Ångström exponent ($å_{abs}$) as a function of the BC / OA mass ratio for selected dust events in the wet season. The black line corresponds to a non-linear least squares fit applied to the data ($y = x^{-0.199} \times 0.632$). The light blue lines correspond to the standard error of the fit.

exceeded several times. In this period, the BrC contribution had a median of 37 % (IQR: 27–47) and showed a significant correlation with CO ($R^2 = 0.47$). This significant increase in the BrC contribution could be related to the relatively short distance between the fire spots and the ATTO site. It can be observed in Fig. 10 that the El Niño influence continued during the dry season 2016, but not as strongly as in 2015. Previous observations have shown that the atmospheric lifetime of BB-emitted BrC is ∼ 1 day due to photolysis and oxidation, which destroy the chromophores (Forrister et al., 2015; Wang et al., 2016b; Wong et al., 2017). Therefore, BrC emitted from fires in the southern borders of the Amazon rainforest, which require ∼ 3 days to be transported to the ATTO site, is likely to be significantly photodegraded and to contribute only weakly to total aerosol light absorption after atmospheric processing.

The BC-to-OA mass ratio during the sampling time had a median of 0.06 (IQR: 0.04–0.10). The ratio BC to OA has been used before to parameterize $å_{abs}$ and ω_0 (Pokhrel et al., 2016; Saleh et al., 2014), but little is known about this relationship for tropical forest emissions. A broader range of the BC-to-OA mass ratio between 2014 and 2016 was observed during the dust episodes in the wet season, including those periods when regional fires were active (IQR: 0.08–0.24). Other periods, like the dry season, with higher BC mass concentrations exhibited a narrower and lower BC-to-OA mass ratio range (IQR: 0.03–0.08). A scatter plot of the absorption wavelength dependence, $å_{abs}$, as a function of the BC-to-OA mass ratio during the northern African LRT events in the wet season can be found in Fig. 11. We have found a trend where $å_{abs}$ increases with decreasing BC-to-OA mass ratio following an exponential function. These results are comparable to those presented by Pokhrel et al. (2016) and Saleh et al. (2014), with slightly lower $å_{abs}$ values in our study, however. This pattern could be related to a dominant presence of primary organic aerosol (POA) that has characteristically lower absorption wavelength dependence compared to SOA (Saleh et al., 2013). However, more experimental studies are required to investigate the optical properties of aerosol produced by burning different tropical forest fuels.

4 Summary and conclusions

This study presents the optical properties of aerosol particles at the remote ATTO site for a measurement period of 5 years (2012–2017). The atmospheric seasonality at ATTO strongly affects aerosol light scattering and absorption, with significant increases from wet to dry season conditions due to intense biomass burning in South America and Africa. The wet season background aerosol was dominated by biogenic particles with occasional interruptions by long-range transported dust and BB aerosols from Africa to ATTO, leading to decreases in scattering Ångström exponent, $å_{sca}$, and single scattering albedo, ω_0 (637 nm). The average ω_0 during the wet season was 0.93 ± 0.04, which is higher than the dry season average of 0.87 ± 0.03. The absorption wavelength dependence, $å_{abs}$, was relatively low, with an average of 0.93 ± 0.16, and varied only slightly between seasons. The highest $å_{abs}$ were measured during BB events, but no effect on $å_{abs}$ was observed due to the presence of dust, most likely due to a size effect, given that after May 2014 absorption coefficients were measured only for sub-micron aerosol particles. The BC mass absorption coefficient (MAC) at 637 nm calculated from MAAP and SP2 measurements agrees with other studies; however, it is higher than "typical" values that are commonly used in the literature to convert σ_{ap} into BC mass concentrations. The calculated wet season MAC average was $11.4 \pm 1.2\,m^2\,g^{-1}$, and increased slightly during the dry season to an average of $12.3 \pm 1.3\,m^2\,g^{-1}$ at 637 nm. These values are consistent with a strong "lensing effect" by organic coatings attached to BC aerosol particles. High OA amounts in the Amazonian atmosphere resulted in low BC-to-OA mass ratios, in the range of 0.04 to 0.10 (IQR). A significant correlation between BC-to-OA mass ratio and $å_{abs}$ was observed during the wet season under the influence of regional and remote BB emissions. The ΔBC / ΔCO enhancement ratios (ER_{BC}) were mostly lower than $8\,ng\,m^{-3}\,ppb^{-1}$, mainly due to the aging and deposition of BB aerosol particles during transport to ATTO. A higher and wider range of ER_{BC} values was observed during the dry season due to the influence of different biomass combustion phases that varied from smoldering to flaming fires.

Theoretical wavelength-dependent BC $å_{abs}$ were calculated and used to estimate the BrC contribution to near-UV (370 nm) light absorption. This approach resulted in medians of 27 % and 22 % BrC contributions in the wet and dry seasons, respectively. Higher BrC contributions were measured during the El Niño period at the end of 2015, when BrC absorption at 370 nm increased to a median of 37 %. We observed that winds coming from ESE directions in the dry season were more likely to bring aerosols with a high absorption wavelength dependence, implying a higher BrC content.

In the case of prolonged drought periods in the Amazon Basin, significant increases in BrC absorption contribution could be expected due to increased fire occurrence. Long-term monitoring of light absorbing aerosol particles is required to reduce uncertainty in global climate models. The data presented here provide a contribution in this direction and can help to understand how different climatic phenomena, like El Niño, can affect the Amazon atmospheric aerosol cycling. Further investigations on the BC mixing state and morphology will be required to improve modeled calculations and BrC retrievals.

Data availability. The data of the key results presented here have been deposited in supplementary data files for use in follow-up studies. They are available in NASA Ames format under https://doi.org/10.17617/3.1r (Saturno et al., 2018b, available data for ATTO BC and BrC study). For data requests beyond the available data, please refer to the corresponding authors.

Appendix A

Table A1. List of frequently used symbols and acronyms.

Description	Acronym	Symbol	Units
Black carbon	BC		
Brown carbon	BrC		
Equivalent black carbon	BC_e		
Refractory black carbon	rBC		
Organic carbon	OC		
Organic aerosol	OA		
Light-absorbing carbonaceous matter	LAC		
ΔBC / ΔCO enhancement ratio	ER_{BC}		
Attenuation coefficient	ATN	σ_{ATN}	m^{-1}
Absorption coefficient		σ_{ap}	m^{-1}
Scattering coefficient		σ_{sp}	m^{-1}
Absorption Ångström exponent	AAE	$\mathring{a}_{abs}$	
Scattering Ångström exponent	SAE	$\mathring{a}_{sca}$	
Wavelength dependence of $\mathring{a}_{abs}$	WDA		
Mass attenuation cross section		α_{atn}	$m^2\,g^{-1}$
(BC) Mass absorption cross section	MAC	α_{abs}	$m^2\,g^{-1}$
Backscattering coefficient		σ_{bsp}	m^{-1}
Single scattering albedo	SSA	ω_0	
Aerosol optical depth	AOD		
Condensation nuclei number concentration ($>$ 10 nm)		N_{CN}	cm^{-3}
Accumulation mode particle number concentration (100–430 nm)		N_{acc}	cm^{-3}
Precipitation at ATTO region of interest (ROI), Fig. 1a		P_{ATTO}	mm
Equivalent potential temperature		θ_e	K
Amazon Tall Tower Observatory	ATTO		
Backward trajectory	BT		
Long-range transport	LRT		
El Niño–Southern Oscillation	ENSO		
Oceanic Niño Index	ONI		
Biomass burning	BB		
Fossil fuel	FF		
Coordinated universal time	UTC		
Local time	LT		
Inter-quartile range	IQR		
Domain of interest, Fig. 2a	DOI		

Supplement. The supplement related to this article is available online at: https://doi.org/10.5194/acp-18-12817-2018-supplement.

Author contributions. JS, BAH, CP, FD, QW, DMZ, JB, SC, YC, XC, JVL, MLP, LVR, DW, SW, PA, UP and MOA designed the research. JS, BAH, CP, FD, QW, DMZ, JB, SC, YC, XC, JD, IHA, TK, JVL, HP, MLP, LVR, PS, DW, SW and MOA performed the measurements and/or contributed to the data analysis. All authors contributed to the discussion and interpretation of the results and to writing the paper.

Competing interests. The authors declare that they have no conflict of interest.

Special issue statement. This article is part of the special issues "Amazon Tall Tower Observatory (ATTO) Special Issue" and "Observations and Modeling of the Green Ocean Amazon (GoAmazon2014/5)". It is not associated with a conference.

Acknowledgements. This work has been supported by the Max Planck Society (MPG) and the Paul Crutzen Graduate School (PCGS). For the operation of the ATTO site, we acknowledge the support by the German Federal Ministry of Education and Research (BMBF contract 01LB1001A) and the Brazilian Ministério da Ciência, Tecnologia e Inovação (MCTI/FINEP contract 01.11.01248.00) as well as the Amazon State University (UEA), FAPEAM, LBA/INPA and SDS/CEUC/RDS-Uatumã. Paulo Artaxo acknowledges support from FAPESP – Fundação de Amparo à Pesquisa do Estado de São Paulo. Jorge Saturno is grateful for the PhD scholarship from the Fundación Gran Mariscal de Ayacucho (Fundayacucho). This paper contains results of research conducted under the Technical/Scientific Cooperation Agreement between the National Institute for Amazonian Research, the State University of Amazonas, and the Max-Planck-Gesellschaft e.V.; the opinions expressed are the entire responsibility of the authors and not of the participating institutions. We highly acknowledge the support by the Instituto Nacional de Pesquisas da Amazônia (INPA). We would like to especially thank all the people involved in the technical, logistical, and scientific support of the ATTO project, in particular Reiner Ditz, Jürgen Kesselmeier, Alberto Quesada, Niro Higuchi, Susan Trumbore, Matthias Sörgel, Thomas Disper, Andrew Crozier, Thomas Klimach, Björn Nillius, Uwe Schulz, Steffen Schmidt, Antonio Ocimar Manzi, Alcides Camargo Ribeiro, Hermes Braga Xavier, Elton Mendes da Silva, Nagib Alberto de Castro Souza, Adi Vasconcelos Brandão, Amaury Rodrigues Pereira, Antonio Huxley Melo Nascimento, Feliciano de Souza Coehlo, Thiago de Lima Xavier, Josué Ferreira de Souza, Roberta Pereira de Souza, Bruno Takeshi, and Wallace Rabelo Costa.

The article processing charges for this open-access publication were covered by the Max Planck Society.

Edited by: Markku Kulmala
Reviewed by: two anonymous referees

References

ACTRIS: ACTRIS Intercomparison Workshop for Integrating Nephelometer and Absorption Photometers, Leipzig, Germany, available at: http://www.wmo-gaw-wcc-aerosol-physics.org/files/ACTRIS-intercomparison-workshop-integrating-nephelometer-and-absorption-photometer-02-03-2013.pdf (last access 1 June 2017), 2014.

Ahlm, L., Nilsson, E. D., Krejci, R., Mårtensson, E. M., Vogt, M., and Artaxo, P.: Aerosol number fluxes over the Amazon rain forest during the wet season, Atmos. Chem. Phys., 9, 9381–9400, https://doi.org/10.5194/acp-9-9381-2009, 2009.

Akagi, S. K., Yokelson, R. J., Wiedinmyer, C., Alvarado, M. J., Reid, J. S., Karl, T., Crounse, J. D., and Wennberg, P. O.: Emission factors for open and domestic biomass burning for use in atmospheric models, Atmos. Chem. Phys., 11, 4039–4072, https://doi.org/10.5194/acp-11-4039-2011, 2011.

Anderson, T. L., Covert, D. S., Marshall, S. F., Laucks, M. L., Charlson, R. J., Waggoner, A. P., Ogren, J. A., Caldow, R., Holm, R. L., Quant, F. R., Sem, G. J., Wiedensohler, A., Ahlquist, N. A., and Bates, T. S.: Performance Characteristics of a High-Sensitivity, Three-Wavelength, Total Scatter/Backscatter Nephelometer, J. Atmos. Ocean. Tech., 13, 967–986, https://doi.org/10.1175/1520-0426(1996)013<0967:PCOAHS>2.0.CO;2, 1996.

Andreae, M. O.: Biomass burning: Its history, use and distribution and its impact on environmental quality and global climate, Glob. Biomass Burn. Atmos. Clim. Biosph. Implic., 15–42, 1991.

Andreae, M. O.: Raising dust in the greenhouse, Nature, 380, 389–390, https://doi.org/10.1038/380389a0, 1996.

Andreae, M. O.: The dark side of aerosols, Nature, 409, 671–672, https://doi.org/10.1038/35055640, 2001.

Andreae, M. O.: Aerosols before pollution, Science, 315, 50–51, https://doi.org/10.1126/science.1136529, 2007.

Andreae, M. O. and Gelencsér, A.: Black carbon or brown carbon? The nature of light-absorbing carbonaceous aerosols, Atmos. Chem. Phys., 6, 3131–3148, https://doi.org/10.5194/acp-6-3131-2006, 2006.

Andreae, M. O. and Merlet, P.: Emission of trace gases and aerosols from biomass burning, Global Biogeochem. Cy., 15, 955–966, https://doi.org/10.1029/2000GB001382, 2001.

Andreae, M. O., Browell, E. V., Garstang, M., Gregory, G. L., Harriss, R. C., Hill, G. F., Jacob, D. J., Pereira, M. C., Sachse, G. W., Setzer, A. W., Dias, P. L. S., Talbot, R. W., Torres, A. L., and Wofsy, S. C.: Biomass-burning emissions and associated haze layers over Amazonia, J. Geophys. Res., 93, 1509–1527, https://doi.org/10.1029/JD093iD02p01509, 1988.

Andreae, M. O., Anderson, B. E., Blake, D. R., Bradshaw, J. D., Collins, J. E., Gregory, G. L., Sachse, G. W., and Shipham, M. C.: Influence of plumes from biomass burning on atmospheric chemistry over the equatorial and tropical South Atlantic during CITE 3, J. Geophys. Res., 99, 12793–12808, https://doi.org/10.1029/94JD00263, 1994.

Andreae, M. O., Artaxo, P., Beck, V., Bela, M., Freitas, S., Gerbig, C., Longo, K., Munger, J. W., Wiedemann, K. T., and Wofsy, S. C.: Carbon monoxide and related trace gases and aerosols over the Amazon Basin during the wet and dry seasons, Atmos. Chem. Phys., 12, 6041–6065, https://doi.org/10.5194/acp-12-6041-2012, 2012.

Andreae, M. O., Acevedo, O. C., Araùjo, A., et al.: The Amazon Tall Tower Observatory (ATTO): overview of pilot measurements on ecosystem ecology, meteorology, trace gases, and aerosols, Atmos. Chem. Phys., 15, 10723–10776, https://doi.org/10.5194/acp-15-10723-2015, 2015.

Ångström, A.: On the Atmospheric Transmission of Sun Radiation and on Dust in the Air, Geogr. Ann., 11, 156–166, https://doi.org/10.2307/519399, 1929.

Aragão, L. E. O., Malhi, Y., Roman-Cuesta, R. M., Saatchi, S., Anderson, L. O., and Shimabukuro, Y. E.: Spatial patterns and fire response of recent Amazonian droughts, Geophys. Res. Lett., 34, 1–5, https://doi.org/10.1029/2006GL028946, 2007.

Aragão, L. E. O., Malhi, Y., Barbier, N., Lima, A., Shimabukuro, Y., Anderson, L., and Saatchi, S.: Interactions between rainfall, deforestation and fires during recent years in the Brazilian Amazonia, Philos. Trans. R. Soc. B Biol. Sci., 363, 1779–1785, https://doi.org/10.1098/rstb.2007.0026, 2008.

Artaxo, P., Martins, J. V., Yamasoe, M. A., Procópio, A. S., Pauliquevis, T. M., Andreae, M. O., Guyon, P., Gatti, L. V., and Cordova Leal, A. M.: Physical and chemical properties of aerosols in the wet and dry seasons in Rondônia, Amazonia, J. Geophys. Res., 107, 8081, https://doi.org/10.1029/2001JD000666, 2002.

Artaxo, P., Rizzo, L. V., Brito, J. F., Barbosa, H. M. J., Arana, A., Sena, E. T., Cirino, G. G., Bastos, W., Martin, S. T., and Andreae, M. O.: Atmospheric aerosols in Amazonia and land use change: from natural biogenic to biomass burning conditions, Faraday Discuss., 165, 203–235, https://doi.org/10.1039/c3fd00052d, 2013.

Barbosa, P. M., Stroppiana, D., Grégoire, J.-M., and Cardoso Pereira, J. M.: An assessment of vegetation fire in Africa (1981–1991): Burned areas, burned biomass, and atmospheric emissions, Global Biogeochem. Cy., 13, 933–950, https://doi.org/10.1029/1999GB900042, 1999.

Bilbao, B. A., Leal, A. V., and Méndez, C. L.: Indigenous Use of Fire and Forest Loss in Canaima National Park, Venezuela, Assessment of and Tools for Alternative Strategies of Fire Management in Pemón Indigenous Lands, Hum. Ecol., 38, 663–673, https://doi.org/10.1007/s10745-010-9344-0, 2010.

Bohren, C. F. and Huffman, D. R.: Absorption and scattering of light by small particles, Wiley, Hoboken, NJ, 1983.

Bond, T. C. and Bergstrom, R. W.: Light Absorption by Carbonaceous Particles?: An Investigative Review, Aerosol Sci. Technol., 40, 27–67, https://doi.org/10.1080/02786820500421521, 2006.

Bond, T. C., Streets, D. G., Yarber, K. F., Nelson, S. M., Woo, J.-H., and Klimont, Z.: A technology-based global inventory of black and organic carbon emissions from combustion, J. Geophys. Res., 109, D14203, https://doi.org/10.1029/2003JD003697, 2004.

Bond, T. C., Doherty, S. J., Fahey, D. W., Forster, P. M., Berntsen, T., DeAngelo, B. J., Flanner, M. G., Ghan, S., Kärcher, B., Koch, D., Kinne, S., Kondo, Y., Quinn, P. K., Sarofim, M. C., Schultz, M. G., Schulz, M., Venkataraman, C., Zhang, H., Zhang, S., Bellouin, N., Guttikunda, S. K., Hopke, P. K., Jacobson, M. Z., Kaiser, J. W., Klimont, Z., Lohmann, U., Schwarz, J. P., Shindell, D., Storelvmo, T., Warren, S. G., and Zender, C. S.: Bounding the role of black carbon in the climate system: A scientific assessment, J. Geophys. Res.-Atmos., 118, 5380–5552, https://doi.org/10.1002/jgrd.50171, 2013.

Brito, J., Rizzo, L. V., Morgan, W. T., Coe, H., Johnson, B., Haywood, J., Longo, K., Freitas, S., Andreae, M. O., and Artaxo, P.: Ground-based aerosol characterization during the South American Biomass Burning Analysis (SAMBBA) field experiment, Atmos. Chem. Phys., 14, 12069–12083, https://doi.org/10.5194/acp-14-12069-2014, 2014.

Cachier, H., Bremond, M.-P., and Buat-Ménard, P.: Determination of atmospheric soot carbon with a simple thermal method, Tellus B, 41, 379–390, https://doi.org/10.1111/j.1600-0889.1989.tb00316.x, 1989.

Caponi, L., Formenti, P., Massabó, D., Di Biagio, C., Cazaunau, M., Pangui, E., Chevaillier, S., Landrot, G., Andreae, M. O., Kandler, K., Piketh, S., Saeed, T., Seibert, D., Williams, E., Balkanski, Y., Prati, P., and Doussin, J.-F.: Spectral- and size-resolved mass absorption efficiency of mineral dust aerosols in the shortwave spectrum: a simulation chamber study, Atmos. Chem. Phys., 17, 7175–7191, https://doi.org/10.5194/acp-17-7175-2017, 2017.

Carbone, S., Brito, J. F., Xu, L., Ng, N. L., Rizzo, L. V., Stern, R., Cirino, G. G., Holanda, B. A., Senna, E., Wolff, S., Saturno, J., Chi, X., Souza, R. A. F., Arana, A., de Sá, M., Pöhlker, M. L., Andreae, M. O., Pöhlker, C., Barbosa, H. M. J., and Artaxo, P.: Long-term chemical composition and source apportionment of submicron aerosol particles in the central Amazon basin (ATTO), Atmos. Chem. Phys. Discuss., in preparation, 2018.

Carslaw, K. S., Lee, L. A., Reddington, C. L., Pringle, K. J., Rap, A., Forster, P. M., Mann, G. W., Spracklen, D. V., Woodhouse, M. T., Regayre, L. A., and Pierce, J. R.: Large contribution of natural aerosols to uncertainty in indirect forcing, Nature, 503, 67–71, https://doi.org/10.1038/nature12674, 2013.

Chand, D., Guyon, P., Artaxo, P., Schmid, O., Frank, G. P., Rizzo, L. V., Mayol-Bracero, O. L., Gatti, L. V., and Andreae, M. O.: Optical and physical properties of aerosols in the boundary layer and free troposphere over the Amazon Basin during the biomass burning season, Atmos. Chem. Phys., 6, 2911–2925, https://doi.org/10.5194/acp-6-2911-2006, 2006.

Chi, X., Winderlich, J., Mayer, J.-C., Panov, A. V., Heimann, M., Birmili, W., Heintzenberg, J., Cheng, Y., and Andreae, M. O.: Long-term measurements of aerosol and carbon monoxide at the ZOTTO tall tower to characterize polluted and pristine air in the Siberian taiga, Atmos. Chem. Phys., 13, 12271–12298, https://doi.org/10.5194/acp-13-12271-2013, 2013.

Chow, J. C., Yu, J. Z., Watson, J. G., Hang Ho, S. S., Bohannan, T. L., Hays, M. D., and Fung, K. K.: The application of thermal methods for determining chemical composition of carbonaceous aerosols: A review, J. Environ. Sci., 42, 1521–1541, https://doi.org/10.1080/10934520701513365, 2007.

Clarke, A. D. and Charlson, R. J.: Radiative Properties of the Background Aerosol: Absorption Component of Extinction, Science, 229, 263–265, https://doi.org/10.1126/science.229.4710.263, 1985.

Cochrane, M. A.: Fire science for rainforests, Nature, 421, 913–919, https://doi.org/10.1038/nature01437, 2003.

Collaud Coen, M., Weingartner, E., Apituley, A., Ceburnis, D., Fierz-Schmidhauser, R., Flentje, H., Henzing, J. S., Jennings, S. G., Moerman, M., Petzold, A., Schmid, O., and Baltensperger, U.: Minimizing light absorption measurement artifacts of the Aethalometer: evaluation of five correction algorithms, Atmos. Meas. Tech., 3, 457–474, https://doi.org/10.5194/amt-3-457-2010, 2010.

Crutzen, P. J. and Andreae, M. O.: Biomass burning in the tropics: Impact on atmospheric chemistry and biogeochemical cycles, Science, 250, 1669–1678, 10.1126/science.250.4988.1669, 1990.

Das, S., Harshvardhan, H., Bian, H., Chin, M., Curci, G., Protonotariou, A. P., Mielonen, T., Zhang, K., Wang, H., and Liu, X.: Biomass burning aerosol transport and vertical distribution over the South African-Atlantic region, J. Geophys. Res.-Atmos., 6391–6415, https://doi.org/10.1002/2016JD026421, 2017.

Davidson, E. A., de Araújo, A. C., Artaxo, P., Balch, J. K., Brown, I. F. C., Bustamante, M. M., Coe, M. T., DeFries, R. S., Keller, M., Longo, M., Munger, J. W., Schroeder, W., Soares-Filho, B. S., Souza, C. M., and Wofsy, S. C.: The Amazon basin in transition, Nature, 481, 321–328, https://doi.org/10.1038/nature10717, 2012.

Denjean, C., Cassola, F., Mazzino, A., Triquet, S., Chevaillier, S., Grand, N., Bourrianne, T., Momboisse, G., Sellegri, K., Schwarzenbock, A., Freney, E., Mallet, M., and Formenti, P.: Size distribution and optical properties of mineral dust aerosols transported in the western Mediterranean, Atmos. Chem. Phys., 16, 1081–1104, https://doi.org/10.5194/acp-16-1081-2016, 2016.

Draxler, R. R. and Hess, G. D.: An overview of the HYSPLIT 4 modelling system for trajectories, dispersion and deposition, Aust. Met. Mag., 47, 295–308, 1998.

Drinovec, L., Mocnik, G., Zotter, P., Prévôt, A. S. H., Ruckstuhl, C., Coz, E., Rupakheti, M., Sciare, J., Müller, T., Wiedensohler, A., and Hansen, A. D. A.: The "dual-spot" Aethalometer: an improved measurement of aerosol black carbon with real-time loading compensation, Atmos. Meas. Tech., 8, 1965–1979, https://doi.org/10.5194/amt-8-1965-2015, 2015.

Dubovik, O., Holben, B., Eck, T. F., Smirnov, A., Kaufman, Y. J., King, M. D., Tanré, D., and Slutsker, I.: Variability of Absorption and Optical Properties of Key Aerosol Types Observed in Worldwide Locations, J. Atmos. Sci., 59, 590–608, 2002.

Falster, D. S., Warton, D. I., and Wright, I. J.: SMATR: Standardised major axis tests and routines, ver 2.0, available at: http://www.bio.mq.edu.au/ecology/SMATR/ (last access: 1 June 2017), 2006.

Favez, O., El Haddad, I., Piot, C., Boréave, A., Abidi, E., Marchand, N., Jaffrezo, J.-L., Besombes, J.-L., Personnaz, M.-B., Sciare, J., Wortham, H., George, C., and D'Anna, B.: Intercomparison of source apportionment models for the estimation of wood burning aerosols during wintertime in an Alpine city (Grenoble, France), Atmos. Chem. Phys., 10, 5295–5314, https://doi.org/10.5194/acp-10-5295-2010, 2010.

Fioletov, V. E., McLinden, C. A., Krotkov, N., Li, C., Joiner, J., Theys, N., Carn, S., and Moran, M. D.: A global catalogue of large SO_2 sources and emissions derived from the Ozone Monitoring Instrument, Atmos. Chem. Phys., 16, 11497–11519, https://doi.org/10.5194/acp-16-11497-2016, 2016.

Fisch, G., Tota, J., Machado, L. A. T., Silva Dias, M. A. F., da F. Lyra, R. F., Nobre, C. A., Dolman, A. J., and Gash, J. H. C.: The convective boundary layer over pasture and forest in Amazonia, Theor. Appl. Climatol., 78, 47–59, https://doi.org/10.1007/s00704-004-0043-x, 2004.

Formenti, P., Andreae, M. O., Lange, L., Roberts, G., Cafmeyer, J., Rajta, I., Maenhaut, W., Holben, B. N., Artaxo, P., and Lelieveld, J.: Saharan dust in Brazil and Suriname during the Large-Scale Biosphere-Atmosphere Experiment in Amazonia (LBA) – Cooperative LBA Regional Experiment (CLAIRE) in March 1998, J. Geophys. Res.-Atmos., 106, 14919–14934, https://doi.org/10.1029/2000JD900827, 2001.

Forrister, H., Liu, J., Scheuer, E., Dibb, J., Ziemba, L., Thornhill, K. L., Anderson, B., Diskin, G., Perring, A. E., Schwarz, J. P., Campuzano-Jost, P., Day, D. A., Palm, B. B., Jimenez, J. L., Nenes, A., and Weber, R. J.: Evolution of brown carbon in wildfire plumes, Geophys. Res. Lett., 42, 4623–4630, https://doi.org/10.1002/2015GL063897, 2015.

Fuller, K. A., Malm, W. C., and Kreidenweis, S. M.: Effects of mixing on extinction by carbonaceous particles, J. Geophys. Res.-Atmos., 104, 15941–15954, https://doi.org/10.1029/1998JD100069, 1999.

Fuzzi, S., Decesari, S., Facchini, M. C., Cavalli, F., Emblico, L., Mircea, M., Andreae, M. O., Trebs, I., Hoffer, A., Guyon, P., Artaxo, P., Rizzo, L. V., Lara, L. L., Pauliquevis, T., Maenhaut, W., Raes, N., Chi, X., Mayol-Bracero, O. L., Soto-García, L. L., Claeys, M., Kourtchev, I., Rissler, J., Swietlicki, E., Tagliavini, E., Schkolnik, G., Falkovich, A. H., Rudich, Y., Fisch, G., and Gatti, L. V.: Overview of the inorganic and organic composition of size-segregated aerosol in Rondônia, Brazil, from the biomass-burning period to the onset of the wet season, J. Geophys. Res.-Atmos., 112, D01201, https://doi.org/10.1029/2005JD006741, 2007.

Garg, S., Chandra, B. P., Sinha, V., Sarda-Esteve, R., Gros, V., and Sinha, B.: Limitation of the Use of the Absorption Angstrom Exponent for Source Apportionment of Equivalent Black Carbon: a Case Study from the North West Indo-Gangetic Plain, Environ. Sci. Technol., 50, 814–824, https://doi.org/10.1021/acs.est.5b03868, 2016.

GES-DISC: Goddard Earth Sciences Data and Information Services Center, available at: https://giovanni.gsfc.nasa.gov/giovanni/, last access: 1 June 2017.

Gläser, G., Wernli, H., Kerkweg, A., and Teubler, F.: The transatlantic dust transport from North Africa to the Americas-Its characteristics and source regions, J. Geophys. Res.-Atmos., 120, 11231–11252, https://doi.org/10.1002/2015JD023792, 2015.

Guyon, P., Graham, B., Beck, J., Boucher, O., Gerasopoulos, E., Mayol-Bracero, O. L., Roberts, G. C., Artaxo, P., and Andreae, M. O.: Physical properties and concentration of aerosol particles over the Amazon tropical forest during background and biomass burning conditions, Atmos. Chem. Phys., 3, 951–967, https://doi.org/10.5194/acp-3-951-2003, 2003a.

Guyon, P., Boucher, O., Graham, B., Beck, J., Mayol-Bracero, O. L., Roberts, G. C., Maenhaut, W., Artaxo, P., and Andreae, M. O.: Refractive index of aerosol particles over the Amazon tropical forest during LBA-EUSTACH 1999, J. Aerosol Sci., 34, 883–907, https://doi.org/10.1016/S0021-8502(03)00052-1, 2003b.

Guyon, P., Graham, B., Roberts, G. C., Mayol-Bracero, O. L., Maenhaut, W., Artaxo, P., and Andreae, M. O.: Sources of optically active aerosol particles over the Amazon forest, Atmos. Environ., 38, 1039–1051, https://doi.org/10.1016/j.atmosenv.2003.10.051, 2004.

Guyon, P., Frank, G. P., Welling, M., Chand, D., Artaxo, P., Rizzo, L., Nishioka, G., Kolle, O., Fritsch, H., Silva Dias, M. A. F., Gatti, L. V., Cordova, A. M., and Andreae, M. O.: Airborne measurements of trace gas and aerosol particle emissions from

biomass burning in Amazonia, Atmos. Chem. Phys., 5, 2989–3002, https://doi.org/10.5194/acp-5-2989-2005, 2005.

Gysel, M., Laborde, M., Olfert, J. S., Subramanian, R., and Gröhn, A. J.: Effective density of Aquadag and fullerene soot black carbon reference materials used for SP2 calibration, Atmos. Meas. Tech., 4, 2851–2858, https://doi.org/10.5194/amt-4-2851-2011, 2011.

Hamilton, D. S., Lee, L. A., Pringle, K. J., Reddington, C. L., Spracklen, D. V., and Carslaw, K. S.: Occurrence of pristine aerosol environments on a polluted planet, P. Natl. Acad. Sci. USA, 111, 18466–18471, https://doi.org/10.1073/pnas.1415440111, 2014.

Hansen, A. D. A., Rosen, H., and Novakov, T.: The aethalometer – An instrument for the real-time measurement of optical absorption by aerosol particles, Sci. Total Environ., 36, 191–196, https://doi.org/10.1016/0048-9697(84)90265-1, 1984.

Hoffer, A., Gelencsér, A., Guyon, P., Kiss, G., Schmid, O., Frank, G. P., Artaxo, P., and Andreae, M. O.: Optical properties of humic-like substances (HULIS) in biomass-burning aerosols, Atmos. Chem. Phys., 6, 3563–3570, https://doi.org/10.5194/acp-6-3563-2006, 2006.

IPCC: Climate Change 2013: The Physical Science Basis, Contribution of Working Group I to the Fifth Assessment Report of the Intergovernmental Panel on Climate Change, edited by: Stocker, T. F., Qin, D., Plattner, G.-K., Tignor, M., Allen, S. K., Boschung, J., Nauels, A., Xia, Y., Bex, V., and Midgley, P. M., Cambridge University Press, Cambridge, UK, New York, NY, USA, 1535 pp., 2013.

Janhäll, S., Andreae, M. O., and Pöschl, U.: Biomass burning aerosol emissions from vegetation fires: particle number and mass emission factors and size distributions, Atmos. Chem. Phys., 10, 1427–1439, https://doi.org/10.5194/acp-10-1427-2010, 2010.

Kirchstetter, T. W., Novakov, T., and Hobbs, P. V.: Evidence that the spectral dependence of light absorption by aerosols is affected by organic carbon, J. Geophys. Res.-Atmos., 109, D21208, https://doi.org/10.1029/2004JD004999, 2004.

Kondo, Y., Matsui, H., Moteki, N., Sahu, L., Takegawa, N., Kajino, M., Zhao, Y., Cubison, M. J., Jimenez, J. L., Vay, S., Diskin, G. S., Anderson, B., Wisthaler, A., Mikoviny, T., Fuelberg, H. E., Blake, D. R., Huey, G., Weinheimer, A. J., Knapp, D. J., and Brune, W. H.: Emissions of black carbon, organic, and inorganic aerosols from biomass burning in North America and Asia in 2008, J. Geophys. Res., 116, D08204, https://doi.org/10.1029/2010JD015152, 2011.

Laborde, M., Crippa, M., Tritscher, T., Jurányi, Z., Decarlo, P. F., Temime-Roussel, B., Marchand, N., Eckhardt, S., Stohl, A., Baltensperger, U., Prévôt, A. S. H., Weingartner, E., and Gysel, M.: Black carbon physical properties and mixing state in the European megacity Paris, Atmos. Chem. Phys., 13, 5831–5856, https://doi.org/10.5194/acp-13-5831-2013, 2013.

Lack, D. A. and Langridge, J. M.: On the attribution of black and brown carbon light absorption using the Ångström exponent, Atmos. Chem. Phys., 13, 10535–10543, https://doi.org/10.5194/acp-13-10535-2013, 2013.

Lack, D. A., Cappa, C. D., Covert, D. S., Baynard, T., Massoli, P., Sierau, B., Bates, T. S., Quinn, P. K., Lovejoy, E. R., and Ravishankara, A. R.: Bias in Filter-Based Aerosol Light Absorption Measurements Due to Organic Aerosol Loading: Evidence from Ambient Measurements, Aerosol Sci. Technol., 42, 1033–1041, https://doi.org/10.1080/02786820802389277, 2008.

Lack, D. A., Bahreini, R., Langridge, J. M., Gilman, J. B., and Middlebrook, A. M.: Brown carbon absorption linked to organic mass tracers in biomass burning particles, Atmos. Chem. Phys., 13, 2415–2422, https://doi.org/10.5194/acp-13-2415-2013, 2013.

Laskin, A., Laskin, J., and Nizkorodov, S. A.: Chemistry of Atmospheric Brown Carbon, Chem. Rev., 115, 4335–4382, https://doi.org/10.1021/cr5006167, 2015.

Lewis, K., Arnott, W. P., Moosmüller, H., and Wold, C. E.: Strong spectral variation of biomass smoke light absorption and single scattering albedo observed with a novel dual-wavelength photoacoustic instrument, J. Geophys. Res., 113, D16203, https://doi.org/10.1029/2007JD009699, 2008.

Lewis, S. L., Brando, P. M., Phillips, O. L., van der Heijden, G. M. F., and Nepstad, D.: The 2010 Amazon Drought, Science, 331, 554–554, https://doi.org/10.1126/science.1200807, 2011.

Liu, D., Flynn, M., Gysel, M., Targino, A., Crawford, I., Bower, K., Choularton, T., Jurányi, Z., Steinbacher, M., Hüglin, C., Curtius, J., Kampus, M., Petzold, A., Weingartner, E., Baltensperger, U., and Coe, H.: Single particle characterization of black carbon aerosols at a tropospheric alpine site in Switzerland, Atmos. Chem. Phys., 10, 7389–7407, https://doi.org/10.5194/acp-10-7389-2010, 2010.

Liu, D., Taylor, J. W., Young, D. E., Flynn, M. J., Coe, H., and Allan, J. D.: The effect of complex black carbon microphysics on the determination of the optical properties of brown carbon, Geophys. Res. Lett., 42, 613–619, https://doi.org/10.1002/2014GL062443, 2015.

Liu, D., Whitehead, J., Alfarra, M. R., Reyes-Villegas, E., Spracklen, D. V., Reddington, C. L., Kong, S., Williams, P. I., Ting, Y.-C., Haslett, S., Taylor, J. W., Flynn, M. J., Morgan, W. T., McFiggans, G., Coe, H., and Allan, J. D.: Black-carbon absorption enhancement in the atmosphere determined by particle mixing state, Nat. Geosci., 10, 184–188, https://doi.org/10.1038/ngeo2901, 2017.

Martin, S. T., Andreae, M. O., Althausen, D., Artaxo, P., Baars, H., Borrmann, S., Chen, Q., Farmer, D. K., Guenther, A., Gunthe, S. S., Jimenez, J. L., Karl, T., Longo, K., Manzi, A., Müller, T., Pauliquevis, T., Petters, M. D., Prenni, A. J., Pöschl, U., Rizzo, L. V., Schneider, J., Smith, J. N., Swietlicki, E., Tota, J., Wang, J., Wiedensohler, A., and Zorn, S. R.: An overview of the Amazonian Aerosol Characterization Experiment 2008 (AMAZE-08), Atmos. Chem. Phys., 10, 11415–11438, https://doi.org/10.5194/acp-10-11415-2010, 2010a.

Martin, S. T., Andreae, M. O., Artaxo, P., Baumgardner, D., Chen, Q., Goldstein, A. H., Guenther, A., Heald, C. L., Mayol-Bracero, O. L., McMurry, P. H., Pauliquevis, T., Pöschl, U., Prather, K. A., Roberts, G. C., Saleska, S. R., Silva Dias, M. A., Spracklen, D. V., Swietlicki, E., and Trebs, I.: Sources and properties of Amazonian aerosol particles, Rev. Geophys., 48, RG2002, https://doi.org/10.1029/2008RG000280, 2010b.

Martin, S. T., Artaxo, P., Machado, L. A. T., Manzi, A. O., Souza, R. A. F., Schumacher, C., Wang, J., Andreae, M. O., Barbosa, H. M. J., Fan, J., Fisch, G., Goldstein, A. H., Guenther, A., Jimenez, J. L., Pöschl, U., Silva Dias, M. A., Smith, J. N., and Wendisch, M.: Introduction: Observations and Modeling of the Green Ocean

Amazon (GoAmazon2014/5), Atmos. Chem. Phys., 16, 4785–4797, https://doi.org/10.5194/acp-16-4785-2016, 2016.

Martin, S. T., Artaxo, P., Machado, L., Manzi, A. O., Souza, R. A. F., Schumacher, C., Wang, J., Biscaro, T., Brito, J., Calheiros, A., Jardine, K., Medeiros, A., Portela, B., de Sá, S. S., Adachi, K., Aiken, A. C., Albrecht, R., Alexander, L., Andreae, M. O., Barbosa, H. M. J., Buseck, P., Chand, D., Comstock, J. M., Day, D. A., Dubey, M., Fan, J., Fast, J., Fisch, G., Fortner, E., Giangrande, S., Gilles, M., Goldstein, A. H., Guenther, A., Hubbe, J., Jensen, M., Jimenez, J. L., Keutsch, F. N., Kim, S., Kuang, C., Laskin, A., McKinney, K., Mei, F., Miller, M., Nascimento, R., Pauliquevis, T., Pekour, M., Peres, J., Petäjä, T., Pöhlker, C., Pöschl, U., Rizzo, L., Schmid, B., Shilling, J. E., Dias, M. A. S., Smith, J. N., Tomlinson, J. M., Tóta, J., and Wendisch, M.: The Green Ocean Amazon Experiment (GoAmazon2014/5) Observes Pollution Affecting Gases, Aerosols, Clouds, and Rainfall over the Rain Forest, B. Am. Meteorol. Soc., 98, 981–997, https://doi.org/10.1175/BAMS-D-15-00221.1, 2017.

Massabò, D., Caponi, L., Bernardoni, V., Bove, M. C., Brotto, P., Calzolai, G., Cassola, F., Chiari, M., Fedi, M. E., Fermo, P., Giannoni, M., Lucarelli, F., Nava, S., Piazzalunga, A., Valli, G., Vecchi, R., and Prati, P.: Multi-wavelength optical determination of black and brown carbon in atmospheric aerosols, Atmos. Environ., 108, 1–12, https://doi.org/10.1016/j.atmosenv.2015.02.058, 2015.

Mikhailov, E. F., Mironova, S., Mironov, G., Vlasenko, S., Panov, A., Chi, X., Walter, D., Carbone, S., Artaxo, P., Heimann, M., Lavric, J., Pöschl, U., and Andreae, M. O.: Long-term measurements (2010–2014) of carbonaceous aerosol and carbon monoxide at the Zotino Tall Tower Observatory (ZOTTO) in central Siberia, Atmos. Chem. Phys., 17, 14365–14392, https://doi.org/10.5194/acp-17-14365-2017, 2017.

Mishchenko, M. I., Dlugach, J. M., Yanovitskij, E. G., and Zakharova, N. T.: Bidirectional reflectance of flat, optically thick particulate layers: an efficient radiative transfer solution and applications to snow and soil surfaces, J. Quant. Spectrosc. Ra., 63, 409–432, https://doi.org/10.1016/S0022-4073(99)00028-X, 1999.

Moosmüller, H., Chakrabarty, R. K., Ehlers, K. M., and Arnott, W. P.: Absorption Ångström coefficient, brown carbon, and aerosols: basic concepts, bulk matter, and spherical particles, Atmos. Chem. Phys., 11, 1217–1225, https://doi.org/10.5194/acp-11-1217-2011, 2011.

Moran-Zuloaga, D., Ditas, F., Walter, D., Saturno, J., Brito, J., Carbone, S., Chi, X., Hrabe de Angelis, I., Baars, H., Godoi, R. H. M., Heese, B., Holanda, B. A., Lavric, J. V., Martin, S. T., Ming, J., Pöhlker, M. L., Ruckteschler, N., Su, H., Wang, Y., Wang, Q., Wang, Z., Weber, B., Wolff, S., Artaxo, P., Pöschl, U., Andreae, M. O., and Pöhlker, C.: Long-term study on coarse mode aerosols in the Amazon rain forest with the frequent intrusion of Saharan dust plumes, Atmos. Chem. Phys., 18, 10055–10088, https://doi.org/10.5194/acp-18-10055-2018, 2018.

Moteki, N. and Kondo, Y.: Method to measure time-dependent scattering cross sections of particles evaporating in a laser beam, J. Aerosol Sci., 39, 348–364, https://doi.org/10.1016/j.jaerosci.2007.12.002, 2008.

Müller, T., Henzing, J. S., de Leeuw, G., Wiedensohler, A., Alastuey, A., Angelov, H., Bizjak, M., Collaud Coen, M., Engström, J. E., Gruening, C., Hillamo, R., Hoffer, A., Imre, K., Ivanow, P., Jennings, G., Sun, J. Y., Kalivitis, N., Karlsson, H., Komppula, M., Laj, P., Li, S.-M., Lunder, C., Marinoni, A., Martins dos Santos, S., Moerman, M., Nowak, A., Ogren, J. A., Petzold, A., Pichon, J. M., Rodriquez, S., Sharma, S., Sheridan, P. J., Teinilä, K., Tuch, T., Viana, M., Virkkula, A., Weingartner, E., Wilhelm, R., and Wang, Y. Q.: Characterization and intercomparison of aerosol absorption photometers: result of two intercomparison workshops, Atmos. Meas. Tech., 4, 245–268, https://doi.org/10.5194/amt-4-245-2011, 2011a.

Müller, T., Laborde, M., Kassell, G., and Wiedensohler, A.: Design and performance of a three-wavelength LED-based total scatter and backscatter integrating nephelometer, Atmos. Meas. Tech., 4, 1291–1303, https://doi.org/10.5194/amt-4-1291-2011, 2011b.

Nepstad, D. C., Stickler, C. M., Filho, B. S., and Merry, F.: Interactions among Amazon land use, forests and climate: prospects for a near-term forest tipping point, Philos. T. Roy. Soc. B, 363, 1737–1746, https://doi.org/10.1098/rstb.2007.0036, 2008.

Ng, N. L., Herndon, S. C., Trimborn, A., Canagaratna, M. R., Croteau, P. L., Onasch, T. B., Sueper, D., Worsnop, D. R., Zhang, Q., Sun, Y. L., and Jayne, J. T.: An Aerosol Chemical Speciation Monitor (ACSM) for Routine Monitoring of the Composition and Mass Concentrations of Ambient Aerosol, Aerosol Sci. Technol., 45, 780–794, https://doi.org/10.1080/02786826.2011.560211, 2011.

Petzold, A. and Schönlinner, M.: Multi-angle absorption photometry – a new method for the measurement of aerosol light absorption and atmospheric black carbon, J. Aerosol Sci., 35, 421–441, https://doi.org/10.1016/j.jaerosci.2003.09.005, 2004.

Petzold, A., Ogren, J. A., Fiebig, M., Laj, P., Li, S.-M., Baltensperger, U., Holzer-Popp, T., Kinne, S., Pappalardo, G., Sugimoto, N., Wehrli, C., Wiedensohler, A., and Zhang, X.-Y.: Recommendations for reporting "black carbon" measurements, Atmos. Chem. Phys., 13, 8365–8379, https://doi.org/10.5194/acp-13-8365-2013, 2013.

Pöhlker, C., Saturno, J., Krüger, M. L., Förster, J.-D., Weigand, M., Wiedemann, K. T., Bechtel, M., Artaxo, P., and Andreae, M. O.: Efflorescence upon humidification? X-ray microspectroscopic in-situ observation of changes in aerosol microstructure and phase state upon hydration, Geophys. Res. Lett., 41, 3681–3689, https://doi.org/10.1002/2014GL059409, 2014.

Pöhlker, C., Walter, D., Paulsen, H., Könemann, T., Rodríguez-Caballero, E., Moran-Zuloaga, D., Brito, J., Carbone, S., Degrendele, C., Després, V. R., Ditas, F., Holanda, B. A., Kaiser, J. W., Lammel, G., Lavric, J. V., Ming, J., Pickersgill, D., Pöhlker, M. L., Praß, M., Ruckteschler, N., Saturno, J., Sörgel, M., Wang, Q., Weber, B., Wolff, S., Artaxo, P., Pöschl, U., and Andreae, M. O.: Land cover and its transformation in the backward trajectory footprint region of the Amazon Tall Tower Observatory, Atmos. Chem. Phys. Discuss., https://doi.org/10.5194/acp-2018-323, in review, 2018.

Pöhlker, M. L., Ditas, F., Saturno, J., Klimach, T., Hrabe de Angelis, I., Araùjo, A. C., Brito, J., Carbone, S., Cheng, Y., Chi, X., Ditz, R., Gunthe, S. S., Holanda, B. A., Kandler, K., Kesselmeier, J., Könemann, T., Krüger, O. O., Lavric, J. V., Martin, S. T., Mikhailov, E., Moran-Zuloaga, D., Rizzo, L. V., Rose, D., Su, H., Thalman, R., Walter, D., Wang, J., Wolff, S., Barbosa, H. M. J., Artaxo, P., Andreae, M. O., Pöschl, U., and Pöhlker, C.: Long-term observations of cloud condensation nuclei over the Amazon rain forest – Part 2: Variability and charac-

teristics of biomass burning, long-range transport, and pristine rain forest aerosols, Atmos. Chem. Phys., 18, 10289–10331, https://doi.org/10.5194/acp-18-10289-2018, 2018.

Pokhrel, R. P., Wagner, N. L., Langridge, J. M., Lack, D. A., Jayarathne, T., Stone, E. A., Stockwell, C. E., Yokelson, R. J., and Murphy, S. M.: Parameterization of single-scattering albedo (SSA) and absorption Ångström exponent (AAE) with EC / OC for aerosol emissions from biomass burning, Atmos. Chem. Phys., 16, 9549–9561, https://doi.org/10.5194/acp-16-9549-2016, 2016.

Pöschl, U., Martin, S. T., Sinha, B., Chen, Q., Gunthe, S. S., Huffman, J. A., Borrmann, S., Farmer, D. K., Garland, R. M., Helas, G., Jimenez, J. L., King, S. M., Manzi, A., Mikhailov, E., Pauliquevis, T., Petters, M. D., Prenni, A. J., Roldin, P., Rose, D., Schneider, J., Su, H., Zorn, S. R., Artaxo, P., and Andreae, M. O.: Rainforest Aerosols as Biogenic Nuclei of Clouds and Precipitation in the Amazon, Science, 329, 1513–1516, https://doi.org/10.1126/science.1191056, 2010.

Prospero, J. M., Glaccum, R. A., and Nees, R. T.: Atmospheric transport of soil dust from Africa to South America, Nature, 289, 570–572, https://doi.org/10.1038/289570a0, 1981.

Raatikainen, T., Brus, D., Hyvärinen, A.-P., Svensson, J., Asmi, E., and Lihavainen, H.: Black carbon concentrations and mixing state in the Finnish Arctic, Atmos. Chem. Phys., 15, 10057–10070, https://doi.org/10.5194/acp-15-10057-2015, 2015.

R Development Core Team: R: A language and environment for statistical computing, available at: http://www.r-project.org (last access: 1 June 2017), 2009.

Reid, J. S., Hobbs, P. V, Ferek, R. J., Blake, D. R., Martins, J. V., Dunlap, M. R., and Liousse, C.: Physical, chemical, and optical properties of regional hazes dominated by smoke in Brazil, J. Geophys. Res.-Atmos., 103, 32059–32080, https://doi.org/10.1029/98JD00458, 1998.

Reid, J. S., Eck, T. F., Christopher, S. A., Koppmann, R., Dubovik, O., Eleuterio, D. P., Holben, B. N., Reid, E. A., and Zhang, J.: A review of biomass burning emissions part III: intensive optical properties of biomass burning particles, Atmos. Chem. Phys., 5, 827–849, https://doi.org/10.5194/acp-5-827-2005, 2005.

Ridley, D. A., Heald, C. L., and Prospero, J. M.: What controls the recent changes in African mineral dust aerosol across the Atlantic?, Atmos. Chem. Phys., 14, 5735–5747, https://doi.org/10.5194/acp-14-5735-2014, 2014.

Rincón, A. G., Guzmán, M. I., Hoffmann, M. R., and Colussi, A. J.: Thermochromism of Model Organic Aerosol Matter, J. Phys. Chem. Lett., 1, 368–373, https://doi.org/10.1021/jz900186e, 2010.

Rizzo, L. V., Correia, A. L., Artaxo, P., Procópio, A. S., and Andreae, M. O.: Spectral dependence of aerosol light absorption over the Amazon Basin, Atmos. Chem. Phys., 11, 8899–8912, https://doi.org/10.5194/acp-11-8899-2011, 2011.

Rizzo, L. V., Artaxo, P., Müller, T., Wiedensohler, A., Paixão, M., Cirino, G. G., Arana, A., Swietlicki, E., Roldin, P., Fors, E. O., Wiedemann, K. T., Leal, L. S. M., and Kulmala, M.: Long term measurements of aerosol optical properties at a primary forest site in Amazonia, Atmos. Chem. Phys., 13, 2391–2413, https://doi.org/10.5194/acp-13-2391-2013, 2013.

Roberts, G. C., Nenes, A., Seinfeld, J. H., and Andreae, M. O.: Impact of biomass burning on cloud properties in the Amazon Basin, J. Geophys. Res., 108, 4062, https://doi.org/10.1029/2001JD000985, 2003.

Saleh, R., Hennigan, C. J., McMeeking, G. R., Chuang, W. K., Robinson, E. S., Coe, H., Donahue, N. M., and Robinson, A. L.: Absorptivity of brown carbon in fresh and photo-chemically aged biomass-burning emissions, Atmos. Chem. Phys., 13, 7683–7693, https://doi.org/10.5194/acp-13-7683-2013, 2013.

Saleh, R., Robinson, E. S., Tkacik, D. S., Ahern, A. T., Liu, S., Aiken, A. C., Sullivan, R. C., Presto, A. A., Dubey, M. K., Yokelson, R. J., Donahue, N. M., and Robinson, A. L.: Brownness of organics in aerosols from biomass burning linked to their black carbon content, Nat. Geosci., 7, 2–5, https://doi.org/10.1038/ngeo2220, 2014.

Salvador, P., Almeida, S. M., Cardoso, J., Almeida-Silva, M., Nunes, T., Cerqueira, M., Alves, C., Reis, M. A., Chaves, P. C., Artíñano, B., and Pio, C.: Composition and origin of PM_{10} in Cape Verde: Characterization of long-range transport episodes, Atmos. Environ., 127, 326–339, https://doi.org/10.1016/j.atmosenv.2015.12.057, 2016.

Sandradewi, J., Prévôt, A. S. H., Szidat, S., Perron, N., Alfarra, M. R., Lanz, V. A., Weingartner, E., and Baltensperger, U.: Using aerosol light absorption measurements for the quantitative determination of wood burning and traffic emission contributions to particulate matter, Environ. Sci. Technol., 42, 3316–3323, https://doi.org/10.1021/es702253m, 2008.

Saturno, J., Pöhlker, C., Massabò, D., Brito, J., Carbone, S., Cheng, Y., Chi, X., Ditas, F., Hrabe de Angelis, I., Morán-Zuloaga, D., Pöhlker, M. L., Rizzo, L. V., Walter, D., Wang, Q., Artaxo, P., Prati, P., and Andreae, M. O.: Comparison of different Aethalometer correction schemes and a reference multi-wavelength absorption technique for ambient aerosol data, Atmos. Meas. Tech., 10, 2837–2850, https://doi.org/10.5194/amt-10-2837-2017, 2017.

Saturno, J., Ditas, F., Penning de Vries, M., Holanda, B. A., Pöhlker, M. L., Carbone, S., Walter, D., Bobrowski, N., Brito, J., Chi, X., Gutmann, A., Hrabe de Angelis, I., Machado, L. A. T., Moran-Zuloaga, D., Rüdiger, J., Schneider, J., Schulz, C., Wang, Q., Wendisch, M., Artaxo, P., Wagner, T., Pöschl, U., Andreae, M. O., and Pöhlker, C.: African volcanic emissions influencing atmospheric aerosols over the Amazon rain forest, Atmos. Chem. Phys., 18, 10391–10405, https://doi.org/10.5194/acp-18-10391-2018, 2018a.

Saturno, J., Holanda, B., Pöhlker, C., Ditas, F., Wang, Q., Moran-Zuloaga, D., Brito, J., Carbone, S., Cheng, Y., Chi, X., Ditas, J., Hoffmann, T., Hrabe de Angelis, I., Könemann, T., Lavric, J., Ma, N., Ming, J., Paulsen, H., Pöhlker, M., Rizzo, L., Schlag, P., Su, H., Walter, D., Wolff, S., Zhang, Y., Artaxo, P., Pöschl, U., and Andreae, M. O.: Available data for ATTO BC and BrC study, Max Planck Society, https://doi.org/10.17617/3.1r, 2018b.

Schkolnik, G., Chand, D., Hoffer, A., Andreae, M. O., Erlick, C., Swietlicki, E., and Rudich, Y.: Constraining the density and complex refractive index of elemental and organic carbon in biomass burning aerosol using optical and chemical measurements, Atmos. Environ., 41, 1107–1118, https://doi.org/10.1016/j.atmosenv.2006.09.035, 2007.

Schuster, G. L., Dubovik, O., Arola, A., Eck, T. F., and Holben, B. N.: Remote sensing of soot carbon – Part 2: Understanding the absorption Ångström exponent, Atmos. Chem. Phys., 16, 1587–1602, https://doi.org/10.5194/acp-16-1587-2016, 2016.

Schwarz, J. P., Gao, R. S., Fahey, D. W., Thomson, D. S., Watts, L. A., Wilson, J. C., Reeves, J. M., Darbeheshti, M., Baumgardner, D. G., Kok, G. L., Chung, S. H., Schulz, M., Hendricks, J., Lauer, A., Kärcher, B., Slowik, J. G., Rosenlof, K. H., Thompson, T. L., Langford, A. O., Loewenstein, M., and Aikin, K. C.: Single-particle measurements of midlatitude black carbon and light-scattering aerosols from the boundary layer to the lower stratosphere, J. Geophys. Res., 111, D16207, https://doi.org/10.1029/2006JD007076, 2006.

Seinfeld, J. H., Bretherton, C., Carslaw, K. S., Coe, H., DeMott, P. J., Dunlea, E. J., Feingold, G., Ghan, S., Guenther, A. B., Kahn, R., Kraucunas, I., Kreidenweis, S. M., Molina, M. J., Nenes, A., Penner, J. E., Prather, K. A., Ramanathan, V., Ramaswamy, V., Rasch, P. J., Ravishankara, A. R., Rosenfeld, D., Stephens, G., and Wood, R.: Improving our fundamental understanding of the role of aerosol–cloud interactions in the climate system, P. Natl. Acad. Sci. USA, 113, 5781–5790, https://doi.org/10.1073/pnas.1514043113, 2016.

Snelling, D. R., Smallwood, G. J., Liu, F., Gülder, Ö. L., and Bachalo, W. D.: A calibration-independent laser-induced incandescence technique for soot measurement by detecting absolute light intensity, Appl. Opt., 44, 6773, https://doi.org/10.1364/AO.44.006773, 2005.

Stephens, M., Turner, N., and Sandberg, J.: Particle Identification by Laser-Induced Incandescence in a Solid-State Laser Cavity, Appl. Opt., 42, 3726, https://doi.org/10.1364/AO.42.003726, 2003.

Stull, R. B.: An Introduction to Boundary Layer Meteorology, Springer, the Netherlands, 1988.

Subramanian, R., Kok, G. L., Baumgardner, D., Clarke, A., Shinozuka, Y., Campos, T. L., Heizer, C. G., Stephens, B. B., de Foy, B., Voss, P. B., and Zaveri, R. A.: Black carbon over Mexico: the effect of atmospheric transport on mixing state, mass absorption cross-section, and BC / CO ratios, Atmos. Chem. Phys., 10, 219–237, https://doi.org/10.5194/acp-10-219-2010, 2010.

Sumlin, B. J., Pandey, A., Walker, M. J., Pattison, R. S., Williams, B. J., and Chakrabarty, R. K.: Atmospheric Photooxidation Diminishes Light Absorption by Primary Brown Carbon Aerosol from Biomass Burning, Environ. Sci. Technol. Lett., 4, 540–545, https://doi.org/10.1021/acs.estlett.7b00393, 2017.

Talbot, R. W., Andreae, M. O., Berresheim, H., Artaxo, P., Garstang, M., Harriss, R. C., Beecher, K. M., and Li, S. M.: Aerosol chemistry during the wet season in central Amazonia: The influence of long-range transport, J. Geophys. Res., 95, 16955, https://doi.org/10.1029/JD095iD10p16955, 1990.

Tasoglou, A., Saliba, G., Subramanian, R., and Pandis, S. N.: Absorption of chemically aged biomass burning carbonaceous aerosol, J. Aerosol Sci., 113, 141–152, https://doi.org/10.1016/j.jaerosci.2017.07.011, 2017.

Tuch, T. M., Haudek, A., Müller, T., Nowak, A., Wex, H., and Wiedensohler, A.: Design and performance of an automatic regenerating adsorption aerosol dryer for continuous operation at monitoring sites, Atmos. Meas. Tech., 2, 417–422, https://doi.org/10.5194/amt-2-417-2009, 2009.

Virkkula, A., Backman, J., Aalto, P. P., Hulkkonen, M., Riuttanen, L., Nieminen, T., dal Maso, M., Sogacheva, L., de Leeuw, G., and Kulmala, M.: Seasonal cycle, size dependencies, and source analyses of aerosol optical properties at the SMEAR II measurement station in Hyytiälä, Finland, Atmos. Chem. Phys., 11, 4445–4468, https://doi.org/10.5194/acp-11-4445-2011, 2011.

Wang, Q., Huang, R.-J., Cao, J., Han, Y., Wang, G., Li, G., Wang, Y., Dai, W., Zhang, R., and Zhou, Y.: Mixing State of Black Carbon Aerosol in a Heavily Polluted Urban Area of China: Implications for Light Absorption Enhancement, Aerosol Sci. Technol., 48, 689–697, https://doi.org/10.1080/02786826.2014.917758, 2014.

Wang, Q., Saturno, J., Chi, X., Walter, D., Lavric, J. V., Moran-Zuloaga, D., Ditas, F., Pöhlker, C., Brito, J., Carbone, S., Artaxo, P., and Andreae, M. O.: Modeling investigation of light-absorbing aerosols in the Amazon Basin during the wet season, Atmos. Chem. Phys., 16, 14775–14794, https://doi.org/10.5194/acp-16-14775-2016, 2016a.

Wang, X., Heald, C. L., Sedlacek, A. J., de Sá, S. S., Martin, S. T., Alexander, M. L., Watson, T. B., Aiken, A. C., Springston, S. R., and Artaxo, P.: Deriving brown carbon from multiwavelength absorption measurements: method and application to AERONET and Aethalometer observations, Atmos. Chem. Phys., 16, 12733–12752, https://doi.org/10.5194/acp-16-12733-2016, 2016b.

Warton, D. I., Wright, I. J., Falster, D. S., and Westoby, M.: Bivariate line-fitting methods for allometry, Biol. Rev. Camb. Philos. Soc., 81, 259–291, https://doi.org/10.1017/S1464793106007007, 2006.

Weingartner, E., Saathoff, H., Schnaiter, M., Streit, N., Bitnar, B., and Baltensperger, U.: Absorption of light by soot particles: determination of the absorption coefficient by means of aethalometers, J. Aerosol Sci., 34, 1445–1463, https://doi.org/10.1016/S0021-8502(03)00359-8, 2003.

Winderlich, J., Chen, H., Gerbig, C., Seifert, T., Kolle, O., Lavric, J. V., Kaiser, C., Höfer, A., and Heimann, M.: Continuous low-maintenance $CO_2/CH_4/H_2O$ measurements at the Zotino Tall Tower Observatory (ZOTTO) in Central Siberia, Atmos. Meas. Tech., 3, 1113–1128, https://doi.org/10.5194/amt-3-1113-2010, 2010.

Womack, C., Manfred, K., Wagner, N., He, Q., Rudich, Y., Brown, S., and Washenfelder, R.: Characterizing the optical properties of brown carbon aerosol from biomass burning using broadband cavity enhanced spectroscopy, in Atmospheric Chemistry Gordon Research Conference, 2017.

Wong, J. P. S., Nenes, A., and Weber, R. J.: Changes in Light Absorptivity of Molecular Weight Separated Brown Carbon Due to Photolytic Aging, Environ. Sci. Technol., 51, 8414–8421, https://doi.org/10.1021/acs.est.7b01739, 2017.

Zanatta, M., Gysel, M., Bukowiecki, N., Müller, T., Weingartner, E., Areskoug, H., Fiebig, M., Yttri, K. E., Mihalopoulos, N., Kouvarakis, G., Beddows, D., Harrison, R. M., Cavalli, F., Putaud, J. P., Spindler, G., Wiedensohler, A., Alastuey, A., Pandolfi, M., Sellegri, K., Swietlicki, E., Jaffrezo, J. L., Baltensperger, U., and Laj, P.: A European aerosol phenomenology-5: Climatology of black carbon optical properties at 9 regional background sites across Europe, Atmos. Environ., 145, 346–364, https://doi.org/10.1016/j.atmosenv.2016.09.035, 2016.

Supplement of Atmos. Chem. Phys., 18, 12817–12843, 2018
https://doi.org/10.5194/acp-18-12817-2018-supplement

Atmospheric Chemistry and Physics Open Access

Supplement of

Black and brown carbon over central Amazonia: long-term aerosol measurements at the ATTO site

Jorge Saturno et al.

Correspondence to: Jorge Saturno (j.saturno@mpic.de) and Christopher Pöhlker (c.pohlker@mpic.de)

Table S1. Aerosol sampling conditions and locations at the ATTO site.

Time period	Location	Inlet tube dimensions	Approx. flow rate (L min^{-1})	Drying system	1 µm cyclone cut for BC (y/n)
Mar 2012 – Sep 2012	Mast *	60 m height 17 mm (0.685 ″) inner diameter	13	Diffusion dryers	n
Sep 2012 – Dec 2013	Walk-up tower **	60 m height 17 mm (0.685 ″) inner diameter	13	Diffusion dryers	n
Dec 2013 – May 2014	Mast *	60 m height 24 mm (0.935 ″) inner diameter	18	Diffusion dryers	n
May 2014 – Jan 2015	Mast *	60 m height 24 mm (0.935 ″) inner diameter	30	Diffusion dryers	y
Jan 2015 – present	Mast *	60 m height 24 mm (0.935 ″) inner diameter	30	Automatic regenerating adsorption aerosol dryer	y

* S 02° 08.602’; W 59° 00.033’, 130 m a.s.l.
** S 02° 08.647’; W 58° 59.992’, 130 m a.s.l.

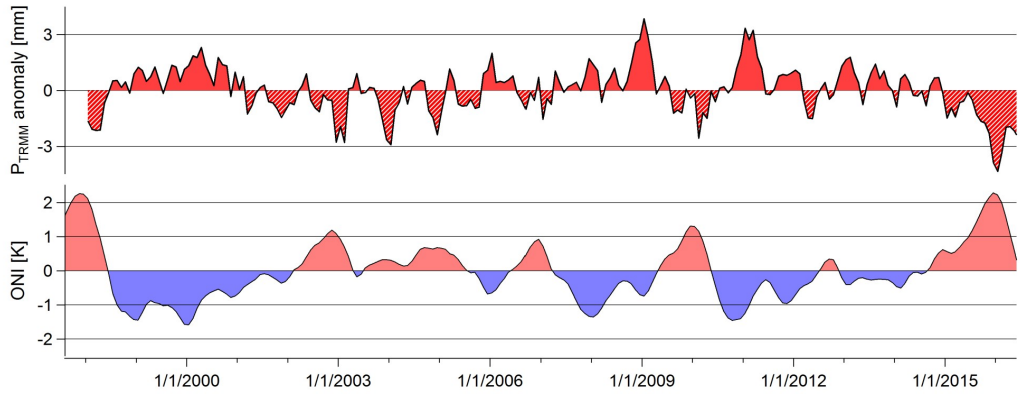

Figure S1. Precipitation anomalies calculated from the Tropical Rainfall Measurement Mission (TRMM) observations along the BT tracks in the ROI ATTO area (top) (see Fig. 1), and Oceanic Niño Index (ONI) (bottom) time series from 1998 to 2016.

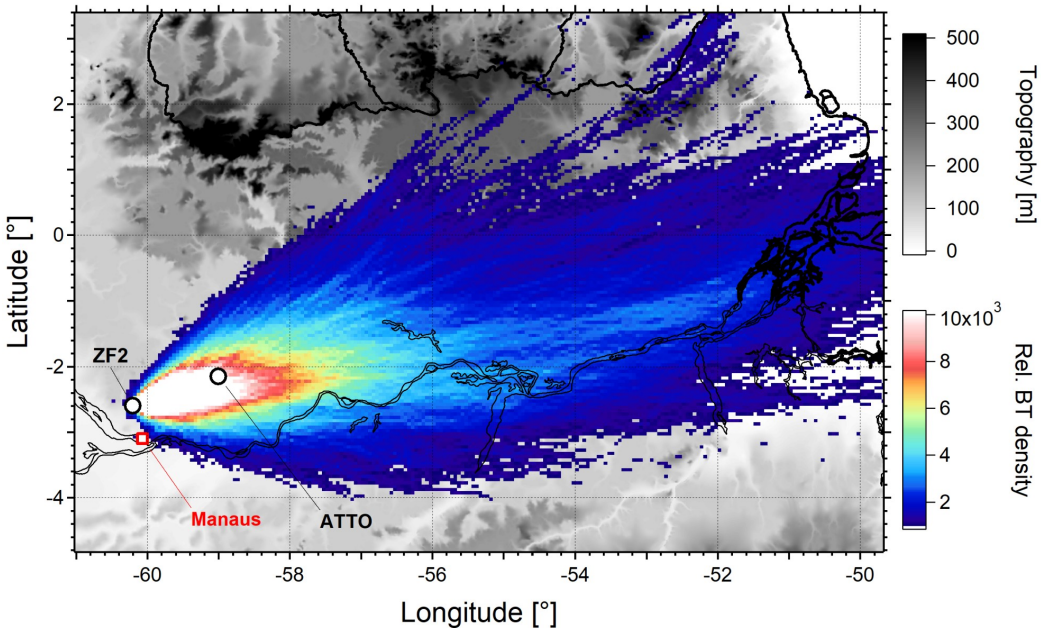

Figure S2. HYPSLIT backward trajectory footprint of the ZF2 site (01 Jan 2014 to 31 Dec 2015) calculated every hour with a starting height of 1000 m. Adapted from Pöhlker et al. (2017).

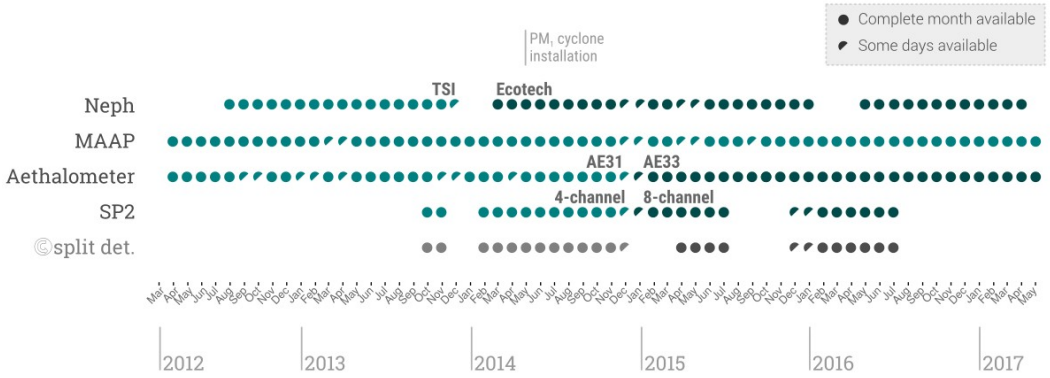

Figure S3. Nephelometer, MAAP, Aethalometer, and SP2 (+ split detector) measurement periods at the ATTO site.

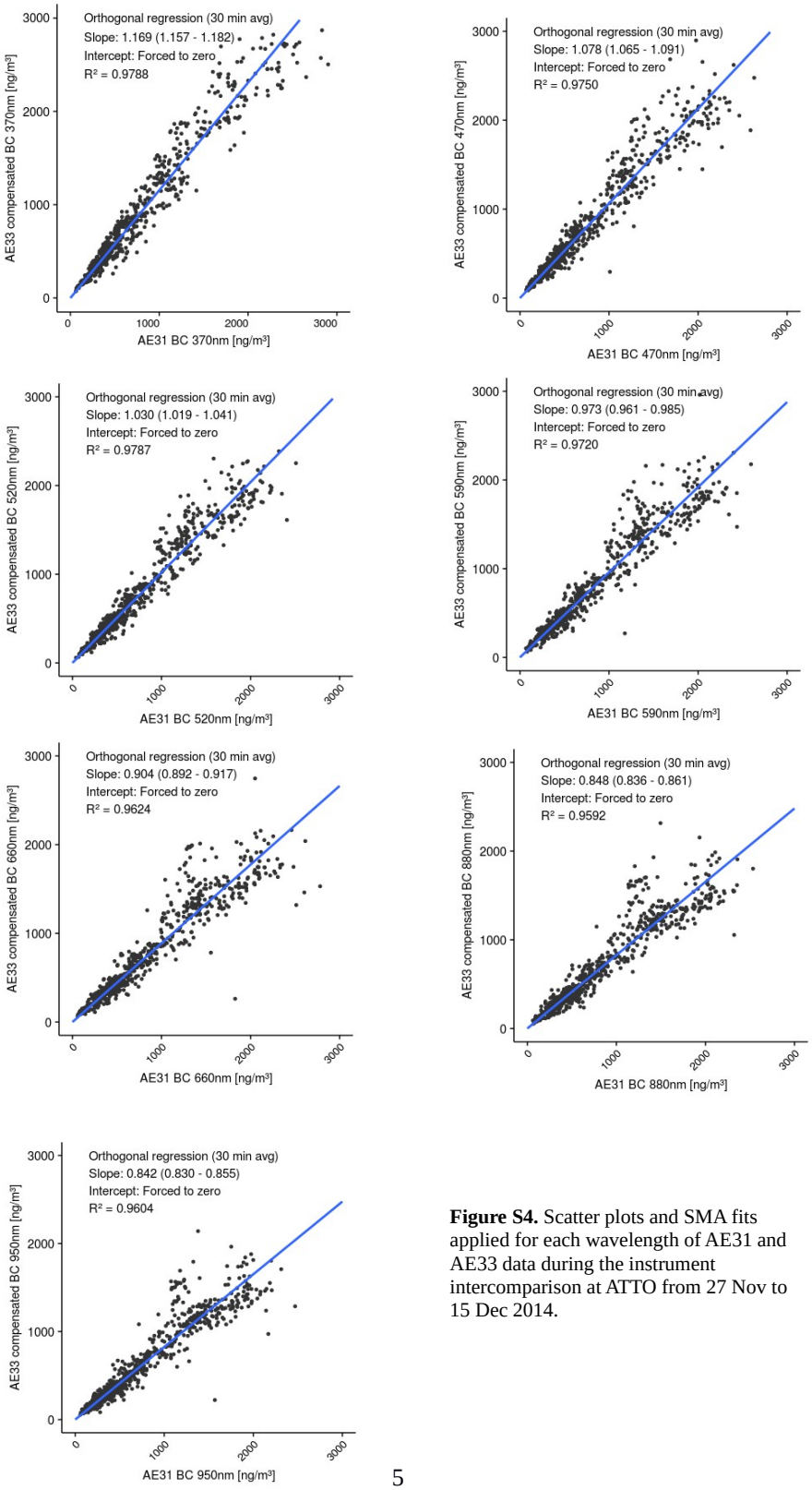

Figure S4. Scatter plots and SMA fits applied for each wavelength of AE31 and AE33 data during the instrument intercomparison at ATTO from 27 Nov to 15 Dec 2014.

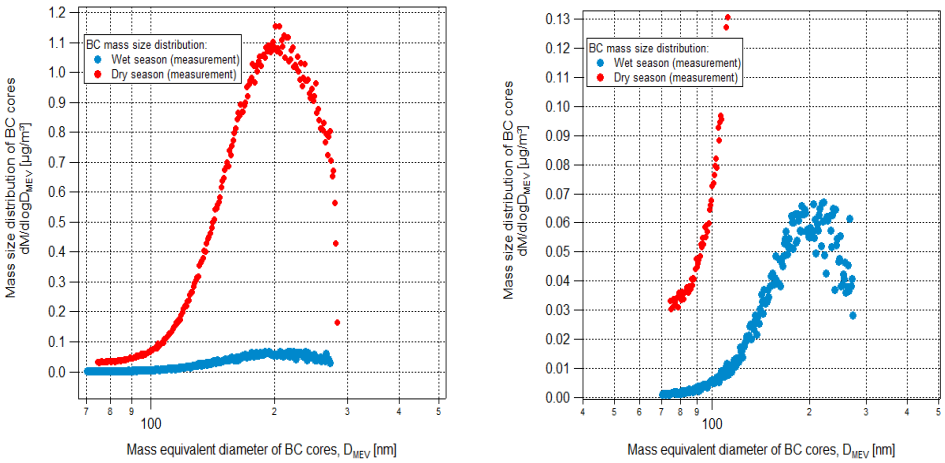

Figure S5. Refractory black carbon mass size distributions observed at the ATTO site on different characteristic days during the wet (blue dots) and the dry (red dots) season in 2014. The right panel shows a zoom into the wet season size distribution.

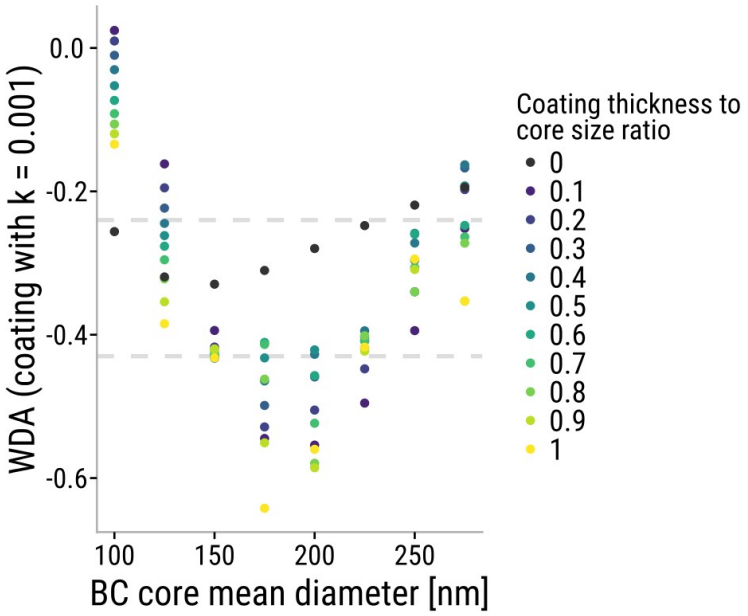

Figure S6. Results of Mie model calculations for pure BC, using a log-normal size distribution with mean = BC geometric mean diameter (GMD), and a standard deviation of 1.45, and internally mixed BC using the core-shell model for monodisperse BC cores with a coating's refractive index of 1.55 - 0.001i. The horizontal dashed lines show the boundaries of the inter-quartile range.

Table S2. Relative overestimation of the BrC contribution to light absorption at 370 nm obtained from Mie model calculations by considering different BC core size ranges and refractive indices of the coating material. The parameters used in this study are shown in bold letters.

BC core size range [nm]	Refractive index of the coating material	Relative overestimation of BrC contribution to σ_{370} (%)
100 – 275	1.55 - 0i	0
100 – 275	**1.55 - 0.001i**	**0**
100 – 275	1.55 - 0.1i	33
100 – 275	1.55 - 0.2i	46
80 – 275	1.55 - 0i	18
80 – 275	1.55 - 0.001i	18
80 – 275	1.55 - 0.1i	44
80 – 275	1.55 - 0.2i	56

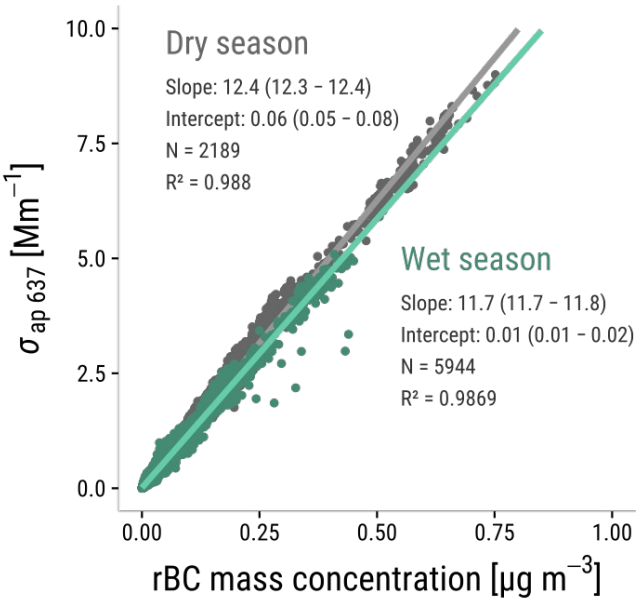

Figure S7. Light absorption coefficient at 637 nm ($\sigma_{ap\ 637}$) vs. rBC mass concentration (30-min averaged data) corresponding to the wet and the dry seasons, in green and gray, respectively. The slopes of the SMA fits correspond to the BC mass absorption cross-section at 637 nm ($\alpha_{abs\ 637}$), inter-quartile ranges are indicated in brackets.

2.2 Influx of African biomass burning aerosol during the Amazonian dry season through layered transatlantic transport of black carbon-rich smoke

This chapter has been published as:
Holanda, B. A.; Pöhlker, M. L.; Walter, D.; Saturno, J.; Sörgel, M.; Ditas, J.; Ditas, F.; Schulz, C.; Franco, M. A.; Wang, Q.; Donth, T.; Artaxo, P.; Barbosa, H. M. J.; Borrmann, S.; Braga, R.; Brito, J.; Cheng, Y.; Dollner, M.; Kaiser, J. W.; Klimach, T.; Knote, C.; Krüger, O. O.; Fütterer, D.; Lavrič, J. V.; Ma, N.; Machado, L. A. T.; Ming, J.; Morais, F. G.; Paulsen, H.; Sauer, D.; Schlager, H.; Schneider, J.; Su, H.; Weinzierl, B.; Walser, A.; Wendisch, M.; Ziereis, H.; Zöger, M.; Pöschl, U.; Andreae, M. O., and Pöhlker, C.: "Influx of african biomass burning aerosol during the amazonian dry season through layered transatlantic transport of black carbon-rich smoke". *Atmos. Chem. Phys.*, 20, 8. (2020), pp. 4757–4785. DOI: 10.5194/acp-20-4757-2020. URL: https://www.atmos-chem-phys.net/20/4757/2020/

Supplementary Material: The Supplementary Material for this article can be found online at: https://doi.org/10.5194/acp-20-4757-2020-supplement

This manuscript includes data sets from the following field experiments:
ATTO and ACRIDICON-CHUVA.

Contribution to this publication by Bruna A. Holanda: I am the first author of this publication and my contribution to this work included the processing and analysis of the ACRIDICON-CHUVA, ATTO, and satellite data sets used here. Furthermore, I have been responsible over several years for conducting the measurements, quality assurance and frequent maintenance of the relevant aerosol instruments at ATTO, which yielded the ATTO long-term data set in this study. Alongside my coauthors, I played a primary role in initiating and designing the research, analyzing the results, preparing figures, and writing the manuscript.

Atmos. Chem. Phys., 20, 4757–4785, 2020
https://doi.org/10.5194/acp-20-4757-2020

Atmospheric Chemistry and Physics Open Access EGU

Influx of African biomass burning aerosol during the Amazonian dry season through layered transatlantic transport of black carbon-rich smoke

Bruna A. Holanda[1,2,3], Mira L. Pöhlker[1], David Walter[1,4], Jorge Saturno[2,a], Matthias Sörgel[2,5], Jeannine Ditas[6,1], Florian Ditas[1,2,b], Christiane Schulz[7,8], Marco Aurélio Franco[3,1], Qiaoqiao Wang[6,2], Tobias Donth[9], Paulo Artaxo[3], Henrique M. J. Barbosa[3], Stephan Borrmann[8,10], Ramon Braga[1], Joel Brito[3,c], Yafang Cheng[1], Maximilian Dollner[11,12], Johannes W. Kaiser[5,d], Thomas Klimach[1], Christoph Knote[13], Ovid O. Krüger[1], Daniel Fütterer[12], Jošt V. Lavrič[4], Nan Ma[6,1], Luiz A. T. Machado[14,1], Jing Ming[1,2], Fernando G. Morais[3], Hauke Paulsen[1], Daniel Sauer[12], Hans Schlager[12], Johannes Schneider[8], Hang Su[1], Bernadett Weinzierl[11,12], Adrian Walser[11,12,13], Manfred Wendisch[9], Helmut Ziereis[12], Martin Zöger[15], Ulrich Pöschl[1], Meinrat O. Andreae[2,16], and Christopher Pöhlker[1,2]

[1]Multiphase Chemistry Department, Max Planck Institute for Chemistry, 55128 Mainz, Germany
[2]Biogeochemistry Department, Max Planck Institute for Chemistry, 55128 Mainz, Germany
[3]Instituto de Fisica, Universidade de Sao Paulo, 05508-090, Sao Paulo, SP, Brazil
[4]Max Planck Institute for Biogeochemistry, 07701 Jena, Germany
[5]Atmospheric Chemistry Department, Max Planck Institute for Chemistry, 55128 Mainz, Germany
[6]Institute for Environmental and Climate Research (ECI), Jinan University, Guangzhou, 511443, China
[7]Experimental Aerosol and Cloud Microphysics Department, TROPOS, Leibniz-Institute for Tropospheric Research, Leipzig, Germany
[8]Particle Chemistry Department, Max Planck Institute for Chemistry, 55128 Mainz, Germany
[9]Leipzig Institute for Meteorology, Leipzig University, Leipzig, Germany
[10]Institute for Physics of the Atmosphere, Johannes Gutenberg University, 55128 Mainz, Germany
[11]University of Vienna, Faculty of Physics, Aerosol Physics and Environmental Physics, 1090 Vienna, Austria
[12]Institute for Atmospheric Physics, German Aerospace Center (DLR), 82234 Oberpfaffenhofen, Germany
[13]Meteorological Institute, Ludwig-Maximilians-Universität, Munich, Germany
[14]National Institute for Space Research (INPE), São José Dos Campos, Brazil
[15]Flight experiments, German Aerospace Center (DLR), 82234 Oberpfaffenhofen, Germany
[16]Scripps Institution of Oceanography, University of California San Diego, La Jolla, California 92093, USA
[a]now at: Physikalisch-Technische Bundesanstalt, 38116 Braunschweig, Germany
[b]now at: Hessisches Landesamt für Naturschutz, Umwelt und Geologie, 65203 Wiesbaden, Germany
[c]now at: IMT Lille Douai, Univ. Lille, SAGE, 59000 Lille, France
[d]now at: Deutscher Wetterdienst, 63067 Offenbach, Germany

Correspondence: Mira L. Pöhlker (m.pohlker@mpic.de) and Christopher Pöhlker (c.pohlker@mpic.de)

Received: 29 August 2019 – Discussion started: 2 September 2019
Revised: 6 January 2020 – Accepted: 4 March 2020 – Published: 24 April 2020

Published by Copernicus Publications on behalf of the European Geosciences Union.

Abstract. Black carbon (BC) aerosols influence the Earth's atmosphere and climate, but their microphysical properties, spatiotemporal distribution, and long-range transport are not well constrained. This study presents airborne observations of the transatlantic transport of BC-rich African biomass burning (BB) smoke into the Amazon Basin using a Single Particle Soot Photometer (SP2) as well as several complementary techniques. We base our results on observations of aerosols and trace gases off the Brazilian coast onboard the HALO (High Altitude and LOng range) research aircraft during the ACRIDICON-CHUVA campaign in September 2014.

During flight AC19 over land and ocean at the northeastern coastline of the Amazon Basin, we observed a BC-rich layer at ~ 3.5 km altitude with a vertical extension of ~ 0.3 km. Backward trajectories suggest that fires in African grasslands, savannas, and shrublands were the main source of this pollution layer and that the observed BB smoke had undergone more than 10 d of atmospheric transport and aging over the South Atlantic before reaching the Amazon Basin. The aged smoke is characterized by a dominant accumulation mode, centered at about 130 nm, with a particle concentration of $N_{acc} = 850 \pm 330\,cm^{-3}$. The rBC particles account for $\sim 15\,\%$ of the submicrometer aerosol mass and $\sim 40\,\%$ of the total aerosol number concentration. This corresponds to a mass concentration range from 0.5 to $2\,\mu g\,m^{-3}$ (1st to 99th percentiles) and a number concentration range from 90 to $530\,cm^{-3}$. Along with rBC, high c_{CO} (150 ± 30 ppb) and c_{O_3} (56 ± 9 ppb) mixing ratios support the biomass burning origin and pronounced photochemical aging of this layer. Upon reaching the Amazon Basin, it started to broaden and to subside, due to convective mixing and entrainment of the BB aerosol into the boundary layer. Satellite observations show that the transatlantic transport of pollution layers is a frequently occurring process, seasonally peaking in August/September.

By analyzing the aircraft observations together with the long-term data from the Amazon Tall Tower Observatory (ATTO), we found that the transatlantic transport of African BB smoke layers has a strong impact on the northern and central Amazonian aerosol population during the BB-influenced season (July to December). In fact, the early BB season (July to September) in this part of the Amazon appears to be dominated by African smoke, whereas the later BB season (October to December) appears to be dominated by South American fires. This dichotomy is reflected in pronounced changes in aerosol optical properties such as the single scattering albedo (increasing from 0.85 in August to 0.90 in November) and the BC-to-CO enhancement ratio (decreasing from 11 to $6\,ng\,m^{-3}\,ppb^{-1}$). Our results suggest that, despite the high fraction of BC particles, the African BB aerosol acts as efficient cloud condensation nuclei (CCN), with potentially important implications for aerosol–cloud interactions and the hydrological cycle in the Amazon.

1 Introduction

Biomass burning (BB) in the African and South American tropics and subtropics represents a globally significant source of atmospheric aerosol particles and trace gases (Andreae, 1991; Andreae et al., 1988; Barbosa et al., 1999; Ichoku and Ellison, 2014; Kaiser et al., 2012; Reddington et al., 2016; van der Werf et al., 2017). A major constituent of BB smoke is black carbon (BC), which is co-emitted along with organic aerosols and inorganic salts in proportions that depend on the fuel type and fire phase (Allen and Miguel, 1995; Andreae, 2019; Andreae and Merlet, 2001; Jen et al., 2019; Levin et al., 2010; Reid et al., 2005). The BC aerosol is a key component in the climate system as it significantly influences the Earth's radiative budget through the so-called direct, semi-direct, and indirect aerosol effects (Bond et al., 2013; Boucher et al., 2016; Brioude et al., 2009; Koch and Del Genio, 2010; IPCC, 2013). Recent studies have classified BC as the second largest contributor to global warming and estimated its direct radiative forcing to be as high as $+1.1\,W\,m^{-2}$, with 90 % uncertainty bounds spanning from $+0.17$ to $+2.1\,W\,m^{-2}$ (Bond et al., 2013, and references therein). This large uncertainty arises from our poor understanding of the BC microphysical properties and its spatiotemporal distribution in the atmosphere (Boucher et al., 2013; Andreae and Ramanathan, 2013). During their typical atmospheric lifetime of several days, BC particles undergo photochemical aging, creating internally mixed BC aerosols via the condensation of low and semi-volatile compounds, coagulation, and cloud processing (Bond et al., 2013; Cubison et al., 2011; Konovalov et al., 2017, 2019; Schwarz et al., 2008; Willis et al., 2016). The formation of non-absorbing or semi-transparent coatings on the BC cores changes the particles' optical properties (Fuller et al., 1999; Moffet and Prather, 2009; Pokhrel et al., 2017; Schnaiter, 2005; Zhang et al., 2015) as well as their ability to act as cloud condensation nuclei (CCN) (Laborde et al., 2013; Liu et al., 2017; Tritscher et al., 2011), which influences their atmospheric transport and lifetime.

The Amazonian atmosphere is strongly influenced by the yearly north–south oscillation of the Intertropical Convergence Zone (ITCZ) (Andreae et al., 2012; Martin et al., 2010; Pöhlker et al., 2019), which causes a pronounced seasonality in aerosol concentrations (e.g., BC and CCN) and other aerosol properties (e.g., single scattering albedo) (Roberts et al., 2001; Roberts, 2003; Martin et al., 2010; Artaxo et al., 2013; Rizzo et al., 2013; Andreae et al., 2015; Pöhlker et al., 2016; Saturno et al., 2018b). This makes the central Amazon Basin an ideal environment to study atmospheric and biogeochemical processes as a function of the highly variable aerosol population. During the wet season (February to May), trace gas and aerosol emissions from the regional biosphere predominantly regulate atmospheric cycling, precipitation patterns, and regional climate (Pöhlker et al., 2012; Pöschl et al., 2010). Average wet season black carbon (BC)

mass concentrations, M_{BC}, are $\sim 0.07\,\mu g\,m^{-3}$, and M_{BC} approaches zero during pristine episodes (Andreae and Gelencsér, 2006; Pöhlker et al., 2018). In contrast, the dry season (August to November) is characterized by intense and persistent BB emissions, changing substantially the atmospheric composition and cycling (Artaxo et al., 2013; Rizzo et al., 2013). Average dry season BC mass concentrations (M_{BC}) in central Amazonia are $\sim 0.4\,\mu g\,m^{-3}$, with peaks reaching $\sim 0.9\,\mu g\,m^{-3}$ (Pöhlker et al., 2018; Saturno et al., 2018b), while in the southern hotspot regions of agriculture-related burning, the average M_{BC} can be as high as $\sim 2.8\,\mu g\,m^{-3}$ (Artaxo et al., 2013).

Several studies have found that the long-range transport (LRT) of long-lived species from Africa plays a major role in the Amazonian atmospheric composition. The transport of dust from distant sources into the heart of the Amazon Basin was first observed in 1977, although Africa was not identified as the source region at the time (Lawson and Winchester, 1979). Subsequently, the plume-wise LRT of African dust and smoke during the Amazonian wet season has been well documented (Ansmann et al., 2009; Baars et al., 2011; Barkley et al., 2019; Moran-Zuloaga et al., 2018; Swap et al., 1992; Talbot et al., 1990; Wang et al., 2016). The LRT of aerosols occurs also during the Amazonian dry season, when smoke from the intense African BB plays a substantial role. The earliest observations of such pollution layers in the free troposphere over the Brazilian coast can be found in ozone (O_3) soundings made from Natal, on the eastern coast of Brazil (5.8° S, 35.2° W), where mixing ratios of ~ 70 ppb were measured with a maximum in the month of September (Kirchhoff et al., 1983; Logan and Kirchhoff, 1986). These measurements were continued over a 10-year period (1978–1988), confirming the climatological presence of a tropospheric O_3 maximum over the Brazilian coast, centered at the 500 hPa pressure level and peaking in the September–October period (Kirchhoff et al., 1991).

The first comprehensive airborne measurements off the South American coast, made in 1989 near Natal, could also attribute these pollution layers to LRT of African BB emissions (Andreae et al., 1994). Additional aircraft campaigns in southern Africa, the tropical South Atlantic, and the Amazon Basin have found pollution layers in the free troposphere with similar characteristics (e.g., Andreae et al., 1988; Diab et al., 1996; Thompson et al., 1996; Bozem et al., 2014; Marenco et al., 2016). Recent studies in the central basin, at the Amazon Tall Tower Observatory (ATTO) and at the northeastern edge of the Amazon, found indications of a significant abundance of African smoke during the Amazonian dry season (Barkley et al., 2019; Pöhlker et al., 2019, 2018; Saturno et al., 2018b; Wang et al., 2016). However, robust quantitative data from observations and/or models (e.g., African BC and CCN fractions in the Amazon Basin) have remained sparse.

This study focusses on the transatlantic transport of African BB smoke into the Amazon Basin by combining in situ aircraft observations, modeling results, and remote sensing data. The core of this work is aircraft observations made within a defined African pollution layer upon its arrival at the South American coast during the ACRIDICON-CHUVA campaign over Amazonia in September 2014 (Wendisch et al., 2016). We focus primarily on the spatiotemporal distribution and advection dynamics of the BB smoke layers by analyzing (i) aerosol and trace gas concentration profiles, (ii) backward trajectories and African BB source regions, (iii) the seasonality of the pollution transport, (iv) the horizontal and vertical extents of the transported layers, and (v) the convective mixing and smoke entrainment from the layers into the planetary boundary layer as they are transported from the ocean into the South American continent. Note that a detailed characterization of the microphysical aerosol properties within the BB smoke layers (e.g., the BC core diameters and mixing state) is beyond the scope of the present work and will be the subject of a separate follow-up study. As a final step of the present study, we integrate its main results into the broader picture of the long-term aerosol observations at the central Amazonian ATTO site to estimate the relevance of African pollution for the aerosol lifecycle in the dry season.

2 Materials and methods

2.1 The ACRIDICON-CHUVA campaign

The data presented here were obtained during flight AC19 of the ACRIDICON-CHUVA aircraft campaign (Machado et al., 2018; Wendisch et al., 2016), which took place over the Atlantic Ocean and the Amazon Basin on 30 September 2014. The main objective of ACRIDICON-CHUVA was to study the interactions between aerosol particles, deep convective clouds, and atmospheric radiation using a broad set of instruments for airborne observations of aerosol physical and chemical properties, trace gases, radiation, and cloud. The measurements were conducted onboard the German HALO (High Altitude and LOng range) research aircraft, operated by the German Aerospace Center (DLR), covering a wide geographic area of the Amazon Basin and probing different pollution states by means of highly resolved atmospheric profiles (altitudes up to 15 km).

2.2 Airborne measurements of aerosol, trace gas, and meteorology during ACRIDICON-CHUVA

Navigation and basic meteorological data (e.g., air pressure, temperature, humidity, and water vapor mixing ratio) were obtained from the BAsic HALO Measurement And Sensor System (BAHAMAS) at 1 s time resolution. BAHAMAS acquires data from air flow and thermodynamic sensors as well as from the aircraft avionics and a high-precision inertial reference system to derive basic meteorological parameters like pressure, temperature, and the 3-D wind vector,

as well as aircraft position and attitude. Water vapor mixing ratio and further derived humidity parameters are measured by SHARC (Sophisticated Hygrometer for Atmospheric ResearCh) based on direct absorption measurement by a tunable diode laser (TDL) system. Typical absolute accuracy of the basic meteorological data is 0.5 K for temperature, 0.3 hPa for pressure, 0.4–0.6 m s^{-1} for wind, and 5 % (+1 ppm) for water vapor mixing ratio. All aerosol concentration data were normalized to standard temperature and pressure (STP, $T_0 =$ 273.15 K, $p_0 = 1013.25$ hPa). Most of the aerosol sampling was conducted through the HALO aerosol submicrometer inlet (HASI), which provides up to 30 L min^{-1} sample air flow divided over four sample lines. The air stream sampled on top of the fuselage is aligned with the inlet using a front shroud and decelerated by a factor of approximately 15, providing near-isokinetic sampling to the aerosol instruments mounted inside the aircraft cabin (Andreae et al., 2018).

The characterization of refractory black carbon (rBC) particles at high time resolution was conducted using an eight-channel Single Particle Soot Photometer (SP2, Droplet Measurement Techniques, Longmont, CO, USA) (Stephens et al., 2003; Schwarz et al., 2006). The instrument measures the time-dependent scattering and incandescence signals produced by single aerosol particles when crossing a Gaussian-shaped laser beam (Nd:YAG; wavelength $\lambda = 1064$ nm) (Schwarz et al., 2006). The avalanche photo-diode (APD) detectors measure at high and low gain stages the aerosol particle light scattering and incandescence in two wavelength ranges ($\lambda = 350$–800 nm and $\lambda = 630$–880 nm). All particles scatter the laser light with an intensity that is proportional to their optical size, from which the optical diameter (D_o) is determined. The instrument detects purely scattering particles in the size range of 200 nm $< D_o <$ 400 nm. Particles containing sufficient mass of rBC absorb the laser light and are heated to their vaporization temperature ($\sim$ 4000 °C), emitting incandescence light. The peak intensity of the incandescence signal is linearly proportional to the mass of rBC in the particle, which is determined after applying a calibration factor (Laborde et al., 2013). Assuming a void-free density of 1.8 g cm^{-3}, the mass-equivalent diameter (D_{MEV}) of rBC cores is calculated from the measured rBC mass (Laborde et al., 2013). The SP2 measurements are sensitive to rBC cores in the nominal size range of 70 nm $< D_{\mathrm{MEV}} <$ 500 nm. The SP2 incandescence signal was calibrated at the beginning, during, and at the end of the campaign, using size-selected fullerene soot particles. The scattering signal was calibrated using spherical polystyrene latex spheres (208, 244, and 288 nm) and ammonium sulfate particles with diameters selected by a differential mobility analyzer (DMA, Grimm Aerosol Technik, Ainring, Germany). The results of all calibrations agreed within their uncertainty ranges, confirming good instrument stability throughout the campaign.

The concentration of condensation nuclei, N_{CN}, was measured using a butanol-based condensation particle counter (CPC, Grimm Aerosol Technik) with a nominal lower cutoff particle diameter of 4 nm. Due to losses in the inlet lines, the effective cutoff diameter was $\sim$ 10 nm at lower atmospheric levels and $\sim$ 20 nm in the upper troposphere. Accordingly, total aerosol concentrations will be represented by $N_{\mathrm{CN,20}}$. An additional CPC with the same cutoff diameter was connected to a thermodenuder, which heats a segment of the sample line to 250 °C. The thermodenuder is used to evaporate the volatile aerosol constituents, such as organics and ammonium sulfate salts, allowing one to quantify the non-volatile (or refractory) particles (e.g., mineral dust, black carbon, sea salt) (Clarke, 1991; Weinzierl et al., 2011). In addition, the particle number size distributions (PNSD) of aerosols in the size range of $D_{\mathrm{p}} = 90$–600 nm were obtained from an Ultra-High Sensitivity Aerosol Spectrometer (UHSAS; Droplet Measurement Technologies, Longmont, CO, USA) (Cai et al., 2008). In this paper, we refer to the total number concentration measured by the UHSAS as the accumulation-mode number concentration, N_{acc}. The ultrafine fraction (f_{fine}) is obtained as the difference between the CPC particle counts, $N_{\mathrm{CN,20}}$, and the N_{acc} obtained by the UHSAS, divided by $N_{\mathrm{CN,20}}$. Likewise, the volatile fraction (f_{vol}) is obtained from the difference between aerosol counts measured by the two CPCs (with and without a thermodenuder) divided by $N_{\mathrm{CN,20}}$.

The CCN concentration, N_{CCN}, was measured with a two-column CCN counter (CCNC, model CCN-200, DMT, Longmont, CO, USA) (Krüger et al., 2014; Roberts and Nenes, 2005; Rose et al., 2008). In this study, we used only the measurements at constant supersaturation ($S = 0.52 \pm 0.05$ %). The activated fraction, $f_{\mathrm{CCN,0.5}}$, was calculated as $N_{\mathrm{CCN,0.5}}$ divided by $N_{\mathrm{CN,20}}$.

A compact time-of-flight aerosol mass spectrometer (C-ToF-AMS, Aerodyne Research, Inc., Billerica, MA, USA) measured the mass concentration of four chemical species (i.e., organics, sulfate, nitrate, and ammonium) of the submicrometer aerosol with a time resolution of 30 s (Drewnick et al., 2005; Schulz et al., 2018). A complete description of the instrument and its operation during the ACRIDICON-CHUVA campaign is given in Schulz et al. (2018) and Andreae et al. (2018).

A dual-cell ultraviolet (UV) absorption detector (TE49C, Thermo Scientific) operating at a wavelength of $\lambda = 254$ nm was used to measure O_3 with a precision of 2 % or 1 ppb. The CO mixing ratio was detected with a fast-response fluorescence instrument (AL5002, Aerolaser, Garmisch, Germany) (Gerbig et al., 1999). NO and total reactive nitrogen, NO_y, were measured by a modified dual-channel chemiluminescence detector (CLD-SR, Ecophysics) in connection with a gold converter (Baehr, 2003; Ziereis et al., 2000). More details on the measurement techniques can be found in Andreae et al. (2018).

The rBC enhancement ratio relative to CO ($\mathrm{EnR}_{\mathrm{BC},M} = \Delta M_{\mathrm{rBC}}/\Delta c_{\mathrm{CO}}$, where Δ is the difference between the concentration of the species in the plume and in the background atmosphere) was obtained by applying a bivariate fit

to the rBC and CO correlation within individual pollution plumes. Analogously, CCN and rBC enhancement ratios relative to total CPC particle counts ($\Delta N_{CCN,0.5}/\Delta N_{CN,20}$ and $\Delta N_{rBC}/\Delta N_{CN,20}$) were obtained by applying a bivariate fit between the respective quantities. Note that the best fit for the c_{CO} vs. M_{rBC} correlation was obtained after multiplying the c_{CO} by a factor such that their means are numerically equivalent and then multiplying the resulting fit parameter by the same factor to obtain the $EnR_{BC,M}$.

2.3 Ground-based aerosol and trace gas measurements at ATTO

The ATTO site was established in 2010/2011 as a research platform for in-depth and long-term measurements of aerosol particles and trace gases as well as meteorological and ecological parameters in the central Amazon rain forest (Andreae et al., 2015). The research site is located 150 km northeast of Manaus, in a region characterized by periodic pristine atmospheric conditions during parts of the wet season vs. strong BB pollution during the dry season (Pöhlker et al., 2016, 2018; Saturno et al., 2018b). The present study includes ATTO data of the aerosol absorption coefficient at $\lambda = 637$ nm, σ_{ap}, using the Multiangle Absorption Photometer (MAAP, model 5012, Thermo Electron Group, Waltham, USA) and the aerosol scattering coefficients, σ_{sp}, using a nephelometer (model Aurora 3000, Ecotech Pty Ltd., Knoxfield, Australia), respectively. The M_{BC_e} was calculated using a mass absorption cross section of $12.3\,m^2\,g^{-1}$ for the dry season, as obtained by Saturno et al. (2018b). The single scattering albedo (SSA), which characterizes the absorption properties of an aerosol population, is defined as scattering divided by total extinction (absorption + scattering). All data were normalized to standard temperature and pressure (STP, $T_0 = 273.15$ K, $p_0 = 1013.25$ hPa). The CCN concentrations at a supersaturation of 0.5 %, $N_{CCN,0.5}$, were calculated using long-term scanning mobility particle sizer (SMPS) data and the κ-Köhler parametrization as described in Pöhlker et al. (2016). For more details about the aerosol optical properties' characterization and CCN observations, we refer the reader to Saturno et al. (2018b) and Pöhlker et al. (2016, 2018), respectively. Further details on CO measurements conducted at the ATTO site can be found in Winderlich et al. (2010) and Andreae et al. (2015). Daily EnR_{BC} was calculated by applying a bivariate regression fit to 30 min averages of ΔBC_e and ΔCO. The 5th percentiles of the BC_e and CO measurements of the corresponding month were used as background values.

2.4 Satellite and ground-based remote sensing

In this study, we used the vertically resolved extinction coefficients (LIDAR Level 2 Version 3 Aerosol Profile product with 5 km horizontal resolution) of the Cloud-Aerosol Lidar with Orthogonal Polarization (CALIOP) lidar system, onboard the Cloud-Aerosol Lidar and Infrared Pathfinder Satellite Observations (CALIPSO) satellite (Winker et al., 2009). The CALIPSO algorithms detect and classify aerosol layers based on their observed physical and optical properties into the subclasses polluted continental, biomass burning (smoke), desert dust, polluted dust, clean continental, and marine aerosol (Omar et al., 2009).

To obtain CO concentrations between the 400 and 600 hPa pressure levels, we used the Atmospheric Infrared Sounder (AIRS) onboard the NASA Aqua satellite available from the Giovanni online data system (https://giovanni.gsfc.nasa.gov/giovanni/, last access: 13 June 2019). Daily averages of aerosol optical depth (AOD) at 550 nm with an original grid resolution of $1^\circ \times 1^\circ$ were obtained from Moderate Resolution Imaging Spectroradiometer (MODIS) aerosol products from the NASA Terra and Aqua satellites (Remer et al., 2005). Finally, AOD at 500 nm (level 2.0) was obtained by direct sun measurements in Ascension Island (7.976° S, 14.415° W), using the CIMEL sunphotometer of the AErosol RObotic NETwork (AERONET, https://aeronet.gsfc.nasa.gov/, last access: 12 March 2019) (Holben et al., 1998).

2.5 Direct radiative forcing at the top of the atmosphere

In this study, we used the library for radiative transfer (LibRadtran) (Emde et al., 2016) with the uvspec tool to calculate the direct radiative forcing at the top of the atmosphere (DRF-TOA) by aerosol particles in the BB layer in the region of the South Atlantic Ocean. To solve the radiative transfer equation, we chose the Discrete Ordinate Radiative Transfer solver (DISORT) 2 (Evans, 1998; Stamnes et al., 2000). The setup for the atmosphere was based on the standard tropical profile (Anderson et al., 1986), which was modified with measurement data. The vertical profiles of the mean aerosol extinction coefficient were calculated based on multi-year (2012–2018) CALIPSO retrievals. The extraterrestrial spectrum was used as described in Gueymard (2004). A wavelength range from 300 to 4000 nm was considered. The ocean was set as the underlying surface. The AOD of the plume was calculated by integrating the mean extinction coefficient over the altitude band of the pollution layer (1–5 km). A SSA of 0.84 was assumed for the smoke layer based on Zuidema et al. (2016) and Sect. 3.5 of the present study. An asymmetry parameter of 0.7 was used based on the typical BC value presented in Cheng et al. (2014). With the above parametrization, we obtained the mean daily value for the DRF-TOA along different longitudes.

2.6 Backward trajectory modeling and fire intensities

The HYbrid Single-Particle Lagrangian Integrated Trajectory (HYSPLIT) model (Stein et al., 2015) was used to obtain systematic and multi-year sets of backward trajectories

(BTs) for the ATTO site as outlined in detail in Pöhlker et al. (2019). The time series of cumulative fire intensity along the BTs (CF_{BT}) was calculated based on (i) an ensemble of filtered 3 d HYSPLIT BTs, started every hour in the time frame between 1 January 2013 and 31 December 2018, at a starting height of 200 m, and (ii) daily georeferenced fire intensity maps, in W m^{-2}, from the Global Fire Assimilation System (GFAS). The GFAS fire intensity maps were obtained as NetCDF3 files with a spatial resolution of 0.1° latitude by 0.1° longitude (0.1° equals roughly 11 km). Only those segments of the individual BTs in convective exchange with the surface/fires (i.e., BT segments with heights < 1000 m) and encountering *en route* convection (i.e., BT segments with sun fluxes > 50 W m^{-2}) were included in the calculation of CF_{BT}. In addition, the individual BTs were terminated upon *en route* occurrence of rain (i.e., for rainfall > 2 mm). Details of the BT data set and filtering can be found in Pöhlker et al. (2019).

We calculated the cumulative fire intensity for each trajectory as follows: every two consecutive points of the original trajectory (1 h time step) build one linear segment of a trajectory with length (L_i) $1 < i < 72$ h (see Fig. S1 in the Supplement). For each trajectory segment, the collection of grid cells (m, n) that the trajectory passes through is computed: this is done by finding all locations along the trajectory for which either the latitude or longitude coordinate is an integer multiplied by 0.1°. To account for the residence time of air mass at each grid cell, the length ($l_{i,j}$) of the trajectory path within the cell (m, n) is calculated, divided by the length of the trajectory segment (L_i) and multiplied by the fire intensity ($F_{m,n}$) corresponding to the grid cell (m, n). This results in the fire intensity weighted by the residence time of the air parcel along the segment. The cumulative fire intensity (cumFire) along every individual BT is calculated by summing up $F_{m,n}$ over the whole trajectory length. Note that as we used 3 d BTs, each trajectory was mapped to the raster of fire intensities of the 3 corresponding days (see the example in Fig. S2). Finally, we summed up the cumulative fire intensities over the 24 BTs for each day in order to obtain the CF_{BT} time series with 1 d time resolution.

The method described above is summarized in the following equations. Let F be a matrix containing fire intensities of size $M \times N$. Let T be a list of K trajectories.

$$\text{cumFire} = \sum_{j} \sum_{i=1}^{72} F_{m,n} \cdot \frac{l_{i,j}}{L_i}, \tag{1}$$

and $l_{i,j}$ is the path of trajectory segment within cell $F_{m,n}$, calculated as follows:

$$l_{i,j} = \sqrt{\left((x_{m+1} - x_m) \cdot \cos\left(\frac{y_{n+1} + y_n}{2}\right)\right)^2 + (y_{n+1} - y_n)^2}. \tag{2}$$

Finally, for the ensemble of 24 trajectories at each day,

$$CF_{BT} = \sum_{k=0}^{24} \text{cumFire}(T_k). \tag{3}$$

2.7 GIS data products and analysis

The analysis of geographic information system (GIS) data sets was conducted with the QGIS software package (Las Palmas version 2.18.2, QGIS development team). The GIS data sets were handled using the coordinate reference of the World Geodetic System from 1984 (WGS84). The following GIS data sets were used in this study: (i) maps of global water bodies obtained from the European Space Agency (ESA) (https://www.esa-landcover-cci.org/?q=node/162, last access: 4 July 2019), (ii) wind fields from the Modern-Era Retrospective analysis for Research and Applications Version 2 model (Merra-2, https://gmao.gsfc.nasa.gov/reanalysis/MERRA-2/, last access: 4 July 2019) obtained through the Giovanni online data system, (iii) land cover maps obtained from ESA (http://maps.elie.ucl.ac.be/CCI/viewer/index.php, last access: 4 July 2019), and (iv) a map of global biomes according to Olson et al. (2001). For further details, we refer the reader to Pöhlker et al. (2019).

3 Results and discussion

The flight track of AC19 followed the direction of the Amazon River from Manaus towards the coast and included cloud-profiling maneuvers over the Atlantic Ocean (Fig. 1). A remarkable observation during AC19 was the strong stratification of the troposphere over the ocean with vertically well-defined and horizontally extended layers, with varying degrees of pollution. Based on contrasting aerosol concentrations, size ranges, and composition, we distinguished an upper and a lower pollution layer (UPL and LPL) with a horizontal clean air mass layer (CL) in between. The layers were discernible visually from the aircraft cockpit (Fig. 2).

In this study, we present the tropospheric stratification for the lowest 5 km of the atmosphere, focusing primarily on aerosol and trace gas properties within the UPL, and contrast them with the properties of the CL, LPL, and marine boundary layer (MBL). Aerosol properties in the upper troposphere during ACRIDICON-CHUVA have been characterized in previous studies (Andreae et al., 2018; Schulz et al., 2018). Upon ascent and descent, the UPL was probed six times at offshore locations[1], right before it reached the South American continent, and two times onshore ∼200–400 km from the coastline (blue squares in Fig. 1). The eight UPL penetrations were several hundred kilometers apart from each other, underlining the large horizontal extent of the layer. Later on the route back to Manaus airport, we observed an active fire

[1]Note that we count the two passages through the layer over the Amazon River delta as offshore.

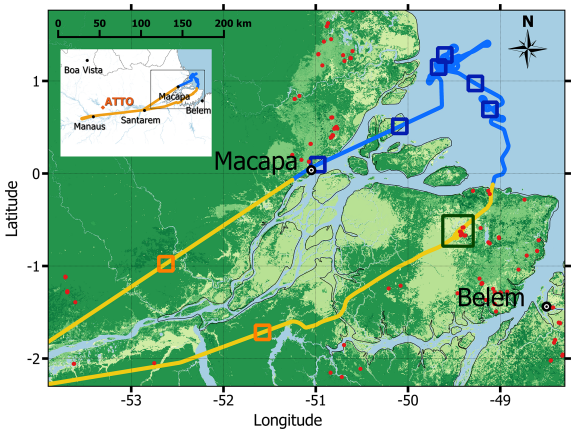

Figure 1. ACRIDICON-CHUVA flight AC19 on 30 September 2014. The squares represent the locations at which the aircraft ascended or descended through the upper pollution layer (UPL) (blue: offshore profiles, orange: inshore profiles). The yellow and blue segments of the flight track correspond to the inshore and offshore sections that were averaged to obtain the profiles in Fig. 3. Red markers indicate fire spots on 30 September 2014 as obtained from INPE (http://www.inpe.br/queimadas/bdqueimadas/, last access: 17 April 2019), and the dark green square represents the location where a fresh BB plume was probed at ∼ 1 km altitude.

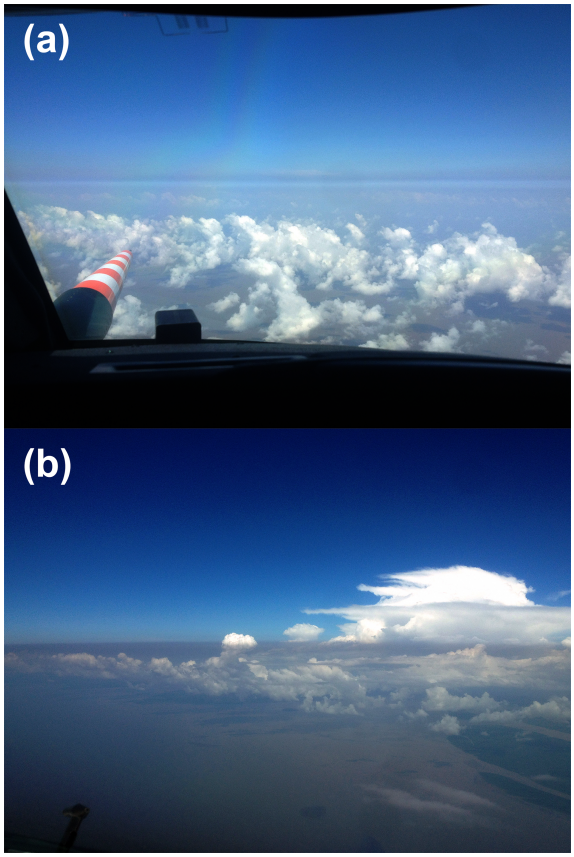

Figure 2. View from the HALO cockpit during flight AC19 on 30 September 2014, showing **(a)** the layering of the troposphere with clearly visible pollution layers as well as a clean layer in between at an offshore location (17:09 UTC) and **(b)** the brownish pollution layer arriving at the Brazilian coastline (16:55 UTC).

plume northwest of Belém (green square in Fig. 1, photo of plume in Fig. S3). This plume was probed at ∼ 1 km above the fire and is expected to be only a few minutes old. Selected aerosol properties at this local, fresh BB plume are contrasted with the UPL aerosol properties.

3.1 Offshore aerosol particle and trace gas profiles

The pronounced tropospheric stratification observed over the Atlantic Ocean near the northeastern margin of the Amazon Basin is illustrated by selected meteorological, trace gas, and aerosol profiles in Fig. 3. In Fig. 3a, the profiles of water vapor mass mixing ratio, q, and potential temperature, θ, show rather small interquartile ranges, indicating comparable q and θ conditions where profiling maneuvers were conducted along the flight track. In relation to q and θ, a well-defined layering – particularly the UPL – clearly emerges in the aerosol particle and trace gas properties (Fig. 3, Table 1). Generally, the profile of θ indicates rather stable conditions along the entire profile, with the UPL being centered at ∼ 3.5 km altitude. For comparison, radiosonde profiles at Belém airport for the same day as flight AC19 are shown in Fig. S4. The stable conditions presumably prevented the pollution from being mixed downwards and further suggest that the UPL is decoupled from the air masses above and below, facilitating an efficient horizontal transport pathway for the pollutants. Moreover, the distinct properties of the UPL, CL, and LPL as outlined below suggest that the corresponding air masses originated from different sources and/or processes and probably reflect different atmospheric aging times (see also Sect. 3.2). For example, shallow convection (or Scu) can increase aerosol at the top of clouds through detrainment.

In terms of aerosol properties, the UPL is characterized by a relative maximum in total number concentrations, $N_{CN,20} = 970 \pm 260\,cm^{-3}$ (mean ± 1 SD, Fig. 3b). Aerosol particles in the accumulation mode dominate the UPL aerosol, as $N_{acc} = 850 \pm 330\,cm^{-3}$ accounts for most of $N_{CN,20}$ (∼ 85 %). This corresponds to a significant drop in the ultrafine particle fraction with $f_{fine} \approx 15\,\%$ within the UPL (Fig. 3b). The aerosols in the UPL are further characterized by a low fraction of volatile particles, f_{vol}, as shown in Fig. 3c. In the atmospheric column, f_{vol} reaches its minimum of $16 \pm 9\,\%$ within the UPL and generally shows a similar profile to f_{fine}, indicating a rather aged plume (Grieshop et al., 2009; Zhou et al., 2017). The particle number size distributions of the UPL aerosol – in comparison

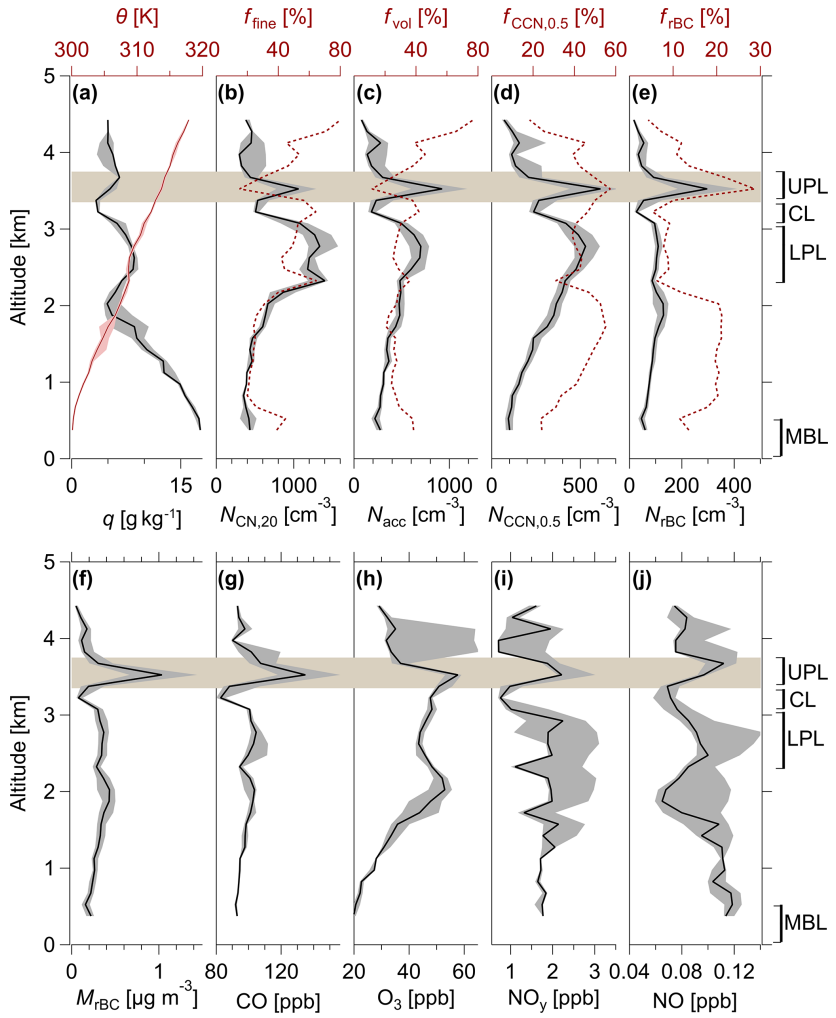

Figure 3. Vertical profiles of selected meteorological, aerosol, and trace gas parameters measured off the Brazilian coast during flight AC19: **(a)** potential temperature, θ, and water vapor mass mixing ratio, q; **(b)** total aerosol particle number concentration, $N_{CN,20}$, and ultrafine particle number fraction, f_{fine}; **(c)** accumulation-mode particle number concentration, N_{acc}, and volatile particle number fraction, f_{vol}; **(d)** CCN number concentration at $S = 0.5\,\%$, $N_{CCN,0.5}$, and activated fraction at $S = 0.5\,\%$, $f_{CCN,0.5}$; **(e)** rBC number concentration, N_{rBC}, and rBC number fraction, $f_{rBC,N}$; and **(f)** rBC mass concentration, M_{rBC}; **(g)** carbon monoxide, c_{CO}; **(h)** ozone, c_{O_3}; **(i)** total reactive nitrogen, c_{NO_y}; and **(j)** nitrogen monoxide, c_{NO}, mole fractions measured off the Brazilian coast during flight AC19. The black lines and shadings represent the median and inter-quartile range calculated for 150 m altitude bins during the flight section off the Brazilian coast (16:50 to 19:07 UTC, blue line in Fig. 1). The brown shaded area represents the approximate vertical location of the upper pollution layer (UPL). The altitudes of the lower pollution layer (LPL), the clean layer (CL), and the marine boundary layer (MBL) are indicated on the right-hand side of the plot. The precise time windows when the UPL, CL, LPL, and MBL were probed are shown in Table S1 of the Supplement.

to the LPL, CL, MBL, and fresh BB aerosols probed during AC19 – are shown in Fig. 4 and summarized in Table 2 (see Fig. S5 for individual PNSDs). A modal diameter of 132 nm was observed for the UPL aerosol, whereas the fresh BB aerosol showed a clearly smaller modal diameter of 124 nm. Further note that the modal diameter in the UPL is smaller than the 220 nm observed directly off the African coast (Weinzierl et al., 2011). The CCN concentrations at $S = 0.5\,\%$, $N_{CCN,0.5}$, show a maximum within the UPL with $N_{CCN,0.5} = 560 \pm 180\,cm^{-3}$ as well as a high CCN fraction, $f_{CCN,0.5} = 60 \pm 6\,\%$ (Fig. 3d).

The N_{acc} within the UPL is lower than at the ATTO site under strongly BB-influenced ($N_{acc,BB} \approx 3400\,cm^{-3}$) and average dry season conditions ($N_{acc,dry} \approx 1300\,cm^{-3}$), yet still substantially higher than under an average wet season at ATTO ($N_{acc,wet} \approx 150\,cm^{-3}$) or pristine rain forest con-

Table 1. Characteristic aerosol and trace gas concentrations in the upper pollution layer (UPL), clean layer (CL), lower pollution layer (LPL), and marine boundary layer (MBL) observed during the AC19 flight section off the Brazilian coast (16:50 to 19:07 UTC; Fig. 1). For comparison, corresponding data from a fresh biomass burning plume (BB, also observed during AC19; see Fig. 1) have been added. Data are summarized as arithmetic mean ± standard deviation (SD) as well as 1st and 99th percentiles (P1 and P99).

	UPL				CL				LPL				MBL				BB			
	mean	SD	P1	P99	mean	SD	P1	P99	mean	SD	P1	P99	mean	SD	P1	P99	mean	SD	P1	P99
$N_{CN,20}$ (cm^{-3})	970	260	400	1500	500	60	450	760	1300	200	750	1750	420	140	220	800	4200	2100	1500	10 500
N_{acc} (cm^{-3})	850	330	260	1550	180	60	90	360	650	140	320	940	230	50	140	330	2700	1400	660	6600
$N_{CCN,0.5}$ (cm^{-3})	560	180	200	920	230	40	170	350	510	90	320	700	95	30	30	200	2000	1100	500	5100
N_{rBC} (cm^{-3})	280	110	90	530	30	12	9	60	110	20	60	190	50	16	24	84	280	110	120	630
f_{fine} (%)	15	14	0	45	65	7	44	79	48	11	27	69	43	13	18	68	37	8	19	61
f_{vol} (%)	16	9	3	40	43	6	25	55	27	7	13	44	39	9	22	62	17	7	2	38
$f_{rBC,N}$ (%)	28	5	17	40	6	2	2	11	9	2	5	14	12	3	5	19	7	2	4	11
$f_{CCN,0.5}$ (%)	60	6	44	71	46	6	34	62	41	8	26	59	23	6	11	38	45	5	31	54
c_{CO} (ppb)	150	30	100	210	83	4	78	101	105	5	96	115	92	1	90	94	162	40	107	277
c_{O_3} (ppb)	56	9	36	71	48	2	46	53	45	2	41	51	21	1	19	23	34	2	31	38
c_{NO_y} (ppb)	2.5	0.8	1.0	4.5	0.9	0.4	0.6	2.0	2.1	0.8	0.8	3.1	1.7	0.1	1.4	1.8	2.1	0.3	1.7	2.9
c_{NO} (ppb)	0.10	0.02	0.06	0.13	0.07	0.01	0.04	0.09	0.10	0.02	0.06	0.15	0.12	0.02	0.09	0.15	0.18	0.06	0.11	0.32
M_{rBC} (µg m^{-3})	1.0	0.4	0.3	2.0	0.09	0.05	0.02	0.25	0.36	0.11	0.17	0.73	0.17	0.07	0.07	0.37	0.70	0.24	0.35	1.36
M_{Org} (µg m^{-3})	2.5	1.2	1.2	4.4	0.91	–	–	–	1.72	0.15	1.57	1.86	−0.02	0.04	−0.08	0.04	4.6	1.6	2.2	7.4
M_{SO_4} (µg m^{-3})	0.86	0.41	0.50	1.60	0.42	–	–	–	0.79	0.02	0.76	0.81	0.22	0.08	0.14	0.33	0.57	0.18	0.38	0.94
M_{NO_3} (µg m^{-3})	0.33	0.26	0.08	0.70	0.04	–	–	–	0.05	0.02	0.03	0.07	0.013	0.012	−0.002	0.025	0.15	0.06	0.05	0.25
M_{NH_4} (µg m^{-3})	0.48	0.23	0.25	0.81	0.25	–	–	–	0.45	0.16	0.31	0.62	0.18	0.11	0.06	0.37	0.33	0.11	0.20	0.56

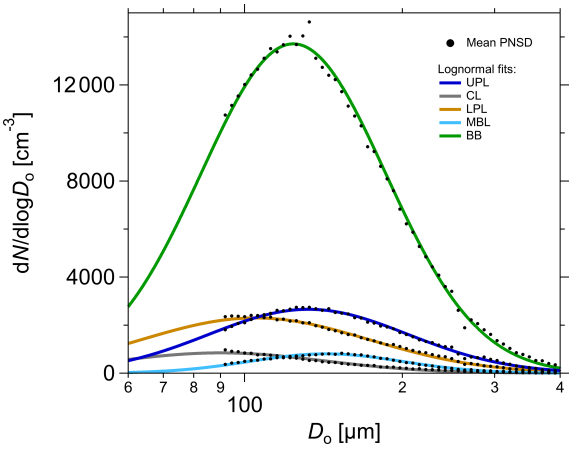

Figure 4. Particle number size distributions (PNSD) measured by the UHSAS for the UPL, CL, LPL, and MBL, as defined in Fig. 3, and the fresh BB plume probed during AC19 (see Fig. 1). The data points (black dots) are fitted by log-normal functions between 90 and 500 nm (Heintzenberg, 1994).

Table 2. Fit parameters of UHSAS-derived aerosol size distributions in Fig. 4, representing different conditions (i.e., layers, plumes) during AC19. A log-normal function (Heintzenberg, 1994) was used to fit a mono-modal size distribution to the mean data points: $\frac{dN}{d\ln d_p} = \frac{A}{\sqrt{2\pi}\ln\sigma_g}\exp\left(-\frac{(\ln d_p - \ln d_0)^2}{2\ln(\sigma_g)^2}\right)$.

	UPL	CL	LPL	MBL	BB
A	2920	970	2890	680	13 930
d_0 (nm)	132	90	105	143	124
σ_g	1.55	1.58	1.65	1.40	1.50
r^2	1.00	0.99	1.00	1.00	1.00

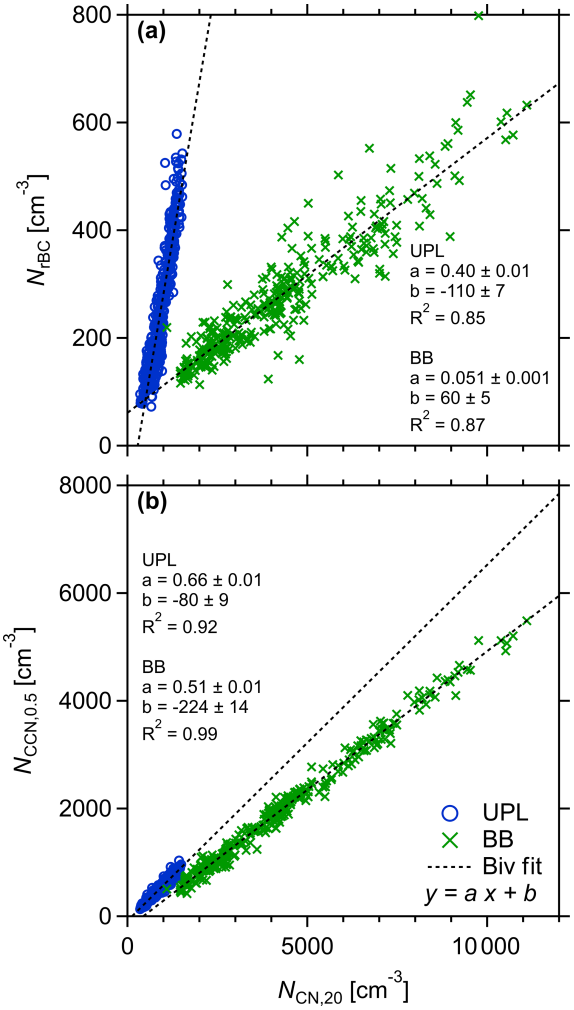

Figure 5. Correlation between **(a)** rBC particle number concentrations (N_{rBC}) and total aerosol ($N_{CN,20}$); and between **(b)** CCN at $S = 0.5\,\%$ ($N_{CCN,0.5}$) and total aerosol ($N_{CN,20}$) in the UPL (blue) and in the fresh biomass burning plume (green). The dashed lines are bivariate linear regressions applied to the data sets.

ditions ($N_{acc,PR} \approx 90\,cm^{-3}$) (Pöhlker et al., 2016, 2018). Remarkably, rBC particles represent a dominant species of the UPL aerosol population in terms of number concentration with $N_{rBC} = 280 \pm 110\,cm^{-3}$, corresponding to an rBC number fraction of $f_{rBC,N} = 28 \pm 5\,\%$ relative to $N_{CN,20}$ (Fig. 3e). The ratio $\Delta N_{rBC}/\Delta N_{CN,20} \approx 40\,\%$ in the UPL is much higher than $\Delta N_{rBC}/\Delta N_{CN,20} \approx 5\,\%$ in the fresh BB plume (Fig. 5a). Visually, the dark color of the layer observable in Fig. 2 corresponds to the high rBC fraction. For comparison, rBC number fractions of 0 %–15 % relative to $N_{CN,20}$ were observed in megacity pollution (Laborde et al., 2013) and $f_{rBC,N} \approx 6\,\%$ in wildfire plumes injected into the lowermost stratosphere in the Northern Hemisphere (Ditas et al., 2018).

In terms of absolute mass concentrations, rBC within the UPL, with $M_{rBC} = 1.0 \pm 0.4\,\mu g\,m^{-3}$ (ranging from 0.5 to $2\,\mu g\,m^{-3}$), approaches the highest BC levels observed at ATTO (M_{BC_e} up to $2.5\,\mu g\,m^{-3}$; Pöhlker et al., 2018; Saturno et al., 2018b). Figure 6 shows the fractions of rBC mass relative to the other main constituents of the submicrometer aerosol (M_{total} = non-refractory + rBC) in the UPL in comparison to the CL, LPL, MBL, and fresh BB values. Organic matter – comprising co-emitted primary as well as secondarily formed organics – accounts for the dominant mass fractions in all layers, with $f_{org,M} \approx 50\,\%$ in the UPL, CL, and, LPL, and as much as 72 % in the fresh BB plume. Generally, the dominance of organic matter is in agreement with previous studies performed at different locations and seasons in the Amazon region (e.g., Brito et al., 2014; Chen et al., 2015; Fuzzi et al., 2006; Martin et al., 2010, 2017; de Sá et al., 2019; Schneider et al., 2011; Schulz et al., 2018; Shrivas-

tava et al., 2019; Talbot et al., 1990). For example, in the southwestern region of the Amazon, which is heavily impacted by BB, organics account for $f_{org,M} > 90\,\%$ in the dry season (Brito et al.2014). Note that the thermal stability of some organic species and tar balls in BB plumes can lead to an underestimation of the $f_{org,M}$ measured by the C-ToF-AMS (Adachi et al., 2018). Further, the organic matter in the UPL is significantly more oxidized than the fresh BB smoke, as shown in Fig. S6. This can be associated with the long aging times and the elevated O_3 mixing ratio in the UPL (Fig. 3h) (Martin et al., 2017). The rBC mass fractions account for $f_{rBC,M} = 15\,\%$ in the UPL and $f_{rBC,M} = 12\,\%$ in the BB plume. A clear difference was observed for the mass fractions of the inorganic constituents sulfate (SO_4^{2-}), ammonium (NH_4^+), and nitrate (NO_3^-), which in sum account for $f_{inorg,M} = 35\,\%$ in the UPL and $f_{inorg,M} = 16\,\%$ in the BB plume. The increased $f_{inorg,M}$ in the UPL can probably be explained by aging-related condensation of the secondarily formed species SO_4^{2-}, NH_4^+, and NO_3^-. On the other hand, the lower $f_{org,M}$ in the UPL compared to the fresh Amazonian BB is related to the evaporation of organics due to fragmentation during the aging over the Atlantic. Note that, despite the higher $\Delta N_{rBC}/\Delta N_{CN,20}$ in the UPL compared to the fresh BB (Fig. 5a), the UPL shows a higher CCN activated fraction ($\Delta N_{CCN,0.5}/\Delta N_{CN,20} = 66\,\%$, Fig. 5b). The high CCN efficiency is likely due to internal mixing of rBC with sulfate, nitrate, and highly oxygenated organic aerosol. These findings, in combination with the UPL's large geographic extent, suggest that it represents an aerosol and CCN reservoir of particular significance for the Amazonian cloud cycling and rainfall formation – i.e., cloud droplet formation and growth.

Regarding trace gases, Fig. 3g–j show absolute maxima in the UPL for the mole fractions of carbon monoxide (c_{CO}), ozone (c_{O_3}), and total reactive nitrogen (c_{NO_y}) as well as a secondary maximum for nitrogen monoxide (c_{NO}). The elevated $c_{CO} = 150 \pm 30$ ppb along with the high M_{rBC} indicates that the UPL air masses originated from BB emissions. Moreover, the ratio between these two co-emitted species can be used as a tracer for the origin and age of BB plumes (Darbyshire et al., 2019; Guyon et al., 2005; Saturno et al., 2018b). The aged UPL is characterized by a higher rBC enhancement ratio, $EnR_{BC,M} = 14.7 \pm 0.6\,ng\,m^{-3}\,ppb^{-1}$, compared to fresh Amazonian BB with $EnR_{BC,M}$ of $6.3 \pm 0.2\,ng\,m^{-3}\,ppb^{-1}$ (Fig. S7). Recent aircraft measurements of African BB pollution over Ascension Island have found similar $EnR_{BC,M} = 11$–$17\,ng\,m^{-3}\,ppb^{-1}$ in the free troposphere (Wu et al., 2020). The ozone as a secondary pollutant also presents a maximum within the UPL ($c_{O_3} = 56 \pm 9$ ppb) and appears to be anti-correlated with NO ($c_{NO} = 0.10 \pm 0.02$ ppb). Therefore, the fact that O_3 and NO_y ($c_{NO_y} = 2.5 \pm 0.8$ ppb) are strongly enhanced in the pollution layers reflects the high photochemical age of the plume. Overall, the trace gas mole fractions within the UPL are consistent with previous aircraft measurements. Over the Atlantic, off the city of Natal, Brazil, Andreae et al. (1994) found similar pollution layers with c_{O_3} and c_{CO} up to 90 and 210 ppb, respectively. The mean mole fraction of NO_y in these plumes was extremely high: 4.4 ± 3.1 ppb, with enhancement ratios, EnR_{NO_y}, in the range 0.018 to 0.108. The EnR_{NO_y} in the UPL (0.019) lies in the lower part of this range. Over Ascension Island, c_{O_3} can be as high as 80 ppb in the lower troposphere (Thompson et al., 1996).

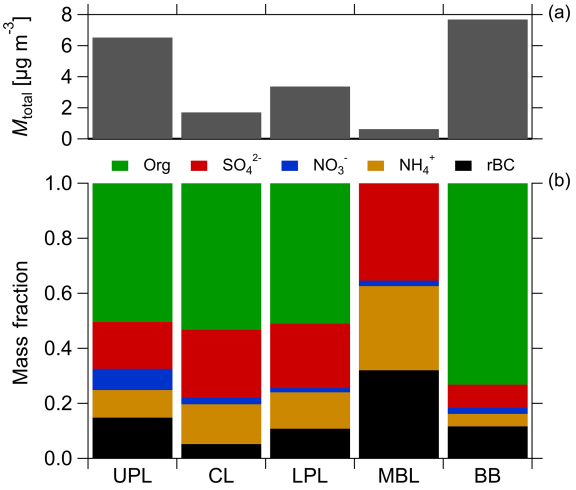

Figure 6. Cumulative mass concentrations of non-refractory submicrometer species (i.e., organic (Org), sulfate (SO_4^{2-}), nitrate (NO_3^-), ammonium (NH_4^+)) and rBC **(a)**; and mass fractions of the respective species to the total mass ($M_{total} = M_{Org} + M_{SO_4} + M_{NO_3} + M_{NH_4} + M_{rBC}$) in the UPL, CL, LPL, and MBL, as defined in Fig. 3, and the fresh BB plumes probed during AC19 (see Fig. 1) **(b)**. Note that no C-ToF-AMS data were available from 17:27 to 19:05 UTC during the offshore section of flight AC19 and, therefore, a reduced number of measurements points are included in the averages. The concentration of organics was below the detection limit in the MBL.

Below the UPL, the atmospheric vertical profile off the Brazilian coast shows a second maximum in aerosol concentrations in the LPL ($N_{CN,20} = 1300 \pm 200\,cm^{-3}$; $N_{acc} = 650 \pm 140\,cm^{-3}$) at altitudes between ~ 2.3 and 3.0 km (Fig. 3). The properties of the UPL and LPL, however, are remarkably different. The LPL shows rather lower concentrations of rBC ($M_{rBC} = 0.36 \pm 0.11\,\mu g\,m^{-3}$ and $N_{rBC} = 110 \pm 20\,cm^{-3}$), CO ($c_{CO} = 105 \pm 5$ ppb), and O_3 ($c_{O_3} = 45 \pm 2$ ppb), which decreases with decreasing altitude. NO_y actually reaches the highest concentrations in this layer, with values up to 3.0 ppb. We assume that the pyrogenic species found in the LPL are also advected from Africa; however, possible influences from urban emissions in Africa and/or South America, for example, should not be neglected. This possibility is supported by the relatively high sulfate content of the aerosol in this layer, which at an average value of $0.79 \pm 0.02\,\mu g\,m^{-3}$ accounts for 23 % of the total aerosol mass concentration (Fig. 6). Sulfur-rich anthropogenic emis-

sions from fossil-fuel combustion may have become mixed with BB emissions by cloud venting over the Gulf of Guinea region (Dajuma et al., 2019).

One interesting aspect of the LPL is that the ultrafine fraction accounts for about half of the aerosol number concentration ($d_0 = 105$ nm; see PNSD in Fig. 4). Likewise, in the LPL the f_{vol} is higher than in the other atmospheric levels. One possible explanation for this is that new particle formation occurs in the detrainment regions around the shallow cumulus, which brings air masses from the marine boundary layer (MBL), containing dimethyl sulfide and SO_2, into the LPL. This phenomenon has previously been reported by several authors (Hegg et al., 1990; Kerminen et al., 2018; Perry and Hobbs, 1994). Direct convective transport of ultrafine particles from the MBL into the LPL is unlikely to be an important source of such particles, as their concentration in the MBL is only about 200 cm^{-3}, well below their concentration in the LPL of about 700 cm^{-3}. In the MBL (with its top at $\sim$ 600 m a.s.l.), the total and accumulation-mode particle concentrations are somewhat lower than in the layers aloft ($N_{CN,20} = 420 \pm 160$ cm^{-3} and $N_{acc} = 230 \pm 50$ cm^{-3}) and present larger diameters ($d_0 = 143$ nm). The MBL appears to be only weakly influenced by the African BB, with $M_{rBC} = 0.17 \pm 0.07$ µg m^{-3} and N_{rBC} accounting for only 10 % of the $N_{CN,20}$. Additionally, the aerosol population in the MBL appears less efficient as CCN, with only 20 % of particles being activated at $S = 0.5$ % (Fig. 3d).

In between the UPL and LPL, the $\sim$ 200 m thick CL was found centered at $\sim$ 3.2 km altitude with relatively dry air as represented by a sharp decrease in q. Such clean layers have been previously observed in the dry season over the African continent and adjacent oceans, specifically in the southeastern Atlantic Ocean, with a few hundred (up to 1 km) meters thickness (Hobbs, 2003). Within the CL, the combustion tracer concentrations M_{rBC}, N_{rBC}, and c_{CO} sharply decrease to 0.09 ± 0.05 µg m^{-3}, 30 ± 12 cm^{-3}, and 83 ± 4 ppb, respectively. We further found $N_{CN,20} = 500 \pm 60$ cm^{-3}, which is comparable to $N_{CN} = 500$ cm^{-3} in another CL as reported by Hobbs (2003). Within the CL, the aerosol size distribution is substantially shifted towards the Aitken mode ($d_0 =$ 90 nm, Fig. 4). The c_{O_3} shows a slight decrease to 48 ± 2 ppb. Hobbs (2003) proposed that the CL derived from the ultraclean upper tropospheric air.

In the vicinity of the western African coast, similar tropospheric stratification was observed in a recent aircraft campaign. Aerosol and trace gas profile measurements over the Gulf of Guinea in July 2016, measured under the influence of aged BB plumes originating in central Africa, revealed two distinct aerosol layers, where the upper one, centered at 3.8 km altitude, was enriched in rBC ($\sim$ 0.3 µg m^{-3}), CO ($\sim$ 340 ppb), and organics ($\sim$ 65 µg m^{-3}) (Denjean et al., 2019; Flamant et al., 2018). Moreover, Weinzierl et al. (2011) reported $f_{vol} = 26$ % (13 %–52 %, p_3–p_{97}) for BB plumes near the western African coast in 2008 during SAMUM-2, which are larger than the f_{vol} within the UPL in this study. Typically, organic aerosol becomes less volatile during atmospheric aging, concurrent with an increase in its O/C ratio (Grieshop et al., 2009; Isaacman-VanWertz et al., 2018; Slowik et al., 2012; Zhou et al., 2017). More recently, from comprehensive measurements on Ascension Island in the middle of the South Atlantic, Zuidema et al. (2018) described a smoke layer over a stratocumulus cloud deck where "shortwave-absorbing aerosol emanating from biomass burning in continental Africa advects westwards over the South Atlantic for approximately one third of the year, from June to October". These previously reported results suggest that the discrete rBC-enriched layer reported here likely formed in the vicinity of the African coast and tapered as it approached the South American continent. In addition, the atmospheric stability facilitated the transport across the South Atlantic towards the Amazon. Further, ongoing studies suggest the existence of a low-level jet with a maximum around 800 hPa ($\sim$ 3 km) induced by changes in boundary layer height during the day (Anselmo et al., 2020). The low-level jet may be the main mechanism transporting the African pollution from the Atlantic Ocean into the Amazon Basin.

3.2 Backward trajectories and potential source regions in Africa

Based on BTs, which reflect the large-scale trade wind circulation patterns, we investigated the origin and age of the UPL up to 10 d prior to its observation. Figure 7a compares BT ensembles – started in the relevant offshore area (i.e., 3° N to 3° S; 52 to 44° W) and during the time period of the UPL observation by the aircraft (i.e., 30 September 2014 18:00 UTC) – for the starting heights at 500 m (representing near-surface conditions), 2500 m (peak of LPL), 3500 m (peak of the UPL), and 5000 m above ground level (well above the UPL). The comparison of the different BT starting heights shows clear differences in air mass advection patterns: specifically, the UPL BTs indicate rather fast and directed air mass movements from easterly directions, whereas the LPL BTs indicated more curvilinear movement from east-southeasterly directions. The fact that the BT patterns diverge is consistent with the different trace gas and aerosol properties shown in Fig. 3, underlining that LPL and UPL represent air masses of different origin and/or atmospheric aging history. Furthermore, the wind fields at about 3500 m illustrate the large-scale meteorology at the UPL altitude. The transatlantic transport time of the UPL air masses was about 10 d according to the BT ensembles.

The fire map in Fig. 7a helps to identify potential source regions of the UPL aerosol. It includes fires within a 5 d window (15 to 20 September 2014) of when the BB-laden air masses likely originated in the African source regions and then started their $\sim$ 10 d journey across the Atlantic Ocean until the aircraft observation on 30 September. Several hotspots of fire activity in central and southern Africa can be found in Fig. 7a$_1$. All of them are located in tropical and

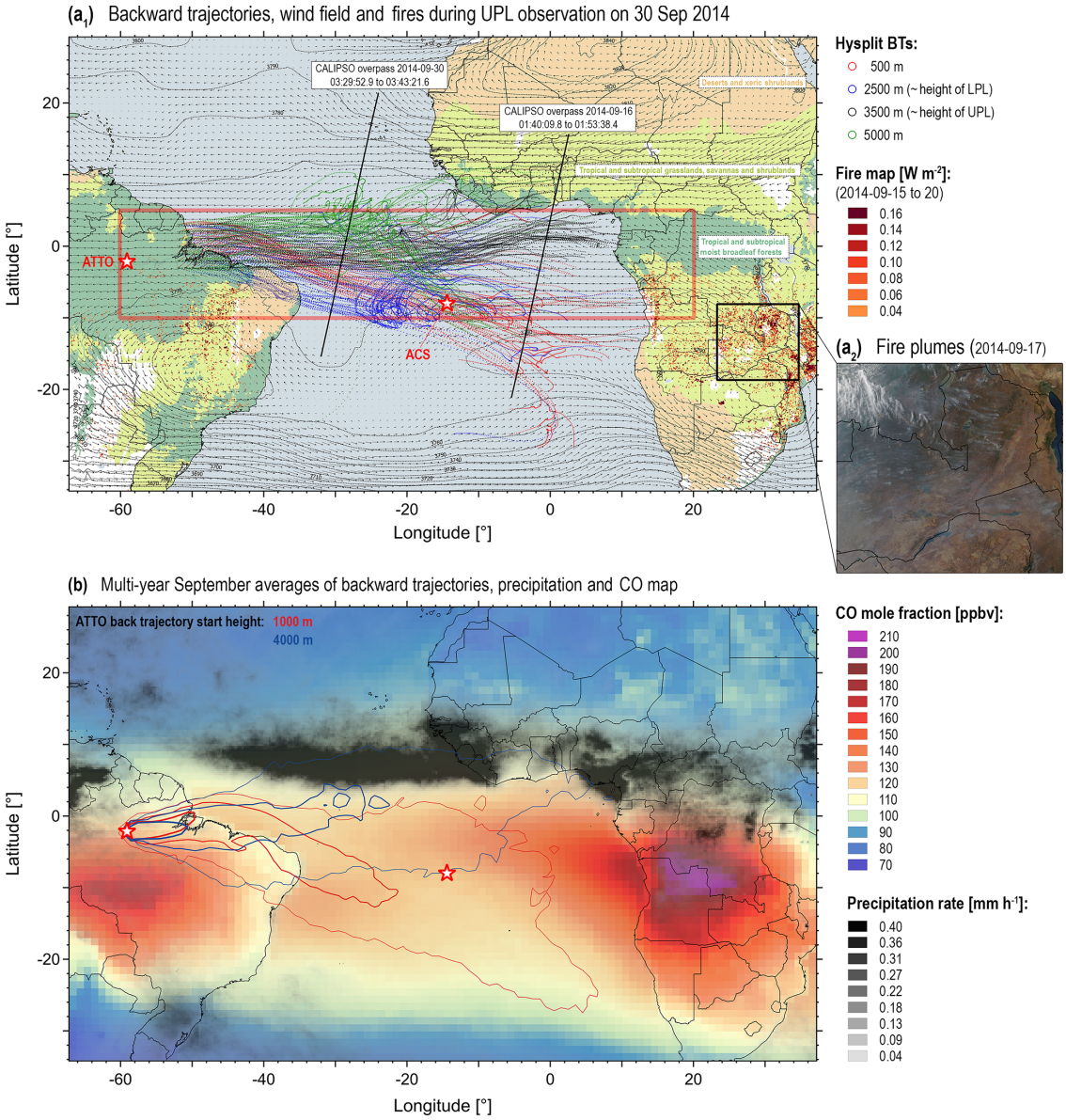

Figure 7. Composite maps combining backward trajectories (BTs) and satellite data products characterizing atmospheric conditions **(a_1)** during flight AC19 on 30 September 2014 in comparison to **(b)** the averages of September observations during multiple years. Panel **(a_1)** shows HYSPLIT 10 d BTs starting at different altitudes (500, 2500, 3500, 5000 m a.g.l.) at 18:00 UTC on 30 September 2014 (similar time and location to the UPL observations during flight AC19). Note that the altitudes where the BTs were initiated include the heights of the sampled UPL and LPL. The fire radiative power (FRP) density (mW m^{-2}), retrieved by the Global Fire Assimilation System (GFAS v1.0) averaged from 15 to 20 September 2014, is also shown as a fire map with $0.1° \times 0.1°$ grid resolution. The orbits of two CALIPSO passages on 30 and 16 September 2014 as shown in Fig. 9 as well as the geographic locations of the ATTO site and Ascension Island are also illustrated. Panel **(a_2)** shows multiple clearly visible fire plumes in the African source region. Panel **(b)** shows multi-year averages of all Septembers for (i) HYSPLIT BT ensembles starting at ATTO (1000 and 4000 m a.g.l.) from 2005 to 2018. Contour lines represent the fraction of occurrence of overpassing trajectories in a specific region as described in Pöhlker et al. (2019). (ii) AIRS-derived CO data products (400 to 600 hPa atmospheric levels) from 2005 to 2018 and (iii) TRMM precipitation from 2005 to 2018. For general illustration, animations (https://climate.nasa.gov/climate_resources/146/video-simulated-clouds-and-aerosols/, last access: 4 July 2019; https://gmao.gsfc.nasa.gov/research/aerosol/modeling/nr1_movie/, last access: 4 July 2019) of the Goddard Earth Observing Model (Version 5, GEOS-5) show that aerosol particles are transported efficiently from Africa to South America and to a lesser extent from South America to Africa (Colarco et al., 2010; Yasunari et al., 2011).

subtropical grasslands, savannas, and shrublands according to Olson et al. (2001). Particularly, the Miombo woodlands are well known as a region of frequent and intense fire activities, mostly driven by human activities (Andela and van der Werf, 2014; Barbosa et al., 1999; Earl et al., 2015). For the time frame of 15 to 20 September 2014, satellite-based natural color reflectance images show the high fire activity through a larger number of clearly visible smoke plumes in the hotspot areas (one example is shown for 19 September 2014 in Fig. 7a$_2$). Note that at the same time, the fire activity in South America is still comparatively low (Fig. 7a$_1$). Overall, the fires, wind field, and BTs in Fig. 7a$_1$ show a coherent picture and suggest that the shown grassland, savanna, and shrubland fires represent the sources for the UPL at the Brazilian coast.

It has been generally assumed – though not shown in detail and quantified yet – that African smoke accounts for a significant fraction of pollution input into the Amazon Basin (Saturno et al., 2018b). Therefore, we complemented the case-specific map in Fig. 7a$_1$, which focuses on the precise time window of flight AC19, by a seasonally averaged map in Fig. 7b, presenting the multi-year September averages of CO (the complete yearly cycle is shown in Fig. S8). The map in Fig. 7b emphasizes the large extent of the African smoke plume (here represented by CO) over the Atlantic area. It further shows good agreement between the CO plume pattern and BT ensembles at the central Amazonian ATTO site, indicating that transatlantic smoke transport is a general and seasonally recurring phenomenon beyond the specific case of the analyzed layer in September 2014. This is supported by in situ measurements made during the Atmospheric Tomography mission (ATom) 2016–2018 flight missions, which showed elevated concentrations of BB aerosols (about 0.1 to 1 µg m^{-3}) over most the of the southern tropical Atlantic in July to October (Schill et al., 2019). Biomass smoke particles were the dominant aerosol fraction in this region between the surface and 4 km altitude. Further note that precipitation rates over the South Atlantic are comparatively low, as shown in Fig. 7b. Accordingly, rain-out and wash-out mechanisms likely do not substantially reduce the BB aerosol population during transport.

3.3 Geographic extent of pollution layers over the Atlantic and direct radiative effects

Satellite-based observations resolve the transatlantic transport of the pollution layers. Figure 8 illustrates the movement of the African aerosol particles across the Atlantic by means of the burning tracer CO, where individual plumes during the dry season of 2014 can be identified. This includes the plume probed at the Brazilian coast during AC19 (marked by a dashed line), which appears to be coincidentally the strongest plume in 2014. Beyond this particular event, several weaker plumes were also observed. Based on Fig. 8, a characteristic transport velocity of $\sim 380\,\mathrm{km\,d^{-1}}$ can be

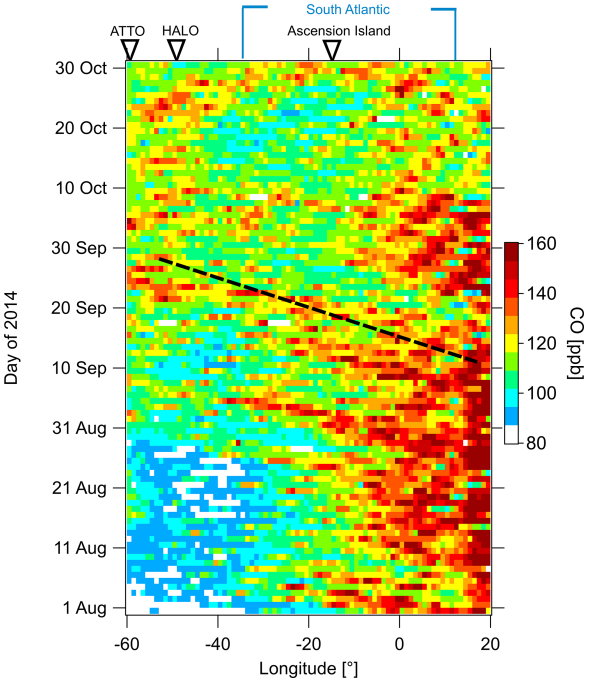

Figure 8. Hovmöller plot of the daily AIRS-derived carbon monoxide (400 to 600 hPa) distributed over the South Atlantic region (60° W to 20° E) from August to October 2014, averaged over the latitudinal band of 10° S to 5° N, corresponding to the region of interest (ROI) highlighted in Fig. 7a$_1$. Several events of transatlantic transport of aerosol from Africa towards South America can be identified. The black dashed line highlights a particularly strong plume originating around 10 September 2014 and arriving in the observational area of AC19 on 30 September.

obtained and, therefore, an aging time of ~ 10 d. Similarly, satellite-based AOD observations can be used to resolve the plume movement as shown in Fig. S9.

The transatlantic transport of the particular BB plume that was probed during AC19 was temporally and geographically close to that of a volcanogenic sulfate-rich plume, whose origin was related to a period of strong activity of the Nyamuragira volcano in the eastern Democratic Republic of the Congo. The associated major SO_2 emissions were oxidized to sulfate during the transatlantic passage (Saturno et al., 2018a). The plume of sulfate-rich aerosols was observed airborne during ACRIDICON-CHUVA flight AC14 on 21 September 2014 in the region from 200 to 400 km south of Manaus as well as by ground-based measurements at ATTO from 21 to 30 September 2014. Importantly, the BB plume probed during AC19 and the volcanogenic plume probed during AC14 were distinct events (i.e., did not occur in the same air masses) since the volcanogenic plume (i) occurred ~ 1 week earlier, (ii) was observed to be strongest between 4 and 5 km, in contrast to 3 to 4 km for the BB

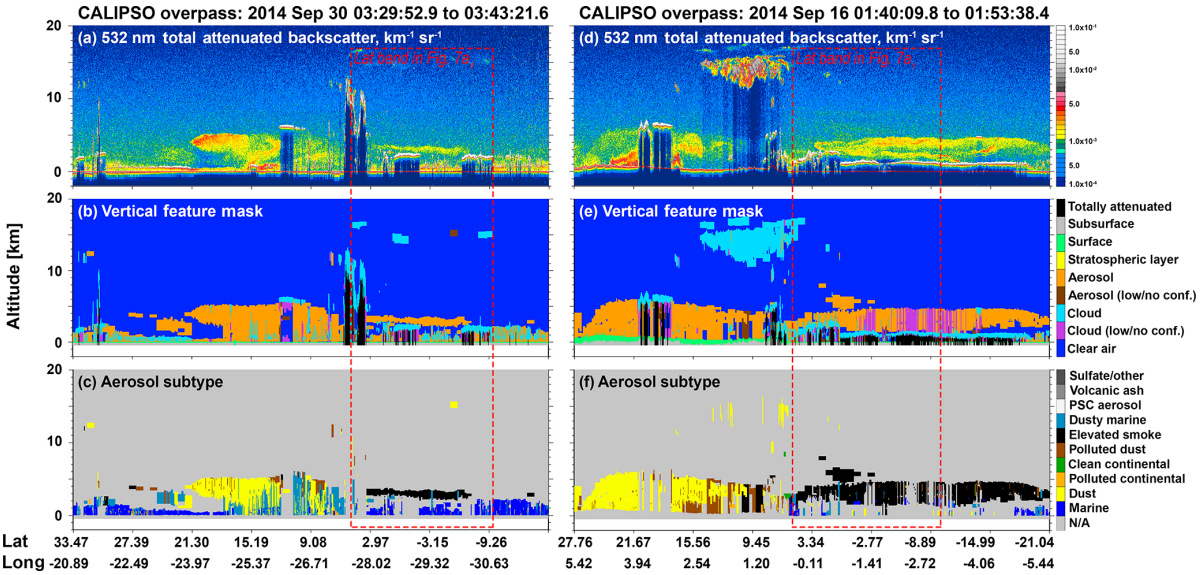

Figure 9. CALIPSO-derived lidar profiles for 16 and 30 September 2014, where African BB plumes were identified over the South Atlantic Ocean. The first profile near the South American coast shows the aerosol layer at similar altitudes to those observed during flight AC19. Satellite orbits for both profiles are shown in Fig. $7a_1$.

plume, and (iii) showed a very low rBC mass concentration. However, the volcanogenic plume can be regarded as a "reference case of the dynamics and conditions of transatlantic aerosol transport from southern Africa to South America" (Saturno et al., 2018a). The temporal coincidence of the volcanogenic and BB plumes suggests that transatlantic aerosol transport was particularly efficient in the second half of September 2014. Moreover, the observation that the single volcanogenic plume significantly influenced the aerosol particle chemical composition, hygroscopicity, and optical properties at ATTO (Saturno et al., 2018a) suggests that the more frequent and presumably stronger African BB plumes likely have a similarly profound impact on the central Amazonian aerosol population, at least during the dry season.

The African BB plumes (particularly the strong event at the end of September) were also observed by the vertically resolved aerosol extinction measurements by the CALIPSO satellite, revealing elevated and vertically defined smoke layers over the South Atlantic. Figure 9 shows two selected CALIPSO passages on 16 and 30 September 2014 (the day of the AC19 flight). More examples of similar layers over the Atlantic Ocean in September 2016 are shown and discussed in Barkley et al. (2019). These passages show exemplary snapshots of the elevated smoke layers at different longitudinal locations: on 16 September 2014 a layer was probed relatively close to the southern African coast, whereas on 30 September 2014 a layer was observed halfway between Ascension Island and the Amazon River delta. For the overpass on 30 September 2014, the layer's N–S extension was about 1200 km and its altitude between 3 and 4 km, which agrees well with the altitude of the UPL observation during flight AC19. For the passage on 16 September 2014, the layer's N–S extension was about 4° N to 20° S (∼ 2800 km) and its altitude between 2 and 5 km. In this context, a dedicated study of Adebiyi and Zuidema (2016) has shown that 45 % of the forward trajectories of satellite-detected smoke plumes in southern Africa exit the continent westwards between 5 and 15° S and are transported westward by the Southern African Easterly Jet (AES-J), overlying a semi-permanent marine stratocumulus deck. Moreover, Fig. 9 suggests that the layer's latitudinal extent decreases as it approaches the South American continent.

In order to constrain the seasonal and vertical aspects of the transatlantic transport, we analyzed the satellite-retrieved aerosol profiles over the South Atlantic Ocean during the dry season of multiple years (2012 to 2018). Figure 10a–c show the extinction coefficients of all CALIPSO overpasses within the region of interest (ROI, as defined in Fig. 7a) averaged over the months of August, September, and October. High aerosol loadings (up to 5 km altitude) in the longitude band from 10 to 20° E correspond to BB emissions over the African continent. Likewise, comparably high extinction coefficients (up to 3 km altitude) are observed due to BB fires in South America (60 to 40° W). Over the South Atlantic from 40° W to 10° E, the maximum extinction coefficient is observed at two different levels of the atmosphere, separated by a relatively clean layer in between. The lower layer (altitude < 1 km) with a pronounced extinction coefficient rep-

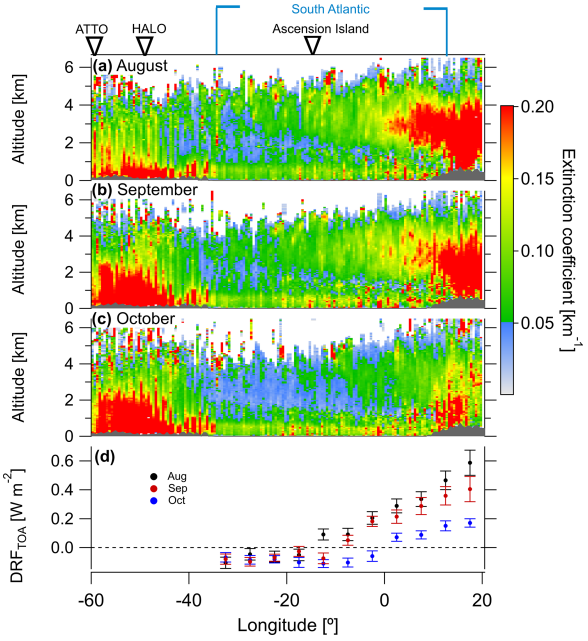

Figure 10. Curtain plot showing the columnar aerosol extinction coefficient at 532 nm, based on multi-year CALIOP data from 2012 to 2018 (only nighttime data). Panels represent monthly averages for the months of **(a)** August, **(b)** September, and **(c)** October within the latitude band from 10° S to 5° N, corresponding to the ROI indicated in Fig. 7a$_1$. The grey shaded area represents the mean surface elevation and depicts boundaries of the African and South American continents. Panel **(d)** shows the daily mean of the direct radiative forcing at the top of the atmosphere (DRF-TOA) exerted by the pollution layer over the South Atlantic Ocean, calculated using the LibRadTran radiative transfer model.

resents the MBL, which is presumably dominated by the (coarse-mode) marine aerosols and is clearly visible throughout the 3 months in Fig. 10. On the other hand, the higher layer (altitudes between 1 and 5 km) represents the African BB aerosol being transported westwards over the Atlantic all the way to South America. The transport pattern stands out in the months of August and September, but is weakened in October, when the remaining BB plumes appear to be mostly/completely removed from the atmosphere halfway before reaching South America. The injection height of BB aerosol in Africa is relatively high due to the AEJ-S, which induces an upward motion directly below the jet, enhancing updrafts over land that lift up BB aerosols to altitudes where they can be efficiently transported over the South Atlantic (Adebiyi and Zuidema, 2016). The vertical location of pollution plumes in the atmosphere is an important parameter, as it can considerably influence its atmospheric lifetime. Aerosol lifted up to higher altitudes tends to be advected over larger distances due to less efficient removal mechanisms (i.e., wet deposition). When leaving the African coast, the smoke layer is present at altitudes between 1.5 and 5 km, but becomes more restricted to higher altitudes (3–5 km) as it moves towards South America. Figure 10 suggests a pronounced thinning of the layer during its movement westwards due to dilution.

The transatlantic transport pattern of African BB, as presented here, is not well represented by the state-of-art atmospheric models. The simulations of the transatlantic transport of BB aerosol by several global aerosol models are able to capture the vertical distribution of aerosol over the African continent, but diverge from the satellite observations as it moves westward over the Atlantic Ocean (Das et al., 2017). In the models, BB aerosol plumes quickly descend to lower levels just off the western African coast, while our observations suggest that they are transported at high altitudes (< 5 km) well above the MBL all the way to the Amazon Basin. After reaching the Brazilian coast, the smoke layer gradually subsides, likely being entrained into the cloud layer below or more deeply mixing into the boundary layer. The effects of the aged pollution plume on radiative and cloud-nucleation properties over the Atlantic and upon arrival in the Amazon Basin are still uncertain.

In order to estimate the direct radiative effect that the African BB layer exerts along its transport over the Atlantic, we used the mean CALIPSO profiles to obtain information about the vertical extent of the plumes. Figure 10d shows the longitudinal profile of DRF-TOA calculated for different AOD values and atmospheric conditions as daily mean values for 3 different months. We observed a decrease in the warming effect of the aerosol towards South America. Near the African coast, a positive DRF-TOA was observed, reaching values as high as $+0.6\,\mathrm{W\,m^{-2}}$ in August, $+0.4\,\mathrm{W\,m^{-2}}$ in September, and $+0.17\,\mathrm{W\,m^{-2}}$ in October. On the other hand, negative DRF-TOA, ranging from -0.03 to $-0.10\,\mathrm{W\,m^{-2}}$, was found through the 3 months for lower AOD values (longitudes $< 5°$ E). The change in sign of the DRF-TOA is mostly a result of the high amount of absorption assumed for the aerosol layer in the simulations (single scattering albedo of 0.84). At higher optical depths, the absorption in the layer dominates, thus causing a positive forcing (warming) at TOA. At low AOD values, on the other hand, the absorption is weaker and the back-scattered radiation dominates the radiative effect, resulting in a negative aerosol radiative forcing at the TOA. Sensitivity cases for different assumptions about aerosol and surface properties are shown in Fig. S10. Our results suggest that the transport of BB smoke across the Atlantic has strong direct effects on the regional radiative balance, which changes from warming to cooling along the way from southern Africa to South America.

3.4 Transport of the pollution layer into the Amazon Basin

An important question for the aerosol cycling in the Amazonian troposphere is how the UPL evolves as it moves from

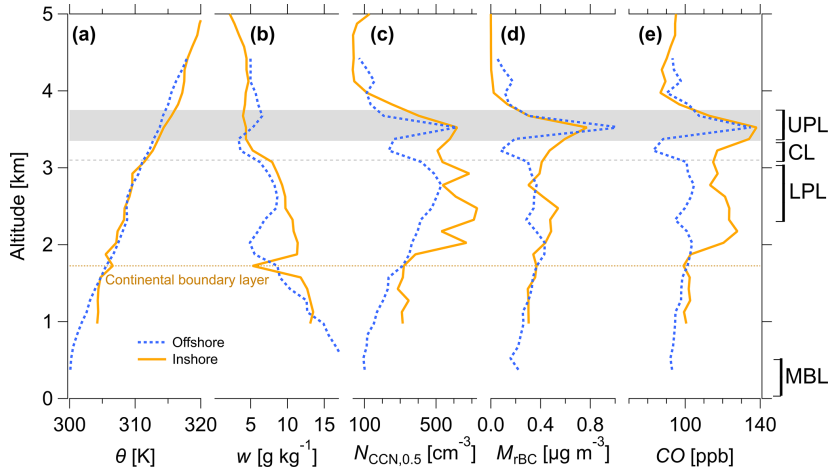

Figure 11. Vertical profiles of selected meteorological, aerosol, and trace gas parameters measured inshore and offshore of the Brazilian coast during AC19: **(a)** potential temperature, θ; **(b)** water vapor mass mixing ratio, w; **(c)** CCN ($S = 0.5\,\%$) number concentration, $N_{\mathrm{CCN},0.5}$; **(d)** rBC mass concentration, M_{rBC}; and **(e)** carbon monoxide mole fraction, c_{CO}. The figure shows the medians calculated for 150 m altitude bins over the flight sections inshore (yellow) and offshore (blue) of the Brazilian coast (as indicated in Fig. 1). The grey shaded area represents the approximate vertical location of the upper pollution layer (UPL) and the grey dashed line the lower limit of the clean layer (CL) observed exclusively during the offshore profiles.

the Atlantic Ocean into the South American continent. With the data available from flight AC19 (six offshore and two onshore penetrations of the UPL, Fig. 1), at least some conclusion can be drawn for the first ~ 400 km of UPL (as well as CL and LPL) transport over land. Figure 11 overlays onshore vs. offshore vertical profiles of selected meteorological, aerosol, and trace gas parameters. Meteorologically, the θ profiles show some divergences between inshore and offshore in the well-mixed continental boundary layer (up to ~ 1.5 km altitude) and in the UPL altitude band. Even stronger differences were found in the q profiles, which show the broadening of the upper dry layer from offshore to onshore profiles. Regarding the CL, the characteristic trace gas and aerosol concentration minima in the offshore profiles mostly disappeared onshore (e.g., for CCN, M_{rBC}, and c_{CO}, Fig. 11c, d, e). This fading of the CL minimum appears to be linked to the evolution of the UPL's vertical structure, which mostly remains intact, showing however a tendency to broaden and subside into the altitude range of the CL (i.e., 3.1 to 3.3 km), likely because of the onset of deeper vertical convective mixing over land. In addition, the inshore profiles also suggest that some BB emissions have been added, as the air masses moved inland because the increased concentrations of CCN, rBC, and CO in the LPL cannot be explained by downward mixing from the UPL alone. This is consistent with the presence of scattered fires in the coastal region (Fig. 1).

In this context note that a pronounced UPL was exclusively observed during flight AC19 (the only flight over the northeastern basin), whereas no comparable stratification was found during the other 13 flights in the central and western parts of the basin (Wendisch et al., 2016). Also, upon ascent after take-off and descent before landing of AC19 at Manaus International Airport, the altitude range (i.e., 3 to 4 km) was probed; however, no clear indications of an UPL were found. This suggests that the UPL started broadening over the first 400 km over the continent and faded away when the air masses reached the central basin in the region of Manaus (~ 1200 km from the coast). Accordingly, we conclude that convective mixing by the abundant cumulus that typically reaches up to 4–6 km over the Amazon prevented a well-defined UPL from being preserved far into the central basin. As a result, the aerosol brought in by the UPL is mixed downwards through convection and then transported further westwards with the boundary layer air masses. Similar downward mixing of BB emissions by convection over land has been reported from the south of western Africa (Dajuma et al., 2019).

3.5 Estimated relevance of the pollution layer for central Amazonian aerosol cycling

Considering the large horizontal extension of the pollution layer, it presumably accounts for an important input of aerosols and trace gases into the Amazon Basin, with potentially strong impacts for cloud microphysics as well as the atmospheric radiative budget. Here we put the experimental results outlined so far into a broader context of multiple years of observations at the central Amazonian ATTO site to estimate the relevance of the pollution layer input for

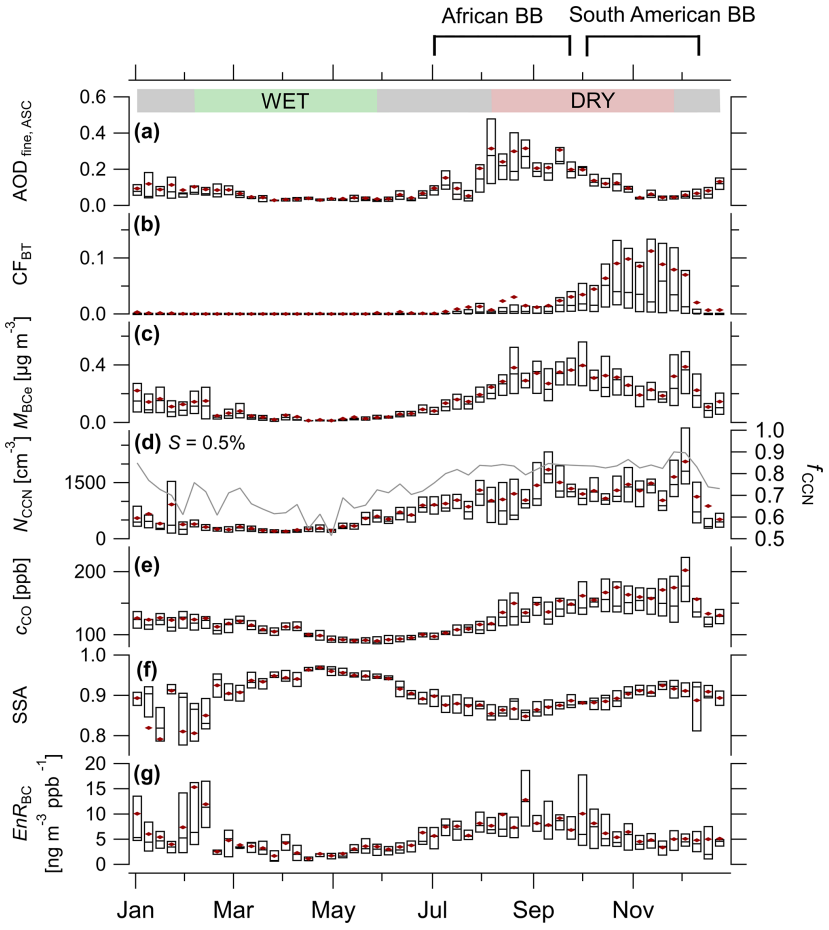

Figure 12. Seasonality of aerosol and trace gas properties based on long-term observations (2013–2018) at Ascension Island **(a)** and at the ATTO site **(b–g)**. The plot shows **(a)** fine-mode aerosol optical depth (AOD_{fine}) at 500 nm retrieved by the AERONET sunphotometer at Ascension Island; **(b)** cumulative fire intensity along the backward trajectories (CF_{BT}) of air masses arriving at the ATTO site (for details, see Sect. 2.6); **(c)** black carbon mass concentration M_{BC_e}; **(e)** CCN concentrations and activated fraction at $S = 0.5\,\%$; **(e)** CO mole fraction; **(f)** single scattering albedo, SSA; and **(g)** BC enhancement ratio, EnR_{BC}. The boxplots represent weekly statistics with the mean (red markers), the median (segment), and the 5th and 75th percentiles (lower and upper box edges) of the long-term daily measurements. The green and red shaded areas represent the wet and dry seasons, with transition periods in between, as defined in Pöhlker et al. (2016). On the top of the figure, markers indicate periods within the BB-influenced part of the year that ATTO is dominated either by the LRT of African BB or by the South American BB.

the central Amazonian aerosol lifecycle. Therefore, Fig. 12 combines the seasonal variability of relevant parameters to assess the interplay of African vs. South American BB emissions for the observed aerosol abundance and properties at ATTO. The influence of African BB transport into the basin is represented by the fine-mode AOD at Ascension Island, $AOD_{fine,ASC}$, based on ~ 20 years of AERONET observations. Note that Ascension Island is located in the main BT path of the transatlantic pollution transport and therefore a well-located observational site *en route* (Fig. $7a_1$). The influence of South American BB for the ATTO observations is represented by a BT data product, CF_{BT}, based on pixel-wise accumulation of fire intensities along individual ATTO BTs over a multi-year period.

Generally, the Amazonian atmosphere is strongly influenced by BB aerosols during the dry season and to a somewhat lower extent during the flanking transition periods, causing significant increases in scattering and absorption coefficients (Rizzo et al., 2013; Saturno et al., 2018b). In Fig. 12, the long-lasting BB influence can be seen by means of the broad seasonal maxima in M_{BC_e}, $N_{CCN,0.5}$, and c_{CO}. The BB-impacted part of the year in the Amazon, including dry season and transition periods, will be called hereafter the BB season. Remarkably, the African BB influence (repre-

Table 3. Characteristic aerosol and trace gas concentrations during the African vs. South American dominated periods of the BB season at the ATTO site: arithmetic mean ± SD, median and inter-quartile range of daily averages from 2013 to 2018.

	African dominated BB[b]					South American dominated BB[c]				
	mean	SD	median	25th perc	75th perc	mean	SD	median	25th perc	75th perc
$N_{CN,20}$ (cm^{-3})	1350	550	1300	900	1700	2000	1000	1800	1400	2300
$N_{CCN,0.5}$ (cm^{-3})	1100	500	1090	750	1400	1800	900	1600	1200	2000
M_{BC_e} ($\mu g\,m^{-3}$)	0.36	0.12	0.33	0.26	0.42	0.41	0.17	0.36	0.29	0.48
c_{CO} (ppb)	140	30	131	120	150	190	70	170	150	200
$f_{CCN,0.5}$ (%)	83	6	84	80	87	87	04	88	84	90
EnR_{BC}[a] ($ng\,m^{-3}\,ppb^{-1}$)	11	6	10	7	14	6	4	5	3	7
SSA (637 nm)	0.85	0.02	0.85	0.84	0.86	0.90	0.03	0.90	0.89	0.93

[a] Daily EnR_{BC} (from 2013 to 2018) was calculated by applying a bivariate fit to 30 min averages of M_{BC_e} and c_{CO} measurements (see Sect. 2.3). [b] To calculate the African BB dominated state, periods with South American fire influences (CF_{BT} > 50th percentile of $CF_{BT,dry}$) and with clean atmospheric conditions (M_{BC_e} < 50th percentile of $M_{BC_e,dry}$) were excluded. [c] To calculate the South American BB dominated state, we selected periods with South American fire influences (CF_{BT} > 50th percentile of $CF_{BT,dry}$) and with polluted atmospheric conditions (M_{BC_e} > 50th percentile of $M_{BC_e,dry}$).

sented by $AOD_{fine,ASC}$) vs. the South American BB influence (represented by CF_{BT}) shows contrasting and complementary seasonal cycles: $AOD_{fine,ASC}$ has its onset in July, peaks in September, and drops again in October (see also Figs. 8 and 10), whereas CF_{BT} has its onset in September, peaks in October/November, and drops towards the beginning of December. The seasonal cycles in M_{BC_e}, $N_{CCN,0.5}$, and c_{CO} vs. $AOD_{fine,ASC}$ and CF_{BT} in Fig. 12 suggest that the Amazonian BB season can be regarded as consisting of an African-smoke dominated period in the first half and an South American-smoke dominated period in the second half of this season. In fact, differences between the first and second halves of the BB season have been found and are summarized in Table 3.

In the first half of the BB season, under predominant African influence, seasonally averaged BB tracer concentrations of $M_{BC_e} = 0.36 \pm 0.12\,\mu g\,m^{-3}$ and $c_{CO} = 140 \pm 30$ ppb were observed, whereas in the second half under predominant South American influence, $M_{BC_e} = 0.41 \pm 0.17\,\mu g\,m^{-3}$ and $c_{CO} = 190 \pm 70$ ppb were somewhat higher. The CCN concentrations increase throughout the dry season, with $N_{CCN,0.5} = 1100 \pm 500\,cm^{-3}$ in the African-BB and $N_{CCN,0.5} = 1800 \pm 900\,cm^{-3}$ in the South American-BB dominated states. In both periods, the BB-derived aerosol particles show high CCN efficiency, with 83 % and 87 % of particle activation at $S = 0.5$ % during the first and second halves of the BB season, respectively. Clearer differences between the two BB properties in the dry season were observed, however, for the SSA and the BC enhancement ratio, EnR_{BC} (Fig. 12 and Table 3). The aerosol was strongly absorbing in August, with a minimum SSA of about 0.85 ± 0.02. Subsequently, the absorption properties decreased towards November with a relative maximum in SSA at about 0.90 ± 0.03. These results are consistent with the large $\Delta N_{rBC}/\Delta N_{CN,20}$ of ∼ 40 % in the African UPL vs. the rather low $\Delta N_{rBC}/\Delta N_{CN,20}$ of ∼ 5 % in an exemplary Amazonian BB plume (Sect. 3.1, Fig. 5a). Moreover, Saturno et al. (2018b) have shown that the brown carbon (BrC) contribution to total absorption becomes increasingly important towards the end of the dry season. This is a further indication of the predominance of regional fires towards the later BB season, given that BrC is quickly photodegraded in the atmosphere after emission, with a typical lifetime of a few days to weeks (Fleming et al., 2020; Wong et al., 2019), comparable to the transport times of African BB emissions across the Atlantic.

In the Amazonian dry season, the EnR_{BC} values span from 3 to 14 $ng\,m^{-3}\,ppb^{-1}$ (daily values), with the highest values occurring under the influence of African plumes and associated with lower SSA (see also Saturno et al., 2018b). The EnR_{BC} decreases from its peak of $11 \pm 6\,ng\,m^{-3}\,ppb^{-1}$ in July–September to a relative minimum of $6 \pm 4\,ng\,m^{-3}\,ppb^{-1}$ around November (Fig. 12g). The high EnR_{BC} in African plumes can be attributed to more flaming combustion in the comparatively dry grassland, savanna, and shrubland vegetation, in contrast to more smoldering combustion of Amazonian deforestation fires in the moist tropical forests. For comparison, Darbyshire et al. (2019) reported, from the SAMBBA aircraft campaign over the southern Amazon Basin, EnR_{BC} of 3 $ng\,m^{-3}\,ppb^{-1}$ in the west associated with more smoldering combustion of pasture and forested areas, in contrast to EnR_{BC} of 12 $ng\,m^{-3}\,ppb^{-1}$ in the eastern part influenced by cerrado fires. Note that differences between ground-based (this section) and aircraft (Sect. 3.1) EnR_{BC} presented in this paper are due to removal processes, combustion phase, and, possibly, the use of different measurement techniques. However, the independent ground-based observations do show a clear decrease in EnR_{BC} from African- to Amazonian-BB dominated states, which is consistent with the aircraft measurements.

4 Summary and conclusions

In this study, we probed an event of African BB being advected into the Amazon Basin with a comprehensive set of instruments for aerosol and trace gas measurements onboard the HALO aircraft during the ACRIDICON-CHUVA campaign in September 2014. Vertical profiles over the Atlantic Ocean and inshore over the northeastern Amazon Basin revealed a horizontally extended rBC-enriched layer (referred to as the UPL) of about 300 m thickness at ~ 3.5 km altitude, which showed strongly elevated aerosol and trace gas concentrations compared to the other atmospheric levels below 6 km. The plume was dominated by aerosol particles in the accumulation-mode size range ($N_{acc} = 850 \pm 330\,cm^{-3}$), peaking at ~ 130 nm diameter, and consisting mostly of particles containing non-volatile material. Remarkably, rBC particles appeared to be a dominant species, with mean number and mass concentrations of $N_{rBC} = 280 \pm 110\,cm^{-3}$ and $M_{rBC} = 1.0 \pm 0.4\,\mu g\,m^{-3}$, respectively. This accounts for $\sim$ 40 % of the total aerosol number and 15 % of the submicrometer aerosol mass concentrations. The UPL also shows high mass fractions of organics (50 %), sulfate (17 %), ammonium (8 %), and nitrate (10 %). Along with rBC, high c_{CO} (150 ± 30 ppb) indicated that the layer originated from biomass burning. Moreover, the advanced photochemical aging of the plume was indicated by the elevated c_{O_3} (56 ± 9 ppb) and by the very high f_{44} measured by the AMS. Despite the large fraction of rBC, the aerosol in the UPL appeared to be very CCN efficient due to internal mixing of rBC with sulfate, nitrate, and oxygenated organic aerosol, with ~ 70 % of particles activated at $S = 0.5$ %.

Backward trajectory analysis and remote sensing observations showed that the layer originated from BB in African grasslands, savannas, and shrublands. Therefore, the aerosol in the pollution layer upon arrival in South America, as probed by aircraft, has experienced at least 10 d of atmospheric aging over the African continent and the Atlantic Ocean. Moreover, multi-year remote sensing observations showed that layered atmospheric structures, and also the westward advection of African BB plumes, are a rather common phenomenon over the South Atlantic during the Amazonian dry season, peaking each year in August and September. Near the African coast, the vertical extent of the layer is a few kilometers, and it narrows down to only a few hundred meters while transported to South America. Based on the remote sensing data, we further calculate the DRF-TOA exerted by the pollution layer as a function of longitude. We found that the aging of the plume leads to a change in the DRF-TOA from a positive (warming) to a negative (cooling) effect as it moves westwards over the Atlantic. While the layered structure prevails all the way across the Atlantic for several days, it becomes quickly mixed vertically just a few hundreds of kilometers after reaching the South American continent. The aerosol particles in the layer are subsequently entrained into the continental boundary layer by convection and large-scale subsidence. We propose that long-range transport of such layers is the main pathway supplying African CCN and highly aged BC into the Amazonian atmosphere.

Long-term (2013–2018) ground-based aerosol measurements at the ATTO site in central Amazonia have demonstrated that long-range transported BB from Africa has a pronounced impact on aerosol particle properties within the dry season. From July to December, the Amazonian atmosphere is strongly influenced by BB aerosols, with corresponding increases in scattering and absorption coefficients (Saturno et al., 2018b; Rizzo et al., 2013), as well as the BB tracers, BC and CO. The interplay of African vs. South American BB emissions at ATTO is expressed by defined seasonal cycles of SSA, which increased from 0.85 in August to 0.90 in November, while EnR_{BC} decreased from 11 ± 6 to $6 \pm 4\,ng\,m^{-3}\,ppb^{-1}$.

This study highlights the importance of the transatlantic transport as a source of highly aged rBC and CCN-active particles to the Amazonian atmosphere, especially the northeastern regions, which are less impacted by anthropogenic pollution and regional fires. This process clearly merits future modeling investigations to assess its effects on regional radiative forcing as well as cloud properties and lifecycle.

Appendix A: List of frequently used symbols and acronyms

Description	Acronym
Aerosol optical depth	AOD
Aerosol Robotic Network	AERONET
Aerosol, Cloud, Precipitation, And Radiation Interactions And Dynamics Of Convective Cloud Systems Campaign	ACRIDICON-CHUVA
Amazon Tall Tower Observatory	ATTO
Atmospheric Infrared Sounder	AIRS
Backward trajectory	BT
Basic HALO Measurement And Sensor System	BAHAMAS
Biomass burning	BB
Black carbon	BC
Clean layer	CL
Cloud condensation nuclei	CCN
Cloud-Aerosol Lidar And Infrared Pathfinder Satellite Observations	CALIPSO
Condensation particle counters	CPC
Coordinated Universal Time	UTC
Compact Time-of-Flight Aerosol Mass Spectrometer	C-ToF-AMS
Fire radiative power	FRP
Long-range transport	LRT
Lower pollution layer	LPL
Marine boundary layer	MBL
Mass Absorption Aerosol Photometer	MAAP
Moderate Resolution Imaging Spectroradiometer	MODIS
Particle number size distributions	PNSD
Refractory black carbon	rBC
Region of interest	ROI
Single Particle Soot Photometer	SP2
Single scattering albedo	SSA
Ultra High Sensitivity Aerosol Spectrometer	UHSAS
Upper pollution layer	UPL

Data availability. The data of the key results presented here have been deposited in associated data files for use in follow-up studies. The HALO aircraft data (named "HALO.dat") and the ATTO data (named "ATTO.dat") used in this study are available in NASA Ames format under https://doi.org/10.17617/3.3r (Holanda et al., 2020a). Additional aircraft data from the ACRIDICON-CHUVA campaign can be found on the HALO database under https://halo-db.pa.op.dlr.de/ (DLR, 2020). Additional ATTO data can be found in the ATTO data portal under https://www.attodata.org/ (ATTO, 2020). The time series with cumulative fire count along backward trajectories (see Sect. 2.6) are available in NASA Ames format (named "H1000_Cer_Rain.dat") under https://doi.org/10.17617/3.3q (Holanda et al., 2020b). For data requests beyond the available data, please refer to the corresponding authors.

Supplement. The supplement related to this article is available online at: https://doi.org/10.5194/acp-20-4757-2020-supplement.

Author contributions. BAH conducted most of the data analysis and wrote the paper. CP, MOA, and UP supervised the work. MAF, QW, TD, JWK, CK, NM, HP, JS, CS, DW, and MW contributed specific parts of the data analysis. MLP, MD, TK, DF, LATM, DS, HS, JS, CS, BW, AW, MW, SB, HZ, MZ, CP, UP, and MOA conducted the measurements during the ACRIDICON-CHUVA campaign. BAH, MLP, JSa MS, FD, OOK, JB, MAF, FGM, JVL, and CP conducted the measurements at the ATTO site. JD, PA, HMJB, LATM, RB, YC, JWK, OOK, JM, and HSu contributed to the data analysis and interpretation through fruitful discussions and by providing valuable comments and ideas. All the authors contributed to the interpretation of the results and writing of the paper.

Competing interests. The authors declare that they have no conflict of interest.

Disclaimer. This paper contains results of research conducted under the Technical/Scientific Cooperation Agreement between the National Institute for Amazonian Research, the State University of Amazonas, and the Max-Planck-Gesellschaft e.V.; the opinions expressed are the entire responsibility of the authors and not of the participating institutions.

Special issue statement. This article is part of the special issue "Amazon Tall Tower Observatory (ATTO) Special Issue". It is not associated with a conference.

Acknowledgements. We recognize the Max Planck Society, the Conselho Nacional de Desenvolvimento Científico e Tecnológico (CNPq, Brazil), and the Max Planck Graduate Center with the Johannes Gutenberg University Mainz (MPGC) for the financial support. We thank the entire ACRIDICON-CHUVA team for the fruitful scientific cooperation. Special thanks goes to the HALO pilots, Steffen Gemsa, Michael Grossrubatscher, and Stefan Grillenbeck. We thank Volker Dreiling, the Sensor and Data Team of DLR Flight Experiments, and the HALO team of the DLR for their cooperation. We acknowledge the generous support of the ACRIDICON-CHUVA campaign by the Max Planck Society, the German Aerospace Center (DLR), FAPESP (São Paulo Research Foundation), and the German Science Foundation (Deutsche Forschungsgemeinschaft, DFG) within the DFG Priority Program "Atmospheric and Earth System Research with the Research Aircraft HALO (High Altitude and Long Range Research Aircraft)". Bernadett Weinzierl, Maximilian Dollner, and Adrian Walser would like to acknowledge funding from the European Research Council under the European Community's Horizon 2020 research and innovation framework program/ERC grant agreement 640458 (A-LIFE). Paulo Artaxo acknowledges FAPESP (Fundação de Amparo à Pesquisa do Estado de São Paulo) grant 2017/17047-0. Marco A. Franco acknowledges the scholarship from CNPq, project 169842/2017-7, for supporting his PhD studies at the University of São Paulo, São Paulo, Brazil, and CAPES, project 88887.368025/2019-00, for supporting 6 months of a sandwich doctorate program at the Max Planck Institute for Chemisty, Mainz, Germany. For the operation of the ATTO site, we acknowledge the support by the Max Planck Society, the German Federal Ministry of Education and Research and the Brazilian Ministério da Ciência, Tecnologia e Inovação as well as the Amazon State University (UEA), FAPEAM, LBA/INPA, and SDS/CEUC/RDS-Uatumã. Special thanks for all the people involved in ATTO project, in particular Susan Trumbore, Carlos Alberto Quesada, Reiner Ditz, Stefan Wolff, Jürgen Kesselmeier, Antonio O. Manzi, Andrew Crozier, Thomas Disper, Alcides Camargo Ribeiro, Hermes Braga Xavier, Nagib Alberto de Castro Souza, Adir Vasconcelos Brandão, Amauri Rodriguês Perreira, Antonio Huxley Melo Nascimento, André Luiz Matos, Delano Campos, Fábio Jorge, Roberta Pereira de Souza, Bruno Takeshi, Wallace Rabelo Costa, Uwe Schultz, Karl Kübler, Olaf Kolle, Martin Hertel, Kerstin Hippler, and Steffen Schmidt. Remote sensing analyses and visualizations used in this study were produced with the Giovanni online data system, developed and maintained by the NASA GES DISC. We acknowledge the National Oceanic and Atmospheric Administration (NOAA) Air Resources Laboratory (ARL) for the HYSPLIT transport and dispersion model. We thank Arthur J. Sedlacek, Daniel Moran-Zuloaga, Maria Praß, Leslie Kremper, Tobias Könemann, Jan-David Förster, Björn Nillius, Anywhere Tsokankunku, and Oliver Lauer for their support and inspiring discussions.

Financial support. This research has been supported by the Max Planck Society, the Max Planck Graduate Center with the Johannes Gutenberg University Mainz (MPGC), the Bundesministerium für Bildung und Forschung (BMBF contracts 01LB1001A, 01LK1602A, 01LK1602B, and 01LG1205E), the Brazilian Ministério da Ciência, Tecnologia e Inovação (MCTI/FINEP contract 01.11.01248.00), the Conselho Nacional de Desenvolvimento Científico e Tecnológico (CNPq, Brazil) (process 200723/2015-4), the FAPESP (Fundação de Amparo à Pesquisa do Estado de São Paulo) (grant no. 2017/17047-0), the CNPq project (grant no. 169842/2017-7), the CAPES project (grant no. 88887.368025/2019-00), and the European Commission, H2020

Research Infrastructures (A-LIFE (grant no. 640458)). This study was also supported by EU Project HAIC under FP7-AAT-2012-3.5.1-1 and by the German Science Foundation within DFG SPP 1294 HALO by contract nos. VO1504/4-1, JU 3059/1-1 and SCHN1138/1-2.

The article processing charges for this open-access publication were covered by the Max Planck Society.

Review statement. This paper was edited by Gilberto Fisch and reviewed by two anonymous referees.

References

Adachi, K., Sedlacek, A. J., Kleinman, L., Chand, D., Hubbe, J. M., and Buseck, P. R.: Volume changes upon heating of aerosol particles from biomass burning using transmission electron microscopy, Aerosol Sci. Tech., 52, 46–56, https://doi.org/10.1080/02786826.2017.1373181, 2018.

Adebiyi, A. A. and Zuidema, P.: The role of the southern African easterly jet in modifying the southeast Atlantic aerosol and cloud environments, Q. J. Roy. Meteor. Soc., 142, 1574–1589, https://doi.org/10.1002/qj.2765, 2016.

Allen, A. G. and Miguel, A. H.: Biomass Burning in the Amazon: Characterization of the Ionic Component of Aerosols Generated from Flaming and Smoldering Rainforest and Savannah, Environ. Sci. Technol., 29, 486–493, https://doi.org/10.1021/es00002a026, 1995.

Andela, N. and van der Werf, G. R.: Recent trends in African fires driven by cropland expansion and El Niño to La Niña transition, Nat. Clim. Change, 4, 791–795, https://doi.org/10.1038/nclimate2313, 2014.

Anderson, G. P., Clough, S. A., Kneizys, F. X., Chetwynd, J. H., and Shettle, E. P.: AFGL (Air Force Geophysical Laboratory) atmospheric constituent profiles (0.120 km), Environmental research papers, USA, 1986.

Andreae, M. O.: Biomass burning: Its history, use and distribution and its impact on environmental quality and global climate, in: Global Biomass Burning: Atmospheric, Climatic and Biospheric Implications, edited by: Levine, J. S., 3–21, MIT Press, Cambridge, Mass., USA, 1991.

Andreae, M. O.: Emission of trace gases and aerosols from biomass burning – an updated assessment, Atmos. Chem. Phys., 19, 8523–8546, https://doi.org/10.5194/acp-19-8523-2019, 2019.

Andreae, M. O. and Gelencsér, A.: Black carbon or brown carbon? The nature of light-absorbing carbonaceous aerosols, Atmos. Chem. Phys., 6, 3131–3148, https://doi.org/10.5194/acp-6-3131-2006, 2006.

Andreae, M. O. and Merlet, P.: Emission of trace gases and aerosols from biomass burning, Global Biogeochem. Cy., 15, 955–966, https://doi.org/10.1029/2000GB001382, 2001.

Andreae, M. O. and Ramanathan, V.: Climate's Dark Forcings, Science, 340, 280–281, https://doi.org/10.1126/science.1235731, 2013.

Andreae, M. O., Browell, E. V., Garstang, M., Gregory, G. L., Harriss, R. C., Hill, G. F., Jacob, D. J., Pereira, M. C., Sachse, G. W., Setzer, A. W., Dias, P. L. S., Talbot, R. W., Torres, A. L., and Wofsy, S. C.: Biomass-burning emissions and associated haze layers over Amazonia, J. Geophys. Res., 93, 1509, https://doi.org/10.1029/JD093iD02p01509, 1988.

Andreae, M. O., Anderson, B. E., Blake, D. R., Bradshaw, J. D., Collins, J. E., Gregory, G. L., Sachse, G. W., and Shipham, M. C.: Influence of plumes from biomass burning on atmospheric chemistry over the equatorial and tropical South Atlantic during CITE 3, J. Geophys. Res., 99, 12793, https://doi.org/10.1029/94JD00263, 1994.

Andreae, M. O., Artaxo, P., Beck, V., Bela, M., Freitas, S., Gerbig, C., Longo, K., Munger, J. W., Wiedemann, K. T., and Wofsy, S. C.: Carbon monoxide and related trace gases and aerosols over the Amazon Basin during the wet and dry seasons, Atmos. Chem. Phys., 12, 6041–6065, https://doi.org/10.5194/acp-12-6041-2012, 2012.

Andreae, M. O., Acevedo, O. C., Araùjo, A., Artaxo, P., Barbosa, C. G. G., Barbosa, H. M. J., Brito, J., Carbone, S., Chi, X., Cintra, B. B. L., da Silva, N. F., Dias, N. L., Dias-Júnior, C. Q., Ditas, F., Ditz, R., Godoi, A. F. L., Godoi, R. H. M., Heimann, M., Hoffmann, T., Kesselmeier, J., Könemann, T., Krüger, M. L., Lavric, J. V., Manzi, A. O., Lopes, A. P., Martins, D. L., Mikhailov, E. F., Moran-Zuloaga, D., Nelson, B. W., Nölscher, A. C., Santos Nogueira, D., Piedade, M. T. F., Pöhlker, C., Pöschl, U., Quesada, C. A., Rizzo, L. V., Ro, C.-U., Ruckteschler, N., Sá, L. D. A., de Oliveira Sá, M., Sales, C. B., dos Santos, R. M. N., Saturno, J., Schöngart, J., Sörgel, M., de Souza, C. M., de Souza, R. A. F., Su, H., Targhetta, N., Tóta, J., Trebs, I., Trumbore, S., van Eijck, A., Walter, D., Wang, Z., Weber, B., Williams, J., Winderlich, J., Wittmann, F., Wolff, S., and Yáñez-Serrano, A. M.: The Amazon Tall Tower Observatory (ATTO): overview of pilot measurements on ecosystem ecology, meteorology, trace gases, and aerosols, Atmos. Chem. Phys., 15, 10723–10776, https://doi.org/10.5194/acp-15-10723-2015, 2015.

Andreae, M. O., Afchine, A., Albrecht, R., Holanda, B. A., Artaxo, P., Barbosa, H. M. J., Borrmann, S., Cecchini, M. A., Costa, A., Dollner, M., Fütterer, D., Järvinen, E., Jurkat, T., Klimach, T., Konemann, T., Knote, C., Krämer, M., Krisna, T., Machado, L. A. T., Mertes, S., Minikin, A., Pöhlker, C., Pöhlker, M. L., Pöschl, U., Rosenfeld, D., Sauer, D., Schlager, H., Schnaiter, M., Schneider, J., Schulz, C., Spanu, A., Sperling, V. B., Voigt, C., Walser, A., Wang, J., Weinzierl, B., Wendisch, M., and Ziereis, H.: Aerosol characteristics and particle production in the upper troposphere over the Amazon Basin, Atmos. Chem. Phys., 18, 921–961, https://doi.org/10.5194/acp-18-921-2018, 2018.

Anselmo, E. M., Shumacher, C., and Machado, L. A. T.: The Amazonian Low-level Jet and its Connection to Convective Cloud Propagation and Evolution, Mon. Weather Rev., submitted, 2020.

Ansmann, A., Baars, H., Tesche, M., Müller, D., Althausen, D., Engelmann, R., Pauliquevis, T., and Artaxo, P.: Dust and smoke transport from Africa to South America: Lidar profiling over Cape Verde and the Amazon rainforest, Geophys. Res. Lett., 36, L11802, https://doi.org/10.1029/2009GL037923, 2009.

Artaxo, P., Rizzo, L. V., Brito, J. F., Barbosa, H. M. J., Arana, A., Sena, E. T., Cirino, G. G., Bastos, W., Martin, S. T., and Andreae, M. O.: Atmospheric aerosols in Amazonia and land use change: from natural biogenic to biomass burning conditions, Faraday Discuss., 165, 203, https://doi.org/10.1039/c3fd00052d, 2013.

ATTO: ATTO data portal, available at: https://www.attodata.org/, last access: 17 April 2020.

Baars, H., Ansmann, A., Althausen, D., Engelmann, R., Artaxo, P., Pauliquevis, T., and Souza, R.: Further evidence for significant smoke transport from Africa to Amazonia, Geophys. Res. Lett., 38, L20802, https://doi.org/10.1029/2011GL049200, 2011.

Baehr, J.: Aircraft observations of NO, NO_y , CO, and O_3 in the upper troposphere from 60° N to 60° S – Interhemispheric differences at mitlatitudes, Geophys. Res. Lett., 30, 1598, https://doi.org/10.1029/2003GL016935, 2003.

Barbosa, P. M., Stroppiana, D., Grégoire, J.-M., and Cardoso Pereira, J. M.: An assessment of vegetation fire in Africa (1981–1991): Burned areas, burned biomass, and atmospheric emissions, Global Biogeochem. Cy., 13, 933–950, https://doi.org/10.1029/1999GB900042, 1999.

Barkley, A. E., Prospero, J. M., Mahowald, N., Hamilton, D. S., Popendorf, K. J., Oehlert, A. M., Pourmand, A., Gatineau, A., Panechou-Pulcherie, K., Blackwelder, P., and Gaston, C. J.: African biomass burning is a substantial source of phosphorus deposition to the Amazon, Tropical Atlantic Ocean, and Southern Ocean, P. Natl. Acad. Sci., 116, 16216–16221, https://doi.org/10.1073/pnas.1906091116, 2019.

Bond, T. C., Doherty, S. J., Fahey, D. W., Forster, P. M., Berntsen, T., Deangelo, B. J., Flanner, M. G., Ghan, S., Kärcher, B., Koch, D., Kinne, S., Kondo, Y., Quinn, P. K., Sarofim, M. C., Schultz, M. G., Schulz, M., Venkataraman, C., Zhang, H., Zhang, S., Bellouin, N., Guttikunda, S. K., Hopke, P. K., Jacobson, M. Z., Kaiser, J. W., Klimont, Z., Lohmann, U., Schwarz, J. P., Shindell, D., Storelvmo, T., Warren, S. G., and Zender, C. S.: Bounding the role of black carbon in the climate system: A scientific assessment, J. Geophys. Res.-Atmos., 118, 5380–5552, https://doi.org/10.1002/jgrd.50171, 2013.

Boucher, O., Randall, D., Artaxo, P., Bretherton, C., Feingold, G., Forster, P., Kerminen, V.-M., Kondo, Y., Liao, H., Lohmann, U., Rasch, P., Satheesh, S. K., Sherwood, S., Stevens, B., and Zhang, X. Y.: Clouds and Aerosols, in: Climate Change 2013: The Physical Science Basis. Contribution of Working Group I to the Fifth Assessment Report of the Intergovernmental Panel on Climate Change, edited by: Stocker, T. F., Qin, D., Plattner, G.-K., Tignor, M., Allen, S. K., Boschung, J., Nauels, A., Xia, Y., Bex, V., and Midgley, P. M., Cambridge University Press, Cambridge, UK and New York, NY, USA, 2013.

Boucher, O., Balkanski, Y., Hodnebrog, Ø., Myhre, C. L., Myhre, G., Quaas, J., Samset, B. H., Schutgens, N., Stier, P., and Wang, R.: Jury is still out on the radiative forcing by black carbon, P. Natl. Acad. Sci. USA, 113, E5092–E5093, https://doi.org/10.1073/pnas.1607005113, 2016.

Bozem, H., Fischer, H., Gurk, C., Schiller, C. L., Parchatka, U., Koenigstedt, R., Stickler, A., Martinez, M., Harder, H., Kubistin, D., Williams, J., Eerdekens, G., and Lelieveld, J.: Influence of corona discharge on the ozone budget in the tropical free troposphere: a case study of deep convection during GABRIEL, Atmos. Chem. Phys., 14, 8917–8931, https://doi.org/10.5194/acp-14-8917-2014, 2014.

Brioude, J., Cooper, O. R., Feingold, G., Trainer, M., Freitas, S. R., Kowal, D., Ayers, J. K., Prins, E., Minnis, P., McKeen, S. A., Frost, G. J., and Hsie, E.-Y.: Effect of biomass burning on marine stratocumulus clouds off the California coast, Atmos. Chem. Phys., 9, 8841–8856, https://doi.org/10.5194/acp-9-8841-2009, 2009.

Brito, J., Rizzo, L. V., Morgan, W. T., Coe, H., Johnson, B., Haywood, J., Longo, K., Freitas, S., Andreae, M. O., and Artaxo, P.: Ground-based aerosol characterization during the South American Biomass Burning Analysis (SAMBBA) field experiment, Atmos. Chem. Phys., 14, 12069–12083, https://doi.org/10.5194/acp-14-12069-2014, 2014.

Cai, Y., Montague, D. C., Mooiweer-Bryan, W., and Deshler, T.: Performance characteristics of the ultra high sensitivity aerosol spectrometer for particles between 55 and 800 nm: Laboratory and field studies, J. Aerosol Sci., 39, 759–769, https://doi.org/10.1016/j.jaerosci.2008.04.007, 2008.

Chen, Q., Farmer, D. K., Rizzo, L. V., Pauliquevis, T., Kuwata, M., Karl, T. G., Guenther, A., Allan, J. D., Coe, H., Andreae, M. O., Pöschl, U., Jimenez, J. L., Artaxo, P., and Martin, S. T.: Submicron particle mass concentrations and sources in the Amazonian wet season (AMAZE-08), Atmos. Chem. Phys., 15, 3687–3701, https://doi.org/10.5194/acp-15-3687-2015, 2015.

Cheng, T., Wu, Y., and Chen, H.: Effects of morphology on the radiative properties of internally mixed light absorbing carbon aerosols with different aging status, Opt. Express, 22, 15904, https://doi.org/10.1364/OE.22.015904, 2014.

Clarke, A. D.: A thermo-optic technique for in situ analysis of size-resolved aerosol physicochemistry, Atmos. Environ. A-Gen., 25, 635–644, https://doi.org/10.1016/0960-1686(91)90061-B, 1991.

Colarco, P., Silva, A., Chin, M., and Diehl, T.: Online simulations of global aerosol distributions in the NASA GEOS 4 model and comparisons to satellite and ground – based aerosol optical depth, J. Geophys. Res.-Atmos., 115, D14207, https://doi.org/10.1029/2009JD012820, 2010.

Cubison, M. J., Ortega, A. M., Hayes, P. L., Farmer, D. K., Day, D., Lechner, M. J., Brune, W. H., Apel, E., Diskin, G. S., Fisher, J. A., Fuelberg, H. E., Hecobian, A., Knapp, D. J., Mikoviny, T., Riemer, D., Sachse, G. W., Sessions, W., Weber, R. J., Weinheimer, A. J., Wisthaler, A., and Jimenez, J. L.: Effects of aging on organic aerosol from open biomass burning smoke in aircraft and laboratory studies, Atmos. Chem. Phys., 11, 12049–12064, https://doi.org/10.5194/acp-11-12049-2011, 2011.

Dajuma, A., Ogunjobi, K. O., Vogel, H., Knippertz, P., Silué, S., N'Datchoh, E. T., Yoboué, V., and Vogel, B.: Cloud-venting induced downward mixing of the Central African biomass burning plume during the West Africa summer monsoon, Atmos. Chem. Phys. Discuss., https://doi.org/10.5194/acp-2019-617, in review, 2019.

Darbyshire, E., Morgan, W. T., Allan, J. D., Liu, D., Flynn, M. J., Dorsey, J. R., O'Shea, S. J., Lowe, D., Szpek, K., Marenco, F., Johnson, B. T., Bauguitte, S., Haywood, J. M., Brito, J. F., Artaxo, P., Longo, K. M., and Coe, H.: The vertical distribution of biomass burning pollution over tropical South America from aircraft in situ measurements during SAMBBA, Atmos. Chem. Phys., 19, 5771–5790, https://doi.org/10.5194/acp-19-5771-2019, 2019.

Das, S., Harshvardhan, H., Bian, H., Chin, M., Curci, G., Protonotariou, A. P., Mielonen, T., Zhang, K., Wang, H., and Liu, X.: Biomass burning aerosol transport and vertical distribution over the South African-Atlantic region, J. Geophys. Res.-Atmos., 122, 6391–6415, https://doi.org/10.1002/2016JD026421, 2017.

Denjean, C., Bourrianne, T., Burnet, F., Mallet, M., Maury, N., Colomb, A., Dominutti, P., Brito, J., Dupuy, R., Sellegri, K., Schwarzenboeck, A., Flamant, C., and Knippertz, P.: Light ab-

sorption properties of aerosols over Southern West Africa, Atmos. Chem. Phys. Discuss., https://doi.org/10.5194/acp-2019-587, in review, 2019.

de Sá, S. S., Rizzo, L. V., Palm, B. B., Campuzano-Jost, P., Day, D. A., Yee, L. D., Wernis, R., Isaacman-VanWertz, G., Brito, J., Carbone, S., Liu, Y. J., Sedlacek, A., Springston, S., Goldstein, A. H., Barbosa, H. M. J., Alexander, M. L., Artaxo, P., Jimenez, J. L., and Martin, S. T.: Contributions of biomass-burning, urban, and biogenic emissions to the concentrations and light-absorbing properties of particulate matter in central Amazonia during the dry season, Atmos. Chem. Phys., 19, 7973–8001, https://doi.org/10.5194/acp-19-7973-2019, 2019.

Diab, R. D., Thompson, A. M., Zunckel, M., Coetzee, G. J. R., Combrink, J., Bodeker, G. E., Fishman, J., Sokolic, F., McNamara, D. P., Archer, C. B., and Nganga, D.: Vertical ozone distribution over southern Africa and adjacent oceans during SAFARI-92, J. Geophys. Res.-Atmos., 101, 23823–23833, https://doi.org/10.1029/96JD01267, 1996.

Ditas, J., Ma, N., Zhang, Y., Assmann, D., Neumaier, M., Riede, H., and Karu, E.: Strong impact of wildfires on the abundance and aging of black carbon in the lowermost stratosphere, P. Natl. Acad. Sci. USA, 115, E11595–E11603, https://doi.org/10.1073/pnas.1806868115, 2018.

DLR: Halo database, available at: https://halo-db.pa.op.dlr.de/, last access: 17 April 2020.

Drewnick, F., Hings, S. S., DeCarlo, P., Jayne, J. T., Gonin, M., Fuhrer, K., Weimer, S., Jimenez, J. L., Demerjian, K. L., Borrmann, S., and Worsnop, D. R.: A New Time-of-Flight Aerosol Mass Spectrometer (TOF-AMS)–Instrument Description and First Field Deployment, Aerosol Sci. Tech., 39, 637–658, https://doi.org/10.1080/02786820500182040, 2005.

Earl, N., Simmonds, I., and Tapper, N.: Weekly cycles of global fires-Associations with religion, wealth and culture, and insights into anthropogenic influences on global climate, Geophys. Res. Lett., 42, 9579–9589, https://doi.org/10.1002/2015GL066383, 2015.

Emde, C., Buras-Schnell, R., Kylling, A., Mayer, B., Gasteiger, J., Hamann, U., Kylling, J., Richter, B., Pause, C., Dowling, T., and Bugliaro, L.: The libRadtran software package for radiative transfer calculations (version 2.0.1), Geosci. Model Dev., 9, 1647–1672, https://doi.org/10.5194/gmd-9-1647-2016, 2016.

Evans, K. F.: The Spherical Harmonics Discrete Ordinate Method for Three-Dimensional Atmospheric Radiative Transfer, J. Atmos. Sci., 55, 429–446, https://doi.org/10.1175/1520-0469(1998)055<0429:TSHDOM>2.0.CO;2, 1998.

Flamant, C., Knippertz, P., Fink, A. H., Akpo, A., Brooks, B., Chiu, C. J., Coe, H., Danuor, S., Evans, M., Jegede, O., Kalthoff, N., Konaré, A., Liousse, C., Lohou, F., Mari, C., Schlager, H., Schwarzenboeck, A., Adler, B., Amekudzi, L., Aryee, J., Ayoola, M., Batenburg, A. M., Bessardon, G., Borrmann, S., Brito, J., Bower, K., Burnet, F., Catoire, V., Colomb, A., Denjean, C., Fosu-Amankwah, K., Hill, P. G., Lee, J., Lothon, M., Maranan, M., Marsham, J., Meynadier, R., Ngamini, J.-B., Rosenberg, P., Sauer, D., Smith, V., Stratmann, G., Taylor, J. W., Voigt, C., and Yoboué, V.: The Dynamics–Aerosol–Chemistry–Cloud Interactions in West Africa Field Campaign: Overview and Research Highlights, B. Am. Meteorol. Soc., 99, 83–104, https://doi.org/10.1175/BAMS-D-16-0256.1, 2018.

Fleming, L. T., Lin, P., Roberts, J. M., Selimovic, V., Yokelson, R., Laskin, J., Laskin, A., and Nizkorodov, S. A.: Molecular composition and photochemical lifetimes of brown carbon chromophores in biomass burning organic aerosol, Atmos. Chem. Phys., 20, 1105–1129, https://doi.org/10.5194/acp-20-1105-2020, 2020.

Fuller, K. A., Malm, W. C., and Kreidenweis, S. M.: Effects of mixing on extinction by carbonaceous particles, J. Geophys. Res.-Atmos., 104, 15941–15954, https://doi.org/10.1029/1998JD100069, 1999.

Fuzzi, S., Andreae, M. O., Huebert, B. J., Kulmala, M., Bond, T. C., Boy, M., Doherty, S. J., Guenther, A., Kanakidou, M., Kawamura, K., Kerminen, V.-M., Lohmann, U., Russell, L. M., and Pöschl, U.: Critical assessment of the current state of scientific knowledge, terminology, and research needs concerning the role of organic aerosols in the atmosphere, climate, and global change, Atmos. Chem. Phys., 6, 2017–2038, https://doi.org/10.5194/acp-6-2017-2006, 2006.

Gerbig, C., Schmitgen, S., Kley, D., Volz-Thomas, A., Dewey, K., and Haaks, D.: An improved fast-response vacuum-UV resonance fluorescence CO instrument, J. Geophys. Res.-Atmos., 104, 1699–1704, https://doi.org/10.1029/1998JD100031, 1999.

Grieshop, A. P., Logue, J. M., Donahue, N. M., and Robinson, A. L.: Laboratory investigation of photochemical oxidation of organic aerosol from wood fires 1: measurement and simulation of organic aerosol evolution, Atmos. Chem. Phys., 9, 1263–1277, https://doi.org/10.5194/acp-9-1263-2009, 2009.

Gueymard, C. A.: The sun's total and spectral irradiance for solar energy applications and solar radiation models, Sol. Energy, 76, 423–453, https://doi.org/10.1016/j.solener.2003.08.039, 2004.

Guyon, P., Frank, G. P., Welling, M., Chand, D., Artaxo, P., Rizzo, L., Nishioka, G., Kolle, O., Fritsch, H., Silva Dias, M. A. F., Gatti, L. V., Cordova, A. M., and Andreae, M. O.: Airborne measurements of trace gas and aerosol particle emissions from biomass burning in Amazonia, Atmos. Chem. Phys., 5, 2989–3002, https://doi.org/10.5194/acp-5-2989-2005, 2005.

Hegg, D. A., Radke, L. F., and Hobbs, P. V.: Particle production associated with marine clouds, J. Geophys. Res., 95, 13917, https://doi.org/10.1029/JD095iD09p13917, 1990.

Heintzenberg, J.: Properties of the Log-Normal Particle Size Distribution, Aerosol Sci. Tech., 21, 46–48, https://doi.org/10.1080/02786829408959695, 1994.

Hobbs, P. V.: Clean air slots amid dense atmospheric pollution in southern Africa, J. Geophys. Res., 108, 1–8, https://doi.org/10.1029/2002JD002156, 2003.

Holanda, B., Pöhlker, C., Pöhlker, M., and Lavrič, J.: ATTO and HALO data related to Holanda et al 2020, Max Planck Society, https://doi.org/10.17617/3.3r, 2020a.

Holanda, B., Pöhlker, C., and Walter, D.: Fire contact of ATTO backward trajectories, Max Planck Society, https://doi.org/10.17617/3.3q, 2020b.

Holben, B. N., Eck, T. F., Slutsker, I., Tanré, D., Buis, J. P., Setzer, A., Vermote, E., Reagan, J. A., Kaufman, Y. J., Nakajima, T., Lavenu, F., Jankowiak, I., and Smirnov, A.: AERONET – A Federated Instrument Network and Data Archive for Aerosol Characterization, Remote Sens. Environ., 66, 1–16, https://doi.org/10.1016/S0034-4257(98)00031-5, 1998.

Ichoku, C. and Ellison, L.: Global top-down smoke-aerosol emissions estimation using satellite fire radiative power

measurements, Atmos. Chem. Phys., 14, 6643–6667, https://doi.org/10.5194/acp-14-6643-2014, 2014.

IPCC: Climate Change 2013: The Physical Science Basis, Contribution of Working Group I to the Fifth Assessment Report of the Intergovernmental Panel on Climate Change, edited by: Stocker, T. F., Qin, D., Plattner, G.-K., Tignor, M., Allen, S. K., Boschung, J., Nauels, A., Xia, Y., Bex, V., and Midgley, P. M., Cambridge University Press, Cambridge, UK, New York, NY, USA, 1535 pp., 2013.

Isaacman-VanWertz, G., Massoli, P., O'Brien, R., Lim, C., Franklin, J. P., Moss, J. A., Hunter, J. F., Nowak, J. B., Canagaratna, M. R., Misztal, P. K., Arata, C., Roscioli, J. R., Herndon, S. T., Onasch, T. B., Lambe, A. T., Jayne, J. T., Su, L., Knopf, D. A., Goldstein, A. H., Worsnop, D. R., and Kroll, J. H.: Chemical evolution of atmospheric organic carbon over multiple generations of oxidation, Nat. Chem., 10, 462–468, https://doi.org/10.1038/s41557-018-0002-2, 2018.

Jen, C. N., Hatch, L. E., Selimovic, V., Yokelson, R. J., Weber, R., Fernandez, A. E., Kreisberg, N. M., Barsanti, K. C., and Goldstein, A. H.: Speciated and total emission factors of particulate organics from burning western US wildland fuels and their dependence on combustion efficiency, Atmos. Chem. Phys., 19, 1013–1026, https://doi.org/10.5194/acp-19-1013-2019, 2019.

Kaiser, J. W., Heil, A., Andreae, M. O., Benedetti, A., Chubarova, N., Jones, L., Morcrette, J.-J., Razinger, M., Schultz, M. G., Suttie, M., and van der Werf, G. R.: Biomass burning emissions estimated with a global fire assimilation system based on observed fire radiative power, Biogeosciences, 9, 527–554, https://doi.org/10.5194/bg-9-527-2012, 2012.

Kerminen, V.-M., Chen, X., Vakkari, V., Petäjä, T., Kulmala, M., and Bianchi, F.: Atmospheric new particle formation and growth: review of field observations, Environ. Res. Lett., 13, 103003, https://doi.org/10.1088/1748-9326/aadf3c, 2018.

Kirchhoff, V. W. J. H., Hilsenrath, E., Motta, A. G., Sahai, Y., and Medrano-B, R. A.: Equatorial ozone characteristics as measured at Natal (5.9° S, 35.2° W), J. Geophys. Res., 88, 6812, https://doi.org/10.1029/JC088iC11p06812, 1983.

Kirchhoff, V. W. J. H., Barnes, R. A., and Torres, A. L.: Ozone climatology at Natal, Brazil, from in situ ozonesonde data, J. Geophys. Res., 96, 10899, https://doi.org/10.1029/91JD01212, 1991.

Koch, D. and Del Genio, A. D.: Black carbon semi-direct effects on cloud cover: review and synthesis, Atmos. Chem. Phys., 10, 7685–7696, https://doi.org/10.5194/acp-10-7685-2010, 2010.

Konovalov, I. B., Beekmann, M., Berezin, E. V., Formenti, P., and Andreae, M. O.: Probing into the aging dynamics of biomass burning aerosol by using satellite measurements of aerosol optical depth and carbon monoxide, Atmos. Chem. Phys., 17, 4513–4537, https://doi.org/10.5194/acp-17-4513-2017, 2017.

Konovalov, I. B., Beekmann, M., Golovushkin, N. A., and Andreae, M. O.: Nonlinear behavior of organic aerosol in biomass burning plumes: a microphysical model analysis, Atmos. Chem. Phys., 19, 12091–12119, https://doi.org/10.5194/acp-19-12091-2019, 2019.

Krüger, M. L., Mertes, S., Klimach, T., Cheng, Y. F., Su, H., Schneider, J., Andreae, M. O., Pöschl, U., and Rose, D.: Assessment of cloud supersaturation by size-resolved aerosol particle and cloud condensation nuclei (CCN) measurements, Atmos. Meas. Tech., 7, 2615–2629, https://doi.org/10.5194/amt-7-2615-2014, 2014.

Laborde, M., Crippa, M., Tritscher, T., Jurányi, Z., Decarlo, P. F., Temime-Roussel, B., Marchand, N., Eckhardt, S., Stohl, A., Baltensperger, U., Prévôt, A. S. H., Weingartner, E., and Gysel, M.: Black carbon physical properties and mixing state in the European megacity Paris, Atmos. Chem. Phys., 13, 5831–5856, https://doi.org/10.5194/acp-13-5831-2013, 2013.

Lawson, D. R. and Winchester, J. W.: Sulfur, potassium, and phosphorus associations in aerosols from South American tropical rain forests, J. Geophys. Res., 84, 3723, https://doi.org/10.1029/JC084iC07p03723, 1979.

Levin, E. J. T., McMeeking, G. R., Carrico, C. M., Mack, L. E., Kreidenweis, S. M., Wold, C. E., Moosmüller, H., Arnott, W. P., Hao, W. M., Collett, J. L., and Malm, W. C.: Biomass burning smoke aerosol properties measured during Fire Laboratory at Missoula Experiments (FLAME), J. Geophys. Res., 115, D18210, https://doi.org/10.1029/2009JD013601, 2010.

Liu, D., Whitehead, J., Alfarra, M. R., Reyes-Villegas, E., Spracklen, D. V., Reddington, C. L., Kong, S., Williams, P. I., Ting, Y. C., Haslett, S., Taylor, J. W., Flynn, M. J., Morgan, W. T., McFiggans, G., Coe, H., and Allan, J. D.: Black-carbon absorption enhancement in the atmosphere determined by particle mixing state, Nat. Geosci., 10, 184–188, https://doi.org/10.1038/ngeo2901, 2017.

Logan, J. A. and Kirchhoff, V. W. J. H.: Seasonal variations of tropospheric ozone at Natal, Brazil, J. Geophys. Res.-Atmos., 91, 7875–7881, https://doi.org/10.1029/JD091iD07p07875, 1986.

Machado, L. A. T., Calheiros, A. J. P., Biscaro, T., Giangrande, S., Silva Dias, M. A. F., Cecchini, M. A., Albrecht, R., Andreae, M. O., Araujo, W. F., Artaxo, P., Borrmann, S., Braga, R., Burleyson, C., Eichholz, C. W., Fan, J., Feng, Z., Fisch, G. F., Jensen, M. P., Martin, S. T., Pöschl, U., Pöhlker, C., Pöhlker, M. L., Ribaud, J.-F., Rosenfeld, D., Saraiva, J. M. B., Schumacher, C., Thalman, R., Walter, D., and Wendisch, M.: Overview: Precipitation characteristics and sensitivities to environmental conditions during GoAmazon2014/5 and ACRIDICON-CHUVA, Atmos. Chem. Phys., 18, 6461–6482, https://doi.org/10.5194/acp-18-6461-2018, 2018.

Marenco, F., Johnson, B., Langridge, J. M., Mulcahy, J., Benedetti, A., Remy, S., Jones, L., Szpek, K., Haywood, J., Longo, K., and Artaxo, P.: On the vertical distribution of smoke in the Amazonian atmosphere during the dry season, Atmos. Chem. Phys., 16, 2155–2174, https://doi.org/10.5194/acp-16-2155-2016, 2016.

Martin, S. T., Andreae, M. O., Artaxo, P., Baumgardner, D., Chen, Q., Goldstein, A. H., Guenther, A., Heald, C. L., Mayol-Bracero, O. L., McMurry, P. H., Pauliquevis, T., Pöschl, U., Prather, K. A., Roberts, G. C., Saleska, S. R., Silva Dias, M. A., Spracklen, D. V., Swietlicki, E., and Trebs, I.: Sources and properties of Amazonian aerosol particles, Rev. Geophys., 48, RG2002, https://doi.org/10.1029/2008RG000280, 2010.

Martin, S. T., Artaxo, P., Machado, L., Manzi, A. O., Souza, R. A. F., Schumacher, C., Wang, J., Biscaro, T., Brito, J., Calheiros, A., Jardine, K., Medeiros, A., Portela, B., De Sá, S. S., Adachi, K., Aiken, A. C., Alblbrecht, R., Alexander, L., Andreae, M. O., Barbosa, H. M. J., Buseck, P., Chand, D., Comstmstmstock, J. M., Day, D. A., Dubey, M., Fan, J., Faststt, J., Fisch, G., Fortner, E., Giangrande, S., Gilllles, M., Goldststein, A. H., Guenther, A., Hubbe, J., Jensen, M., Jimenez, J. L., Keutstsch, F. N., Kim, S., Kuang, C., Laskskin, A., McKinney, K., Mei, F., Millller, M., Nascimento, R., Pauliquevis, T., Pekour, M., Peres, J., Petäjä, T.,

Pöhlklker, C., Pöschl, U., Rizzo, L., Schmid, B., Shilllling, J. E., Silva Dias, M. A., Smith, J. N., Tomlmlinson, J. M., Tóta, J., and Wendisch, M.: The green ocean amazon experiment (GOAMAZON2014/5) observes pollution affecting gases, aerosols, clouds, and rainfall over the rain forest, B. Am. Meteorol. Soc., 98, 981–997, https://doi.org/10.1175/BAMS-D-15-00221.1, 2017.

Moffet, R. C. and Prather, K. A.: In-situ measurements of the mixing state and optical properties of soot with implications for radiative forcing estimates, P. Natl. Acad. Sci. USA, 106, 11872–11877, https://doi.org/10.1073/pnas.0900040106, 2009.

Moran-Zuloaga, D., Ditas, F., Walter, D., Saturno, J., Brito, J., Carbone, S., Chi, X., Hrabě de Angelis, I., Baars, H., Godoi, R. H. M., Heese, B., Holanda, B. A., Lavrič, J. V., Martin, S. T., Ming, J., Pöhlker, M. L., Ruckteschler, N., Su, H., Wang, Y., Wang, Q., Wang, Z., Weber, B., Wolff, S., Artaxo, P., Pöschl, U., Andreae, M. O., and Pöhlker, C.: Long-term study on coarse mode aerosols in the Amazon rain forest with the frequent intrusion of Saharan dust plumes, Atmos. Chem. Phys., 18, 10055–10088, https://doi.org/10.5194/acp-18-10055-2018, 2018.

Olson, D. M., Dinerstein, E., Wikramanayake, E. D., Burgess, N. D., Powell, G. V. N., Underwood, E. C., D'amico, J. A., Itoua, I., Strand, H. E., Morrison, J. C., Loucks, C. J., Allnutt, T. F., Ricketts, T. H., Kura, Y., Lamoreux, J. F., Wettengel, W. W., Hedao, P., and Kassem, K. R.: Terrestrial Ecoregions of the World: A New Map of Life on Earth, Bioscience, 51, 933, https://doi.org/10.1641/0006-3568(2001)051[0933:teotwa]2.0.co;2, 2001.

Omar, A. H., Winker, D. M., Kittaka, C., Vaughan, M. A., Liu, Z., Hu, Y., Trepte, C. R., Rogers, R. R., Ferrare, R. A., Lee, K. P., Kuehn, R. E., and Hostetler, C. A.: The CALIPSO automated aerosol classification and lidar ratio selection algorithm, J. Atmos. Ocean. Tech., 26, 1994–2014, https://doi.org/10.1175/2009JTECHA1231.1, 2009.

Perry, K. D. and Hobbs, P. V.: Further evidence for particle nucleation in clear air adjacent to marine cumulus clouds, J. Geophys. Res., 99, 22803, https://doi.org/10.1029/94JD01926, 1994.

Pöhlker, C., Wiedemann, K. T., Sinha, B., Shiraiwa, M., Gunthe, S. S., Smith, M., Su, H., Artaxo, P., Chen, Q., Cheng, Y., Elbert, W., Gilles, M. K., Kilcoyne, A. L. D., Moffet, R. C., Weigand, M., Martin, S. T., Pöschl, U., and Andreae, M. O.: Biogenic Potassium Salt Particles as Seeds for Secondary Organic Aerosol in the Amazon, Science, 337, 1075–1078, https://doi.org/10.1126/science.1223264, 2012.

Pöhlker, C., Walter, D., Paulsen, H., Könemann, T., Rodríguez-Caballero, E., Moran-Zuloaga, D., Brito, J., Carbone, S., Degrendele, C., Després, V. R., Ditas, F., Holanda, B. A., Kaiser, J. W., Lammel, G., Lavrič, J. V., Ming, J., Pickersgill, D., Pöhlker, M. L., Praß, M., Löbs, N., Saturno, J., Sörgel, M., Wang, Q., Weber, B., Wolff, S., Artaxo, P., Pöschl, U., and Andreae, M. O.: Land cover and its transformation in the backward trajectory footprint region of the Amazon Tall Tower Observatory, Atmos. Chem. Phys., 19, 8425–8470, https://doi.org/10.5194/acp-19-8425-2019, 2019.

Pöhlker, M. L., Pöhlker, C., Ditas, F., Klimach, T., Hrabe de Angelis, I., Araújo, A., Brito, J., Carbone, S., Cheng, Y., Chi, X., Ditz, R., Gunthe, S. S., Kesselmeier, J., Könemann, T., Lavrič, J. V., Martin, S. T., Mikhailov, E., Moran-Zuloaga, D., Rose, D., Saturno, J., Su, H., Thalman, R., Walter, D., Wang, J., Wolff, S., Barbosa, H. M. J., Artaxo, P., Andreae, M. O., and Pöschl, U.: Long-term observations of cloud condensation nuclei in the Amazon rain forest – Part 1: Aerosol size distribution, hygroscopicity, and new model parametrizations for CCN prediction, Atmos. Chem. Phys., 16, 15709–15740, https://doi.org/10.5194/acp-16-15709-2016, 2016.

Pöhlker, M. L., Ditas, F., Saturno, J., Klimach, T., Hrabě de Angelis, I., Araùjo, A. C., Brito, J., Carbone, S., Cheng, Y., Chi, X., Ditz, R., Gunthe, S. S., Holanda, B. A., Kandler, K., Kesselmeier, J., Könemann, T., Krüger, O. O., Lavrič, J. V., Martin, S. T., Mikhailov, E., Moran-Zuloaga, D., Rizzo, L. V., Rose, D., Su, H., Thalman, R., Walter, D., Wang, J., Wolff, S., Barbosa, H. M. J., Artaxo, P., Andreae, M. O., Pöschl, U., and Pöhlker, C.: Long-term observations of cloud condensation nuclei over the Amazon rain forest – Part 2: Variability and characteristics of biomass burning, long-range transport, and pristine rain forest aerosols, Atmos. Chem. Phys., 18, 10289–10331, https://doi.org/10.5194/acp-18-10289-2018, 2018.

Pokhrel, R. P., Beamesderfer, E. R., Wagner, N. L., Langridge, J. M., Lack, D. A., Jayarathne, T., Stone, E. A., Stockwell, C. E., Yokelson, R. J., and Murphy, S. M.: Relative importance of black carbon, brown carbon, and absorption enhancement from clear coatings in biomass burning emissions, Atmos. Chem. Phys., 17, 5063–5078, https://doi.org/10.5194/acp-17-5063-2017, 2017.

Pöschl, U., Martin, S. T., Sinha, B., Chen, Q., Gunthe, S. S., Huffman, J. A., Borrmann, S., Farmer, D. K., Garland, R. M., Helas, G., Jimenez, J. L., King, S. M., Manzi, A., Mikhailov, E., Pauliquevis, T., Petters, M. D., Prenni, A. J., Roldin, P., Rose, D., Schneider, J., Su, H., Zorn, S. R., Artaxo, P., and Andreae, M. O.: Rainforest Aerosols as Biogenic Nuclei of Clouds and Precipitation in the Amazon, Science, 329, 1513–1516, https://doi.org/10.1126/science.1191056, 2010.

Reddington, C. L., Spracklen, D. V., Artaxo, P., Ridley, D. A., Rizzo, L. V., and Arana, A.: Analysis of particulate emissions from tropical biomass burning using a global aerosol model and long-term surface observations, Atmos. Chem. Phys., 16, 11083–11106, https://doi.org/10.5194/acp-16-11083-2016, 2016.

Reid, J. S., Koppmann, R., Eck, T. F., and Eleuterio, D. P.: A review of biomass burning emissions part II: intensive physical properties of biomass burning particles, Atmos. Chem. Phys., 5, 799–825, https://doi.org/10.5194/acp-5-799-2005, 2005.

Remer, L. A., Kaufman, Y. J., Tanré, D., Mattoo, S., Chu, D. A., Martins, J. V., Li, R.-R., Ichoku, C., Levy, R. C., Kleidman, R. G., Eck, T. F., Vermote, E., and Holben, B. N.: The MODIS Aerosol Algorithm, Products, and Validation, J. Atmos. Sci., 62, 947–973, https://doi.org/10.1175/JAS3385.1, 2005.

Rizzo, L. V., Artaxo, P., Müller, T., Wiedensohler, A., Paixão, M., Cirino, G. G., Arana, A., Swietlicki, E., Roldin, P., Fors, E. O., Wiedemann, K. T., Leal, L. S. M., and Kulmala, M.: Long term measurements of aerosol optical properties at a primary forest site in Amazonia, Atmos. Chem. Phys., 13, 2391–2413, https://doi.org/10.5194/acp-13-2391-2013, 2013.

Roberts, G. C.: Impact of biomass burning on cloud properties in the Amazon Basin, J. Geophys. Res., 108, 4062, https://doi.org/10.1029/2001JD000985, 2003.

Roberts, G. C. and Nenes, A.: A continuous-flow streamwise thermal-gradient CCN chamber for atmospheric measurements, Aerosol Sci. Tech., 39, 206–221, https://doi.org/10.1080/027868290913988, 2005.

Roberts, G. C., Andreae, M. O., Zhou, J., and Artaxo, P.: Cloud condensation nuclei in the Amazon Basin: "marine" conditions over a continent?, Geophys. Res. Lett., 28, 2807–2810, https://doi.org/10.1029/2000GL012585, 2001.

Rose, D., Gunthe, S. S., Mikhailov, E., Frank, G. P., Dusek, U., Andreae, M. O., and Pöschl, U.: Calibration and measurement uncertainties of a continuous-flow cloud condensation nuclei counter (DMT-CCNC): CCN activation of ammonium sulfate and sodium chloride aerosol particles in theory and experiment, Atmos. Chem. Phys., 8, 1153–1179, https://doi.org/10.5194/acp-8-1153-2008, 2008.

Saturno, J., Ditas, F., Penning de Vries, M., Holanda, B. A., Pöhlker, M. L., Carbone, S., Walter, D., Bobrowski, N., Brito, J., Chi, X., Gutmann, A., Hrabe de Angelis, I., Machado, L. A. T., Moran-Zuloaga, D., Rüdiger, J., Schneider, J., Schulz, C., Wang, Q., Wendisch, M., Artaxo, P., Wagner, T., Pöschl, U., Andreae, M. O., and Pöhlker, C.: African volcanic emissions influencing atmospheric aerosols over the Amazon rain forest, Atmos. Chem. Phys., 18, 10391–10405, https://doi.org/10.5194/acp-18-10391-2018, 2018a.

Saturno, J., Holanda, B. A., Pöhlker, C., Ditas, F., Wang, Q., Moran-Zuloaga, D., Brito, J., Carbone, S., Cheng, Y., Chi, X., Ditas, J., Hoffmann, T., Hrabe de Angelis, I., Könemann, T., Lavrič, J. V., Ma, N., Ming, J., Paulsen, H., Pöhlker, M. L., Rizzo, L. V., Schlag, P., Su, H., Walter, D., Wolff, S., Zhang, Y., Artaxo, P., Pöschl, U., and Andreae, M. O.: Black and brown carbon over central Amazonia: long-term aerosol measurements at the ATTO site, Atmos. Chem. Phys., 18, 12817–12843, https://doi.org/10.5194/acp-18-12817-2018, 2018b.

Schill, G. P., Froyd, K. D., Bian, H., Brock, C. B., Ray, E., Hornbrook, R. S., Hills, A. J., Apel, E. C., Chen, M., Colarco, P., and Murphy, D. M.: The ubiquity of dilute, aged smoke in the global remote troposphere and its effect on climate, Nat. Geosci., in preparation, 2019.

Schnaiter, M.: Absorption amplification of black carbon internally mixed with secondary organic aerosol, J. Geophys. Res., 110, D19204, https://doi.org/10.1029/2005JD006046, 2005.

Schneider, J., Freutel, F., Zorn, S. R., Chen, Q., Farmer, D. K., Jimenez, J. L., Martin, S. T., Artaxo, P., Wiedensohler, A., and Borrmann, S.: Mass-spectrometric identification of primary biological particle markers and application to pristine submicron aerosol measurements in Amazonia, Atmos. Chem. Phys., 11, 11415–11429, https://doi.org/10.5194/acp-11-11415-2011, 2011.

Schulz, C., Schneider, J., Amorim Holanda, B., Appel, O., Costa, A., de Sá, S. S., Dreiling, V., Fütterer, D., Jurkat-Witschas, T., Klimach, T., Knote, C., Krämer, M., Martin, S. T., Mertes, S., Pöhlker, M. L., Sauer, D., Voigt, C., Walser, A., Weinzierl, B., Ziereis, H., Zöger, M., Andreae, M. O., Artaxo, P., Machado, L. A. T., Pöschl, U., Wendisch, M., and Borrmann, S.: Aircraft-based observations of isoprene-epoxydiol-derived secondary organic aerosol (IEPOX-SOA) in the tropical upper troposphere over the Amazon region, Atmos. Chem. Phys., 18, 14979–15001, https://doi.org/10.5194/acp-18-14979-2018, 2018.

Schwarz, J. P., Gao, R. S., Fahey, D. W., Thomson, D. S., Watts, L. A., Wilson, J. C., Reeves, J. M., Darbeheshti, M., Baumgardner, D. G., Kok, G. L., Chung, S. H., Schulz, M., Hendricks, J., Lauer, A., Kärcher, B., Slowik, J. G., Rosenlof, K. H., Thompson, T. L., Langford, A. O., Loewenstein, M., and Aikin, K. C.: Single-particle measurements of midlatitude black carbon and light-scattering aerosols from the boundary layer to the lower stratosphere, J. Geophys. Res.-Atmos., 111, 1–15, https://doi.org/10.1029/2006JD007076, 2006.

Schwarz, J. P., Gao, R. S., Spackman, J. R., Watts, L. A., Thomson, D. S., Fahey, D. W., Ryerson, T. B., Peischl, J., Holloway, J. S., Trainer, M., Frost, G. J., Baynard, T., Lack, D. A., de Gouw, J. A., Warneke, C., and Del Negro, L. A.: Measurement of the mixing state, mass, and optical size of individual black carbon particles in urban and biomass burning emissions, Geophys. Res. Lett., 35, 1–5, https://doi.org/10.1029/2008GL033968, 2008.

Shrivastava, M., Andreae, M. O., Artaxo, P., Barbosa, H. M. J., Berg, L. K., Brito, J., Ching, J., Easter, R. C., Fan, J., Fast, J. D., Feng, Z., Fuentes, J. D., Glasius, M., Goldstein, A. H., Alves, E. G., Gomes, H., Gu, D., Guenther, A., Jathar, S. H., Kim, S., Liu, Y., Lou, S., Martin, S. T., McNeill, V. F., Medeiros, A., de Sá, S. S., Shilling, J. E., Springston, S. R., Souza, R. A. F., Thornton, J. A., Isaacman-VanWertz, G., Yee, L. D., Ynoue, R., Zaveri, R. A., Zelenyuk, A., and Zhao, C.: Urban pollution greatly enhances formation of natural aerosols over the Amazon rainforest, Nat. Commun., 10, 1046, https://doi.org/10.1038/s41467-019-08909-4, 2019.

Slowik, J. G., Wong, J. P. S., and Abbatt, J. P. D.: Real-time, controlled OH-initiated oxidation of biogenic secondary organic aerosol, Atmos. Chem. Phys., 12, 9775–9790, https://doi.org/10.5194/acp-12-9775-2012, 2012.

Stamnes, K., Tsay, S.-C., Wiscombe, W., and Laszlo, I.: DISORT, A General-Purpose Fortran Program for Discrete Ordinate-Method Radiative Transfer in Scattering and Emitting Layered Media: Documentation of Methodology, Tech. rep., Dept. of Physics and Engineering Physics, Stevens Institute of Technology, Hoboken, NJ 07030, 2000.

Stein, A. F., Draxler, R. R., Rolph, G. D., Stunder, B. J. B., Cohen, M. D., and Ngan, F.: NOAA's HYSPLIT Atmospheric Transport and Dispersion Modeling System, B. Am. Meteorol. Soc., 96, 2059–2077, https://doi.org/10.1175/BAMS-D-14-00110.1, 2015.

Stephens, M., Turner, N., and Sandberg, J.: Particle identification by laser-induced incandescence in a solid-state laser cavity, Appl. Optics, 42, 3726–36, https://doi.org/10.1364/AO.42.003726, 2003.

Swap, R., Garstang, M., Greco, S., Talbot, R., and Kallberg, P.: Saharan dust in the Amazon Basin, Tellus B, 44, 133–149, https://doi.org/10.1034/j.1600-0889.1992.t01-1-00005.x, 1992.

Talbot, R. W., Andreae, M. O., Berresheim, H., Artaxo, P., Garstang, M., Harriss, M., Beecher, K. M., and Li, S.-M.: Aerosol Chemistry During the Wet Season in Central Amazonia?: The Influence of Long-Range Transport, J. Geophys. Res., 95, 16955–16969, 1990.

Thompson, A. M., Diab, R. D., Bodeker, G. E., Zunckel, M., Coetzee, G. J. R., Archer, C. B., McNamara, D. P., Pickering, K. E., Combrink, J., Fishman, J., and Nganga, D.: Ozone over southern Africa during SAFARI-92/TRACE A, J. Geophys. Res.-Atmos., 101, 23793–23807, https://doi.org/10.1029/95JD02459, 1996.

Tritscher, T., Jurányi, Z., Martin, M., Chirico, R., Gysel, M., Heringa, M. F., DeCarlo, P. F., Sierau, B., Prévôt, A. S. H., Weingartner, E., and Baltensperger, U.: Changes of hygroscopicity and morphology during ageing of diesel soot, Environ. Res. Lett., 6, 034026, https://doi.org/10.1088/1748-9326/6/3/034026, 2011.

Wang, Q., Saturno, J., Chi, X., Walter, D., Lavric, J. V., Moran-Zuloaga, D., Ditas, F., Pöhlker, C., Brito, J., Carbone, S., Artaxo, P., and Andreae, M. O.: Modeling investigation of light-absorbing aerosols in the Amazon Basin during the wet season, Atmos. Chem. Phys., 16, 14775–14794, https://doi.org/10.5194/acp-16-14775-2016, 2016.

Weinzierl, B., Sauer, D., Esselborn, M., Petzold, A., Veira, A., Rose, M., Mund, S., Wirth, M., Ansmann, A., Tesche, M., Gross, S., and Freudenthaler, V.: Microphysical and optical properties of dust and tropical biomass burning aerosol layers in the Cape Verde region-an overview of the airborne in situ and lidar measurements during SAMUM-2, Tellus B, 63, 589–618, https://doi.org/10.1111/j.1600-0889.2011.00566.x, 2011.

Wendisch, M., Pöschl, U., Andreae, M. O., MacHado, L. A. T., Albrecht, R., Schlager, H., Rosenfeld, D., Martin, S. T., Abdelmonem, A., Afchine, A., Araujo, A. C., Artaxo, P., Aufmhoff, H., Barbosa, H. M. J., Borrmann, S., Braga, R., Buchholz, B., Cecchini, M. A., Costa, A., Curtius, J., Dollner, M., Dorf, M., Dreiling, V., Ebert, V., Ehrlich, A., Ewald, F., Fisch, G., Fix, A., Frank, F., Futterer, D., Heckl, C., Heidelberg, F., Huneke, T., Jakel, E., Jarvinen, E., Jurkat, T., Kanter, S., Kastner, U., Kenntner, M., Kesselmeier, J., Klimach, T., Knecht, M., Kohl, R., Kolling, T., Kramer, M., Kruger, M., Krisna, T. C., Lavric, J. V., Longo, K., Mahnke, C., Manzi, A. O., Mayer, B., Mertes, S., Minikin, A., Molleker, S., Munch, S., Nillius, B., Pfeilsticker, K., Pohlker, C., Roiger, A., Rose, D., Rosenow, D., Sauer, D., Schnaiter, M., Schneider, J., Schulz, C., De Souza, R. A. F., Spanu, A., Stock, P., Vila, D., Voigt, C., Walser, A., Walter, D., Weigel, R., Weinzierl, B., Werner, F., Yamasoe, M. A., Ziereis, H., Zinner, T., and Zoger, M.: Acridicon-chuva campaign: Studying tropical deep convective clouds and precipitation over amazonia using the New German research aircraft HALO, B. Am. Meteorol. Soc., 97, 1885–1908, https://doi.org/10.1175/BAMS-D-14-00255.1, 2016.

van der Werf, G. R., Randerson, J. T., Giglio, L., van Leeuwen, T. T., Chen, Y., Rogers, B. M., Mu, M., van Marle, M. J. E., Morton, D. C., Collatz, G. J., Yokelson, R. J., and Kasibhatla, P. S.: Global fire emissions estimates during 1997–2016, Earth Syst. Sci. Data, 9, 697–720, https://doi.org/10.5194/essd-9-697-2017, 2017.

Willis, M. D., Healy, R. M., Riemer, N., West, M., Wang, J. M., Jeong, C.-H., Wenger, J. C., Evans, G. J., Abbatt, J. P. D., and Lee, A. K. Y.: Quantification of black carbon mixing state from traffic: implications for aerosol optical properties, Atmos. Chem. Phys., 16, 4693–4706, https://doi.org/10.5194/acp-16-4693-2016, 2016.

Winderlich, J., Chen, H., Gerbig, C., Seifert, T., Kolle, O., Lavrič, J. V., Kaiser, C., Höfer, A., and Heimann, M.: Continuous low-maintenance $CO_2/CH_4/H_2O$ measurements at the Zotino Tall Tower Observatory (ZOTTO) in Central Siberia, Atmos. Meas. Tech., 3, 1113–1128, https://doi.org/10.5194/amt-3-1113-2010, 2010.

Winker, D. M., Vaughan, M. A., Omar, A., Hu, Y., Powell, K. A., Liu, Z., Hunt, W. H., and Young, S. A.: Overview of the CALIPSO Mission and CALIOP Data Processing Algorithms, J. Atmos. Ocean. Tech., 26, 2310–2323, https://doi.org/10.1175/2009JTECHA1281.1, 2009.

Wong, J. P. S., Tsagkaraki, M., Tsiodra, I., Mihalopoulos, N., Violaki, K., Kanakidou, M., Sciare, J., Nenes, A., and Weber, R. J.: Atmospheric evolution of molecular-weight-separated brown carbon from biomass burning, Atmos. Chem. Phys., 19, 7319–7334, https://doi.org/10.5194/acp-19-7319-2019, 2019.

Wu, H., Taylor, J. W., Szpek, K., Langridge, J., Williams, P. I., Flynn, M., Allan, J. D., Abel, S. J., Pitt, J., Cotterell, M. I., Fox, C., Davies, N. W., Haywood, J., and Coe, H.: Vertical variability of the properties of highly aged biomass burning aerosol transported over the southeast Atlantic during CLARIFY-2017, Atmos. Chem. Phys. Discuss., https://doi.org/10.5194/acp-2020-197, in review, 2020.

Yasunari, T. J., Koster, R. D., Lau, K. M., Aoki, T., Sud, Y. C., Yamazaki, T., Motoyoshi, H., and Kodama, Y.: Influence of dust and black carbon on the snow albedo in the NASA Goddard Earth Observing System version 5 land surface model, J. Geophys. Res.-Atmos., 116, D02210, https://doi.org/10.1029/2010JD014861, 2011.

Zhang, J., Liu, J., Tao, S., and Ban-Weiss, G. A.: Long-range transport of black carbon to the Pacific Ocean and its dependence on aging timescale, Atmos. Chem. Phys., 15, 11521–11535, https://doi.org/10.5194/acp-15-11521-2015, 2015.

Zhou, S., Collier, S., Jaffe, D. A., Briggs, N. L., Hee, J., Sedlacek III, A. J., Kleinman, L., Onasch, T. B., and Zhang, Q.: Regional influence of wildfires on aerosol chemistry in the western US and insights into atmospheric aging of biomass burning organic aerosol, Atmos. Chem. Phys., 17, 2477–2493, https://doi.org/10.5194/acp-17-2477-2017, 2017.

Ziereis, H., Schlager, H., Schulte, P., van Velthoven, P. F. J., and Slemr, F.: Distributions of NO, NO_x, and NO_y in the upper troposphere and lower stratosphere between 28° and 61° N during POLINAT 2, J. Geophys. Res.-Atmos., 105, 3653–3664, https://doi.org/10.1029/1999JD900870, 2000.

Zuidema, P., Redemann, J., Haywood, J., Wood, R., Piketh, S., Hipondoka, M., and Formenti, P.: Smoke and Clouds above the Southeast Atlantic: Upcoming Field Campaigns Probe Absorbing Aerosol's Impact on Climate, B. Am. Meteorol. Soc., 97, 1131–1135, https://doi.org/10.1175/BAMS-D-15-00082.1, 2016.

Zuidema, P., Sedlacek, A. J., Flynn, C., Springston, S., Delgadillo, R., Zhang, J., Aiken, A. C., Koontz, A., and Muradyan, P.: The Ascension Island Boundary Layer in the Remote Southeast Atlantic is Often Smoky, Geophys. Res. Lett., 45, 4456–4465, https://doi.org/10.1002/2017GL076926, 2018.

Supplement of Atmos. Chem. Phys., 20, 4757–4785, 2020
https://doi.org/10.5194/acp-20-4757-2020-supplement

Atmospheric Chemistry and Physics Open Access

Supplement of

Influx of African biomass burning aerosol during the Amazonian dry season through layered transatlantic transport of black carbon-rich smoke

Bruna A. Holanda et al.

Correspondence to: Mira L. Pöhlker (m.pohlker@mpic.de) and Christopher Pöhlker (c.pohlker@mpic.de)

Table S1. List of time sections in which the UPL, CL, LPL MBL and BB were sampled during flight AC19.

	Time window	
Offshore profile	16:50:00	19:07:00
UPL	16:21:50	16:22:40
	16:54:22	16:55:02
	17:08:22	17:09:00
	18:02:46	18:03:09
	18:03:47	18:04:18
	18:10:35	18:12:15
	18:34:32	18:35:47
	18:42:51	18:43:39
	18:47:50	18:48:04
	19:58:00	19:58:39
CL	17:09:08	17:09:30
	18:02:04	18:02:39
	18:36:08	18:38:42
	18:40:16	18:42:44
	18:43:43	18:44:24
	18:47:21	18:47:43
LPL	16:52:03	16:53:18
	17:10:00	17:11:37
	17:56:43	17:57:16
	17:57:33	17:58:15
	17:58:31	18:00:08
	18:54:33	18:55:51
MBL	17:23:14	17:27:28
Fresh BB	19:24:03	19:24:37
	19:24:49	19:25:08
	19:25:44	19:27:02
	19:27:11	19:28:16
	19:30:09	19:30:46
	19:32:24	19:34:03
	19:18:24	19:18:45

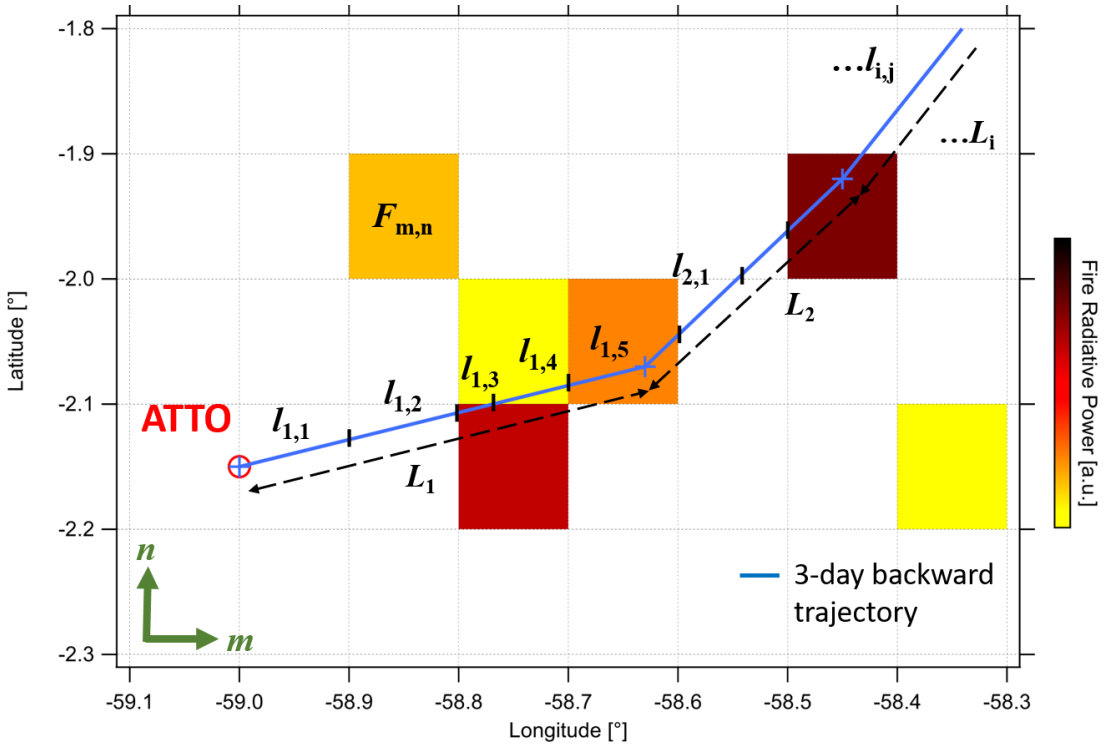

Figure S1. Sketch illustrating the initiation of a three-day BT starting at the ATTO site (red circle) mapped to the raster of fire intensities.

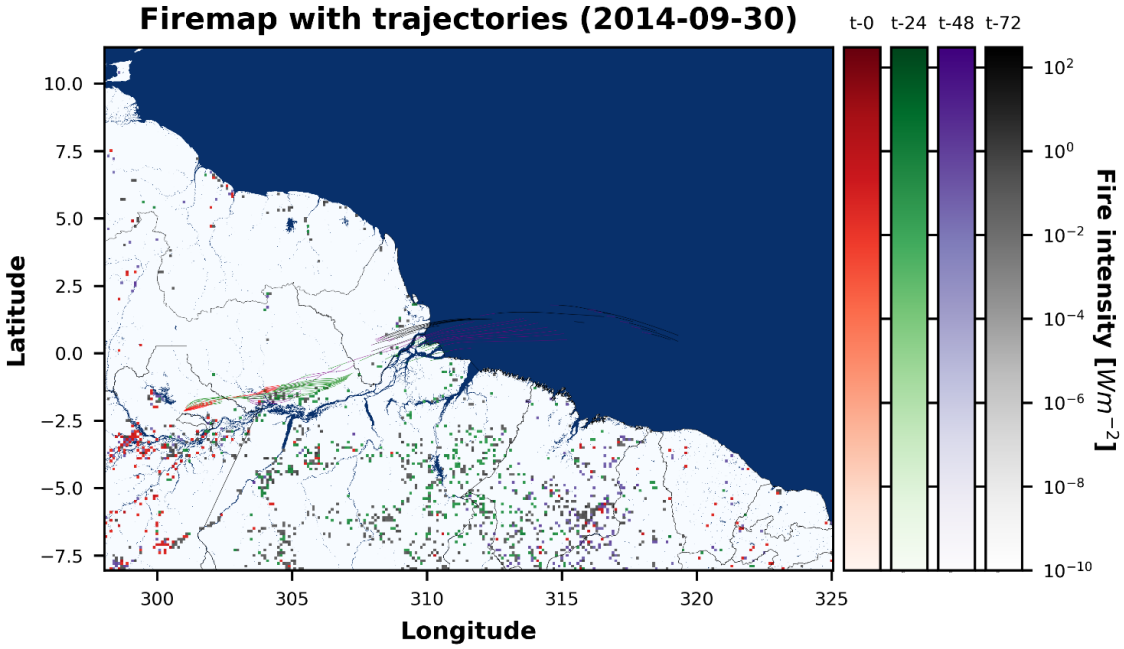

Figure S2. Ensemble of three-day HYSPLIT BTs, starting at every hour at the ATTO site (1000 m a.s.l.) on 30 September 2014 and corresponding daily fire intensity maps (W m^{-2}) from the Global Fire Assimilation System (GFAS).

Figure S3. View from the HALO cockpit, showing the active fire plumes (intersected at ~1 km above ground) during flight AC19 at 19:20 UTC on 30 September 2014. See also fire map in Fig. 1.

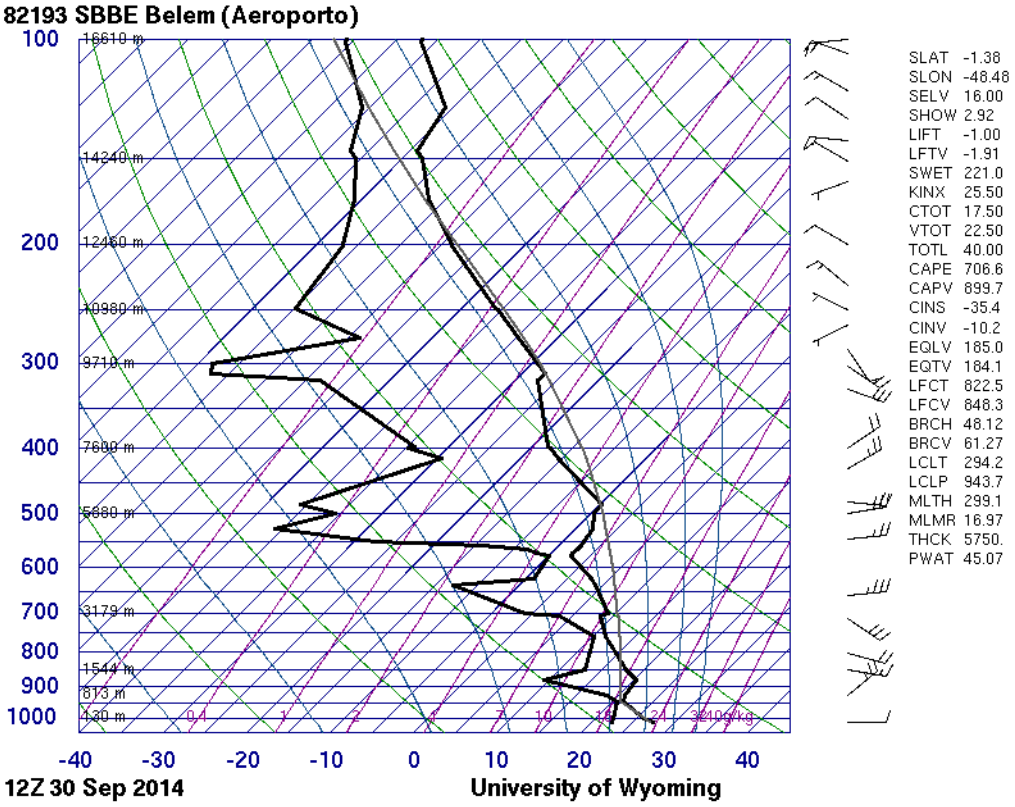

Figure S4. Radiosonde sounding at Belem Airport (see Fig 1.) on 30 September 2014 at 12:00 UTC, provided Wyoming University (http://weather.uwyo.edu/upperair/sounding.html, last access on 06 August 2019). The sounding shows similar tropospheric stratification as presented in Fig. 3. The first layer (top around 1000 m) is associated with the boundary layer, the second (top around 3200 m) is related to the shallow clouds top and the third one (around 5000 m) is the large scale inversion.

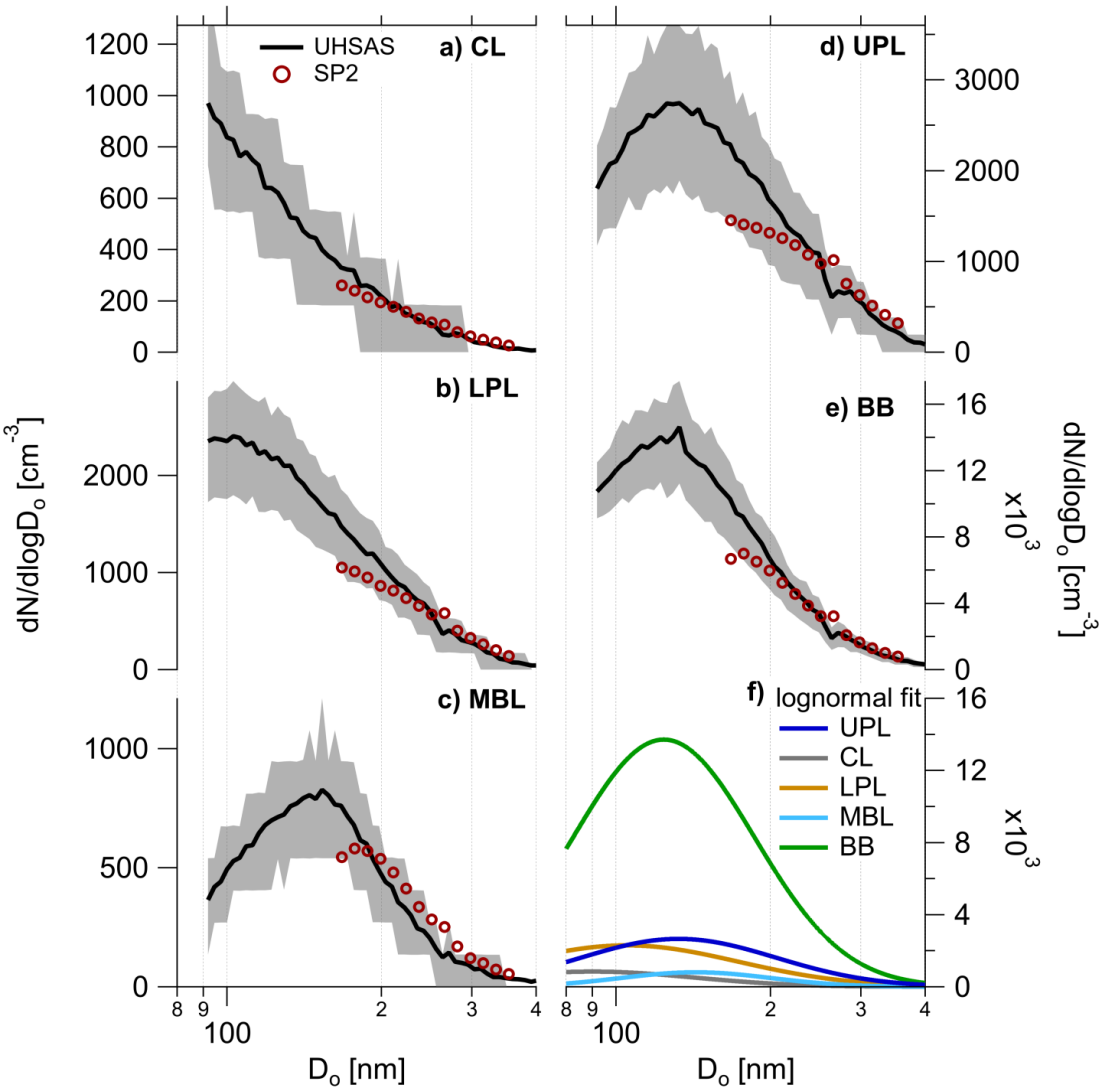

Figure S5. Particle number size distributions (median and interquartile range) derived from the UHSAS and SP2 (rBC + SC) for the **(a)** CL, **(b)** LPL, **(c)** MPL, **(d)** UPL and **(e)** fresh BB plume probed during flight AC19. Panel **(f)** shows the curve fits of the UHSAS data points.

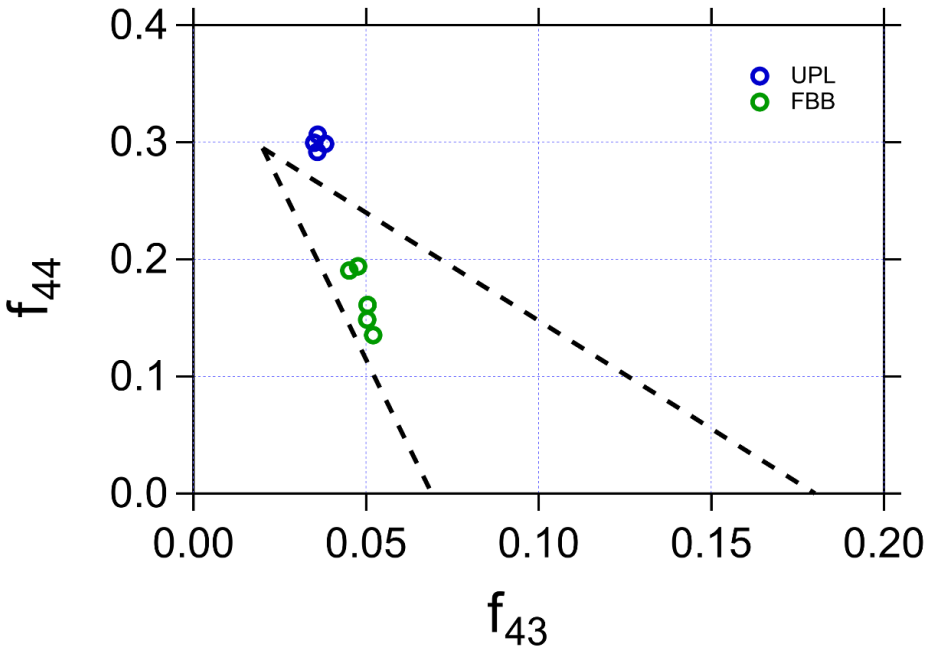

Figure S6. Scatterplot of the ratios f_{43} (m/z 43 to total organic signal) against f_{44} (m/z 44 to total organic signal) expressing the photochemical aging of the organic aerosol measured by the C-ToF-AMS. The blue and green markers correspond to measurements within the UPL and fresh BB, respectively. The signal at m/z 44 relates mostly to CO_2^+ ions and the m/z 43 signal to $C_2H_3O^+$ ions. The triangular region (dashed lines) in the f_{44} vs. f_{43} space defines the boundaries within which most of the organic aerosol was found in previous studies and can be used as a guide to characterize oxidized organic components: data in the upper left represent more oxidized organics vs. the less oxidized organics in the lower right (Ng et al., 2010; Schulz et al., 2018).

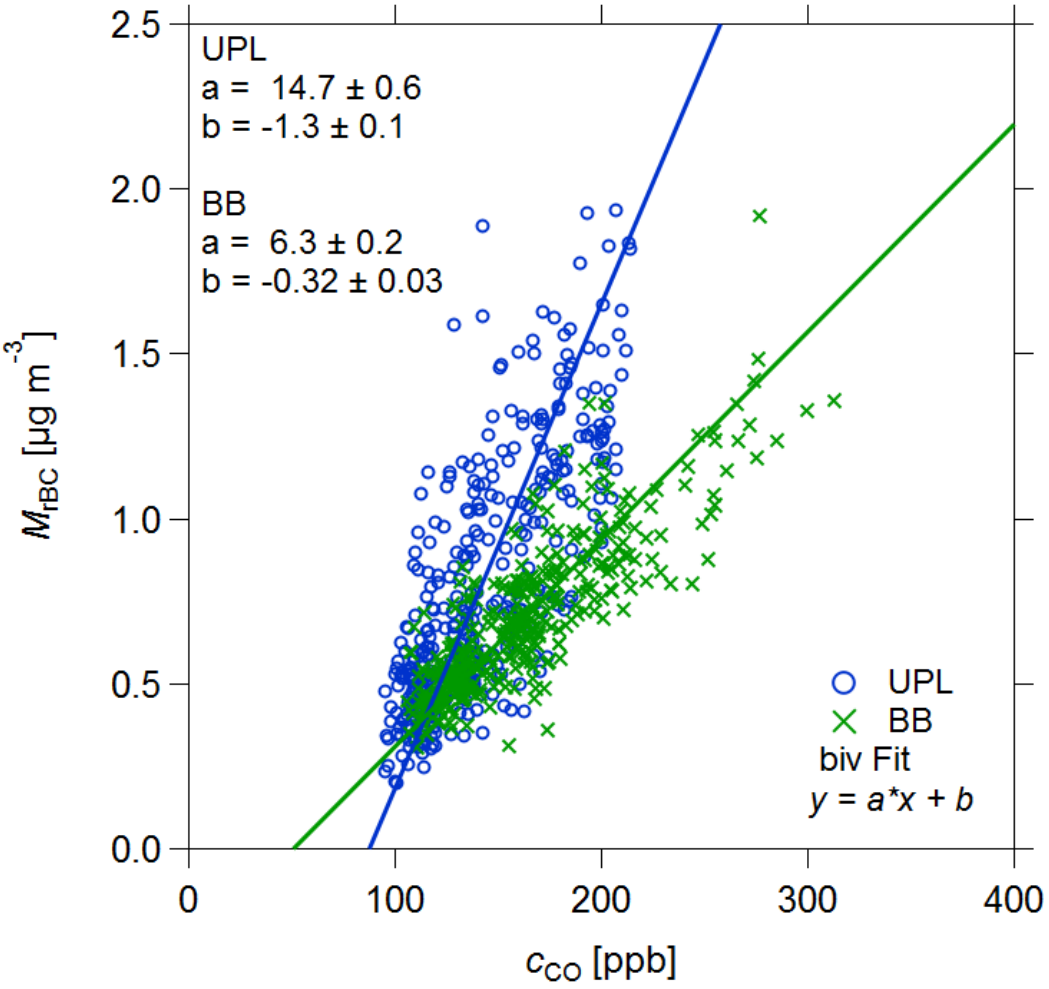

Figure S7. Correlation between Δc_{CO} and ΔM_{rBC} within the upper pollution layer (UPL) and fresh biomass burning (BB) plume probed during AC19. A bivariate regression fit was applied to the data set in order to obtain the BC enhancement ration, EnR_{BC}.

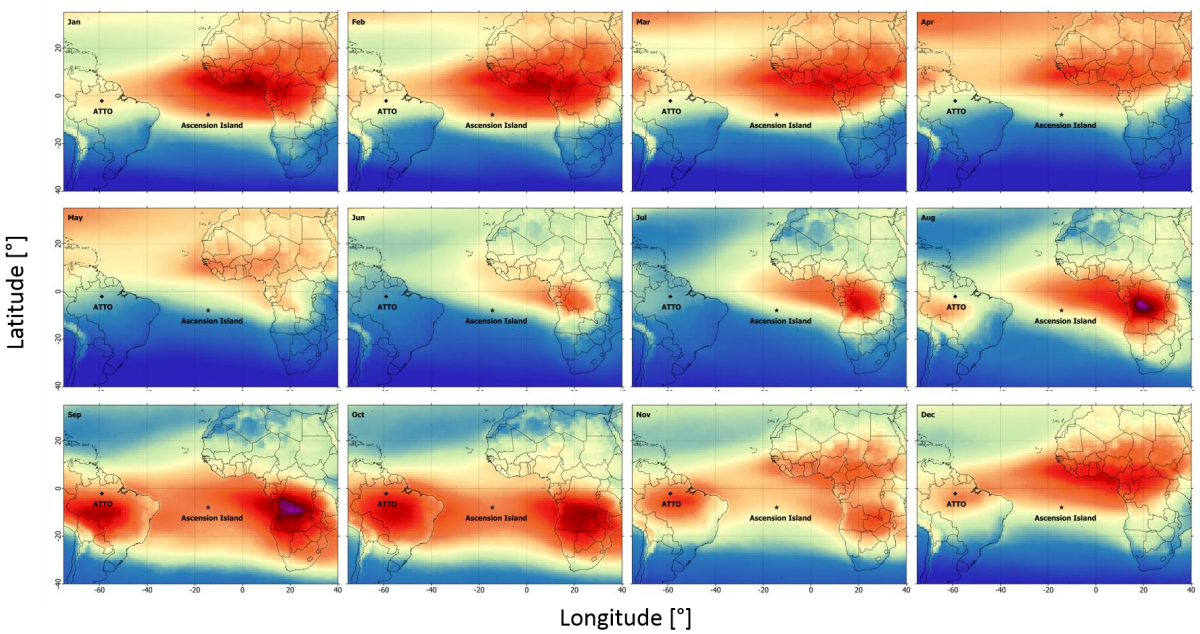

Figure S8. Monthly distribution of AIRS-derived carbon monoxide (400 to 600 hPa) over the Southern Hemisphere. The map shows averages over multiple years (2005-2018).

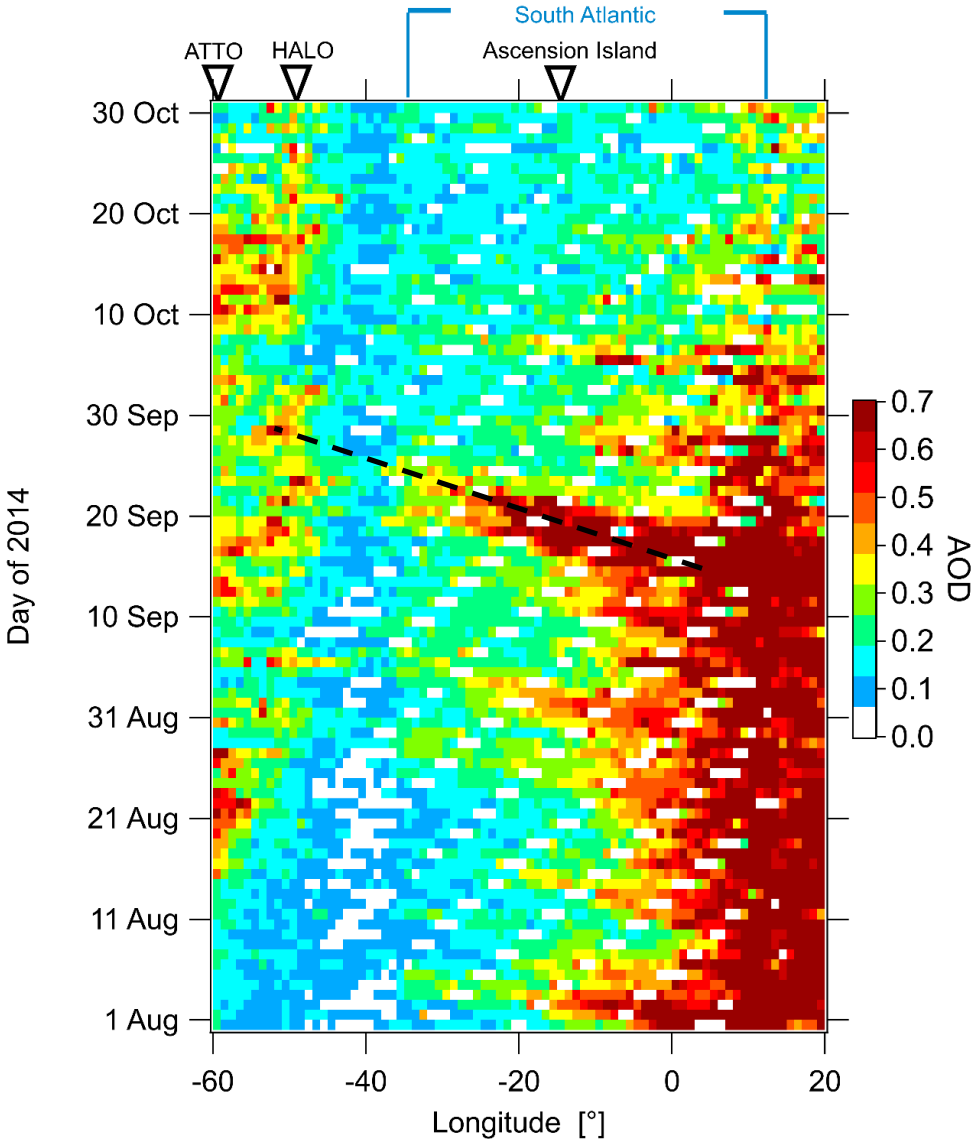

Figure S9. Hovmöller plot of the daily MODIS AOD (550 nm) distributed over the South Atlantic region (60 ºW to 20 ºE) from August to October 2014, averaged over the latitudinal band of 10º S to 5º N, corresponding to the region of interest (ROI) highlighted in Fig. 7a. Several events of transatlantic transport of aerosol from Africa towards South America can be easily identified, with the strongest plume starting approximately on 15 September 2014. A dashed line for this particular event is also shown in the picture, which arrives at a time close to our observations on AC19 on 30 September 2014. Westwards of 35 ºW, the AOD levels are

increasingly influenced by the South American continent, which masks the AOD signals of the transported African pollution as it approaches the South American continent.

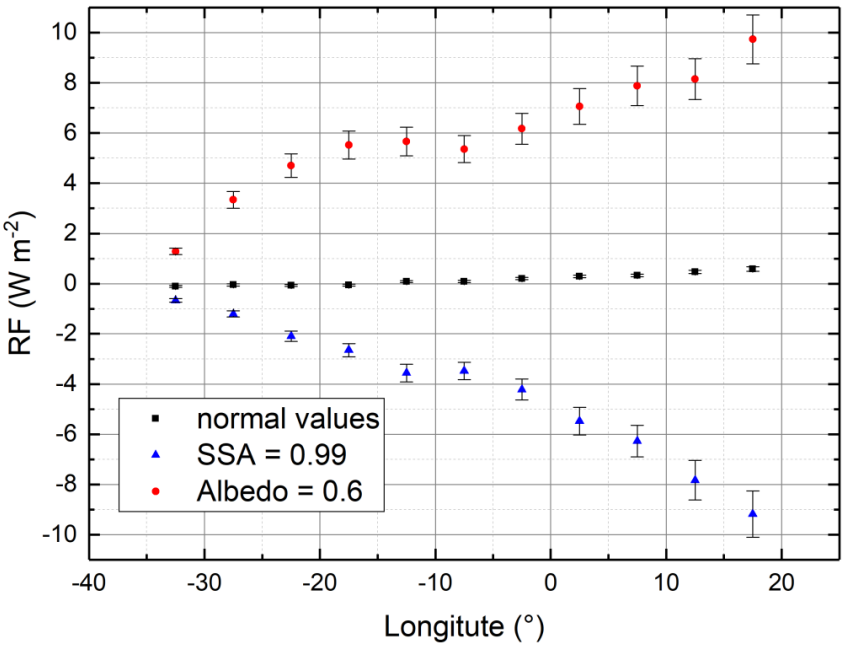

Figure S10. Sensitivity tests showing the DRF-TOA changes due to different assumptions in the aerosol and surface properties, comparing with the original DRF-TOA estimation. The simulations show that if the aerosol layer is mostly scattering (SSA = 0.99), a general cooling (back-scattering by the layer) is observed. On the other hand, if the absorbing ocean is replaced by a higher surface albedo (0.6), a warming effect by the layer is observed due to the downward radiation that is scattered back and forth between the aerosol layer and the surface.

2.3 African smoke over the Amazon rain forest

This chapter contains the final draft of a manuscript that will soon be submitted to a peer reviewed journal.

This manuscript includes data sets from the following field experiments:
ATTO, ACRIDICON-CHUVA and CAFE-Africa.

Contribution to this chapter by Bruna A. Holanda: I am the first author of this manuscript and my personal contribution to this work includes the processing and analysis of the ATTO, ACRIDICON-CHUVA, and CAFE-Africa data sets. I have been responsible over several years for conducting the measurements, quality assurance and frequent maintenance of the relevant aerosol instruments at ATTO, which yielded the long-term data sets presented in this study. Furthermore, I participate in the CAFE-Africa aircraft campaign in Cape Verde in 2018. I wrote the scripts for an automated processing of the ~ 4 Tb of SP2 data in this study. I further developed and optimized the black carbon source assignment method, which is the backbone of this work. Alongside my coauthors, I played the primary role in initiating and designing the research, analyzing the results, preparing figures, and writing the manuscript.

African smoke over the Amazon rain forest

Bruna A. Holanda[1], Marco A. Franco[1,2], David Walter[1,3,c], Meinrat O. Andreae[4,5], Paulo Artaxo[2], Samara Carbone[6], Yafang Cheng[1], Sourangsu Chowdhury[7], Florian Ditas[1,a], Martin Gysel-Beer[8], Thomas Klimach[1], Leslie A. Kremper[1], Ovid O. Krüger[1], Jost V. Lavric[3,d], Jos Lelieveld[7], Chaoqun Ma[1], Luiz A. T. Machado[1,2], Fernando G. Morais[2], Robin L. Modini[8], Andrea Pozzer[7], Jorge Saturno[1,b], Hang Su[1], Manfred Wendisch[9], Stefan Wolff[1], Mira L. Pöhlker[1,9,10], Ulrich Pöschl[1], and Christopher Pöhlker[1,4]

[1]Multiphase Chemistry Department, Max Planck Institute for Chemistry, 55128 Mainz, Germany
[2]Institute of Physics, University of São Paulo, São Paulo 05508-900, Brazil
[3]Department of Biogeochemical Processes, Max Planck Institute for Biogeochemistry, 07701 Jena, Germany
[4]Biogeochemistry Department, Max Planck Institute for Chemistry, 55128 Mainz, Germany
[5]Scripps Institution of Oceanography, University of California San Diego, La Jolla, CA 92037, USA
[6]Federal University of Uberlândia, Uberlândia-MG, 38408-100, Brazil
[7]Atmospheric Chemistry Department, Max Planck Institute for Chemistry, 55128 Mainz, Germany
[8]Laboratory of Atmospheric Chemistry, Paul Scherrer Institute, 5232 Villigen PSI, Switzerland
[9]Leipzig Institute for Meteorology, Leipzig University, Leipzig, Germany
[10]Experimental Aerosol and Cloud Microphysics Department, Leibniz Institute for Tropospheric Research, Leipzig, Germany
[a]now at: Hessian Agency for Nature Conservation, Environment and Geology, 65203 Wiesbaden, Germany
[b]now at: Physikalisch-Technische Bundesanstalt, 38116 Braunschweig, Germany
[c]now at: Climate Geochemistry Department, Max Planck Institute for Chemistry, 55128 Mainz, Germany
[d]now at: Acoem Ecotech, 1492 Ferntree Gully Road, Knoxfield VIC 3180, Melbourne, Australia

Correspondence: Christopher Pöhlker (c.pohlker@mpic.de)

Abstract. Smoke from vegetation fires, comprising black carbon (BC) along with organic and inorganic aerosols, widely affects atmospheric circulation, radiation transfer, and the water cycle. Over the Amazon rain forest, the smoke is not only defined by regional fires but also receive a large fraction from Africa through long-range transport. Here we quantify and characterize this African smoke fraction in central Amazonia. The African contribution follows a clear seasonality and episodically accounts for up to 90 % of the BC mass. In terms of annual means, the BC mass even exceeds the South American fraction. Both smoke regimes are further characterized by distinctly different physico-chemical and optical properties. While the African BC influx and the anticipated impact on radiation transfer are large, the associated African contribution to the total particle (CN) and cloud condensation nuclei (CCN) burden is comparatively small, relative to South American fires. We found a good agreement between our results and three global circulation models, although in some case African contribution to the Amazon is largely underestimated, emphasizing the need to improve the representation of transatlantic aerosol transport as well as emission schemes.

1 Introduction

The widespread fires in the Amazon basin in recent years aroused public concerns worldwide. In August 2019, a smoke layer, which was several kilometers thick and temporarily covered the entire western basin, caused a 'black rain' event even in São Paulo city 2500 km away [1]. Since 2019, the number of fires in the Amazon increased significantly relative to the previous years and, thus, we have witnessed a trend reversal after a continuous and more than one-decade long decline in deforestation rates and burning activities [2, 3].

Biomass burning became frequent and ubiquitous in the Amazon over recent decades since fire is the tool of choice for land clearing and management in agricultural expansion, infrastructure development, and mining [4]. The emitted biomass burning aerosols comprise black carbon (BC), organic and inorganic particles as well as gaseous species of different volatility [5, 6]. The smoke alters the radiation balance of the atmosphere through absorption and scattering of solar radiation and further affects the intense (re)cycling of water between biosphere and atmosphere [7, 8]. Under smoky conditions, the concentrations of aerosol particles and cloud condensation nuclei (CCN) in the Amazon exceed the natural background by up to two orders of magnitude [9, 10]. This has consequences, for instance, through the so called "cloud burning" effect, in which the light absorbing smoke cools the surface and correspondingly heats the BC-enriched air layers above. This leads to a stabilization of the boundary layer up to an inhibition of shallow convective cloud formation [11, 12]. Another important process is the influence of the smoke on clouds and precipitation through perturbations of cloud microphysical processes, including a cloud droplet size reduction, a delay of the precipitation onset in the clouds to higher altitudes, a corresponding suppression of low-level rainout as well as an invigoration of the updrafts, leading to intense thunderstorms and extreme weather events [13–15]. This, in turn, modifies the aerosol population and creates a complex system with feedback mechanisms [16, 17]. Because of its atmospheric significance, the properties and roles of biomass burning smoke in the Amazon have been investigated intensely [18–21].

This picture gets more complicated by the fact that the Amazonian atmosphere is not only influenced by fires in the rain forest and nearby biomes [1], but also to a large degree by the transatlantic transport of smoke, dust, and other emissions from Africa, which is one of the strongest aerosol sources worldwide [24–28]. The fires in Africa are mostly ignited by humans for land clearing and agricultural waste burning [29, 30]. Accordingly, the Amazon receives African aerosols essentially all year long, as it is located 'downwind' of the African continent in the large-scale trade wind circulation [23]. Figure $1A_1$ shows conceptually the spatiotemporal patterns of African aerosol transport into the Amazon: From December to April, northeasterly air masses transport large amounts of Saharan dust and smoke from African fires north of the equator (i.e., in the Sahel and West Africa) towards the Amazon [31, 32]. From August to November, southeasterly air masses transport large amounts of smoke from African fires south of the equator towards the Amazon [22, 33, 34]. Since the African smoke influx appears to be

[1] Brazil comprises six continental biomes: Amazônia, Cerrado, Caatinga, Mata Atlântica, Pantanal and Pampa (see e.g., https://www.globalforestwatch.org/, last access 16 Mar 2021). As shown in Fig. S3, the ATTO footprint region covers four of them (in the order of their relevance for the ATTO measurements): Amazônia, Cerrado, Caatinga, and Mata Atlântica [23].

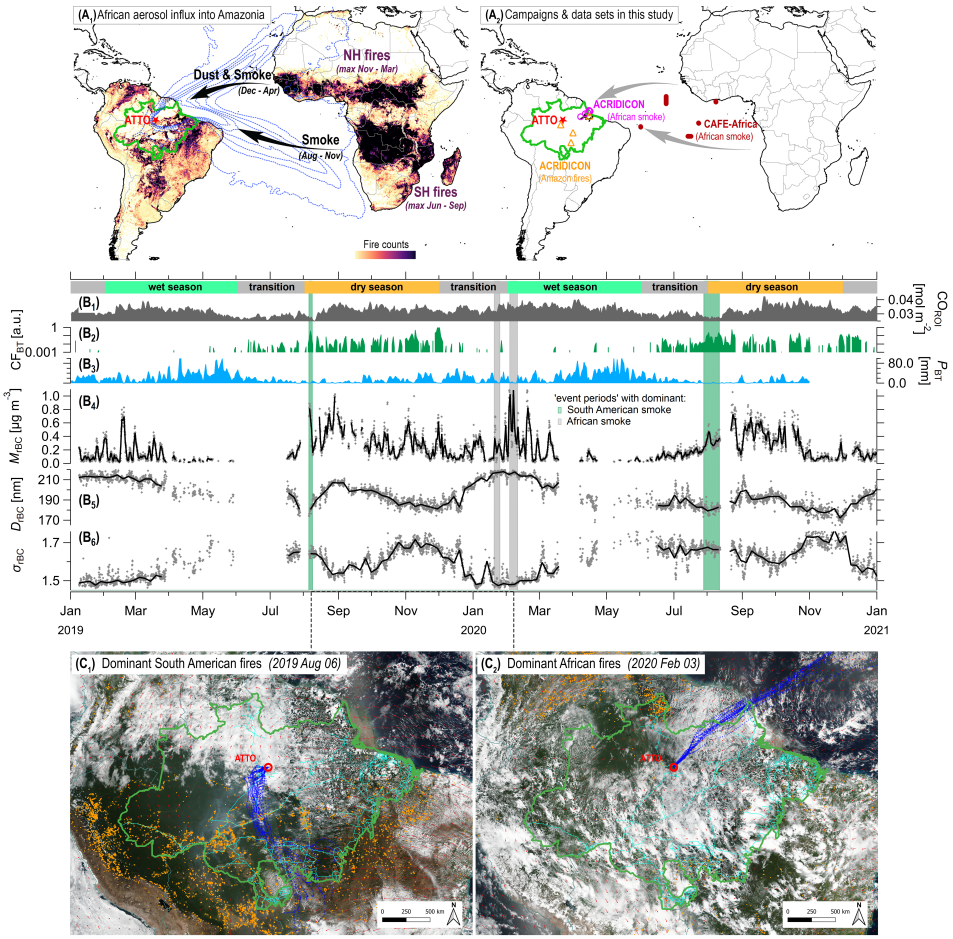

Figure 1. **(A$_1$)** Backward trajectory (BT) ensemble (2011-2020, HYSPLIT, 10 days) starting at 200 m a.g.l. at ATTO in combination with density map of fire counts for same time frame. **(A$_2$)** Geographical location of the ATTO site and the regions where biomass burning plumes were probed with the HALO aircraft. **(B$_1$)** As proxy for African smoke influx into the Amazon: satellite-derived CO concentration in offshore region of interest in front of Brazilian coast (ROI$_{\text{offshore}}$, Sect. S1.5). **(B$_2$)** As proxy for periods with intense South American smoke influence: cumulative number of fires, CF_{BT}, along the 3-day BTs starting at 200 m at ATTO according to [22]. **(B$_3$)** As proxy for aerosol wet scavenging in air masses arriving at ATTO: cumulative precipitation, P_{BT}, along the 3-day BTs according to [23]. **(B$_4$ – B$_6$)** Time series of mass concentration, M_{rBC}, geometric mean diameter, D_{rBC}, and geometric standard deviation, σ_{rBC}, derived from monomodal fitting of 3 h averaged rBC mass size distributions. Green and gray vertical shadings indicate ATTO 'event periods' with dominant influence of South American (i.e., 28 Jul – 11 Aug 2020) vs African smoke (i.e., 20 – 23 Jan & 03 – 09 Feb 2020). **(C)** Satellite views with fire maps of selected days when ATTO was under dominant influence of biomass burning pollution from **(C$_1$)** South America, on 06 August 2019; and **(C$_2$)** Africa, on 03 February 2020.

the rule, rather than the exception, the biomass burning pollution over the Amazon can be regarded as a mixture from South American and African fires with a high spatiotemporal variability. This raises the following fundamental questions:

1. What are the respective contributions and seasonality of South American and African biomass burning smoke to the aerosol burden in (central) Amazonia?
2. How does smoke from both continents differ in terms of microphysical and optical properties and how does this relate to climate-relevant processes, such as the atmospheric radiative transfer as well as aerosol-cloud interactions?
3. Is the influx of African smoke into Amazonia correctly represented in global aerosol models?

Based on measurements of refractory black carbon (rBC)[2] mass in single particles at the Amazon Tall Tower Observatory (ATTO) in central Amazonia [36] during the intense burning seasons 2019 and 2020, complemented by aircraft data in key regions indicated in Fig. $1A_2$, these questions are answered here.

2 Results and discussion

While some aerosols from distant (intercontinental) sources, such as mineral dust, Atlantic marine or African volcanogenic aerosols, have peculiar physicochemical properties that facilitate their identification within the aerosol mixture in the Amazon [e.g., 26, 31], distinguishing the African biomass burning smoke after transatlantic transport from the regional Amazonian smoke is more challenging. [37] showed that differences in the microphysical properties of the BC particles (core size and coating thickness) can be used for a smoke source appointment. Here, we present a related approach to apportion biomass burning smoke over the Amazon based solely on the BC core mass size distribution. For this purpose, we analyzed two full seasonal cycles of rBC data measured at ATTO (see Sect. S1.1). The time series of the rBC mas concentration and core properties – specifically the geometric mean diameters (D_{rBC}) and geometric standard deviation (σ_{rBC}) of the 3-h averaged rBC mass size distributions (Fig. $1B_{4–6}$) – show a pronounced seasonality and high variability, which we hypothesize to be modulated by the relative contributions of sources. To verify that, we searched for days with dominant advection of either African or South Americam smoke by combining the rBC data with daily composite maps – such as the ones in Fig. 1C, showing satellite images of fire plumes, fire maps, wind fields, and backward trajectories. We identified a certain number of 'event periods' with preponderance of either African or South American smoke, as described in the following.

A characteristic period with mostly South American smoke at ATTO spanned from 06 to 11 August 2019 and from 28 July to 11 August 2020 with elevated rBC mass concentration (green shading in Fig. 1B). In this period, the carbon monoxide (CO) concentrations over the ocean (Fig. $1B_1$), just before reaching the coast, was at a minimum suggesting low advection of African smoke at the same time that a maximum in fire counts along the backward trajectory (BT) footprint was observed (Fig. $1B_2$).

[2]Refractory black carbon (rBC) refers to the carbonaceous fraction of particulate matter that is insoluble and vaporizes at temperatures near 4000 K, which can be measured based on laser-induced incandescence methods [35]

Figure 1C$_1$ shows an example of southerly winds transporting dense smoke from fire hotspots along the large highways into the central basin on 06 August 2019. The heavy smoke could visually be traced from the fires to ATTO in satellite images (further example days in Fig. S10 and Fig. S11). A characteristic episode of mostly African smoke at ATTO with M_{rBC} exceeding $1\,\mu\mathrm{g\,m^{-3}}$ occurred from 20 to 23 January and 03 to 09 February 2020 (gray shading in Fig. 1B). These days belong to the early Amazonian wet season, when fire occurrence in the Amazon, and specifically along the ATTO BT footprint, approaches its minimum due to frequent and intense rainfall and therefore, smoke from South American fires can be largely excluded (see Fig. 1B$_2$ and B$_3$). The high M_{rBC} can be therefore explained by long-range transport of African aerosol plumes, which bring a mixture of dust and smoke and occur prominently between December and April as outlined in detail in [31]. Figure 1C$_2$ shows rather straight northeasterly trajectories and strong winds that correspond to the typical air mass advection patterns of long-range transport of African aerosols [see 31].

We found statistically robust differences in the rBC microphysical properties between the 'event periods' with preponderant African or South American smoke. Figure Fig. S5 and S6A shows that the African rBC cores were significantly larger ($D_{\mathrm{rBC,Afr}} = 216 \pm 2\,\mathrm{nm}$, mean $\pm$ SD) and their mass size distribution narrower ($\sigma_{\mathrm{rBC,Afr}} = 1.48 \pm 0.01$) than the South American rBC cores ($D_{\mathrm{rBC,SAm}} = 181 \pm 3\,\mathrm{nm}$ and $\sigma_{\mathrm{rBC,SAm}} = 1.67 \pm 0.02$). These trends were found to be consistent throughout the entire ATTO data set analyzed here (for a detailed description, see Sect. S1.3). The finding that African and South American smoke in the ATTO footprint region are characterized by consistently different rBC signatures allows to deconvolute the superposition of both smoke populations in the Amazon through a bimodal lognormal fitting of the rBC mass size distributions [38]. The position ($D_{\mathrm{rBC,i}}$) and width ($\sigma_{\mathrm{rBC,i}}$) of one African (Afr) and one South American (SAm) mode were constrained according to the respective monomodal fit parameters presented in Fig. S6A, while the rBC mass concentration of each mode ($A_{\mathrm{rBC,i}}$) was a free parameter. Examples of individual bimodal fits are shown in Fig. S7. Note that, by applying the bimodal fit, we additionally assume that biomass burning in Africa and in South America are the only two sources providing BC particles to the ATTO site. It means that potential emission sources such as urban pollution (for example from Manaus city, see [39, 40], do not significantly contribute to rBC mass concentration at ATTO, which is justified according to [41] and model simulations in Fig. S18. Based on these fits, the African ($M_{\mathrm{rBC,Afr}}$) and South American ($M_{\mathrm{rBC,SAm}}$) fractional contributions to the total M_{rBC} were derived from the integral of the corresponding mode. The resulting time series of the separated influence of African vs South American rBC based on this approach, the deconvolution method, is shown in Fig. 2. A detailed description of the procedure can be found in Sect. S1.3.

Figure 2A & B shows the time series of the rBC mass fractions as well as absolute rBC mass concentrations attributed to African and South American fires based on the bimodal fitting of the rBC mass size distributions. Generally, for large parts of the year, biomass burning aerosols – either from South American and/or African sources – are present in the Amazonian atmosphere, while pristine episodes ($M_{\mathrm{rBC}} < 0.01\,\mu\mathrm{g\,m^{-3}}$) are comparatively short and rare (about 15 % of the days analyzed here) [see also 10]. The rBC mass concentration attributed to the South American fires, $M_{\mathrm{rBC,SAm}}$, is elevated from July to November, presenting a seasonal maximum in the late dry season when $M_{\mathrm{rBC,SAm}}$ reaches up to $0.8\,\mu\mathrm{g\,m^{-3}}$, corresponding to more than 80 % of the total rBC mass. Within the studied period, an average of $M_{\mathrm{rBC,SAm,dry}} = 0.27 \pm 0.15\,\mu\mathrm{g\,m^{-3}}$ was

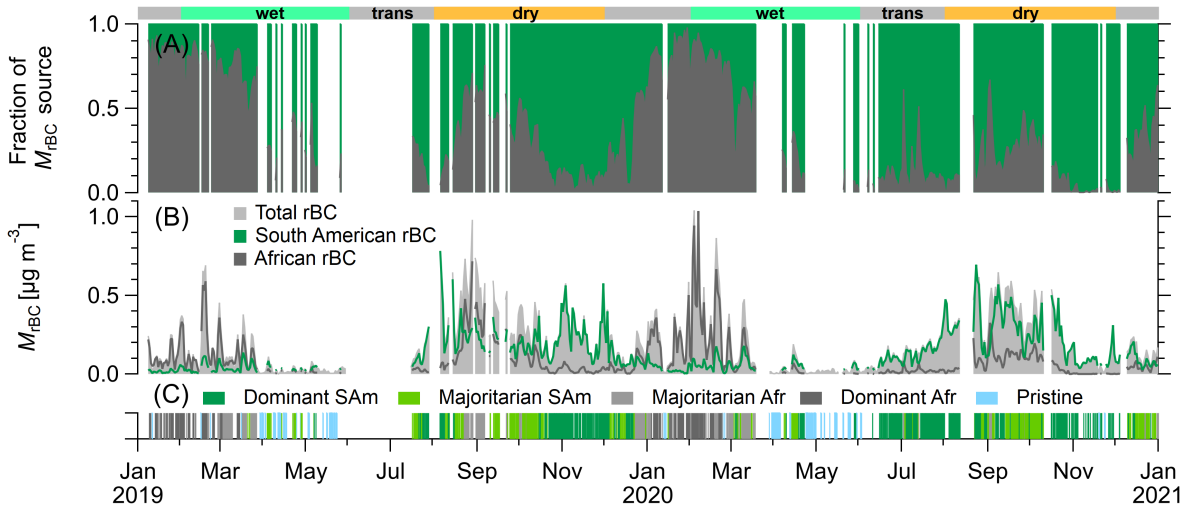

Figure 2. Relative **(A)** and absolute **(B)** contributions of African vs South American biomass burning to total rBC mass concentration at ATTO in 2019 and 2020. **(A)** has been obtained from **(B)** by normalizing to total rBC. **(C)** Coloured bar code represents five flags for dominant and majoritarian South American influence, dominant and majoritarian African influence as well as pristine aerosol conditions.

obtained for the dry season. Some minor and sporadic contributions from SAm fires were observed during the wet season, with an average of $M_{\mathrm{rBC,SAm,wet}} = 0.07 \pm 0.04\,\mu\mathrm{g\,m^{-3}}$. Also the African smoke is present for most of the year and contributes substantially to the BC burden over the Amazon. The African influence has two maxima: the highest fraction, up to 90 %, occurred between January and March, when the wet season long-range transport from African dust and smoke typically peaks [see 31]. During this time, sharp peaks in $M_{\mathrm{rBC,Afr}}$ up to $1.2\,\mu\mathrm{g\,m^{-3}}$ can be easily observed. For comparison, the maximum $M_{\mathrm{rBC,Afr}}$ observed at ATTO is about half of that observed in the concentrated layers of African smoke arriving at the Brazilian coast after transatlantic transport [22]. The average wet season mass concentration $M_{\mathrm{rBC,Afr,wet}} = 0.21 \pm 0.25\,\mu\mathrm{g\,m^{-3}}$ is comparable to dry season average values. The secondary maximum (up to 60 %) of African influence occurs in August and September, when the dry season long-range transport of African smoke peaks [see 22], with an average mass concentration of $M_{\mathrm{rBC,Afr,dry}} = 0.10 \pm 0.12\,\mu\mathrm{g\,m^{-3}}$. We note that the seasonality of the South American and African smoke contributions agrees well with (*i*) the satellite-derived CO mixing ratio averaged over the region of interest ($\mathrm{ROI_{offshore}}$) in the westerly trade winds at the South American coast (Fig. $1\mathrm{B_1}$), which is a marker for the extent of long-range transport of African biomass burning emissions, and (*ii*) the accumulated number of fires along the backward trajectories ($\mathrm{CF_{BT}}$, Fig. $1\mathrm{B_2}$), which is a marker for the abundance of fires relatively close to ATTO.

The source assignment of biomass burning smoke in Fig. 2 allows to classify the atmospheric conditions at ATTO based on the relative contributions of both sources (or the absence of them) in order to analyze the physico-chemical and optical aerosol properties. We chose the following regimes:

- **Dominant South American influence**: $(M_{\mathrm{rBC,SAm}}/M_{\mathrm{rBC}}) > 0.85$
- **Majoritarian South American influence**: $0.5 < (M_{\mathrm{rBC,SAm}}/M_{\mathrm{rBC}}) < 0.85$
- **Majoritarian African influence**: $0.5 < (M_{\mathrm{rBC,Afr}}/M_{\mathrm{rBC}}) < 0.85$
- **Dominant African influence**: $(M_{\mathrm{rBC,Afr}}/M_{\mathrm{rBC}}) > 0.85$
- **Pristine**: $M_{\mathrm{rBC}} < 0.01\,\mu\mathrm{g\,m^{-3}}$ according to definition in [10]

Figure 2C illustrates the time series of this source classification and Fig. 3 provides a statistical summary of selected aerosol parameters for each pollution regime. The pristine atmospheric conditions serve as a reference case.

Generally, open vegetation fires always combine flaming and smoldering combustion, while the relative contributions of both are highly variable and strongly depend on fuel and environmental conditions [5]. The carbon monoxide (CO) concentration and especially the enhancement ratio between BC and CO ($\Delta\mathrm{BC}/\Delta\mathrm{CO}$) are established markers for the extent of smoldering involved. Here, we found comparatively high values of $\Delta\mathrm{BC}/\Delta\mathrm{CO} = 23.7 \pm 4.0\,\mathrm{ng\,m^{-3}ppb^{-1}}$ (Fig. S13A) for the African-dominated smoke, suggesting mostly flaming combustion, which is in line with the relatively dry vegetation mixture at the fire locations in Africa (see Fig. S4). In contrast, rather low values of $\Delta\mathrm{BC}/\Delta\mathrm{CO} = 4.5 \pm 0.2\,\mathrm{ng\,m^{-3}ppb^{-1}}$ were observed for the South American-dominated smoke, suggesting a more smoldering combustion, which is consistent with the rather moist fuel in the ATTO footprint region (Fig. S3).

Microphysical, chemical and optical aerosol parameters in Fig. 3 show significant differences with gradual transitions between the African- and South American-dominated states. The average M_{rBC} varies between $0.25\,\mu\mathrm{g\,m^{-3}}$ for a dominant South American influence and $0.48\,\mu\mathrm{g\,m^{-3}}$ for a dominant African BB influence, which is both well above the pristine background state (Fig. 3A). Despite the large distance between both continents, the average African influence on M_{rBC} in the central Amazon Basin appears to be equal – or even higher – than the South American influence for the studied period. While strongly affecting the BC mass, the influence of African smoke on the total particle (CN) and cloud condensation nuclei (CCN) number concentration is, on the other hand, rather small compared to that of South American biomass burning aerosols (Fig. 3B). The N_{CN} and N_{CCN} at a supersaturation of 0.3 % (retrieved from [42] parametrization) is on average about a factor of 5 higher for South American than for African-dominated conditions ($N_{\mathrm{CN,Afr}} \approx 300\,\mathrm{cm^{-3}}$ and $N_{\mathrm{CCN,Afr}} \approx 180\,\mathrm{cm^{-3}}$, respectively). The fact that African-dominated and pristine conditions differ strongly in M_{rBC} (Fig. 3A) and only weakly in N_{CN} (Fig. 3B) underlines that M_{rBC} is a more reliable aerosol marker for clean atmospheric conditions in the Amazon than N_{CN} [10]. The corresponding rBC and total number size distribution (PNSD), which underline the higher rBC fraction in the African smoke, are shown in Fig. S14. The fact that African smoke is much richer in rBC relative to non-absorbing material is reflected in the rBC mass and number fractions (Fig. S13B–D), which is significantly higher for African than for South American-dominated

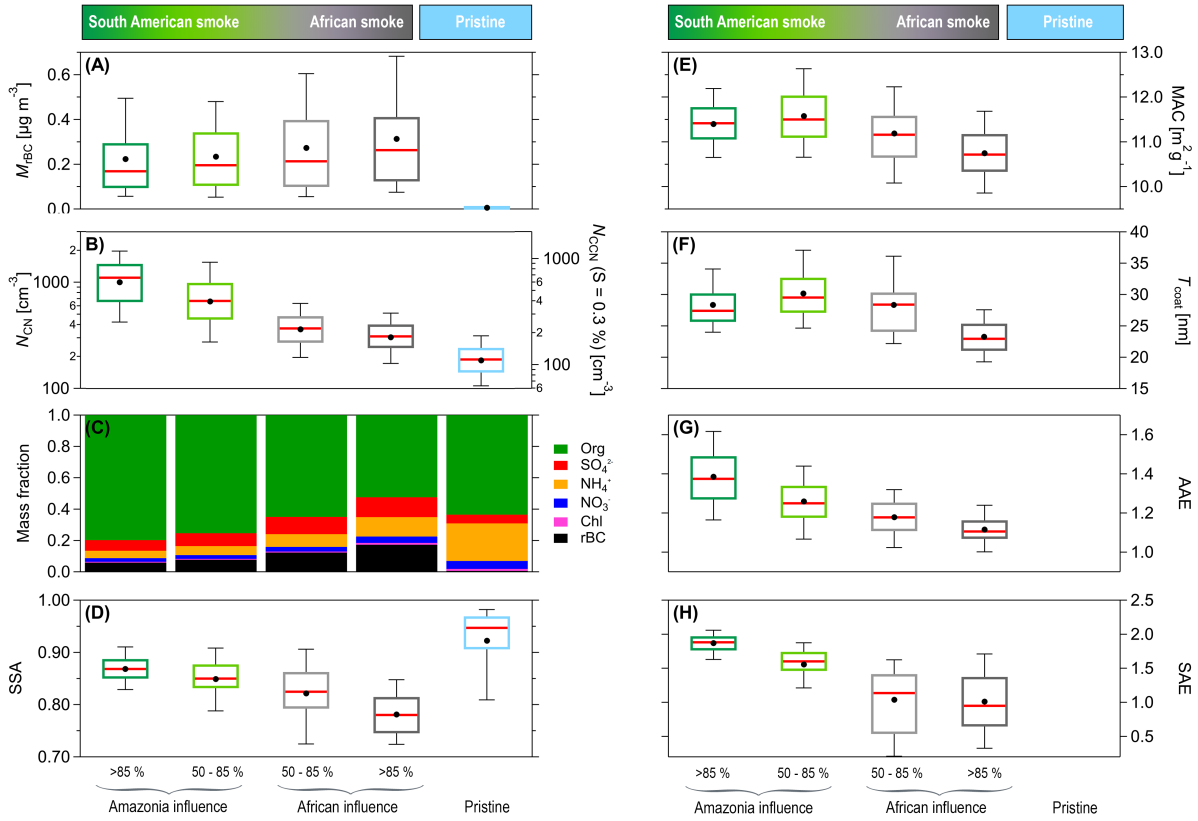

Figure 3. Statistical analysis of the aerosol parameters at the ATTO site for the periods dominated by Amazonian biomass burning (green) and African BB (grey) and mixed regimes: **(A)** rBC mass concentration measured by the SP2, M_{rBC}; **(B)** particle number concentration, N_{CN} (left axis) and cloud condensation nuclei number concentration N_{CCN} at a supersaturation of 0.3 % (right axis); **(C)** mass fraction of the non-refractory submicrometer species (Organic, Sulfate, Ammonium, Nitrate, Chloride) and rBC; **(D)** single scattering albedo at 637 nm, SSA; **(E)** mass absorption cross section at 637 nm, MAC; **(F)** coating thickness, T_{coat}, for particles with $\sim 180 < d_{\mathrm{MEV}} < 220\,\mathrm{nm}$; **(G)** absorption Ängstrom exponent, AAE, calculated from Eq.S6; **(H)** scattering Ängstrom exponent, SAE, calculated from S5 using the wavelength pair 450 and 635 nm. The boxes shows the 25$^{\mathrm{th}}$ and 75$^{\mathrm{th}}$ percentiles, the marker and horizontal bar represents the mean and median, respectively, and the whiskers represent the 9$^{\mathrm{th}}$ and 91$^{\mathrm{st}}$ percentiles. The time series of all variables, including eventual data gaps that affects the number of data points used to compose the box plots, are shown in Fig. S2.

episodes. In African plumes, rBC is the second most abundant species of the PM1 ($f_{\mathrm{rBC,Afr}} = 18 \pm 8\,\%$) after the organics ($f_{\mathrm{Org,Afr}} = 52 \pm 8\,\%$), while the inorganic species SO_4^{2-}, NH_4^+, NO_3^- and Cl^- contributes to $13 \pm 3\,\%$, $12 \pm 5\,\%$, $4 \pm 2\,\%$ and $1.0 \pm 0.6\,\%$ of PM1, respectively. The enriched BC in African fires are related, among other factors, to more flaming controlled combustion — i.e. the BC emissions are proportionally higher already at the sources (see [43]) – and tends to further increase

during the transatlantic transport due to the loss of organics by photo bleaching. The rBC mass fraction decreases toward the South American dominated regime, $f_{\mathrm{rBC,SAm}} = 6 \pm 2\,\%$, while the organics is by far the dominant fraction contributing to PM1, $f_{\mathrm{Org,SAm}} = 80 \pm 5\,\%$.

The level of chemical oxidation of the organic aerosol can be inferred from key organic fragments (m/z 43, 44) presented in Fig. S15. These results suggest that African smoke is more oxidized as it shows the highest f44 signals (corresponding mostly to the fragment CO_2^+) at the same time that the f43 signals (most likely related to the fragment $C_2H_3O^+$) are the lowest. Further, the main levoglucosan fragment $f60$ (mostly ions $C_2H_4O^+$), often used as a marker for biomass burning [44], quickly degrades in the atmosphere within the first few hours after emission. In all biomass burning regimes at ATTO, the f60 lies close to the reference value of 0.3 ± 0.06 for negligible or completely oxidized biomass-burning PM1 [44], meaning that all BB plumes probed at ATTO have aged for at least 9 –12 h in the atmosphere before reaching the remote ATTO site (see the $f60$ decay curve in [43]). Our results from ATTO are consistent with chemical composition from previous studies over the Amazon Basin [45–48] and in African plumes over the South Atlantic [e.g. 43, 49]. For further information see supplementary material.

The optical properties of the biomass burning smoke are essential for the regional radiative balance and are determined by microphysical particle properties [50, and references therein]. Clear differences in the optical properties were found between the African- and South American-dominated states. The single scattering albedo (SSA) characterizes the overall absorption strength of an aerosol population. Here, we found a lower absorption for the South American-dominated state with $\mathrm{SSA_{SAm}} = 0.86\,(0.84 - 0.88)$ at 637 nm than for the African-dominated state with $\mathrm{SSA_{Afr}} = 0.77\,(0.74 - 0.79)$ at 637 nm. These results are consistent with previous studies suggesting a drop in SSA due to the influx of African aerosol into the Amazon basin [21, 22, 26]. The higher SSA for the South American relative to the African smoke corresponds to a lower f_{rBC} and, thus larger fraction of non-absorbing particles (Fig. S13E). Our African SSA is slightly higher than the SSA values between 0.65 and 0.76 (at 660 nm) measured over western Africa by [51], which presumably results from the additional mixing with the rain forest background aerosol, dust and/or marine aerosol at ATTO (see Fig. 3, C and D). The lower SSA for African smoke was observed across the entire wavelength range analyzed here, which shows a quasi-linear decrease in SSA towards higher wavelengths (Fig. S16), in agreement with previous studies [51–53]. For the pristine case, a comparatively high SSA at 637 nm was obtained $\mathrm{SSA_{Pr}} = 0.92\,(0.86 - 0.95)$, which does not reach unity, probably due to the presence of a certain fractions of absorbing biogenic aerosols (e.g., pigmented spores) [e.g., 54].

The mass absorption coefficient (MAC, at 637 nm) – a fundamental input parameter for radiative transfer models – ranges from $\mathrm{MAC_{Afr}} = 9.5\,(9.1 - 9.9)\,\mathrm{m^2\,g^{-1}}$ for African-dominated conditions to $\mathrm{MAC_{SAm}} = 11.2\,(10.8 - 11.6)\,\mathrm{m^2\,g^{-1}}$ for South American-dominated conditions (Fig. 3E). This range includes the averages of $11.4 \pm 1.2\,\mathrm{m^2\,g^{-1}}$ and $12.3 \pm 1.3\,\mathrm{m^2\,g^{-1}}$ that [26] reported for the Amazonian wet and dry seasons, respectively. Considering that all absorption at 637 nm is attributed to the black carbon, the mean MAC values in Fig. 3E exceed the reference value of $\mathrm{MAC_{ref}} = 6.5 \pm 1.0\,\mathrm{m^2\,g^{-1}}$ at 637 nm for uncoated BC significantly [55]. We found an absorption enhancement ($E_{\mathrm{abs}} = \mathrm{MAC}/\mathrm{MAC_{ref}}$) between $E_{\mathrm{abs}} = 1.3$ for the African smoke and $E_{\mathrm{abs}} = 1.9$ for the South American smoke. An $E_{\mathrm{abs}} > 1$ is typically caused by the presence of coatings onto

the BC cores through the so-called lensing effect [56, 57] (see positive correlation between coating thickness and MAC at 637 nm in Fig. S17). The rather high E_{abs} values are related to the observation that the majority of rBC particles exhibit a substantial coating, regardless of the source. The fresher South American smoke was characterized by thicker average coatings with $T_{coat,SAm} = 30\,(27 - 32)$ nm (for $\sim 180 < d_{MEV} < 220$ nm), compared to the aged African smoke with $T_{coat,Afr} = 23\,(21 - 25)$ nm (Fig. 3F).

Besides the coating-related lensing effect, an apparent absorption enhancement at shorter wavelengths can also be related to the presence of brown carbon (BrC), which is the fraction of organic aerosol that absorbs radiation, especially in the ultraviolet (UV) range [58]. Overall, we found that the absorption by South American smoke has stronger wavelength dependence as expressed by the higher absorption Ängstrom exponent (AAE) in Fig. 3G. The average $AAE_{SAm} = 1.40\,(1.29 - 1.50)$ in South American plumes indicates the strong presence of BrC in the nearby deforestation fires whereas the much older African smoke is characterized by lower values of $AAE_{Afr} = 1.12\,(1.05 - 1.22)$, indicating negligible BrC contribution.

The spectral dependence of the scattering coefficient, expressed as the scattering Angstrom exponent (SAE, using the wavelength pair 450 and 635 nm in Eq. S5) is associated with the size distribution of the aerosol particles [59]. We found the highest SAE values for the relatively fresh South American smoke with $SAE_{SAm} = 1.99\,(1.93 - 2.05)$, which are characterized by a quite narrow distribution (Fig. 3H). For African smoke, the SAE is significantly lower with $SAE_{Af} = 0.82\,(0.38 - 1.00)$, which falls within the SAE range of $0.59 - 1.64$ (median of 1.07) reported by [51] for African BB layers over the Atlantic and is further consistent with the overall larger particles diameter (Fig. S14). The large variability in SAE observed for the African smoke is associated with the co-transported mineral dust and sea spray aerosol in the long-range transported plumes during the wet season [31].

The experimental rBC mass concentration at ATTO as well as the African and South American fractions in Fig. 2 were compared against model simulations using the EMAC [60–62] and CAM-chem [63, 64] global models. Figure 4A shows that the total measured rBC – which includes African and South American influences – and the standard model output yield a moderate positive correlation, with Pearson's coefficient of $R = 0.55$ and $R = 0.51$ for EMAC and CAM-chem, respectively (see linear regressions in Fig. S20). Generally, the default model runs underestimate the measured BC with a mean bias of 25% in EMAC and 19% in CAM-chem. Further and more important, the models does not capture the temporal variability well. Especially some of the large peaks in BC concentration, such as in August – September 2019 and January – March 2020 corresponding to periods with strong advection of African smoke, are essentially absent in both model results. Remarkably, a much better agreement is obtained by comparing the model runs in which African emissions were switched off with the rBC mass concentration attributed to the South American fires (Fig. 4B). For the South American smoke, both models performed well, yielding a strong positive correlation coefficient of $R \sim 0.70$ in EMAC and CAM-chem. The absolute concentrations of the modelled BC are a factor ~ 1.1 higher than observations, but the temporal variability is captured convincingly in both models. The magnitude of African BC in the models was derived from the difference between the *STD* and *NOBBafr* runs, and compared with the African-attributed rBC at ATTO in Fig. 4C, yielding a moderate positive correlation ($R = 0.58$ and $R = 0.55$) with the African BB at ATTO. This result highlights that the seasonal variability of African smoke is also well

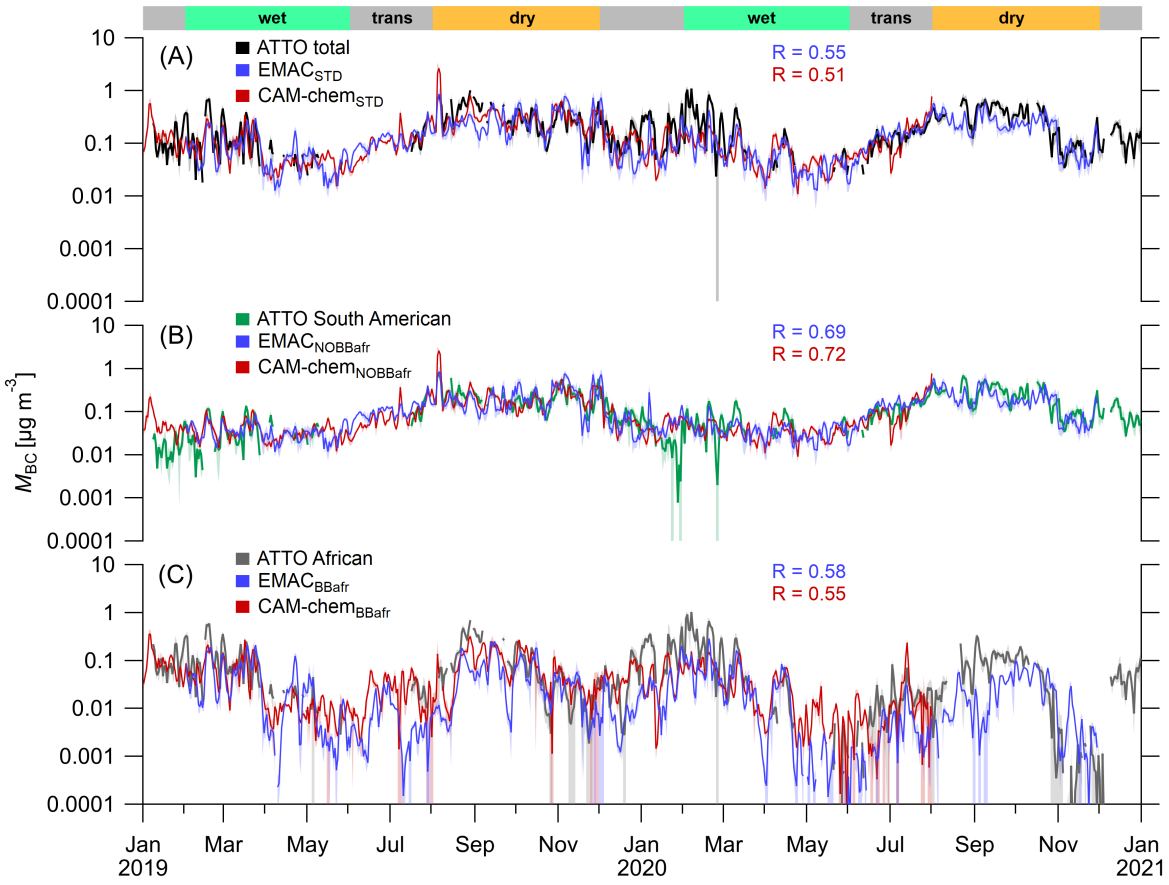

Figure 4. Comparison between observations and model simulations using EMAC and CESM. Time series of total BC mass concentration (M_{rBC}, black line) measured at ATTO versus standard model runs (M_{STD}); **(B)** South American-attributed ($M_{rBC,SAm}$, green) versus $M_{NOBBafr}$ model runs; and **(C)** African-attributed ($M_{rBC,Afr}$, gray) versus M_{BBafr} = (M_{STD} - $M_{NOBBafr}$) model runs (see subsection S1.10 and subsection S1.11). The time series are daily averages with colored shading as standard deviations. Legend specifies the correlation coefficients (R) for relationship between experimental and model data depicted in Fig. S20.

220 captured in the models, however the absolute concentrations are underestimated by a factor of 2 in EMAC with mean bias of 60%, while CAM-chem performed slightly better, with mean bias of 50%. The underestimation of biomass burning emissions inventories over African continent can be responsible for the discrepancies between models and observations [65]. This is in line with previous studies showing that a correct representation of the transatlantic smoke transport in various models has been particularly challenging due to several factors such as uncertainties in fire emission inventories, wet scavenging, plume rise
225 and subsidence parameterizations. [e.g., 66–71]. Nevertheless, the good correlation between model and observations further

underlines that rBC classification based on microphysical particle properties as applied here is a robust approach. Therefore, our dataset can serve as largely improved experimental basis for future model investigations of aerosol-cloud-radiation interactions over the Amazon Basin.

Author contributions. BH and CP designed the study. BH, DW, OK, LAK, MAF, FD, JS collected and analyzed the ATTO aerosol data. DW and JVL collected and analyzed the ATTO carbon monoxide data. SW, FM, PA provided essential scientific support for the broad range of ATTO measurements. BH, OK, MP, MOA, MW, LATM, JL played key roles and/or collected and analyzed the data in the course of the ACRIDICON-CHUVA and CAFE-Africa aircraft campaigns. BH wrote the paper, supported by CP. All authors contributed to the discussion of the results as well as the finalization of the manuscript. UP, MOA, CP supervised the study.

Competing interests. The authors declare that they have no conflict of interest.

Disclaimer. This paper contains results of research conducted under the Technical/Scientific Cooperation Agreement between the National Institute for Amazonian Research, the State University of Amazonas, and the Max-Planck-Gesellschaft e.V.; the opinions expressed are the entire responsibility of the authors and not of the participating institutions.

Acknowledgements. This research has been supported by the Max Planck Society, the Max Planck Graduate Center with the Johannes Gutenberg University Mainz (MPGC), the Bundesministerium für Bildung und Forschung (BMBF contracts 01LB1001A, 01LK1602A, and 01LK1602B), the Brazilian Ministério da Ciência, Tecnologia e Inovação (MCTI/FINEP contract 01.11.01248.00), the Conselho Nacional de Desenvolvimento Científico e Tecnológico (CNPq, Brazil) (process 200723/2015-4), the FAPESP (Fundação de Amparo à Pesquisa do Estado de São Paulo) (grant no. 2017/17047-0), the CNPq project (grant no. 169842/2017-7), the CAPES project (grant no. 88887.368025/2019-00), and the European Commission, H2020 Research Infrastructures (A-LIFE (grant no. 640458)). For the operation of the ATTO site, we acknowledge the support by the Max Planck Society, the German Federal Ministry of Education and Research and the Brazilian Ministério da Ciência, Tecnologia e Inovação as well as the Amazon State University (UEA), FAPEAM, LBA/INPA, and SDS/CEUC/RDS-Uatumã. We would like to especially thank all the people involved in the technical, logistical, and scientific support of the ATTO project, in particular Susan Trumbore, Carlos Alberto Quesada, Reiner Ditz, Jürgen Kesselmeier, Thomas Klimach, Björn Nillius, Antonio O. Manzi, Thomas Disper, Hermes Braga Xavier, Nagib Alberto de Castro Souza, Adir Vasconcelos Brandão, Amauri Rodriguês Perreira, André Luiz Matos, Fábio Jorge, Fernando Goncalves Morais, Roberta Pereira de Souza, Bruno Takeshi, Uwe Schultz, Karl Kübler, Olaf Kolle, Martin Hertel, Kerstin Hippler, and Steffen Schmidt. In particular, we would like to thank Andrew Crozier, Sam Jones, Delano Campos, Juarez Viegas, Wallace Rabelo Costa, and Antonio Huxley Melo Nascimento for the frequent maintenance and troubleshooting of the ATTO instrument. A special thanks goes to Mouaz Kazziha for GIS data management and help in the preparation of the composite maps. Remote sensing analyses and visualizations used in this study were produced with the Giovanni online data system, developed and maintained by the NASA GES DISC. We acknowledge the National Oceanic and Atmospheric Administration (NOAA) Air Resources Laboratory (ARL) for the HYSPLIT transport and dispersion model. We further acknowledge the use of imagery from the NASA Worldview application (https://worldview.earthdata.nasa.gov), part of the NASA Earth Observing System Data and Information System (EOSDIS).

Data availability. The dataset presented here are available in NASA Ames format under https://doi.org/10.xxxxx/xx (Holanda et al., 2020c). Additional ATTO data can be found in the ATTO data portal under https://www.attodata.org/ (ATTO, 2020). The time series with cumulative fire count along backward trajectories (see Sect. 2.6) are available in NASA Ames format (named "H1000_Cer_Rain.dat") under https://doi.org/10.17617/3.3q (Holanda et al., 2020b). For data requests beyond the available data, please refer to the corresponding authors.

References

[1] Guilherme Martins Pereira, Sofia Ellen da Silva Caumo, Adriana Grandis, Emerson Queiroz Mota do Nascimento, Alexandre Lima Correia, Henrique de Melo Jorge Barbosa, Marta Angela Marcondes, Marcos Silveira Buckeridge, and Pérola de Castro Vasconcellos. Physical and chemical characterization of the 2019 "black rain" event in the Metropolitan Area of São Paulo, Brazil. *Atmospheric Environment*, 248:118229, mar 2021.

[2] Jos Barlow, Erika Berenguer, Rachel Carmenta, and Filipe França. Clarifying Amazonia's burning crisis. *Global Change Biology*, 26(2):319–321, feb 2020.

[3] H. Escobar. Deforestation in the brazilian amazon is still rising sharply. *Science*, 369(6504):613–613, 2020.

[4] Eric A. Davidson, Alessandro C. de Araujo, Paulo Artaxo, Jennifer K. Balch, I. Foster Brown, Mercedes M. C. Bustamante, Michael T. Coe, Ruth S. DeFries, Michael Keller, Marcos Longo, J. William Munger, Wilfrid Schroeder, Britaldo S. Soares-Filho, Jr. Souza, Carlos M., and Steven C. Wofsy. The amazon basin in transition. *Nature*, 481(7381):321–328, 2012.

[5] J. M. Lobert and J. Wamatz. *Emissions from the combustion process in vegetation*, pages 15–37. John Wiley, New York, 1993.

[6] M. O. Andreae. Emission of trace gases and aerosols from biomass burning – an updated assessment. *Atmospheric Chemistry and Physics*, 19(13):8523–8546, 2019.

[7] E. Salati and P. B. Vose. Amazon Basin: A System in Equilibrium. *Science*, 225(4658):129–138, jul 1984.

[8] Fred Pearce. Weather makers. *Science*, 368(6497):1302, 2020.

[9] Jorge Saturno, Bruna A. Holanda, Christopher Pöhlker, Florian Ditas, Qiaoqiao Wang, Daniel Moran-Zuloaga, Joel Brito, Samara Carbone, Yafang Cheng, Xuguang Chi, Jeannine Ditas, Thorsten Hoffmann, Isabella Hrabe de Angelis, Tobias Könemann, Jošt V. Lavrič, Nan Ma, Jing Ming, Hauke Paulsen, Mira L. Pöhlker, Luciana V. Rizzo, Patrick Schlag, Hang Su, David Walter, Stefan Wolff, Yuxuan Zhang, Paulo Artaxo, Ulrich Pöschl, and Meinrat O. Andreae. Black and brown carbon over central Amazonia: long-term aerosol measurements at the ATTO site. *Atmospheric Chemistry and Physics*, 18(17):12817–12843, sep 2018.

[10] M. L. Pöhlker, F. Ditas, J. Saturno, T. Klimach, I. Hrabě de Angelis, A. C. Araùjo, J. Brito, S. Carbone, Y. Cheng, X. Chi, R. Ditz, S. S. Gunthe, B. A. Holanda, K. Kandler, J. Kesselmeier, T. Könemann, O. O. Krüger, J. V. Lavrič, S. T. Martin,

E. Mikhailov, D. Moran-Zuloaga, L. V. Rizzo, D. Rose, H. Su, R. Thalman, D. Walter, J. Wang, S. Wolff, H. M. J. Barbosa, P. Artaxo, M. O. Andreae, U. Pöschl, and C. Pöhlker. Long-term observations of cloud condensation nuclei over the amazon rain forest – part 2: Variability and characteristics of biomass burning, long-range transport, and pristine rain forest aerosols. *Atmos. Chem. Phys.*, 18(14):10289–10331, 2018.

[11] I. Koren, Y. J. Kaufman, L. A. Remer, and J. V. Martins. Measurement of the effect of amazon smoke on inhibition of cloud formation. *Science*, 303(5662):1342–1345, 2004.

[12] L. Liu, Y. Cheng, S. Wang, C. Wei, M. Pöhlker, C. Pöhlker, P. Artaxo, M. Shrivastava, M. O. Andreae, U. Pöschl, and H. Su. Impact of biomass burning aerosols on radiation, clouds, and precipitation over the amazon: relative importance of aerosol–cloud and aerosol–radiation interactions. *Atmos. Chem. Phys.*, 20:13283–13301, 2020.

[13] M. O. Andreae, D. Rosenfeld, P. Artaxo, A. A. Costa, G. P. Frank, K. M. Longo, and M. A. F. Silva-Dias. Smoking rain clouds over the amazon. *Science*, 303(5662):1337–1342, 2004.

[14] Graham Feingold. On smoke suppression of clouds in Amazonia. *Geophysical Research Letters*, 32(2):L02804, 2005.

[15] D. Rosenfeld, U. Lohmann, G. B. Raga, C. D. O'Dowd, M. Kulmala, S. Fuzzi, A. Reissell, and M. O. Andreae. Flood or drought: How do aerosols affect precipitation? *Science*, 321(5894):1309–1313, 2008.

[16] L. A. Toledo Machado, M. A. Franco, L. A. Kremper, F. Ditas, M. O. Andreae, P. Artaxo, M. A. Cecchini, B. A. Holanda, M. L. Pöhlker, I. Saraiva, S. Wolff, U. Pöschl, and C. Pöhlker. How weather events modify aerosol particle size distributions in the amazon boundary layer. *Atmospheric Chemistry and Physics Discussions*, 2021:1–31, 2021.

[17] M. A. Franco, F. Ditas, L. A. Kremper, L. A. T. Machado, M. O. Andreae, A. Araújo, H. M. J. Barbosa, J. F. de Brito, S. Carbone, B. A. Holanda, F. G. Morais, J. P. Nascimento, M. L. Pöhlker, L. V. Rizzo, M. Sá, J. Saturno, D. Walter, S. Wolff, U. Pöschl, P. Artaxo, and C. Pöhlker. Occurrence and growth of sub-50 nm aerosol particles in the amazonian boundary layer. *Atmospheric Chemistry and Physics Discussions*, 2021:1–36, 2021.

[18] E. Darbyshire, W. T. Morgan, J. D. Allan, D. Liu, M. J. Flynn, J. R. Dorsey, S. J. O'Shea, D. Lowe, K. Szpek, F. Marenco, B. T. Johnson, S. Bauguitte, J. M. Haywood, J. F. Brito, P. Artaxo, K. M. Longo, and H. Coe. The vertical distribution of biomass burning pollution over tropical south america from aircraft in situ measurements during sambba. *Atmos. Chem. Phys.*, 19(9):5771–5790, 2019.

[19] Manfred Wendisch, Ulrich Pöschl, Meinrat O. Andreae, Luiz A. T. Machado, Rachel Albrecht, Hans Schlager, Daniel Rosenfeld, Scot T. Martin, Ahmed Abdelmonem, Armin Afchine, Alessandro C. Araùjo, Paulo Artaxo, Heinfried Aufmhoff, Henrique M. J. Barbosa, Stephan Borrmann, Ramon Braga, Bernhard Buchholz, Micael Amore Cecchini, Anja Costa, Joachim Curtius, Maximilian Dollner, Marcel Dorf, Volker Dreiling, Volker Ebert, André Ehrlich, Florian Ewald, Gilberto Fisch, Andreas Fix, Fabian Frank, Daniel Fütterer, Christopher Heckl, Fabian Heidelberg, Tilman Hüneke, Evelyn Jäkel, Emma Järvinen, Tina Jurkat, Sandra Kanter, Udo Kästner, Mareike Kenntner, Jürgen Kesselmeier,

Thomas Klimach, Matthias Knecht, Rebecca Kohl, Tobias Kölling, Martina Krämer, Mira Krüger, Trismono Candra Krisna, Jost V. Lavric, Karla Longo, Christoph Mahnke, Antonio O. Manzi, Bernhard Mayer, Stephan Mertes, Andreas Minikin, Sergej Molleker, Steffen Münch, Björn Nillius, Klaus Pfeilsticker, Christopher Pöhlker, Anke Roiger, Diana Rose, Dagmar Rosenow, Daniel Sauer, Martin Schnaiter, Johannes Schneider, Christiane Schulz, Rodrigo A. F. de Souza, Antonio Spanu, Paul Stock, Daniel Vila, Christiane Voigt, Adrian Walser, David Walter, Ralf Weigel, Bernadett Weinzierl, Frank Werner, Marcia A. Yamasoe, Helmut Ziereis, Tobias Zinner, and Martin Zöger. Acridicon–chuva campaign: Studying tropical deep convective clouds and precipitation over amazonia using the new german research aircraft halo. *Bulletin of the American Meteorological Society*, 97(10):1885–1908, 2016.

[20] Leoc Aragao, Y. Malhi, N. Barbier, A. Lima, Y. Shimabukuro, L. Anderson, and S. Saatchi. Interactions between rainfall, deforestation and fires during recent years in the brazilian amazonia. *Philosophical Transactions of the Royal Society B-Biological Sciences*, 363(1498):1779–1785, 2008.

[21] P. Artaxo, L. V. Rizzo, J. F. Brito, H. M. J. Barbosa, A. Arana, E. T. Sena, G. G. Cirino, W. Bastos, S. T. Martin, and M. O. Andreae. Atmospheric aerosols in amazonia and land use change: from natural biogenic to biomass burning conditions. *Faraday Discussions*, 165:203–235, 2013.

[22] B. A. Holanda, M. L. Pöhlker, D. Walter, J. Saturno, M. Sörgel, J. Ditas, F. Ditas, C. Schulz, M. A. Franco, Q. Wang, T. Donth, P. Artaxo, H. M. J. Barbosa, S. Borrmann, R. Braga, J. Brito, Y. Cheng, M. Dollner, J. W. Kaiser, T. Klimach, C. Knote, O. O. Krüger, D. Fütterer, J. V. Lavrič, N. Ma, L. A. T. Machado, J. Ming, F. G. Morais, H. Paulsen, D. Sauer, H. Schlager, J. Schneider, H. Su, B. Weinzierl, A. Walser, M. Wendisch, H. Ziereis, M. Zöger, U. Pöschl, M. O. Andreae, and C. Pöhlker. Influx of african biomass burning aerosol during the amazonian dry season through layered transatlantic transport of black carbon-rich smoke. *Atmos. Chem. Phys.*, 20(8):4757–4785, 2020.

[23] C. Pöhlker, D. Walter, H. Paulsen, T. Könemann, E. Rodríguez-Caballero, D. Moran-Zuloaga, J. Brito, S. Carbone, C. Degrendele, V. R. Després, F. Ditas, B. A. Holanda, J. W. Kaiser, G. Lammel, J. V. Lavrič, J. Ming, D. Pickersgill, M. L. Pöhlker, M. Praß, N. Löbs, J. Saturno, M. Sörgel, Q. Wang, B. Weber, S. Wolff, P. Artaxo, U. Pöschl, and M. O. Andreae. Land cover and its transformation in the backward trajectory footprint region of the amazon tall tower observatory. *Atmos. Chem. Phys.*, 19(13):8425–8470, 2019.

[24] H. Baars, A. Ansmann, D. Althausen, R. Engelmann, B. Heese, D. Mller, P. Artaxo, M. Paixao, T. Pauliquevis, and R. Souza. Aerosol profiling with lidar in the Amazon Basin during the wet and dry season. *Journal of Geophysical Research Atmospheres*, 117(21):1–16, 2012.

[25] Qiaoqiao Wang, Jorge Saturno, Xuguang Chi, David Walter, Jost V. Lavric, Daniel Moran-Zuloaga, Florian Ditas, Christopher Pöhlker, Joel Brito, Samara Carbone, Paulo Artaxo, and Meinrat O. Andreae. Modeling investigation of light-absorbing aerosols in the Amazon Basin during the wet season. *Atmospheric Chemistry and Physics*, 16(22):14775–14794, 2016.

[26] Jorge Saturno, Florian Ditas, Marloes Penning De Vries, Bruna A. Holanda, Mira L. Pöhlker, Samara Carbone, David Walter, Nicole Bobrowski, Joel Brito, Xuguang Chi, Alexandra Gutmann, Isabella Hrabe De Angelis, Luiz A.T. Machado, Daniel Moran-Zuloaga, Julian Rüdiger, Johannes Schneider, Christiane Schulz, Qiaoqiao Wang, Manfred Wendisch, Paulo Artaxo, Thomas Wagner, Ulrich Pöschl, Meinrat O. Andreae, and Christopher Pöhlker. African volcanic emissions influencing atmospheric aerosols over the Amazon rain forest. *Atmospheric Chemistry and Physics*, 18(14):10391–10405, 2018.

[27] Anne E. Barkley, Joseph M. Prospero, Natalie Mahowald, Douglas S. Hamilton, Kimberly J. Popendorf, Amanda M. Oehlert, Ali Pourmand, Alexandre Gatineau, Kathy Panechou-Pulcherie, Patricia Blackwelder, and Cassandra J. Gaston. African biomass burning is a substantial source of phosphorus deposition to the Amazon, Tropical Atlantic Ocean, and Southern Ocean. *Proceedings of the National Academy of Sciences*, 116(33):16216–16221, aug 2019.

[28] H. Baars, A. Ansmann, D. Althausen, R. Engelmann, P. Artaxo, T. Pauliquevis, and R. Souza. Further evidence for significant smoke transport from africa to amazonia. *Geophysical Research Letters*, 38:L20802, 2011.

[29] Meinrat O. Andreae. Biomass burning: Its history, use and distribution and its impact on environmental quality and global climate. *Global Biomass Burning: Atmospheric, Climatic and Biospheric Implications, edited by J. S. Levine*, MIT Press,:pp. 3–21, 1991.

[30] Sally Archibald, A. Carla Staver, and Simon A. Levin. Evolution of human-driven fire regimes in Africa. *Proceedings of the National Academy of Sciences of the United States of America*, 109(3):847–852, 2012.

[31] Daniel Moran-Zuloaga, Florian Ditas, David Walter, Jorge Saturno, Joel Brito, Samara Carbone, Xuguang Chi, Isabella Hrabě De Angelis, Holger Baars, Ricardo H M Godoi, Birgit Heese, Bruna A Holanda, Jošt V. Lavrič, Scot Martin, Jing Ming, Mira L Pöhlker, Nina Ruckteschler, Hang Su, Yaqiang Wang, Qiaoqiao Wang, Zhibin Wang, Bettina Weber, Stefan Wolff, Paulo Artaxo, Ulrich Pöschl, Meinrat Andreae, and Christopher Pöhlker. Long-term study on coarse mode aerosols in the Amazon rain forest with the frequent intrusion of Saharan dust plumes. *Atmospheric Chemistry and Physics*, 18(13):10055–10088, 2018.

[32] R. Swap, M. Garstang, S. Greco, R. Talbot, and P. Kallberg. Saharan dust in the amazon basin. *Tellus Series B-Chemical and Physical Meteorology*, 44(2):133–149, 1992.

[33] J. Saturno, B. A. Holanda, C. Pöhlker, F. Ditas, Q. Wang, D. Moran-Zuloaga, J. Brito, S. Carbone, Y. Cheng, X. Chi, J. Ditas, T. Hoffmann, I. Hrabe de Angelis, T. Könemann, J. V. Lavrič, N. Ma, J. Ming, H. Paulsen, M. L. Pöhlker, L. V. Rizzo, P. Schlag, H. Su, D. Walter, S. Wolff, Y. Zhang, P. Artaxo, U. Pöschl, and M. O. Andreae. Black and brown carbon over central amazonia: long-term aerosol measurements at the atto site. *Atmos. Chem. Phys.*, 18(17):12817–12843, 2018.

[34] Adeyemi A. Adebiyi and Paquita Zuidema. The role of the southern African easterly jet in modifying the southeast Atlantic aerosol and cloud environments. *Quarterly Journal of the Royal Meteorological Society*, 142(697):1574–1589, 2016.

[35] A. Petzold, J. A. Ogren, M. Fiebig, P. Laj, S.-M. Li, U. Baltensperger, T. Holzer-Popp, S. Kinne, G. Pappalardo, N. Sugimoto, C. Wehrli, A. Wiedensohler, and X.-Y. Zhang. Recommendations for reporting "black carbon" measurements. *Atmospheric Chemistry and Physics*, 13(16):8365–8379, 2013.

[36] M. O. Andreae, O. C. Acevedo, A. Araùjo, P. Artaxo, C. G. G. Barbosa, H. M. J. Barbosa, J. Brito, S. Carbone, X. Chi, B. B. L. Cintra, N. F. da Silva, N. L. Dias, C. Q. Dias-Júnior, F. Ditas, R. Ditz, A. F. L. Godoi, R. H. M. Godoi, M. Heimann, T. Hoffmann, J. Kesselmeier, T. Könemann, M. L. Krüger, J. V. Lavric, A. O. Manzi, D. Moran-Zuloaga, A. C. Nölscher, D. Santos Nogueira, M. T. F. Piedade, C. Pöhlker, U. Pöschl, L. V. Rizzo, C. U. Ro, N. Ruckteschler, L. D. A. Sá, M. D. O. Sá, C. B. Sales, R. M. N. D. Santos, J. Saturno, J. Schöngart, M. Sörgel, C. M. de Souza, R. A. F. de Souza, H. Su, N. Targhetta, J. Tóta, I. Trebs, S. Trumbore, A. van Eijck, D. Walter, Z. Wang, B. Weber, J. Williams, J. Winderlich, F. Wittmann, S. Wolff, and A. M. Yáñez-Serrano. The amazon tall tower observatory (atto): overview of pilot measurements on ecosystem ecology, meteorology, trace gases, and aerosols. *Atmos. Chem. Phys.*, 15:10723–10776, 2015.

[37] D. Liu, J. D. Allan, D. E. Young, H. Coe, D. Beddows, Z. L. Fleming, M. J. Flynn, M. W. Gallagher, R. M. Harrison, J. Lee, A. S. H. Prevot, J. W. Taylor, J. Yin, P. I. Williams, and P. Zotter. Size distribution, mixing state and source apportionment of black carbon aerosol in london during wintertime. *Atmospheric Chemistry and Physics*, 14(18):10061–10084, 2014.

[38] Jost Heintzenberg. Properties of the log-normal particle size distribution. *Aerosol Science and Technology*, 21(1):46–48, 1994.

[39] S. T. Martin, M. O. Andreae, P. Artaxo, D. Baumgardner, Q. Chen, A. H. Goldstein, A. Guenther, C. L. Heald, O. L. Mayol-Bracero, P. H. McMurry, T. Pauliquevis, U. Poschl, K. A. Prather, G. C. Roberts, S. R. Saleska, M. A. S. Dias, D. V. Spracklen, E. Swietlicki, and I. Trebs. Sources and properties of amazonian aerosol particles. *Reviews of Geophysics*, 48:RG2002, 2010.

[40] S.T. Martin, P. Artaxo, L. Machado, A.O. Manzi, R.A.F. Souza, C. Schumacher, J. Wang, T. Biscaro, J. Brito, A. Calheiros, K. Jardine, A. Medeiros, B. Portela, S.S. de Sá, K. Adachi, A.C. Aiken, R. Albrecht, L. Alexander, M.O. Andreae, H.M.J. Barbosa, P. Buseck, D. Chand, J.M. Comstock, D.A. Day, M. Dubey, J. Fan, J. Fast, G. Fisch, E. Fortner, S. Giangrande, M. Gilles, A.H. Goldstein, A. Guenther, J. Hubbe, M. Jensen, J.L. Jimenez, F.N. Keutsch, S. Kim, C. Kuang, A. Laskin, K. McKinney, F. Mei, M. Miller, R. Nascimento, T. Pauliquevis, M. Pekour, J. Peres, T. Petäjä, C. Pöhlker, U. Pöschl, L. Rizzo, B. Schmid, J.E. Shilling, M.A. Silva Dias, J.N. Smith, J.M. Tomlinson, J. Tóta, and M. Wendisch. The green ocean amazon experiment (goamazon2014/5) observes pollution affecting gases, aerosols, clouds, and rainfall over the rain forest. *Bulletin of the American Meteorological Society*, 0(0):null, 2016.

[41] Christopher Pöhlker, David Walter, Hauke Paulsen, Tobias Könemann, Emilio Rodríguez-caballero, Daniel Moran-zuloaga, Joel Brito, Samara Carbone, Céline Degrendele, Viviane R Després, Florian Ditas, Mira L Pöhlker, Maria Praß,

Nina Löbs, Jorge Saturno, Matthias Sörgel, Qiaoqiao Wang, Bettina Weber, Stefan Wolff, Paulo Artaxo, Ulrich Pöschl, and Meinrat O Andreae. Land cover and its transformation in the backward trajectory footprint region of the Amazon Tall Tower Observatory. *Atmospheric Chemistry and Physics*, pages 8425–8470, 2019.

[42] Mira L. Pöhlker, Christopher Pöhlker, Florian Ditas, Thomas Klimach, Isabella Hrabe De Angelis, Alessandro Araújo, Joel Brito, Samara Carbone, Yafang Cheng, Xuguang Chi, Reiner Ditz, Sachin S. Gunthe, Jürgen Kesselmeier, Tobias Könemann, Jošt V. Lavrič, Scot T. Martin, Eugene Mikhailov, Daniel Moran-Zuloaga, Diana Rose, Jorge Saturno, Hang Su, Ryan Thalman, David Walter, Jian Wang, Stefan Wolff, Henrique M.J. Barbosa, Paulo Artaxo, Meinrat O. Andreae, and Ulrich Pöschl. Long-term observations of cloud condensation nuclei in the Amazon rain forest - Part 1: Aerosol size distribution, hygroscopicity, and new model parametrizations for CCN prediction. *Atmospheric Chemistry and Physics*, 16(24):15709–15740, 2016.

[43] H. Wu, J. W. Taylor, J. M. Langridge, C. Yu, J. D. Allan, K. Szpek, M. I. Cotterell, P. I. Williams, M. Flynn, P. Barker, C. Fox, G. Allen, J. Lee, and H. Coe. Rapid transformation of ambient absorbing aerosols from west african biomass burning. *Atmospheric Chemistry and Physics*, 21(12):9417–9440, 2021.

[44] M. J. Cubison, A. M. Ortega, P. L. Hayes, D. K. Farmer, D. Day, M. J. Lechner, W. H. Brune, E. Apel, G. S. Diskin, J. A. Fisher, H. E. Fuelberg, A. Hecobian, D. J. Knapp, T. Mikoviny, D. Riemer, G. W. Sachse, W. Sessions, R. J. Weber, A. J. Weinheimer, A. Wisthaler, and J. L. Jimenez. Effects of aging on organic aerosol from open biomass burning smoke in aircraft and laboratory studies. *Atmospheric Chemistry and Physics*, 11(23):12049–12064, dec 2011.

[45] Christiane Schulz, Johannes Schneider, Bruna Amorim Holanda, Oliver Appel, Anja Costa, Suzane S. de Sá, Volker Dreiling, Daniel Fütterer, Tina Jurkat-Witschas, Thomas Klimach, Martina Krämer, Scot T. Martin, Stephan Mertes, Mira L. Pöhlker, Daniel Sauer, Christiane Voigt, Bernadett Weinzierl, Helmut Ziereis, Martin Zöger, Meinrat O. Andreae, Paulo Artaxo, Luiz A. T. Machado, Ulrich Pöschl, Manfred Wendisch, and Stephan Borrmann. Aircraft-based observations of isoprene epoxydiol-derived secondary organic aerosol (IEPOX-SOA) in the tropical upper troposphere over the Amazon region. *Atmospheric Chemistry and Physics Discussions*, pages 1–32, apr 2018.

[46] S. S. de Sá, B. B. Palm, P. Campuzano-Jost, D. A. Day, W. Hu, G. Isaacman-VanWertz, L. D. Yee, J. Brito, S. Carbone, I. O. Ribeiro, G. G. Cirino, Y. Liu, R. Thalman, A. Sedlacek, A. Funk, C. Schumacher, J. E. Shilling, J. Schneider, P. Artaxo, A. H. Goldstein, R. A. F. Souza, J. Wang, K. A. McKinney, H. Barbosa, M. L. Alexander, J. L. Jimenez, and S. T. Martin. Urban influence on the concentration and composition of submicron particulate matter in central amazonia. *Atmospheric Chemistry and Physics*, 18(16):12185–12206, 2018.

[47] S. S. de Sá, L. V. Rizzo, B. B. Palm, P. Campuzano-Jost, D. A. Day, L. D. Yee, R. Wernis, G. Isaacman-VanWertz, J. Brito, S. Carbone, Y. J. Liu, A. Sedlacek, S. Springston, A. H. Goldstein, H. M. J. Barbosa, M. L. Alexander, P. Artaxo, J. L. Jimenez, and S. T. Martin. Contributions of biomass-burning, urban, and biogenic emissions to the concentrations and light-absorbing properties of particulate matter in central amazonia during the dry season. *Atmospheric Chemistry and Physics*, 19(12):7973–8001, 2019.

[48] J. Brito, L. V. Rizzo, W. T. Morgan, H. Coe, B. Johnson, J. Haywood, K. Longo, S. Freitas, M. O. Andreae, and P. Artaxo. Ground-based aerosol characterization during the South American Biomass Burning Analysis (SAMBBA) field experiment. *Atmospheric Chemistry and Physics*, 14(22):12069–12083, nov 2014.

[49] Jonathan W Taylor, Huihui Wu, Kate Szpek, Keith Bower, Ian Crawford, Michael J Flynn, Paul I. Williams, James Dorsey, Justin M. Langridge, Michael I. Cotterell, Cathryn Fox, Nicholas W. Davies, Jim M. Haywood, and Hugh Coe. Absorption closure in highly aged biomass burning smoke. *Atmospheric Chemistry and Physics*, 20(19):11201–11221, sep 2020.

[50] T. C. Bond, S. J. Doherty, D. W. Fahey, P. M. Forster, T. Berntsen, B. J. Deangelo, M. G. Flanner, S. Ghan, B. Kärcher, D. Koch, S. Kinne, Y. Kondo, P. K. Quinn, M. C. Sarofim, M. G. Schultz, M. Schulz, C. Venkataraman, H. Zhang, S. Zhang, N. Bellouin, S. K. Guttikunda, P. K. Hopke, M. Z. Jacobson, J. W. Kaiser, Z. Klimont, U. Lohmann, J. P. Schwarz, D. Shindell, T. Storelvmo, S. G. Warren, and C. S. Zender. Bounding the role of black carbon in the climate system: A scientific assessment. *Journal of Geophysical Research Atmospheres*, 118(11):5380–5552, 2013.

[51] Cyrielle Denjean, Thierry Bourrianne, Frederic Burnet, Marc Mallet, Nicolas Maury, Aurélie Colomb, Pamela Dominutti, Joel Brito, Régis Dupuy, Karine Sellegri, Alfons Schwarzenboeck, Cyrille Flamant, and Peter Knippertz. Light absorption properties of aerosols over Southern West Africa. *Atmospheric Chemistry and Physics Discussions*, pages 1–40, aug 2019.

[52] Huihui Wu, Jonathan W. Taylor, Kate Szpek, Justin M. Langridge, Paul I. Williams, Michael Flynn, James D. Allan, Steven J. Abel, Joseph Pitt, Michael I. Cotterell, Cathryn Fox, Nicholas W. Davies, Jim Haywood, and Hugh Coe. Vertical variability of the properties of highly aged biomass burning aerosol transported over the southeast Atlantic during CLARIFY-2017. *Atmospheric Chemistry and Physics*, 20(21):12697–12719, nov 2020.

[53] Paquita Zuidema, Jens Redemann, James Haywood, Robert Wood, Stuart Piketh, Martin Hipondoka, and Paola Formenti. Smoke and Clouds above the Southeast Atlantic: Upcoming Field Campaigns Probe Absorbing Aerosol's Impact on Climate. *Bulletin of the American Meteorological Society*, 97(7):1131–1135, jul 2016.

[54] J. A. Huffman, B. Sinha, R. M. Garland, A. Snee-Pollmann, S. S. Gunthe, P. Artaxo, S. T. Martin, M. O. Andreae, and U. Pöschl. Biological aerosol particle concentrations and size distributions measured in pristine tropical rainforest air during amaze-08. *Atmos. Chem. Phys.*, 12(24):11997–12019, 2012.

[55] Tami C. Bond and Robert W. Bergstrom. Light Absorption by Carbonaceous Particles: An Investigative Review. *Aerosol Science and Technology*, 40(1):27–67, jan 2006.

[56] Jinfeng Yuan, Robin Lewis Modini, Marco Zanatta, Andreas B. Herber, Thomas Müller, Birgit Wehner, Laurent Poulain, Thomas Tuch, Urs Baltensperger, and Martin Gysel-Beer. Variability in the mass absorption cross section of black carbon (BC) aerosols is driven by BC internal mixing state at a central European background site (Melpitz, Germany) in winter. *Atmospheric Chemistry and Physics*, 21(2):635–655, jan 2021.

[57] Kirk A. Fuller, William C. Malm, and Sonia M. Kreidenweis. Effects of mixing on extinction by carbonaceous particles. *Journal of Geophysical Research: Atmospheres*, 104(D13):15941–15954, jul 1999.

[58] J. C. Corbin, H. Czech, D. Massabò, F. Buatier de Mongeot, G. Jakobi, F. Liu, P. Lobo, C. Mennucci, A. A. Mensah, J. Orasche, S. M. Pieber, A. S. H. Prévôt, B. Stengel, L.-L. Tay, M. Zanatta, R. Zimmermann, I. El Haddad, and M. Gysel. Infrared-absorbing carbonaceous tar can dominate light absorption by marine-engine exhaust. *npj Climate and Atmospheric Science*, 2(1):12, dec 2019.

[59] Gregory L. Schuster, Oleg Dubovik, and Brent N. Holben. Angstrom exponent and bimodal aerosol size distributions. *Journal of Geophysical Research*, 111(D7):D07207, 2006.

[60] P. Jöckel, H. Tost, A. Pozzer, M. Kunze, O. Kirner, C. A. M. Brenninkmeijer, S. Brinkop, D. S. Cai, C. Dyroff, J. Eckstein, F. Frank, H. Garny, K.-D. Gottschaldt, P. Graf, V. Grewe, A. Kerkweg, B. Kern, S. Matthes, M. Mertens, S. Meul, M. Neumaier, M. Nützel, S. Oberländer-Hayn, R. Ruhnke, T. Runde, R. Sander, D. Scharffe, and A. Zahn. Earth system chemistry integrated modelling (escimo) with the modular earth submodel system (messy) version 2.51. *Geoscientific Model Development*, 9(3):1153–1200, 2016.

[61] P. Jöckel, A. Kerkweg, A. Pozzer, R. Sander, H. Tost, H. Riede, A. Baumgaertner, S. Gromov, and B. Kern. Development cycle 2 of the Modular Earth Submodel System (MESSy2). *Geosci. Model Dev.*, 3(2):717–752, Dec 2010.

[62] A. Pozzer, A. de Meij, K. J. Pringle, H. Tost, U. M. Doering, J. van Aardenne, and J. Lelieveld. Distributions and regional budgets of aerosols and their precursors simulated with the EMAC chemistry-climate model. *Atmos. Chem. Phys.*, 12(2):961–987, Jan 2012.

[63] G. Danabasoglu, J.-F. Lamarque, J. Bacmeister, D. A. Bailey, A. K. DuVivier, J. Edwards, L. K. Emmons, J. Fasullo, R. Garcia, A. Gettelman, C. Hannay, M. M. Holland, W. G. Large, P. H. Lauritzen, D. M. Lawrence, J. T. M. Lenaerts, K. Lindsay, W. H. Lipscomb, M. J. Mills, R. Neale, K. W. Oleson, B. Otto-Bliesner, A. S. Phillips, W. Sacks, S. Tilmes, L. van Kampenhout, M. Vertenstein, A. Bertini, J. Dennis, C. Deser, C. Fischer, B. Fox-Kemper, J. E. Kay, D. Kinnison, P. J. Kushner, V. E. Larson, M. C. Long, S. Mickelson, J. K. Moore, E. Nienhouse, L. Polvani, P. J. Rasch, and W. G. Strand. The community earth system model version 2 (cesm2). *Journal of Advances in Modeling Earth Systems*, 12(2):e2019MS001916, 2020. e2019MS001916 2019MS001916.

[64] Louisa K. Emmons, Rebecca H. Schwantes, John J. Orlando, Geoff Tyndall, Douglas Kinnison, Jean-François Lamarque, Daniel Marsh, Michael J. Mills, Simone Tilmes, Charles Bardeen, Rebecca R. Buchholz, Andrew Conley, Andrew Gettelman, Rolando Garcia, Isobel Simpson, Donald R. Blake, Simone Meinardi, and Gabrielle Pétron. The chemistry mechanism in the community earth system model version 2 (cesm2). *Journal of Advances in Modeling Earth Systems*, 12(4):e2019MS001882, 2020. e2019MS001882 2019MS001882.

[65] Ruben Ramo, Ekhi Roteta, Ioannis Bistinas, Dave van Wees, Aitor Bastarrika, Emilio Chuvieco, and Guido R. van der Werf. African burned area and fire carbon emissions are strongly impacted by small fires undetected by coarse resolution satellite data. *Proceedings of the National Academy of Sciences*, 118(9), 2021.

[66] Sampa Das, H. Harshvardhan, Huisheng Bian, Mian Chin, Gabriele Curci, Anna P. Protonotariou, Tero Mielonen, Kai Zhang, Hailong Wang, and Xiaohong Liu. Biomass burning aerosol transport and vertical distribution over the South African-Atlantic region. *Journal of Geophysical Research: Atmospheres*, 122(12):6391–6415, 2017.

[67] Marianne T. Lund, Bjørn H. Samset, Ragnhild B. Skeie, Duncan Watson-Parris, Joseph M. Katich, Joshua P. Schwarz, and Bernadett Weinzierl. Short Black Carbon lifetime inferred from a global set of aircraft observations. *npj Climate and Atmospheric Science*, 1(1):1–8, 2018.

[68] Marc Mallet, Pierre Nabat, Paquita Zuidema, Jens Redemann, Andrew Mark Sayer, Martin Stengel, Sebastian Schmidt, Sabrina Cochrane, Sharon Burton, Richard Ferrare, Kerry Meyer, Pablo Saide, Hiren Jethva, Omar Torres, Robert Wood, David Saint Martin, Romain Roehrig, and Christina Hsu. Simulation of the transport , vertical distribution , optical properties and radiative impact of smoke aerosols with the ALADIN regional climate model during the ORACLES-2016 and LASIC experiments. pages 4963–4990, 2019.

[69] G. P. Schill, K. D. Froyd, H. Bian, A. Kupc, C. Williamson, C. A. Brock, E. Ray, R. S. Hornbrook, A. J. Hills, E. C. Apel, M. Chin, P. R. Colarco, and D. M. Murphy. Widespread biomass burning smoke throughout the remote troposphere. *Nature Geoscience*, 13:422–427, 2020.

[70] Y. Shinozuka, P. E. Saide, G. A. Ferrada, S. P. Burton, R. Ferrare, S. J. Doherty, H. Gordon, K. Longo, M. Mallet, Y. Feng, Q. Wang, Y. Cheng, A. Dobracki, S. Freitag, S. G. Howell, S. LeBlanc, C. Flynn, M. Segal-Rosenhaimer, K. Pistone, J. R. Podolske, E. J. Stith, J. R. Bennett, G. R. Carmichael, A. da Silva, R. Govindaraju, R. Leung, Y. Zhang, L. Pfister, J.-M. Ryoo, J. Redemann, R. Wood, and P. Zuidema. Modeling the smoky troposphere of the southeast atlantic: a comparison to oracles airborne observations from september of 2016. *Atmospheric Chemistry and Physics*, 20(19):11491–11526, 2020.

[71] Therese S. Carter, Colette L. Heald, Christopher D. Cappa, Jesse H. Kroll, Teresa L. Campos, Hugh Coe, Michael I. Cotterell, Nicholas W. Davies, Delphine K. Farmer, Cathyrn Fox, Lauren A. Garofalo, Lu Hu, Justin M. Langridge, Ezra J. T. Levin, Shane M. Murphy, Rudra P. Pokhrel, Yingjie Shen, Kate Szpek, Jonathan W. Taylor, and Huihui Wu. Investigating carbonaceous aerosol and its absorption properties from fires in the western united states (we-can) and southern africa (oracles and clarify). *Journal of Geophysical Research: Atmospheres*, 126(15):e2021JD034984, 2021. e2021JD034984 2021JD034984.

Supplementary Materials for African smoke over the Amazon rain forest

Bruna A. Holanda[1], Marco A. Franco[1,2], David Walter[1,3,c], Meinrat O. Andreae[4,5], Paulo Artaxo[2], Samara Carbone[6], Yafang Cheng[1], Sourangsu Chowdhury[7], Florian Ditas[1,a], Martin Gysel-Beer[8], Thomas Klimach[1], Leslie A. Kremper[1], Ovid O. Krüger[1], Jost V. Lavric[3,d], Jos Lelieveld[7], Chaoqun Ma[1], Luiz A. T. Machado[1,2], Fernando G. Morais[2], Robin L. Modini[8], Andrea Pozzer[7], Jorge Saturno[1,b], Hang Su[1], Manfred Wendisch[9], Stefan Wolff[1], Mira L. Pöhlker[1,9,10], Ulrich Pöschl[1], and Christopher Pöhlker[1,4,*]

[1]Multiphase Chemistry Department, Max Planck Institute for Chemistry, 55128 Mainz, Germany

[2]Institute of Physics, University of São Paulo, São Paulo 05508-900, Brazil

[3]Department of Biogeochemical Processes, Max Planck Institute for Biogeochemistry, 07701 Jena, Germany

[4]Biogeochemistry Department, Max Planck Institute for Chemistry, 55128 Mainz, Germany

[5]Scripps Institution of Oceanography, University of California San Diego, La Jolla, CA 92037, USA

[6]Federal University of Uberlândia, Uberlândia-MG, 38408-100, Brazil

[7]Atmospheric Chemistry Department, Max Planck Institute for Chemistry, 55128 Mainz, Germany

[8]Laboratory of Atmospheric Chemistry, Paul Scherrer Institute, 5232 Villigen PSI, Switzerland

[9]Leipzig Institute for Meteorology, Leipzig University, Leipzig, Germany

[10]Experimental Aerosol and Cloud Microphysics Department, Leibniz Institute for Tropospheric Research, Leipzig, Germany

[a]now at: Hessian Agency for Nature Conservation, Environment and Geology, 65203 Wiesbaden, Germany

[b]now at: Physikalisch-Technische Bundesanstalt, 38116 Braunschweig, Germany

[c]now at: Climate Geochemistry Department, Max Planck Institute for Chemistry, 55128 Mainz, Germany

[d]now at: Acoem Ecotech, 1492 Ferntree Gully Road, Knoxfield VIC 3180, Melbourne, Australia

[*]Corresponding author: C. Pöhlker. E-mail: c.pohlker@mpic.de

This manuscript was compiled on October 4, 2021

Contents

S1 Materials and Methods

S1.1 ATTO aerosol and trace gas measurements and data processing

The Amazon Tall Tower Observatory (ATTO, https://www.attoproject.org, last access 30 Aug 2021) is located in the central Amazon basin in a region with largely untouched primary rain forest (2.146° S, 59.006° W, 130 m above sea level, ∼150 km northeast of Manaus, Brazil). Details on atmospheric, geographic, and ecological conditions at the ATTO site and on its footprint region can be found elsewhere [1, 2]. Since 2012, the site has been operated for long-term and in-depth investigations of meteorology, trace gases, atmospheric aerosols, and rain forest ecology [e.g., 3–6]. The measurements presented here span two full seasonal cycles, from January 2019 to December 2020. The results were obtained from a broad set of aerosol instruments, sampling from the 325 m inlet height at the tall tower. The sample air reached the air-conditioned laboratory container with the instruments through a stain-less steel tube (finetron tubes, Dockweiler AG, Neustadt-Glewe, Germany, outer diameter 25 mm , inner diameter 22.1 mm), equipped with a total suspended matter inlet head. The total air flow rate in the tube was 35 L min^{-1}. A transmission curve, specifying particles losses due to diffusion, sedimentation, and impaction in the inlet tube is shown in Fig. S1 [see also 7, 8]. Particle losses in the size range most relevant for this work (i.e., ∼50 nm to ∼1 µm are <5 %. In the laboratory container, an custom-build isokinetic split distributed the sample air to the individual instruments. The sample air was dried by an automated condensation dryer to a relative humidity <40 %. All particle data were corrected for standard temperature and pressure (STP, 273.15 K, 1013.25 hPa). All data was averaged to 3-h time resolution. The data processing was conducted with IGOR Pro (version 8.04, Wavemetrics, Inc., Portland, OR, USA).

Refractory black carbon (rBC) particles were measured by an 8-channel single particle soot photometer (SP2, S/N 12, Droplet Measurement Technologies, Longmont, USA). The instrument measures the time-dependent scattering and incandescence signals produced by single aerosol particles when crossing an intense laser beam with a Gaussian beam profile (Nd:YAG; $\lambda = 1064\,\mathrm{nm}$) [9, 10]. All particles crossing the laser beam scatter light, which is detected by avalanche photodetectors (APD). The intensity of the scattered signal is proportional to the particle scattering cross section, from which its optical diameter (D_p) can be determined. Pure scattering particles (SC) do not absorb light and therefore remain unaffected by the passage through the beam. The particles containing rBC, however, absorb the laser light and are quickly heated to their vaporization temperature ($\sim$4000 °C), which initiates the emission of incandescence light. The peak intensity of the incandescent signal is proportional to the rBC mass in the particles (regardless the coating). Thus, the mass-equivalent diameters of the individual rBC cores ($\mathrm{d_{MEV}}$) are calculated by assuming a void-free sphere with a BC material density of $1.8\,\mathrm{g\,cm^{-3}}$ [11]. The SP2 is sensitive to rBC-free particles in the optical size range of about $180 < D_p < 400\,\mathrm{nm}$ and to rBC cores in the size range of about $80 < d_\mathrm{MEV} < 500\,\mathrm{nm}$, with a counting efficiency close to unity. Calibrations of the incandescence and scattering channels were performed periodically (i.e., in intervals of 2-3 months) using size-selected fullerene soot (Sigma-Aldrich Inc.) and ammonium sulfate (Sigma-Aldrich Inc.) particles, respectively. Particles were generated with an aerosol nebulizer (Droplet Measurement Technologies), dried by a diffusion drier, and size-selected by a differential mobility analyzer (DMA, Grimm Aerosol Technik, Ainring, Germany). During the long-term ATTO measurements, the SP2 software was set to record 1 in every 10 particles. The data were processed with the Paul-Scherrer Institute (PSI) SP2 toolkit [12]. Further details on the SP2 operation at ATTO can be found in Saturno *et al.* [13].

When an internally mixed particle, with rBC core and non-absorbing coating, crosses the laser beam, the rBC-related light absorption causes rapid heating and, thus, initiates a sequential evaporation of the entire particle. First, the non-refractory coating evaporates causing a shrinkage of the particle diameter and its scattering cross section. This is followed by the evaporation of the rBC core [14]. The optical size of the whole particle prior to evaporation can be determined by fitting of a Gaussian to the leading-edge-only (LEO-fit) of the 'early' scattering signal before the particle starts to evaporate [14]. The coating thickness is determined from the SP2's reconstructed scattering and incandescence signals, assuming a spherical concentric core-shell morphology for the Mie calculations [11]. The coating thickness (T_coat) is then calculated based on the difference between the optical diameter (D_p) determined from the LEO fit and the mass equivalent diameter of the rBC cores (d_MEV) according to

$$T_\mathrm{coat} = \frac{D_\mathrm{p} - d_\mathrm{MEV}}{2} \tag{S1}$$

For the Mie calculations, we used the refractive indices of $1.75 + 0.43\mathrm{i}$ for the core and and $1.50 + 0\mathrm{i}$ for the coating, following Yuan *et al.* [15] and Motos *et al.* [16]. The chosen values provide good agreement between the optical diameter of the rBC cores (from the LEO-fit) and the mass equivalent diameter. The coating-thickness analysis in this study includes T_coat values from rBC cores in the size range $180 > d_\mathrm{MEV} > 220\,\mathrm{nm}$.

The total aerosol particle number concentration for particles >6 nm (N_CN) was measured by a Condensation Particle Counter (CPC, model 5412, Grimm Aerosol Technik, Ainring, Germany). Particle number size distributions in the size range of $10-400\,\mathrm{nm}$ were measured by a Scanning Mobility Particle Sizer (SMPS, classifier models 3080, 3082; CPC models 3772, 3750; Neutralizer model 3077; DMA model 3081; TSI Inc. Shoreview, MN, USA). Details on the SMPS measurements at ATTO can be found elsewhere [17**?** , 18]. The SMPS data was processed with the Aerosol Instrument Manager software (AIM, version 10, TSI Inc.). Note that during the period from 01 August to 30 September 2019, the SMPS at the 325 m inlet had technical issues and, therefore, SMPS (model 3080) data from the 60 m inlet line at the 80 m mast was used instead [for further details see 18]. In terms of overall aerosol variability, the sampling heights at 325 m vs 60 m show no pronounced differences (i.e., concentration levels and mode diameters). Thus, the overall aerosol trends in the SMPS contour plots in Fig. S2 are appropriately captured also in the 60 m data. The CCN number concentration at a supersaturation $S = 0.3\,\%$, $N_\mathrm{CCN}(S = 0.3\,\%)$, was calculated from the N_CN data using the κ-Köhler parametrization and annually averaged error function (erf) fit parameters presented in Pöhlker *et al.* [19].

Carbon monoxide (CO) mixing ratios were measured with a Picarro cavity ring-down spectrometer (G1302 analyzer, Picarro Inc., Santa Clara, USA) at five different sampling heights on the 80 m walk-up tower. Here, we used CO data measured at 79 m height. Meteorological parameters such as temperature (Θ), relative humidity (RH), air pressure (p), precipitation rates (P), wind speed and wind direction were measured with a compact weather station (Lufft, WS600-LMB, G. Lufft Mess- und Regeltechnik GmbH, Fellbach, Germany) at a height of 321 m on the tall tower.

Aerosol chemical composition was analyzed with an Aerosol Chemical Speciation Monitor (ACSM, Aerodyne Research Inc., Billerica, MA, USA) at the 60 m height of the 80 m walk-up tower. The instrument measures the major aerosol constituents organics (Org), sulfate (SO_4^{2-}), nitrate (NO_3^-), ammonium (NH_4^+), and chloride (Cl^-) [20]. Data below the following detection limits of the ACSM (measured as described by [20]) were filtered out:: 0.2 µg m^{-3} for Org, 0.015 µg m^{-3} for SO_4^{2-}, 0.16 µg m^{-3} for NH_4^+, 0.013 µg m^{-3} for NO_3^-, and 0.01 µg m^{-3} for Cl^-. The ACSM data coverage during the wet seasons of 2019 and 2020 is comparatively sparse due to technical issues, affecting the statistical analysis of periods with dominant African smoke influence. Despite the reduced statistics, the obtained results are robust and consistent with previous observations over the Amazon basin [21–23] as well as over the South Atlantic Ocean [24–26]. The total submicrometer aerosol mass (M_{PM1}) was determined as the sum of all ACSM-measured species as well as the SP2-derived rBC mass M_{rBC}.

The aerosol absorption coefficient (σ_{abs}) at $\lambda = 637$ nm was measured by a Multi-Angle Absorption Photometer (MAAP, model 5012, Thermo Electron Group, Waltham, USA). In addition, σ_{abs} at 7 wavelengths (370, 470, 520, 590, 637, 660, 880 and 950 nm) were measured by an aethalometer (model AE33, Aerosol d.o.o., Ljubljana, Slovenia). A correction scheme to account for instrument artefacts was applied to the aethalometer data [3, 27, 28]. The corrections to account for multiple scattering effects use MAAP data as a reference absorption measurement [28]. The aerosol scattering coefficients (σ_{scat}) at 3 wavelengths (450, 525, 635 nm) were measured by a nephelometer (model Aurora 3000, Ecotech Pty Ltd., Knoxfield, Australia). The instruments (i.e., nephelometer, aethalometer, MAAP) were installed behind a PM1 cyclone (URG, model URG-2000-30EHB, Chapel Hill, USA), which defined a sharp particle size cut-point towards larger diameters. Details on the nephelometer, aethalometer, and MAAP measurements at ATTO can be found in Saturno *et al.* [3, 28]. The single scattering albedo (SSA), was calculated by dividing the scattering coefficient by total extinction according to

$$\mathrm{SSA}(\lambda) = \frac{\sigma_{\mathrm{sca}}(\lambda)}{\sigma_{\mathrm{sca}}(\lambda) + \sigma_{\mathrm{abs}}(\lambda)} \tag{S2}$$

The mass absorption cross section (MAC) represents the total light absorption per mass of rBC and is used in climate models to convert mass concentration into absorption [29]. The MAC at different wavelengths was derived from the light absorption coefficient, measured by the MAAP and AE33, and the rBC mass concentration, measured by the SP2, as follows

$$\mathrm{MAC}(\lambda) = \frac{\sigma_{\mathrm{abs}}(\lambda)}{M_{\mathrm{rBC}}} \tag{S3}$$

The wavelength dependence of aerosol light absorption or scattering is described by the Ångström exponent. The absorption and scattering Ångström exponents (AAE and SAE) between a wavelength pair can be determined as follows:

$$\mathrm{AAE}(\lambda_1, \lambda_2) = -\frac{\ln(\sigma_{\mathrm{abs}}(\lambda_1)/\sigma_{\mathrm{abs}}(\lambda_2))}{\ln(\lambda_1/\lambda_2)} \tag{S4}$$

and

$$\mathrm{SAE}(\lambda_1, \lambda_2) = -\frac{\ln(\sigma_{\mathrm{sca}}(\lambda_1)/\sigma_{\mathrm{sca}}(\lambda_2))}{\ln(\lambda_1/\lambda_2))} \tag{S5}$$

Several recent studies followed the wavelength pair approach to calculate AAE [e.g. 15, 25, 30]. As an alternative approach [3], we applied a linear fit to the logarithm of the absorption or scattering coefficients vs the logarithm

of the wavelength across the entire wavelength range to obtain the AAE and SAE as follows

$$\ln(\sigma_{\mathrm{abs}}) = -\mathrm{AAE} \cdot \ln(\lambda) + \ln(k_0) \tag{S6}$$

and

$$\ln(\sigma_{\mathrm{sca}}) = -\mathrm{SAE} \cdot \ln(\lambda) + \ln(k_0) \tag{S7}$$

Linear fits with $R^2 < 0.95$ were excluded from the analysis.

S1.2 Aircraft measurements

Selected rBC data from two aircraft campaigns were used in this study. The measurements were conducted onboard the German High Altitude and LOng Range (HALO) research aircraft (https://www.dlr.de/content/de/missionen/halo.html, last access 30 Aug 2021), operated by the German Aerospace Center (DLR). During both campaigns, the same set of instruments in the HALO-CCN-Rack was used, which supports the direct comparability of both datasets [for details, see 31]. The ACRIDICON–CHUVA (Aerosol, Cloud, Precipitation, And Radiation Interactions And Dynamics Of Convective Cloud Systems) campaign was conducted in September and October 2014, covering a large extent of the Amazon basin and the offshore region at the northeastern Brazilian coast (approx. 12° S – 2° N, 79° W – 49° W). The CAFE-Africa (Chemistry of the Atmosphere Field Experiment in Africa) campaign took place in August and September 2018 over the central and southern Atlantic Ocean and Western Africa with base at Sal international airport, Cabo Verde (16.75° N, 22.95° W). In this study, we focused on the CAFE-Africa flights CA04, CA05, CA12, CA13 and CA15 over the South Atlantic Ocean (approx. 10° S – 15° N, 35° E – 5° E) where African biomass burning layers were intensively probed. Detailed information on the ACRIDICON–CHUVA and CAFE-Africa campaigns can be found elsewhere [21, 31–34]. The regions/locations where biomass burning plumes were encountered are shown in Fig. 1.

S1.3 Biomass burning aerosol source assignment

Previous studies indicated – and the present study strongly supports – that the biomass burning smoke in the Amazon can be regarded as a mixture from South American and African fires with a high spatiotemporal variability of both influences [e.g., 7, 35–40]. Related to the approach by Liu *et al.* [41], we used differences in the rBC microphysical properties for a source assignment of the biomass burning smoke measured at ATTO. The overall ATTO time series of the geometric mean diameters (D_{rBC}) and geometric standard deviation (σ_{rBC}), retrieved from 3-h averaged rBC mass size distributions, in relation to the M_{rBC} for the 2-year period analyzed here are shown in Fig. 1B. As shown in Fig. S6A, we found that the D_{rBC} and the σ_{rBC} for the 'event periods' with dominant African or South American BB influences have statistically different properties, which allow a discrimination of both smoke fractions. We found that smoke from South American fires – which refers especially to fires in the ATTO footprint region as shown in Fig. S3 and Pöhlker *et al.* [42] – is characterized by comparatively small rBC cores (i.e., $175 < D_{\mathrm{rBC}} < 185\,\mu\mathrm{m}$) as well as a comparatively broad rBC core size distribution (i.e., $1.64 < \sigma_{\mathrm{rBC}} < 1.69$). In contrast, the aged and transatlantically transported smoke from African fires is characterized by comparatively large rBC cores (i.e., $210 < D_{\mathrm{rBC}} < 220\,\mu\mathrm{m}$) as well as a comparatively narrow rBC core size distribution ($1.47 < \sigma_{\mathrm{rBC}} < 1.49$).

These differences in D_{rBC} and σ_{rBC} appear to be remarkably robust throughout the 2–year time series analyzed here (see also Sect. S2.2). For illustration, Fig. S5 shows the characteristic shape of the rBC core size distributions for the ATTO periods with a predominant influence of either South American or African fires highlighted in Fig. 1B. Further, Fig. S6 summarizes the statistics of D_{rBC} and σ_{rBC} for all ground-based and aircraft campaigns addressed in this study. A remarkable agreement was obtained between the rBC distributions at ATTO and from two complementary aircraft campaigns over the Amazon (ACRIDICON-CHUVA), and over the Atlantic Ocean (CAFE-Africa). During ACRIDICON-CHUVA, two distinctly different conditions were probed: First, defined pollution layer(s) at ~3.5 km altitude, in which smoke from southern Africa was transported across the

Table S1: Statistical analysis of the fit parameters obtained by applying a monomodal fit to the individual BC mass size distributions. The ATTO size distributions was averaged to 3-h and the HALO data to 10 seconds prior to applying the fitting.

		ATTO periods		ACRIDICON-CHUVA		CAFE-Africa						SAMBBA	
		SAm	Afr	Amz	Afr LRT	all	CA04	CA05	CA12	CA13	CA15	Amz	Cerrado
D_{rBC}	Avg	181	217	180	202	226	225	227	219	231	221	179	192
	Std	3	2	8	8	8	5	5	7	8	9	4	9
	P09	176	215	173	193	217	220	221	214	219	214	174	185
	P25	179	216	176	197	221	222	223	217	224	217	177	189
	P50	181	217	180	201	225	225	226	219	232	219	179	192
	P75	183	218	184	206	230	227	229	222	237	223	181	195
	P91	185	219	190	214	237	229	234	225	240	227	184	199
σ_{rBC}	Avg	1.66	1.48	1.59	1.49	1.49	1.50	1.49	1.51	1.48	1.50	1.49	1.52
	Std	0.02	0.01	0.03	0.04	0.04	0.03	0.03	0.04	0.03	0.04	0.03	0.04
	P09	1.64	1.47	1.56	1.44	1.45	1.48	1.45	1.48	1.44	1.46	1.45	1.49
	P25	1.65	1.47	1.57	1.46	1.48	1.49	1.47	1.50	1.46	1.48	1.47	1.50
	P50	1.66	1.48	1.59	1.48	1.49	1.50	1.49	1.52	1.48	1.50	1.49	1.52
	P75	1.67	1.48	1.60	1.51	1.51	1.51	1.51	1.53	1.50	1.52	1.51	1.54
	P91	1.69	1.49	1.62	1.54	1.53	1.52	1.53	1.55	1.52	1.55	1.53	1.56
	N	126	92	13	297	1968	516	310	262	630	250	153	814

Atlantic, were analyzed as outlined in [35]. Under these conditions pure African smoke after $10-15$ days of transport was probed off the Brazilian coast prior to being mixed into the convective boundary layer over the Amazon. In this layer, we found averages of $D_{\mathrm{rBC,AC,Afr}} = 205 \pm 8$ nm and $\sigma_{\mathrm{rBC,AC,Af}} = 1.50 \pm 0.02$. Second, four fresh biomass burning plumes were probed directly over fires in the Amazon, which therefore represent reference cases for pure and fresh Amazonian smoke. For these plumes, averages of $D_{\mathrm{rBC,AC,SAm}} = 181$ nm and $\sigma_{\mathrm{rBC,AC,SAm}} = 1.65$ were obtained. During CAFE-Africa, the transatlantic transport of African smoke was sampled at different locations over the ocean (see Fig. 1A$_2$), yielding averages of $D_{\mathrm{rBC,CA,Afr}} = 223 \pm 5$ nm and $\sigma_{\mathrm{rBC,CA,Afr}} = 1.50 \pm 0.02$. The D_{rBC} and σ_{rBC} from the aircraft and ATTO data agree remarkably well, suggesting that the smoke from African and South American fires can be represented by generalized rBC signatures.

In previous studies, differences in the rBC size distributions have been related either to differences in the combustion and emission process, which includes fuel types, fuel moisture content, and flaming vs smoldering conditions, or to differences in atmospheric transport and aging, which can be driven by coagulation or size-dependent particle removal through rain-out [e.g., 11, 43–47]. Below, we summarize the observations suggesting that the contrasting rBC signatures measured at ATTO (i.e., D_{rBC} and σ_{rBC}) are likely defined by the fuel and combustion conditions and, thus appear to be largely source-specific. (*i*) The rBC mass size distribution of African smoke measured at ATTO agrees well with our aircraft measurements over the Atlantic Ocean closer to the African coast (see Fig. S5), suggesting that transatlantic transport does not change the rBC signature to a significant extent. In fact, on the way to South America, the African smoke travels typically $10-15$ days within highly stratified aerosol layers up to 5.5 km height over the Atlantic Ocean [7, 35, 37, 48, 49]. Over the ocean, the atmospheric circulation follows the St. Helena high pressure system, and, therefore, African smoke encounters few precipitation clouds during transatlantic transport. In addition, the number concentration of rBC particles in these smoke layers are too low (~ 100's cm^{-3}) for self-coagulation to be an important process on these timescales [50]. (*ii*) We found a consistent rBC signature for transatlantically transported smoke from Northern Africa, measured at ATTO in the wet season, and Southern Africa, measured by the aircraft in the dry season (Fig. S5). This is consistent with similar average fuel mixtures in Northern and Southern Africa (Fig. S4 C$_2$ and D$_2$), comprising mostly dry vegetation (i.e., deciduous open and closed forests, shrublands, and herbaceous landscapes) and suggesting a dominance of a flaming fire regime [51]. (*iii*) When the smoke layers are advected over the South American continent, where convection sets in, large scale subsidence or downdrafts from convection distributes the African aerosol vertically over the continental mixed layer changing the concentrations at the ATTO site. Still, no noticeable size selection due to rain-out on the way from the offshore region to the ATTO site as suggested by the cumulative rain along BT (Fig. 1B$_3$). (*iv*) The fuel mixture in the ATTO BT footprint region on the South American continent differs clearly from the African fuel mixture (compare Fig. S4 and Fig. S3). Here, fires in evergreen rain forest regions in the Amazonia followed by fires in Cerrado are the most relevant for ATTO according to sensitivity model runs in Fig. S19. The transport time of the smoke from fires in the footprint region to ATTO is between 1 to 4 days and the smoke is transported

within a well mixed layer up to 3.5 km altitude [see Fig. S12 and 49].

Given that mixed smoke conditions in central Amazonia – and probably also the entire basin – are the rule rather than the exception and that South American vs African smoke is characterized by robust differences in rBC properties (Fig. S6), the D_{rBC} and σ_{rBC} time series in Fig. 1 can be deconvoluted quantitatively as mixed South American and African influences. Therefore, we conducted a bimodal fitting to the rBC mass size distribution time series after averaging it to 3-h time bins. The fit was applied across the rBC size range from 90 to 500 nm. The following function according to Heintzenberg [52] has been used

$$f(d_{\mathrm{MEV}}) = \frac{A_{\mathrm{rBC,SAm}}}{\sqrt{2\pi} log(\sigma_{\mathrm{rBC,SAm}})} \exp\left[-\frac{(log(d_{\mathrm{MEV}}) - logD_{\mathrm{rBC,SAm}})^2}{2log^2(\sigma_{\mathrm{rBC,SAm}})}\right] + \frac{A_{\mathrm{rBC,Afr}}}{\sqrt{2\pi} log(\sigma_{\mathrm{rBC,Afr}})} \exp\left[-\frac{(log(d_{\mathrm{MEV}}) - logD_{\mathrm{rBC,Afr}})^2}{2log^2(\sigma_{\mathrm{rBC,Afr}})}\right] \tag{S8}$$

with the fit parameters $D_{\mathrm{rBC,i}}$ as geometric mean diameter, $\sigma_{\mathrm{rBC,i}}$ as geometric standard deviation, and $A_{\mathrm{rBC,i}}$ as the rBC mass concentration at $D_{\mathrm{rBC,i}}$. The bimodal fit comprised one 'African (Afr) mode' and one 'South American (SAm) mode'. The fit parameters $D_{\mathrm{rBC,i}}$ and $\sigma_{\mathrm{rBC,i}}$ were constrained according to the rBC properties for largely 'pure' African and South American smoke (Fig. S6). Specifically, the following constraints were used for the African mode:

- $A_{\mathrm{rBC,Afr}}$ was a free parameter
- $D_{\mathrm{rBC,Afr}}$ was constrained within the range from 215 to 219 nm
- $\sigma_{\mathrm{rBC,Afr}}$ was constrained within the range from 1.47 to 1.49

The following constraints were used for the South American mode:

- $A_{\mathrm{rBC,SAm}}$ was a free parameter
- $D_{\mathrm{rBC,SAm}}$ was constrained within the range from 176 to 185 nm
- $\sigma_{\mathrm{rBC,SAm}}$ was constrained within the range from 1.64 to 1.69

For illustration, examples of bimodal-fitted rBC size distributions for different mixed smoke conditions are shown in Fig. S7.

Based on the bimodal fits, the African ($M_{\mathrm{rBC,Afr}}$) vs South American ($M_{\mathrm{rBC,SAm}}$) contributions to the total M_{rBC} were quantified as the integral mass concentrations of rBC cores of the corresponding modes. The resulting time series of the separated influence of African vs South American rBC based on this approach is shown in Fig. 2. Further, the aerosol properties at ATTO were classified into the following five pollution regimes:

- **Dominant South American influence**: $M_{\mathrm{rBC,SAm}}/M_{\mathrm{rBC}} > 0.85$
- **Majoritarian South American influence**: $0.5 < M_{\mathrm{rBC,SAm}}/M_{\mathrm{rBC}} < 0.85$
- **Majoritarian African influence**: $0.5 < M_{\mathrm{rBC,Afr}}/M_{\mathrm{rBC}} < 0.85$
- **Dominant African influence**: $M_{\mathrm{rBC,Afr}}/M_{\mathrm{rBC}} > 0.85$
- **Pristine**: $M_{\mathrm{rBC}} < 0.01\,\mu\mathrm{g\,m^{-3}}$ according to definition in [53]

Note that the number of modes (n) fitted in Equation S8 can be in principle as high as the number of different combustion sources, given that they are characterized by different microphysical rBC properties. For simplicity, we assume here that biomass burning in Africa and in South America are the only two (major) sources providing BC particles to ATTO. This means that other rBC sources, such as urban pollution e.g. from Manaus city, do not contribute significantly, which is justified according to Pöhlker *et al.* [42].

S1.4 Backward trajectories

The backward trajectory (BT) analysis is based on the Hybrid Single-Particle Lagrangian Integrated Trajectory model (HYSPLIT, NOAA-ARL) with meteorological input data from the Global Data Assimilation System [54, 55]. The 1 d as well as 3 d BTs in the composite maps (e.g., Fig. 1) were calculated with GDAS meteorological input data at 0.25° resolution. A starting height of 200 m a.g.l. (above ground level) was chosen. For a systematic ATTO-related BT analysis, refer to Pöhlker *et al.* [42].

S1.5 Proxy for African smoke influx into the Amazon: satellite-derived CO mixing concentration in offshore region in front of South American coast

To estimate the influx of air masses carrying African biomass burning emissions into the Amazon basin, the carbon monoxide (CO) data from the satellite Sentinel-5P (vertically integrated CO column density in $\mathrm{mol\,m^{-2}}$; OFFL L3 product; obtained through Google Earth Engine, https://code.earthengine.google.com/, last access 30 Aug 2021) within an offshore region of interest ($\mathrm{ROI_{offshore}}$) located at the northeastern coast of South America was used. The $\mathrm{ROI_{offshore}}$ and the corresponding CO data ($\mathrm{CO_{ROI}}$) are shown in Fig. S8. In the steady westerly trade winds [35, 42], the influx of African smoke into the central Amazon passes through the $\mathrm{ROI_{offshore}}$, which makes $\mathrm{CO_{ROI}}$ a useful (qualitative) marker for its seasonality. For typical air mass velocities (obtained from the length of the BTs), the average transport time from the center of the $\mathrm{ROI_{offshore}}$ to ATTO is about 3.2 days. Accordingly, the $\mathrm{CO_{ROI}}$ time series was shifted by 3.2 days. Note that this average shift is just an approximation since the offset time can vary quite significantly from ~ 2 to ~ 5 days.

S1.6 Proxy for periods with intense South American smoke influence at ATTO: cumulative number of fires along backward trajectories

The time series of cumulative fire intensity along the BTs ($\mathrm{CF_{BT}}$) was calculated based on (i) an ensemble of filtered 3 d HYSPLIT BTs, started every hour in the time frame between 1 January 2019 and 31 December 2020, at a starting height of 200 m, and (ii) daily georeferenced fire intensity maps, in $\mathrm{W\,m^{-2}}$, from the Global Fire Assimilation System (GFAS). Detailed information on this procedure can be found in [35]. The GFAS fire intensity maps were obtained as NetCDF3 files with a spatial resolution of 0.1° latitude by 0.1° longitude. Only those segments of the individual BTs in convective exchange with the surface/fires (i.e., BT segments with heights <1000 m) and encountering *en route* convection (i.e., BT segments with sun fluxes $>50\,\mathrm{W\,m^{-2}}$ were included in the calculation of $\mathrm{CF_{BT}}$. In addition, the individual BTs were terminated upon *en route* occurrence of rain (i.e., for rainfall >2 mm. Details of the BT data set and filtering can be found in [42].

S1.7 Proxy for aerosol wet scavenging in air masses arriving at ATTO: cumulative precipitation along backward trajectories

Precipitation data, which was available through GDAS and the HYSPLIT model for every data point of the BTs, was used to calculate the cumulative precipitation, P_{BT}, for every individual 3-day BT. The resulting P_{BT} time series represents the amount of rain that the air masses experienced during their last 3 days of transport towards ATTO. Accordingly, P_{BT} reflects the extent of rain-related aerosol scavenging of the arriving air masses. For details, refer to [7] and [42].

S1.8 Geographic information system (GIS) data and processing

The analysis of geographic information system (GIS) data sets was conducted with the QGIS software package (version 3.12, QGIS development team, https://www.qgis.org/, last access 31 Aug 2021) using the coordinate

reference of the World Geodetic System from 1984 (WGS84). The following GIS data sets have been used in this study:

- **Land cover**: The land cover data was obtained from the Copernicus Global Land Service and data was downloaded under https://land.copernicus.eu/global/products/lc (last access 06 Feb 2021).
- **Fire maps**: The satellite-detected fires were obtained from the Instituto Nacional de Pesquisas Espaciais (INPE), available under http://queimadas.dgi.inpe.br/queimadas/portal (last access 31 Aug 2021). Only fires from the NASA satellites Terra and Aqua we taken into account here.
- **Wind vector fields**: Wind vectors were calculated based on data from the Modern-Era Retrospective analysis for Research and Applications Version 2 model (Merra-2, https://gmao.gsfc.nasa.gov/reanalysis/MERRA-2/, last access: 06 Feb 2021) obtained through the Giovanni online data system (https://giovanni.gsfc.nasa.gov/giovanni/, last access 06 Feb 2021).
- **Corrected reflectance satellite images**: Satellite images (here from Suomi NPP / VIIRS) were downloaded as GeoTiff files from the NASA's EOSDIS Worldview (https://worldview.earthdata.nasa.gov, last access: 06 Feb 2021).
- **Global water bodies**: Maps of global water bodies were obtained from the European Space Agency (ESA) (https://www.esa-landcover-cci.org/?q=node/162, last access: 15 June 2020).
- **Major roads**: The GIS information on highways and roads in the Amazon Basin were retrieved from the OpenStreetMap (OSM) data set (https://www.openstreetmap.org, last access 13 Dec 2020) and the Amazonian road network from CRS maps (http://maps.csr.ufmg.br, last access 13 Dec 2020).
- **Brazilian biomes**: The GIS data specifying the geographic extent of the Brazilian biomes Amazônia, Cerrado, Caatinga, and Mata Atlântica were obtained from Global Forest Watch (https://data.globalforestwatch.org, last access 16 Mar 2021).

S1.9 Analysis of fires per land cover type to determine mixture of burnt fuels/vegetation

In QGIS, the INPE fire maps (from the satellites Aqua and Terra only) for 2019 were projected onto the Copernicus land cover maps for 2019. The detected fires were classified into the established 22 land cover categories. The seasonality in the occurrence of land-cover-specific fires was then analyzed for the year 2019 to create Fig. S4 and Fig. S3. For Africa, this analysis was further separated into the Northern vs Southern hemisphere of the continent. For South America – and specifically for the ATTO-relevant footprint region – the fire maps were further subdivided into the biome regions Amazônia, Cerrado, Caatinga, and Mata Atlântica. Based on this seasonal data for 2019, the following periods were highlighted in Pie charts: (i) Average fire/fuel mixture in Northern Africa between January and March, which corresponds to the peak of long-range transport of African dust and smoke into the Amazon during the wet season as outlined in [7] (Fig. S4C2). (ii) Average fire/fuel mixture in Southern Africa between August and September, which corresponds to the peak of long-range transport of African smoke into the Amazon during the dry season as outlined in [35] (Fig. S4D2). (iii) Average fire/fuel mixtures in the ATTO footprint region in South America – separated into the four relevant biomes Amazônia, Cerrado, Caatinga, and Mata Atlântica – between August and September, which corresponds to the peak of biomass burning in the Amazon as outlined in [42] (Fig. S3C2–F2).

S1.10 EMAC model

We used the EMAC global atmospheric chemistry model at T63 grid, engulfing the ATTO station horizontal, which has a spectral resolution of 1.8° × 1.8°, with 47 hybrid vertical levels up to 0.01 hPa [56–60]. The 5th generation European Centre Hamburg general circulation model (ECHAM5) was used as the base atmospheric model.

Multiple submodels in EMAC illustrate the tropospheric and stratospheric processes and their interaction with the biosphere. We used the Modular Earth Submodel System (MESSy, v.2.55, [57, 61]) to link submodels that describe emission, aerosol formation, atmospheric chemistry, clouds and other processes in the base model. The GMXe (Global Modal Aerosol Extension) submodel [62] simulates the microphysical processes in aerosols and the gas/aerosol portioning. There are two main modes in GMXe, namely hydrophilic and hydrophobic. The hydrophilic mode encompasses aerosols in the entire size spectrum (coarse, accumulation, Aitken and nucleation), while the hydrophobic mode does not include the nucleation mode. We updated the assumptions in the GMXe by emitting black carbon in accumulation and Aitken modes following a recent study [63]. The ORACLE (Organic Aerosol Composition and Evolution) submodel [64, 65] was used to simulate the atmospheric evolution, composition and transport of organic aerosols. The AEROPT (AERosol OPTical properties) submodel [58, 66–68], was used to simulate the aerosol optical properties. AEROPT assumes the aerosol components in each mode to be spherical, well mixed and with volume averaged refractive indices. The gas phase and heterogeneous chemistry was simulated with the MECCA submodel [69, 70]. To enable the high-frequency output of data from the model at the geographic coordinates of ATTO, we implemented the SCOUT [57] submodel. Apart from these submodels, the following MESSy submodels were enabled, AIRSEA, BIOBURN, CLOUD, CLOUDOPT, CONVEC, CVTRANS, DDEP, E5VDIFF, H2O, JVAL, LNOX, OFFEMIS, ONEMIS, ORBIT, SCAV, SEDI, SORBIT, SURFACE, TNUDGE and TROPOP. Explicit description of each of these submodels can be found in the MESSy submodel list (https://www.messy-interface.org/current/auto/messy_submodels.html, last access 28 July 2021).

The EMAC global simulations, nudged towards the ERA-5 meteorological re-analyses, were performed from January 2019 to November 2020. Over the past decade, EMAC model simulations of aerosols and trace gases have been extensively assessed against ground measurements and satellite retrievals [71–77]. Here, we use the monthly varying Community Emissions Data System (CEDS) anthropogenic emission inventory of 2014, [78] at $0.5^\circ \times 0.5^\circ$ resolution for the primary emitted species, i.e. SO_2 (sulfur dioxide), NH_3 (ammonia), CO (carbon monoxide), NO_2 (oxides of nitrogen), BC, OC (organic carbon), and NMVOCs (non methane volatile organic compounds). The CEDS emission inventory includes eight broad anthropogenic source sectors – transportation (TRA), industrial combustion and processes (IND), power generation (PGN), residential and commercial combustion (RES), waste incineration (WST), agricultural waste burning (AWB), agricultural soils (AGS) and shipping (SHP). Biomass burning emissions were obtained from the Global Fire Assimilation System (GFAS) inventory [79] for the study period, with updated emission factors for fire types and chemical species from [80]. The emissions data were then pre-processed and vertically distributed in six emission heights following [58]. Besides the standard simulation (STD) with all emissions in all geographies turned on, we performed five sensitivity simulations:

(a) **NOANTH:** with emissions from TRA, IND, PGN, RES, WST, AWB, AGS and SHP switched off to quantify the impact of these anthropogenic sources on the ATTO site.

(b) **NOBB:** with zero biomass burning emissions globally, which indicates the influence of all biomass burning emissions over the ATTO site.

(c) **NOBBafr:** with zero biomass burning emissions over the African continent. This test run helps to identify the impact of transported BC from African continent in the Amazon.

(d) **NOBBcer:** with zero biomass burning emissions from Cerrado biome.

(e) **NOBBcaa:** zero biomass burning emission over from Caatinga biome. The two last runs test the influence of savanna-like fires in Caatinga and Cerrado may have an influence on the rBC classification scheme presented in this study.

Further, the BC influences attributed to anthropogenic pollution (ANTH), biomass burning (BB), Africa fires (BBafr), Cerrado fires (BBcer), Caatinga fires (BBcaa) and Amazonia fires (BBamz) were calculated as follow:

(a) **ANTH:** STD - NOANTH

(b) **BB:** STD - NOBB

(c) **BBafr:** STD - NOBBafr

(d) **BBcer:** STD - NOBBcer

(e) **BBcaa:** STD - NOBBcaa

(f) **BBamz:** STD - NOBB - NOBBafr - NOBBcer - NOBBcaa. This is an approximation for the fires in Amazonia since *BBamz* may have a contribution from BB from the rest of the world. However, this contribution is very small and can be ignored for our analysis.

To evaluate the ability of the models in reproducing the BC observations at ATTO, we calculated the mean bias (MB) of the model as follows:

$$\mathrm{MB}(\%) = \frac{\frac{\sum_{i=1}^{N} O_i}{N} - \frac{\sum_{i=1}^{N} M_i}{N}}{\frac{\sum_{i=1}^{N} O_i}{N}} * 100 \tag{S9}$$

where N is the number of observations, M_i and O_i are the model and observation values at each time step i, respectively.

S1.11 CAM-chem model

The Community Atmosphere Model with Chemistry (CAM-chem, v.6.3) was implemented to simulate the contribution from African biomass burning to the black carbon concentration at ATTO site. The CAM-chem is an active atmosphere component of the Community Earth System Model (CESM) [81] in which a Finite Volume (FV) dynamical core [82] was coupled with Model for Ozone and Related chemical Tracers with Tropospheric and Stratospheric chemistry (MOZART-TS1) [83] and four-mode version of the Modal Aerosol Module (MAM4) [84]. The CAM-chem was run with horizontal resolution of $0.94° \times 0.94°$, and 56 levels vertical levels to $\sim$45 km while its model meteorology (including winds, surface pressure, and temperature) was nudged toward MERRA2 reanalysis (https://doi.org/10.5065/XVAQ-2X07, last access 18 August 2021). Lower boundary condition about sea and sea ice were prescribed with the merged Hadley-OI sea surface temperature and sea ice concentration data [85].

CAM-chem has a full consideration of different processes that affect aerosol properties include new particle formation, gas- and aqueous-phase chemistry, dry deposition and gravitational settling, water uptake, in cloud (nucleation) and below-cloud scavenging, and release from evaporated cloud and raindrops. Anthropogenic emission of BC was extracted from Community Emissions Data System (CEDS) [86] while biomass burning emission was provided by Quick Fire Emissions Dataset (QFED) [87]. Both anthropogenic and biomass burning BC was emitted into the first model layer without considering plume rise.

The standard model simulation (CAM-chem$_{\mathrm{STD}}$) was carried with all emissions in all geographies activated. Simulated mass concentration of BC was then interpolated to the ATTO station position to compare with the observations. Also, to quantify the contribution of African biomass burning, a parallel experiment (CAM-chem$_{\mathrm{NOBBafr}}$) was performed by zeroing out biomass burning emission over African continent. Both the two simulations were run from October 2018 to July 2020 while results of the first 3 months were not used for spin-up.

S1.12 MERRA-2 model

Modern-Era Retrospective analysis for Research and Applications v.2 (MERRA-2) simulated BC mass concentration was retrieved over the bounding area ($-60 < \mathrm{Lon} < -58.125° E$; $-2.5 < \mathrm{Lat} < -1.5° N$) that includes the ATTO site. The area-averaged of black carbon surface mass concentration with 1 hour time resolution was

obtained from the Giovanni platform (https://giovanni.gsfc.nasa.gov/giovanni/, last access: 23 March 2021). The MERRA-2 provides near-real-time climate analysis, in which aerosol and meteorological observations are jointly assimilated within a global data assimilation system [88]. The Goddard Global Ozone Chemistry Aerosol Radiation and Transport (GOCART) model [89, 90] coupled with the Goddard Earth Observing System version 5 (GEOS-5) atmospheric model [91] treats the sources, sinks, and chemistry of five externally mixed aerosol species, including dust, sea salt, black carbon (hydrophobic and hydrophilic), organic carbon, and sulfate. The GEOS-5 model runs on 0.625° × 0.5° latitude–longitude grids and 72 vertical layers from the surface to 0.01 hPa [92–94].

Biomass burning emissions of organic carbon, black carbon, and SO_2 aerosols in MERRA-2 derive from a variety of inventories over the course of the reanalysis. Since 2010, MERRA-2 utilizes the Quick Fire Emissions Dataset (QFED) version 2.4-r6 [87] which draws on the cloud correction method used in the Global Fire Assimilation System (GFAS; [95]) and employs a treatment of emissions from nonobserved land areas [87]. The fire locations and fire radiative power (FRP) are obtained from MODerate Resolution Imaging Spectroradiometer MODIS level-2 fire and geolocation products. Level-2 fire products are gridded at 0.3125° × 0.25° latitude–longitude resolution and combined in order to create daily mean emissions at the same resolution. The losses for all aerosol types include dry deposition (including gravitational settling), large-scale wet removal, and convective scavenging. The model-generated precipitation is corrected with observations prior to affect the wet deposition of aerosols over land and ocean [96]. Aerosol hygroscopic growth depends on simulated relative humidity and is considered in computations of particle fall velocity, deposition velocity, and optical parameters. Numerous studies have demonstrated the skill of the GOCART aerosol module in simulating AOD and other observable aerosol properties [e.g. 90, 97–99].

S2 Supplementary Text

S2.1 Amazonian deforestation rates and fire counts

The long-term time series of deforestation rates in the Amazon are shown in Fig. S2. The continuous decrease in deforestation rates from about 2004 until about 2014/15 is clearly visible [compare also 100]. The relative maximum in deforestation rates 2015/16 can be associated with the comparatively strong El Niño during these years, which is typically associated with drought conditions in the central basin [42]. Over 2017 and 2018, deforestation rates stagnated. Since 2019, deforestation rates underwent a steep rise.

S2.2 Biomass burning aerosol source assignment

The biomass burning aerosol source assignment as described in subsection S1.3 is the backbone of the present study and has, therefore been evaluated and verified carefully. Outlined below are results and arguments that support that the source assignment is robust and quantitative:

1. By means of daily composite maps, combining fires counts, total reflectance satellite images, backward trajectories from ATTO, and reanalysis wind vector fields, days with a preponderance of either African or South American BB influence were identified. Examples of such maps are shown in (Fig. 1C, S10, S11) An illustrative example for 'pure' African BB influence is the 03 February 2020 as shown in Fig. 1D, which is representative for the time window between 20-23 January and 03-09 February 2020 (highlighted as gray shading in Fig. 1B). These days belong to the Amazonian wet season, which is characterized by a minimum in fire occurrence in the Amazon as well as strong rainfall and efficient aerosol scavenging. Accordingly, an influence from Amazonian fires can be largely neglected as shown in previous studies [e.g., 7, 38, 42, 101]. Yet, the 03 February was characterized by rather strongly polluted conditions at ATTO (i.e., $M_{\mathrm{rBC}} = 0.48 \pm 0.33\,\mu\mathrm{g\,m^{-3}}$, mean ± SD), which can be explained by long-range transport of African smoke [7]. Figure 1C shows the relatively 'straight', northeasterly backward trajectories, which correspond with the typical air mass advection pattern for long-range transport as outlined in [7]. The

fire map shows no indications that the trajectories passed over fires in Amazonia. An additional example for 'pure' African BB influence on the central Amazon is shown in Fig. S11.

2. A characteristic polluted episode at ATTO ($M_{\mathrm{rBC}} = 0.32 \pm 0.08\,\mu\mathrm{g\,m^{-3}}$) with 'pure' South American BB influence spanned from 28 July to 11 August 2020 (see green shading in Fig. 1B). As an example, the 01 August 2020 in Fig. 1C shows the overall air mass advection patterns. During this time, southerly winds brought dense smoke from fire hotspots along the highways BR-230 and BR-163 to ATTO. The smoke could visually be traced in the satellite images (see Fig. $1C_1$ and Fig. S10). Further, the influence of African BB was low during this episode since the long-range transport from Africa is associated with easterly rather than southerly advections. Also the CO concentrations in the $\mathrm{ROI_{offshore}}$ off the Brazilian coast show a minimum during this time as shown in (Fig. S8b).

3. In the course of the ACRIDICON-CHUVA aircraft campaign over the Amazon basin in the dry season 2014 [102], smoke layers over the Atlantic ocean were observed, which could be attributed to the long-range transport of BB emissions from Southern Africa [35]. As these smoke layer were probed off the South American coast in steady westerly wind fields, they were unaffected by fires in the Amazon and, thus indeed represent the properties of the aged African smoke prior to mixing with the Amazonian smoke upon arrival over the continent. The rBC properties observed within the smoke layer correspond exactly with the rBC properties during periods at ATTO that were dominated by African BB influence as shown in Fig. 1.

4. Analysis of plume-wise variability of rBC properties in two-year time series from ATTO.

5. Generally, our observations are consistent with the typical D_{rBC} range of ~170 to ~230 nm in biomass burning plumes from previous laboratory and field studies [e.g., 11, 25, 30, 45, 46, 103].

Moreover, while African smoke is transported within (highly) stratified aerosol layers up to 5.5 km height over the Atlantic, the Amazon smoke is transported horizontally within a well-mixed layer up to 3.5 km [49]. Therefore we consider that the African smoke did not undergo relevant wet scavenging neither during horizontal transport nor over the South American continent prior to reaching the ATTO site (as suggested in Fig. 1B), which could influence the rBC mode diameter [44]. We assume also that no significant coagulational growth of rBC cores take place during horizontal transport. Because BC number concentration within this study are in the order of $\sim 100\,\mathrm{s\,cm^{-3}}$, BC self coagulation, that would lead to larger core diameters over time, is rather a weak process influencing BC size distribution within the time scale from days to weeks of atmospheric aging [50, 104]. Even in measurements closer to the source, when particle concentration are orders of magnitude higher, no significant increase in D_{rBC} was observed [24, 25].

References

[1] C. Pöhlker, D. Walter, H. Paulsen, T. Könemann, E. Rodríguez-Caballero, D. Moran-Zuloaga, J. Brito, S. Carbone, C. Degrendele, V. R. Després, F. Ditas, B. A. Holanda, J. W. Kaiser, G. Lammel, J. V. Lavrič, J. Ming, D. Pickersgill, M. L. Pöhlker, M. Praß, N. Löbs, J. Saturno, M. Sörgel, Q. Wang, B. Weber, S. Wolff, P. Artaxo, U. Pöschl, and M. O. Andreae. Land cover and its transformation in the backward trajectory footprint region of the amazon tall tower observatory. *Atmos. Chem. Phys.*, 19(13):8425–8470, 2019.

[2] M. O. Andreae, O. C. Acevedo, A. Araùjo, P. Artaxo, C. G. G. Barbosa, H. M. J. Barbosa, J. Brito, S. Carbone, X. Chi, B. B. L. Cintra, N. F. da Silva, N. L. Dias, C. Q. Dias-Júnior, F. Ditas, R. Ditz, A. F. L. Godoi, R. H. M. Godoi, M. Heimann, T. Hoffmann, J. Kesselmeier, T. Könemann, M. L. Krüger, J. V. Lavric, A. O. Manzi, D. Moran-Zuloaga, A. C. Nölscher, D. Santos Nogueira, M. T. F. Piedade, C. Pöhlker, U. Pöschl, L. V. Rizzo, C. U. Ro, N. Ruckteschler, L. D. A. Sá, M. D. O. Sá, C. B. Sales, R. M. N. D. Santos, J. Saturno, J. Schöngart, M. Sörgel, C. M. de Souza, R. A. F. de Souza, H. Su, N. Targhetta, J. Tóta, I. Trebs, S. Trumbore, A. van Eijck, D. Walter, Z. Wang, B. Weber, J. Williams, J. Winderlich,

F. Wittmann, S. Wolff, and A. M. Yáñez-Serrano. The amazon tall tower observatory (atto): overview of pilot measurements on ecosystem ecology, meteorology, trace gases, and aerosols. *Atmos. Chem. Phys.*, 15:10723–10776, 2015.

[3] J. Saturno, B. A. Holanda, C. Pöhlker, F. Ditas, Q. Wang, D. Moran-Zuloaga, J. Brito, S. Carbone, Y. Cheng, X. Chi, J. Ditas, T. Hoffmann, I. Hrabe de Angelis, T. Könemann, J. V. Lavrič, N. Ma, J. Ming, H. Paulsen, M. L. Pöhlker, L. V. Rizzo, P. Schlag, H. Su, D. Walter, S. Wolff, Y. Zhang, P. Artaxo, U. Pöschl, and M. O. Andreae. Black and brown carbon over central amazonia: long-term aerosol measurements at the atto site. *Atmos. Chem. Phys.*, 18(17):12817–12843, 2018.

[4] A. M. Yáñez-Serrano, A. C. Nölscher, E. Bourtsoukidis, E. Gomes Alves, L. Ganzeveld, B. Bonn, S. Wolff, M. Sa, M. Yamasoe, J. Williams, M. O. Andreae, and J. Kesselmeier. Monoterpene chemical speciation in a tropical rainforest:variation with season, height, and time of dayat the amazon tall tower observatory (atto). *Atmos. Chem. Phys.*, 18(5):3403–3418, 2018.

[5] S. Botía, C. Gerbig, J. Marshall, J. V. Lavric, D. Walter, C. Pöhlker, B. Holanda, G. Fisch, A. C. de Araújo, M. O. Sá, P. R. Teixeira, A. F. Resende, C. Q. Dias-Junior, H. van Asperen, P. S. Oliveira, M. Stefanello, and O. C. Acevedo. Understanding nighttime methane signals at the amazon tall tower observatory (atto). *Atmos. Chem. Phys.*, 20(11):6583–6606, 2020.

[6] N. Löbs, C. G. G. Barbosa, S. Brill, D. Walter, F. Ditas, M. de Oliveira Sá, A. C. de Araújo, L. R. de Oliveira, R. H. M. Godoi, S. Wolff, M. Piepenbring, J. Kesselmeier, P. Artaxo, M. O. Andreae, U. Pöschl, C. Pöhlker, and B. Weber. Aerosol measurement methods to quantify spore emissions from fungi and cryptogamic covers in the amazon. *Atmos. Meas. Tech.*, 13(1):153–164, 2020.

[7] Daniel Moran-Zuloaga, Florian Ditas, David Walter, Jorge Saturno, Joel Brito, Samara Carbone, Xuguang Chi, Isabella Hrabě De Angelis, Holger Baars, Ricardo H M Godoi, Birgit Heese, Bruna A Holanda, Jošt V. Lavrič, Scot Martin, Jing Ming, Mira L Pöhlker, Nina Ruckteschler, Hang Su, Yaqiang Wang, Qiaoqiao Wang, Zhibin Wang, Bettina Weber, Stefan Wolff, Paulo Artaxo, Ulrich Pöschl, Meinrat Andreae, and Christopher Pöhlker. Long-term study on coarse mode aerosols in the Amazon rain forest with the frequent intrusion of Saharan dust plumes. *Atmospheric Chemistry and Physics*, 18(13):10055–10088, 2018.

[8] S. L. von der Weiden, F. Drewnick, and S. Borrmann. Particle loss calculator – a new software tool for the assessment of the performance of aerosol inlet systems. *Atmos. Meas. Tech.*, 2(2):479–494, 2009.

[9] Michelle Stephens, Nelson Turner, and Jon Sandberg. Particle identification by laser-induced incandescence in a solid-state laser cavity. *Applied optics*, 42(19):3726–36, 2003.

[10] Joshua P. Schwarz, R. S. Gao, D. W. Fahey, D. S. Thomson, L. A. Watts, J. C. Wilson, J. M. Reeves, M. Darbeheshti, D. G. Baumgardner, G. L. Kok, S. H. Chung, M. Schulz, J. Hendricks, A. Lauer, B. Kärcher, J. G. Slowik, K. H. Rosenlof, T. L. Thompson, A. O. Langford, M. Loewenstein, and K. C. Aikin. Single-particle measurements of midlatitude black carbon and light-scattering aerosols from the boundary layer to the lower stratosphere. *Journal of Geophysical Research Atmospheres*, 111(16):1–15, 2006.

[11] M. Laborde, M. Crippa, T. Tritscher, Z. Jurányi, P. F. Decarlo, B. Temime-Roussel, N. Marchand, S. Eckhardt, A. Stohl, U. Baltensperger, A. S.H. Prévôt, E. Weingartner, and M. Gysel. Black carbon physical properties and mixing state in the European megacity Paris. *Atmospheric Chemistry and Physics*, 13(11):5831–5856, 2013.

[12] M Gysel-Beer and J Corbin. SP2 toolkit 4.115 (Igor7) (Version 4.115). http://doi.org/10.5281/zenodo.3575186/, 2019.

[13] Jorge Saturno, Bruna A. Holanda, Christopher Pöhlker, Florian Ditas, Qiaoqiao Wang, Daniel Moran-Zuloaga, Joel Brito, Samara Carbone, Yafang Cheng, Xuguang Chi, Jeannine Ditas, Thorsten Hoffmann, Isabella Hrabe de Angelis, Tobias Könemann, Jošt V. Lavrič, Nan Ma, Jing Ming, Hauke Paulsen, Mira L.

Pöhlker, Luciana V. Rizzo, Patrick Schlag, Hang Su, David Walter, Stefan Wolff, Yuxuan Zhang, Paulo Artaxo, Ulrich Pöschl, and Meinrat O. Andreae. Black and brown carbon over central Amazonia: long-term aerosol measurements at the ATTO site. *Atmospheric Chemistry and Physics*, 18(17):12817–12843, sep 2018.

[14] R. S. Gao, J. P. Schwarz, K. K. Kelly, D. W. Fahey, L. a. Watts, T. L. Thompson, J. R. Spackman, J. G. Slowik, E. S. Cross, J.-H. Han, P. Davidovits, T. B. Onasch, and D. R. Worsnop. A Novel Method for Estimating Light-Scattering Properties of Soot Aerosols Using a Modified Single-Particle Soot Photometer. *Aerosol Science and Technology*, 41(2):125–135, 2007.

[15] Jinfeng Yuan, Robin Lewis Modini, Marco Zanatta, Andreas B. Herber, Thomas Müller, Birgit Wehner, Laurent Poulain, Thomas Tuch, Urs Baltensperger, and Martin Gysel-Beer. Variability in the mass absorption cross section of black carbon (BC) aerosols is driven by BC internal mixing state at a central European background site (Melpitz, Germany) in winter. *Atmospheric Chemistry and Physics*, 21(2):635–655, jan 2021.

[16] Ghislain Motos, Joel C. Corbin, Julia Schmale, Rob L. Modini, Michele Bertò, Piotr Kupiszewski, Urs Baltensperger, and Martin Gysel-Beer. Black Carbon Aerosols in the Lower Free Troposphere are Heavily Coated in Summer but Largely Uncoated in Winter at Jungfraujoch in the Swiss Alps. *Geophysical Research Letters*, 47(14):1–10, 2020.

[17] L. A. Toledo Machado, M. A. Franco, L. A. Kremper, F. Ditas, M. O. Andreae, P. Artaxo, M. A. Cecchini, B. A. Holanda, M. L. Pöhlker, I. Saraiva, S. Wolff, U. Pöschl, and C. Pöhlker. How weather events modify aerosol particle size distributions in the amazon boundary layer. *Atmospheric Chemistry and Physics Discussions*, 2021:1–31, 2021.

[18] M. L. Pöhlker, C. Pöhlker, T. Klimach, I. Hrabe de Angelis, H. M. J. Barbosa, J. Brito, S. Carbone, Y. Cheng, X. Chi, F. Ditas, R. Ditz, S. S. Gunthe, J. Kesselmeier, T. Könemann, J. V. Lavrič, S. T. Martin, D. Moran-Zuloaga, D. Rose, J. Saturno, H. Su, R. Thalman, D. Walter, J. Wang, S. Wolff, P. Artaxo, M. O. Andreae, and U. Pöschl. Long-term observations of cloud condensation nuclei in the amazon rain forest – part 1: Aerosol size distribution, hygroscopicity, and new model parameterizations for ccn prediction. *Atmos. Chem. Phys.*, 16:15709–15740, 2016.

[19] Mira L. Pöhlker, Christopher Pöhlker, Florian Ditas, Thomas Klimach, Isabella Hrabe De Angelis, Alessandro Araújo, Joel Brito, Samara Carbone, Yafang Cheng, Xuguang Chi, Reiner Ditz, Sachin S. Gunthe, Jürgen Kesselmeier, Tobias Könemann, Jošt V. Lavrič, Scot T. Martin, Eugene Mikhailov, Daniel Moran-Zuloaga, Diana Rose, Jorge Saturno, Hang Su, Ryan Thalman, David Walter, Jian Wang, Stefan Wolff, Henrique M.J. Barbosa, Paulo Artaxo, Meinrat O. Andreae, and Ulrich Pöschl. Long-term observations of cloud condensation nuclei in the Amazon rain forest - Part 1: Aerosol size distribution, hygroscopicity, and new model parametrizations for CCN prediction. *Atmospheric Chemistry and Physics*, 16(24):15709–15740, 2016.

[20] N. L. Ng, S. C. Herndon, A. Trimborn, M. R. Canagaratna, P. L. Croteau, T. B. Onasch, D. Sueper, D. R. Worsnop, Q. Zhang, Y. L. Sun, and J. T. Jayne. An aerosol chemical speciation monitor (acsm) for routine monitoring of the composition and mass concentrations of ambient aerosol. *Aerosol Science and Technology*, 45(7):780–794, 2011.

[21] Christiane Schulz, Johannes Schneider, Bruna Amorim Holanda, Oliver Appel, Anja Costa, Suzane S. de Sá, Volker Dreiling, Daniel Fütterer, Tina Jurkat-Witschas, Thomas Klimach, Martina Krämer, Scot T. Martin, Stephan Mertes, Mira L. Pöhlker, Daniel Sauer, Christiane Voigt, Bernadett Weinzierl, Helmut Ziereis, Martin Zöger, Meinrat O. Andreae, Paulo Artaxo, Luiz A. T. Machado, Ulrich Pöschl, Manfred Wendisch, and Stephan Borrmann. Aircraft-based observations of isoprene epoxydiol-derived secondary organic aerosol (IEPOX-SOA) in the tropical upper troposphere over the Amazon region. *Atmospheric Chemistry and Physics Discussions*, pages 1–32, apr 2018.

[22] S. S. de Sá, B. B. Palm, P. Campuzano-Jost, D. A. Day, W. Hu, G. Isaacman-VanWertz, L. D. Yee, J. Brito, S. Carbone, I. O. Ribeiro, G. G. Cirino, Y. Liu, R. Thalman, A. Sedlacek, A. Funk, C. Schumacher, J. E. Shilling, J. Schneider, P. Artaxo, A. H. Goldstein, R. A. F. Souza, J. Wang, K. A. McKinney, H. Barbosa, M. L. Alexander, J. L. Jimenez, and S. T. Martin. Urban influence on the concentration and composition of submicron particulate matter in central amazonia. *Atmospheric Chemistry and Physics*, 18(16):12185–12206, 2018.

[23] S. S. de Sá, L. V. Rizzo, B. B. Palm, P. Campuzano-Jost, D. A. Day, L. D. Yee, R. Wernis, G. Isaacman-VanWertz, J. Brito, S. Carbone, Y. J. Liu, A. Sedlacek, S. Springston, A. H. Goldstein, H. M. J. Barbosa, M. L. Alexander, P. Artaxo, J. L. Jimenez, and S. T. Martin. Contributions of biomass-burning, urban, and biogenic emissions to the concentrations and light-absorbing properties of particulate matter in central amazonia during the dry season. *Atmospheric Chemistry and Physics*, 19(12):7973–8001, 2019.

[24] H. Wu, J. W. Taylor, J. M. Langridge, C. Yu, J. D. Allan, K. Szpek, M. I. Cotterell, P. I. Williams, M. Flynn, P. Barker, C. Fox, G. Allen, J. Lee, and H. Coe. Rapid transformation of ambient absorbing aerosols from west african biomass burning. *Atmospheric Chemistry and Physics*, 21(12):9417–9440, 2021.

[25] Jonathan W Taylor, Huihui Wu, Kate Szpek, Keith Bower, Ian Crawford, Michael J Flynn, Paul I. Williams, James Dorsey, Justin M. Langridge, Michael I. Cotterell, Cathryn Fox, Nicholas W. Davies, Jim M. Haywood, and Hugh Coe. Absorption closure in highly aged biomass burning smoke. *Atmospheric Chemistry and Physics*, 20(19):11201–11221, sep 2020.

[26] Huihui Wu, Jonathan W. Taylor, Kate Szpek, Justin M. Langridge, Paul I. Williams, Michael Flynn, James D. Allan, Steven J. Abel, Joseph Pitt, Michael I. Cotterell, Cathryn Fox, Nicholas W. Davies, Jim Haywood, and Hugh Coe. Vertical variability of the properties of highly aged biomass burning aerosol transported over the southeast Atlantic during CLARIFY-2017. *Atmospheric Chemistry and Physics*, 20(21):12697–12719, nov 2020.

[27] M. Collaud Coen, E. Weingartner, A. Apituley, D. Ceburnis, R. Fierz-Schmidhauser, H. Flentje, J. S. Henzing, S. G. Jennings, M. Moerman, A. Petzold, O. Schmid, and U. Baltensperger. Minimizing light absorption measurement artifacts of the aethalometer: evaluation of five correction algorithms. *Atmos. Meas. Tech.*, 3(2):457–474, 2010.

[28] J. Saturno, C. Pöhlker, D. Massabò, J. Brito, S. Carbone, Y. Cheng, X. Chi, F. Ditas, I. Hrabě de Angelis, D. Morán-Zuloaga, M. L. Pöhlker, L. V. Rizzo, D. Walter, Q. Wang, P. Artaxo, P. Prati, and M. O. Andreae. Comparison of different aethalometer correction schemes and a reference multi-wavelength absorption technique for ambient aerosol data. *Atmos. Meas. Tech.*, 10(8):2837–2850, 2017.

[29] T. C. Bond, S. J. Doherty, D. W. Fahey, P. M. Forster, T. Berntsen, B. J. Deangelo, M. G. Flanner, S. Ghan, B. Kärcher, D. Koch, S. Kinne, Y. Kondo, P. K. Quinn, M. C. Sarofim, M. G. Schultz, M. Schulz, C. Venkataraman, H. Zhang, S. Zhang, N. Bellouin, S. K. Guttikunda, P. K. Hopke, M. Z. Jacobson, J. W. Kaiser, Z. Klimont, U. Lohmann, J. P. Schwarz, D. Shindell, T. Storelvmo, S. G. Warren, and C. S. Zender. Bounding the role of black carbon in the climate system: A scientific assessment. *Journal of Geophysical Research Atmospheres*, 118(11):5380–5552, 2013.

[30] E. Darbyshire, W. T. Morgan, J. D. Allan, D. Liu, M. J. Flynn, J. R. Dorsey, S. J. O'Shea, D. Lowe, K. Szpek, F. Marenco, B. T. Johnson, S. Bauguitte, J. M. Haywood, J. F. Brito, P. Artaxo, K. M. Longo, and H. Coe. The vertical distribution of biomass burning pollution over tropical south america from aircraft in situ measurements during sambba. *Atmos. Chem. Phys.*, 19(9):5771–5790, 2019.

[31] Manfred Wendisch, Ulrich Poschl, Meinrat O. Andreae, Luiz A.T. MacHado, Rachel Albrecht, Hans Schlager, Daniel Rosenfeld, Scot T. Martin, Ahmed Abdelmonem, Armin Afchine, Alessandro C. Araujo, Paulo Artaxo, Heinfried Aufmhoff, Henrique M.J. Barbosa, Stephan Borrmann, Ramon Braga, Bernhard Buchholz, Micael Amore Cecchini, Anja Costa, Joachim Curtius, Maximilian Dollner, Marcel Dorf, Volker Dreiling, Volker Ebert, Andre Ehrlich, Florian Ewald, Gilberto Fisch, Andreas Fix, Fabian Frank, Daniel

Futterer, Christopher Heckl, Fabian Heidelberg, Tilman Huneke, Evelyn Jakel, Emma Jarvinen, Tina Jurkat, Sandra Kanter, Udo Kastner, Mareike Kenntner, Jurgen Kesselmeier, Thomas Klimach, Matthias Knecht, Rebecca Kohl, Tobias Kolling, Martina Kramer, Mira Kruger, Trismono Candra Krisna, Jost V. Lavric, Karla Longo, Christoph Mahnke, Antonio O. Manzi, Bernhard Mayer, Stephan Mertes, Andreas Minikin, Sergej Molleker, Steffen Munch, Bjorn Nillius, Klaus Pfeilsticker, Christopher Pohlker, Anke Roiger, Diana Rose, Dagmar Rosenow, Daniel Sauer, Martin Schnaiter, Johannes Schneider, Christiane Schulz, Rodrigo A.F. De Souza, Antonio Spanu, Paul Stock, Daniel Vila, Christiane Voigt, Adrian Walser, David Walter, Ralf Weigel, Bernadett Weinzierl, Frank Werner, Marcia A. Yamasoe, Helmut Ziereis, Tobias Zinner, and Martin Zoger. Acridicon-chuva campaign: Studying tropical deep convective clouds and precipitation over amazonia using the New German research aircraft HALO. *Bulletin of the American Meteorological Society*, 97(10):1885–1908, 2016.

[32] Meinrat O. Andreae, Armin Afchine, Rachel Albrecht, Bruna Amorim Holanda, Paulo Artaxo, Henrique M. J. Barbosa, Stephan Borrmann, Micael A. Cecchini, Anja Costa, Maximilian Dollner, Daniel Fütterer, Emma Järvinen, Tina Jurkat, Thomas Klimach, Tobias Konemann, Christoph Knote, Martina Krämer, Trismono Krisna, Luiz A. T. Machado, Stephan Mertes, Andreas Minikin, Christopher Pöhlker, Mira L. Pöhlker, Ulrich Pöschl, Daniel Rosenfeld, Daniel Sauer, Hans Schlager, Martin Schnaiter, Johannes Schneider, Christiane Schulz, Antonio Spanu, Vinicius B. Sperling, Christiane Voigt, Adrian Walser, Jian Wang, Bernadett Weinzierl, Manfred Wendisch, and Helmut Ziereis. Aerosol characteristics and particle production in the upper troposphere over the Amazon Basin. *Atmospheric Chemistry and Physics*, 18(2):921–961, jan 2018.

[33] I. Tadic, C. Nussbaumer, B. Bohn, H. Harder, D. Marno, M. Martinez, F. Obersteiner, U. Parchatka, A. Pozzer, R. Rohloff, M. Zöger, J. Lelieveld, and H. Fischer. Central role of nitric oxide in ozone production in the upper tropical troposphere over the atlantic ocean and west africa. *Atmospheric Chemistry and Physics Discussions*, 2021:1–24, 2021.

[34] J. Schneider, R. Weigel, T. Klimach, A. Dragoneas, O. Appel, A. Hünig, S. Molleker, F. Köllner, H.-C. Clemen, O. Eppers, P. Hoppe, P. Hoor, C. Mahnke, M. Krämer, C. Rolf, J.-U. Grooß, A. Zahn, F. Obersteiner, F. Ravegnani, A. Ulanovsky, H. Schlager, M. Scheibe, G. S. Diskin, J. P. DiGangi, J. B. Nowak, M. Zöger, and S. Borrmann. Aircraft-based observation of meteoric material in lower-stratospheric aerosol particles between 15 and 68° n. *Atmospheric Chemistry and Physics*, 21(2):989–1013, 2021.

[35] B. A. Holanda, M. L. Pöhlker, D. Walter, J. Saturno, M. Sörgel, J. Ditas, F. Ditas, C. Schulz, M. A. Franco, Q. Wang, T. Donth, P. Artaxo, H. M. J. Barbosa, S. Borrmann, R. Braga, J. Brito, Y. Cheng, M. Dollner, J. W. Kaiser, T. Klimach, C. Knote, O. O. Krüger, D. Fütterer, J. V. Lavrič, N. Ma, L. A. T. Machado, J. Ming, F. G. Morais, H. Paulsen, D. Sauer, H. Schlager, J. Schneider, H. Su, B. Weinzierl, A. Walser, M. Wendisch, H. Ziereis, M. Zöger, U. Pöschl, M. O. Andreae, and C. Pöhlker. Influx of african biomass burning aerosol during the amazonian dry season through layered transatlantic transport of black carbon-rich smoke. *Atmos. Chem. Phys.*, 20(8):4757–4785, 2020.

[36] H. Baars, A. Ansmann, D. Althausen, R. Engelmann, B. Heese, D. Mller, P. Artaxo, M. Paixao, T. Pauliquevis, and R. Souza. Aerosol profiling with lidar in the Amazon Basin during the wet and dry season. *Journal of Geophysical Research Atmospheres*, 117(21):1–16, 2012.

[37] Qiaoqiao Wang, Jorge Saturno, Xuguang Chi, David Walter, Jost V. Lavric, Daniel Moran-Zuloaga, Florian Ditas, Christopher Pöhlker, Joel Brito, Samara Carbone, Paulo Artaxo, and Meinrat O. Andreae. Modeling investigation of light-absorbing aerosols in the Amazon Basin during the wet season. *Atmospheric Chemistry and Physics*, 16(22):14775–14794, 2016.

[38] Jorge Saturno, Florian Ditas, Marloes Penning De Vries, Bruna A. Holanda, Mira L. Pöhlker, Samara Carbone, David Walter, Nicole Bobrowski, Joel Brito, Xuguang Chi, Alexandra Gutmann, Isabella Hrabe De Angelis, Luiz A.T. Machado, Daniel Moran-Zuloaga, Julian Rüdiger, Johannes Schneider, Christiane Schulz, Qiaoqiao Wang, Manfred Wendisch, Paulo Artaxo, Thomas Wagner, Ulrich Pöschl, Meinrat O.

Andreae, and Christopher Pöhlker. African volcanic emissions influencing atmospheric aerosols over the Amazon rain forest. *Atmospheric Chemistry and Physics*, 18(14):10391–10405, 2018.

[39] Anne E. Barkley, Joseph M. Prospero, Natalie Mahowald, Douglas S. Hamilton, Kimberly J. Popendorf, Amanda M. Oehlert, Ali Pourmand, Alexandre Gatineau, Kathy Panechou-Pulcherie, Patricia Blackwelder, and Cassandra J. Gaston. African biomass burning is a substantial source of phosphorus deposition to the Amazon, Tropical Atlantic Ocean, and Southern Ocean. *Proceedings of the National Academy of Sciences*, 116(33):16216–16221, aug 2019.

[40] B. A. Holanda, M. L. Pöhlker, D. Walter, J. Saturno, M. Sörgel, J. Ditas, F. Ditas, C. Schulz, M. A. Franco, Q. Wang, T. Donth, P. Artaxo, H. M. J. Barbosa, S. Borrmann, R. Braga, J. Brito, Y. Cheng, M. Dollner, J. W. Kaiser, T. Klimach, C. Knote, O. O. Krüger, D. Fütterer, J. V. Lavrič, N. Ma, L. A. T. Machado, J. Ming, F. G. Morais, H. Paulsen, D. Sauer, H. Schlager, J. Schneider, H. Su, B. Weinzierl, A. Walser, M. Wendisch, H. Ziereis, M. Zöger, U. Pöschl, M. O. Andreae, and C. Pöhlker. Influx of african biomass burning aerosol during the amazonian dry season through layered transatlantic transport of black carbon-rich smoke. *Atmos. Chem. Phys.*, 20(8):4757–4785, 2020.

[41] D. Liu, J. D. Allan, D. E. Young, H. Coe, D. Beddows, Z. L. Fleming, M. J. Flynn, M. W. Gallagher, R. M. Harrison, J. Lee, A. S. H. Prevot, J. W. Taylor, J. Yin, P. I. Williams, and P. Zotter. Size distribution, mixing state and source apportionment of black carbon aerosol in london during wintertime. *Atmospheric Chemistry and Physics*, 14(18):10061–10084, 2014.

[42] Christopher Pöhlker, David Walter, Hauke Paulsen, Tobias Könemann, Emilio Rodríguez-caballero, Daniel Moran-zuloaga, Joel Brito, Samara Carbone, Céline Degrendele, Viviane R Després, Florian Ditas, Mira L Pöhlker, Maria Praß, Nina Löbs, Jorge Saturno, Matthias Sörgel, Qiaoqiao Wang, Bettina Weber, Stefan Wolff, Paulo Artaxo, Ulrich Pöschl, and Meinrat O Andreae. Land cover and its transformation in the backward trajectory footprint region of the Amazon Tall Tower Observatory. *Atmospheric Chemistry and Physics*, pages 8425–8470, 2019.

[43] Joshua P. Schwarz, R. S. Gao, J. R. Spackman, L. A. Watts, D. S. Thomson, D. W. Fahey, T. B. Ryerson, J. Peischl, J. S. Holloway, M. Trainer, G. J. Frost, T. Baynard, D. A. Lack, J. A. de Gouw, C. Warneke, and L. A. Del Negro. Measurement of the mixing state, mass, and optical size of individual black carbon particles in urban and biomass burning emissions. *Geophysical Research Letters*, 35(13):1–5, 2008.

[44] N Moteki, Y Kondo, N Oshima, N Takegawa, M Koike, K Kita, H Matsui, and M Kajino. Size dependence of wet removal of black carbon aerosols during transport from the boundary layer to the free troposphere. *Geophysical Research Letters*, 39:2–5, 2012.

[45] A. A. May, G. R. McMeeking, T. Lee, J. W. Taylor, J. S. Craven, I. Burling, A. P. Sullivan, S. Akagi, J. L. Collett, M. Flynn, H. Coe, S. P. Urbanski, J. H. Seinfeld, R. J. Yokelson, and S. M. Kreidenweis. Aerosol emissions from prescribed fires in the united states: A synthesis of laboratory and aircraft measurements. *Journal of Geophysical Research-Atmospheres*, 119(20):11826–11849, 2014.

[46] Amara L Holder, Gayle S W Hagler, Johanna Aurell, Michael D Hays, and Brian K Gullett. Particulate matter and black carbon optical properties and emission factors from prescribed fires in the southeastern United States. *Journal of Geophysical Research: Atmospheres*, 121(7):3465–3483, apr 2016.

[47] Ghislain Motos, Julia Schmale, Joel C. Corbin, Rob L. Modini, Nadine Karlen, Michele Bertò, Urs Baltensperger, and Martin Gysel-Beer. Cloud droplet activation properties and scavenged fraction of black carbon in liquid-phase clouds at the high-alpine research station Jungfraujoch (3580ma.s.l.). *Atmospheric Chemistry and Physics*, 19(6):3833–3855, 2019.

[48] M. O. Andreae, E. V. Browell, M. Garstang, G. L. Gregory, R. C. Harriss, G. F. Hill, D. J. Jacob, M. C. Pereira, G. W. Sachse, A. W. Setzer, P. L. Silva Dias, R. W. Talbot, A. L. Torres, and S. C. Wofsy. Biomass-burning emissions and associated haze layers over Amazonia. *Journal of Geophysical Research*, 93(D2):1509, 1988.

[49] Albert Ansmann, Holger Baars, Matthias Tesche, Detlef Müller, Dietrich Althausen, Ronny Engelmann, Theotonio Pauliquevis, and Paulo Artaxo. Dust and smoke transport from Africa to South America: Lidar profiling over Cape Verde and the Amazon rainforest. *Geophysical Research Letters*, 36(11):L11802, jun 2009.

[50] L. Fierce, N. Riemer, and T. C. Bond. Explaining variance in black carbon's aging timescale. *Atmospheric Chemistry and Physics*, 15(6):3173–3191, 2015.

[51] J. M. Lobert and J. Wamatz. *Emissions from the combustion process in vegetation*, pages 15–37. John Wiley, New York, 1993.

[52] Jost Heintzenberg. Properties of the log-normal particle size distribution. *Aerosol Science and Technology*, 21(1):46–48, 1994.

[53] M. L. Pöhlker, F. Ditas, J. Saturno, T. Klimach, I. Hrabě de Angelis, A. C. Araùjo, J. Brito, S. Carbone, Y. Cheng, X. Chi, R. Ditz, S. S. Gunthe, B. A. Holanda, K. Kandler, J. Kesselmeier, T. Könemann, O. O. Krüger, J. V. Lavrič, S. T. Martin, E. Mikhailov, D. Moran-Zuloaga, L. V. Rizzo, D. Rose, H. Su, R. Thalman, D. Walter, J. Wang, S. Wolff, H. M. J. Barbosa, P. Artaxo, M. O. Andreae, U. Pöschl, and C. Pöhlker. Long-term observations of cloud condensation nuclei over the amazon rain forest – part 2: Variability and characteristics of biomass burning, long-range transport, and pristine rain forest aerosols. *Atmos. Chem. Phys.*, 18(14):10289–10331, 2018.

[54] R. R. Draxler and G. D. Hess. An overview of the hysplit_4 modelling system for trajectories, dispersion and deposition. *Australian Meteorological Magazine*, 47(4):295–308, 1998.

[55] A. F. Stein, R. R. Draxler, G. D. Rolph, B. J. B. Stunder, M. D. Cohen, and F. Ngan. Noaa's hysplit atmospheric transport and dispersion modeling system. *Bulletin of the American Meteorological Society*, 96(12):2059–2077, 2015.

[56] P. Jöckel, H. Tost, A. Pozzer, M. Kunze, O. Kirner, C. A. M. Brenninkmeijer, S. Brinkop, D. S. Cai, C. Dyroff, J. Eckstein, F. Frank, H. Garny, K.-D. Gottschaldt, P. Graf, V. Grewe, A. Kerkweg, B. Kern, S. Matthes, M. Mertens, S. Meul, M. Neumaier, M. Nützel, S. Oberländer-Hayn, R. Ruhnke, T. Runde, R. Sander, D. Scharffe, and A. Zahn. Earth system chemistry integrated modelling (escimo) with the modular earth submodel system (messy) version 2.51. *Geoscientific Model Development*, 9(3):1153–1200, 2016.

[57] P. Jöckel, A. Kerkweg, A. Pozzer, R. Sander, H. Tost, H. Riede, A. Baumgaertner, S. Gromov, and B. Kern. Development cycle 2 of the Modular Earth Submodel System (MESSy2). *Geosci. Model Dev.*, 3(2):717–752, Dec 2010.

[58] A. Pozzer, A. de Meij, K. J. Pringle, H. Tost, U. M. Doering, J. van Aardenne, and J. Lelieveld. Distributions and regional budgets of aerosols and their precursors simulated with the EMAC chemistry-climate model. *Atmos. Chem. Phys.*, 12(2):961–987, Jan 2012.

[59] P. Jöckel, R. Sander, A. Kerkweg, H. Tost, and J. Lelieveld. Technical Note: The Modular Earth Submodel System (MESSy) - a new approach towards Earth System Modeling. *Atmos. Chem. Phys.*, 5(2):433–444, Feb 2005.

[60] Jos Lelieveld, Klaus Klingmueller, Andrea Pozzer, Ulrich Poeschl, Mohammed Fnais, Andreas Daiber, and Thomas Muenzel. Cardiovascular disease burden from ambient air pollution in Europe reassessed using novel hazard ratio functions. *Eur Heart J*, 40(20):1590–1596, May 2019.

[61] Christof G. Beer, Johannes Hendricks, Mattia Righi, Bernd Heinold, Ina Tegen, Silke Groß, Daniel Sauer, Adrian Walser, and Bernadett Weinzierl. Modelling mineral dust emissions and atmospheric dispersion with MADE3 in EMAC v2.54. *Geosci. Model Dev.*, 13(9):4287–4303, Sep 2020.

[62] K. J. Pringle, H. Tost, S. Message, B. Steil, D. Giannadaki, A. Nenes, C. Fountoukis, P. Stier, E. Vignati, and J. Lelieveld. Description and evaluation of GMXe: a new aerosol submodel for global simulations (v1). *Geosci. Model Dev.*, 3(2):391–412, Sep 2010.

[63] Pauli Paasonen, Kaarle Kupiainen, Zbigniew Klimont, Antoon Visschedijk, Hugo A. C. Denier van der Gon, and Markus Amann. Continental anthropogenic primary particle number emissions. *Atmos. Chem. Phys.*, 16(11):6823–6840, Jun 2016.

[64] A. P. Tsimpidi, V. A. Karydis, A. Pozzer, S. N. Pandis, and J. Lelieveld. ORACLE (v1.0): module to simulate the organic aerosol composition and evolution in the atmosphere. *Geosci. Model Dev.*, 7(6):3153–3172, Dec 2014.

[65] Alexandra P. Tsimpidi, Vlassis A. Karydis, Andrea Pozzer, Spyros N. Pandis, and Jos Lelieveld. ORACLE 2-D (v2.0): an efficient module to compute the volatility and oxygen content of organic aerosol with a global chemistry–climate model. *Geosci. Model Dev.*, 11(8):3369–3389, Aug 2018.

[66] A. Lauer, V. Eyring, J. Hendricks, P. Jöckel, and U. Lohmann. Global model simulations of the impact of ocean-going ships on aerosols, clouds, and the radiation budget. *Atmos Chem Phys*, 7(19):5061–5079, Oct 2007.

[67] Simone Dietmüller, Patrick Jöckel, Holger Tost, Markus Kunze, Catrin Gellhorn, Sabine Brinkop, Christine Frömming, Michael Ponater, Benedikt Steil, Axel Lauer, and Johannes Hendricks. A new radiation infrastructure for the Modular Earth Submodel System (MESSy, based on version 2.51). *Geosci Model Dev*, 9(6):2209–2222, Jun 2016.

[68] Klaus Klingmüller, Jos Lelieveld, Vlassis A. Karydis, and Georgiy L. Stenchikov. Direct radiative effect of dust–pollution interactions. *Atmos Chem Phys*, 19(11):7397–7408, Jun 2019.

[69] R. Sander, A. Kerkweg, P. Jöckel, and J. Lelieveld. Technical note: The new comprehensive atmospheric chemistry module MECCA. *Atmos. Chem. Phys.*, 5(2):445–450, Feb 2005.

[70] Rolf Sander, Andreas Baumgaertner, David Cabrera-Perez, Franziska Frank, Sergey Gromov, Jens-Uwe Grooß, Hartwig Harder, Vincent Huijnen, Patrick Jöckel, Vlassis A. Karydis, Kyle E. Niemeyer, Andrea Pozzer, Hella Riede, Martin G. Schultz, Domenico Taraborrelli, and Sebastian Tauer. The community atmospheric chemistry box model CAABA/MECCA-4.0. *Geosci. Model Dev.*, 12(4):1365–1385, Apr 2019.

[71] J. Lelieveld, C. Brühl, P. Jöckel, B. Steil, P. J. Crutzen, H. Fischer, M. A. Giorgetta, P. Hoor, M. G. Lawrence, R. Sausen, and H. Tost. Stratospheric dryness: model simulations and satellite observations. *Atmos Chem Phys*, 7(5):1313–1332, Feb 2007.

[72] A. Kerkweg, R. Sander, H. Tost, and P. Jöckel. Technical note: Implementation of prescribed (OFFLEM), calculated (ONLEM), and pseudo-emissions (TNUDGE) of chemical species in the Modular Earth Submodel System (MESSy). *Atmos. Chem. Phys.*, 6(11):3603–3609, Sep 2006.

[73] J. Lelieveld, K. Klingmueller, A. Pozzer, R. T. Burnett, A. Haines, and V. Ramanathan. Effects of fossil fuel and total anthropogenic emission removal on public health and climate. *Proc Natl Acad Sci U.S.A*, 116(15):7192–7197, Apr 2019.

[74] C. Brühl, J. Lelieveld, H. Tost, M. Höpfner, and N. Glatthor. Stratospheric sulfur and its implications for radiative forcing simulated by the chemistry climate model EMAC. *J Geophys Res Atmos*, 120(5):2103–2118, Mar 2015.

[75] A. Pozzer, A. de Meij, J. Yoon, H. Tost, A. K. Georgoulias, and M. Astitha. AOD trends during 2001–2010 from observations and model simulations. *Atmos Chem Phys*, 15(10):5521–5535, May 2015.

[76] Peter H. Zimmermann, Carl A. M. Brenninkmeijer, Andrea Pozzer, Patrick Jöckel, Franziska Winterstein, Andreas Zahn, Sander Houweling, and Jos Lelieveld. Model simulations of atmospheric methane (1997–2016) and their evaluation using NOAA and AGAGE surface and IAGOS-CARIBIC aircraft observations. *Atmos Chem Phys*, 20(9):5787–5809, May 2020.

[77] Sourangsu Chowdhury, Andy Haines, Klaus Klingmüller, Vinod Kumar, Andrea Pozzer, Chandra Venkataraman, Christian Witt, and Jos Lelieveld. Global and national assessment of the incidence of asthma in children and adolescents from major sources of ambient NO2. *Environ Res Lett*, 16(3):035020, Mar 2021.

[78] Rachel M. Hoesly, Steven J. Smith, Leyang Feng, Zbigniew Klimont, Greet Janssens-Maenhout, Tyler Pitkanen, Jonathan J. Seibert, Linh Vu, Robert J. Andres, Ryan M. Bolt, Tami C. Bond, Laura Dawidowski, Nazar Kholod, June-ichi Kurokawa, Meng Li, Liang Liu, Zifeng Lu, Maria Cecilia P. Moura, Patrick R. O'Rourke, and Qiang Zhang. Historical (1750–2014) anthropogenic emissions of reactive gases and aerosols from the Community Emissions Data System (CEDS). *Geosci. Model Dev.*, 11(1):369–408, Jan 2018.

[79] J. W. Kaiser, A. Heil, M. O. Andreae, A. Benedetti, N. Chubarova, L. Jones, J.-J. Morcrette, M. Razinger, M. G. Schultz, M. Suttie, and G. R. van der Werf. Biomass burning emissions estimated with a global fire assimilation system based on observed fire radiative power. *Biogeosciences*, 9(1):527–554, Jan 2012.

[80] M. O. Andreae. Emission of trace gases and aerosols from biomass burning – an updated assessment. *Atmospheric Chemistry and Physics*, 19(13):8523–8546, 2019.

[81] G. Danabasoglu, J.-F. Lamarque, J. Bacmeister, D. A. Bailey, A. K. DuVivier, J. Edwards, L. K. Emmons, J. Fasullo, R. Garcia, A. Gettelman, C. Hannay, M. M. Holland, W. G. Large, P. H. Lauritzen, D. M. Lawrence, J. T. M. Lenaerts, K. Lindsay, W. H. Lipscomb, M. J. Mills, R. Neale, K. W. Oleson, B. Otto-Bliesner, A. S. Phillips, W. Sacks, S. Tilmes, L. van Kampenhout, M. Vertenstein, A. Bertini, J. Dennis, C. Deser, C. Fischer, B. Fox-Kemper, J. E. Kay, D. Kinnison, P. J. Kushner, V. E. Larson, M. C. Long, S. Mickelson, J. K. Moore, E. Nienhouse, L. Polvani, P. J. Rasch, and W. G. Strand. The community earth system model version 2 (cesm2). *Journal of Advances in Modeling Earth Systems*, 12(2):e2019MS001916, 2020. e2019MS001916 2019MS001916.

[82] Shian-Jiann Lin and Richard B. Rood. An explicit flux-form semi-lagrangian shallow-water model on the sphere. *Quarterly Journal of the Royal Meteorological Society*, 123(544):2477–2498, 1997.

[83] Louisa K. Emmons, Rebecca H. Schwantes, John J. Orlando, Geoff Tyndall, Douglas Kinnison, Jean-François Lamarque, Daniel Marsh, Michael J. Mills, Simone Tilmes, Charles Bardeen, Rebecca R. Buchholz, Andrew Conley, Andrew Gettelman, Rolando Garcia, Isobel Simpson, Donald R. Blake, Simone Meinardi, and Gabrielle Pétron. The chemistry mechanism in the community earth system model version 2 (cesm2). *Journal of Advances in Modeling Earth Systems*, 12(4):e2019MS001882, 2020. e2019MS001882 2019MS001882.

[84] X. Liu, P.-L. Ma, H. Wang, S. Tilmes, B. Singh, R. C. Easter, S. J. Ghan, and P. J. Rasch. Description and evaluation of a new four-mode version of the modal aerosol module (mam4) within version 5.3 of the community atmosphere model. *Geoscientific Model Development*, 9(2):505–522, 2016.

[85] James W. Hurrell, James J. Hack, Dennis Shea, Julie M. Caron, and James Rosinski. A new sea surface temperature and sea ice boundary dataset for the community atmosphere model. *Journal of Climate*, 21(19):5145 – 5153, 2008.

[86] R. M. Hoesly, S. J. Smith, L. Feng, Z. Klimont, G. Janssens-Maenhout, T. Pitkanen, J. J. Seibert, L. Vu, R. J. Andres, R. M. Bolt, T. C. Bond, L. Dawidowski, N. Kholod, J.-I. Kurokawa, M. Li, L. Liu, Z. Lu, M. C. P. Moura, P. R. O'Rourke, and Q. Zhang. Historical (1750–2014) anthropogenic emissions of reactive gases and aerosols from the community emissions data system (ceds). *Geoscientific Model Development*, 11(1):369–408, 2018.

[87] A. S. Darmenov and A. da Silva. The Quick Fire Emissions Dataset (QFED)—Documentation of versions 2.1, 2.2 and 2.4. *NASA//TM-2015-104606*, 38(NASA Global Modeling and Assimilation Office):183 pp, 2015.

[88] Ronald Gelaro, Will McCarty, Max J. Suárez, Ricardo Todling, Andrea Molod, Lawrence Takacs, Cynthia A. Randles, Anton Darmenov, Michael G. Bosilovich, Rolf Reichle, Krzysztof Wargan, Lawrence Coy, Richard Cullather, Clara Draper, Santha Akella, Virginie Buchard, Austin Conaty, Arlindo M. da Silva, Wei Gu, Gi-Kong Kim, Randal Koster, Robert Lucchesi, Dagmar Merkova, Jon Eric Nielsen, Gary Partyka, Steven Pawson, William Putman, Michele Rienecker, Siegfried D. Schubert, Meta Sienkiewicz, and Bin Zhao. The Modern-Era Retrospective Analysis for Research and Applications, Version 2 (MERRA-2). *Journal of Climate*, 30(14):5419–5454, jul 2017.

[89] Mian Chin, Paul Ginoux, Stefan Kinne, Omar Torres, Brent N. Holben, Bryan N. Duncan, Randall V. Martin, Jennifer A. Logan, Akiko Higurashi, and Teruyuki Nakajima. Tropospheric Aerosol Optical Thickness from the GOCART Model and Comparisons with Satellite and Sun Photometer Measurements. *Journal of the Atmospheric Sciences*, 59(3):461–483, feb 2002.

[90] Peter Colarco, Arlindo da Silva, Mian Chin, and Thomas Diehl. Online simulations of global aerosol distributions in the NASA GEOS-4 model and comparisons to satellite and ground-based aerosol optical depth. *Journal of Geophysical Research*, 115(D14):D14207, jul 2010.

[91] M.M. Rienecker, M.J. Suarez, R. Todling, J. Bacmeister, L. Takacs, H.-C. Liu, W. Gu, M. Sienkiewicz, R.D. Koster, R. Gelaro, I. Stajner, and J.E. Nielsen. The GEOS-5 Data Assimilation System—Documentation of versions 5.0.1, 5.1.0, and 5.2.0. *NASA/TM–2008–104606*, 27(Technical Report Series on Global Modeling and Data Assimilation):118 pp, 2008.

[92] Cynthia A Randles. The MERRA-2 Aerosol Assimilation. *NASA Technical Report*, 45(December), 2016.

[93] C. A. Randles, A. M. da Silva, V. Buchard, P. R. Colarco, A. Darmenov, R. Govindaraju, A. Smirnov, B. Holben, R. Ferrare, J. Hair, Y. Shinozuka, and C. J. Flynn. The MERRA-2 Aerosol Reanalysis, 1980 Onward. Part I: System Description and Data Assimilation Evaluation. *Journal of Climate*, 30(17):6823–6850, sep 2017.

[94] V. Buchard, C. A. Randles, A. M. da Silva, A. Darmenov, P. R. Colarco, R. Govindaraju, R. Ferrare, J. Hair, A. J. Beyersdorf, L. D. Ziemba, and H. Yu. The MERRA-2 Aerosol Reanalysis, 1980 Onward. Part II: Evaluation and Case Studies. *Journal of Climate*, 30(17):6851–6872, sep 2017.

[95] J. W. Kaiser, A. Heil, M. O. Andreae, A. Benedetti, N. Chubarova, L. Jones, J.-J. Morcrette, M. Razinger, M. G. Schultz, M. Suttie, and G. R. van der Werf. Biomass burning emissions estimated with a global fire assimilation system based on observed fire radiative power. *Biogeosciences*, 9(1):527–554, jan 2012.

[96] Rolf H. Reichle, Q. Liu, Randal D. Koster, Clara S. Draper, Sarith P. P. Mahanama, and Gary S. Partyka. Land Surface Precipitation in MERRA-2. *Journal of Climate*, 30(5):1643–1664, mar 2017.

[97] E. Nowottnick, P. Colarco, R. Ferrare, G. Chen, S. Ismail, B. Anderson, and E. Browell. Online simulations of mineral dust aerosol distributions: Comparisons to NAMMA observations and sensitivity to dust emission parameterization. *Journal of Geophysical Research*, 115(D3):D03202, feb 2010.

[98] E. Nowottnick, P. Colarco, A. da Silva, D. Hlavka, and M. McGill. The fate of saharan dust across the atlantic and implications for a central american dust barrier. *Atmospheric Chemistry and Physics*, 11(16):8415–8431, aug 2011.

[99] H. Bian, P. R. Colarco, M. Chin, G. Chen, J. M. Rodriguez, Q. Liang, D. Blake, D. A. Chu, A. da Silva, A. S. Darmenov, G. Diskin, H. E. Fuelberg, G. Huey, Y. Kondo, J. E. Nielsen, X. Pan, and A. Wisthaler. Source attributions of pollution to the Western Arctic during the NASA ARCTAS field campaign. *Atmospheric Chemistry and Physics*, 13(9):4707–4721, may 2013.

[100] Jos Barlow, Erika Berenguer, Rachel Carmenta, and Filipe França. Clarifying Amazonia's burning crisis. *Global Change Biology*, 26(2):319–321, feb 2020.

[101] C. Pöhlker, K. T. Wiedemann, B. Sinha, M. Shiraiwa, S. S. Gunthe, M. Smith, H. Su, P. Artaxo, Q. Chen, Y. F. Cheng, W. Elbert, M. K. Gilles, A. L. D. Kilcoyne, R. C. Moffet, M. Weigand, S. T. Martin, U. Pöschl, and M. O. Andreae. Biogenic potassium salt particles as seeds for secondary organic aerosol in the amazon. *Science*, 337(6098):1075–1078, 2012.

[102] Manfred Wendisch, Ulrich Pöschl, Meinrat O. Andreae, Luiz A. T. Machado, Rachel Albrecht, Hans Schlager, Daniel Rosenfeld, Scot T. Martin, Ahmed Abdelmonem, Armin Afchine, Alessandro C. Araùjo, Paulo Artaxo, Heinfried Aufmhoff, Henrique M. J. Barbosa, Stephan Borrmann, Ramon Braga, Bernhard Buchholz, Micael Amore Cecchini, Anja Costa, Joachim Curtius, Maximilian Dollner, Marcel Dorf, Volker Dreiling, Volker Ebert, André Ehrlich, Florian Ewald, Gilberto Fisch, Andreas Fix, Fabian Frank, Daniel Fütterer, Christopher Heckl, Fabian Heidelberg, Tilman Hüneke, Evelyn Jäkel, Emma Järvinen, Tina Jurkat, Sandra Kanter, Udo Kästner, Mareike Kenntner, Jürgen Kesselmeier, Thomas Klimach, Matthias Knecht, Rebecca Kohl, Tobias Kölling, Martina Krämer, Mira Krüger, Trismono Candra Krisna, Jost V. Lavric, Karla Longo, Christoph Mahnke, Antonio O. Manzi, Bernhard Mayer, Stephan Mertes, Andreas Minikin, Sergej Molleker, Steffen Münch, Björn Nillius, Klaus Pfeilsticker, Christopher Pöhlker, Anke Roiger, Diana Rose, Dagmar Rosenow, Daniel Sauer, Martin Schnaiter, Johannes Schneider, Christiane Schulz, Rodrigo A. F. de Souza, Antonio Spanu, Paul Stock, Daniel Vila, Christiane Voigt, Adrian Walser, David Walter, Ralf Weigel, Bernadett Weinzierl, Frank Werner, Marcia A. Yamasoe, Helmut Ziereis, Tobias Zinner, and Martin Zöger. Acridicon–chuva campaign: Studying tropical deep convective clouds and precipitation over amazonia using the new german research aircraft halo. *Bulletin of the American Meteorological Society*, 97(10):1885–1908, 2016.

[103] Jeannine Ditas, Nan Ma, Yuxuan Zhang, Denise Assmann, Marco Neumaier, Hella Riede, Einar Karu, Jonathan Williams, Dieter Scharffe, Qiaoqiao Wang, Jorge Saturno, Joshua P. Schwarz, Joseph M. Katich, Gavin R. McMeeking, Andreas Zahn, Markus Hermann, Carl A. M. Brenninkmeijer, Meinrat O. Andreae, Ulrich Pöschl, Hang Su, and Yafang Cheng. Strong impact of wildfires on the abundance and aging of black carbon in the lowermost stratosphere. *Proceedings of the National Academy of Sciences*, 115(50):E11595, 2018.

[104] J. H. Seinfeld and S. N. Pandis. *Atmospheric Chemistry and Physics: From Air Pollution to Climate Change*. John Wiley & Sons, Inc., 2006.

[105] Amy K Hodgson, William T Morgan, Sebastian O Shea, Stéphane Bauguitte, James D Allan, Eoghan Darbyshire, Michael J Flynn, Dantong Liu, James Lee, Ben Johnson, Jim M Haywood, Karla M Longo, Paulo E Artaxo, and Hugh Coe. Near-field emission profiling of tropical forest and Cerrado fires in Brazil during SAMBBA 2012. pages 5619–5638, 2018.

[106] Celso H. L. Silva Junior, Ana C. M. Pessoa, Nathalia S. Carvalho, Joao B. C. Reis, Liana O. Anderson, and Luiz E. O. C. Aragao. The brazilian amazon deforestation rate in 2020 is the greatest of the decade. *Nature Ecology & Evolution*, 5(2):144–145, 2021.

[107] N. L. Ng, M. R. Canagaratna, Q. Zhang, J. L. Jimenez, J. Tian, I. M. Ulbrich, J. H. Kroll, K. S. Docherty, P. S. Chhabra, R. Bahreini, S. M. Murphy, J. H. Seinfeld, L. Hildebrandt, N. M. Donahue, P. F. Decarlo, V. A. Lanz, A. S.H. Prévôt, E. Dinar, Y. Rudich, and D. R. Worsnop. Organic aerosol components observed in Northern Hemispheric datasets from Aerosol Mass Spectrometry. *Atmospheric Chemistry and Physics*, 10(10):4625–4641, 2010.

[108] C. Schulz, J. Schneider, B. A. Holanda, O. Appel, A. Costa, S. S. de Sá, V. Dreiling, D. Fütterer, T. Jurkat-Witschas, T. Klimach, M. Krämer, S. T. Martin, S. Mertes, M. L. Pöhlker, D. Sauer, C. Voigt, B. Weinzierl, H. Ziereis, M. Zöger, M. O. Andreae, P. Artaxo, L. A. T. Machado, U. Pöschl, M. Wendisch, and S. Borrmann. Aircraft-based observations of isoprene epoxydiol-derived secondary organic aerosol

(iepox-soa) in the tropical upper troposphere over the amazon region. *Atmos. Chem. Phys. Discuss.*, 2018:1–32, 2018.

[109] M. J. Cubison, A. M. Ortega, P. L. Hayes, D. K. Farmer, D. Day, M. J. Lechner, W. H. Brune, E. Apel, G. S. Diskin, J. A. Fisher, H. E. Fuelberg, A. Hecobian, D. J. Knapp, T. Mikoviny, D. Riemer, G. W. Sachse, W. Sessions, R. J. Weber, A. J. Weinheimer, A. Wisthaler, and J. L. Jimenez. Effects of aging on organic aerosol from open biomass burning smoke in aircraft and laboratory studies. *Atmospheric Chemistry and Physics*, 11(23):12049–12064, dec 2011.

[110] K. Pistone, J. Redemann, S. Doherty, P. Zuidema, S. Burton, B. Cairns, S. Cochrane, R. Ferrare, C. Flynn, S. Freitag, S. G. Howell, M. Kacenelenbogen, S. LeBlanc, X. Liu, K. S. Schmidt, A. J. Sedlacek III, M. Segal-Rozenhaimer, Y. Shinozuka, S. Stamnes, B. van Diedenhoven, G. Van Harten, and F. Xu. Intercomparison of biomass burning aerosol optical properties from in situ and remote-sensing instruments in oracles-2016. *Atmospheric Chemistry and Physics*, 19(14):9181–9208, 2019.

[111] Cyrielle Denjean, Thierry Bourrianne, Frederic Burnet, Marc Mallet, Nicolas Maury, Aurélie Colomb, Pamela Dominutti, Joel Brito, Régis Dupuy, Karine Sellegri, Alfons Schwarzenboeck, Cyrille Flamant, and Peter Knippertz. Light absorption properties of aerosols over Southern West Africa. *Atmospheric Chemistry and Physics Discussions*, pages 1–40, aug 2019.

S3 Supplementary Figures

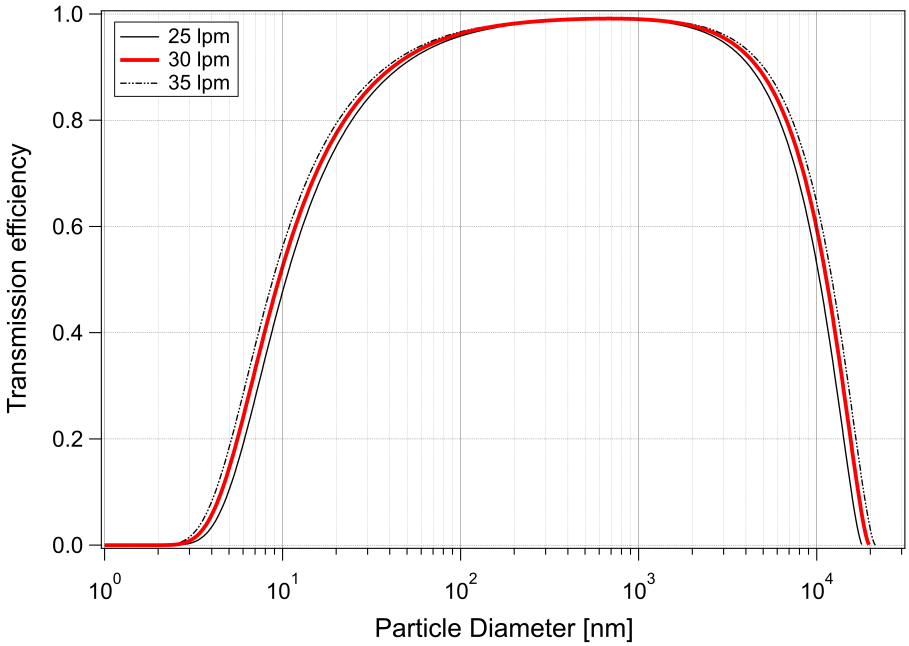

Figure S1: Calculated transmission efficiency of the 325 m aerosol inlet at the tall tower at ATTO. The transmission curve was calculated for three different sample air flow rates in the main inlet tube by using the particle loss calculator (PLC, version 2.0) developed by von der Weiden *et al.* [8]. Refer also to Supplementary materials in Moran *et al.* [7].

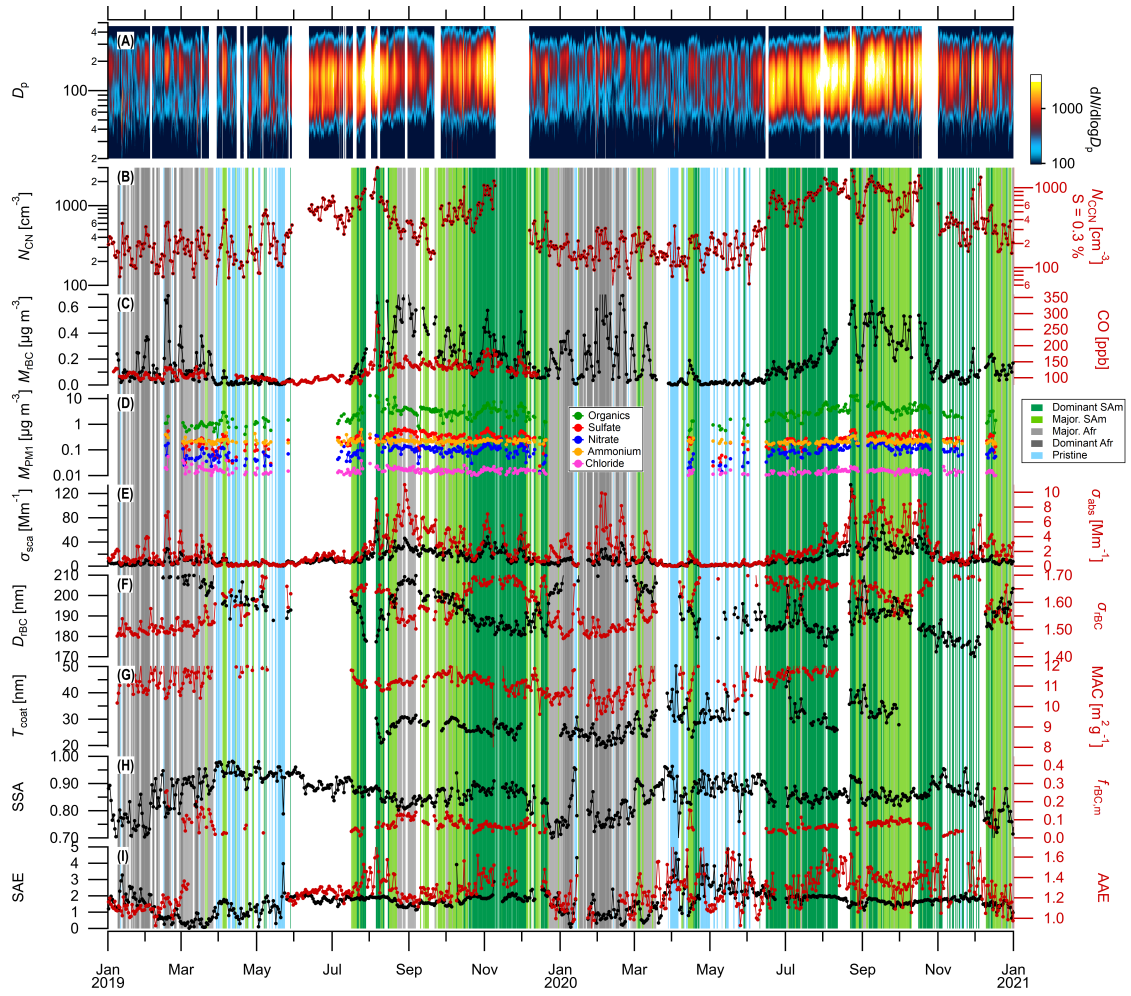

Figure S2: Time series of trace gas and aerosol parameters at ATTO in time period from Jan 2019 to Dec 2020. Data shown here was used as input for Box-Whisker plots in Fig. 3. The following specific datasets are shown: SMPS-derived particle number size distribution; total number concentration of particles >6 nm (N_{CN}); cloud condensation nuclei (CCN) number concentration at a supersaturation of 0.3 % ($N_{\mathrm{CCN}}(S = 0.3\,\%)$); rBC mass concentration measured by the SP2 (M_{rBC}); carbon monoxide (CO) mixing ratio; mass concentration of ACSM-measured submicrometer species organics (Org), sulfate ($SO_4{}^{2-}$), nitrate ($NO_3{}^{-}$), ammonium ($NH_4{}^{+}$), and chloride (Cl^{-}); scattering coefficient at 550 nm (σ_{sca}); absorption coefficient at 637 nm (σ_{abs}); coating thickness (T_{coat}) of rBC-containing particles with $\sim 180 < d_{\mathrm{MEV}} < 220$ nm; mass absorption cross section (MAC) at 637 nm; single scattering albedo (SSA) at 637 nm; rBC mass fration ($f_{rBC,m}$); absorption Ångström exponent (AAE) calculated from Eq.S6; scattering Ångström exponent (SAE) calculated from S5 using the wavelength pair 450 and 635 nm. Green and gray background shading shows flag conditions that were either dominated by African or South American smoke according to Sect. S1.3 (see legend).

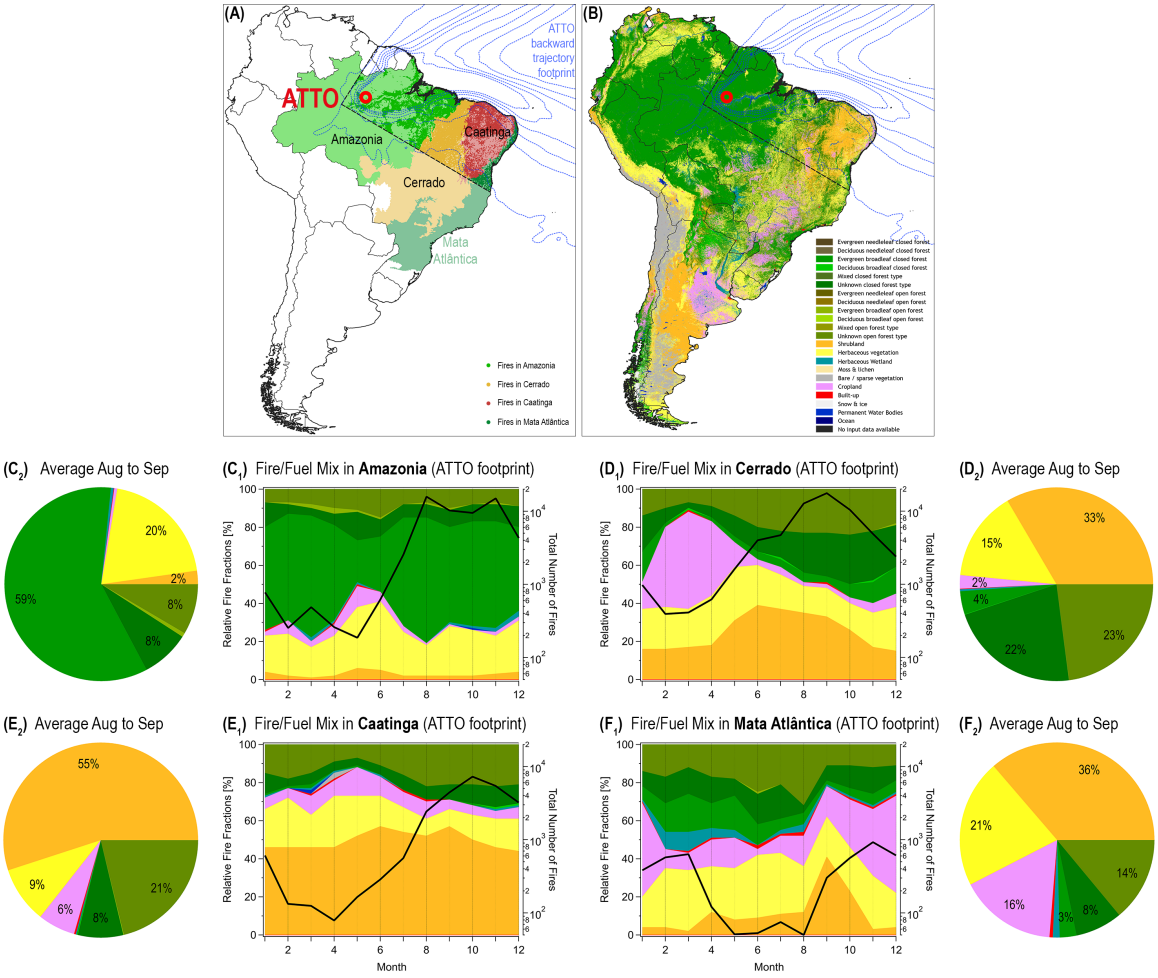

Figure S3: Average fire/fuel mixtures in ATTO footprint region on South America continent in 2019, separated into biomes Amazonia, Cerrado, Caatinga, and Mata Atlântica. Fire map (**A**) and land cover map (**B**) were combined to calculate seasonal cycle of fire counts per land cover category ($\mathbf{C}_1$, $\mathbf{D}_1$, $\mathbf{E}_1$, and $\mathbf{F}_1$). Black solid lines in $\mathbf{C}_1$, $\mathbf{D}_1$, $\mathbf{E}_1$, and $\mathbf{F}_1$ show total number of detected fires. Pie charts in $\mathbf{C}_2$, $\mathbf{D}_2$, $\mathbf{E}_2$, and $\mathbf{F}_2$ emphasize average fire/fuel mixtures in the ATTO footprint-relevant region in biomes Amazonia, Cerrado, Caatinga, and Mata Atlantica between August and September, which corresponds to the peak of biomass burning in the Amazon. Dashed black polygon line in **(A)** marks approximate region of ATTO footprint (compare blue isolines as backward trajectory contours). For further details, refer to Sect. S1.9.

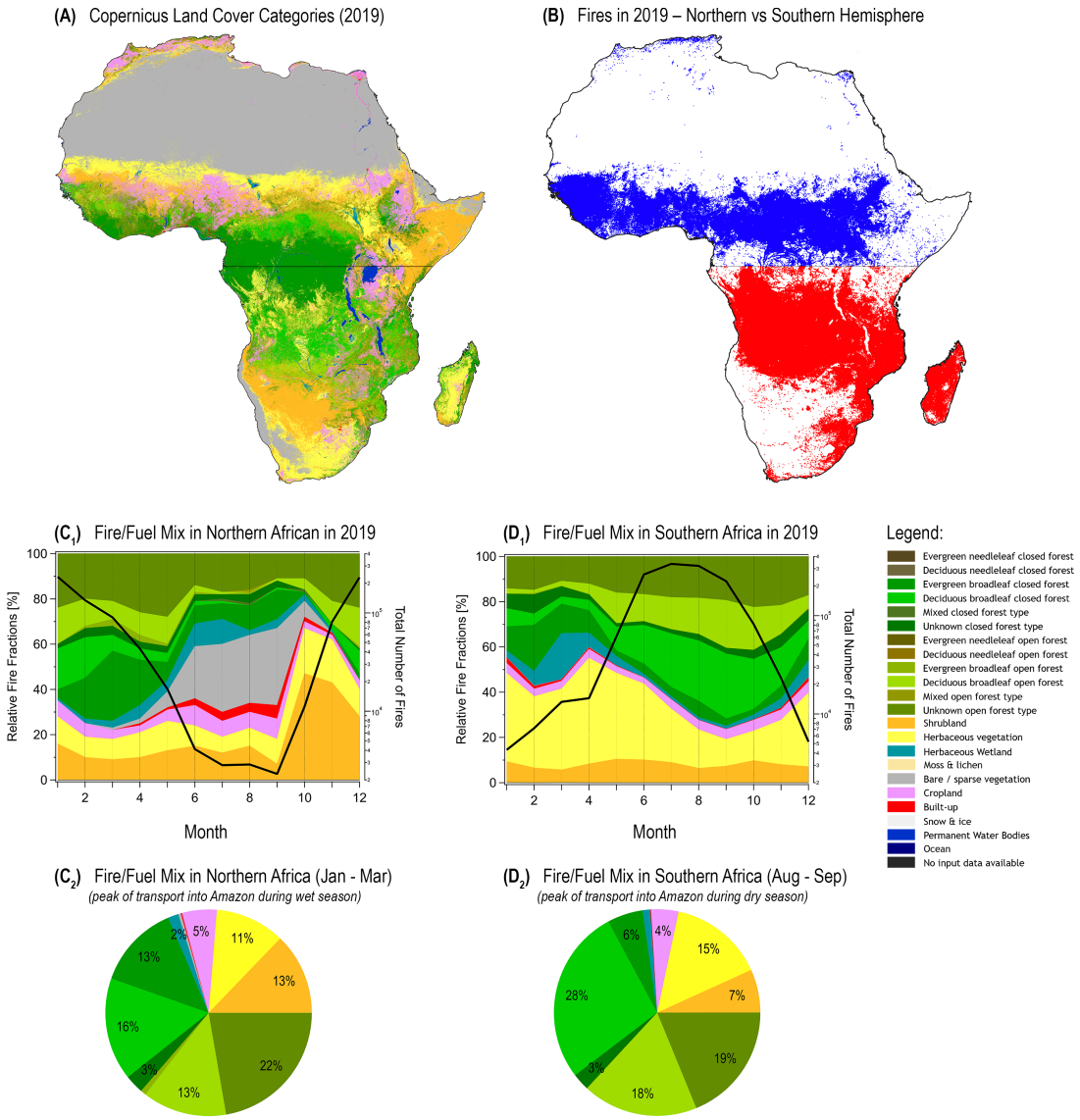

Figure S4: Average fire/fuel mixtures in Africa in 2019, separated into the Northern vs Southern hemispheres. Land cover map (**A**) and fire map (**B**) were combined to calculate seasonal cycle of fire counts per land cover category ($\mathbf{C}_1$ and $\mathbf{D}_1$). Black solid lines in $\mathbf{C}_1$ and $\mathbf{D}_1$ show total number of detected fires. Pie charts in $\mathbf{C}_2$ and $\mathbf{D}_2$ emphasize (i) average fire/fuel mixture in Northern Africa between January and March, which corresponds to the peak of long-range transport of African smoke into the Amazon during the wet season and (ii) average fire/fuel mixture in Southern Africa between August and September, which corresponds to the peak of long-range transport of African smoke into the Amazon during the dry season. For further details, refer to Sect. S1.9.

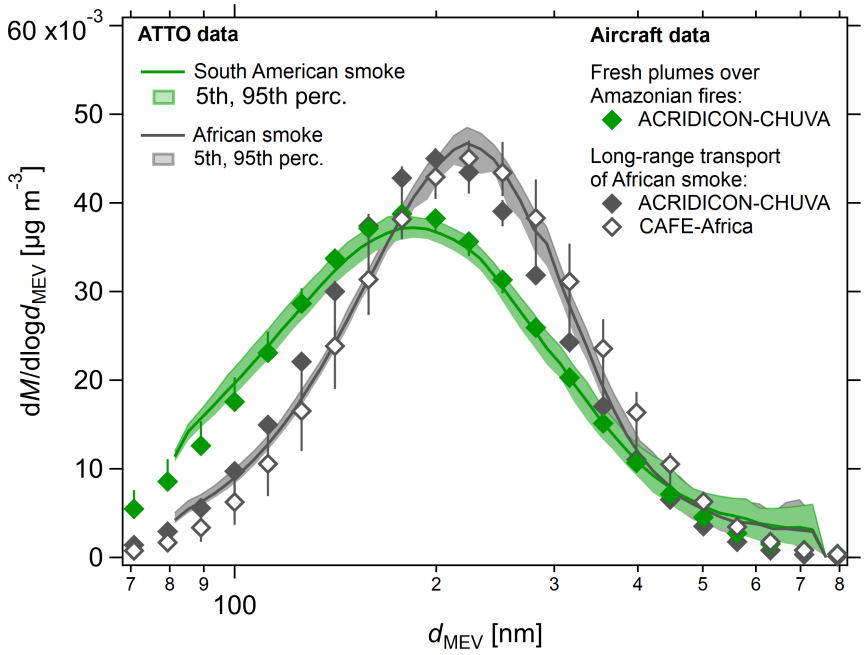

Figure S5: Figure emphasizing the characteristic differences in the normalized rBC mass size distributions under predominant African (gray) vs South American smoke conditions (compare Sect. S1.3). It further shows the good agreement between the ATTO and aircraft data sets. Solid lines show average values and shadings represent 5^{th} to 95^{th} percentile ranges of rBC distributions during ATTO event periods as highlighted in Fig. 1B. For comparison, corresponding aircraft data from ACRIDICON-CHUVA and CAFE-Africa campaigns (see Sect. S1.2) for selected flight segments are shown with markers representing average values and the error bars representing 5^{th} to 95^{th} percentile ranges.

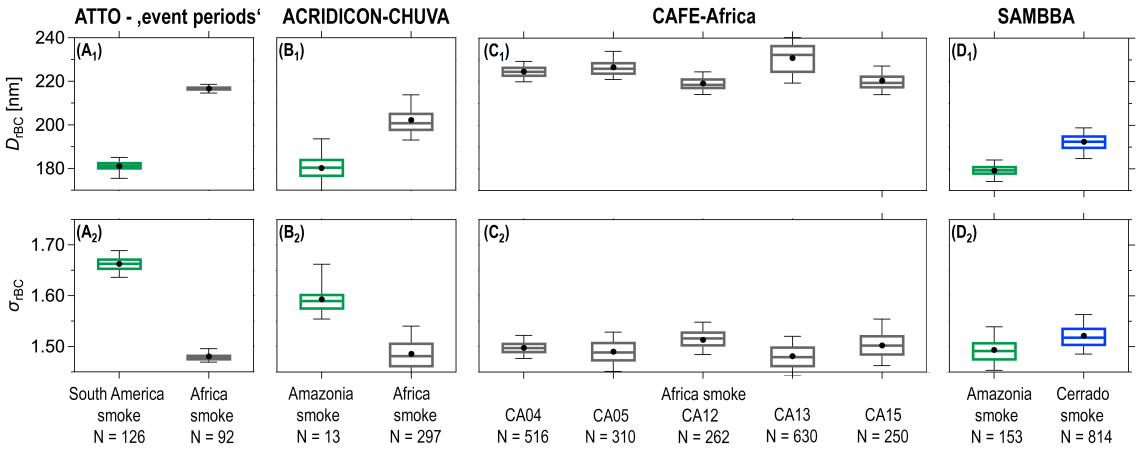

Figure S6: Statistics of the fit parameters geometric mean diameter (D_{rBC}) and geometric standard deviation (σ_{rBC}) from fitted rBC mass size distributions during characteristic conditions of ATTO and aircraft measurements, emphasizing the clear differences in rBC microphysical properties between African and South American smoke. ($\mathbf{A_1}$ and $\mathbf{A_2}$) ATTO event periods as highlighted in Fig. 1B. ($\mathbf{B_1}$ and $\mathbf{B_2}$) Smoke conditions during ACRIDICON-CHUVA [31] – specifically layer of long-range transported African smoke as well as fresh Amazonian fires plumes as analyzed in Holanda *et al.* [40]. ($\mathbf{C_1}$ and $\mathbf{C_2}$) African smoke probed over Atlantic Ocean during CAFE-Africa – here separated into the five flights that probed relevant smoke conditions. ($\mathbf{D_1}$ and $\mathbf{D_2}$) For further comparison, fresh smoke over fire in Amazonian rain forest vs fire in Cerrado savanna region probed during SAMBBA campaign according to Hodgson *et al.* [105]. In box-whisker plots, the horizontal lines represent the medians, circular markers the means, boxes the 25$^{\mathrm{th}}$ and 75$^{\mathrm{th}}$ percentiles, and the whiskers the 9$^{\mathrm{th}}$ and 91$^{\mathrm{st}}$ percentiles. Below, N specifies the number of data points used to compose the box-whisker plots with one data point representing a 10 s-averaged rBC mass size distribution.

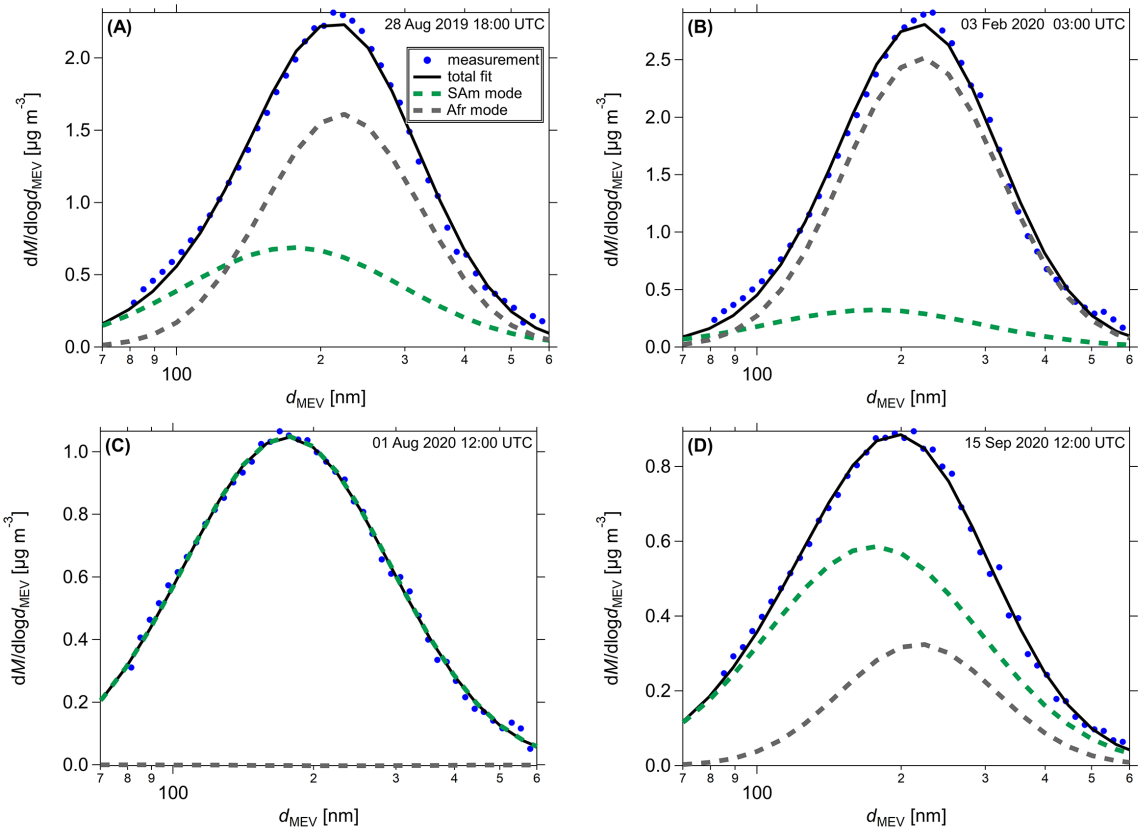

Figure S7: Examples of bimodal fits of 3 h-averaged ATTO rBC mass size distributions. The fit comprises an African (Afr) mode and a South American (SAm) mode with constraints for the fit parameters D_{rBC} and σ_{rBC} as outlied in Sect. S1.3.

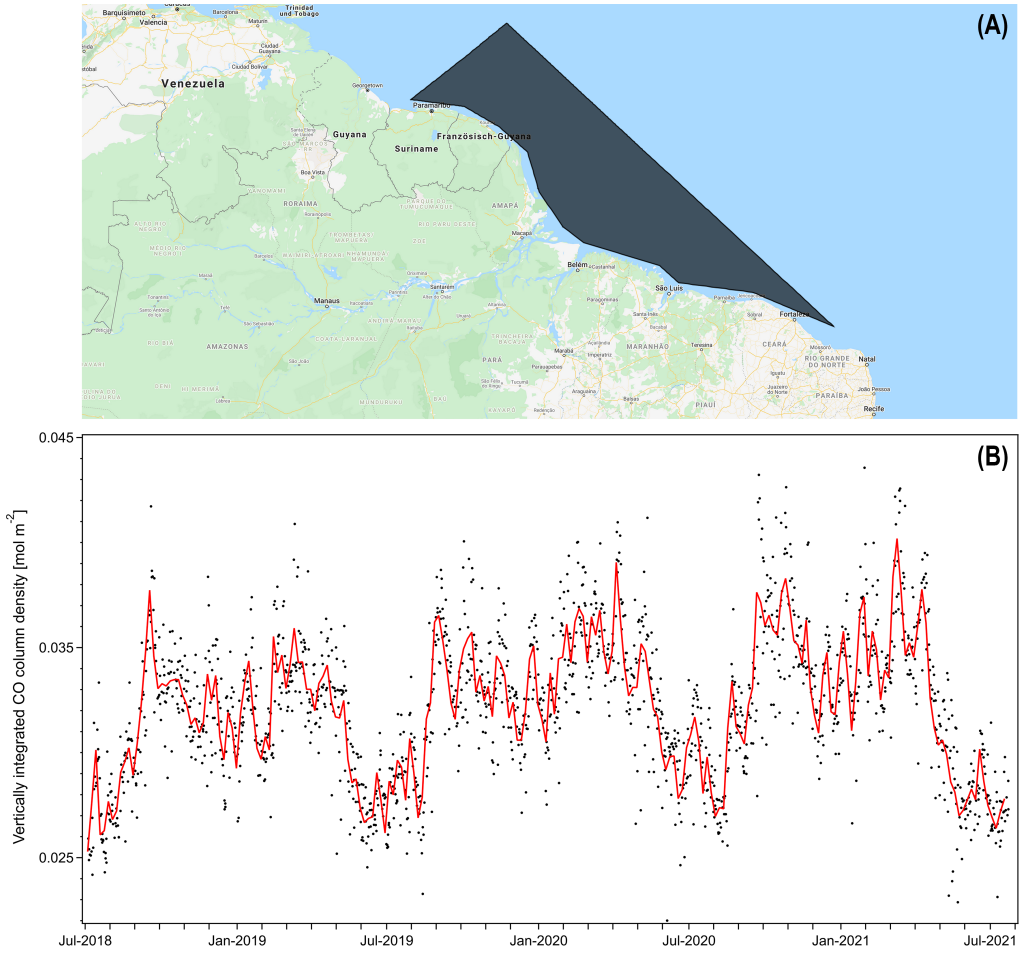

Figure S8: Satellite-derived vertically integrated CO column density in offshore region of interest ($ROI_{offshore}$) in front of South American coast as proxy for African smoke influx into the Amazon. **(A)** Map showing location and shape of the $ROI_{offshore}$. **(B)** Corresponding time series of vertically integrated CO column density (CO_{ROI}) within $ROI_{offshore}$. The figure shows individual data points (black dots) and the 5-day averages (solid lines). For details refer to Sect. S1.5.

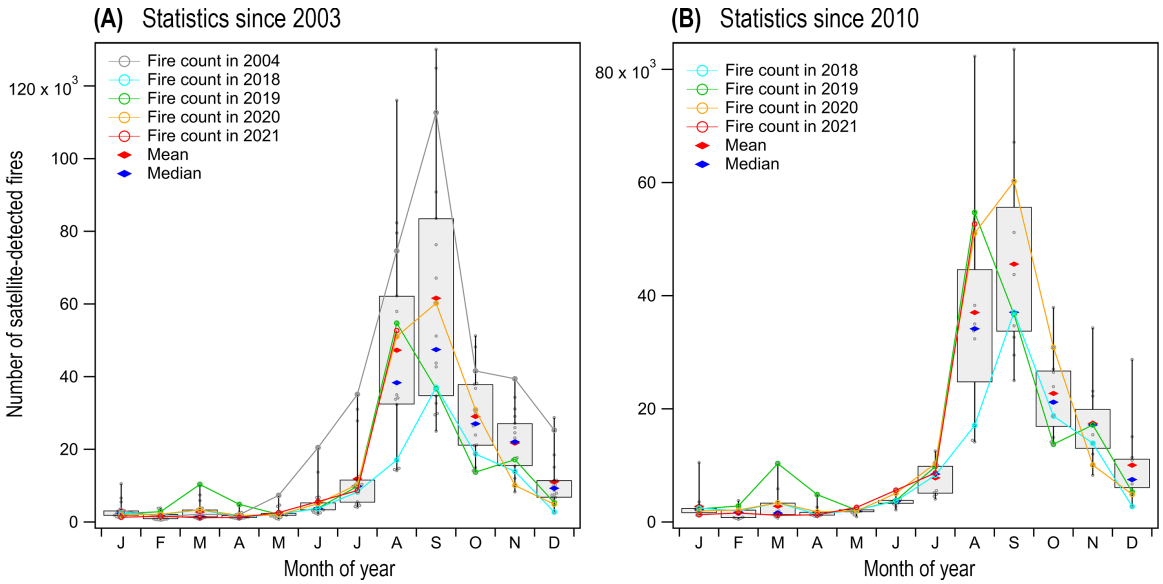

Figure S9: Increase of detected fires in recent years in Amazonia, emphasized by Box-Whisker plots with seasonal cycle in number of satellite-detected fires for two time frames: **(A)** from 2003-01-01 to 2021-08-31 and **(B)** from 2010-01-01 to 2021-08-31. Fire count has been derived from Brazilian National Institute for Space Research data (Instituto Nacional de Pesquisas Espaciais, INPE, http://queimadas.dgi.inpe.br/queimadas/bdqueimadas, last access 28 July 2021). From all satellites used in the INPE data, only the NASA satellites Terra and Aqua were used here because both span the longest continuous time period and allowed to calculate multi-year anomalies. The boxes specify the interquartile range with the median as blue diamond marker and the mean as red diamond marker. The whiskers specify the minimum and maximum values. Fire counts of individual years are highlighted as colored open circular markers: (i) 2004 as one of the years with strongest fire activity, also corresponding to peaking deforestation rates in the Amazon [106]; (ii) 2018 as a year with comparatively low fire activities; (iii) 2019 and 2020 as the years of interest of the present study, which both show significant increases in fire counts relative to the previous years; (iv) 2021 showing the most recent situation.

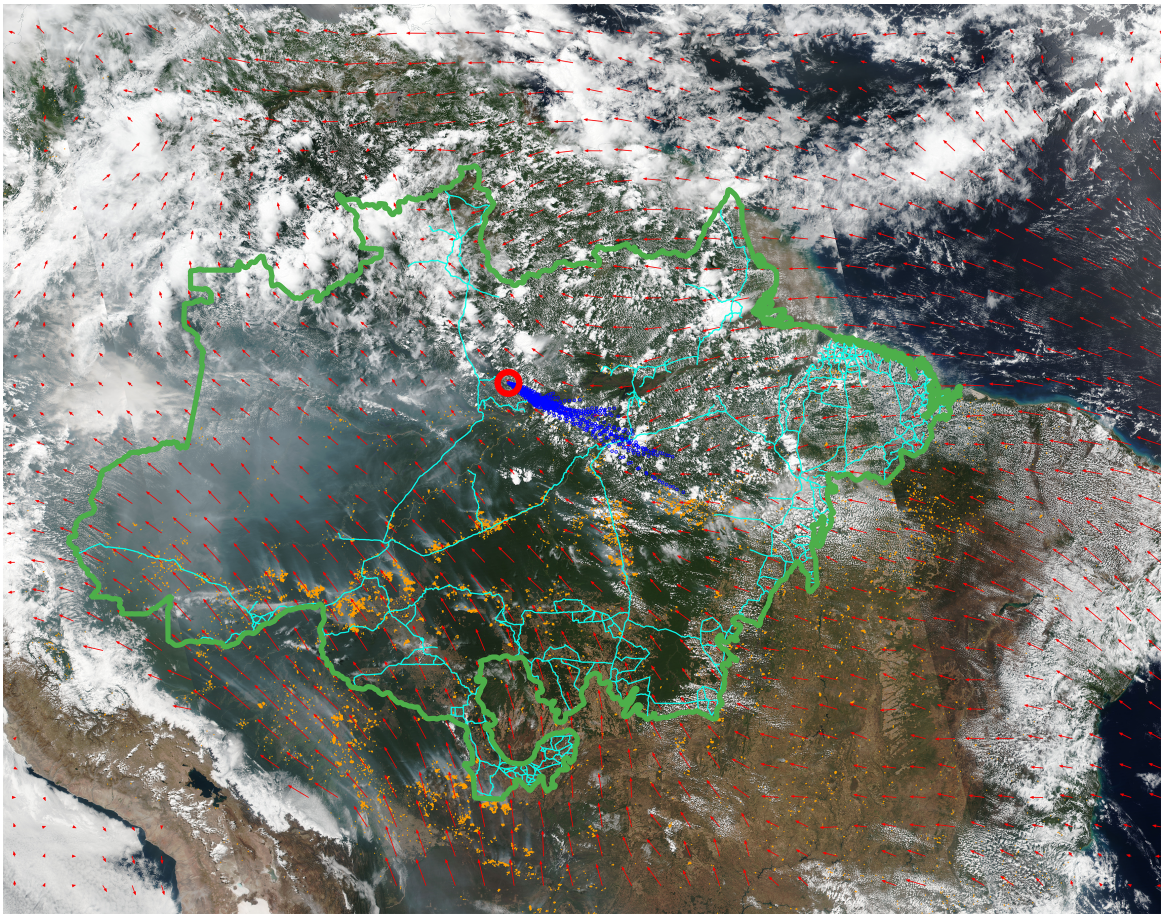

Figure S10: Smoke cover over western Amazon during period of intense burning on 14 August 2019, here visualized as composite map of (i) corrected reflectance satellite images showing cloud cover and smoke plumes, (ii) individual detected fires shown as yellow points, (iii) wind vectors (red) at 950 hPa showing overall wind fields in agreement with HYSPLIT 1 d backward trajectory (BT) ensembles (blue), started at the ATTO site (red circle). Green boundary shows legal Amazon region. Blue lines show major highways in the Amazon basin.

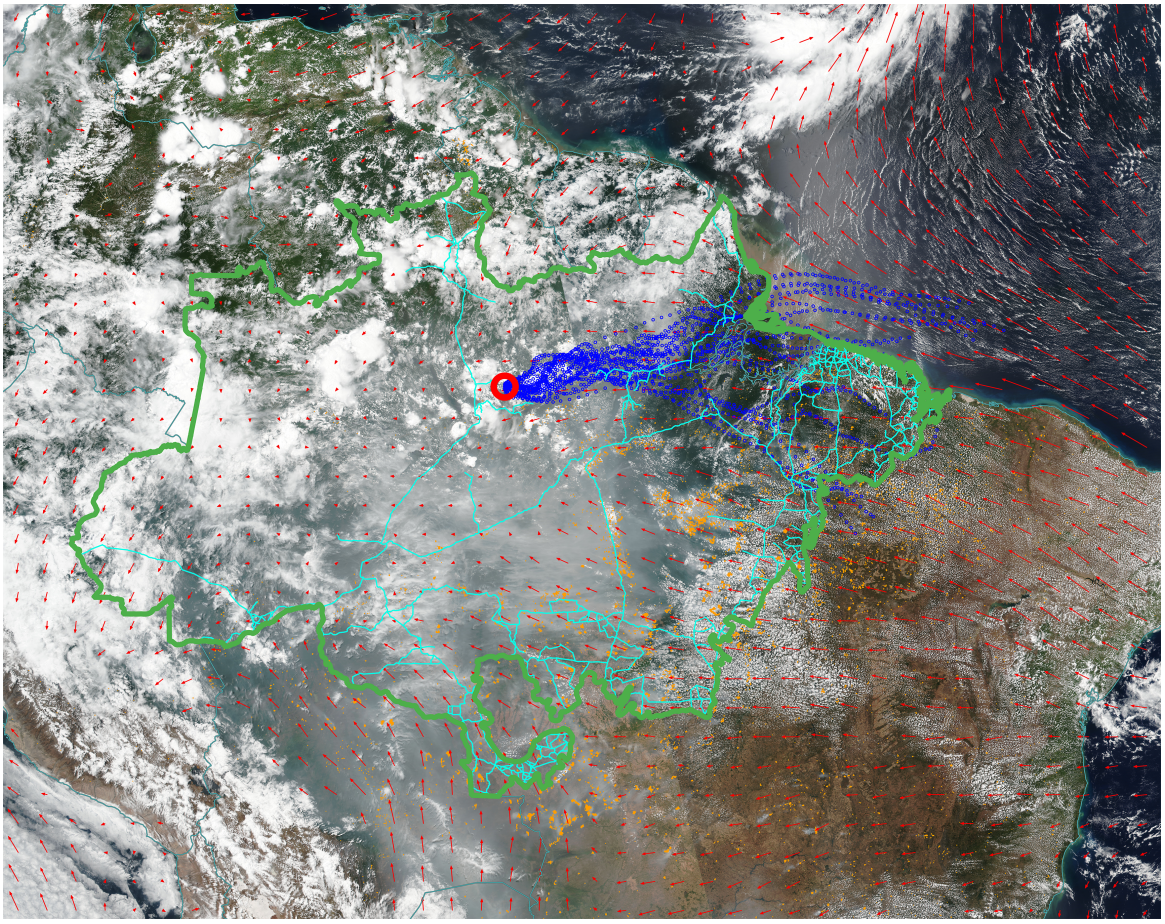

Figure S11: Smoke cover over western Amazon during period of intense burning on 15 September 2020, here visualized as composite map of (i) corrected reflectance satellite images showing cloud cover and smoke plumes, (ii) individual detected fires shown as yellow points, (iii) wind vectors (red) at 950 hPa showing overall wind fields in agreement with HYSPLIT 1 d backward trajectory (BT) ensembles (blue), started at the ATTO site (red circle). Green boundary shows legal Amazon region. Blue lines show major highways in the Amazon basin.

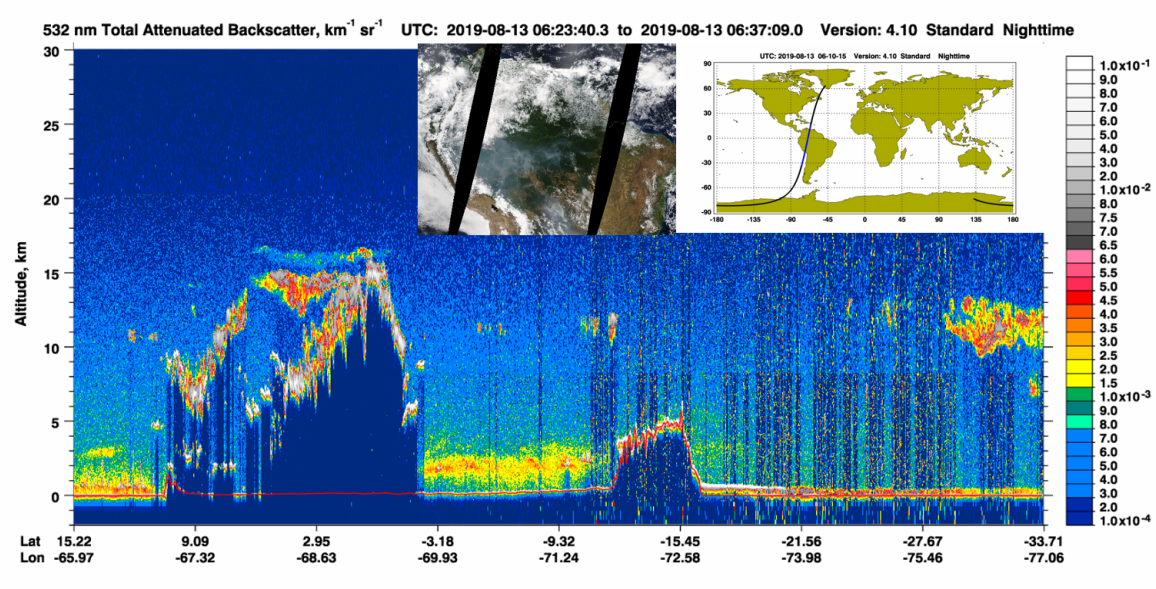

Figure S12: Exemplary lidar profiles from CALIPSO (https://www-calipso.larc.nasa.gov/, last access 04 Sep 2021) passage on 13 August 2019 over the smoky western Amazon basin showing enrichment of the smoke in the lower 2 to 3 km of the atmosphere. The CALIPSO orbit for this particular scene is shown in the upper right corner. Further, true color image of the same day is shown in the upper middle.

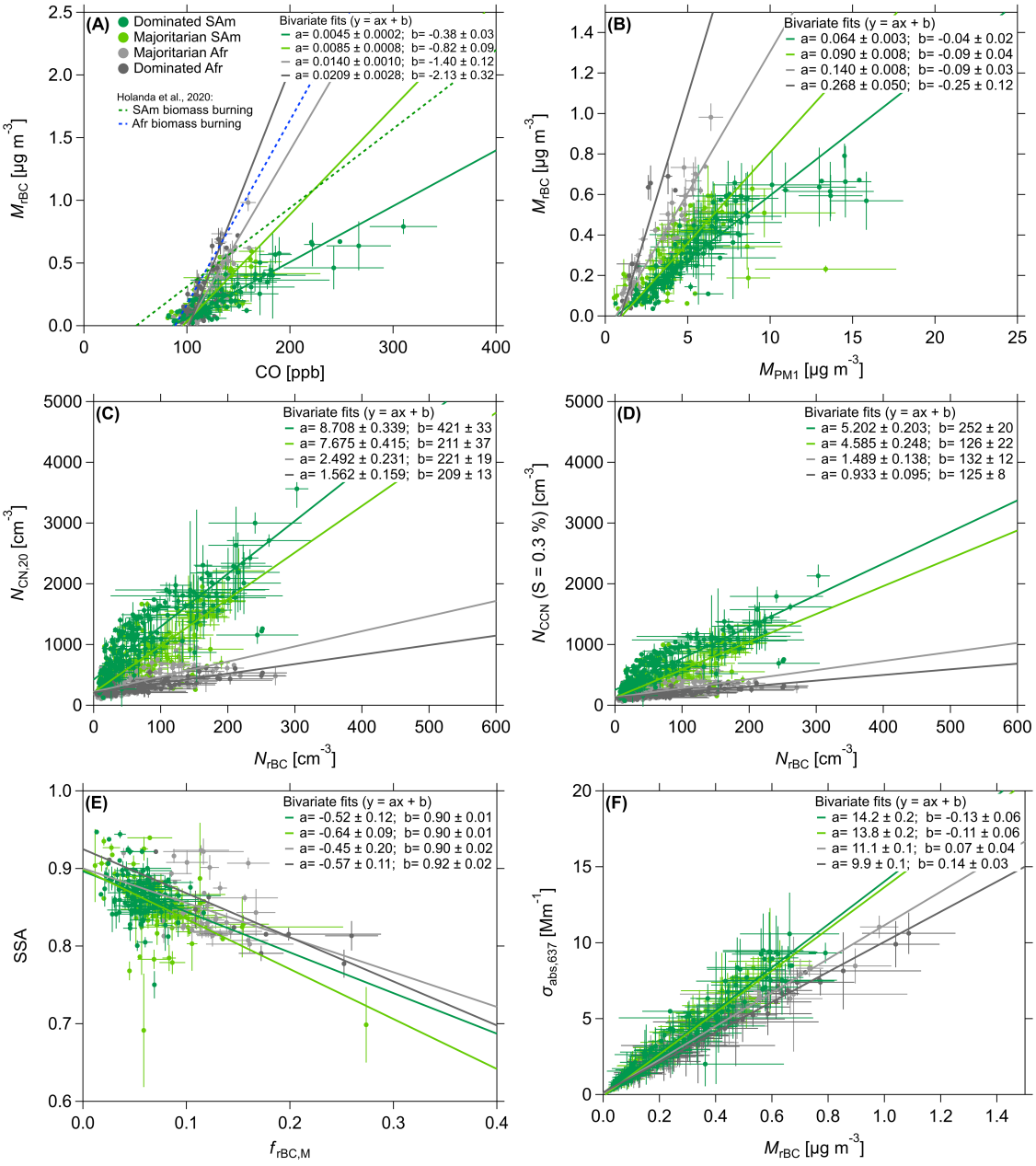

Figure S13: Correlations between selected aerosol and trace gas parameters, separated into into the four categories of dominant or majoritarian South American influence vs dominant or majoritarian African influence. Specifically shown are **(A)** black carbon mass concentration (M_{rBC}) vs carbon monoxide (CO); **(B)** M_{rBC} vs total submicrometer aerosol mass (M_{PM1}) derived from SP2 and ACSM; **(C)** total particle number concentration with $D_{\mathrm{p}} > 20$ nm ($N_{\mathrm{CN},20}$) vs black carbon number concentration (N_{rBC}); **(D)** cloud condensation nuclei number concentration N_{CCN} at a supersaturation of 0.3 % vs N_{rBC}; **(E)** single scattering albedo (SSA) at 637 nm vs rBC mass fraction ($f_{\mathrm{rBC,M}}$); and **(F)** absorption coefficient ($\sigma_{\mathrm{abs},637}$) at 637 nm vs M_{rBC}, defining the mass absorption cross section (MAC) at 637 nm according to Eq. S3. The solid lines represent linear orthogonal distance regression (ODR) fits applied to the daily averaged data with error bars showing the standard deviations. Further shown in **(A)** as dashed lines are previous results from a related study by Holanda *et al.* [40].

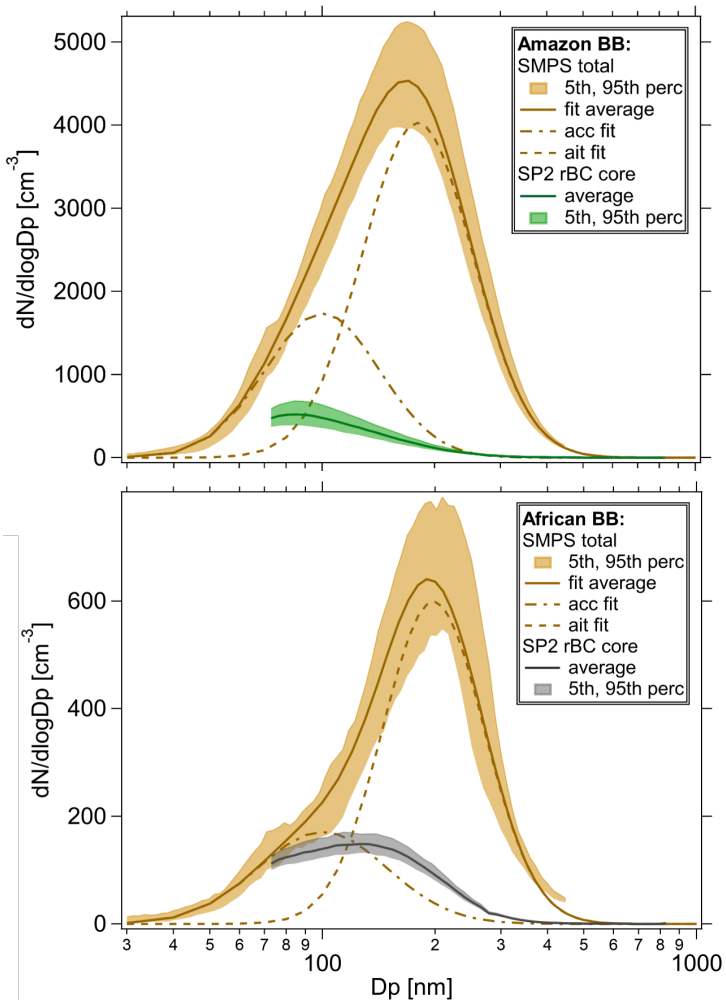

Figure S14: Number size distributions of SP2-derived rBC cores and SMPS-derived total particles at ATTO under predominant South American influence (upper panel) and predominant African influence (lower panel). Solid lines represent the fitted log-normal function with shadings as the corresponding 5^{th} to 95^{th} percentile ranges. .

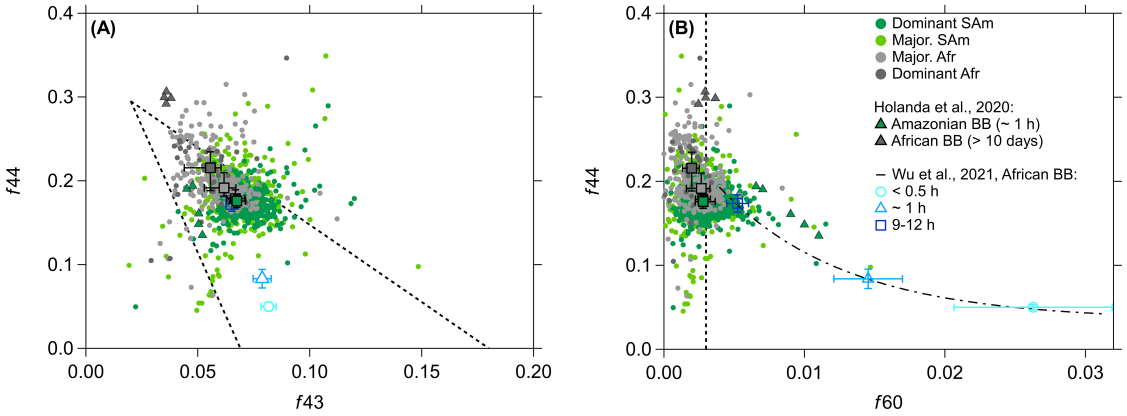

Figure S15: ACSM results reflecting the extent of photo-chemical aging of the organic aerosol constituents and confirming that the African smoke at ATTO is strongly aged, whereas the South American smoke is comparatively fresh. **(A)** Scatter plot of the ratios $f43$ (m/z 43 to total organic signal) against $f44$ (m/z 44 to total organic signal) with the m/z 44 signal relating mostly to CO_2^+ ions and the m/z 43 signal to $C_2H_3O^+$ ions. The triangular region (dashed lines) in the $f44$ vs $f43$ space defines the boundaries within which most of the organic aerosol was found in previous studies [107, 108]. Data in the upper left represent more oxidized organics vs the less oxidized organics in the lower right. **(B)** Scatter plot of the ratios $f44$ (m/z 44 to total organic signal) against $f60$ (m/z 60 to total organic signal) with the m/z 60 signal relating to the biomass burning tracer levoglucosan. Vertical dashed line in **(B)** represents reference value for negligible influence of comparatively fresh smoke according to Cubison *et al.* [109], either because biomass burning influence is absent or levoglucosan has been completely oxidized. Curved dashed line in **(B)** represents temporal evolution in $f44$ vs $f60$ space of smoke upon aging right after emission according to Wu *et al.* [24]. Further shown are the markers from our previous study [40] showing aged African and rather fresh Amazonian smoke.

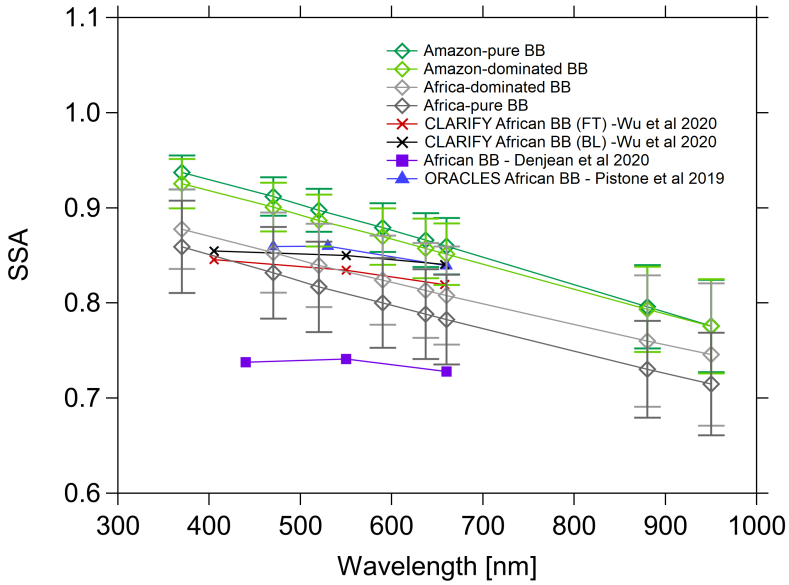

Figure S16: Wavelength dependence of single scattering albedo (SSA) for the four categories of smoke conditions at ATTO, which are dominant or majoritarian South American influence vs dominant or majoritarian African influence. For comparison, SSA values in African smoke plumes from the previous campaigns CLARIFY [26], ORACLES [110] and DACCIWA [111] are shown as well. The SSA at the 7 wavelengths was calculated by interpolating the SAE derived from the measured scattering coefficient at 3 wavelengths.

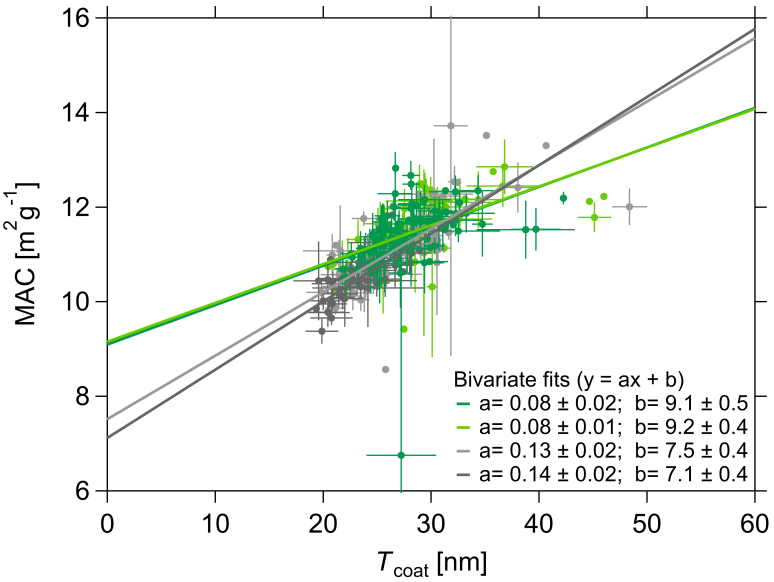

Figure S17: Relationship between mass absorption cross section (MAC) at 637 nm and the average coating thickness (T_{coat}) on rBC cores in the diameter range $180 < d_{\mathrm{MEV}} < 220$ nm for the four categories of smoke conditions at ATTO, which are dominant or majoritarian South American influence vs dominant or majoritarian African influence. Compare also Fig. S13F.

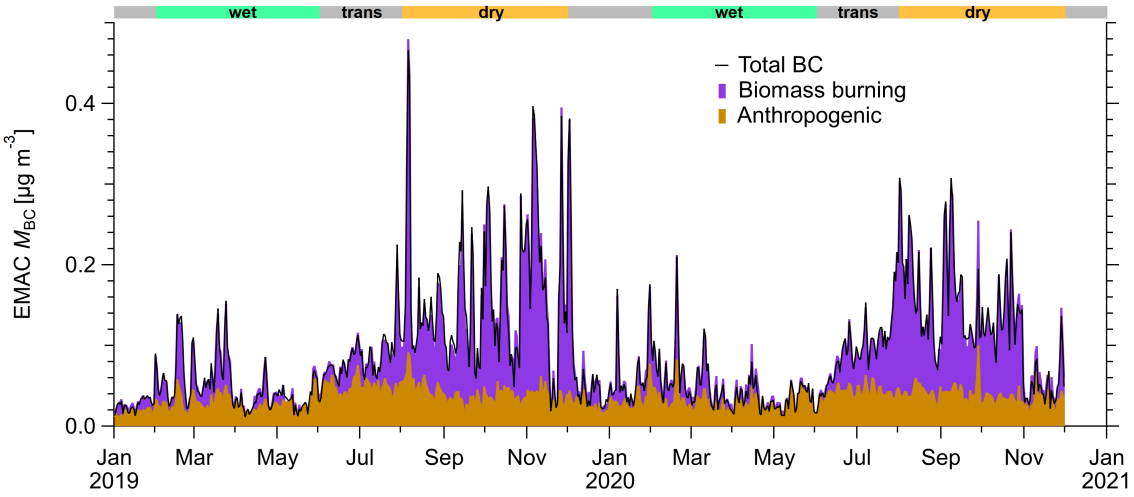

Figure S18: EMAC model sensitivity simulation discriminating the contributions of biomass burning and (other) anthropogenic emissions to the total BC mass concentrations, M_{BC}, at ATTO. The total M_{BC} (black solid line) represents the EMAC standard simulation (STD). Results correspond to the sensitivity test NOANTH as outlined in detail in Sect. S1.10. The anthropogenic sources that were switched on and off here comprise transportation (TRA), industrial combustion and processes (IND), power generation (PGN), residential and commercial combustion (RES), waste incineration (WST), agricultural waste burning (AWB), agricultural soils (AGS), and shipping (SHP).

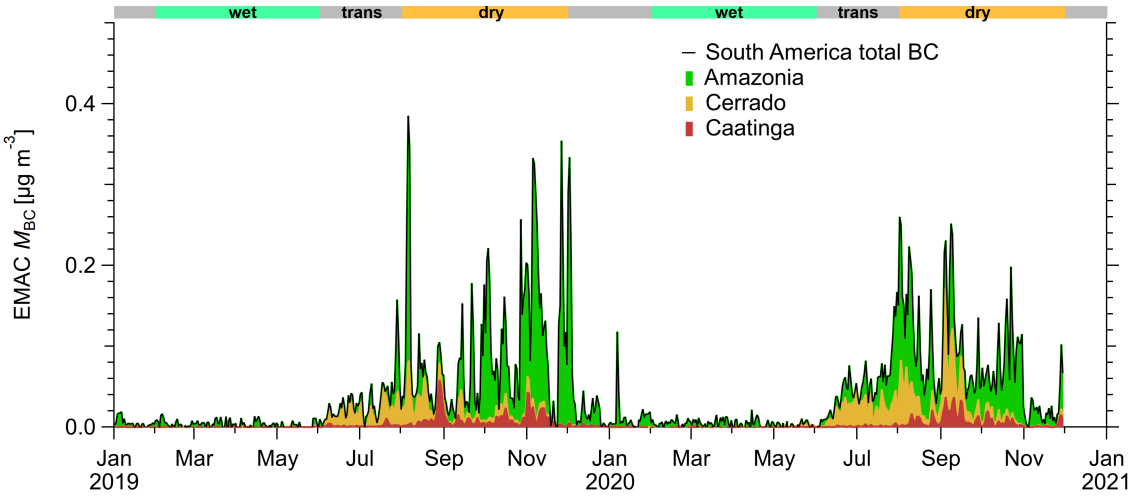

Figure S19: EMAC model sensitivity simulation discriminating the contributions of fires in the Brazilian biomes Amazonia, Cerrado, and Caatinga to the total BC mass concentrations, M_{BC}, at ATTO. The total M_{BC} (black solid line) represents the EMAC standard simulation (STD). Results further include the model runs NOBBcer (zero biomass burning emissions from Cerrado), NOBBcaa (zero biomass burning emission over from Caatinga) as well as NOBB, NOBBafr as outlined in detail in Sect. S1.10. The geographic extent of the ecoregions relative to the ATTO footprint is shown in Fig. S3.

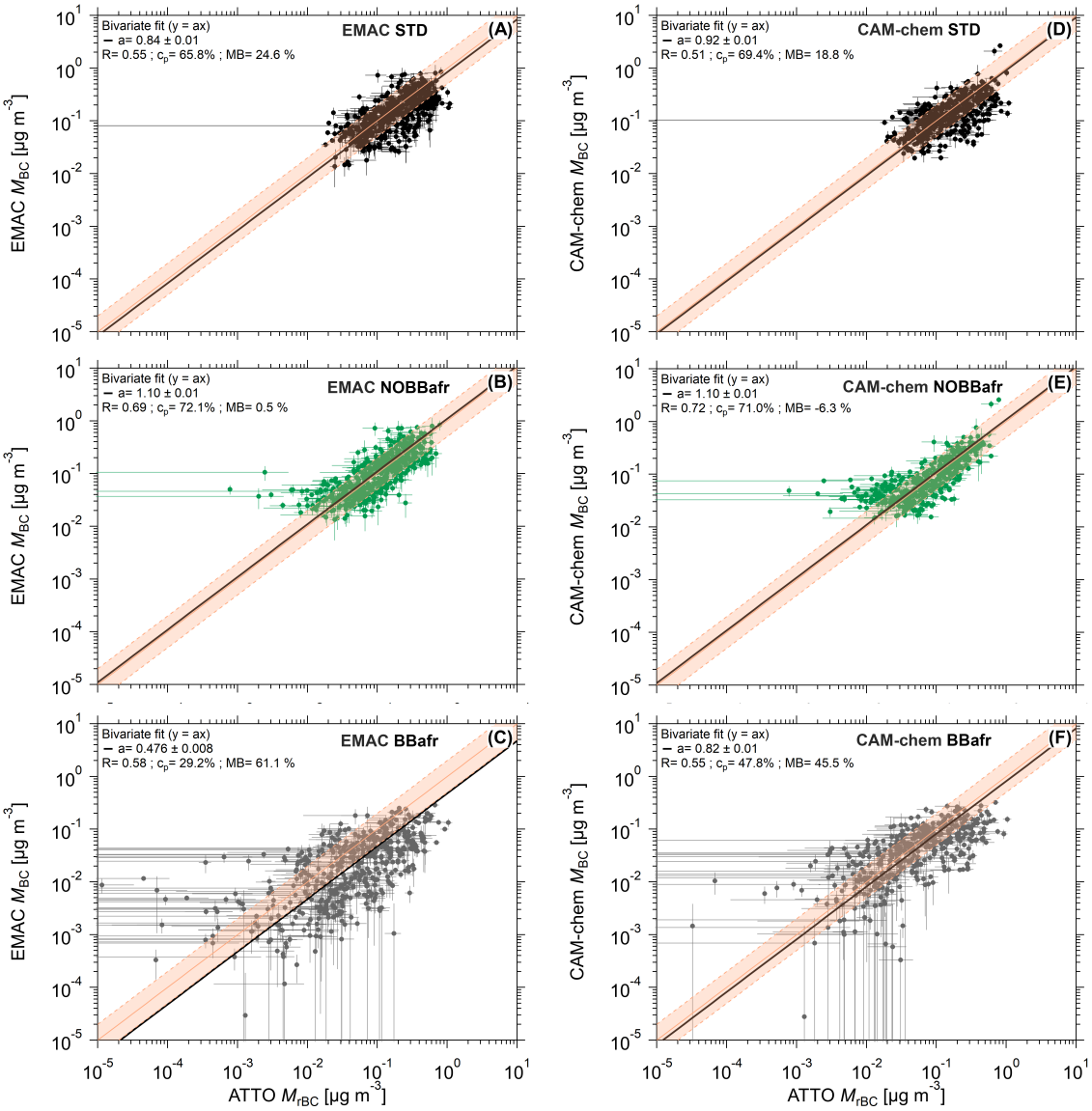

Figure S20: Correlations between measured and modelled BC mass concentrations (M_{BC}) at ATTO , in relation to corresponding time series in Fig. **??**. The following cases are shown: **A** and **D**: total BC (black markers, STD model runs), **B** and **E**: the South American BC fraction (green markers, NOBBafr model runs), and **C** and **F**: the African BC fraction (gray markers, model run BBafr = STD - NOBBafr). EMAC (**A**–**C**, see subsection S1.10) and CAM-chem (**D**–**F**, see subsection S1.11) model results are compared here. Shaded area represents the region between the 1:2 and 2:1 lines. Specified in the individual panels are the fit parameters, the correlation coefficient (R), the percentage of data points (c_{p}) that falls in between the 1:2 and 2:1 lines, and the mean bias between model and observation (MB).

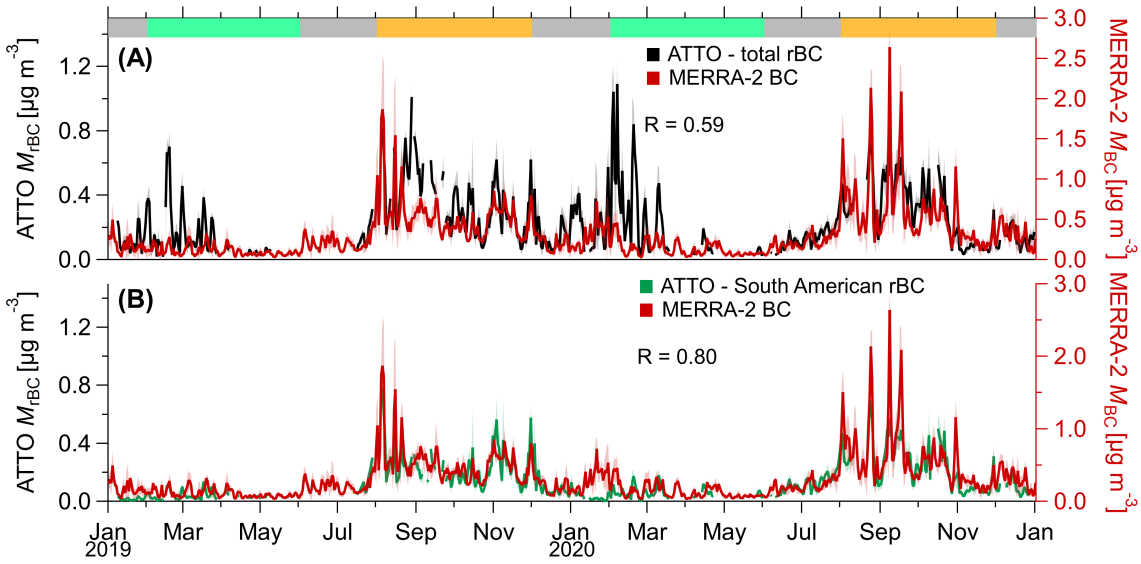

Figure S21: Comparison between model and observations. Time series of total (M_{rBC}, black line) as well as South American ($M_{\mathrm{rBC,SAm}}$, green) BC mass concentration measured at ATTO (data from Fig. 2) and modelled BC surface mass concentration from MERRA-2 model ($M_{\mathrm{BC,MERRA}}$, red) averaged over the area that includes ATTO ($-60 < \mathrm{Lon} < -58.125\,^{\circ}\mathrm{E}$; $-2.5 < \mathrm{Lat} < -1.5\,^{\circ}\mathrm{N}$). All time series show daily averages with colored shading as standard deviation. Legend specifies the Pearson's R for relationship between experimental and model data.

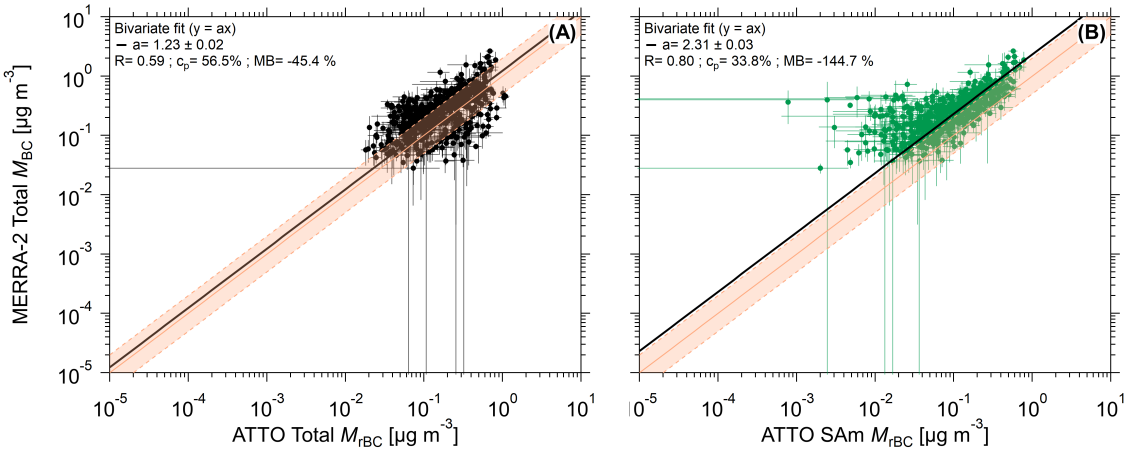

Figure S22: Correlations between measured and modelled BC mass concentrations (M_{BC}) at ATTO, in relation to corresponding time series in Fig. S21. Beyond Fig. S20, here the agreement with the model MERRA-2 is shown. The following cases are shown: **A**: total BC (black markers) and **B**: the South American BC fraction (green markers). Note that only the total BC at ATTO was modelled with MERRA-2. Shaded area represents the region between the 1:2 and 2:1 lines. Specified in the individual panels are the fit parameters, the correlation coefficient (R), the percentage of data points (c_{p}) that falls in between the 1:2 and 2:1 lines, and the mean bias between model and observation (MB).

2.4 Atmospheric processing of African biomass burning aerosols over the Tropical Atlantic Ocean and their spatial distribution over the Amazon Basin

This chapter contains a manuscript draft in early stage that will be submitted to a peer-reviewed journal.

This manuscript includes data sets from the following field experiments:
ACRIDICON-CHUVA and CAFE-Africa.

Contribution to this chapter by Bruna A. Holanda: This manuscript is currently in preparation and my personal contribution includes the processing, quality assurance and analysis of the ACRIDICON-CHUVA and CAFE-Africa data sets. I participate in the CAFE-Africa aircraft campaign in Cape Verde in 2018, being responsible for operating the aerosol measurements during the scientific flights, as well as performing frequent maintenance and calibrations. I wrote the scripts for a systematic and automated processing of the SP2 data set presented in this study. Together with my coauthors, I initiated and designed the research. I took the lead for analyzing the results, preparing figures, and writing the manuscript.

Atmospheric processing of African biomass burning aerosols over the Tropical Atlantic Ocean and their spatial distribution over the Amazon Basin

Bruna A. Holanda[1], Ovid O. Krüger[1], Meinrat O. Andreae[2,3], Thomas Klimach[1], David Walter[1,4], Ulrich Pöschl[1], Mira L. Pöhlker[1,5,6], Christopher Pöhlker[1,2], and potential further coauthors, especially from the ACRIDICON-CHUVA and CAFE-Africa teams, to be involved upon finalization of this manuscript draft

[1]Multiphase Chemistry Department, Max Planck Institute for Chemistry, 55128 Mainz, Germany
[2]Biogeochemistry Department, Max Planck Institute for Chemistry, 55128 Mainz, Germany
[3]Scripps Institution of Oceanography, University of California San Diego, La Jolla, CA 92037, USA
[4]Climate Geochemistry Department, Max Planck Institute for Chemistry, 55128 Mainz, Germany
[5]Leipzig Institute for Meteorology, Leipzig University, Leipzig, Germany
[6]Experimental Aerosol and Cloud Microphysics Department, Leibniz Institute for Tropospheric Research, Leipzig, Germany

Correspondence: Christopher Pöhlker (c.pohlker@mpic.de)

Abstract. Biomass burning in the tropics is a globally important source of black carbon particles (BC), which affects atmospheric circulation, cloud properties and water cycling. The Amazon rain forest is an ecosystem of global significance for climate and biodiversity, nevertheless, it has been subject to severe and increasing burning and deforestation activities. In addition to the regional fire emissions, the long-range transport of biomass burning smoke from Africa contributes greatly to the Amazonian aerosol population. Yet, the transport of African smoke over the Atlantic Ocean and its influx into the Amazon Basin remains underestimated in global models. In this study, we present vertically resolved BC measurements across a wide area over the South Atlantic Ocean and the Amazon Basin, based on aircraft observations. We present the mass concentrations, BC core size distributions, and BC coating thicknesses in relation to geography, altitude, and atmospheric aging. Further, we quantify the African and South American smoke contributions along a north-south transect across the Amazon basin. With that, we expect to gain new insights on the evolution of the BC particles in order to improve model capabilities to represent the sources, transport, and sinks of the transatlantic transport of African smoke and thus, access its climate effects.

+++ Early and preliminary manuscript draft +++

1 Introduction

Biomass burning is a major source of atmospheric black carbon (BC) worldwide, which is emitted together with gases of different volatility as well as organic and inorganic aerosols species (e.g., Andreae, 2019). The BC particles are of particular climate-relevance as they affect the Earth's radiation balance and act as cloud condensation nuclei (CCN) in the formation and development of clouds and precipitation (Bond et al., 2013; Stocker et al., 2013; Andreae and Rosenfeld, 2008). The atmospheric life cycle of BC particles is complex and dynamic. After emission from a variety of combustion sources, the particles undergo atmospheric aging, which changes, e.g., their optical and hygroscopic properties and, thus, their atmospheric significance (e.g., Pokhrel et al., 2016; Cappa et al., 2012; Liu et al., 2013). A prominent example is the formation of a coating on the BC cores through the condensation of co-emitted or atmospherically formed semi- and low-volatility compounds (Moffet and Prather, 2009; Adachi et al., 2020).

Africa and South America are global hotspots of biomass burning (Crutzen and Andreae, 1990). Accordingly, atmospheric processes over both continents, including the tropical Atlantic Ocean in between, are heavily influenced by biomass burning smoke (Andreae et al., 1988, 2015; Zuidema et al., 2018; Wu et al., 2020). In previous studies, we have shown that the African smoke is efficiently transported across the Atlantic in the westerly trade wind circulation and strongly affects aerosol processes in the Amazon, including aerosol optical properties and the cloud condensation nuclei (CCN) budget (e.g., Saturno et al., 2018a; Pöhlker et al., 2018; Holanda et al., 2020). In fact, the Amazon receives African smoke essentially all year long (Holanda et al., 2021). This underlines that beyond the annually reoccurring transport of Saharan dust into the Amazon (e.g., Swap et al., 1992; Moran-Zuloaga et al., 2017) also the transatlantic transport of African smoke is an aerosol influx of major significance, which has to be taken into account in the analysis and modelling of the Amazonian aerosol life cycle. This is all the more important since global models tend to underestimate the smoke transport across the Atlantic (e.g., Lund et al., 2018; Carter et al., 2021; Shinozuka et al., 2020).

To quantify the fraction of African smoke in the Amazon and, thus, to assess its relevance for the local atmospheric processes, we have developed an approach to distinguish between the South American and African smoke fractions (Holanda et al., 2021). This analysis is based on characteristic microphysical differences in the BC core size distribution. Specifically, we found that the African BC cores are significantly larger and that their size distribution is narrower than BC cores from fires in the Amazon and adjacent ecoregions. These differences remain sufficiently unchanged during atmospheric transport and processing so that the smoke contributions from both continents can be separated in a deconvolution of BC core size distributions. With this approach, we found that at the Amazon Tall Tower Observatory (ATTO) in the central basin, the African smoke accounts for up to 90 % of the BC mass in the wet season and for up to 60 % in the dry season. The microphysical properties and quantities of BC at ATTO were found to be in remarkably good agreement with selected flight segments of the aircraft mission ACRIDICON-CHUVA over the Amazon (Wendisch et al., 2016) and CAFE-Africa over the Atlantic Ocean (Tadic et al., 2021).

This study builds on Holanda et al. (2021) and applies the microphysical deconvolution of African and South American smoke systematically to the entire ACRIDICON-CHUVA data set. With this approach, we address the following general questions:

1. How do the vertical distribution and properties of the African biomass burning aerosols evolve during their transport across the Atlantic prior to reaching South America?
2. How widely is the African smoke distributed in terms of latitude, longitude, and altitude? Can a north-south gradient over the Amazon basin be resolved?
3. Which conclusions can be drawn on the influence of the African smoke on the Amazonian radiation balance and hydrological cycle?

2 Methods and Analysis

2.1 HALO aircraft missions

Airborne aerosol measurements used in this study were conducted onboard the HALO (High Altitude and LOng Range) research aircraft over the Amazon Basin and the tropical Atlantic in the course of two field experiments.

- The ACRIDICON-CHUVA campaign (Aerosol, Cloud, Precipitation, and Radiation Interactions and Dynamics of Convective Cloud Systems–Cloud Processes of the Main Precipitation Systems in Brazil: A Contribution to Cloud Resolving Modeling and to the Global Precipitation Measurement) took place during the dry season month of September 2014 over the Amazon Basin. Details on the mission's instrumentation and objectives can be found in Wendisch et al. (2016), along with further studies of potential interest (Cecchini et al., 2017; Andreae et al., 2018; Campos Braga et al., 2021). In Holanda et al. (2020), the observed transatlantic transport of African biomass burning aerosols in defined black carbon-rich layers is addressed in detail.
- The CAFE-Africa campaign (Chemistry of the Atmosphere: Field Experiment in Africa) took place in August 2018 over the Atlantic Ocean in the outflow region of the African continent. Further details on the mission can be found in Schneider et al. (2021) and Tadic et al. (2021).

The map with the flight track and sampling regions of both campaigns are depicted in Fig. 1.

2.2 Aerosol measurements

Data at 1-Hz time resolution were collected from the HALO aerosol submicrometer inlet (HASI) with the HALO-CCN rack (Andreae et al., 2018), which includes an eight-channel Single Particle Soot Photometer (SP2, Droplet Measurement Techniques, Longmont, USA) to measure refractory black carbon (rBC) concentrations and properties as well as a dual-column continuous-flow stream-wise thermal gradient CCN counter (CCNC-200, Droplet Measurement Techniques). Details on both instruments can be found elsewhere (e.g., Stephens et al., 2003; Roberts and Nenes, 2005; Schwarz et al., 2006; Rose et al.,

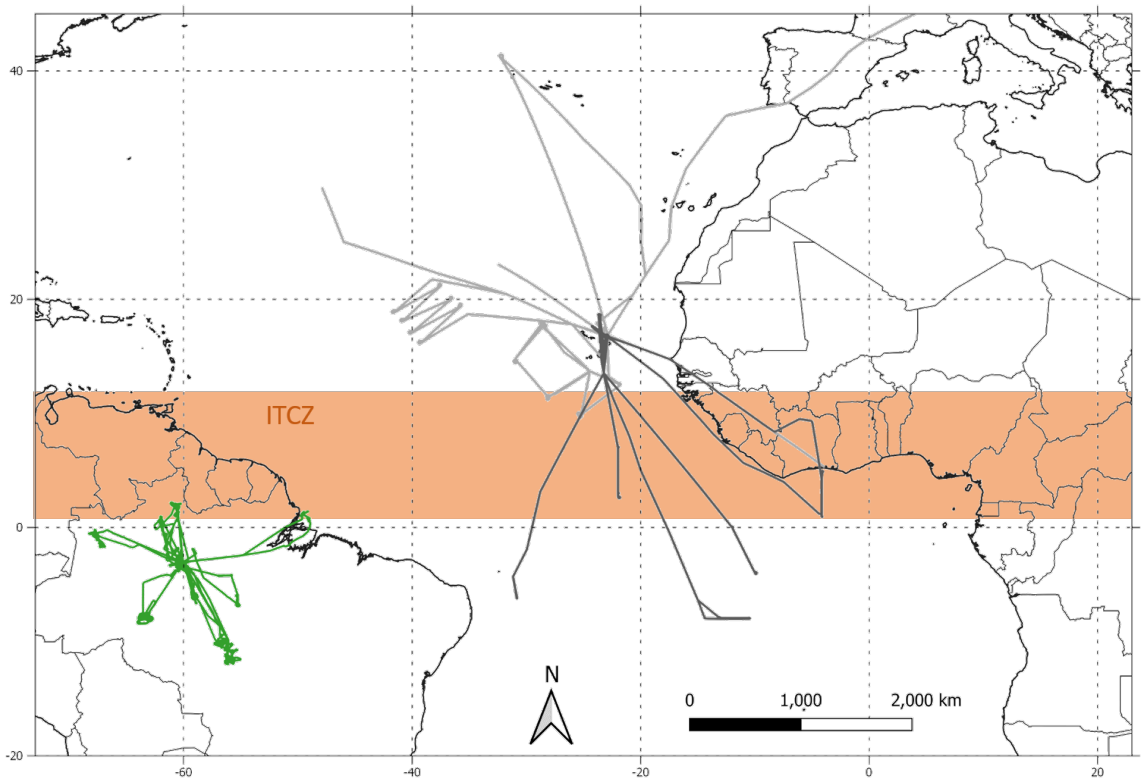

Figure 1. Map with the flight tracks of the ACRIDICON-CHUVA (green) and the CAFE-Africa campaigns with the HALo aircraft. The red shaded area indicates the approximate location of the Intertropical Convergence Zone (ITCZ).

2008; Laborde et al., 2013). The SP2 data analysis as well as the approach to discriminate African vs South American smoke are described elsewhere (Saturno et al., 2018a; Holanda et al., 2021). All concentration data was normalized to standard temperature and pressure (STP, $T_0 = 273.15\,\mathrm{K}$ and $p_0 = 1013.25\,\mathrm{hPa}$) and averaged over 1-min time step prior to analysis.

3 Results and Discussion

3.1 Vertical and longitudinal distribution of rBC mass over the Tropical Atlantic

Figure 2 presents the vertical profiles of the rBC mass concentration (M_{rBC}) over the tropical Atlantic Ocean for the individual flights conducted during the CAFE-Africa campaign in west-to-east order. Accordingly, the panels represent regions with different distances from Africa, and therefore, different aging times during the transatlantic transport. Biomass burning smoke was ubiquitous over the entire South Atlantic region that was probed with the aircraft. It extended horizontally over thousands of kilometers during the aircraft campaign period. The smoke is confined in atmospheric layers within the lowest 6 km of the atmosphere (see yellow shading). The thickness and height of the horizontal layers and BC concentrations depend on the sampled region. The observed rBC mass concentration were comparatively high, spanning from peak concentrations of $\sim 4\,\mu\mathrm{g\,m^{-3}}$ during flight CA04 to peak concentrations of $\sim 2\,\mu\mathrm{g\,m^{-3}}$ at the closest point to South America during flight CA05.

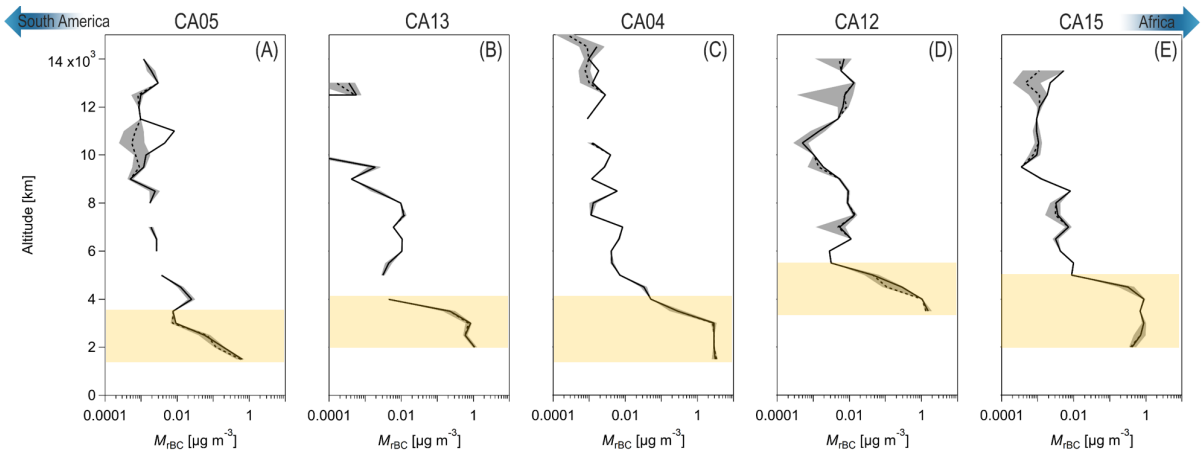

Figure 2. Vertical profiles of measured black carbon mass concentrations, M_{rBC}, at a range of locations over the South Atlantic Ocean during the CAFE-Africa mission during August and September 2018. Every panel represents one research flight in a certain geographic region (i.e.,CA05, CA13, CA04, CA12, and CA15) and the panels represent a west **(A)** to east **(E)** transect. The plots show the mean (solid lines), median (dashed lines), 25$^{\mathrm{th}}$ and 75$^{\mathrm{th}}$ percentiles (shading) calculated for 500 m altitude bins of the 1-min averaged data. The yellow shaded area indicates the approximate location of the biomass burning aerosol layer.

The microphysical properties of the rBC particles in the African outflow for the lower 6 km are shown in Fig. 3. The rBC mass size distributions peak at comparatively large diameters ($210 < D_{\mathrm{rBC}} < 240\,\mathrm{nm}$) and are further characterized by a comparatively narrow distribution ($1.45 < \sigma_{\mathrm{rBC}} < 1.55$) (compare the complementary results for the ATTO site in Holanda et al., 2021). A rather small variability in the parameters D_{rBC} and σ_{rBC} was observed across the different flights as well as

for different altitudes (e.g., flights CA12 vs CA13). The extent of the variability observed in D_{rBC} can probably be related to different source regions and, therefore, different mixtures of burnt fuel/vegetation and/or different aging times of the smoke. In terms of mixing state, the rBC particles showed moderately thick coatings (T_{coat}), spanning from 35 to 45 nm. The lowest coating thickness was obtained during flight CA05, which was closest to the South American coast. Generally, the T_{coat} levels obtained in this study are larger than for the aged African smoke at ATTO within the Amazonian boundary layer (i.e., 20–25 nm) as shown in Holanda et al. (2021). This observation might imply that the coating thickness is reduced in the course of the transatlantic transport, e.g., through a photo-degradation of organics matter condensed onto the rBC cores, but then increases again when the particles are exposed to condensable vapors in the Amazonian boundary layer. The ongoing analysis will likely yield further insights here.

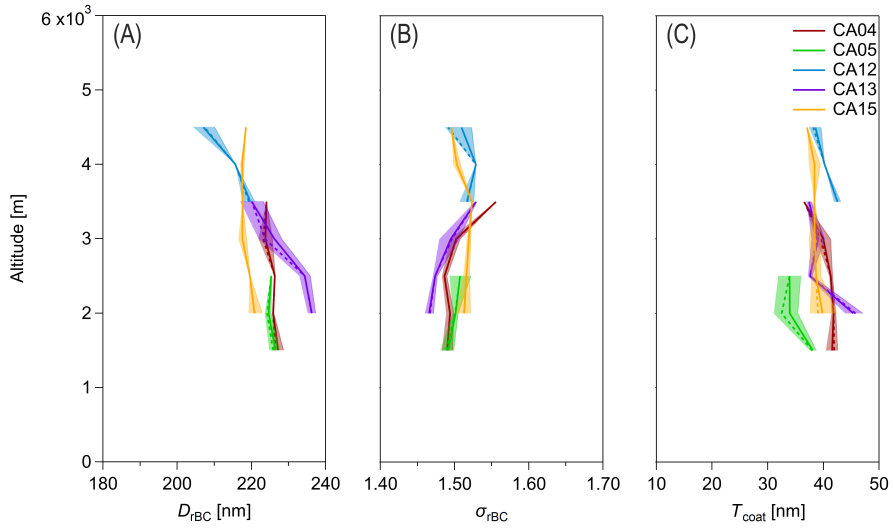

Figure 3. Vertical profiles of rBC microphysical properties measured at a range of longitudes over the South Atlantic Ocean during the CAFE-Africa mission during August and September 2018: **(A)** geometric mean diameters (D_{rBC}); **(B)** geometric standard deviation (σ_{rBC}) of the core size distributions; and **(C)** coating thickness (T_{coat}) of rBC-containing particles within the size range $\sim 180 < d_{\mathrm{MEV}} < 220$ nm. The plots show the mean (solid lines), median (dashed lines), 25$^{\mathrm{th}}$ and 75$^{\mathrm{th}}$ percentiles (shading) calculated for 500 m altitude bins of the 1-min averaged data.

3.2 Vertical and latitudinal distribution of rBC mass over the Amazon Basin

Figure 4 shows the vertical profiles of M_{rBC} along a north-south transect over the Amazon. The northern Amazon region covers Lat $> 1.8°$S, the central $1.8°S <$ Lat $< 7.2°$S, and the southern Amazon Lat $< 7.2°S$). Similar to the M_{rBC} profiles over the South Atlantic region in Fig. 2, most of the M_{rBC} is concentrated in the lowest 5 km of the atmosphere, where concentrations

105 are two to three orders of magnitude higher than in the altitudes above. The southern Amazon is clearly the most polluted region, with M_{rBC} reaching up to $1\,\mu\mathrm{g\,m^{-3}}$ (1-min averages), while the northern Amazon, which is generally less affected by human activities, showed lower M_{rBC} of up to $\sim 0.3\,\mu\mathrm{g\,m^{-3}}$. Since the aircraft campaign took place in September, which is the month with the strongest advection of African smoke through long-range transport (compare consistent observations in Saturno et al., 2018b; Holanda et al., 2020, 2021), the BC burden over the Amazon was likely influenced to a significant extent
110 by biomass burning emission in Africa. The African influence is discussed in more detail in Sect. 3.3.

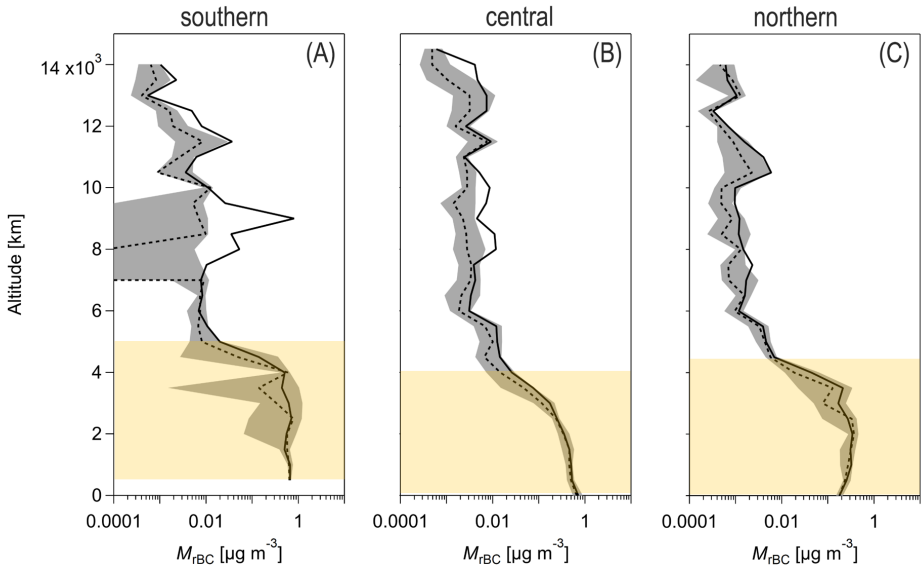

Figure 4. Vertical profiles of measured black carbon mass concentration, M_{rBC}, over **(C)** the northern (Lat $> 1.8^\circ S$), **(B)** central ($1.8^\circ S <$ Lat $< 7.2^\circ S$), and **(A)** southern (Lat $< 7.2^\circ S$) regions of the Amazon Basin during the ACRIDICON-CHUVA mission in September and October 2014. The plots show the mean (solid lines), median (dashed lines), 25^{th} and 75^{th} percentiles (shading) calculated for $500\,\mathrm{m}$ altitude bins of the 1-min averaged data. The yellow shaded area indicates the approximate location of the biomass burning aerosol layer.

The rBC microphysical properties over the Amazon Basin were more variable than the corresponding measurements over the South Atlantic (see Fig. 3. This probably indicates higher levels of mixing of the smoke from different sources as well as different aging histories affecting rBC properties. The vertical profiles of D_{rBC}, σ_{rBC} and T_{coat} are shown in Fig. 5. The modal diameter of rBC cores ranges between $190 < D_{\mathrm{rBC}} > 210\,\mathrm{nm}$, which is lower than the values measured in aged African
115 smoke. Moreover, the broader distributions ($\sigma_{\mathrm{rBC}} \sim 1.63$) were found at all atmospheric levels in the southern Basin, while the northern region presents the narrowest distributions ($\sigma_{\mathrm{rBC}} \sim 1.5$). These trends in M_{rBC} and σ_{rBC} are consistent with Holanda et al. (2021). The coating thickness observed during the ACRIDICON–CHUVA is in the same range observed at the ATTO site according to Holanda et al. (2021). The lowest coating thickness were found in the southern part of the basin at high altitudes.

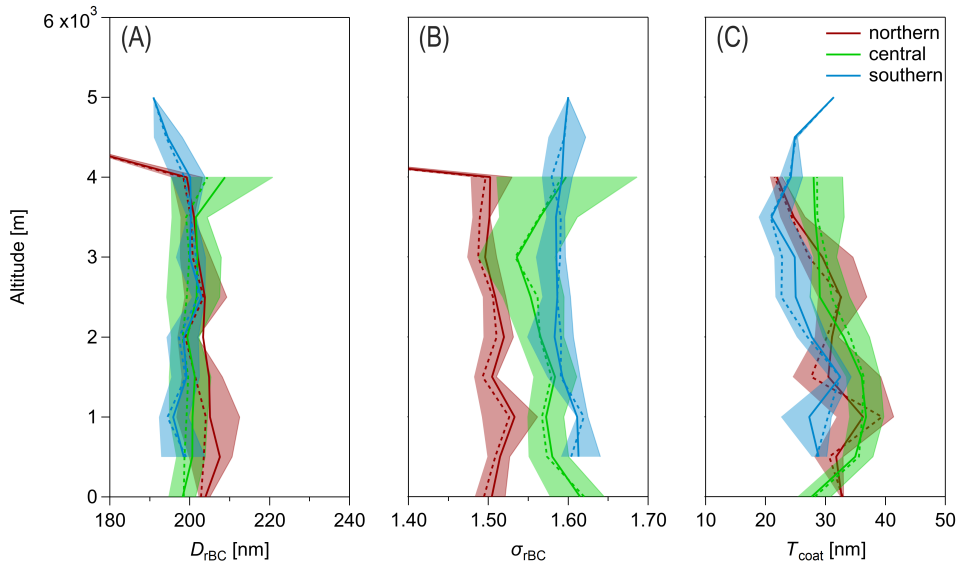

Figure 5. Vertical profiles of rBC microphysical properties measured over the northern, central and southern regions of the Amazon Basin: **(A)** geometric mean diameters (D_{rBC}); **(B)** the geometric standard deviation (σ_{rBC}) of the core size distributions; and **(C)** coating thickness (T_{coat}) of rBC-containing particles within the size range $\sim 180 < d_{\mathrm{MEV}} < 220\,\mathrm{nm}$. The plots show the statistical parameters: mean (solid lines), median (dashed lines), 25^{th} and 75^{th} percentiles (shading) calculated for $500\,\mathrm{m}$ altitude bins of the 1-min averaged data.

3.3 The African biomass burning smoke over the Amazon basin

To investigate the fraction and spatial distribution of the African rBC in the overall smoke burden over the Amazon during the dry season, we used the approach from Holanda et al. (2021) to apportion the African contribution relative to the smoke from South American fires. By using this approach, we hypothesize that the BC mass size distribution is source-specific and unalterable upon atmospheric aging and wet removal, and that the BC population over he Amazon is a superposition of two independent sources. The result of this approach is shown in the latitude-altitude curtain plot in Fig. 6A, which illustrates the spatial distribution of the African rBC fraction over the Amazon. It suggests that the African smoke is more significant in the northern region, contributing more than $50\,\%$ of the rBC burden for all altitudes below $5\,\mathrm{km}$, whereas its fractional contribution decreases towards the southern part of the basin as the burning activities in South America increase along the same north-to-south transect.

The absolute rBC concentrations attributed to African and South American smoke for the southern, central and northern regions are shown in Fig. 6B–D. In the northern region – which includes the offshore flight AC19 as analyzed in detail in Holanda et al. (2020) – the vertical distribution of M_{rBC} attributed to African emissions are, on average, two times larger than the South

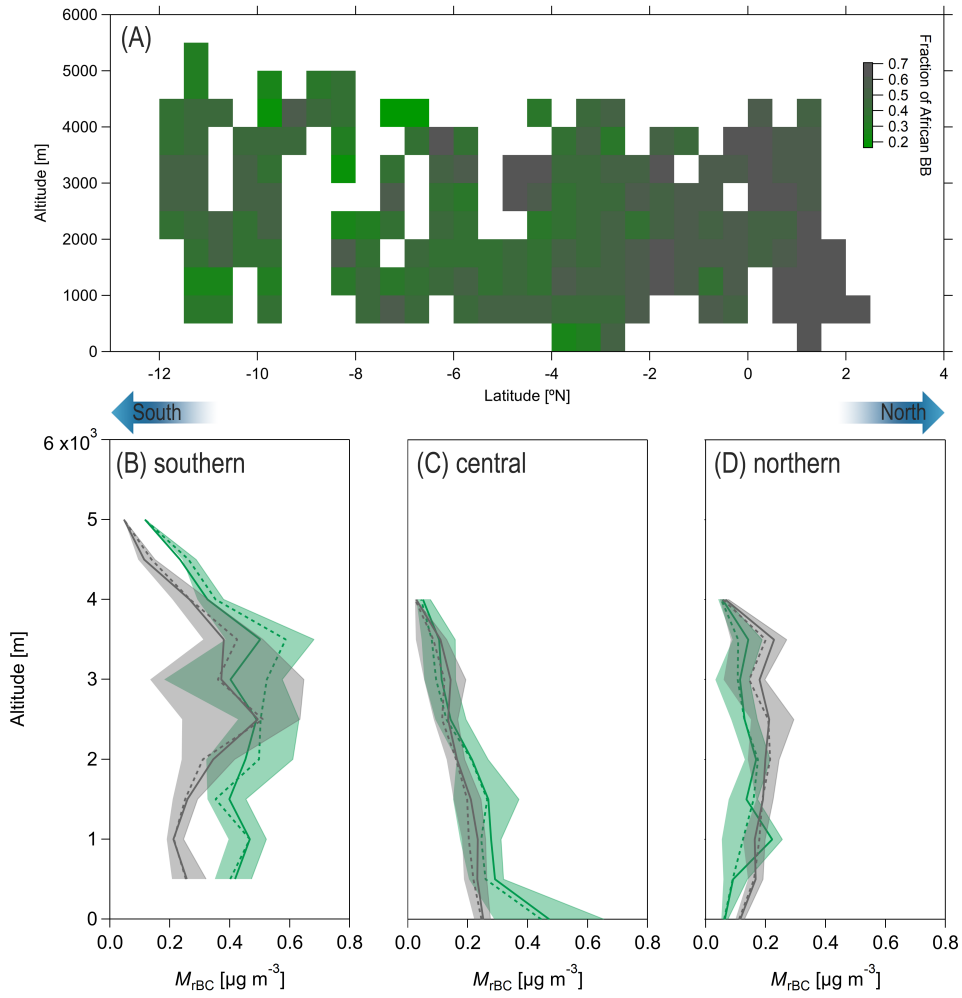

Figure 6. Latitude-altitude curtain plot of the fractional contribution of African rBC over the Amazon Basin shown in **(A)**, according to the classification approach presented in Holanda et al. (2021). Further shown are the absolute rBC mass concentrations attributed to South America (green) and Africa (grey) sources averaged over the **(B)** southern; **(C)** central and **(D)** northern regions of the Amazon Basin probed during the ACRIDICON–CHUVA campaign in September and October 2014. The profiles show the statistical parameters: mean (solid lines), median (dashed lines), 25^{th} and 75^{th} percentiles (shading) calculated for $500\,\text{m}$ altitude bins of the 1-min averaged data.

American contributions of $\sim 0.1\,\mu\text{g}\,\text{m}^{-3}$, with both sources showing rather stable concentrations up to $5\,\text{km}$ (Fig. 6D). The peak in the African rBC fraction at 3.5 km as well as the peak in the South American rBC fraction at 1 km altitude are consistent with the observations of an aged African pollution layer and fresh biomass burning in the Amazon as described in Holanda

et al. (2020). In the central Amazon region – which includes the ATTO site (Andreae et al., 2015; Saturno et al., 2018a) – the South American smoke is dominant, with larger concentrations than the in northern region during this particular period (Fig. 6C). Note however, that the large peak at the lowest altitude could in principle be biased by the influence of the Manaus city plume and airport, which remains to be investigated in the ongoing analysis. Remarkably, a pronounced layer attributed to Africa smoke was observed between 2 to 4 km altitude over southern Amazon (Fig. 6B). In this layer, M_{rBC} reaches up to $\sim 0.6\,\mu\mathrm{g\,m^{-3}}$ (75$^{\mathrm{th}}$ percentile) and sharply decreases at lower levels. The South American rBC is equally important at high altitudes, also contributing to up to $\sim 0.6\,\mu\mathrm{g\,m^{-3}}$ but this concentrations remains elevated also at lower altitudes.

4 Conclusions and outlook

This manuscript represents the current, though yet preliminary, state of the ongoing analysis of the extended ACRIDICON-CHUVA and CAFE-Africa data sets. The analysis shown here so far represents the backbone of a publication that is being written. A strength of the combination of both campaigns is that the same set of instruments with a continuous and consistent calibration history and data processing has been used, which ensures comparability of the result across all flights. Based on the results so far from the size-resolved rBC profiles up to an altitude of 15 km over a large geographic areas over the Amazon Basin and South Atlantic Ocean, the following (preliminary) conclusions can be drawn:

- The position of the rBC mass size distributions of the African smoke peaks at larger diameter than the corresponding South American distribution. Further the African is narrower than the South American distribution. Both, agrees well with observations at the Amazon Tall Tower Observatory (ATTO) in Holanda et al. (2021).
- The transatlantic transport of the African smoke occurs in layers in the free troposphere (consistent with Holanda et al., 2020) and does not alter the rBC size distribution to a significant extent.
- The significant larger core diameters observed in aged African biomass burning could be a result of the ascent of the plumes over Africa due to in-cloud processing. The values presented in this study are also larger than values reported in (Wu et al., 2021) for fresh biomass burning plumes in western Africa. However, further aerosol profiling over the African continent is needed to address this question.
- The coating thickness on the rBC core tends to decrease with atmospheric aging in the course of the transatlantic transport.
- The fractional contribution of African rBC is largest in the northern Amazon and decreases towards the southern Amazon, which is strongly affected by deforestation fires and, thus, enhanced local biomass burning emissions. The largest concentrations of biomass burning aerosols were observed in the southern Amazon since the influences of South American and African smoke adds up here.

Beyond the results and conclusions presented so far, the following specific steps will be part of the further data analysis:

- In addition to the SP2 data analyzed, the complementary trace gas and aerosol data from both aircraft missions will be analyzed and implemented in this manuscript for comparison.
- Remote sensing data (i.e., satellite data) will be involved for a validation of the results.
- The aircraft data presented here will be compared with a detailed literature synthesis of studies on previous (aircraft) missions over African, South America and/or the Atlantic region (e.g. Taylor et al., 2020; Wu et al., 2021; Hodgson et al., 2018). Ideally, this comparison starts at the raw SP2 data (if available) to ensure comparability of the results. Note, however, that only few of such studies exist so far.
- The experimental aircraft results presented here will be compared to global model results to investigate whether the sources, transport, and sinks are appropriately covered in the models. The modelling support will further allow to conduct sensitivity studies that will strongly support the interpretation of the experimental results.

References

Adachi, K., Oshima, N., Gong, Z., de Sá, S., Bateman, A. P., Martin, S. T., de Brito, J. F., Artaxo, P., Cirino, G. G., Sedlacek III, A. J., and Buseck, P. R.: Mixing states of Amazon basin aerosol particles transported over long distances using transmission electron microscopy, Atmospheric Chemistry and Physics, 20, 11 923–11 939, https://doi.org/10.5194/acp-20-11923-2020, https://acp.copernicus.org/articles/20/11923/2020/, 2020.

Andreae, M. and Rosenfeld, D.: Aerosol–cloud–precipitation interactions. Part 1. The nature and sources of cloud-active aerosols, Earth-Science Reviews, 89, 13–41, https://doi.org/10.1016/j.earscirev.2008.03.001, http://linkinghub.elsevier.com/retrieve/pii/S0012825208000317, 2008.

Andreae, M. O.: Emission of trace gases and aerosols from biomass burning – an updated assessment, Atmospheric Chemistry and Physics, 19, 8523–8546, https://doi.org/10.5194/acp-19-8523-2019, https://acp.copernicus.org/articles/19/8523/2019/, 2019.

Andreae, M. O., Browell, E. V., Garstang, M., Gregory, G. L., Harriss, R. C., Hill, G. F., Jacob, D. J., Pereira, M. C., Sachse, G. W., Setzer, A. W., Dias, P. L. S., Talbot, R. W., Torres, A. L., and Wofsy, S. C.: Biomass-burning emissions and associated haze layers over Amazonia, Journal of Geophysical Research, 93, 1509, https://doi.org/10.1029/JD093iD02p01509, http://doi.wiley.com/10.1029/JD093iD02p01509, 1988.

Andreae, M. O., Acevedo, O. C., Araùjo, A., Artaxo, P., Barbosa, C. G., Barbosa, H. M., Brito, J., Carbone, S., Chi, X., Cintra, B. B., Da Silva, N. F., Dias, N. L., Dias-Júnior, C. Q., Ditas, F., Ditz, R., Godoi, A. F., Godoi, R. H., Heimann, M., Hoffmann, T., Kesselmeier, J., Könemann, T., Krüger, M. L., Lavric, J. V., Manzi, A. O., Lopes, A. P., Martins, D. L., Mikhailov, E. F., Moran-Zuloaga, D., Nelson, B. W., Nölscher, A. C., Santos Nogueira, D., Piedade, M. T., Pöhlker, C., Pöschl, U., Quesada, C. A., Rizzo, L. V., Ro, C. U., Ruckteschler, N., Sá, L. D., De Oliveira Sá, M., Sales, C. B., Dos Santos, R. M., Saturno, J., Schöngart, J., Sörgel, M., De Souza, C. M., De Souza, R. A., Su, H., Targhetta, N., Tóta, J., Trebs, I., Trumbore, S., Van Eijck, A., Walter, D., Wang, Z., Weber, B., Williams, J., Winderlich, J., Wittmann, F., Wolff, S., and Yáñez-Serrano, A. M.: The Amazon Tall Tower Observatory (ATTO): Overview of pilot measurements on ecosystem ecology, meteorology, trace gases, and aerosols, Atmospheric Chemistry and Physics, 15, 10 723–10 776, https://doi.org/10.5194/acp-15-10723-2015, 2015.

Andreae, M. O., Afchine, A., Albrecht, R., Holanda, B. A., Artaxo, P., Barbosa, H. M. J., Borrmann, S., Cecchini, M. A., Costa, A., Dollner, M., Fütterer, D., Järvinen, E., Jurkat, T., Klimach, T., Konemann, T., Knote, C., Krämer, M., Krisna, T., Machado, L. A. T., Mertes, S., Minikin, A., Pöhlker, C., Pöhlker, M. L., Pöschl, U., Rosenfeld, D., Sauer, D., Schlager, H., Schnaiter, M., Schneider, J., Schulz, C., Spanu, A., Sperling, V. B., Voigt, C., Walser, A., Wang, J., Weinzierl, B., Wendisch, M., and Ziereis, H.: Aerosol characteristics and particle production in the upper troposphere over the Amazon Basin, Atmospheric Chemistry and Physics, 18, 921–961, https://doi.org/10.5194/acp-18-921-2018, https://www.atmos-chem-phys.net/18/921/2018/, 2018.

Bond, T. C., Doherty, S. J., Fahey, D. W., Forster, P. M., Berntsen, T., Deangelo, B. J., Flanner, M. G., Ghan, S., Kärcher, B., Koch, D., Kinne, S., Kondo, Y., Quinn, P. K., Sarofim, M. C., Schultz, M. G., Schulz, M., Venkataraman, C., Zhang, H., Zhang, S., Bellouin, N., Guttikunda, S. K., Hopke, P. K., Jacobson, M. Z., Kaiser, J. W., Klimont, Z., Lohmann, U., Schwarz, J. P., Shindell, D., Storelvmo, T., Warren, S. G., and Zender, C. S.: Bounding the role of black carbon in the climate system: A scientific assessment, Journal of Geophysical Research Atmospheres, 118, 5380–5552, https://doi.org/10.1002/jgrd.50171, 2013.

Campos Braga, R., Rosenfeld, D., Krüger, O. O., Ervens, B., Holanda, B. A., Wendisch, M., Krisna, T., Pöschl, U., Andreae, M. O., Voigt, C., and Pöhlker, M. L.: Linear relationship between effective radius and precipitation water content near the top of convective clouds,

Atmospheric Chemistry and Physics Discussions, 2021, 1–16, https://doi.org/10.5194/acp-2021-295, https://acp.copernicus.org/preprints/acp-2021-295/, 2021.

Cappa, C. D., Onasch, T. B., Massoli, P., Worsnop, D. R., Bates, T. S., Cross, E. S., Davidovits, P., Hakala, J., Hayden, K. L., Jobson, B. T., Kolesar, K. R., Lack, D. A., Lerner, B. M., Li, S.-M., Mellon, D., Nuaaman, I., Olfert, J. S., Petaja, T., Quinn, P. K., Song, C., Subramanian, R., Williams, E. J., and Zaveri, R. A.: Radiative Absorption Enhancements Due to the Mixing State of Atmospheric Black Carbon, Science, 337, 1078–1081, https://doi.org/10.1126/science.1223447, http://www.sciencemag.org/cgi/doi/10.1126/science.1223447, 2012.

Carter, T. S., Heald, C. L., Cappa, C. D., Kroll, J. H., Campos, T. L., Coe, H., Cotterell, M. I., Davies, N. W., Farmer, D. K., Fox, C., Garofalo, L. A., Hu, L., Langridge, J. M., Levin, E. J. T., Murphy, S. M., Pokhrel, R. P., Shen, Y., Szpek, K., Taylor, J. W., and Wu, H.: Investigating Carbonaceous Aerosol and Its Absorption Properties From Fires in the Western United States (WE-CAN) and Southern Africa (ORACLES and CLARIFY), Journal of Geophysical Research: Atmospheres, 126, e2021JD034 984, https://doi.org/https://doi.org/10.1029/2021JD034984, https://agupubs.onlinelibrary.wiley.com/doi/abs/10.1029/2021JD034984, e2021JD034984 2021JD034984, 2021.

Cecchini, M. A., Machado, L. A. T., Andreae, M. O., Martin, S. T., Albrecht, R. I., Artaxo, P., Barbosa, H. M. J., Borrmann, S., Fütterer, D., Jurkat, T., Mahnke, C., Minikin, A., Molleker, S., Pöhlker, M. L., Pöschl, U., Rosenfeld, D., Voigt, C., Weinzierl, B., and Wendisch, M.: Sensitivities of Amazonian clouds to aerosols and updraft speed, Atmospheric Chemistry and Physics, 17, 10 037–10 050, https://doi.org/10.5194/acp-17-10037-2017, https://acp.copernicus.org/articles/17/10037/2017/, 2017.

Crutzen, P. J. and Andreae, M. O.: Biomass Burning in the Tropics: Impact on Atmospheric Chemistry and Biogeochemical Cycles, Science, 250, 1669–1678, https://doi.org/10.1126/science.250.4988.1669, https://science.sciencemag.org/content/250/4988/1669, 1990.

Hodgson, A. K., Morgan, W. T., Shea, S. O., Bauguitte, S., Allan, J. D., Darbyshire, E., Flynn, M. J., Liu, D., Lee, J., Johnson, B., Haywood, J. M., Longo, K. M., Artaxo, P. E., and Coe, H.: Near-field emission profiling of tropical forest and Cerrado fires in Brazil during SAMBBA 2012, pp. 5619–5638, 2018.

Holanda, B. A., Pöhlker, M. L., Walter, D., Saturno, J., Sörgel, M., Ditas, J., Ditas, F., Schulz, C., Franco, M. A., Wang, Q., Donth, T., Artaxo, P., Barbosa, H. M. J., Borrmann, S., Braga, R., Brito, J., Cheng, Y., Dollner, M., Kaiser, J. W., Klimach, T., Knote, C., Krüger, O. O., Fütterer, D., Lavrič, J. V., Ma, N., Machado, L. A. T., Ming, J., Morais, F. G., Paulsen, H., Sauer, D., Schlager, H., Schneider, J., Su, H., Weinzierl, B., Walser, A., Wendisch, M., Ziereis, H., Zöger, M., Pöschl, U., Andreae, M. O., and Pöhlker, C.: Influx of African biomass burning aerosol during the Amazonian dry season through layered transatlantic transport of black carbon-rich smoke, Atmos. Chem. Phys., 20, 4757–4785, https://doi.org/10.5194/acp-20-4757-2020, https://www.atmos-chem-phys.net/20/4757/2020/, 2020.

Holanda, B. A., Franco, M. A., Walter, D., Andreae, M. O., Artaxo, P., Carbone, S., Cheng, Y., Chowdhury, S., Ditas, F., Gysel-Beer, M., Klimach, T., Kremper, L. A., Krüger, O. O., Lavric, J. V., Lelieveld, J., Ma, C., Machado, L. A. T., Morais, F. G., Modini, R. L., Pozzer, A., Saturno, J., Su, H., Wendisch, M., Wolff, S., Pöhlker, M. L., Pöschl, U., and Pöhlker, C.: African smoke over the Amazon rain forest, to be submitted, 2021.

Laborde, M., Crippa, M., Tritscher, T., Jurányi, Z., Decarlo, P. F., Temime-Roussel, B., Marchand, N., Eckhardt, S., Stohl, A., Baltensperger, U., Prévôt, A. S., Weingartner, E., and Gysel, M.: Black carbon physical properties and mixing state in the European megacity Paris, Atmospheric Chemistry and Physics, 13, 5831–5856, https://doi.org/10.5194/acp-13-5831-2013, 2013.

Liu, D., Allan, J., Whitehead, J., Young, D., Flynn, M., Coe, H., McFiggans, G., Fleming, Z. L., and Bandy, B.: Ambient black carbon particle hygroscopic properties controlled by mixing state and composition, Atmospheric Chemistry and Physics, 13, 2015–2029, https://doi.org/10.5194/acp-13-2015-2013, https://acp.copernicus.org/articles/13/2015/2013/, 2013.

Lund, M. T., Samset, B. H., Skeie, R. B., Watson-Parris, D., Katich, J. M., Schwarz, J. P., and Weinzierl, B.: Short Black Carbon lifetime inferred from a global set of aircraft observations, npj Climate and Atmospheric Science, 1, 1–8, https://doi.org/10.1038/s41612-018-0040-x, http://dx.doi.org/10.1038/s41612-018-0040-x, 2018.

Moffet, R. C. and Prather, K. A.: In-situ measurements of the mixing state and optical properties of soot with implications for radiative forcing estimates, Proceedings of the National Academy of Sciences of the United States of America, 106, 11 872–11 877, https://doi.org/10.1073/pnas.0900040106, 2009.

Moran-Zuloaga, D., Ditas, F., Walter, D., Saturno, J., Brito, J., Carbone, S., Chi, X., Hrabě de Angelis, I., Baars, H., Godoi, R. H. M., Heese, B., Holanda, B. A., Lavrič, J. V., Martin, S. T., Ming, J., Pöhlker, M., Ruckteschler, N., Su, H., Wang, Y., Wang, Q., Wang, Z., Weber, B., Wolff, S., Artaxo, P., Pöschl, U., Andreae, M. O., and Pöhlker, C.: Long-term study on coarse mode aerosols in the Amazon rain forest with the frequent intrusion of Saharan dust plumes, Atmospheric Chemistry and Physics Discussions, pp. 1–52, https://doi.org/10.5194/acp-2017-1043, https://www.atmos-chem-phys-discuss.net/acp-2017-1043/, 2017.

Pöhlker, M. L., Ditas, F., Saturno, J., Klimach, T., Hrabě De Angelis, I., Araùjo, A. C., Brito, J., Carbone, S., Cheng, Y., Chi, X., Ditz, R., Gunthe, S. S., Holanda, B. A., Kandler, K., Kesselmeier, J., Könemann, T., Krüger, O. O., Lavric, J. V., Martin, S. T., Mikhailov, E., Moran-Zuloaga, D., Rizzo, L. V., Rose, D., Su, H., Thalman, R., Walter, D., Wang, J., Wolff, S., Barbosa, H. M., Artaxo, P., Andreae, M. O., Pöschl, U., and Pöhlker, C.: Long-term observations of cloud condensation nuclei over the Amazon rain forest - Part 2: Variability and characteristics of biomass burning, long-range transport, and pristine rain forest aerosols, Atmospheric Chemistry and Physics, 18, 10 289–10 331, https://doi.org/10.5194/acp-18-10289-2018, 2018.

Pokhrel, R. P., Wagner, N. L., Langridge, J. M., Lack, D. A., Jayarathne, T., Stone, E. A., Stockwell, C. E., Yokelson, R. J., and Murphy, S. M.: Parameterization of single-scattering albedo (SSA) and absorption Ångström exponent (AAE) with EC/OC for aerosol emissions from biomass burning, Atmospheric Chemistry and Physics, 16, 9549–9561, https://doi.org/10.5194/acp-16-9549-2016, 2016.

Roberts, G. C. and Nenes, A.: A continuous-flow streamwise thermal-gradient CCN chamber for atmospheric measurements, Aerosol Science and Technology, 39, 206–221, https://doi.org/10.1080/027868290913988, 2005.

Rose, D., Gunthe, S. S., Mikhailov, E., Frank, G. P., Dusek, U., Andreae, M. O., and Pöschl, U.: Calibration and measurement uncertainties of a continuous-flow cloud condensation nuclei counter (DMT-CCNC): CCN activation of ammonium sulfate and sodium chloride aerosol particles in theory and experiment, Atmospheric Chemistry and Physics, 8, 1153–1179, https://doi.org/10.5194/acp-8-1153-2008, 2008.

Saturno, J., Ditas, F., De Vries, M. P., Holanda, B. A., Pöhlker, M. L., Carbone, S., Walter, D., Bobrowski, N., Brito, J., Chi, X., Gutmann, A., De Angelis, I. H., Machado, L. A., Moran-Zuloaga, D., Rüdiger, J., Schneider, J., Schulz, C., Wang, Q., Wendisch, M., Artaxo, P., Wagner, T., Pöschl, U., Andreae, M. O., and Pöhlker, C.: African volcanic emissions influencing atmospheric aerosols over the Amazon rain forest, Atmospheric Chemistry and Physics, 18, 10 391–10 405, https://doi.org/10.5194/acp-18-10391-2018, 2018a.

Saturno, J., Holanda, B. A., Pöhlker, C., Ditas, F., Wang, Q., Moran-Zuloaga, D., Brito, J., Carbone, S., Cheng, Y., Chi, X., Ditas, J., Hoffmann, T., Hrabe de Angelis, I., Könemann, T., Lavrič, J. V., Ma, N., Ming, J., Paulsen, H., Pöhlker, M. L., Rizzo, L. V., Schlag, P., Su, H., Walter, D., Wolff, S., Zhang, Y., Artaxo, P., Pöschl, U., and Andreae, M. O.: Black and brown carbon over central Amazonia: long-term aerosol measurements at the ATTO site, Atmospheric Chemistry and Physics, 18, 12 817–12 843, https://doi.org/10.5194/acp-18-12817-2018, https://www.atmos-chem-phys-discuss.net/acp-2017-1097/https://www.atmos-chem-phys.net/18/12817/2018/, 2018b.

Schneider, J., Weigel, R., Klimach, T., Dragoneas, A., Appel, O., Hünig, A., Molleker, S., Köllner, F., Clemen, H.-C., Eppers, O., Hoppe, P., Hoor, P., Mahnke, C., Krämer, M., Rolf, C., Grooß, J.-U., Zahn, A., Obersteiner, F., Ravegnani, F., Ulanovsky, A., Schlager, H., Scheibe, M., Diskin, G. S., DiGangi, J. P., Nowak, J. B., Zöger, M., and Borrmann, S.: Aircraft-based observation of meteoric material in lower-

stratospheric aerosol particles between 15 and 68° N, Atmospheric Chemistry and Physics, 21, 989–1013, https://doi.org/10.5194/acp-21-989-2021, https://acp.copernicus.org/articles/21/989/2021/, 2021.

Schwarz, J. P., Gao, R. S., Fahey, D. W., Thomson, D. S., Watts, L. A., Wilson, J. C., Reeves, J. M., Darbeheshti, M., Baumgardner, D. G., Kok, G. L., Chung, S. H., Schulz, M., Hendricks, J., Lauer, A., Kärcher, B., Slowik, J. G., Rosenlof, K. H., Thompson, T. L., Langford, A. O., Loewenstein, M., and Aikin, K. C.: Single-particle measurements of midlatitude black carbon and light-scattering aerosols from the boundary layer to the lower stratosphere, Journal of Geophysical Research Atmospheres, 111, 1–15, https://doi.org/10.1029/2006JD007076, 2006.

Shinozuka, Y., Saide, P. E., Ferrada, G. A., Burton, S. P., Ferrare, R., Doherty, S. J., Gordon, H., Longo, K., Mallet, M., Feng, Y., Wang, Q., Cheng, Y., Dobracki, A., Freitag, S., Howell, S. G., LeBlanc, S., Flynn, C., Segal-Rosenhaimer, M., Pistone, K., Podolske, J. R., Stith, E. J., Bennett, J. R., Carmichael, G. R., da Silva, A., Govindaraju, R., Leung, R., Zhang, Y., Pfister, L., Ryoo, J.-M., Redemann, J., Wood, R., and Zuidema, P.: Modeling the smoky troposphere of the southeast Atlantic: a comparison to ORACLES airborne observations from September of 2016, Atmospheric Chemistry and Physics, 20, 11 491–11 526, https://doi.org/10.5194/acp-20-11491-2020, https://acp.copernicus.org/articles/20/11491/2020/, 2020.

Stephens, M., Turner, N., and Sandberg, J.: Particle identification by laser-induced incandescence in a solid-state laser cavity., Applied optics, 42, 3726–36, https://doi.org/10.1364/AO.42.003726, http://www.ncbi.nlm.nih.gov/pubmed/12868806, 2003.

Stocker, T. F., Allen, S. K., Bex, V., and Midgley, P. M.: Climate Change 2013 The Physical Science Basis Working Group I Contribution to the Fifth Assessment Report of the Intergovernmental Panel on Climate Change Edited by, 2013.

Swap, R., Garstang, M., Greco, S., Talbot, R., and Kallberg, P.: Saharan dust in the Amazon Basin, Tellus B, 44, 133–149, https://doi.org/10.1034/j.1600-0889.1992.t01-1-00005.x, http://www.tellusb.net/index.php/tellusb/article/view/15434, 1992.

Tadic, I., Nussbaumer, C., Bohn, B., Harder, H., Marno, D., Martinez, M., Obersteiner, F., Parchatka, U., Pozzer, A., Rohloff, R., Zöger, M., Lelieveld, J., and Fischer, H.: Central role of nitric oxide in ozone production in the upper tropical troposphere over the Atlantic Ocean and West Africa, Atmospheric Chemistry and Physics Discussions, 2021, 1–24, https://doi.org/10.5194/acp-2021-52, https://acp.copernicus.org/preprints/acp-2021-52/, 2021.

Taylor, J. W., Wu, H., Szpek, K., Bower, K., Crawford, I., Flynn, M. J., Williams, P. I., Dorsey, J., Langridge, J. M., Cotterell, M. I., Fox, C., Davies, N. W., Haywood, J. M., and Coe, H.: Absorption closure in highly aged biomass burning smoke, Atmospheric Chemistry and Physics, 20, 11 201–11 221, https://doi.org/10.5194/acp-20-11201-2020, https://acp.copernicus.org/articles/20/11201/2020/, 2020.

Wendisch, M., Poschl, U., Andreae, M. O., MacHado, L. A., Albrecht, R., Schlager, H., Rosenfeld, D., Martin, S. T., Abdelmonem, A., Afchine, A., Araujo, A. C., Artaxo, P., Aufmhoff, H., Barbosa, H. M., Borrmann, S., Braga, R., Buchholz, B., Cecchini, M. A., Costa, A., Curtius, J., Dollner, M., Dorf, M., Dreiling, V., Ebert, V., Ehrlich, A., Ewald, F., Fisch, G., Fix, A., Frank, F., Futterer, D., Heckl, C., Heidelberg, F., Huneke, T., Jakel, E., Jarvinen, E., Jurkat, T., Kanter, S., Kastner, U., Kenntner, M., Kesselmeier, J., Klimach, T., Knecht, M., Kohl, R., Kolling, T., Kramer, M., Kruger, M., Krisna, T. C., Lavric, J. V., Longo, K., Mahnke, C., Manzi, A. O., Mayer, B., Mertes, S., Minikin, A., Molleker, S., Munch, S., Nillius, B., Pfeilsticker, K., Pohlker, C., Roiger, A., Rose, D., Rosenow, D., Sauer, D., Schnaiter, M., Schneider, J., Schulz, C., De Souza, R. A., Spanu, A., Stock, P., Vila, D., Voigt, C., Walser, A., Walter, D., Weigel, R., Weinzierl, B., Werner, F., Yamasoe, M. A., Ziereis, H., Zinner, T., and Zoger, M.: Acridicon-chuva campaign: Studying tropical deep convective clouds and precipitation over amazonia using the New German research aircraft HALO, Bulletin of the American Meteorological Society, 97, 1885–1908, https://doi.org/10.1175/BAMS-D-14-00255.1, 2016.

Wu, H., Taylor, J. W., Szpek, K., Langridge, J. M., Williams, P. I., Flynn, M., Allan, J. D., Abel, S. J., Pitt, J., Cotterell, M. I., Fox, C., Davies, N. W., Haywood, J., and Coe, H.: Vertical variability of the properties of highly aged biomass burning aerosol transported over

the southeast Atlantic during CLARIFY-2017, Atmospheric Chemistry and Physics, 20, 12 697–12 719, https://doi.org/10.5194/acp-20-12697-2020, https://acp.copernicus.org/articles/20/12697/2020/, 2020.

Wu, H., Taylor, J. W., Langridge, J. M., Yu, C., Allan, J. D., Szpek, K., Cotterell, M. I., Williams, P. I., Flynn, M., Barker, P., Fox, C., Allen, G., Lee, J., and Coe, H.: Rapid transformation of ambient absorbing aerosols from West African biomass burning, Atmospheric Chemistry and Physics, 21, 9417–9440, https://doi.org/10.5194/acp-21-9417-2021, https://acp.copernicus.org/articles/21/9417/2021/, 2021.

Zuidema, P., Sedlacek, A. J., Flynn, C., Springston, S., Delgadillo, R., Zhang, J., Aiken, A. C., Koontz, A., and Muradyan, P.: The Ascension Island Boundary Layer in the Remote Southeast Atlantic is Often Smoky, Geophysical Research Letters, 45, 4456–4465, https://doi.org/10.1002/2017GL076926, http://doi.wiley.com/10.1002/2017GL076926, 2018.

2.5 Co-variability of black carbon and cloud condensation nuclei in different polluted environments

This chapter contains a manuscript draft in early stage that will be submitted to a peer-reviewed journal.

This manuscript includes data sets from the following field experiments:
ATTO, ACRIDICON-CHUVA, EMERGE-Europe, EMERGE-Asia, CAFE-Africa and CAFE-Europe.

Contribution to this chapter by Bruna A. Holanda: This manuscript is currently in preparation and my personal contribution includes the processing, quality assurance and analysis of the SP2 and CCN data sets from the 5 flight campaigns with HALO. I actively participate in 4 of them, being responsible for operating the aerosol measurements during the scientific flights, performing frequent maintenance and calibrations. I wrote the scripts for a systematic processing of the SP2 data set presented in this study. Together with my coauthors, I initiated and designed the research, analyzed the results, prepared figures, and wrote the manuscript.

Co-variability of black carbon and cloud condensation nuclei in different polluted environments

Bruna A. Holanda[1], Ovid Krüger[1], Karine Chevalier[1,a], David Walter[1,2], Thomas Klimach[1], Meinrat O. Andreae[1,7], Ulrich Pöschl[1], Christopher Pöhlker[1], Mira L. Pöhlker[1,6,8], and potential further coauthors, especially from the ACRIDICON-CHUVA, EMeRGe, and CAFE teams, to be involved upon finalization of this manuscript draft

[1]Multiphase Chemistry Department, Max Planck Institute for Chemistry, 55128 Mainz, Germany
[2]Climate Geochemistry Department, Max Planck Institute for Chemistry, 55128 Mainz, Germany
[3]Atmospheric Chemistry Department, Max Planck Institute for Chemistry, 55128 Mainz, Germany
[4]Institute of Environmental Physics, University of Bremen, 28359 Bremen, Germany
[5]Institute of Physics, University of São Paulo, São Paulo 05508-900, Brazil
[6]Leipzig Institute for Meteorology, Leipzig University, Leipzig, Germany
[7]Scripps Institution of Oceanography, University of California San Diego, La Jolla, CA 92037, USA
[8]Experimental Aerosol and Cloud Microphysics Department, Leibniz Institute for Tropospheric Research, Leipzig, Germany
[a]now at TÜV SÜD Industrie Serivce GmbH, 68167 Mannheim, Germany

Correspondence: Bruna A. Holanda (b.holanda@mpic.de), Mira L. Pöhlker (m.pohlker@mpic.de)

Abstract. Linear relationships between black carbon (BC) and cloud condensation nuclei (CCN) concentrations at a supersaturation of $0.38\,\%$ were observed for different pollution sources in the course of five measurement campaigns with the high altitude and long range HALO aircraft. Characteristic CCN to BC regimes were obtained for lightly aged biomass burning (BB) smoke over the Amazon basin, highly aged BB smoke from Africa over the Atlantic Ocean, and urban pollution over Europe. The CCN to BC ratio for urban emissions in Europe was $\Delta\mathrm{CCN}/\Delta\mathrm{BC} \approx 20 \cdot 10^9$ $\mu\mathrm{g}^{-1}$ which is 20 times higher than for highly aged African BB smoke with $\Delta\mathrm{CCN}/\Delta\mathrm{BC} \approx 0.5 \cdot 10^9$ $\mu\mathrm{g}^{-1}$. Lightly aged Amazonian BB smoke with $\Delta\mathrm{CCN}/\Delta\mathrm{BC} \approx 2.7 \cdot 10^9$ $\mu\mathrm{g}^{-1}$ had a 5 times higher ratio than the African smoke. The CCN to BC relationships are remarkably consistent across different continents and measurement periods. The BC-CCN regimes defined here can potentially be used as tool for aerosol source apportionment of anthropogenic pollution, to update emissions inventories in atmospheric models, and supply a framework for the assumption of BC and CCN concentrations in regions with limited in-situ measurements.

+++ Early and preliminary manuscript draft +++

1 Introduction

Atmospheric pollution, comprising a complex mixture of several gaseous and aerosol species, is a major threat humanity is facing since begin of industrialization (e.g., Liu et al., 2020a; Schwartz, 1994). Most of human activities, such as domestic heating, traffic, or biomass burning (BB) include combustion processes that release significant amounts of aerosol particles to the atmosphere (Bond et al., 2013; Hoesly et al., 2018). Black carbon (BC) along with organic and inorganic particles are main constituents of combustion aerosols (Pöschl, 2005; Bond et al., 2013). The particle size distributions as well as optical and physicochemical properties are highly dependent on the burnt fuel, combustion temperature, oxygen supply as well as particle coagulation and removal processes in the fresh smoke (e.g., Bond et al., 2013; May et al., 2014). Biomass burning accounts for a major fraction of the combustion-related emissions globally (Andreae and Merlet, 2001; Andreae, 2019). The emitted particles can stay airborne for days or weeks and, thus, undergo transcontinental transport (e.g., Holanda et al., 2020, 2021). The atmospheric residence time can even span to months or years, if the smoke is injected into the lower stratosphere via strong convective updrafts over high intensity fires (e.g., Ditas et al., 2018; Ohneiser et al., 2020).

While being transported in the atmosphere, combustion aerosols can affect atmospheric circulation, the water cycle, and the climate system (e.g., Andreae and Rosenfeld, 2008; Rosenfeld et al., 2014, 2008; Bellouin et al., 2020; Naik et al., 2021 in press). They influence the radiative balance by absorbing and scattering solar radiation (Samset et al., 2013). They further alter or even inhibit cloud formation and development through a heating of the atmosphere in layers enriched with absorbing particles and a corresponding cooling of the surface (Koren et al., 2004; Liu et al., 2020b). Finally, aerosols from combustion processes act as cloud condensation nuclei (CCN) and influence cloud droplet number concentrations, cloud albedo and precipitation (Twomey, 1977; Ramanathan et al., 2001; Andreae, 2004; Spracklen et al., 2011; Pöhlker et al., 2021). The ability of aerosol particles to act as CCN is primarily determined by the water vapor supersaturation and particle size with variations in the particles' chemical compositions and corresponding hygroscopicity playing a secondary role (Dusek et al., 2006; Andreae and Rosenfeld, 2008). The number concentration of CCN, N_{CCN}, as a function of supersturation is an essential quantity in cloud microphysics (e.g., Twomey and Wojciechowski, 1969; Campos Braga et al., 2021a).

In ambient aerosol observations, it is typically challenging to distinguish between natural and anthropogenic BC or CCN populations, especially because atmospheric processing alters the physical and chemical appearance (e.g. size, morphology) of the particles profoundly. Further, under polluted atmospheric conditions, the influences from urban and biomass burning emissions are often mixed. Thus, it is difficult to relate the contribution of certain combustion sources to observed increases in BC and/or CCN concentrations. Nevertheless, quantitative knowledge on the emission and co-variability of BC and CCN – as aerosol classes of fundamental climate-relevance – in relation to specific source types would largely expand our knowledge on the human influence on the climate system (e.g., Chen et al., 2010; Bauer et al., 2010).

In this study, we pursued a comprehensive approach by merging BC and CCN data from five aircraft missions around the world (Fig. 1). The missions probed a wide variety of conditions with particular focus on megacity plumes and biomass burning emis-

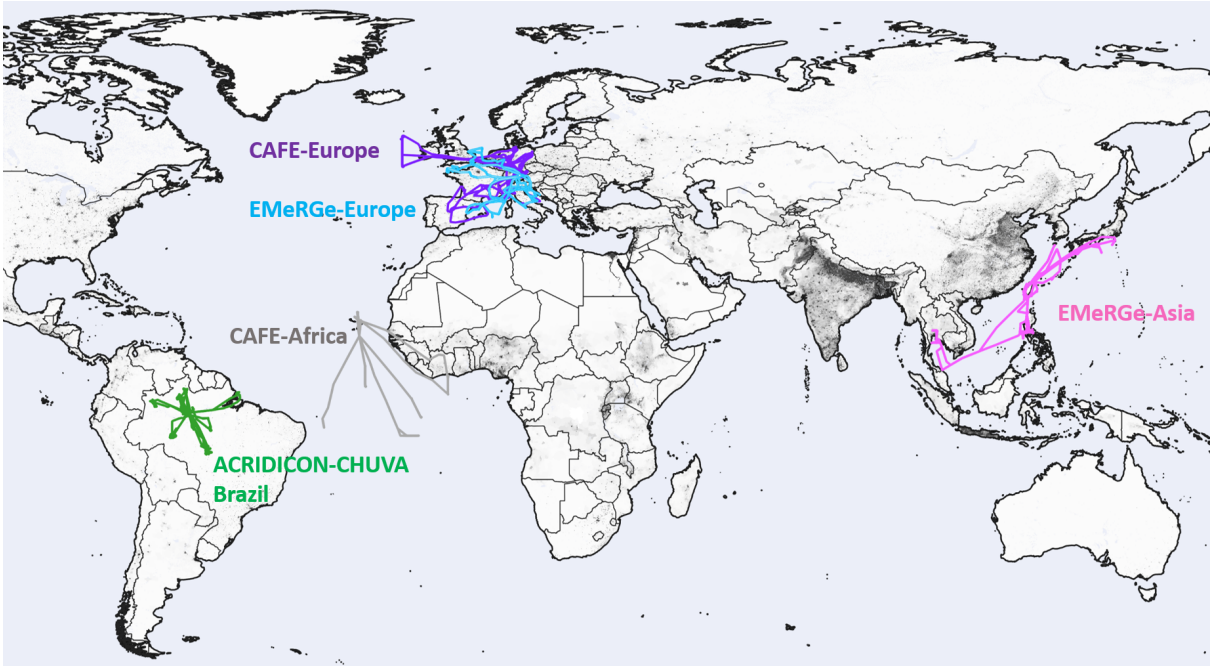

Figure 1. Flight tracks of all five HALO aircraft campaigns analyzed in this study (see Sect. 2.1). The missions probed atmospheric conditions in South America, Europe, East and Southeast Asia as well as over the Southern and Equatorial Atlantic Ocean. Gray shading represents the population density map from https://sedac.ciesin.columbia.edu/data/set/gpw-v4-population-density-rev11 (last access 06 Sep 2021).

sions. We found remarkably distinct and comparatively tight correlations between BC to CCN as a function of the dominant combustion aerosol sources. This study explores the properties of these regimes in the BC-CCN space and their potential as an aerosol classification approach in routine aerosol analyses. The regimes can be broadly categorized in highly aged BB smoke, lightly aged BB smoke, and urban pollution, yielding corresponding ratios of CCN relative to BC, $\Delta CCN/\Delta BC$, according to Andreae (2019). They have been defined based on flight episodes, during which the atmospheric pollution state was particularly defined by one predominant type or source. Subsequently, several case studies were analyzed to investigate mixed pollution conditions as well as the influence of atmospheric ageing. The BC-CCN regimes defined here could advance the observation and modelling of anthropogenic aerosol emissions (i) as an efficient tool for combustion aerosol sources assignment and plume tracking, (ii) to estimate BC or CCN concentrations in other measurements if only one of these parameters has been measured, and/or (iii) to simplify and improve emission inventories in atmospheric models through updated enhancement or emission ratios.

2 Methods

2.1 HALO aircraft measurement missions

Airborne measurements of BC and CCN number concentrations were performed under different atmospheric conditions and over contrasting environments worldwide. The measurements were conducted onboard the HALO (High Altitude and LOng Range) research aircraft (https://www.dlr.de/content/de/missionen/halo.html, last access 30 Aug 2021), operated by the German Aerospace Center (DLR). The data sets presented in this study were collected with the same instrumentation during five HALO campaigns, covering four continents, the Tropical Atlantic Ocean and the Western Pacific off the Asian continent (Fig. 1). The specific campaigns along with the scientific goals are outlined hereinafter:

- **ACRIDICON-CHUVA, 2014**: Aerosol, Cloud, Precipitation, and Radiation Interactions and Dynamics of Convective Cloud Systems–Cloud Processes of the Main Precipitation Systems in Brazil: A Contribution to Cloud Resolving Modeling and to the Global Precipitation Measurement. Measuring over the Amazon Basin were conducted during the dry season in September 2014. We measured Amazon background regions, oceanic aerosol, the arc of deforestation in the Amazon rain forest, and highly aged long-range transported (LRT) BB smoke from Africa (Andreae et al., 2018; Holanda et al., 2020; Cecchini et al., 2017; Campos Braga et al., 2021b; Wendisch et al., 2016). In this study we used all data measured in the arc of deforestation to probe lighlty aged Amazonian BB smoke. Also in the case study section, we used two measurement flights, showing the influx of highly aged African BB in the Amazon.

- **EMeRGe-EU, 2017**: Effect of Megacities on the Transport and Transformation of Pollutants on the Regional to Global Scales in Europe. Urban and BB emissions over Europe were measured in July 2017 (Andrés Hernández et al., 2021; Krüger et al., 2021). Selected measurements were analysed, in the case study section.

- **EMeRGe-Asia, 2018**: Effect of Megacities on the Transport and Transformation of Pollutants on the Regional to Global Scale in Asia. Urban and BB emissions over Asia were measured in March and April 2018. Selected measurements were analysed, in the case study section.

- **CAFE-Africa, 2018**: Chemistry of the Atmosphere: Field Experiment in Africa. Measuring mainly over the Atlantic Ocean with strong African BB influence in August 2018 (Schneider et al., 2021; Tadic et al., 2021). Flight segments with African BB aerosol in different aging states were used in this study. These data were used to derive a typical signature of highly aged BB from Africa.

- **CAFE-EU, 2020**: Chemistry of the Atmosphere: Field Experiment in Europe during COVID-19 confinements. Aim of this campaign was to observe urban emissions over Europe during the COVID-19 pandemic confinements in May and June 2020 (Voigt et al., 2021; Krüger et al., 2021). Krüger et al. (2021) revealed a reduction of 40 % for M_{rBC}. During the measurement period we did not encounter BB emissions from wildfires or domestic heating emissions from wood burning. Data from low approaches and selected urban plumes were used to derive the signature of unperturbed urban emissions.

General navigation and meteorological data were obtained at 1 Hz time resolution from the basic HALO measurement and sensor system (BAHAMAS). Near-isokinetic aerosol sampling was conducted using the HALO aerosol submicrometer inlet (HASI). Details on the general sampling setup can be found elsewhere (Andreae et al., 2018; Holanda et al., 2020; Schulz et al., 2018; Wendisch et al., 2016). All aerosol concentration data was normalized to standard temperature and pressure (STP, $T_0 = 273.15$ K and $p_0 = 1013.25$ hPa). The data were collected at 1 Hz time resolution and averaged to 1 minute time resolution for the analysis.

2.1.1 Black carbon measurements

The refractory black carbon (rBC) was measured with an eight-channel Single Particle Soot Photometer (SP2, Droplet Measurement Techniques, Longmont, USA). The SP2 quantifies rBC and non-absorbing particles using laser-induced incandescence and light scattering, respectively (Stephens et al., 2003; Schwarz et al., 2006). Particles with a rBC core absorb the laser light and evaporate. The emitted incandescence signal is linearly proportional to the mass of the rBC in single particles (Laborde et al., 2013). The count of the rBC signals equals N_{rBC}, while the mass retrieved with the incandescence signal is referred as M_{rBC}. The SP2 used for this study is sensitive to rBC cores in the size range between 80 to 500 nm, mass-equivalent diameter ($\mathrm{d_{MEV}}$), assuming a density of $1.8\,\mathrm{g\,cm^{-3}}$. Note that the lower instrumental cutoff falls above a substantial fraction of N_{rBC} in fresh urban emissions (Pileci et al., 2021; Schwarz et al., 2008; Reddington et al., 2013). The SP2 number-detection efficiency at sea level pressure is close to unity for d_{MEV} 90 nm (Schwarz et al., 2010). The uncertainty for SP2 measurements is 5 % for N_{rBC} and 10 % for M_{rBC} (Laborde et al., 2012). Details on the instrumental setup and calibration procedures can be found in Holanda et al. (2020) and Andreae et al. (2018).

The data was processed with the Paul-Scherrer Institute (PSI) SP2 toolkit (Gysel-Beer and Corbin, 2019). All data was averaged to 1-min time step and a monomodal fit was applied to the 1-min averaged rBC mass size distribution from which the geometric mean diameters (D_{rBC}) and the geometric standard deviation (σ_{rBC}) was obtained. Only rBC data with successful fit ($R^2 > 0.75$) or with $M_{\mathrm{rBC}} > 0.01\,\mu\mathrm{g\,m^{-3}}$ are included in the study.

2.1.2 Cloud condensation nuclei measurements

The CCN number concentration, N_{CCN}, was measured with a dual-column continuous-flow stream-wise thermal gradient CCN counter (CCNC-200, Droplet Measurement Techniques) (e.g., Roberts and Nenes, 2005; Rose et al., 2008). The CCNC-200 consists of two columns, in which particles with a critical supersaturation below the instrumental supersaturation (S) form water droplets. One of the two columns was operated at a constant S providing N_{CCN} in 1 Hz resolution ($S = 0.38\,\%$ for CAFE-EU, CAFE-Africa, EMeRGe-EU, EMeRGe-Asia and $S = 0.53\,\%$ for ACRIDICON-CHUVA). The different S does not strongly affect the N_{CCN} to N_{rBC} ratio, due to the non-exponential increase of N_{CCN} above $S \sim 0.35\,\%$ for Amazonian BB aerosols (Pöhlker et al., 2018; Andreae et al., 2018). While Pöhlker et al. (2018) show this generally for BB aerosol measured in the Amazon, Andreae et al. (2018) reveals the characteristic steep increase reaching its maximum activation at $S \sim 0.35\,\%$

with data from the same flights as used in this paper. A custom-made constant pressure inlet with little particle losses in the CCN relevant size ranges was used to maintain a constant pressure and, thus, S in the instrument (Molleker et al., 2020). The instrument was calibrated before and after the campaigns according to Rose et al. (2008). The error in S is estimated to be in the range of 10 % (Pöhlker et al., 2016) and in $N_{CCN} \sim 10\,\%$ (Krüger et al., 2014).

2.2 Backward trajectories and MODIS data products

The backward trajectories (BT) were calculated with the HYSPLIT package (version 4, Revision 664, October 2014) (Stein et al., 2015; Rolph et al., 2017). BTs were calculated every 1-min along the aircraft flight track (longitude, latitude, altitude). Only BTs below $10\,\mathrm{km}$ altitude were included. The rainfall is the precipitation along the BTs (compare Pöhlker et al., 2019). Information retrieved from the BT analysis are combined with the Moderate Resolution Imaging Spectroradiometer (MODIS) "Fires and Thermal Anomalies (Day and Night)" and "Corrected Reflectance (True Color)" product, downloaded at https://worldview.earthdata.nasa.gov/ (last access 06 Sep 2021).

2.3 Selection of characteristic atmospheric conditions

Plumes with a predominant contribution of specific combustion aerosol sources were identified as outlined below to defined distinct regimes of aerosol properties in the BC-CCN scatter plots. Here we first present the selected plumes where we encountered stable conditions of one single combustion aerosol source (3.1). Second we show the criteria for plume selection in more diverse atmospheric conditions, where we either had comparably few data points or a superposition of different pollution sources (3.2):

- **Urban pollution:** A focal point of the CAFE-EU aircraft campaign was the investigation of urban pollution at low altitudes over a variety of European cities. During the time the campaign took place, biomass emissions did not affect the flights to a significant extent, according to satellite-based fire maps and associate BTs. For our analysis we only included the city plumes with high CCN levels (i.e., $N_{\mathrm{CCN}} > 1000\,\mathrm{cm}^{-3}$). In total, 62 1-min averages fulfilled this criteria.

- **Lightly aged Amazonian BB:** The smoke from fires in the Amazon was investigated during ACRIDICON-CHUVA. We select the flights AC12 and AC13 (18 and 19 September 2014) over the deforestation area and selected the periods where the rBC geometric mean diameter is smaller than $195\,\mathrm{nm}$, which corresponds mostly to measurements below 2 km altitude. In total, 70 1-min averages fulfilled this criterion.

- **Highly aged African BB:** The westerly outflow of highly aged African BB smoke over the Atlantic Ocean – which also reaches the Amazon eventually – was probed during CAFE-Africa. Flight segments were selected according to the geographic area, restricted to the South Atlantic Ocean with latitude $< 9.5\,^{\circ}$ and longitude $< 0\,^{\circ}$. This area was chosen

in order to avoid influences of urban pollution from Western Africa or mineral dust in higher latitudes (Holanda et al., 2021). In total, 305 1-min averages fulfilled these criteria.

Plumes with more diverse atmospheric conditions, where we either had comparably few data points or a superposition of different pollution sources. These plumes are shown in the case study section (3.2) and classified based on the three predefined regimes. The selection criteria is given in Table 1 and the criteria listed below:

- **Case studies on lightly aged BB smoke over Europe and Asia:** We defined BB plumes based on the strongly increased M_{rBC} and N_{rBC} within our measurements and on information from the corresponding flight reports. The specific data selection criteria can be found in Table 1.
- **Case study on highly aged African BB smoke over the Amazon:** For African BB emissions transported into the Amazon basin, the deconvolution method presented in Holanda et al. (2021) (with the same parameters and constraints) was applied to discriminate African vs South American smoke. Therefore, a bimodal fit was applied to every rBC mass size distribution. Two distinctive flight segments of the ACRIDICON-CHUVA flight AC07 (06 September 2014) agreed with the size distribution of African smoke. In total, 21 1-min averages fulfilled these criteria.
- **Case study on highly aged African BB over the Brazilian shore:** For the LRT African BB smoke encountered over the Brazilian shore we used the plumes identified in Holanda et al. (2020). The event day of particular relevance was 30 September 2014, during ACRIDICON-CHUVA flight AC19. In total, 87 1-minute averages fulfilled these criteria.
- **Case studies on urban pollution over Europe and Asia:** The outflow of mega populated centers were selected according to following criteria (i) specific measurement flights, (ii) geographical coordinates, (iii) elevated M_{rBC} and (iv) analysis of backward trajectories. The parameters for the specific case studies are summarized in Table 1.

Table 1. Selected BB and urban plumes during aircraft mission in Europe and Asia with relevant parameters. Number of observations is the total count of 1-minute averages shown in the respective BC-CCN scatter plot.

Case study denomination	Figure	Flight date	Flight	M_{rBC} [$\mu g\,m^{-3}$]	Latitude [°]	Longitude [°]	Altitude [m]	Observations number
BB dominated plumes								
Thailand	4	12 March 2018	E-A-03			< 104.0		170
Thailand	4	07 April 2018	E-A-14			< 104.0		
Marseille pure BB	5A	24 July 2017	E-EU-07	> 0.23	< 43.2			13
Marseille BB and urban	5A	24 July 2017	E-EU-07	> 0.23	> 43.2			7
Portugal BB	6	28 July 2017	E-EU-09		< 44.0	< 10.0	> 2200	103
Italian and Croatian aged BB	7	20 July 2017	E-EU-06		< 42.0	< 12.6	> 1000	14
Urban dominated plumes								
Barcelona urban	10	20 July 2017	E-EU-09		< 44.0	< 10.0	< 2200	74
Nagoya urban	11	30 March 2018	E-A-13		> 137.0			66
Rome urban mixed 1	12	11 July 2017	E-EU-03		$42.0 < \mathrm{Lat} < 44.5$	$13.0 < \mathrm{Lon} < 16.0$		105
Rome urban mixed 2	12	20 July 2017	E-EU-06		$42.0 < \mathrm{Lat} < 44.5$	$13.0 < \mathrm{Lon} < 16.0$		
London urban 1	13A	17 July 2017	E-EU-05			< 0		135
London urban 2	13A	26 July 2017	E-EU-08		> 52.0			
Po Valley urban mix 1	13B	11 July 2017	E-EU-03		$44.6 < \mathrm{Lat} < 46.0$	> 9.0		134
Po Valley urban mix 2	13B	20 July 2017	E-EU-06		$44.6 < \mathrm{Lat} < 46.0$	> 9.0		
China urban 1	14	22 March 2018	E-A-07		$25.0 < \mathrm{Lat} < 33.0$			513
China urban 2	14	24 March 2018	E-A-08		$25.0 < \mathrm{Lat} < 33.0$			
China urban 3	14	26 March 2018	E-A-09		$25.0 < \mathrm{Lat} < 33.0$			

3 Results and discussion

3.1 Definition of BC to CCN regimes

The relationship of N_{CCN} to both, M_{rBC} and N_{rBC}, for particularly defined pollution conditions is addressed here. We used measurement data focusing on defined combustion sources to obtain distinctive BC to CCN regimes as reference for the further analysis (see Sect.2.3). For the three characteristic cases shown in Fig. 2, the BC and CCN concentrations are linearly and well correlated ($R^2 > 0.8$), emphasizing that combustion processes are responsible for the observed CCN increases. Furthermore, the linear relationship between BC and CCN is consistent across several measurement flights, i.e. for independent plume intercepts originating from the same combustion source. This indicates a source-specific relationship without a pronounced influence of aerosol aging.

We found the highest N_{CCN} produced per N_{rBC} and M_{rBC} for urban pollution plumes over several European cities. The measurement period ranged from May to June 2020, without significant BB activities in Europe. Therefore, the N_{CCN} to M_{rBC} and

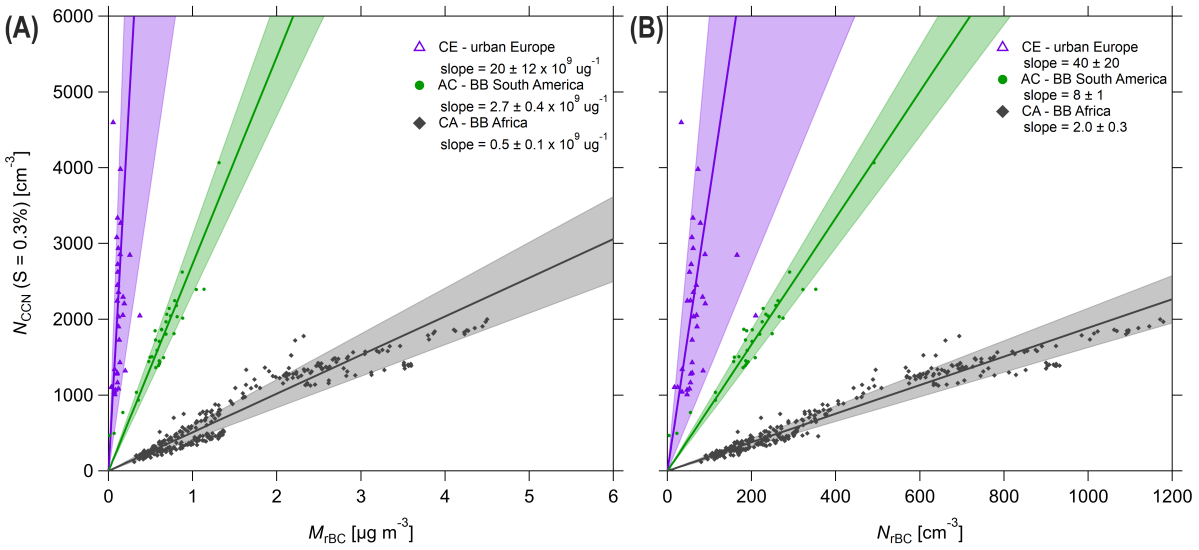

Figure 2. Relationships between **(A)** N_{CCN} and M_{rBC}; and **(B)** N_{CCN} and N_{rBC} for the selected pollution conditions: urban pollution (violet), lightly aged Amazonian BB (green) and highly aged African BB (grey). The solid lines represent linear orthogonal distance regression (ODR) applied to the 1-min averaged data (as markers) with shadings representing $\pm$ one standard deviation. The fit parameters of the regressions are shown in Table 2.

Table 2. The fit parameters of the ODR fits presented in Fig. 2: slope $\pm$ standard deviation (SD), R^2 and the number of observations (N) shown in the respective BC-CCN scatter plot.

	Urban	Lightly aged BB	Highly aged BB
ΔCCN/ΔBC $\pm$ SD [$\cdot 10^9$ µg^{-1}]	20 ± 12	2.7 ± 0.4	0.5 ± 0.1
R^2	0.90	0.99	0.97
N	62	70	305

N_{rBC} regime presented here is representative of pure anthropogenic emissions, which includes to a significant degree emissions from traffic and energy production (Krüger et al., 2021).

For urban pollution, N_{CCN} is the highest from all observations presented in this study, reaching up to $\sim 4600\,\mathrm{cm}^{-3}$, while M_{rBC} does not exceed $\sim 0.2\,\mu\mathrm{g\,cm}^{-3}$, and N_{rBC} $\sim 160\,\mathrm{cm}^{-3}$. Resulting in a $\Delta\mathrm{CCN}/\Delta\mathrm{BC} \approx 20 \pm 12 \cdot 10^9\ \mu\mathrm{g}^{-1}$. The relatively low BC values partly result from the comparably small size of rBC particles in urban pollution (Schwarz et al., 2006, 2008; Reddington et al., 2013; Liu et al., 2014), which entail that a large fraction of N_{rBC} is below the lower SP2 detection limit and, thus, remains undetected here. As shown in Fig. 3, fresh urban emissions are characterized by a broad size distribution with small rBC cores (median $D_{\mathrm{rBC}} = 137\,\mathrm{nm}$ and median $\sigma_{\mathrm{rBC}} = 2.0$).

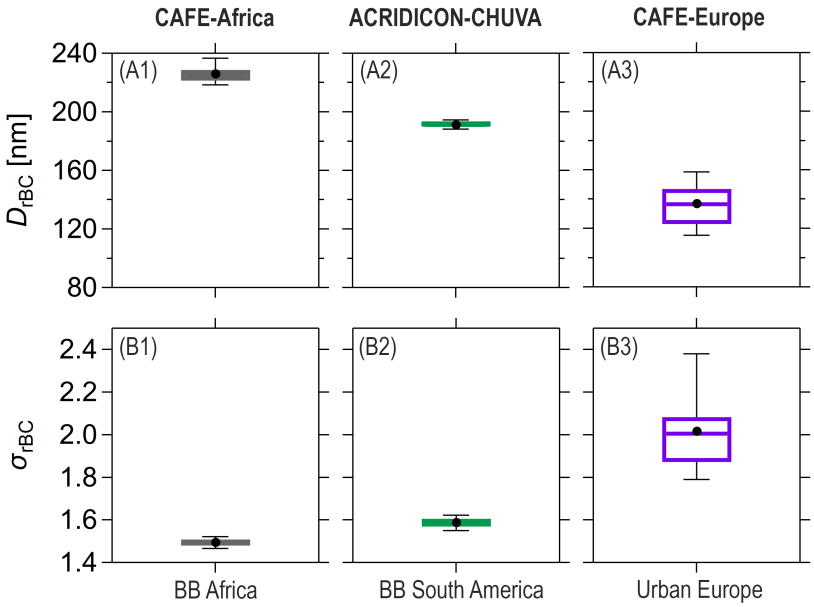

Figure 3. Properties of rBC cores during pollution conditions shown in Fig. 2, showing significant differences in agreement with Holanda et al. (2021). Specifically, geometric mean diameters, D_{rBC}, in **(A)** and (B) the geometric standard deviation, σ_{rBC}, in **(A)** are shown, both retrieved from lognormal fits of 1 minute averaged rBC mass size distributions for the different pollution conditions presented in Fig. 2. In the box-whisker plots, the horizontal bars represent the median, circles the mean, boxes the 25$^{\mathrm{th}}$ and 75$^{\mathrm{th}}$ percentiles, and whiskers the 9$^{\mathrm{th}}$ and 91$^{\mathrm{th}}$ percentiles.

Lightly aged BB smoke over the Amazon rain forest was intensively probed during the ACRIDICON-CHUVA campaign. In the measurement period (September 2014), African long-range transported BB smoke comprises a large fraction of the Amazon's aerosol burden (Saturno et al., 2018; Holanda et al., 2020, 2021). Therefore, we only selected periods when emissions from regional fires in the Amazonian were dominant. Most of the selected data set was collected within the PBL and over the southern region known as 'Arc of Deforestation'. These measurements fall within a defined region showing a lower slope than urban emissions of $\Delta\mathrm{CCN}/\Delta\mathrm{BC} \approx 2.7 \pm 0.4 \cdot 10^9$ µg^{-1} (Fig. 2A and B). Figure 3B shows the characteristic fit parameters of the M_{rBC} size distribution obtained for the lightly aged Amazonian BB plumes, with $D_{\mathrm{rBC}} = 195\,\mathrm{nm}$ and narrow $\sigma_{\mathrm{rBC}} = 1.6$. These observations are consistent with previous studies (Holanda et al., 2020, 2021).

Smoke layers of African BB at different aging states were encountered across vast geographical locations over the tropical South Atlantic during the CAFE-Africa campaign. The highly aged BB aerosol undergoing transatlantic transport represents the lower end of the N_{CCN} to M_{rBC} regimes ($\Delta\mathrm{CCN}/\Delta\mathrm{BC} \approx 0.5 \pm 0.1 \cdot 10^9$ µg^{-1}). An enhanced M_{rBC} and N_{rBC} to total aerosol based on aircraft measurements have been previously reported (Wu et al., 2020, 2021). The longer is the traveling time

over the Atlantic Ocean, the more is the dilution with relatively cleaner air masses in the free troposphere, causing a decrease in absolute aerosol concentrations towards South America. Nevertheless, the ratio of N_{CCN} to M_{rBC} and N_{rBC} remained almost unaffected. Beside its larger fraction of absorbing particles, highly aged African smoke also has large rBC core diameters ($D_{rBC} = 225\,nm$) and narrow distribution ($\sigma_{rBC} = 1.5$), as shown in Fig. 3. These sizes observed for aircraft data are in good agreement with ground based measurements in the central Amazon, as discussed in Holanda et al. (2021).

3.2 Case studies

The BC to CCN regimes defined in Sect. 3.1 were compared to a variety of case studies, covering a broad range of additional conditions. For example, the EMeRGe-Europe and EMeRGe-Asia campaigns were broadly characterized by mixtures of urban pollution and BB smoke. These conditions and further case studies are presented and the characteristic regimes from Fig. 2 are shown as reference lines in all corresponding plots. Despite the large variety of aerosol sources and atmospheric conditions probed, including the influence of particle aging, all case studies agree remarkably well with the BC-CCN regimes.

Beside the fresh BB smoke probed in Brazil during ACRIDICON-CHUVA, we also measured lightly aged smoke plumes in the lower troposphere over Europe and Asia. The plumes presented in the following are (i) lightly aged BB in the Golf of Thailand originated from forest fires in Cambodia and Vietnam (Fig. 4), (ii) lightly aged BB smoke near Marseille (Fig. 5), (iii) lightly aged BB from Portugal, measured over Spain (Fig. 6), and (iv) lightly aged BB smoke measured over the Tyrrhenian Sea (Fig. 7). Beside the lightly aged BB we also show data for highly aged African BB measured over the Amazon and the coast of Brazil (Fig. 8).

Two BB plumes were probed over the Gulf of Thailand during the ferry flights on 12 March and 07 April 2018 of the EMeRGe-Asia campaign. Both plumes match the lower end of the N_{CCN} to M_{rBC} regime found for the Amazonian BB (Fig. 4A). Like in Brazil, fire is a frequently used tool for land clearing in the highlands of Vietnam and Cambodia. The MODIS fire maps in Fig. 4B reveal some fire clusters in the transition area of agricultural used terrains and the native rain forest (Fig. 4B, A2A). Thus, the BB plumes we measured over the Gulf of Thailand likely originated from deforestation and agricultural fires. The plumes were intercepted between 1500 and 2000 m altitude and some hundreds of kilometers far from the emissions sources, and thus, have aged for one and two days in the atmosphere prior to the measurements (Fig. 4C, A2B). Remarkable is the good agreement between the two measurements even though for the second flight encountered cloudy conditions and precipitation (Fig. A2B).

A BB smoke plume was encountered two times (once over the continent and once over the Mediterranean) during the flight 7 of the EMeRGe-Europe campaign on 24 July 2017. Figure 5B shows fire spots close to Marseille, France that likely originated from the burn of subtropical forests. We measured the smoke plume nearby their emission source, thus we probed relatively fresh smoke conditions. Figure 5A reveals an excellent agreement between the BB smoke over the Mediterranean and the

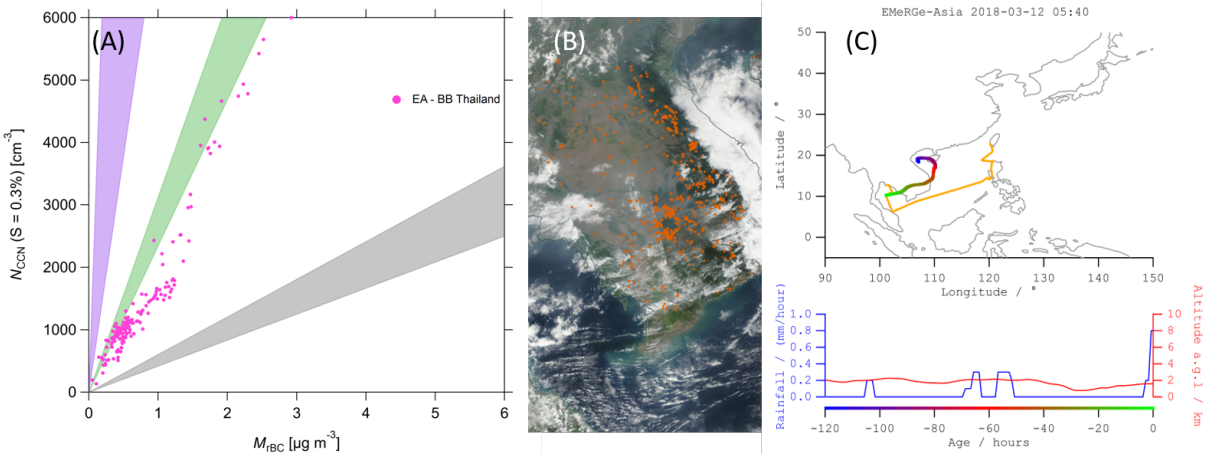

Figure 4. **(A)** Relationship between N_{CCN} and M_{rBC} for BB emissions in Southeast Asia, measured over the Gulf of Thailand during two measurement flights (12 March and 07 April 2018). The plumes are emitted from BB fires in Vietnam and Cambodia with evergreen broad leaf forest vegetation, savannas as dominant combustion fuels. **(B)** MODIS "Corrected Reflectance (True Color)" image for 10 March 2018, two days prior to measurement flight. Red dots indicate "Fires and Thermal Anomalies (Day and Night)". **(C)** HYSPLIT BT for measurements of BB plume. The color-code indicates time passed prior to measurement, suggesting a plume age of one to two days. Note, BT and MODIS image for the flight on 07 April 2018 can be found in appendix (Fig. A2).

lightly aged BB over the Amazon (green shading). For the BB smoke measured over land, however, a higher CCN-BC ratio is observed, falling in between the lightly aged BB smoke (green) and the urban pollution (violet) fields in the BC-CCN space. This may result from intrusions of urban pollution from nearby metropolitan area of Marseille with a population above 3 million and France's largest cargo harbor (https://www.marseille-port.fr/en). These observations highlight the sensitivity of the N_{CCN} to M_{rBC} ratio to addition of pollution from other strong aerosol sources.

Similarly, a higher N_{CCN} to M_{rBC} ratio is observed for BB smoke originated in Portugal (Fig. 6A), especially for relatively low concentrations. For the higher end of M_{rBC}, the ratio agrees well with lightly aged amazonian BB. The main combustion fuels of the Portuguese fires were savanna, grassland and evergreen needle-forest. The fires inflamed five days prior to our measurement flight. The higher N_{CCN} observed in this roughly one day aged plume (Fig. 6C) may result from mixing of the BB emissions with urban pollution from predominantly Madrid. Nevertheless, we find a clear difference to the N_{CCN} to M_{rBC} ratio between this plume, containing predominately BB smoke and the outflow of Barcelona (Fig. 10).

Over the Tyrrhenian Sea we measured roughly two days aged BB smoke from fires in Southern Italy and Croatia during EMeRGe-Europe (Fig. 7). The N_{CCN} to M_{rBC} ratio for this lightly aged BB emissions falls below the ratio found for the BB smoke close to Marseille (Fig. 5) and the range found for lightly aged Amazonian BB smoke (Fig. 2). The main combustion fuels of the BB fires are savannas in Italy and grasslands in Croatia. Thus a drift towards a lower CCN fraction is in good

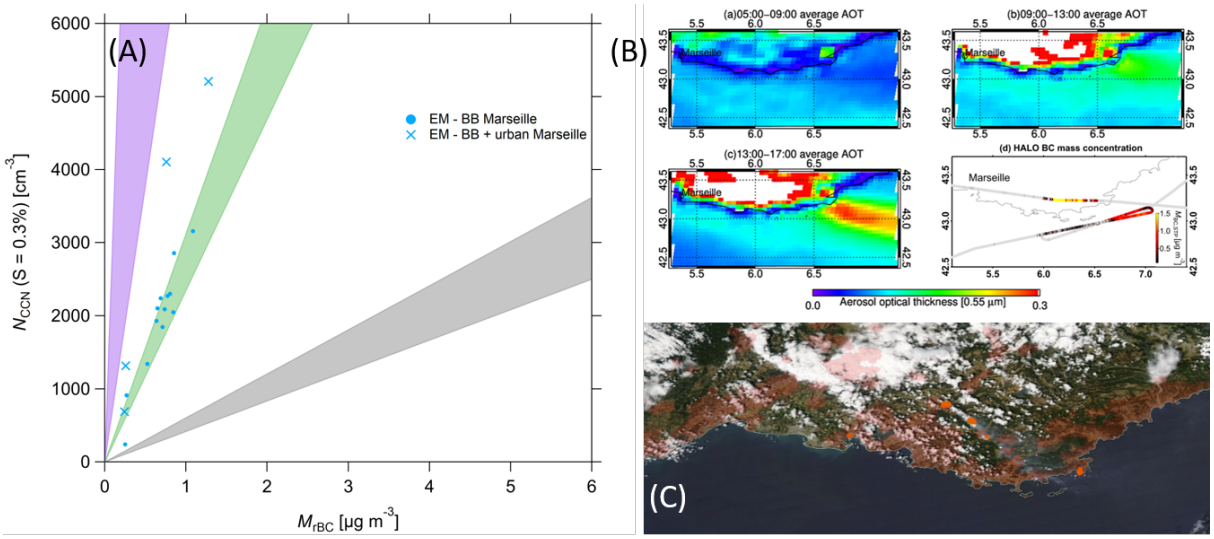

Figure 5. (A) Relationship between N_{CCN} and M_{rBC} for BB emissions in Southern Europe, measured over France and the Mediterranean close to Marseille (24 July 2017). (B)(a - c) Aerosol optical thickness at $0.55\,\mu m$ as retrieved from SEVIRI from 05:00 to 17:00 UTC on 24 July 2017. **(B)**(d) E-EU-07 flight track, color-coded with M_{rBC}. For better contrast, the scale for M_{rBC} ranges from 0.1 to $1.5\,\mu g\,m^{-3}$. Grey color on flight track indicates values below $0.1\,\mu g\,m^{-3}$. M_{rBC} reached values up to $7\,\mu g\,m^{-3}$ at the French coast. Figure adapted from Andrés Hernández et al. (2021). **(C)** MODIS "Corrected Reflectance (True Color)" image for 24 July 2017, the day of measurement flight. Red dots indicate "Fires and Thermal Anomalies (Day and Night)". The grey shading emerging from fire dots is the image of smoke plumes. The red shading gives "Human Built-up And Settlement Extent" showing the high density of urban settlements at BB origin.

agreement with the African BB. These fires show nicely the importance of the combustion fuel on the composition of the plumes.

Highly aged African BB smoke was probed in the northern Amazon Basin during flight AC07 (06 September 2014) and near the Brazilian coast during flight AC19 (30 September 2014) of the ACRIDICON-CHUVA campaign. The African smoke over South America was encountered mainly in defined and stable atmospheric layers with high aerosol concentrations (see Holanda et al. (2020)) as well as after downward mixing into the marine and continental boundary layer. As shown in Fig. 8, many of the data points fall within the region defined as highly aged BB (grey shading). These plumes, even though lower in overall concentration, agree remarkably well with the CAFE-Africa measurements. The points that fall above the grey field correspond to measurements in the marine or Amazonian boundary layers, where the sea salt and biogenic emissions from the Amazon rain forest contribute to the overall CCN burden. Nevertheless, consistent N_{CCN} to M_{rBC} ratios were obtained between independent measurement regions and different campaigns taken 4 years apart from each other. This result indicate that most of the processing in African BB plumes happens during the transport from the sources to the sampling regions over the Atlantic

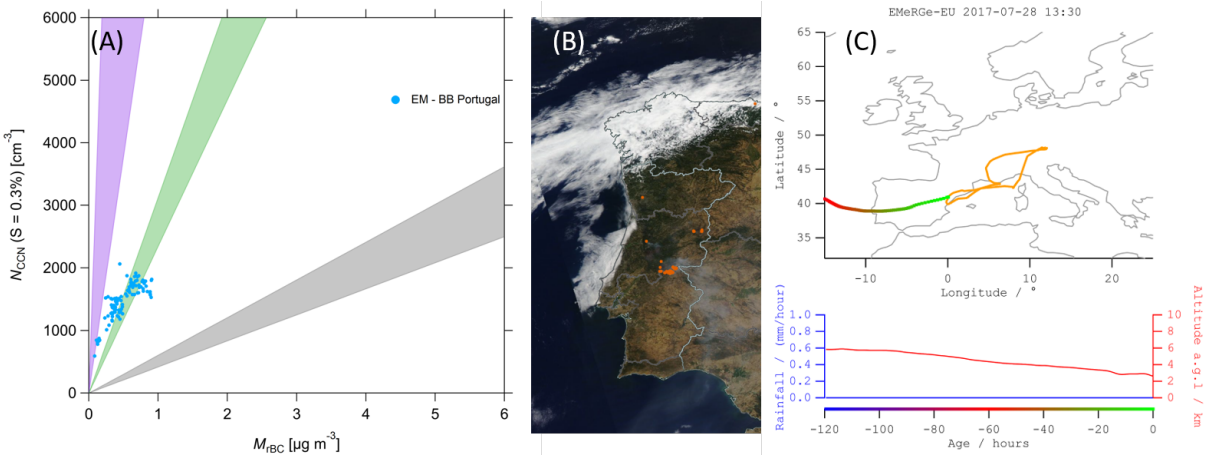

Figure 6. (A) Relationship between N_{CCN} and M_{rBC} for BB emissions in Southern Europe, measured over Spain. The plumes are emitted from BB fires in Portugal, where savannas, grassland and evergreen needle-forests are the dominant combustion fuels. The day of measurement was 28 July 2017. **(B)** MODIS "Corrected Reflectance (True Color)" image for 27 July 2017, one day prior to measurement flight. Red dots indicate "Fires and Thermal Anomalies (Day and Night)". The grey shading emerging from fire dots is the image of smoke plumes. **(C)** HYSPLIT BT for measurements of BB plume. The color-code indicates time passed prior to measurement, suggesting a plume age of about one day.

(within the first minutes after emission and during plume lifting to high altitudes) and there is no detectable further processing between the CAFE-Africa region and Brazil. The lower concentrations with larger distance to emission source are likely due to dilution of the smoke layers. Other processes than that (e.g. cloud processing and wet and dry scavenging), would likely change the ratio between N_{CCN} and M_{rBC}.

No significant processing of African BB is observed even after the plume is mixed down into the boundary layer in central Amazon. Figure 9 shows N_{CCN} to M_{rBC} rations for the lightly aged regional and highly aged African BB influences measured at the ATTO site (Holanda et al. (2021)). Also the ground-based measurements agree well with the regimes identified with the aircraft data. For the separation of the ATTO data the deconvolution method presented in Holanda et al. (2021) was applied. The N_{CCN} is retrieved from the aerosol size distribution (Pöhlker et al., 2018) while M_{rBC} is measured with an different SP2. The good agreement between the HALO aircraft data, with a good spatial resolution and the ground based measurements, with good temporal resolution across different seasons, reveals the robustness of the typical N_{CCN} to M_{rBC} regimes introduced in this study.

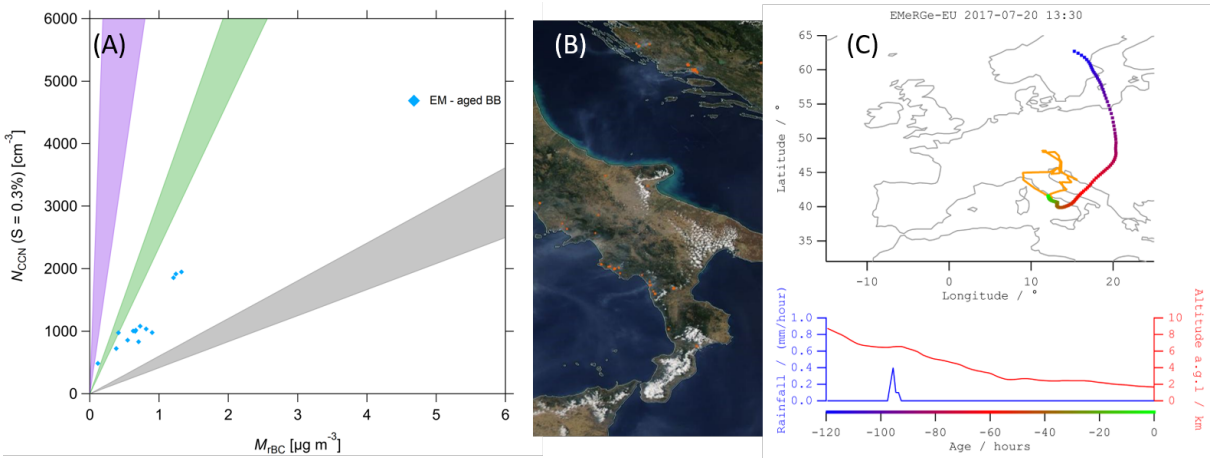

Figure 7. (A) Relationship between N_{CCN} and M_{rBC} for BB emissions in Southern Europe, measured over the Tyrrhenian Sea close to Rome. The plumes are emitted from BB fires in Italy and Croatia, where savannas and grassland are the dominant combustion fuels. The day of measurement was 20 July 2017. **(B)** MODIS "Corrected Reflectance (True Color)" image for 18 July 2017, two days prior to measurement flight. Red dots indicate "Fires and Thermal Anomalies (Day and Night)". The grey shading emerging from fire dots is the image of smoke plumes. **(C)** HYSPLIT BT for measurements of BB plume. The color-code indicates time passed prior to measurement, suggesting a plume age between two and three days.

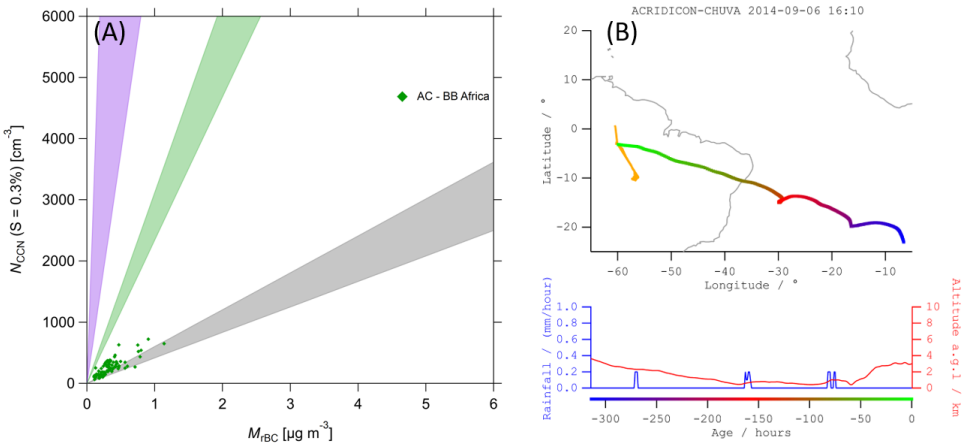

Figure 8. (A) Relationship between N_{CCN} and M_{rBC} for BB emissions from African fires, measured over the Amazon rain forest on 06 September 2014 and the Brazilian coast on 30 September 2014. **(B)** HYSPLIT BT calculated 315 hours backward. The color-code indicates time passed prior to measurement, showing that the plume roughly travelled four days over Brazil prior to measurement. Note, the BT for the second plume can be found in the appendix A4

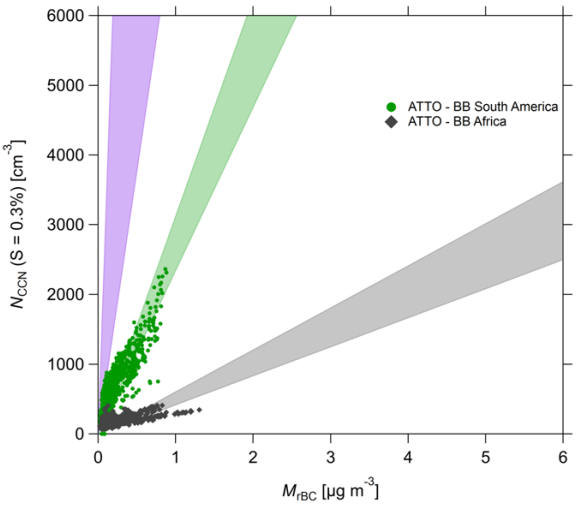

Figure 9. Relationship between N_{CCN} and M_{rBC} for South American BB emissions (green dots) and African BB smoke (black squares) at the ATTO site. Figure adapted from Holanda et al. (2021), further details and methods can be found therein.

In the following we show some urban plumes measured during EMeRGe-Europe and EMeRGe-Asia. (i) urban emissions from Barcelona (Fig. 10), (ii) urban emissions from Nagoya, Japan (Fig. 11), (iii) mixed urban and lightly aged BB emissions from Rome and the Po Valley (Fig. 12, 13B), (iv) the London outflow (Fig. 13A), and (v) urban pollution emitted from Shanghai and Beijing with potential BB influence (Fig. 14).

The city plume of Barcelona measured in 2017 during EMeRGe-Europe (Fig. 10A) shows a comparable N_{CCN} to M_{rBC} ratio to the reference regime for urban pollution (violet shading). During the measurement period, there were BB emissions in Portugal affecting the lower troposphere of the Iberian peninsula (Fig. 6). These BB emissions may also have affected our observations slightly. The good agreement between the measurements from 2017 and 2020, however, suggests urban pollution as dominating source. Also the air mass probed is likely not directly affected by the BB fires in Portugal (Fig. 10B).

The urban pollution measured in the outflow of Ise Bay, downwind of the metropolitan area of Nagoya shows comparable N_{CCN} and M_{rBC} properties as we encountered in fresh European pollution during CAFE-EU (Fig. 11). The metropolitan area of Nagoya is one of Japans major industrial centres and has more than 9 million inhabitants with one of Japan's highest population densities. As for the observations of BB influenced urban pollution in Europe (Fig. 12, 13B), there might be some impact of LRT BB from cropland fires in China. The satellite image reveals a smoke layer on the measurement day in proximity to the measurements (Fig. 11B, C). Nevertheless, a large fraction of the observed CCN is expected to originate from urban emissions in Nagoya metropolitan area. Also the shorter distance to the source region may explain the high CCN concentration within

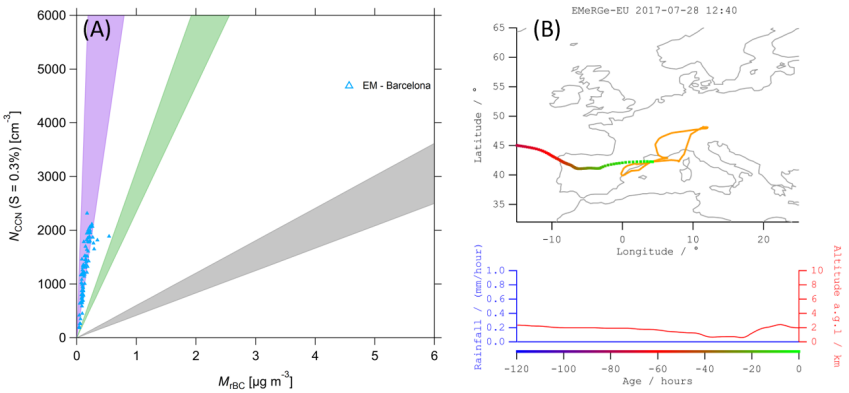

Figure 10. **(A)** Relationship between N_{CCN} and M_{rBC} for urban emissions from Barcelona. The plume was measured over the Mediterranean close to Barcelona (20 July 2017). **(B)** HYSPLIT BT for measurements of the Barcelona plume. The color-code indicates time passed prior to measurement, suggesting a plume age of only few hours.

the Japanese plume. Beside that, the Ise Bay plume was measured within the PBL, while LRT of BB smoke occurs at higher altitudes above the PBL (Holanda et al., 2020, 2021).

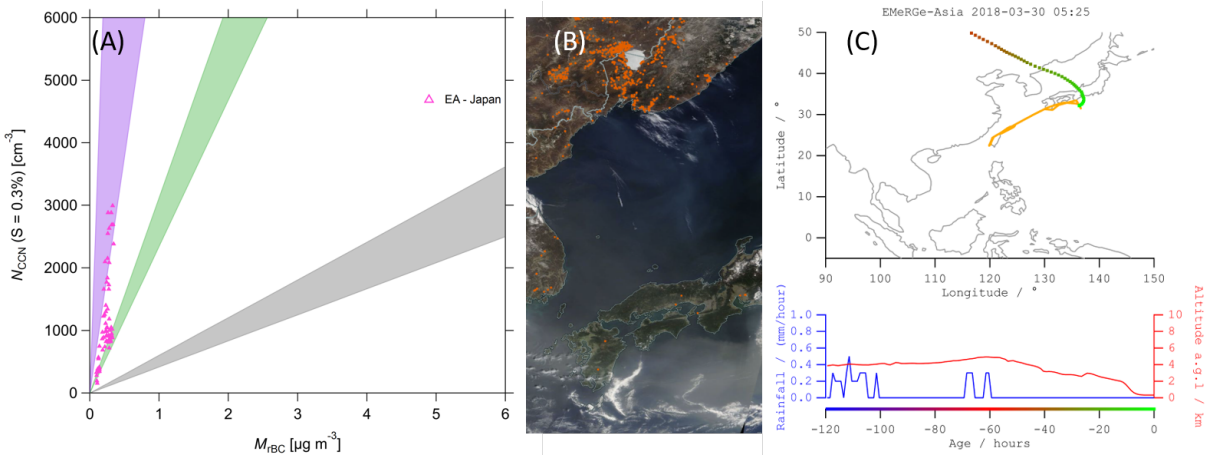

Figure 11. **(A)** Relationship between N_{CCN} and M_{rBC} for urban emissions from metropolitan area of Nagoya (30 March 2018). **(B)** MODIS "Corrected Reflectance (True Color)" image for the day of measurement. Red dots indicate "Fires and Thermal Anomalies (Day and Night)". The grey shading over the ocean is possibly BB and urban smoke from China. **(C)** HYSPLIT BT for measurements of plume. The color-code indicates time passed prior to measurement, suggesting a fresh emissions with few hours residence time.

The observed N_{CCN} to M_{rBC} ratio for the urban plumes of Rome and the Po Valley probed in 2017 during EMeRGe-Europe, diverges strongly from the observations in 2020 (Fig. 12A, 13B). This might relate to the low influence of BB aerosols during the 2020 measurements, while BB emissions were widespread in European in the summer of 2017. These BB emissions contribute to a background of regional haze in the lower troposphere, which is likely responsible for the lower N_{CCN} to M_{rBC} ratio for the measurements taken in 2017. Nevertheless, there is a good agreement between the results for Rome and the Po Valley with the observations of very relatively fresh BB emissions mixed with urban emissions from the Marseille metropolitan area (Fig. 5A). These results illustrate the relevance that BB emissions have on the atmospheric BC burden, strongly influencing the hygroscopic and radiative properties of pollution plumes from some of Europe's largest metropolitan areas.

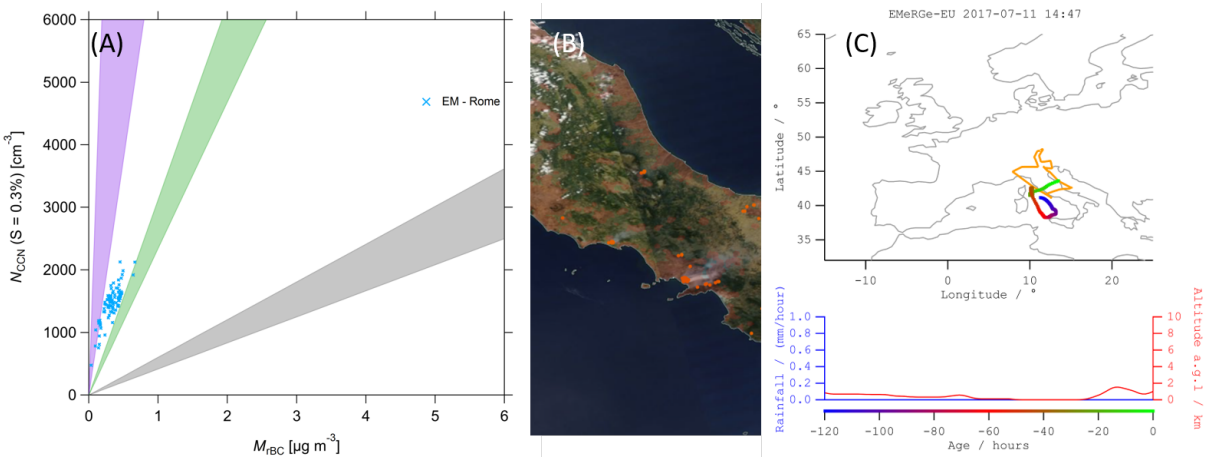

Figure 12. (A) Relationship between N_{CCN} and M_{rBC} for mixed urban and BB emissions in Southern Europe, measured over the Adriatic Sea downwind of Rome. The data is from two measurement flights (11 and 20 July 2017). The BB plumes are emitted from fires in Italy, where savannas and mixed forests are the dominant combustion fuels. **(B)** MODIS "Corrected Reflectance (True Color)" image for 11.07.2017, the day of measurement flight. Red dots indicate "Fires and Thermal Anomalies (Day and Night)". The grey shading emerging from fire dots is the image of smoke plumes. The red shading gives "Human Built-up And Settlement Extent" showing the high density of urban settlements at BB origin. **(C)** HYSPLIT BT for measurements mixed plume. The color-code indicates time passed prior to measurement, suggesting a plume age around one day.

The observed N_{CCN} to M_{rBC} ratio for the urban plumes of London probed during two measurement flights on 17 and 26 July 2017 (Fig. 13A) reveals lower N_{CCN} vs. M_{rBC} ratios compared to the reference region for urban pollution (violet shading). Unlike to the 2020 measurements, we measured the emissions from London mostly above the PBL. Thus, processes in the PBL may strongly alter the N_{CCN} to M_{rBC} ratio for urban pollution. The good agreement between the two independent measurements of the London plume (Fig. 13A, A1) right above the PBL imply some cloud processing as potential sink of CCN. The data points fall between the reference regimes of urban and lightly aged BB emissions, however, there is no indication for BB

influence and the BT analysis clearly suggests the metropolitan area of London as source region (Fig. A1), therefore the overlay with lightly aged BB emissions may be a coincidence. Note the good agreement between the slopes of the London plume for $N_{\mathrm{CCN}} < 1000\,\mathrm{cm}^{-3}$ and the pollution measured close to Nagoya (11.

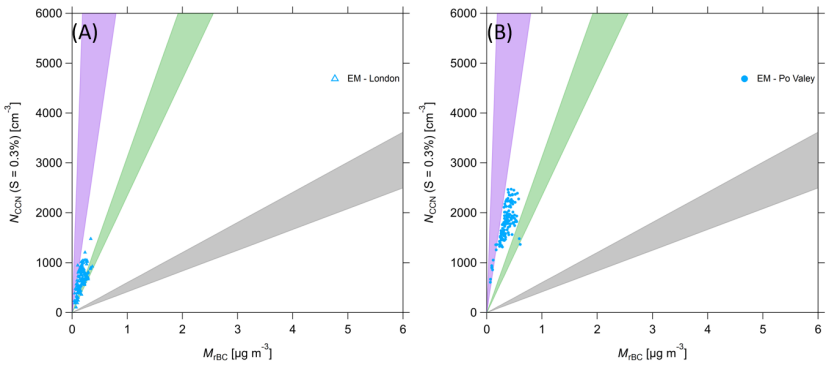

Figure 13. (A) Relationship between N_{CCN} and M_{rBC} for urban emissions from London. The data is from two measurement flights (17 and 26 July 2017). **(B)** Relationship between N_{CCN} and M_{rBC} for mixed urban and BB emissions in Southern Europe, measured over the Po Valley, the Adriatic Sea. The data is from two measurement flights (11 and 20 July 2017).

For the outflow of China's largest cities, Shanghai and Beijing, measured over the East China Sea during EMeRGe-Asia, we find a lower N_{CCN} to M_{rBC} ratio than for fresher urban emissions in Europe. We measured the Chinese outflow over the East China Sea during three consecutive measurement flights (22, 24 and 26 of March 2018). Backward trajectory analysis suggest that urban haze originated mostly in Shanghai, with some contribution of more aged pollution from Beijing (Fig. 14C and A3). Beside urban pollution, also aged BB smoke from cropland fires may contributes to the measured plumes (Fig. 14B). These fires started 5 days prior to the first measurement flight and lasted over all three flights. While the urban pollution travelled one to three days prior to the measurements, the BB emissions were aged around five days (Fig. 14C and A3). The MODIS satellite image reveals a probable mixing of the two pollution types (Fig. 14B). The constant aerosol conditions for this mixed urban and BB emissions from China over four days time period are remarkable.

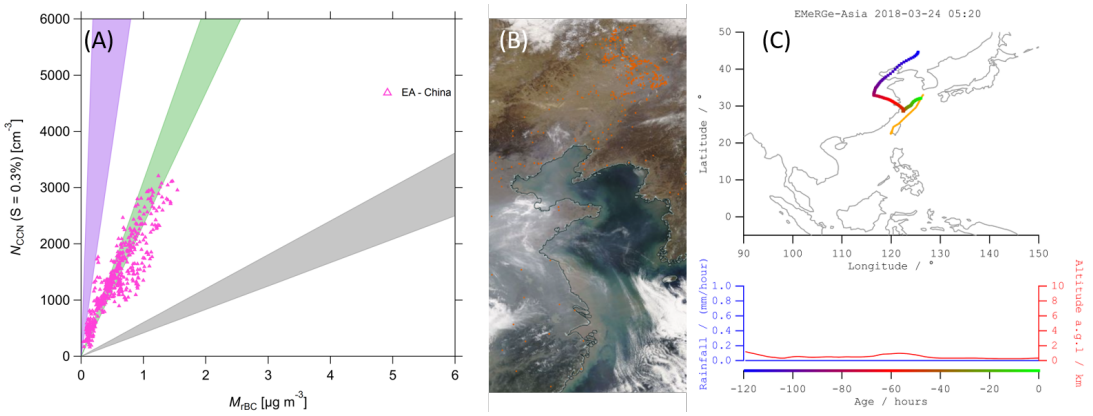

Figure 14. (A) Relationship between N_{CCN} and M_{rBC} for Chinese emissions, measured over the East China Sea downwind of Shanghai and Beijing. The data is from three measurement flights (22, 24 and 26 of March 2018). **(B)** MODIS "Corrected Reflectance (True Color)" image for 22 March 2018. Red dots indicate "Fires and Thermal Anomalies (Day and Night)". Croplands are the dominant combustion fuel for these fires. The grey shading shows the urban and BB smoke mixing over the East China Sea. **(C)** HYSPLIT BT for measurements mixed plume. The color-code indicates time passed prior to measurement, suggesting a plume age around two days for the urban pollution and five days for the BB emissions.

4 Summary and conclusions

We found distinct regimes between the absorbing and initially hydrophobic BC and the scattering and hygroscopic CCN aerosol for the most relevant sources of combustion. The regimes we found correspond to urban emissions within the planetary boundary layer (PBL) in high emission-standards countries, lightly aged biomass burning (BB) smoke from evergreen broadleaf forest vegetation and savannas and highly aged long-range transported (LRT) BB smoke from Africa. Beside that we show how mixing of different aerosol sources influences the N_{CCN} to M_{rBC} ratio. The results for Amazon rain forest and African LRT smoke over the Amazon are confirmed with independent long-term measurements at the ATTO site (Holanda et al., 2021).

There are clear differences in the N_{CCN} to M_{rBC} regimes for urban and BB emissions. The direct effects on cloud physics are primarily a function of N_{CCN}, and thus likely not strongly altered by CCN to BC ratios. However, semi-direct effects where the BC-rich smoke can either accelerate the evaporation of the clouds (so called "cloud burning") or prevent cloud formation by creating warm layers aloft can alter aerosol-cloud interactions and residence times of the BC-richer BB smoke. A more detailed analysis on the impact of the CCN to BC ratios found in this study on cloud physics, removal processes and thus on the atmospheric residence time is desirable.

Urban pollution within the PBL is N_{CCN} dominated. We found consistent ratios for Europe (2017 and 2020) and Japan (2018). The largest influence on urban plumes is observed between measurements taken in the PBL and above. Based on this observa-

tion we assume the lifting from the PBL to the free troposphere as a major driver for the composition of urban plumes. Beside the transformation of the plume by itself, mixing with BB emissions reduces the N_{CCN} to M_{rBC} ratio by introducing large amounts of BC with relatively little N_{CCN}.

Lightly aged BB smoke from evergreen broadleaf forest vegetation and savannas have higher M_{rBC} compared to urban pollution. Our study shows consistent observations for the Amazon rain forest (2014), Southern Europe (2017) and Southeast Asia (2018). These lightly aged BB emissions play regionally a crucial role in pollution levels and superpose with other aerosol and especially urban pollution within the PBL and the lower troposphere. In our analysis we can discriminate typical N_{CCN} to M_{rBC} regimes for plumes with atmospheric residence times of up to four days. Nevertheless, we do not find evidence or clear indications for removal processes of these smoke layers. In fact we reveal consistent data for two plumes in Southeast Asia showing no impact on cloudiness and precipitation. Thus the atmospheric residence time of this lightly aged BB smoke may exceeds previous assumptions (Lund et al., 2018). However, further analysis considering thermodynamic conditions and the meteorological situation during the smoke emission and transport is needed to understand the importance of removal processes and the smoke layers atmospheric residence time.

Highly aged African BB smoke provides the lower end of the N_{CCN} to M_{rBC} regimes in this study. As outlined in Holanda et al. (2020, 2021) African BB smoke after LRT has only little influence on N_{CCN} while is strongly enhanced in M_{rBC}. The relatively larger BC fraction in these plumes favors the rather unperturbed transport of the smoke layers over long distances. Clouds and precipitation also form at low N_{CCN}. While the BC can lead to self-lofting of the smoke plumes and can move them into dry and non-convecting regions of the FT, without cloud formation. Also, the large-scale subsidence in the descending arm of the Hadley cell suppresses wet removal. This characteristics make these BC-rich layers rather inert and enables transport over large distances with high atmospheric residence times. Beside the clear distinction between the ratio of N_{CCN} to M_{rBC}, also the mass equivalent core diameter $\mathrm{M_{MEV}}$ of the BC particles shows a clear difference to the other combustion aerosol sources discussed in this study. This difference in $\mathrm{D_{MEV}}$ was successfully employed (see Holanda et al., 2021) to separate BB emissions from the Amazon and Africa over the Central Amazon.

Appendix A

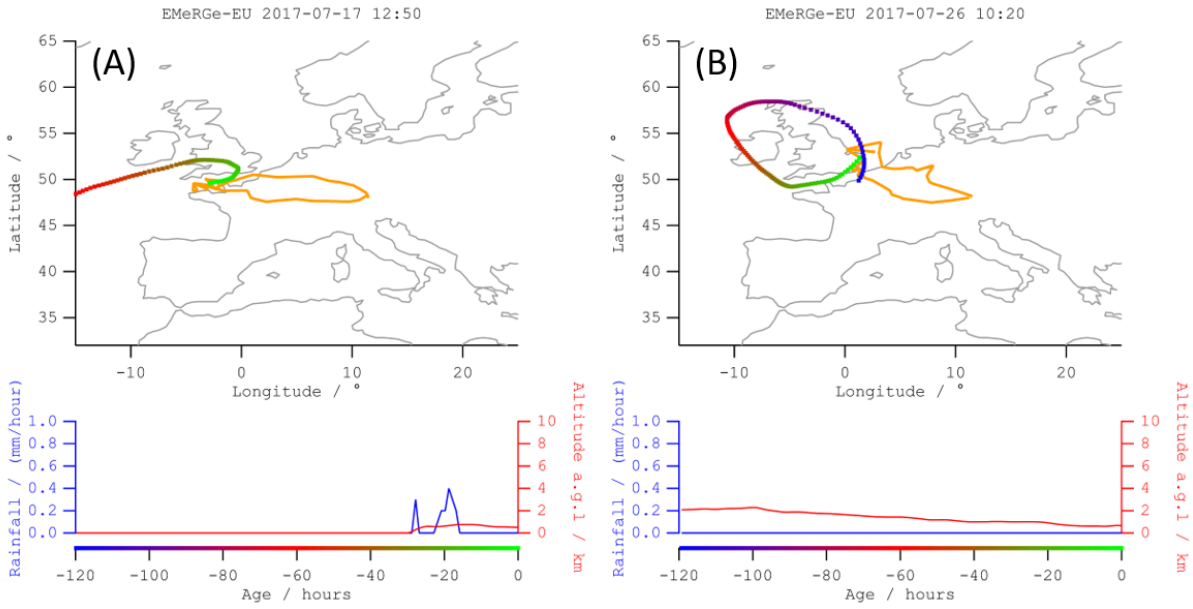

Figure A1. HYSPLIT BT for measurements of the London plume. The color-code indicates time passed prior to measurement. **(A)** shows the measurements conducted 17 July 2017, with an approximate plume age below one day. **(B)** shows the measurements from 26 July 2017 with fresher emissions, aged approximately less than 10 hours.

Competing interests. The authors declare that they have no known competing interests that could have influenced the work reported in this paper.

Acknowledgements. We recognize the Max Planck Society, the Conselho Nacional de Desenvolvimento Científico e Tecnológico (CNPq, Brazil), and the Max Planck Graduate Center with the Johannes Gutenberg University Mainz (MPGC) for the financial support. We thank the entire ACRIDICON-CHUVA, EMeRGe-Europe and - Asia, CAFE-Africa, and CAFE-EU team for the fruitful scientific cooperation. Special thanks goes to the HALO pilots, Steffen Gemsa, Michael Grossrubatscher, Marc Puskeiler, and Stefan Grillenbeck. We thank Volker Dreiling, the Sensor and Data Team of DLR Flight Experiments, and the HALO team of the DLR for their cooperation. We acknowledge the generous support of the ACRIDICON-CHUVA campaign by the Max Planck Society, the German Aerospace Center (DLR), FAPESP (São Paulo Research Foundation), and the German Science Foundation (Deutsche Forschungsgemeinschaft, DFG) within the DFG Priority Program “Atmospheric and Earth System Research with the Research Aircraft HALO (High Altitude and Long Range Research Aircraft)”.

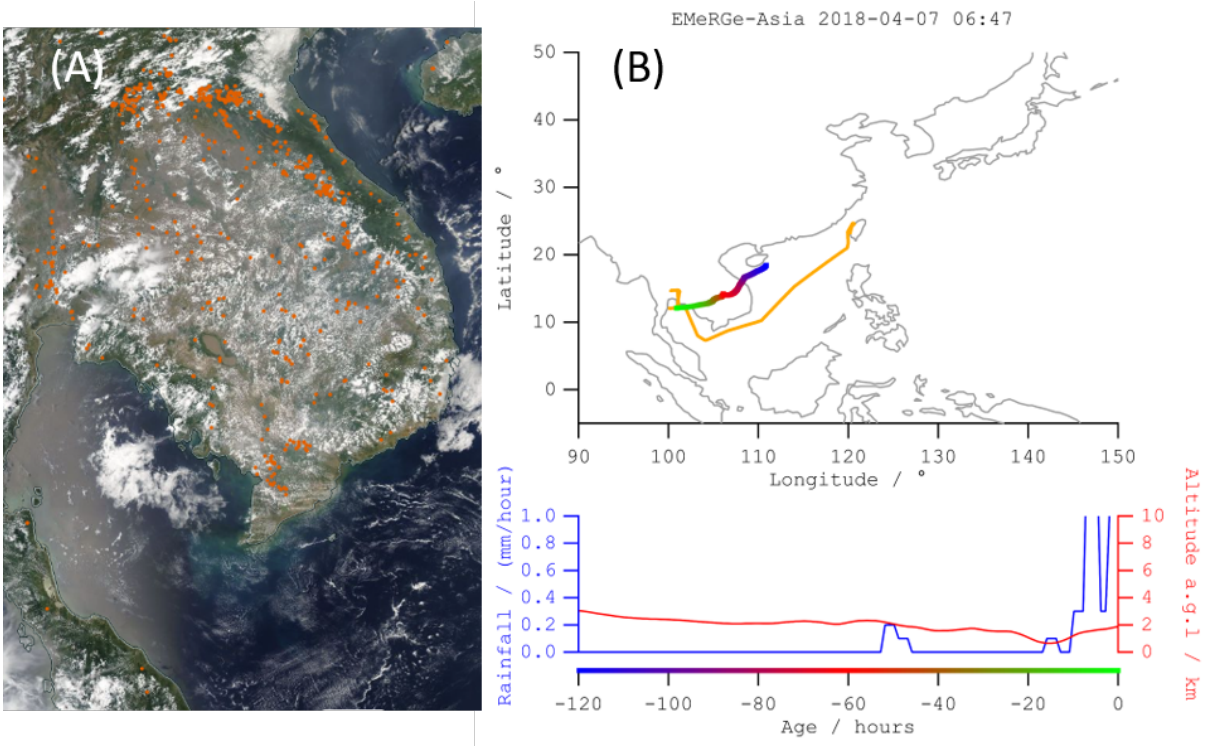

Figure A2. (A) MODIS "Corrected Reflectance (True Color)" image for 05 April 2018, two days prior to measurement flight. Red dots indicate "Fires and Thermal Anomalies (Day and Night)". **(B)** HYSPLIT BT for measurements of BB plume. The color-code indicates time passed prior to measurement, suggesting a plume age of one to two days.

For the EMeRGe campaigns we thank the HALO flight organisation, permissions and related the DLR-FX and the HALO EMeRGe team. Special thanks to Lisa Kaser, Frank Probst, Michael Großrubatscher, Stefan Grillenbeck, Marc Puskeiler, for flight coordination and planning, to Alexander Wolf, and Thomas Leder, the flight engineers and to the BAHAMAS team. The authors also thank enviscope GmbH in particular of Nicole Brehm and Rolf 1554 Maser for the support during the integration and preparation phase of the IOP in Europe

We acknowledge the National Oceanic and Atmospheric Administration (NOAA) Air Resources Laboratory (ARL) for the HYSPLIT transport and dispersion model.

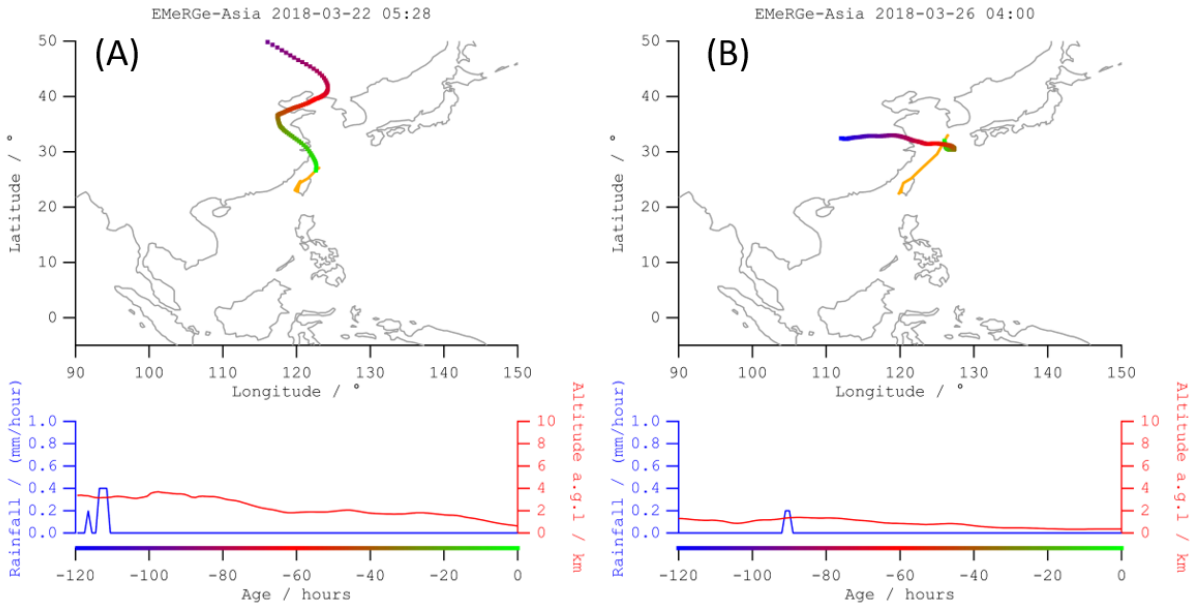

Figure A3. HYSPLIT BT for measurements of Chinese plumes. The color-code indicates time passed prior to measurement. **(A)** shows the measurements conducted 22 March 2018, with an approximate plume age around one day for Shanghai, two days for Beijing and four days for agricultural BB. **(B)** shows the measurements from 26 March 2018, with three to four days residential time from Shanghai.

References

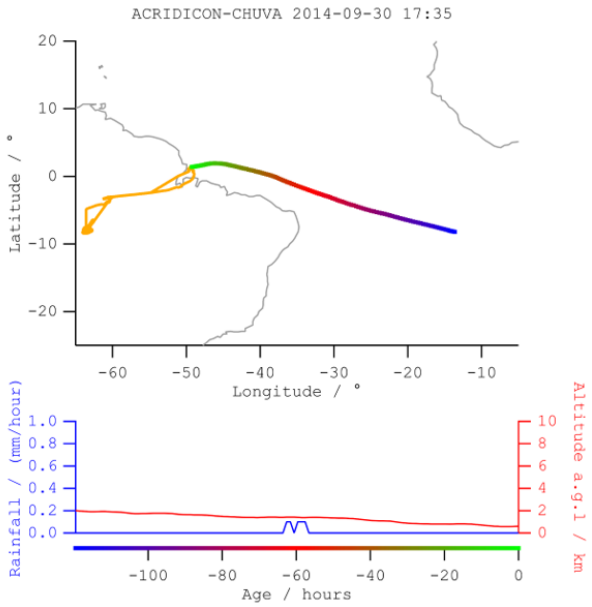

Figure A4. HYSPLIT BT for measurements of African BB plumes at Brazilian coast. The color-code indicates time passed prior to measurement.

References

Andreae, M. and Rosenfeld, D.: Aerosol–cloud–precipitation interactions. Part 1. The nature and sources of cloud-active aerosols, Earth-Science Reviews, 89, 13–41, https://doi.org/10.1016/j.earscirev.2008.03.001, http://linkinghub.elsevier.com/retrieve/pii/S0012825208000317, 2008.

Andreae, M. O.: Smoking Rain Clouds over the Amazon, Science, 303, 1337–1342, https://doi.org/10.1126/science.1092779, http://www.sciencemag.org/cgi/doi/10.1126/science.1092779https://www.sciencemag.org/lookup/doi/10.1126/science.1092779, 2004.

Andreae, M. O.: Emission of trace gases and aerosols from biomass burning – an updated assessment, Atmospheric Chemistry and Physics, 19, 8523–8546, https://doi.org/10.5194/acp-19-8523-2019, https://acp.copernicus.org/articles/19/8523/2019/, 2019.

Andreae, M. O. and Merlet, P.: Emission of trace gases and aerosols from biomass burning, Global Biogeochemical Cycles, 15, 955–966, https://doi.org/10.1029/2000GB001382, http://doi.wiley.com/10.1029/2000GB001382, 2001.

Andreae, M. O., Afchine, A., Albrecht, R., Holanda, B. A., Artaxo, P., Barbosa, H. M. J., Borrmann, S., Cecchini, M. A., Costa, A., Dollner, M., Fütterer, D., Järvinen, E., Jurkat, T., Klimach, T., Konemann, T., Knote, C., Krämer, M., Krisna, T., Machado, L. A. T., Mertes, S., Minikin, A., Pöhlker, C., Pöhlker, M. L., Pöschl, U., Rosenfeld, D., Sauer, D., Schlager, H., Schnaiter, M., Schneider, J., Schulz, C., Spanu, A., Sperling, V. B., Voigt, C., Walser, A., Wang, J., Weinzierl, B., Wendisch, M., and Ziereis, H.: Aerosol characteristics and particle production in the upper troposphere over the Amazon Basin, Atmospheric Chemistry and Physics, 18, 921–961, https://doi.org/10.5194/acp-18-921-2018, https://www.atmos-chem-phys.net/18/921/2018/, 2018.

Andrés Hernández, M. D., Hilboll, A., Ziereis, H., Förster, E., Krüger, O. O., Kaiser, K., Schneider, J., Barnaba, F., Vrekoussis, M., Schmidt, J., Huntrieser, H., Blechschmidt, A.-M., George, M., Nenakhov, V., Klausner, T., Holanda, B. A., Wolf, J., Eirenschmalz, L., Krebsbach, M., Pöhlker, M. L., Hedegaard, A. B., Mei, L., Pfeilsticker, K., Liu, Y., Koppmann, R., Schlager, H., Bohn, B., Schumann, U., Richter, A., Schreiner, B., Sauer, D., Baumann, R., Mertens, M., Jöckel, P., Kilian, M., Stratmann, G., Pöhlker, C., Campanelli, M., Pandolfi, M., Sicard, M., Gomez-Amo, J. L., Pujadas, M., Bigge, K., Kluge, F., Schwarz, A., Daskalakis, N., Walter, D., Zahn, A., Pöschl, U., Bönisch, H., Borrmann, S., Platt, U., and Burrows, J. P.: Overview: On the transport and transformation of pollutants in the outflow of major population centres – observational data from the EMeRGe European intensive operational period in summer 2017, Atmospheric Chemistry and Physics Discussions, 2021, 1–81, https://doi.org/10.5194/acp-2021-500, https://acp.copernicus.org/preprints/acp-2021-500/, 2021.

Bauer, S. E., Menon, S., Koch, D., Bond, T. C., and Tsigaridis, K.: A global modeling study on carbonaceous aerosol microphysical characteristics and radiative effects, Atmospheric Chemistry and Physics, 10, 7439–7456, https://doi.org/10.5194/acp-10-7439-2010, 2010.

Bellouin, N., Quaas, J., Gryspeerdt, E., Kinne, S., Stier, P., Watson-Parris, D., Boucher, O., Carslaw, K. S., Christensen, M., Daniau, A. L., Dufresne, J. L., Feingold, G., Fiedler, S., Forster, P., Gettelman, A., Haywood, J. M., Lohmann, U., Malavelle, F., Mauritsen, T., McCoy, D. T., Myhre, G., Mülmenstädt, J., Neubauer, D., Possner, A., Rugenstein, M., Sato, Y., Schulz, M., Schwartz, S. E., Sourdeval, O., Storelvmo, T., Toll, V., Winker, D., and Stevens, B.: Bounding Global Aerosol Radiative Forcing of Climate Change, Reviews of Geophysics, 58, 1–45, https://doi.org/10.1029/2019RG000660, 2020.

Bond, T. C., Doherty, S. J., Fahey, D. W., Forster, P. M., Berntsen, T., Deangelo, B. J., Flanner, M. G., Ghan, S., Kärcher, B., Koch, D., Kinne, S., Kondo, Y., Quinn, P. K., Sarofim, M. C., Schultz, M. G., Schulz, M., Venkataraman, C., Zhang, H., Zhang, S., Bellouin, N., Guttikunda, S. K., Hopke, P. K., Jacobson, M. Z., Kaiser, J. W., Klimont, Z., Lohmann, U., Schwarz, J. P., Shindell, D., Storelvmo, T., Warren, S. G., and Zender, C. S.: Bounding the role of black carbon in the climate system: A scientific assessment, Journal of Geophysical Research Atmospheres, 118, 5380–5552, https://doi.org/10.1002/jgrd.50171, 2013.

Campos Braga, R., Ervens, B., Rosenfeld, D., Andreae, M. O., Förster, J.-D., Fütterer, D., Hernández Pardo, L., Holanda, B. A., Jurkat, T., Krüger, O. O., Lauer, O., Machado, L. A. T., Pöhlker, C., Sauer, D., Voigt, C., Walser, A., Wendisch, M., Pöschl, U., and Pöhlker, M. L.: Cloud droplet number closure for tropical convective clouds during the ACRIDICON–CHUVA campaign, Atmospheric Chemistry and Physics Discussions, 2021, 1–17, https://doi.org/10.5194/acp-2021-80, https://acp.copernicus.org/preprints/acp-2021-80/, 2021a.

Campos Braga, R., Rosenfeld, D., Krüger, O. O., Ervens, B., Holanda, B. A., Wendisch, M., Krisna, T., Pöschl, U., Andreae, M. O., Voigt, C., and Pöhlker, M. L.: Linear relationship between effective radius and precipitation water content near the top of convective clouds, Atmospheric Chemistry and Physics Discussions, 2021, 1–16, https://doi.org/10.5194/acp-2021-295, https://acp.copernicus.org/preprints/acp-2021-295/, 2021b.

Cecchini, M. A., Machado, L. A. T., Andreae, M. O., Martin, S. T., Albrecht, R. I., Artaxo, P., Barbosa, H. M. J., Borrmann, S., Fütterer, D., Jurkat, T., Mahnke, C., Minikin, A., Molleker, S., Pöhlker, M. L., Pöschl, U., Rosenfeld, D., Voigt, C., Weinzierl, B., and Wendisch, M.: Sensitivities of Amazonian clouds to aerosols and updraft speed, Atmospheric Chemistry and Physics, 17, 10 037–10 050, https://doi.org/10.5194/acp-17-10037-2017, https://acp.copernicus.org/articles/17/10037/2017/, 2017.

Chen, W. T., Lee, Y. H., Adams, P. J., Nenes, A., and Seinfeld, J. H.: Will black carbon mitigation dampen aerosol indirect forcing?, Geophysical Research Letters, 37, 1–5, https://doi.org/10.1029/2010GL042886, 2010.

Ditas, J., Ma, N., Zhang, Y., Assmann, D., Neumaier, M., Riede, H., and Karu, E.: Strong impact of wildfires on the abundance and aging of black carbon in the lowermost stratosphere, https://doi.org/10.1073/pnas.1806868115, 2018.

Dusek, U., Frank, G. P., Hildebrandt, L., Curtius, J., Schneider, J., Walter, S., Chand, D., Drewnick, F., Hings, S., Jung, D., Borrmann, S., and Andreae, M. O.: Size matters more than chemistry for cloud-nucleating ability of aerosol particles, Science, 312, 1375–1378, https://doi.org/10.1126/science.1125261, <GotoISI>://WOS:000237961600054, 2006.

Gysel-Beer, M. and Corbin, J.: SP2 toolkit 4.115 (Igor7) (Version 4.115), http://doi.org/10.5281/zenodo.3575186/, 2019.

Hoesly, R. M., Smith, S. J., Feng, L., Klimont, Z., Janssens-Maenhout, G., Pitkanen, T., Seibert, J. J., Vu, L., Andres, R. J., Bolt, R. M., Bond, T. C., Dawidowski, L., Kholod, N., Kurokawa, J.-I., Li, M., Liu, L., Lu, Z., Moura, M. C. P., O'Rourke, P. R., and Zhang, Q.: Historical (1750–2014) anthropogenic emissions of reactive gases and aerosols from the Community Emissions Data System (CEDS), Geoscientific Model Development, 11, 369–408, https://doi.org/10.5194/gmd-11-369-2018, https://gmd.copernicus.org/articles/11/369/2018/, 2018.

Holanda, B. A., Pöhlker, M. L., Walter, D., Saturno, J., Sörgel, M., Ditas, J., Ditas, F., Schulz, C., Franco, M. A., Wang, Q., Donth, T., Artaxo, P., Barbosa, H. M. J., Borrmann, S., Braga, R., Brito, J., Cheng, Y., Dollner, M., Kaiser, J. W., Klimach, T., Knote, C., Krüger, O. O., Fütterer, D., Lavrič, J. V., Ma, N., Machado, L. A. T., Ming, J., Morais, F. G., Paulsen, H., Sauer, D., Schlager, H., Schneider, J., Su, H., Weinzierl, B., Walser, A., Wendisch, M., Ziereis, H., Zöger, M., Pöschl, U., Andreae, M. O., and Pöhlker, C.: Influx of African biomass burning aerosol during the Amazonian dry season through layered transatlantic transport of black carbon-rich smoke, Atmos. Chem. Phys., 20, 4757–4785, https://doi.org/10.5194/acp-20-4757-2020, https://www.atmos-chem-phys.net/20/4757/2020/, 2020.

Holanda, B. A., Franco, M. A., Walter, D., Andreae, M. O., Artaxo, P., Carbone, S., Cheng, Y., Chowdhury, S., Ditas, F., Gysel-beer, M., Klimach, T., Kremper, L. A., Krüger, O. O., Lavric, J. V., Lelieveld, J., Ma, C., Machado, L. A. T., Morais, F. G., Modini, R. L., Pozzer, A., Saturno, J., Su, H., Wendisch, M., Wolff, S., Pöhlker, M. L., Pöschl, U., and Pöhlker, C.: African smoke over the Amazon rain forest, to be submitted, 2021.

Koren, I., Kaufman, Y. J., Remer, L. A., and Martins, J. V.: Measurement of the effect of Amazon smoke on inhibition of cloud formation, Science, 303, 1342–1345, https://doi.org/10.1126/science.1089424, <GotoISI>://WOS:000189238600043, 2004.

Krüger, M. L., Mertes, S., Klimach, T., Cheng, Y. F., Su, H., Schneider, J., Andreae, M. O., Pöschl, U., and Rose, D.: Assessment of cloud supersaturation by size-resolved aerosol particle and cloud condensation nuclei (CCN) measurements, Atmospheric Measurement Techniques, 7, 2615–2626, https://doi.org/10.5194/amt-7-2615-2014, 2014.

Krüger, O. O., Holanda, B. A., Chowdhury, S., Pozzer, A., Walter, D., Pöhlker, C., Dolores, M., Hernández, A., Burrows, J. P., Lelieveld, J., Quaas, J., Pöschl, U., and Pöhlker, M. L.: Reduction in black carbon aerosol concentrations and emissions during the COVID-19 lockdown quantified by aircraft measurements over Europe, to be submitted, 2021.

Laborde, M., Mertes, P., Zieger, P., Dommen, J., Baltensperger, U., and Gysel, M.: Sensitivity of the Single Particle Soot Photometer to different black carbon types, Atmospheric Measurement Techniques, 5, 1031–1043, https://doi.org/10.5194/amt-5-1031-2012, 2012.

Laborde, M., Crippa, M., Tritscher, T., Jurányi, Z., Decarlo, P. F., Temime-Roussel, B., Marchand, N., Eckhardt, S., Stohl, A., Baltensperger, U., Prévôt, A. S., Weingartner, E., and Gysel, M.: Black carbon physical properties and mixing state in the European megacity Paris, Atmospheric Chemistry and Physics, 13, 5831–5856, https://doi.org/10.5194/acp-13-5831-2013, 2013.

Liu, D., Allan, J. D., Young, D. E., Coe, H., Beddows, D., Fleming, Z. L., Flynn, M. J., Gallagher, M. W., Harrison, R. M., Lee, J., Prevot, A. S., Taylor, J. W., Yin, J., Williams, P. I., and Zotter, P.: Size distribution, mixing state and source apportionment of black carbon aerosol in London during winter time, Atmospheric Chemistry and Physics, 14, 10 061–10 084, https://doi.org/10.5194/acp-14-10061-2014, 2014.

Liu, D., He, C., Schwarz, J. P., and Wang, X.: Lifecycle of light-absorbing carbonaceous aerosols in the atmosphere, npj Climate and Atmospheric Science, 3, https://doi.org/10.1038/s41612-020-00145-8, http://dx.doi.org/10.1038/s41612-020-00145-8, 2020a.

Liu, L., Cheng, Y., Wang, S., Wei, C., Pöhlker, M., Pöhlker, C., Artaxo, P., Shrivastava, M., Andreae, M. O., Pöschl, U., and Su, H.: Impact of biomass burning aerosols on radiation, clouds, and precipitation over the Amazon: relative importance of aerosol–cloud

and aerosol–radiation interactions, Atmos. Chem. Phys., 20, 13 283–13 301, https://doi.org/10.5194/acp-20-13283-2020, https://acp.copernicus.org/preprints/acp-2020-191/, 2020b.

Lund, M. T., Samset, B. H., Skeie, R. B., Watson-Parris, D., Katich, J. M., Schwarz, J. P., and Weinzierl, B.: Short Black Carbon lifetime inferred from a global set of aircraft observations, npj Climate and Atmospheric Science, 1, 1–8, https://doi.org/10.1038/s41612-018-0040-x, http://dx.doi.org/10.1038/s41612-018-0040-x, 2018.

May, A. A., McMeeking, G. R., Lee, T., Taylor, J. W., Craven, J. S., Burling, I., Sullivan, A. P., Akagi, S., Collett, J. L., Flynn, M., Coe, H., Urbanski, S. P., Seinfeld, J. H., Yokelson, R. J., and Kreidenweis, S. M.: Aerosol emissions from prescribed fires in the United States: A synthesis of laboratory and aircraft measurements, Journal of Geophysical Research: Atmospheres, 119, 11,826–11,849, https://doi.org/10.1002/2014JD021848, http://doi.wiley.com/10.1002/2014JD021848, 2014.

Molleker, S., Helleis, F., Klimach, T., Appel, O., Dragoneas, A., Gurk, C., Hünig, A., Köllner, F., Rubach, F., Schulz, C., Schneider, J., and Borrmann, S.: Application of an O-ring pinch device as a constant-pressure inlet (CPI) for airborne sampling, Atmospheric Measurement Techniques, 13, 3651–3660, https://doi.org/10.5194/amt-13-3651-2020, 2020.

Naik, V., Szopa, S., Adhikary, B., Artaxo, P., Berntsen, T., Collins, W. D., Fuzzi, S., Gallardo, L., Kiendler Scharr, A., Klimont, Z., Liao, H., Unger, N., and Zanis, P.: IPCC, 2021: Climate Change 2021: The Physical Science Basis. Contribution of Working Group I to the Sixth Assessment Report of the Intergovernmental Panel on Climate Change, Cambridge University Press, Cambridge, United Kingdom and New York, NY, USA, https://doi.org/xxx, 2021 in press.

Ohneiser, K., Ansmann, A., Baars, H., Seifert, P., Barja, B., Jimenez, C., Radenz, M., Teisseire, A., Floutsi, A., Haarig, M., Foth, A., Chudnovsky, A., Engelmann, R., Zamorano, F., Bühl, J., and Wandinger, U.: Smoke of extreme Australian bushfires observed in the stratosphere over Punta Arenas, Chile, in January 2020: optical thickness, lidar ratios, and depolarization ratios at 355 and 532 nm, Atmospheric Chemistry and Physics, 20, 8003–8015, https://doi.org/10.5194/acp-20-8003-2020, https://acp.copernicus.org/articles/20/8003/2020/, 2020.

Pileci, R. E., Modini, R. L., Bertò, M., Yuan, J., Corbin, J. C., Marinoni, A., Henzing, B., Moerman, M. M., Putaud, J. P., Spindler, G., Wehner, B., Müller, T., Tuch, T., Trentini, A., Zanatta, M., Baltensperger, U., and Gysel-Beer, M.: Comparison of co-located refractory black carbon (rBC) and elemental carbon (EC) mass concentration measurements during field campaigns at several European sites, Atmospheric Measurement Techniques, 14, 1379–1403, https://doi.org/10.5194/amt-14-1379-2021, https://amt.copernicus.org/articles/14/1379/2021/, 2021.

Pöhlker, C., Walter, D., Paulsen, H., Könemann, T., Rodríguez-caballero, E., Moran-zuloaga, D., Brito, J., Carbone, S., Degrendele, C., Després, V. R., Ditas, F., Pöhlker, M. L., Praß, M., Löbs, N., Saturno, J., Sörgel, M., Wang, Q., Weber, B., Wolff, S., Artaxo, P., Pöschl, U., and Andreae, M. O.: Land cover and its transformation in the backward trajectory footprint region of the Amazon Tall Tower Observatory, Atmospheric Chemistry and Physics, pp. 8425–8470, 2019.

Pöhlker, M. L., Pöhlker, C., Ditas, F., Klimach, T., De Angelis, I. H., Araújo, A., Brito, J., Carbone, S., Cheng, Y., Chi, X., Ditz, R., Gunthe, S. S., Kesselmeier, J., Könemann, T., Lavrič, J. V., Martin, S. T., Mikhailov, E., Moran-Zuloaga, D., Rose, D., Saturno, J., Su, H., Thalman, R., Walter, D., Wang, J., Wolff, S., Barbosa, H. M., Artaxo, P., Andreae, M. O., and Pöschl, U.: Long-term observations of cloud condensation nuclei in the Amazon rain forest - Part 1: Aerosol size distribution, hygroscopicity, and new model parametrizations for CCN prediction, Atmospheric Chemistry and Physics, 16, 15 709–15 740, https://doi.org/10.5194/acp-16-15709-2016, 2016.

Pöhlker, M. L., Ditas, F., Saturno, J., Klimach, T., Hrabě De Angelis, I., Araùjo, A. C., Brito, J., Carbone, S., Cheng, Y., Chi, X., Ditz, R., Gunthe, S. S., Holanda, B. A., Kandler, K., Kesselmeier, J., Könemann, T., Krüger, O. O., Lavric, J. V., Martin, S. T., Mikhailov, E., Moran-Zuloaga, D., Rizzo, L. V., Rose, D., Su, H., Thalman, R., Walter, D., Wang, J., Wolff, S., Barbosa, H. M., Artaxo, P., Andreae,

M. O., Pöschl, U., and Pöhlker, C.: Long-term observations of cloud condensation nuclei over the Amazon rain forest - Part 2: Variability and characteristics of biomass burning, long-range transport, and pristine rain forest aerosols, Atmospheric Chemistry and Physics, 18, 10 289–10 331, https://doi.org/10.5194/acp-18-10289-2018, 2018.

Pöhlker, M. L., Zhang, M., Campos Braga, R., Krüger, O. O., Pöschl, U., and Ervens, B.: Aitken mode particles as CCN in aerosol- And updraft-sensitive regimes of cloud droplet formation, Atmospheric Chemistry and Physics, 21, 11 723–11 740, https://doi.org/10.5194/acp-21-11723-2021, 2021.

Pöschl, U.: Atmospheric aerosols: Composition, transformation, climate and health effects, Angewandte Chemie - International Edition, 44, 7520–7540, https://doi.org/10.1002/anie.200501122, 2005.

Ramanathan, V., Crutzen, P. J., Kiehl, J. T., and Rosenfeld, D.: Aerosols : A Major, 294, 2119–2124, 2001.

Reddington, C. L., McMeeking, G., Mann, G. W., Coe, H., Frontoso, M. G., Liu, D., Flynn, M., Spracklen, D. V., and Carslaw, K. S.: The mass and number size distributions of black carbon aerosol over Europe, Atmospheric Chemistry and Physics, 13, 4917–4939, https://doi.org/10.5194/acp-13-4917-2013, 2013.

Roberts, G. C. and Nenes, A.: A continuous-flow streamwise thermal-gradient CCN chamber for atmospheric measurements, Aerosol Science and Technology, 39, 206–221, https://doi.org/10.1080/027868290913988, 2005.

Rolph, G., Stein, A., and Stunder, B.: Real-time Environmental Applications and Display sYstem: READY, Environmental Modelling & Software, 95, 210–228, https://doi.org/https://doi.org/10.1016/j.envsoft.2017.06.025, https://www.sciencedirect.com/science/article/pii/S1364815217302360, 2017.

Rose, D., Gunthe, S. S., Mikhailov, E., Frank, G. P., Dusek, U., Andreae, M. O., and Pöschl, U.: Calibration and measurement uncertainties of a continuous-flow cloud condensation nuclei counter (DMT-CCNC): CCN activation of ammonium sulfate and sodium chloride aerosol particles in theory and experiment, Atmospheric Chemistry and Physics, 8, 1153–1179, https://doi.org/10.5194/acp-8-1153-2008, 2008.

Rosenfeld, D., Lohmann, U., Raga, G. B., O'Dowd, C. D., Kulmala, M., Fuzzi, S., Reissell, A., and Andreae, M. O.: Flood or drought: How do aerosols affect precipitation?, Science, 321, 1309–1313, https://doi.org/10.1126/science.1160606, <GotoISI>://WOS:000258914300038, 2008.

Rosenfeld, D., Andreae, M. O., Asmi, A., Chin, M., de Leeuw, G., Donovan, D. P., Kahn, R., Kinne, S., Kivekas, N., Kulmala, M., Lau, W., Schmidt, K. S., Suni, T., Wagner, T., Wild, M., and Quaas, J.: Global observations of aerosol-cloud-precipitation-climate interactions, Reviews of Geophysics, 52, 750–808, https://doi.org/10.1002/2013rg000441, <GotoISI>://WOS:000348452000005, 2014.

Samset, B. H., Myhre, G., Schulz, M., Balkanski, Y., Bauer, S., Berntsen, T. K., Bian, H., Bellouin, N., Diehl, T., Easter, R. C., Ghan, S. J., Iversen, T., Kinne, S., Kirkeväg, A., Lamarque, J. F., Lin, G., Liu, X., Penner, J. E., Seland, O., Skeie, R. B., Stier, P., Takemura, T., Tsigaridis, K., and Zhang, K.: Black carbon vertical profiles strongly affect its radiative forcing uncertainty, Atmospheric Chemistry and Physics, 13, 2423–2434, https://doi.org/10.5194/acp-13-2423-2013, 2013.

Saturno, J., Ditas, F., De Vries, M. P., Holanda, B. A., Pöhlker, M. L., Carbone, S., Walter, D., Bobrowski, N., Brito, J., Chi, X., Gutmann, A., De Angelis, I. H., Machado, L. A., Moran-Zuloaga, D., Rüdiger, J., Schneider, J., Schulz, C., Wang, Q., Wendisch, M., Artaxo, P., Wagner, T., Pöschl, U., Andreae, M. O., and Pöhlker, C.: African volcanic emissions influencing atmospheric aerosols over the Amazon rain forest, Atmospheric Chemistry and Physics, 18, 10 391–10 405, https://doi.org/10.5194/acp-18-10391-2018, 2018.

Schneider, J., Weigel, R., Klimach, T., Dragoneas, A., Appel, O., Hünig, A., Molleker, S., Köllner, F., Clemen, H.-C., Eppers, O., Hoppe, P., Hoor, P., Mahnke, C., Krämer, M., Rolf, C., Grooß, J.-U., Zahn, A., Obersteiner, F., Ravegnani, F., Ulanovsky, A., Schlager, H., Scheibe, M., Diskin, G. S., DiGangi, J. P., Nowak, J. B., Zöger, M., and Borrmann, S.: Aircraft-based observation of meteoric material in lower-

stratospheric aerosol particles between 15 and 68° N, Atmospheric Chemistry and Physics, 21, 989–1013, https://doi.org/10.5194/acp-21-989-2021, https://acp.copernicus.org/articles/21/989/2021/, 2021.

Schulz, C., Schneider, J., Amorim Holanda, B., Appel, O., Costa, A., de Sá, S. S., Dreiling, V., Fütterer, D., Jurkat-Witschas, T., Klimach, T., Krämer, M., Martin, S. T., Mertes, S., Pöhlker, M. L., Sauer, D., Voigt, C., Weinzierl, B., Ziereis, H., Zöger, M., Andreae, M. O., Artaxo, P., Machado, L. A. T., Pöschl, U., Wendisch, M., and Borrmann, S.: Aircraft-based observations of isoprene epoxydiol-derived secondary organic aerosol (IEPOX-SOA) in the tropical upper troposphere over the Amazon region, Atmospheric Chemistry and Physics Discussions, pp. 1–32, https://doi.org/10.5194/acp-2018-232, https://www.atmos-chem-phys-discuss.net/acp-2018-232/, 2018.

Schwartz, J.: Air Pollution and Daily Mortality: A Review and Meta Analysis, Environmental Research, 64, 36–52, https://doi.org/https://doi.org/10.1006/enrs.1994.1005, https://www.sciencedirect.com/science/article/pii/S001393518471005X, 1994.

Schwarz, J. P., Gao, R. S., Fahey, D. W., Thomson, D. S., Watts, L. A., Wilson, J. C., Reeves, J. M., Darbeheshti, M., Baumgardner, D. G., Kok, G. L., Chung, S. H., Schulz, M., Hendricks, J., Lauer, A., Kärcher, B., Slowik, J. G., Rosenlof, K. H., Thompson, T. L., Langford, A. O., Loewenstein, M., and Aikin, K. C.: Single-particle measurements of midlatitude black carbon and light-scattering aerosols from the boundary layer to the lower stratosphere, Journal of Geophysical Research Atmospheres, 111, 1–15, https://doi.org/10.1029/2006JD007076, 2006.

Schwarz, J. P., Gao, R. S., Spackman, J. R., Watts, L. A., Thomson, D. S., Fahey, D. W., Ryerson, T. B., Peischl, J., Holloway, J. S., Trainer, M., Frost, G. J., Baynard, T., Lack, D. A., de Gouw, J. A., Warneke, C., and Del Negro, L. A.: Measurement of the mixing state, mass, and optical size of individual black carbon particles in urban and biomass burning emissions, Geophysical Research Letters, 35, 1–5, https://doi.org/10.1029/2008GL033968, 2008.

Schwarz, J. P., Spackman, J. R., Gao, R. S., Perring, A. E., Cross, E., Onasch, T. B., Ahern, A., Wrobel, W., Davidovits, P., Olfert, J., Dubey, M. K., Mazzoleni, C., and Fahey, D. W.: The Detection Efficiency of the Single Particle Soot Photometer, Aerosol Science and Technology, 44, 612–628, https://doi.org/10.1080/02786826.2010.481298, https://doi.org/10.1080/02786826.2010.481298, 2010.

Spracklen, D. V., Carslaw, K. S., Pöschl, U., Rap, A., and Forster, P. M.: Global cloud condensation nuclei influenced by carbonaceous combustion aerosol, Atmospheric Chemistry and Physics, 11, 9067–9087, https://doi.org/10.5194/acp-11-9067-2011, 2011.

Stein, A. F., Draxler, R. R., Rolph, G. D., Stunder, B. J. B., Cohen, M. D., and Ngan, F.: NOAA's HYSPLIT Atmospheric Transport and Dispersion Modeling System, Bulletin of the American Meteorological Society, 96, 2059–2077, https://doi.org/10.1175/BAMS-D-14-00110.1, http://journals.ametsoc.org/doi/10.1175/BAMS-D-14-00110.1, 2015.

Stephens, M., Turner, N., and Sandberg, J.: Particle identification by laser-induced incandescence in a solid-state laser cavity., Applied optics, 42, 3726–36, https://doi.org/10.1364/AO.42.003726, http://www.ncbi.nlm.nih.gov/pubmed/12868806, 2003.

Tadic, I., Nussbaumer, C., Bohn, B., Harder, H., Marno, D., Martinez, M., Obersteiner, F., Parchatka, U., Pozzer, A., Rohloff, R., Zöger, M., Lelieveld, J., and Fischer, H.: Central role of nitric oxide in ozone production in the upper tropical troposphere over the Atlantic Ocean and West Africa, Atmospheric Chemistry and Physics Discussions, 2021, 1–24, https://doi.org/10.5194/acp-2021-52, https://acp.copernicus.org/preprints/acp-2021-52/, 2021.

Twomey, S.: The Influence of Pollution on the Shortwave Albedo of Clouds, Journal of the Atmospheric Sciences, 34, 1149–1152, https://doi.org/10.1175/1520-0469(1977)034<1149:TIOPOT>2.0.CO;2, https://doi.org/10.1175/1520-0469(1977)034<1149:TIOPOT>2.0.CO;2, 1977.

Twomey, S. and Wojciechowski, T. A.: Observations of the geographical variation of cloud nuclei, Journal of the Atmospheric Sciences, 26, 684–&, <GotoISI>://WOS:A1969D832200009, 1969.

Voigt, C., Lelieveld, J., Schlager, H., Schneider, J., Curtius, J., Meerkötter, R., Sauer, D., Bugliaro, L., Bohn, B., Crowley, J., Erbertseder, T., Groß, S., Li, Q., Mertens, M., Pöhlker, M., Pozzer, A., Schumann, U., Tomsche, L., Williams, J., Zahn, A., Andreae, M., Borrmann, M., Bräuer, T., Dörich, R., Dörnbrack, A., Edtbauer, A., Ernle, L., Fischer, H., Giez, A., Granzin, M., Grewe, V., Hahn, V., Harder, H., Heinritzi, M., Holanda, B., Jöckel, P., Kaiser, K., Krüger, O., Lucke, J., Marsing, A., Martin, A., Matthes, S., Pöhlker, C., Pöschl, U., Reifenbergand, S., Ringsdorf, A., Scheibe, M., Tadic, I., Zauner-Wieczorek, M., Henke, R., and Rapp, M.: BLUESKY aircraft mission reveals reduction in atmospheric pollution during the 2020 Corona lockdown, Bulletin of the American Meteorological Society, - submitted, 2021.

Wendisch, M., Poschl, U., Andreae, M. O., MacHado, L. A., Albrecht, R., Schlager, H., Rosenfeld, D., Martin, S. T., Abdelmonem, A., Afchine, A., Araujo, A. C., Artaxo, P., Aufmhoff, H., Barbosa, H. M., Borrmann, S., Braga, R., Buchholz, B., Cecchini, M. A., Costa, A., Curtius, J., Dollner, M., Dorf, M., Dreiling, V., Ebert, V., Ehrlich, A., Ewald, F., Fisch, G., Fix, A., Frank, F., Futterer, D., Heckl, C., Heidelberg, F., Huneke, T., Jakel, E., Jarvinen, E., Jurkat, T., Kanter, S., Kastner, U., Kenntner, M., Kesselmeier, J., Klimach, T., Knecht, M., Kohl, R., Kolling, T., Kramer, M., Kruger, M., Krisna, T. C., Lavric, J. V., Longo, K., Mahnke, C., Manzi, A. O., Mayer, B., Mertes, S., Minikin, A., Molleker, S., Munch, S., Nillius, B., Pfeilsticker, K., Pohlker, C., Roiger, A., Rose, D., Rosenow, D., Sauer, D., Schnaiter, M., Schneider, J., Schulz, C., De Souza, R. A., Spanu, A., Stock, P., Vila, D., Voigt, C., Walser, A., Walter, D., Weigel, R., Weinzierl, B., Werner, F., Yamasoe, M. A., Ziereis, H., Zinner, T., and Zoger, M.: Acridicon-chuva campaign: Studying tropical deep convective clouds and precipitation over amazonia using the New German research aircraft HALO, Bulletin of the American Meteorological Society, 97, 1885–1908, https://doi.org/10.1175/BAMS-D-14-00255.1, 2016.

Wu, H., Taylor, J. W., Szpek, K., Langridge, J. M., Williams, P. I., Flynn, M., Allan, J. D., Abel, S. J., Pitt, J., Cotterell, M. I., Fox, C., Davies, N. W., Haywood, J., and Coe, H.: Vertical variability of the properties of highly aged biomass burning aerosol transported over the southeast Atlantic during CLARIFY-2017, Atmospheric Chemistry and Physics, 20, 12 697–12 719, https://doi.org/10.5194/acp-20-12697-2020, https://acp.copernicus.org/articles/20/12697/2020/, 2020.

Wu, H., Taylor, J. W., Langridge, J. M., Yu, C., Allan, J. D., Szpek, K., Cotterell, M. I., Williams, P. I., Flynn, M., Barker, P., Fox, C., Allen, G., Lee, J., and Coe, H.: Rapid transformation of ambient absorbing aerosols from West African biomass burning, Atmospheric Chemistry and Physics, 21, 9417–9440, https://doi.org/10.5194/acp-21-9417-2021, https://acp.copernicus.org/articles/21/9417/2021/, 2021.

CHAPTER 3

Conclusions and Outlook

Conclusions

The Amazon rain forest is an ecosystem of global significance for climate and biodiversity. Nevertheless, it has been subject of severe and, since recently again, increasing deforestation activities and fire occurrence. The heavy smoke from vegetation fires affects the dynamics of atmospheric circulation, cloud properties and, the atmospheric (re)cycling of water. In addition to the regional fire emissions, the long-range transport of biomass burning from Africa contributes to the Amazonian aerosol population. Using a broad set of ground-based and aircraft measurements, this dissertation presents one of the most comprehensive characterization of the occurrence and properties of biomass burning aerosols over the Amazon Basin. Although episodes of long-range transport of African smoke across the Atlantic Ocean and over South America has been documented before, this work provides the first quantitative and comprehensive assessment of the African aerosol burden over the Amazon Basin.

Among the large spectrum of measurements presented here, a major finding of this PhD project relates to distinct differences in the rBC microphysical properties between comparatively fresh South American and highly aged African biomass burning smoke. Specifically, the African rBC cores were found to be significantly larger and their mass size distribution narrower than the South American rBC cores. These trends were first observed with aircraft measurements and were found to be consistent with ground-based measurements at ATTO. Based on this finding, a classification scheme for discriminating South American and African smoke influences over Amazonia was introduced. The method was successfully applied over two years period of continuous SP2 measurements at ATTO and validated using satellite data and global model BC simulations. The African BB is present most of the year, accounting up to 90 % of the BC burden in the wet season and up to 60 % in the dry season.

The variability in BC microphysical properties and mixing state directly affect the way an aerosol population interacts with the radiation. Overall, the BC particles within biomass burning plumes were found to be coated, with the South American BC exhibiting, on average, thicker coatings than the African BC. The coatings on the BC cores lead to more absorption per unit of BC mass, resulting in enhanced BC absorption by a factor of 1.9 and 1.3 in South American and African plumes, respectively. Further, stronger absorption at shorter wavelengths was observed within South American plumes, as expressed by larger AAE, indicating the presence of BrC. The presence of BC and/or BrC in both types of biomass burning plumes cause a decrease in SSA at 637 nm in comparison with the pristine values of 0.92 over the Amazon. The African smoke population is much more absorbing, yielding a SSA at 637 nm of 0.77, which is lower than the SSA of 0.86 obtained in South American plumes. The low albedo is related to the fact that African plumes contains more BC relative to total particles, both in terms of mass and number concentrations.

Finally, this dissertation explores the importance of the different biomass burning sources in supplying cloud condensation nuclei particles to the Amazon Basin. A linear relationship between BC and CCN was obtained, with characteristic slope for the different BB plumes. The African biomass burning presents the lowest CCN to BC ratio (between 1 – 2 CCN per BC particle) while this ratio is about 5 times larger in South American plumes, suggesting that they influence cloud formation and cloud properties differently. Remarkably, the characteristic CCN to BC ratio in all African BB observations was very stable in spite of being probed at the diverse locations and

atmospheric aging times. Therefore, it appears to be unaffected by the horizontal transport in the free troposphere over the Atlantic, or by the downward transport deep into the Amazonian boundary layer.

Future research perspectives

This dissertation shows that the microphysics of BC particles can be an useful parameter to track biomass burning plumes and discriminate them upon mixing with additional sources. The deconvolution method introduced here was shown to be robust approach to apportion BC over the Amazon Basin and has the potential to be used beyond. In view of the increase in frequency and intensity of biomass burning events worldwide, exploring the potential of these approach in further environments represents an interesting direction of research.

Furthermore, the new insights obtained into the life cycle of biomass burning aerosols in the Amazonian atmosphere as well as the extended data sets presented in this dissertation are a basis for targeted follow-up model studies to address important open questions. This relates, for instance, to the radiative affects of aerosol-radiation and aerosol-cloud interactions of South American smoke, on the one hand, and African smoke, on the other. Further, the data allows to validate essential processes in global models, such as the accurate description of the long-range transport of African aerosols across the Atlantic.

Bibliography

Ackerman, A. S.; Toon, O. B.; Taylor, J. P.; Johnson, D. W.; Hobbs, P. V., and Ferek, R. J.: "Effects of aerosols on cloud albedo: evaluation of twomey's parameterization of cloud susceptibility using measurements of ship tracks". *Journal of the Atmospheric Sciences*, 57, 16. (2000), pp. 2684 –2695. DOI: 10.1175/1520-0469(2000)057<2684:EOAOCA>2.0.CO;2. URL: https://journals.ametsoc.org/view/journals/atsc/57/16/1520-0469_2000_057_2684_eoaoca_2.0.co_2.xml.

Adebiyi, A. A. and Zuidema, P.: "The role of the southern African easterly jet in modifying the southeast Atlantic aerosol and cloud environments". *Quarterly Journal of the Royal Meteorological Society*, 142, 697. (2016), pp. 1574–1589. DOI: 10.1002/qj.2765.

Andreae, M. O.: "Correlation between cloud condensation nuclei concentration and aerosol optical thickness in remote and polluted regions". *Atmospheric Chemistry and Physics*, 9, 2. (2009), pp. 543–556. DOI: 10.5194/acp-9-543-2009. URL: https://acp.copernicus.org/articles/9/543/2009/.

Andreae, M. O.: "Emission of trace gases and aerosols from biomass burning – an updated assessment". *Atmospheric Chemistry and Physics*, 19, 13. (2019), pp. 8523–8546. DOI: 10.5194/acp-19-8523-2019. URL: https://acp.copernicus.org/articles/19/8523/2019/.

Andreae, M. O.; Acevedo, O. C.; Araùjo, A.; Artaxo, P.; Barbosa, C. G.; Barbosa, H. M.; Brito, J.; Carbone, S.; Chi, X.; Cintra, B. B.; Da Silva, N. F.; Dias, N. L.; Dias-Júnior, C. Q.; Ditas, F.; Ditz, R.; Godoi, A. F.; Godoi, R. H.; Heimann, M.; Hoffmann, T.; Kesselmeier, J.; Könemann, T.; Krüger, M. L.; Lavric, J. V.; Manzi, A. O.; Lopes, A. P.; Martins, D. L.; Mikhailov, E. F.; Moran-Zuloaga, D.; Nelson, B. W.; Nölscher, A. C.; Santos Nogueira, D.; Piedade, M. T.; Pöhlker, C.; Pöschl, U.; Quesada, C. A.; Rizzo, L. V.; Ro, C. U.; Ruckteschler, N.; Sá, L. D.; De Oliveira Sá, M.; Sales, C. B.; Dos Santos, R. M.; Saturno, J.; Schöngart, J.; Sörgel, M.; De Souza, C. M.; De Souza, R. A.; Su, H.; Targhetta, N.; Tóta, J.; Trebs, I.; Trumbore, S.; Van Eijck, A.; Walter, D.; Wang, Z.; Weber, B.; Williams, J.; Winderlich, J.; Wittmann, F.; Wolff, S., and Yáñez-Serrano, A. M.: "The Amazon Tall Tower Observatory (ATTO): Overview of pilot measurements on ecosystem ecology, meteorology, trace gases, and aerosols". *Atmospheric Chemistry and Physics*, 15, 18. (2015), pp. 10723–10776. DOI: 10.5194/acp-15-10723-2015.

Andreae, M. O.; Afchine, A.; Albrecht, R.; Holanda, B. A.; Artaxo, P.; Barbosa, H. M. J.; Borrmann, S.; Cecchini, M. A.; Costa, A.; Dollner, M.; Fütterer, D.; Järvinen, E.; Jurkat, T.; Klimach, T.; Konemann, T.; Knote, C.; Krämer, M.; Krisna, T.; Machado, L. A. T.; Mertes, S.; Minikin, A.; Pöhlker, C.; Pöhlker, M. L.; Pöschl, U.; Rosenfeld,

D.; Sauer, D.; Schlager, H.; Schnaiter, M.; Schneider, J.; Schulz, C.; Spanu, A.; Sperling, V. B.; Voigt, C.; Walser, A.; Wang, J.; Weinzierl, B.; Wendisch, M., and Ziereis, H.: "Aerosol characteristics and particle production in the upper troposphere over the amazon basin". *Atmospheric Chemistry and Physics*, 18, 2. (2018), pp. 921–961. DOI: 10.5194/acp-18-921-2018. URL: https://acp.copernicus.org/articles/18/921/2018/.

Andreae, M. O.; Artaxo, P.; Beck, V.; Bela, M.; Freitas, S.; Gerbig, C.; Longo, K.; Munger, J. W.; Wiedemann, K. T., and Wofsy, S. C.: "Carbon monoxide and related trace gases and aerosols over the Amazon Basin during the wet and dry seasons". *Atmospheric Chemistry and Physics*, 12, 13. (2012), pp. 6041–6065. DOI: 10.5194/acp-12-6041-2012. URL: https://www.atmos-chem-phys.net/12/6041/2012/.

Andreae, M. O. and Gelencsér, A.: "Black carbon or brown carbon? The nature of light-absorbing carbonaceous aerosols". *Atmospheric Chemistry and Physics*, 6, 10. (2006), pp. 3131–3148. DOI: 10.5194/acp-6-3131-2006. URL: http://www.atmos-chem-phys.net/6/3131/2006/.

Andreae, M. O. and Ramanathan, V.: "Climate's Dark Forcings". *Science*, 340, 6130. (2013), pp. 280–281. DOI: 10.1126/science.1235731. URL: http://www.sciencemag.org/cgi/doi/10.1126/science.1235731.

Andreae, M. O.: "Aerosols before pollution". *Science*, 315, 5808. (2007), pp. 50–51. DOI: 10.1126/science.1136529. eprint: https://science.sciencemag.org/content/315/5808/50.full.pdf. URL: https://science.sciencemag.org/content/315/5808/50.

Andreae, M. O. and Crutzen, P. J.: "Atmospheric aerosols: biogeochemical sources and role in atmospheric chemistry". *Science*, 276, 5315. (1997), pp. 1052–1058. DOI: 10.1126/science.276.5315.1052. eprint: https://science.sciencemag.org/content/276/5315/1052.full.pdf. URL: https://science.sciencemag.org/content/276/5315/1052.

Andreae, M. and Rosenfeld, D.: "Aerosol–cloud–precipitation interactions. Part 1. The nature and sources of cloud-active aerosols". *Earth-Science Reviews*, 89, 1-2. (2008), pp. 13–41. DOI: 10.1016/j.earscirev.2008.03.001. URL: http://linkinghub.elsevier.com/retrieve/pii/S0012825208000317.

Andrés Hernández, M. D.; Hilboll, A.; Ziereis, H.; Förster, E.; Krüger, O. O.; Kaiser, K.; Schneider, J.; Barnaba, F.; Vrekoussis, M.; Schmidt, J.; Huntrieser, H.; Blechschmidt, A.-M.; George, M.; Nenakhov, V.; Klausner, T.; Holanda, B. A.; Wolf, J.; Eirenschmalz, L.; Krebsbach, M.; Pöhlker, M. L.; Hedegaard, A. B.; Mei, L.; Pfeilsticker, K.; Liu, Y.; Koppmann, R.; Schlager, H.; Bohn, B.; Schumann, U.; Richter, A.; Schreiner, B.; Sauer, D.; Baumann, R.; Mertens, M.; Jöckel, P.; Kilian, M.; Stratmann, G.; Pöhlker, C.; Campanelli, M.; Pandolfi, M.; Sicard, M.; Gomez-Amo, J. L.; Pujadas, M.; Bigge, K.; Kluge, F.; Schwarz, A.; Daskalakis, N.; Walter, D.; Zahn, A.; Pöschl, U.; Bönisch, H.; Borrmann, S.; Platt, U., and Burrows, J. P.: "Overview: on the transport and transformation of pollutants in the outflow of major population centres – observational data from the emerge european intensive operational period in summer 2017". *Atmospheric Chemistry and Physics Discussions*, 2021. (2021), pp. 1–81. DOI: 10.5194/acp-2021-500. URL: https://acp.copernicus.org/preprints/acp-2021-500/.

Artaxo, P.: "Working together for amazonia". *Science*, 363, 6425. (2019), pp. 323–323. DOI: 10.1126/science.aaw6986. eprint: https://science.sciencemag.org/content/363/6425/323.full.pdf. URL: https://science.sciencemag.org/content/363/6425/323.

Artaxo, P.; Rizzo, L. V.; Brito, J. F.; Barbosa, H. M. J.; Arana, A.; Sena, E. T.; Cirino, G. G.; Bastos, W.; Martin, S. T., and Andreae, M. O.: "Atmospheric aerosols in Amazonia and land use change: from natural biogenic to biomass burning conditions". *Faraday Discussions*, 165. (2013), p. 203. DOI: 10.1039/c3fd00052d. URL: http://xlink.rsc.org/?DOI=c3fd00052d.

Baars, H.; Ansmann, A.; Althausen, D.; Engelmann, R.; Artaxo, P.; Pauliquevis, T., and Souza, R.: "Further evidence for significant smoke transport from africa to amazonia". *Geophysical Research Letters*, 38. (2011), p. L20802. DOI: L2080210.1029/2011gl049200. URL: <GotoISI>://WOS:000296157100002.

Baars, H.; Ansmann, A.; Althausen, D.; Engelmann, R.; Heese, B.; Mller, D.; Artaxo, P.; Paixao, M.; Pauliquevis, T., and Souza, R.: "Aerosol profiling with lidar in the Amazon Basin during the wet and dry season". *Journal of Geophysical Research Atmospheres*, 117, 21. (2012), pp. 1–16. DOI: 10.1029/2012JD018338.

Barkley, A. E.; Prospero, J. M.; Mahowald, N.; Hamilton, D. S.; Popendorf, K. J.; Oehlert, A. M.; Pourmand, A.; Gatineau, A.; Panechou-Pulcherie, K.; Blackwelder, P., and Gaston, C. J.: "African biomass burning is a substantial source of phosphorus deposition to the Amazon, Tropical Atlantic Ocean, and Southern Ocean". *Proceedings of the National Academy of Sciences*, 116, 33. (2019), pp. 16216–16221. DOI: 10.1073/pnas.1906091116. URL: http://www.pnas.org/lookup/doi/10.1073/pnas.1906091116.

Bohren, C. F. and Huffman, D. R.: "Frontmatter". In: *Absorption and Scattering of Light by Small Particles*. John Wiley & Sons, Ltd, 1998. ISBN: 9783527618156. DOI: https://doi.org/10.1002/9783527618156.fmatter. eprint: https://onlinelibrary.wiley.com/doi/pdf/10.1002/9783527618156. URL: https://onlinelibrary.wiley.com/doi/abs/10.1002/9783527618156.

Bond, T. C.; Doherty, S. J.; Fahey, D. W.; Forster, P. M.; Berntsen, T.; Deangelo, B. J.; Flanner, M. G.; Ghan, S.; Kärcher, B.; Koch, D.; Kinne, S.; Kondo, Y.; Quinn, P. K.; Sarofim, M. C.; Schultz, M. G.; Schulz, M.; Venkataraman, C.; Zhang, H.; Zhang, S.; Bellouin, N.; Guttikunda, S. K.; Hopke, P. K.; Jacobson, M. Z.; Kaiser, J. W.; Klimont, Z.; Lohmann, U.; Schwarz, J. P.; Shindell, D.; Storelvmo, T.; Warren, S. G., and Zender, C. S.: "Bounding the role of black carbon in the climate system: A scientific assessment". *Journal of Geophysical Research Atmospheres*, 118, 11. (2013), pp. 5380–5552. DOI: 10.1002/jgrd.50171. arXiv: arXiv:1011.1669v3.

Botía, S.; Gerbig, C.; Marshall, J.; Lavric, J. V.; Walter, D.; Pöhlker, C.; Holanda, B.; Fisch, G.; Araújo, A. C. de; Sá, M. O.; Teixeira, P. R.; Resende, A. F.; Dias-Junior, C. Q.; Asperen, H. van; Oliveira, P. S.; Stefanello, M., and Acevedo, O. C.: "Understanding nighttime methane signals at the amazon tall tower observatory (atto)". *Atmos. Chem. Phys.*, 20, 11. (2020), pp. 6583–6606. DOI: 10.5194/acp-20-6583-2020. URL: https://acp.copernicus.org/articles/20/6583/2020/.

Boucher, O.; Randall, D.; Artaxo, P.; Bretherton, C.; Feingold, G.; Forster, P.; Kerminen, V.-M.; Kondo, Y.; Liao, H.; Lohmann, U.; Rasch, P.; Satheesh, S.; Sherwood, S.; Stevens, B., and Zhang, X.: "Clouds and aerosols". In: *Climate Change 2013: The Physical Science Basis. Contribution of Working Group I to the Fifth Assessment Report of the Intergovernmental Panel on Climate Change*. Ed. by T. Stocker; D. Qin; G.-K. Plattner; M. Tignor; S. Allen; J. Boschung; A. Nauels; Y. Xia; V. Bex, and P. Midgley. Cambridge, United Kingdom and New York, NY, USA: Cambridge University Press, 2013. Chap. 7, 571–658. ISBN: ISBN 978-1-107-66182-0. DOI: 10.1017/CBO9781107415324.016. URL: www.climatechange2013.org.

Cappa, C. D.; Onasch, T. B.; Massoli, P.; Worsnop, D. R.; Bates, T. S.; Cross, E. S.; Davidovits, P.; Hakala, J.; Hayden, K. L.; Jobson, B. T.; Kolesar, K. R.; Lack, D. A.; Lerner, B. M.; Li, S.-M.; Mellon, D.; Nuaaman, I.; Olfert, J. S.; Petaja, T.; Quinn, P. K.; Song, C.; Subramanian, R.; Williams, E. J., and Zaveri, R. A.: "Radiative Absorption Enhancements Due to the Mixing State of Atmospheric Black Carbon". *Science*, 337, 6098. (2012), pp. 1078–1081. DOI: 10.1126/science.1223447. arXiv: arXiv:1011.1669v3. URL: http://www.sciencemag.org/cgi/doi/10.1126/science.1223447.

Carslaw, K. S.; Gordon, H.; Hamilton, D. S.; Johnson, J. S.; Regayre, L. A.; Yoshioka, M., and Pringle, K. J.: "Aerosols in the pre-industrial atmosphere". *Current Climate Change Reports*, 3, 1. (2017), pp. 1–15. DOI: 10.1007/s40641-017-0061-2. URL: https://doi.org/10.1007/s40641-017-0061-2.

Carter, T. S.; Heald, C. L.; Cappa, C. D.; Kroll, J. H.; Campos, T. L.; Coe, H.; Cotterell, M. I.; Davies, N. W.; Farmer, D. K.; Fox, C.; Garofalo, L. A.; Hu, L.; Langridge, J. M.; Levin, E. J. T.; Murphy, S. M.; Pokhrel, R. P.; Shen, Y.; Szpek, K.; Taylor, J. W., and Wu, H.: "Investigating carbonaceous aerosol and its absorption properties from fires in the western united states (we-can) and southern africa (oracles and clarify)". *Journal of Geophysical Research: Atmospheres*, 126, 15. (2021). e2021JD034984 2021JD034984, e2021JD034984. DOI: https://doi.org/10.1029/2021JD034984. eprint: https://agupubs.onlinelibrary.wiley.com/doi/pdf/10.1029/2021JD034984. URL: https://agupubs.onlinelibrary.wiley.com/doi/abs/10.1029/2021JD034984.

Crutzen, P. J.: *The Anthropocene*. Ed. by E. E. and K. T. Berlin, Heidelberg: Earth System Science in the Anthropocene. Springer, 2006. URL: https://doi.org/10.1007/3-540-26590-2_3.

Davidson, E. A.; Araujo, A. C. de; Artaxo, P.; Balch, J. K.; Brown, I. F.; Bustamante, M. M. C.; Coe, M. T.; DeFries, R. S.; Keller, M.; Longo, M.; Munger, J. W.; Schroeder, W.; Soares-Filho, B. S.; Souza Carlos M., J., and Wofsy, S. C.: "The amazon basin in transition". *Nature*, 481, 7381. (2012), pp. 321–328. DOI: 10.1038/nature10717. URL: <GotoISI>://WOS:000299210600034.

Després, V.; Huffman, J.; Burrows, S. M.; Hoose, C.; Safatov, A.; Buryak, G.; Fröhlich-Nowoisky, J.; Elbert, W.; Andreae, M.; Pöschl, U., and Jaenicke, R.: "Primary biological aerosol particles in the atmosphere: a review". *Tellus B: Chemical and Physical Meteorology*, 64, 1. (2012), p. 15598. DOI: 10.3402/tellusb.v64i0.15598. eprint: https://doi.org/10.3402/tellusb.v64i0.15598. URL: https://doi.org/10.3402/tellusb.v64i0.15598.

Ditas, J.; Ma, N.; Zhang, Y.; Assmann, D.; Neumaier, M.; Riede, H., and Karu, E.: "Strong impact of wildfires on the abundance and aging of black carbon in the lowermost stratosphere". September 2011. (2018). DOI: 10.1073/pnas.1806868115.

Escobar, H.: "Deforestation in the brazilian amazon is still rising sharply". *Science*, 369, 6504. (2020), pp. 613–613. URL: <GotoISI>://WOS:000559184400018.

Fierce, L.; Riemer, N., and Bond, T. C.: "Explaining variance in black carbon's aging timescale". *Atmospheric Chemistry and Physics*, 15, 6. (2015), pp. 3173–3191. DOI: 10.5194/acp-15-3173-2015. URL: https://acp.copernicus.org/articles/15/3173/2015/.

Fröhlich-Nowoisky, J.; Kampf, C. J.; Weber, B.; Huffman, J. A.; Pöhlker, C.; Andreae, M. O.; Lang-Yona, N.; Burrows, S. M.; Gunthe, S. S.; Elbert, W.; Su, H.; Hoor, P.; Thines, E.; Hoffmann, T.; Després, V. R., and Pöschl, U.: "Bioaerosols in the earth system: climate, health, and ecosystem interactions". *Atmospheric Research*, 182. (2016), pp. 346–376. DOI: https://doi.org/10.1016/j.atmosres.2016.07.018. URL: https://www.sciencedirect.com/science/article/pii/S0169809516301995.

Fuller, K. A.; Malm, W. C., and Kreidenweis, S. M.: "Effects of mixing on extinction by carbonaceous particles". *Journal of Geophysical Research: Atmospheres*, 104, D13. (1999), pp. 15941–15954. DOI: 10.1029/1998JD100069. URL: http://doi.wiley.com/10.1029/1998JD100069.

Gao, R. S.; Schwarz, J. P.; Kelly, K. K.; Fahey, D. W.; Watts, L. a.; Thompson, T. L.; Spackman, J. R.; Slowik, J. G.; Cross, E. S.; Han, J.-H.; Davidovits, P.; Onasch, T. B., and Worsnop, D. R.: "A Novel Method for Estimating Light-Scattering Properties of Soot Aerosols Using a Modified Single-Particle Soot Photometer". *Aerosol Science and Technology*, 41, 2. (2007), pp. 125–135. DOI: 10.1080/02786820601118398. URL: http://www.tandfonline.com/doi/abs/10.1080/02786820601118398.

Hallquist, M.; Wenger, J. C.; Baltensperger, U.; Rudich, Y.; Simpson, D.; Claeys, M.; Dommen, J.; Donahue, N. M.; George, C.; Goldstein, A. H.; Hamilton, J. F.; Herrmann, H.; Hoffmann, T.; Iinuma, Y.; Jang, M.; Jenkin, M. E.; Jimenez, J. L.; Kiendler-Scharr, A.; Maenhaut, W.; McFiggans, G.; Mentel, T. F.; Monod, A.; Prévôt, A. S. H.; Seinfeld, J. H.; Surratt, J. D.; Szmigielski, R., and Wildt, J.: "The formation, properties and impact of secondary organic aerosol: current and emerging issues". *Atmospheric Chemistry and Physics*, 9, 14. (2009), pp. 5155–5236. DOI: 10.5194/acp-9-5155-2009. URL: https://acp.copernicus.org/articles/9/5155/2009/.

Hansen, J. E. and Travis, L. D.: "Light scattering in planetary atmospheres". *Space Science Reviews*, 16, 4. (1974), pp. 527–610. DOI: 10.1007/BF00168069. URL: https://doi.org/10.1007/BF00168069.

Holanda, B. A.; Pöhlker, M. L.; Walter, D.; Saturno, J.; Sörgel, M.; Ditas, J.; Ditas, F.; Schulz, C.; Franco, M. A.; Wang, Q.; Donth, T.; Artaxo, P.; Barbosa, H. M. J.; Borrmann, S.; Braga, R.; Brito, J.; Cheng, Y.; Dollner, M.; Kaiser, J. W.; Klimach, T.; Knote, C.; Krüger, O. O.; Fütterer, D.; Lavrič, J. V.; Ma, N.; Machado, L. A. T.; Ming, J.; Morais, F. G.; Paulsen, H.; Sauer, D.; Schlager, H.; Schneider, J.; Su, H.; Weinzierl, B.; Walser, A.; Wendisch, M.; Ziereis, H.; Zöger, M.; Pöschl, U.; Andreae, M. O., and Pöhlker, C.: "Influx of african biomass burning aerosol during the amazonian dry season through layered transatlantic transport of black carbon-

rich smoke". *Atmos. Chem. Phys.*, 20, 8. (2020), pp. 4757–4785. DOI: 10.5194/acp-20-4757-2020. URL: https://www.atmos-chem-phys.net/20/4757/2020/.

Holanda, B. A.; Franco, M. A.; Walter, D.; Andreae, M. O.; Artaxo, P.; Carbone, S.; Cheng, Y.; Chowdhury, S.; Ditas, F.; Gysel-beer, M.; Klimach, T.; Kremper, L. A.; Krüger, O. O.; Lavric, J. V.; Lelieveld, J.; Ma, C.; Machado, L. A. T.; Morais, F. G.; Modini, R. L.; Pozzer, A.; Saturno, J.; Su, H.; Wendisch, M.; Wolff, S.; Pöhlker, M. L.; Pöschl, U., and Pöhlker, C.: "African smoke over the Amazon rain forest". to be submitted. 2021.

Kulmala, M.: "How particles nucleate and grow". *Science*, 302, 5647. (2003), pp. 1000–1001. DOI: 10.1126/science.1090848. URL: <GotoISI>://WOS:000186396300034.

Laj, P. et al.: "A global analysis of climate-relevant aerosol properties retrieved from the network of global atmosphere watch (gaw) near-surface observatories". *Atmospheric Measurement Techniques*, 13, 8. (2020), pp. 4353–4392. DOI: 10.5194/amt-13-4353-2020. URL: https://amt.copernicus.org/articles/13/4353/2020/.

Laurance, W. F.; Goosem, M., and Laurance, S. G. W.: "Impacts of roads and linear clearings on tropical forests". *Trends in Ecology & Evolution*, 24, 12. (2009), pp. 659–669. DOI: 10.1016/j.tree.2009.06.009. URL: <GotoISI>://WOS:000272278000004.

Lelieveld, J.; Klingmueller, K.; Pozzer, A.; Poeschl, U.; Fnais, M.; Daiber, A., and Muenzel, T.: "Cardiovascular disease burden from ambient air pollution in Europe reassessed using novel hazard ratio functions". *Eur Heart J*, 40, 20. (2019), pp. 1590–1596. DOI: 10.1093/eurheartj/ehz135.

Lenton, T. M.; Held, H.; Kriegler, E.; Hall, J. W.; Lucht, W.; Rahmstorf, S., and Schellnhuber, H. J.: "Tipping elements in the earth's climate system". *Proceedings of the National Academy of Sciences*, 105, 6. (2008), pp. 1786–1793. DOI: 10.1073/pnas.0705414105. eprint: https://www.pnas.org/content/105/6/1786.full.pdf. URL: https://www.pnas.org/content/105/6/1786.

Liu, D.; Allan, J.; Whitehead, J.; Young, D.; Flynn, M.; Coe, H.; McFiggans, G.; Fleming, Z. L., and Bandy, B.: "Ambient black carbon particle hygroscopic properties controlled by mixing state and composition". *Atmospheric Chemistry and Physics*, 13, 4. (2013), pp. 2015–2029. DOI: 10.5194/acp-13-2015-2013. URL: https://acp.copernicus.org/articles/13/2015/2013/.

Lobert, J. M. and Wamatz, J.: "Emissions from the combustion process in vegetation". In: *Fire in the Environment: The Ecological, Atmospheric and Climatic Importance of Vegetation Fires*. Ed. by P. J. Crutzen and J. G. Goldammer. New York: John Wiley, 1993, pp. 15–37.

Lund, M. T.; Samset, B. H.; Skeie, R. B.; Watson-Parris, D.; Katich, J. M.; Schwarz, J. P., and Weinzierl, B.: "Short Black Carbon lifetime inferred from a global set of aircraft observations". *npj Climate and Atmospheric Science*, 1, 1. (2018), pp. 1–8. DOI: 10.1038/s41612-018-0040-x. URL: http://dx.doi.org/10.1038/s41612-018-0040-x.

Löbs, N.; Barbosa, C. G. G.; Brill, S.; Walter, D.; Ditas, F.; Oliveira Sá, M. de; Araújo, A. C. de; Oliveira, L. R. de; Godoi, R. H. M.; Wolff, S.; Piepenbring, M.; Kesselmeier, J.; Artaxo, P.; Andreae, M. O.; Pöschl, U.; Pöhlker, C., and Weber, B.: "Aerosol measurement methods to quantify spore emissions from fungi and cryptogamic covers in the amazon". *Atmos. Meas. Tech.*, 13, 1. (2020), pp. 153–164. DOI: 10.5194/amt-13-153-2020. URL: https://www.atmos-meas-tech.net/13/153/2020/.

Machado, L. A. T.; Calheiros, A. J. P.; Biscaro, T.; Giangrande, S.; Silva Dias, M. A. F.; Cecchini, M. A.; Albrecht, R.; Andreae, M. O.; Araujo, W. F.; Arttaxo, P.; Borrmann, S.; Braga, R.; Burleyson, C.; Eichholz, C. W.; Fan, J.; Feng, Z.; Fisch, G. F.; Jensen, M. P.; Martin, S. T.; Pöschl, U.; Pöhlker, C.; Pöhlker, M. L.; Ribaud, J.-F.; Rosenfeld, D.; Saraiva, J. M. B.; Schumacher, C.; Thalman, R.; Walter, D., and Wendisch, M.: "Overview: Precipitation Characteristics and Sensitivities to the Environmental Conditions during GoAmazon2014/5 and ACRIDICON-CHUVA". *Atmospheric Chemistry and Physics Discussions*. (2017), pp. 1–41. DOI: 10.5194/acp-2017-990. URL: https://www.atmos-chem-phys-discuss.net/acp-2017-990/.

Martin, S. T.; Andreae, M. O.; Artaxo, P.; Baumgardner, D.; Chen, Q.; Goldstein, A. H.; Guenther, A.; Heald, C. L.; Mayol-Bracero, O. L.; McMurry, P. H.; Pauliquevis, T.; Pöschl, U.; Prather, K. A.; Roberts, G. C.; Saleska, S. R.; Silva Dias, M. A.; Spracklen, D. V.; Swietlicki, E., and Trebs, I.: "Sources and properties of Amazonian aerosol particles". *Reviews of Geophysics*, 48, 2. (2010), RG2002. DOI: 10.1029/2008RG000280. URL: http://doi.wiley.com/10.1029/2008RG000280.

Monastersky, R.: "Anthropocene: the human age". *Nature*, 519, 7542. (2015), pp. 144–147. DOI: 10.1038/519144a. URL: https://doi.org/10.1038/519144a.

Moran-Zuloaga, D.; Ditas, F.; Walter, D.; Saturno, J.; Brito, J.; Carbone, S.; Chi, X.; Angelis, I. Hrabě de; Baars, H.; Godoi, R. H. M.; Heese, B.; Holanda, B. A.; Lavrič, J. V.; Martin, S. T.; Ming, J.; Pöhlker, M. L.; Ruckteschler, N.; Su, H.; Wang, Y.; Wang, Q.; Wang, Z.; Weber, B.; Wolff, S.; Artaxo, P.; Pöschl, U.; Andreae, M. O., and Pöhlker, C.: "Long-term study on coarse mode aerosols in the amazon rain forest with the frequent intrusion of saharan dust plumes". *Atmos. Chem. Phys.*, 18, 13. (2018), pp. 10055–10088. DOI: 10.5194/acp-18-10055-2018. URL: https://www.atmos-chem-phys.net/18/10055/2018/.

Moteki, N. and Kondo, Y.: "Effects of mixing state on black carbon measurements by laser-induced incandescence". *Aerosol Science and Technology*, 41, 4. (2007), pp. 398–417. DOI: 10.1080/02786820701199728. eprint: https://doi.org/10.1080/02786820701199728. URL: https://doi.org/10.1080/02786820701199728.

Mülmenstädt, J and Feingold, G: "The radiative forcing of aerosol–cloud interactions in liquid clouds: wrestling and embracing uncertainty". *Current Climate Change Reports*, 4, 1. (2018), pp. 23–40. DOI: 10.1007/s40641-018-0089-y. URL: https://doi.org/10.1007/s40641-018-0089-y.

Naik, V.; Szopa, S.; Adhikary, B.; Artaxo, P.; Berntsen, T.; Collins, W. D.; Fuzzi, S.; Gallardo, L.; Kiendler Scharr, A.; Klimont, Z.; Liao, H.; Unger, N., and Zanis, P.: *Climate Change 2021: The Physical Science Basis. Contribution of Working Group I to the Sixth Assessment Report of the Intergovernmental Panel on Climate Change*. Ed. by V. Masson-Delmotte; P. Zhai; A. Pirani; S. L. Connors; C. Péan; S. Berger; N. Caud; Y. Chen; L. Goldfarb; M. I. Gomis; M. Huang; K. Leitzell; E. Lonnoy; J. B. R. Matthews; T. K. Maycock; T. Waterfield; O. Yelekçi; R. Yu, and B. Zhou. Cambridge University Press, 2021. In Press.

Ohneiser, K.; Ansmann, A.; Baars, H.; Seifert, P.; Barja, B.; Jimenez, C.; Radenz, M.; Teisseire, A.; Floutsi, A.; Haarig, M.; Foth, A.; Chudnovsky, A.; Engelmann, R.; Zamorano, F.; Bühl, J., and Wandinger, U.: "Smoke of extreme australian bushfires observed in the stratosphere over punta arenas, chile, in january 2020: optical thickness, lidar ratios, and depolarization ratios at 355 and 532.1667emnm". *Atmospheric Chemistry and Physics*, 20, 13. (2020), pp. 8003–8015. DOI: 10.5194/acp-20-8003-2020. URL: https://acp.copernicus.org/articles/20/8003/2020/.

Patrick Arnott, W.; Moosmüller, H.; Fred Rogers, C.; Jin, T., and Bruch, R.: "Photoacoustic spectrometer for measuring light absorption by aerosol: instrument description". *Atmospheric Environment*, 33, 17. (1999), pp. 2845–2852. DOI: https://doi.org/10.1016/S1352-2310(98)00361-6. URL: https://www.sciencedirect.com/science/article/pii/S1352231098003616.

Pileci, R. E.; Modini, R. L.; Bertò, M.; Yuan, J.; Corbin, J. C.; Marinoni, A.; Henzing, B.; Moerman, M. M.; Putaud, J. P.; Spindler, G.; Wehner, B.; Müller, T.; Tuch, T.; Trentini, A.; Zanatta, M.; Baltensperger, U., and Gysel-Beer, M.: "Comparison of colocated refractory black carbon (rbc) and elemental carbon (ec) mass concentration measurements during field campaigns at several european sites". *Atmospheric Measurement Techniques*, 14, 2. (2021), pp. 1379–1403. DOI: 10.5194/amt-14-1379-2021. URL: https://amt.copernicus.org/articles/14/1379/2021/.

Pöschl, U.: "Atmospheric aerosols: Composition, transformation, climate and health effects". *Angewandte Chemie - International Edition*, 44, 46. (2005), pp. 7520–7540. DOI: 10.1002/anie.200501122.

Pöschl, U. and Shiraiwa, M.: "Multiphase chemistry at the atmosphere–biosphere interface influencing climate and public health in the anthropocene". *Chemical Reviews*, 115, 10. (2015). PMID: 25856774, pp. 4440–4475. DOI: 10.1021/cr500487s. eprint: https://doi.org/10.1021/cr500487s. URL: https://doi.org/10.1021/cr500487s.

Pöhlker, C.; Walter, D.; Paulsen, H.; Könemann, T.; Rodríguez-Caballero, E.; Moran-Zuloaga, D.; Brito, J.; Carbone, S.; Degrendele, C.; Després, V. R.; Ditas, F.; Holanda, B. A.; Kaiser, J. W.; Lammel, G.; Lavrič, J. V.; Ming, J.; Pickersgill, D.; Pöhlker, M. L.; Praß, M.; Löbs, N.; Saturno, J.; Sörgel, M.; Wang, Q.; Weber, B.; Wolff, S.; Artaxo, P.; Pöschl, U., and Andreae, M. O.: "Land cover and its transformation in the backward trajectory footprint region of the amazon tall tower observatory". *Atmos. Chem. Phys.*, 19, 13. (2019), pp. 8425–8470. DOI: 10.5194/acp-19-8425-2019. URL: https://www.atmos-chem-phys.net/19/8425/2019/.

Pöhlker, C.; Wiedemann, K. T.; Sinha, B.; Shiraiwa, M.; Gunthe, S. S.; Smith, M.; Su, H.; Artaxo, P.; Chen, Q.; Cheng, Y. F.; Elbert, W.; Gilles, M. K.; Kilcoyne, A. L. D.; Moffet, R. C.; Weigand, M.; Martin, S. T.; Pöschl, U., and Andreae, M. O.: "Biogenic potassium salt particles as seeds for secondary organic aerosol in the amazon". *Science*, 337, 6098. (2012), pp. 1075–1078. DOI: 10.1126/science.1223264. URL: <GotoISI>://WOS:000308125800041.

Pöschl, U.; Martin, S. T.; Sinha, B.; Chen, Q.; Gunthe, S. S.; Huffman, J. A.; Borrmann, S.; Farmer, D. K.; Garland, R. M.; Helas, G.; Jimenez, J. L.; King, S. M.; Manzi, A.; Mikhailov, E.; Pauliquevis, T.; Petters, M. D.; Prenni, A. J.; Roldin, P.; Rose, D.; Schneider, J.; Su, H.; Zorn, S. R.; Artaxo, P., and Andreae, M. O.: "Rainforest aerosols as biogenic nuclei of clouds and precipitation in the amazon". *Sci-*

ence, 329, 5998. (2010), pp. 1513–1516. DOI: 10.1126/science.1191056. URL: <GotoISI>://000281869000038.

Ramanathan, V. and Carmichael, G.: "Global and regional climate changes due to black carbon". *Nature Geoscience*, 1, 4. (2008), pp. 221–227. DOI: 10.1038/ngeo156. URL: https://doi.org/10.1038/ngeo156.

Rizzo, L. V.; Artaxo, P.; Müller, T.; Wiedensohler, A.; Paixão, M.; Cirino, G. G.; Arana, A.; Swietlicki, E.; Roldin, P.; Fors, E. O.; Wiedemann, K. T.; Leal, L. S. M., and Kulmala, M.: "Long term measurements of aerosol optical properties at a primary forest site in Amazonia". *Atmospheric Chemistry and Physics*, 13, 5. (2013), pp. 2391–2413. DOI: 10.5194/acp-13-2391-2013.

Rosenfeld, D.; Andreae, M. O.; Asmi, A.; Chin, M.; Leeuw, G. de; Donovan, D. P.; Kahn, R.; Kinne, S.; Kivekas, N.; Kulmala, M.; Lau, W.; Schmidt, K. S.; Suni, T.; Wagner, T.; Wild, M., and Quaas, J.: "Global observations of aerosol-cloud-precipitation-climate interactions". *Reviews of Geophysics*, 52, 4. (2014), pp. 750–808. DOI: 10.1002/2013rg000441. URL: <GotoISI>://WOS:000348452000005.

Rosenfeld, D.; Lohmann, U.; Raga, G. B.; O'Dowd, C. D.; Kulmala, M.; Fuzzi, S.; Reissell, A., and Andreae, M. O.: "Flood or drought: how do aerosols affect precipitation?" *Science*, 321, 5894. (2008), pp. 1309–1313. DOI: 10.1126/science.1160606. URL: <GotoISI>://WOS:000258914300038.

Samset, B. H.; Myhre, G.; Schulz, M.; Balkanski, Y.; Bauer, S.; Berntsen, T. K.; Bian, H.; Bellouin, N.; Diehl, T.; Easter, R. C.; Ghan, S. J.; Iversen, T.; Kinne, S.; Kirkevåg, A.; Lamarque, J.-F.; Lin, G.; Liu, X.; Penner, J. E.; Seland, Ø.; Skeie, R. B.; Stier, P.; Takemura, T.; Tsigaridis, K., and Zhang, K.: "Black carbon vertical profiles strongly affect its radiative forcing uncertainty". *Atmospheric Chemistry and Physics*, 13, 5. (2013), pp. 2423–2434. DOI: 10.5194/acp-13-2423-2013. URL: https://acp.copernicus.org/articles/13/2423/2013/.

Saturno, J.; Ditas, F.; Vries, M. Penning de; Holanda, B. A.; Pöhlker, M. L.; Carbone, S.; Walter, D.; Bobrowski, N.; Brito, J.; Chi, X.; Gutmann, A.; Angelis, I. Hrabe de; Machado, L. A. T.; Moran-Zuloaga, D.; Rüdiger, J.; Schneider, J.; Schulz, C.; Wang, Q.; Wendisch, M.; Artaxo, P.; Wagner, T.; Pöschl, U.; Andreae, M. O., and Pöhlker, C.: "African volcanic emissions influencing atmospheric aerosols over the amazon rain forest". *Atmos. Chem. Phys.*, 18, 14. (2018), pp. 10391–10405. DOI: 10.5194/acp-18-10391-2018. URL: https://www.atmos-chem-phys.net/18/10391/2018/.

Saturno, J.; Holanda, B. A.; Pöhlker, C.; Ditas, F.; Wang, Q.; Moran-Zuloaga, D.; Brito, J.; Carbone, S.; Cheng, Y.; Chi, X.; Ditas, J.; Hoffmann, T.; Angelis, I. Hrabe de; Könemann, T.; Lavrič, J. V.; Ma, N.; Ming, J.; Paulsen, H.; Pöhlker, M. L.; Rizzo, L. V.; Schlag, P.; Su, H.; Walter, D.; Wolff, S.; Zhang, Y.; Artaxo, P.; Pöschl, U., and Andreae, M. O.: "Black and brown carbon over central amazonia: long-term aerosol measurements at the atto site". *Atmos. Chem. Phys.*, 18, 17. (2018), pp. 12817–12843. DOI: 10.5194/acp-18-12817-2018. URL: https://www.atmos-chem-phys.net/18/12817/2018/.

Schill, G. P.; Froyd, K. D.; Bian, H.; Kupc, A.; Williamson, C.; Brock, C. A.; Ray, E.; Hornbrook, R. S.; Hills, A. J.; Apel, E. C.; Chin, M.; Colarco, P. R., and Murphy, D. M.: "Widespread biomass burning smoke throughout the remote troposphere". *Nature Geoscience*, 13. (2020), pp. 422–427. DOI: 10.1038/s41561-020-0586-1. URL: https://doi.org/10.1038/s41561-020-0586-1.

Schwarz, J. P.; Spackman, J. R.; Fahey, D. W.; Gao, R. S.; Lohmann, U.; Stier, P.; Watts, L. A.; Thomson, D. S.; Lack, D. A.; Pfister, L.; Mahoney, M. J.; Baumgardner, D.; Wilson, J. C., and Reeves, J. M.: "Coatings and their enhancement of black carbon light absorption in the tropical atmosphere". *Journal of Geophysical Research Atmospheres*, 113, 3. (2008), pp. 1–10. DOI: 10.1029/2007JD009042.

Seinfeld, J. H. and Pandis, S. N.: *Atmospheric Chemistry and Physics: From Air Pollution to Climate Change*. John Wiley & Sons, Inc., 2006, p. 1232. ISBN: 9780471720188. DOI: 10.1063/1.882420.

Shinozuka, Y.; Saide, P. E.; Ferrada, G. A.; Burton, S. P.; Ferrare, R.; Doherty, S. J.; Gordon, H.; Longo, K.; Mallet, M.; Feng, Y.; Wang, Q.; Cheng, Y.; Dobracki, A.; Freitag, S.; Howell, S. G.; LeBlanc, S.; Flynn, C.; Segal-Rosenhaimer, M.; Pistone, K.; Podolske, J. R.; Stith, E. J.; Bennett, J. R.; Carmichael, G. R.; Silva, A. da; Govindaraju, R.; Leung, R.; Zhang, Y.; Pfister, L.; Ryoo, J.-M.; Redemann, J.; Wood, R., and Zuidema, P.: "Modeling the smoky troposphere of the southeast atlantic: a comparison to oracles airborne observations from september of 2016". *Atmospheric Chemistry and Physics*, 20, 19. (2020), pp. 11491–11526. DOI: 10.5194/acp-20-11491-2020. URL: https://acp.copernicus.org/articles/20/11491/2020/.

Shiraiwa, M.; Ueda, K.; Pozzer, A.; Lammel, G.; Kampf, C. J.; Fushimi, A.; Enami, S.; Arangio, A. M.; Fröhlich-Nowoisky, J.; Fujitani, Y.; Furuyama, A.; Lakey, P. S. J.; Lelieveld, J.; Lucas, K.; Morino, Y.; Pöschl, U.; Takahama, S.; Takami, A.; Tong, H.; Weber, B.; Yoshino, A., and Sato, K.: "Aerosol health effects from molecular to global scales". *Environmental Science & Technology*, 51, 23. (2017). PMID: 29111690, pp. 13545–13567. DOI: 10.1021/acs.est.7b04417. eprint: https://doi.org/10.1021/acs.est.7b04417. URL: https://doi.org/10.1021/acs.est.7b04417.

Slowik, J. G.; Cross, E. S.; Han, J.-H.; Davidovits, P.; Onasch, T. B.; Jayne, J. T.; Williams, L. R.; Canagaratna, M. R.; Worsnop, D. R.; Chakrabarty, R. K.; Moosmüller, H.; Arnott, W. P.; Schwarz, J. P.; Gao, R.-S.; Fahey, D. W.; Kok, G. L., and Petzold, A.: "An Inter-Comparison of Instruments Measuring Black Carbon Content of Soot Particles". *Aerosol Science and Technology*, 41, 3. (2007), pp. 295–314. DOI: 10.1080/02786820701197078. URL: http://www.tandfonline.com/doi/abs/10.1080/02786820701197078.

Steffen, W.; Grinevald, J.; Crutzen, P., and McNeill, J.: "The anthropocene: conceptual and historical perspectives". *Philosophical Transactions of the Royal Society A: Mathematical, Physical and Engineering Sciences*, 369, 1938. (2011), pp. 842–867. DOI: 10.1098/rsta.2010.0327. eprint: https://royalsocietypublishing.org/doi/pdf/10.1098/rsta.2010.0327. URL: https://royalsocietypublishing.org/doi/abs/10.1098/rsta.2010.0327.

Stephens, M.; Turner, N., and Sandberg, J.: "Particle identification by laser-induced incandescence in a solid-state laser cavity." *Applied optics*, 42, 19. (2003), pp. 3726–36. DOI: 10.1364/AO.42.003726. URL: http://www.ncbi.nlm.nih.gov/pubmed/12868806.

Stjern, C. W.; Samset, B. H.; Myhre, G.; Forster, P. M.; Hodnebrog, Andrews, T.; Boucher, O.; Faluvegi, G.; Iversen, T.; Kasoar, M.; Kharin, V.; Kirkevåg, A.; Lamarque, J.-F.; Olivié, D.; Richardson, T.; Shawki, D.; Shindell, D.; Smith, C. J.; Takemura, T., and Voulgarakis, A.: "Rapid adjustments cause weak surface temperature response to increased black carbon concentrations". *Journal of Geophysical*

Research: Atmospheres, 122, 21. (2017), pp. 11,462–11,481. DOI: https://doi.org/10.1002/2017JD027326. eprint: https://agupubs.onlinelibrary.wiley.com/doi/pdf/10.1002/2017JD027326. URL: https://agupubs.onlinelibrary.wiley.com/doi/abs/10.1002/2017JD027326.

Thornhill, G. D.; Collins, W. J.; Kramer, R. J.; Olivié, D.; Skeie, R. B.; O'Connor, F. M.; Abraham, N. L.; Checa-Garcia, R.; Bauer, S. E.; Deushi, M.; Emmons, L. K.; Forster, P. M.; Horowitz, L. W.; Johnson, B.; Keeble, J.; Lamarque, J.-F.; Michou, M.; Mills, M. J.; Mulcahy, J. P.; Myhre, G.; Nabat, P.; Naik, V.; Oshima, N.; Schulz, M.; Smith, C. J.; Takemura, T.; Tilmes, S.; Wu, T.; Zeng, G., and Zhang, J.: "Effective radiative forcing from emissions of reactive gases and aerosols – a multi-model comparison". *Atmospheric Chemistry and Physics*, 21, 2. (2021), pp. 853–874. DOI: 10.5194/acp-21-853-2021. URL: https://acp.copernicus.org/articles/21/853/2021/.

Twomey, S.: "Pollution and the planetary albedo". *Atmospheric Environment (1967)*, 8, 12. (1974), pp. 1251–1256. DOI: https://doi.org/10.1016/0004-6981(74)90004-3. URL: https://www.sciencedirect.com/science/article/pii/0004698174900043.

Twomey, S.: "The influence of pollution on the shortwave albedo of clouds". *Journal of Atmospheric Sciences*, 34, 7. (1977), pp. 1149 –1152. DOI: 10.1175/1520-0469(1977)034<1149:TIOPOT>2.0.CO;2. URL: https://journals.ametsoc.org/view/journals/atsc/34/7/1520-0469_1977_034_1149_tiopot_2_0_co_2.xml.

Voigt, C.; Lelieveld, J.; Schlager, H.; Schneider, J.; Curtius, J.; Meerkötter, R.; Sauer, D.; Bugliaro, L.; Bohn, B.; Crowley, J.; Erbertseder, T.; Groß, S.; Li, Q.; Mertens, M.; Pöhlker, M.; Pozzer, A.; Schumann, U.; Tomsche, L.; Williams, J.; Zahn, A.; Andreae, M.; Borrmann, M.; Bräuer, T.; Dörich, R.; Dörnbrack, A.; Edtbauer, A.; Ernle, L.; Fischer, H.; Giez, A.; Granzin, M.; Grewe, V.; Hahn, V.; Harder, H.; Heinritzi, M.; Holanda, B.; Jöckel, P.; Kaiser, K.; Krüger, O.; Lucke, J.; Marsing, A.; Martin, A.; Matthes, S.; Pöhlker, C.; Pöschl, U.; Reifenbergand, S.; Ringsdorf, A.; Scheibe, M.; Tadic, I.; Zauner-Wieczorek, M.; Henke, R., and Rapp, M.: "BLUESKY aircraft mission reveals reduction in atmospheric pollution during the 2020 Corona lockdown". *Bulletin of the American Meteorological Society, - submitted*. (2021).

Wang, Q.; Saturno, J.; Chi, X.; Walter, D.; Lavric, J. V.; Moran-Zuloaga, D.; Ditas, F.; Pöhlker, C.; Brito, J.; Carbone, S.; Artaxo, P., and Andreae, M. O.: "Modeling investigation of light-absorbing aerosols in the Amazon Basin during the wet season". *Atmospheric Chemistry and Physics*, 16, 22. (2016), pp. 14775–14794. DOI: 10.5194/acp-16-14775-2016.

Weingartner, E.; Burtscher, H., and Baltensperger, U.: "Hygroscopic properties of carbon and diesel soot particles". *Atmospheric Environment*, 31, 15. (1997), pp. 2311–2327. DOI: https://doi.org/10.1016/S1352-2310(97)00023-X. URL: https://www.sciencedirect.com/science/article/pii/S135223109700023X.

Wendisch, M.; Poschl, U.; Andreae, M. O.; MacHado, L. A.; Albrecht, R.; Schlager, H.; Rosenfeld, D.; Martin, S. T.; Abdelmonem, A.; Afchine, A.; Araujo, A. C.; Artaxo, P.; Aufmhoff, H.; Barbosa, H. M.; Borrmann, S.; Braga, R.; Buchholz, B.; Cecchini, M. A.; Costa, A.; Curtius, J.; Dollner, M.; Dorf, M.; Dreiling, V.; Ebert, V.; Ehrlich, A.; Ewald, F.; Fisch, G.; Fix, A.; Frank, F.; Futterer, D.; Heckl, C.; Heidelberg, F.; Huneke, T.; Jakel, E.; Jarvinen, E.; Jurkat, T.; Kanter, S.; Kastner, U.; Kenntner, M.; Kesselmeier, J.; Klimach, T.; Knecht, M.; Kohl, R.; Kolling, T.; Kramer, M.; Kruger,

M.; Krisna, T. C.; Lavric, J. V.; Longo, K.; Mahnke, C.; Manzi, A. O.; Mayer, B.; Mertes, S.; Minikin, A.; Molleker, S.; Munch, S.; Nillius, B.; Pfeilsticker, K.; Pohlker, C.; Roiger, A.; Rose, D.; Rosenow, D.; Sauer, D.; Schnaiter, M.; Schneider, J.; Schulz, C.; De Souza, R. A.; Spanu, A.; Stock, P.; Vila, D.; Voigt, C.; Walser, A.; Walter, D.; Weigel, R.; Weinzierl, B.; Werner, F.; Yamasoe, M. A.; Ziereis, H.; Zinner, T., and Zoger, M.: "Acridicon-chuva campaign: Studying tropical deep convective clouds and precipitation over amazonia using the New German research aircraft HALO". *Bulletin of the American Meteorological Society*, 97, 10. (2016), pp. 1885–1908. DOI: 10.1175/BAMS-D-14-00255.1.

Yuan, J.; Modini, R. L.; Zanatta, M.; Herber, A. B.; Müller, T.; Wehner, B.; Poulain, L.; Tuch, T.; Baltensperger, U., and Gysel-Beer, M.: "Variability in the mass absorption cross section of black carbon (BC) aerosols is driven by BC internal mixing state at a central European background site (Melpitz, Germany) in winter". *Atmospheric Chemistry and Physics*, 21, 2. (2021), pp. 635–655. DOI: 10.5194/acp-21-635-2021. URL: https://acp.copernicus.org/articles/21/635/2021/.

Yáñez-Serrano, A. M.; Nölscher, A. C.; Bourtsoukidis, E.; Gomes Alves, E.; Ganzeveld, L.; Bonn, B.; Wolff, S.; Sa, M.; Yamasoe, M.; Williams, J.; Andreae, M. O., and Kesselmeier, J.: "Monoterpene chemical speciation in a tropical rainforest:variation with season, height, and time of dayat the amazon tall tower observatory (atto)". *Atmos. Chem. Phys.*, 18, 5. (2018), pp. 3403–3418. DOI: 10.5194/acp-18-3403-2018. URL: https://www.atmos-chem-phys.net/18/3403/2018/.

Zhang, R.; Khalizov, A. F.; Pagels, J.; Zhang, D.; Xue, H., and McMurry, P. H.: "Variability in morphology, hygroscopicity, and optical properties of soot aerosols during atmospheric processing". *Proceedings of the National Academy of Sciences*, 105, 30. (2008), pp. 10291–10296. DOI: 10.1073/pnas.0804860105. eprint: https://www.pnas.org/content/105/30/10291.full.pdf. URL: https://www.pnas.org/content/105/30/10291.

Zuberi, B.; Johnson, K. S.; Aleks, G. K.; Molina, L. T.; Molina, M. J., and Laskin, A.: "Hydrophilic properties of aged soot". *Geophysical Research Letters*, 32, 1. (2005). DOI: https://doi.org/10.1029/2004GL021496. eprint: https://agupubs.onlinelibrary.wiley.com/doi/pdf/10.1029/2004GL021496. URL: https://agupubs.onlinelibrary.wiley.com/doi/abs/10.1029/2004GL021496.

Personal List of Publications

Holanda, B. A.; Pöhlker, M. L.; Walter, D.; Saturno, J.; Sörgel, M.; Ditas, J.; Ditas, F.; Schulz, C.; Franco, M. A.; Wang, Q.; Donth, T.; Artaxo, P.; Barbosa, H. M. J.; Borrmann, S.; Braga, R.; Brito, J.; Cheng, Y.; Dollner, M.; Kaiser, J. W.; Klimach, T.; Knote, C.; Krüger, O. O.; Fütterer, D.; Lavrič, J. V.; Ma, N.; Machado, L. A. T.; Ming, J.; Morais, F. G.; Paulsen, H.; Sauer, D.; Schlager, H.; Schneider, J.; Su, H.; Weinzierl, B.; Walser, A.; Wendisch, M.; Ziereis, H.; Zöger, M.; Pöschl, U.; Andreae, M. O., and Pöhlker, C.: "Influx of african biomass burning aerosol during the amazonian dry season through layered transatlantic transport of black carbon-rich smoke". *Atmos. Chem. Phys.*, 20, 8. (2020), pp. 4757–4785. DOI: 10.5194/acp-20-4757-2020. URL: https://www.atmos-chem-phys.net/20/4757/2020/

Holanda, Bruna A; Franco, M. A.; Walter, D.; Andreae, M. O.; Artaxo, P.; Carbone, S.; Cheng, Y.; Chowdhury, S.; Ditas, F.; Gysel-Beer, M.; Klimach, T.; Kremper, L. A.; Krüger, O. O.; Lavric, J. V.; Lelieveld, J.; Ma, C.; Machado, L. A. T.; Morais, F. G.; Modini, R. L.; Pozzer, A.; Saturno, J.; Su, H.; Wendisch, M.; Wolff, S.; Pöhlker, M. L.; Pöschl, U., and Pöhlker, C.: "African smoke over the Amazon rain forest". (2021). to be submitted

Pfannerstill, E. Y.; Reijrink, N. G.; Edtbauer, A.; Ringsdorf, A.; Zannoni, N.; Araújo, A.; Ditas, F.; Holanda, B. A.; Sá, M. O.; Tsokankunku, A.; Walter, D.; Wolff, S.; Lavrič, J. V.; Pöhlker, C.; Sörgel, M., and Williams, J.: "Total oh reactivity over the amazon rainforest: variability with temperature, wind, rain, altitude, time of day, season, and an overall budget closure". *Atmospheric Chemistry and Physics*, 21, 8. (2021), pp. 6231–6256. DOI: 10.5194/acp-21-6231-2021. URL: https://acp.copernicus.org/articles/21/6231/2021/

Stevens, B.; Bony, S.; Farrell, D.; Ament, F.; Blyth, A.; Fairall, C.; Karstensen, J.; Quinn, P. K.; Speich, S.; Acquistapace, C.; Aemisegger, F.; Albright, A. L.; Bellenger, H.; Bodenschatz, E.; Caesar, K.-A.; Chewitt-Lucas, R.; Boer, G. de; Delanoë, J.; Denby, L.; Ewald, F.; Fildier, B.; Forde, M.; George, G.; Gross, S.; Hagen, M.; Hausold, A.; Heywood, K. J.; Hirsch, L.; Jacob, M.; Jansen, F.; Kinne, S.; Klocke, D.; Kölling, T.; Konow, H.; Lothon, M.; Mohr, W.; Naumann, A. K.; Nuijens, L.; Olivier, L.; Pincus, R.; Pöhlker, M.; Reverdin, G.; Roberts, G.; Schnitt, S.; Schulz, H.; Siebesma, A. P.; Stephan, C. C.; Sullivan, P.; Touzé-Peiffer, L.; Vial, J.; Vogel, R.; Zuidema, P.; Alexander, N.; Alves, L.; Arixi, S.; Asmath, H.; Bagheri, G.; Baier, K.; Bailey, A.; Baranowski, D.; Baron, A.; Barrau, S.; Barrett, P. A.; Batier, F.; Behrendt, A.; Bendinger, A.; Beucher, F.; Bigorre, S.; Blades, E.; Blossey, P.; Bock, O.; Böing, S.; Bosser, P.; Bourras, D.; Bouruet-Aubertot, P.; Bower, K.; Branellec, P.; Branger, H.; Brennek, M.; Brewer, A.; Brilouet, P.-E.; Brügmann, B.; Buehler, S. A.; Burke, E.; Burton, R.; Calmer, R.; Canonici, J.-C.; Carton, X.; Cato Jr., G.; Charles, J. A.; Chazette, P.; Chen, Y.; Chilinski, M. T.; Choularton, T.; Chuang, P.; Clarke,

S.; Coe, H.; Cornet, C.; Coutris, P.; Couvreux, F.; Crewell, S.; Cronin, T.; Cui, Z.; Cuypers, Y.; Daley, A.; Damerell, G. M.; Dauhut, T.; Deneke, H.; Desbios, J.-P.; Dörner, S.; Donner, S.; Douet, V.; Drushka, K.; Dütsch, M.; Ehrlich, A.; Emanuel, K.; Emmanouilidis, A.; Etienne, J.-C.; Etienne-Leblanc, S.; Faure, G.; Feingold, G.; Ferrero, L.; Fix, A.; Flamant, C.; Flatau, P. J.; Foltz, G. R.; Forster, L.; Furtuna, I.; Gadian, A.; Galewsky, J.; Gallagher, M.; Gallimore, P.; Gaston, C.; Gentemann, C.; Geyskens, N.; Giez, A.; Gollop, J.; Gouirand, I.; Gourbeyre, C.; Graaf, D. de; Groot, G. E. de; Grosz, R.; Güttler, J.; Gutleben, M.; Hall, K.; Harris, G.; Helfer, K. C.; Henze, D.; Herbert, C.; Holanda, B., et al.: "Eurec^{4}a". *Earth System Science Data*, 13, 8. (2021), pp. 4067–4119. DOI: 10.5194/essd-13-4067-2021. URL: https://essd.copernicus.org/articles/13/4067/2021/

Toledo Machado, L. A.; Franco, M. A.; Kremper, L. A.; Ditas, F.; Andreae, M. O.; Artaxo, P.; Cecchini, M. A.; Holanda, B. A.; Pöhlker, M. L.; Saraiva, I.; Wolff, S.; Pöschl, U., and Pöhlker, C.: "How weather events modify aerosol particle size distributions in the amazon boundary layer". *Atmospheric Chemistry and Physics Discussions*, 2021. (2021), pp. 1–31. DOI: 10.5194/acp-2021-314. URL: https://acp.copernicus.org/preprints/acp-2021-314/

Franco, M. A.; Ditas, F.; Kremper, L. A.; Machado, L. A. T.; Andreae, M. O.; Araújo, A.; Barbosa, H. M. J.; Brito, J. F. de; Carbone, S.; Holanda, B. A.; Morais, F. G.; Nascimento, J. P.; Pöhlker, M. L.; Rizzo, L. V.; Sá, M.; Saturno, J.; Walter, D.; Wolff, S.; Pöschl, U.; Artaxo, P., and Pöhlker, C.: "Occurrence and growth of sub 50 nm aerosol particles in the amazonian boundary layer". *Atmospheric Chemistry and Physics Discussions*, 2021. (2021), pp. 1–36. DOI: 10.5194/acp-2021-765. URL: https://acp.copernicus.org/preprints/acp-2021-765/

Andrés Hernández, M. D.; Hilboll, A.; Ziereis, H.; Förster, E.; Krüger, O. O.; Kaiser, K.; Schneider, J.; Barnaba, F.; Vrekoussis, M.; Schmidt, J.; Huntrieser, H.; Blechschmidt, A.-M.; George, M.; Nenakhov, V.; Klausner, T.; Holanda, B. A.; Wolf, J.; Eirenschmalz, L.; Krebsbach, M.; Pöhlker, M. L.; Hedegaard, A. B.; Mei, L.; Pfeilsticker, K.; Liu, Y.; Koppmann, R.; Schlager, H.; Bohn, B.; Schumann, U.; Richter, A.; Schreiner, B.; Sauer, D.; Baumann, R.; Mertens, M.; Jöckel, P.; Kilian, M.; Stratmann, G.; Pöhlker, C.; Campanelli, M.; Pandolfi, M.; Sicard, M.; Gomez-Amo, J. L.; Pujadas, M.; Bigge, K.; Kluge, F.; Schwarz, A.; Daskalakis, N.; Walter, D.; Zahn, A.; Pöschl, U.; Bönisch, H.; Borrmann, S.; Platt, U., and Burrows, J. P.: "Overview: on the transport and transformation of pollutants in the outflow of major population centres – observational data from the emerge european intensive operational period in summer 2017". *Atmospheric Chemistry and Physics Discussions*, 2021. (2021), pp. 1–81. DOI: 10.5194/acp-2021-500. URL: https://acp.copernicus.org/preprints/acp-2021-500/

Braga, R. C.; Rosenfeld, D.; Krüger, O. O.; Ervens, B.; Holanda, B. A.; Wendisch, M.; Krisna, T.; Pöschl, U.; Andreae, M. O.; Voigt, C., and Pöhlker, M. L.: "Linear relationship between effective radius and precipitation water content near the top of convective clouds: measurement results from acridicon–chuva campaign". *Atmospheric Chemistry and Physics*, 21, 18. (2021), pp. 14079–14088. DOI: 10.5194/acp-21-14079-2021. URL: https://acp.copernicus.org/articles/21/14079/2021/

Campos Braga, R.; Ervens, B.; Rosenfeld, D.; Andreae, M. O.; Förster, J.-D.; Fütterer, D.; Hernández Pardo, L.; Holanda, B. A.; Jurkat, T.; Krüger, O. O.; Lauer, O.; Machado, L. A. T.; Pöhlker, C.; Sauer, D.; Voigt, C.; Walser, A.; Wendisch, M.;

Pöschl, U., and Pöhlker, M. L.: "Cloud droplet number closure for tropical convective clouds during the acridicon–chuva campaign". *Atmospheric Chemistry and Physics Discussions*, 2021. (2021), pp. 1–17. DOI: 10.5194/acp-2021-80. URL: https://acp.copernicus.org/preprints/acp-2021-80/

Krüger, O. O.; Holanda, B. A.; Chowdhury, S; Pozzer, A; Walter, D; Pöhlker, C; Dolores, M. H. A.; Burrows, J. P.; Lelieveld, J; Quaas, J; Pöschl, U, and Pöhlker, M. L.: "Reduction in black carbon aerosol concentrations and emissions during the covid-19 lockdown quantified by aircraft measurements over europe". (2021, in preparation)

Voigt, C.; Lelieveld, J.; Schlager, H.; Schneider, J.; Curtius, J.; Meerkötter, R.; Sauer, D.; Bugliaro, L.; Bohn, B.; Crowley, J.; Erbertseder, T.; Groß, S.; Li, Q.; Mertens, M.; Pöhlker, M.; Pozzer, A.; Schumann, U.; Tomsche, L.; Williams, J.; Zahn, A.; Andreae, M.; Borrmann, M.; Bräuer, T.; Dörich, R.; Dörnbrack, A.; Edtbauer, A.; Ernle, L.; Fischer, H.; Giez, A.; Granzin, M.; Grewe, V.; Hahn, V.; Harder, H.; Heinritzi, M.; Holanda, Bruna; Jöckel, P.; Kaiser, K.; Krüger, O.; Lucke, J.; Marsing, A.; Martin, A.; Matthes, S.; Pöhlker, C.; Pöschl, U.; Reifenbergand, S.; Ringsdorf, A.; Scheibe, M.; Tadic, I.; Zauner-Wieczorek, M.; Henke, R., and Rapp, M.: "BLUESKY aircraft mission reveals reduction in atmospheric pollution during the 2020 Corona lockdown". *Bulletin of the American Meteorological Society, - submitted*. (2021)

Artaxo, P.; Hansson, H. C.; Andreae, M. O.; Bäck, J.; Alves, E. G.; Barbosa, H. M. J.; Bender, F.; Bourtsoukidis, E.; Carbone, S.; Chi, J.; Després, V. R.; Ditas, F.; Ezhova, E.; Hasselquist, N. J.; Heintzenberg, J.; Holanda, B. A.; Guenther, A.; Hakola, H.; Heikkinen, L.; Kerminen, V. M.; Kontkanen, J.; Krejci, R.; Kulmala, M.; Lavric, J. V.; Leeuw, G. de; Lehtipalo, K.; Machado, L. A. T.; McFiggans, G.; Franco, M. A. M.; Mohr, C.; Morgan, W.; Nilsson, M. B.; Peichl, M.; Petäjä, T.; Praß, M.; Pöhlker, C.; Pöhlker, M. L.; Pöschl, U.; Von Randow, C.; Riipinen, I.; Rinne, J.; Rizzo, L. V.; Rosenfeld, D.; Silva Dias, M. Assunção Faus da; Sogacheva, L.; Stier, P.; Swietlicki, E.; Sörgel, M.; Tunved, P.; Virkkula, A.; Wang, J.; Weber, B.; Yáñez-Serrano, A. M., and Zieger, P.: "Tropical and boreal forests – atmosphere interactions, a review". *submitted.* (2019)

Botía, S.; Gerbig, C.; Marshall, J.; Lavric, J. V.; Walter, D.; Pöhlker, C.; Holanda, B.; Fisch, G.; Araújo, A. C. de; Sá, M. O.; Teixeira, P. R.; Resende, A. F.; Dias-Junior, C. Q.; Asperen, H. van; Oliveira, P. S.; Stefanello, M., and Acevedo, O. C.: "Understanding nighttime methane signals at the amazon tall tower observatory (atto)". *Atmospheric Chemistry and Physics*, 20, 11. (2020), pp. 6583–6606. DOI: 10.5194/acp-20-6583-2020. URL: https://acp.copernicus.org/articles/20/6583/2020/

Pöhlker, C.; Walter, D.; Paulsen, H.; Könemann, T.; Rodríguez-Caballero, E.; Moran-Zuloaga, D.; Brito, J.; Carbone, S.; Degrendele, C.; Després, V. R.; Ditas, F.; Holanda, B. A.; Kaiser, J. W.; Lammel, G.; Lavrič, J. V.; Ming, J.; Pickersgill, D.; Pöhlker, M. L.; Praß, M.; Löbs, N.; Saturno, J.; Sörgel, M.; Wang, Q.; Weber, B.; Wolff, S.; Artaxo, P.; Pöschl, U., and Andreae, M. O.: "Land cover and its transformation in the backward trajectory footprint region of the amazon tall tower observatory". *Atmos. Chem. Phys.*, 19, 13. (2019), pp. 8425–8470. DOI: 10.5194/acp-19-8425-2019. URL: https://www.atmos-chem-phys.net/19/8425/2019/

Saturno, J.; Holanda, B. A.; Pöhlker, C.; Ditas, F.; Wang, Q.; Moran-Zuloaga, D.; Brito, J.; Carbone, S.; Cheng, Y.; Chi, X.; Ditas, J.; Hoffmann, T.; Angelis, I. Hrabe de; Könemann, T.; Lavrič, J. V.; Ma, N.; Ming, J.; Paulsen, H.; Pöhlker, M. L.;

Rizzo, L. V.; Schlag, P.; Su, H.; Walter, D.; Wolff, S.; Zhang, Y.; Artaxo, P.; Pöschl, U., and Andreae, M. O.: "Black and brown carbon over central amazonia: long-term aerosol measurements at the atto site". *Atmos. Chem. Phys.*, 18, 17. (2018), pp. 12817–12843. DOI: 10.5194/acp-18-12817-2018. URL: https://www.atmos-chem-phys.net/18/12817/2018/

Pöhlker, M. L.; Ditas, F.; Saturno, J.; Klimach, T.; Angelis, I. Hrabě de; Araùjo, A. C.; Brito, J.; Carbone, S.; Cheng, Y.; Chi, X.; Ditz, R.; Gunthe, S. S.; Holanda, B. A.; Kandler, K.; Kesselmeier, J.; Könemann, T.; Krüger, O. O.; Lavrič, J. V.; Martin, S. T.; Mikhailov, E.; Moran-Zuloaga, D.; Rizzo, L. V.; Rose, D.; Su, H.; Thalman, R.; Walter, D.; Wang, J.; Wolff, S.; Barbosa, H. M. J.; Artaxo, P.; Andreae, M. O.; Pöschl, U., and Pöhlker, C.: "Long-term observations of cloud condensation nuclei over the amazon rain forest – part 2: variability and characteristics of biomass burning, long-range transport, and pristine rain forest aerosols". *Atmos. Chem. Phys.*, 18, 14. (2018), pp. 10289–10331. DOI: 10.5194/acp-18-10289-2018. URL: https://www.atmos-chem-phys.net/18/10289/2018/

Andreae, M. O.; Afchine, A.; Albrecht, R.; Holanda, B. A.; Artaxo, P.; Barbosa, H. M. J.; Borrmann, S.; Cecchini, M. A.; Costa, A.; Dollner, M.; Fütterer, D.; Järvinen, E.; Jurkat, T.; Klimach, T.; Konemann, T.; Knote, C.; Krämer, M.; Krisna, T.; Machado, L. A. T.; Mertes, S.; Minikin, A.; Pöhlker, C.; Pöhlker, M. L.; Pöschl, U.; Rosenfeld, D.; Sauer, D.; Schlager, H.; Schnaiter, M.; Schneider, J.; Schulz, C.; Spanu, A.; Sperling, V. B.; Voigt, C.; Walser, A.; Wang, J.; Weinzierl, B.; Wendisch, M., and Ziereis, H.: "Aerosol characteristics and particle production in the upper troposphere over the amazon basin". *Atmospheric Chemistry and Physics*, 18, 2. (2018), pp. 921–961. DOI: 10.5194/acp-18-921-2018. URL: https://acp.copernicus.org/articles/18/921/2018/

Schulz, C.; Schneider, J.; Holanda, B. A.; Appel, O.; Costa, A.; Sá, S. S. de; Dreiling, V.; Fütterer, D.; Jurkat-Witschas, T.; Klimach, T.; Knote, C.; Krämer, M.; Martin, S. T.; Mertes, S.; Pöhlker, M. L.; Sauer, D.; Voigt, C.; Walser, A.; Weinzierl, B.; Ziereis, H.; Zöger, M.; Andreae, M. O.; Artaxo, P.; Machado, L. A. T.; Pöschl, U.; Wendisch, M., and Borrmann, S.: "Aircraft-based observations of isoprene-epoxydiol-derived secondary organic aerosol (iepox-soa) in the tropical upper troposphere over the amazon region". *Atmospheric Chemistry and Physics*, 18, 20. (2018), pp. 14979–15001. DOI: 10.5194/acp-18-14979-2018. URL: https://acp.copernicus.org/articles/18/14979/2018/

Moran-Zuloaga, D.; Ditas, F.; Walter, D.; Saturno, J.; Brito, J.; Carbone, S.; Chi, X.; Angelis, I. Hrabě de; Baars, H.; Godoi, R. H. M.; Heese, B.; Holanda, B. A.; Lavrič, J. V.; Martin, S. T.; Ming, J.; Pöhlker, M. L.; Ruckteschler, N.; Su, H.; Wang, Y.; Wang, Q.; Wang, Z.; Weber, B.; Wolff, S.; Artaxo, P.; Pöschl, U.; Andreae, M. O., and Pöhlker, C.: "Long-term study on coarse mode aerosols in the amazon rain forest with the frequent intrusion of saharan dust plumes". *Atmos. Chem. Phys.*, 18, 13. (2018), pp. 10055–10088. DOI: 10.5194/acp-18-10055-2018. URL: https://www.atmos-chem-phys.net/18/10055/2018/

Saturno, J.; Ditas, F.; Vries, M. Penning de; Holanda, B. A.; Pöhlker, M. L.; Carbone, S.; Walter, D.; Bobrowski, N.; Brito, J.; Chi, X.; Gutmann, A.; Angelis, I. Hrabe de; Machado, L. A. T.; Moran-Zuloaga, D.; Rüdiger, J.; Schneider, J.; Schulz, C.; Wang, Q.; Wendisch, M.; Artaxo, P.; Wagner, T.; Pöschl, U.; Andreae, M. O., and Pöhlker, C.: "African volcanic emissions influencing atmospheric aerosols over the amazon

rain forest". *Atmos. Chem. Phys.*, 18, 14. (2018), pp. 10391–10405. DOI: 10.5194/acp-18-10391-2018. URL: https://www.atmos-chem-phys.net/18/10391/2018/